Dune Transformations Driven by Vegetation Change Arising from Environmental and Anthropogenic Impacts

Yan, Na

Awarding institution:
King's College London

PhD Thesis

Dune Transformations Driven by Vegetation Change Arising from Environmental and Anthropogenic Impacts

Na Yan

Department of Geography

King's College London

Abstract

Parabolic dunes are one of a few common aeolian landforms that are highly controlled by eco-geomorphic interactions. Parabolic dunes, on the one hand, can be developed from highly mobile dune landforms, barchans for instance, in an ameliorated vegetation condition; or on the other hand, they can be reactivated and transformed back into mobile dunes due to vegetation deterioration. The development and transformations of parabolic dunes are also highly sensitive to changes in many environmental factors such as precipitation, temperature, wind regime, as well as changes in land management and other anthropogenic factors. The eco-geomorphic interrelationships and fundamental mechanisms controlling the dune transformations, however, are incompletely understood.

This study combines fieldwork investigation, remote sensing, and Cellular Automaton modelling, to explore both: 1) the dune stabilisation and barchan-to-parabolic dune transformation, as well as 2) the dune reactivation and parabolic-to-barchan dune transformation, under the influence of climatic changes (e.g., drought stress and wind energy), and human disturbance (e.g., grazing activity). Extensive suites of simulations are used to explore boundary conditions, parameter controls, and external forces on both dune transformations. The results show that the characteristics of vegetation play an essential role in the processes of dune transformations, in particular, the species (annual grasses vs. perennial shrubs) and their capabilities of withstanding wind erosion and sand burial. This study has introduced a dune stabilising index (S_*) that captures the interactions between key parameters and establishes the linkage between the system controls and the geometry of a stabilising dune. The dune surface erodibility significantly influences the threshold of climatic forces that reactivates an initial vegetated parabolic dune and transforms its lobe into a mobile barchan dune with arm remnants left behind. The Extended-DECAL can be easily adapted to a different dune system to explore various scenarios under the changes in both natural and anthropogenic controls and to assist in planning judicious land-management practices.

Contents

List of Figures

List of Tables

Acknowledgements

I would like express my heartfelt gratitude to Dr Andreas Baas, who is an inspirational, supportive, and patient supervisor. I appreciate all his contributions, which have made my Ph.D. research a stimulating experience. I would not have achieved this without his dedication to every detail. Likewise, I would like to thank my second supervisor, Professor Nick Drake, who provided me with his valuable supports and advice on remote sensing. I would also like to thank, Professor Hasi Eerdun and his research team at Beijing Normal University. My fieldwork would not be possible without their assistance.

I gratefully acknowledge the funding sources that made my Ph.D. achievable. I was funded by the Graduate School Studentship and the King's Overseas Research Studentship. My fieldwork was also aided by the Dudley Stamp Memorial Award from the Royal Geographical Society (with IBG) and the Postgraduate Research Grant from the British Society for Geomorphology.

As always, I wish to thank my beloved parents for their unconditional love and supports. Last but not least, I would like to extend my appreciations to my colleagues at King's College London, especially Seon Young Lee, Nuttavikhom Phanthuwongpakdee, Louis Raymondin, Briony Turner, Thomas Smith, Junhuan Zhang, Faith Taylor, Joel Gill, Leo Zurita, for their supports throughout the quest toward completing my thesis. To anyone I have not mentioned by name, due to the lack of paper, I value all your help.

Chapter 1

Introduction

Desertification and associated land degradation in dry regions is responsible for increased emission and reduced sink of atmospheric carbon, currently accounting for about 4% of global emissions (Lal, 2001; Millennium Ecosystem Assessment, 2005). Land degradation and vegetation loss also result in severe reduction of global food production (Scherr and Yadav, 1996). Projections of future climatic change, in particular increases in temperature and drought severity and decreases in freshwater availability expected in various regions around the world (IPCC, 2013; Maestre et al., 2012), raise concerns that aeolian activity and desertification may be exacerbated by more active dune transformations, particularly the remobilisation of dunes that are currently stabilised by vegetation and/or biogenic crusts (Ashkenazy et al., 2012; Forman et al., 1992; Lancaster, 1997; Le Houérou, 1996; Muhs and Maat, 1993; Muhs et al., 1996; Thomas et al., 2005; Thomas and Leason, 2005). Relatively small changes in climatological parameters may contribute to an abrupt change in vegetation cover and catastrophic shifts between states of eco-geomorphic systems in which ecological variables and geomorphic variables interact each other on different spatiotemporal scales and together control the overall system behaviour (Bhiry et al., 2011; Lavee et al., 1998; Muckersie and Shepherd, 1995; Rietkerk et al., 2004; Sole, 2007; Yizhaq et al., 2007; Yizhaq et al., 2009).

Despite a growing awareness of great sensitivity of aeolian landforms to vegetation change as well as the diverse feedback between vegetation and sand erosion and burial, the complex eco-geomorphic interrelations between vegetation and dune landforms are not completely understood. Parabolic dunes, for example, are common aeolian landforms that are strongly controlled by eco-geomorphic interactions. Such dunes often form where there is an adequate sand supply, unidirectional wind regime, and moderate vegetation cover (Hugenholtz, 2010; Hugenholtz et al., 2008; Lancaster, 1995; McKee and Bigarella, 1979). Under ameliorating vegetation conditions, parabolic dunes can develop from highly mobile non-vegetated dunes such as barchans (Hart et al., 2012; Reitz et al., 2010; Tsoar and Blumberg, 2002). When the vegetation cover decreases, however, parabolic dunes can be transformed back to highly mobile, non-parabolic dunes (Anton and Vincent, 1986; Hack, 1941). The development

and transformations of parabolic dunes are also highly sensitive to changes in many environmental factors such as precipitation (Landsberg, 1956; Stetler and Gaylord, 1996), temperature (Wolfe and Hugenholtz, 2009), wind strength and variability (Hesp, 2002; Tsoar et al., 2009), as well as to changes in land management and other anthropogenic factors (Hesp, 2001; Tsoar and Blumberg, 2002). Yet, to date, there has been no detailed research on the development of parabolic dunes and their potential dune transformations under the impacts of environmental fluctuations and climatic change as well as anthropogenic pressure.

Within the context described above, the aim of this research is to understand the fundamental mechanisms and environmental controls that govern the transformations from barchan dunes into parabolic dunes as well as from parabolic dunes into barchan dunes. It is achieved through a cellular automaton model that is informed by real-world data from fieldwork investigations and Remote Sensing imagery interpretations. Various functionalities (seasonality, environmental change, and grazing pressure) incorporated in the model can be easily adapted to other environments and vegetation types in a different dune system, and can serve as a tool to assist in understanding eco-geomorphologic interactions of a system and assist in exploring possible future scenarios influenced by both natural and anthropogenic controls.

Eleven chapters are included in this thesis. After reviewing the previous work in terms of the mutual responsive relationship between vegetation and dune transformations over a range of spatial and temporal scales in Chapter 2, objectives and specific research questions are proposed in Chapter 3. Then, Chapter 4 firstly introduces the geographic setting and historical context of the study region, and then analyses the climatic context and the ecological context. The methodology and results of the empirical field study investigated in 2011 and 2012 and remote sensing image interpretations are presented in Chapter 5 and Chapter 6 respectively. Afterwards, Chapter 7 introduces the algorithm of the Extended-DECAL model, and Chapter 8 presents default settings of system parameters, and defines terminology involved in the analysis of modelling results. Chapter 9 fully explores the environmental controls of the barchan-to-parabolic dune transformations. Chapter 10 subsequently examines how climatic change and anthropogenic pressure can lead to the reactivation of parabolic dunes and their transformations into barchans. General discussion and conclusions are finally presented in Chapter 11.

References

Anton, D., Vincent, P., 1986. Parabolic dunes of the Jafurah Desert, Eastern Province, Saudi Arabia. Journal of Arid Environments, 11(3), 187-198.

Ashkenazy, Y., Yizhaq, H., Tsoar, H., 2012. Sand dune mobility under climate change in the Kalahari and Australian deserts. Climatic Change, 112(3-4), 901-923.

Bhiry, N., Delwaide, A., Allard, M., Begin, Y., Filion, L., Lavoie, M., Nozais, C., Payette, S., Pienitz, R., Saulnier-Talbot, E., Vincent, W.F., 2011. Environmental change in the Great Whale River region, Hudson Bay: Five decades of multidisciplinary research by Centre d'etudes nordiques (CEN). Ecoscience, 18(3), 182-203.

Forman, S.L., Goetz, A.F.H., Yuhas, R.H., 1992. Large-scale stabilized dunes on the High Plains of Colorado: Understanding the landscape response to Holocene climates with the aid of images from space. Geology, 20(2), 145-148.

Hack, J.T., 1941. Dunes of the Western Navajo Country. Geogr. Rev., 31(2), 240-263.

Hart, A.T., Hilton, M.J., Wakes, S.J., Dickinson, K.J.M., 2012. The Impact of Ammophila arenaria Foredune Development on Downwind Aerodynamics and Parabolic Dune Development. Journal of Coastal Research, 112-122.

Hesp, P.A., 2001. The Manawatu Dunefield: Environmental Change and Human Impacts. New Zealand Geographer, 57(2), 33-40.

Hesp, P.A., 2002. Foredunes and blowouts: initiation, geomorphology and dynamics. Geomorphology, 48(1-3), 245-268.

Hugenholtz, C.H., 2010. Topographic changes of a supply-limited inland parabolic sand dune during the incipient phase of stabilization. Earth Surface Processes and Landforms, 35(14), 1674-1681.

Hugenholtz, C.H., Wolfe, S.A., Moorman, B.J., 2008. Effects of sand supply on the morphodynamics and stratigraphy of active parabolic dunes, Bigstick Sand Hills, southwestern Saskatchewan. Can. J. Earth Sci., 45(3), 321-335.

IPCC, 2013. Climate change 2013: the physical science basis. Contribution of working group I to the fifth assessment report of the intergovernmental panel on climate change. Cambridge University Press, New York.

Lal, R., 2001. Potential of Desertification Control to Sequester Carbon and Mitigate the Greenhouse Effect. Climatic Change, 51(1), 35-72.

Lancaster, N., 1995. Geomorphology of Desert Dunes. Routledge, London.

Lancaster, N., 1997. Response of eolian geomorphic systems to minor climate change: Examples from the southern Californian deserts. Geomorphology, 19(3-4), 333-347.

Landsberg, S.Y., 1956. The orientation of dunes in Britain and Denmark in relation to wind. Geographical Journal, 122(2), 176-189.

Lavee, H., Imeson, A.C., Sarah, P., 1998. The impact of climate change on geomorphology and desertification along a mediterranean-arid transect. Land Degradation & Development, 9(5), 407-422.

Le Houérou, H.N., 1996. Climate change, drought and desertification. Journal of Arid Environments, 34(2), 133-185.

Maestre, F.T., Salguero-Gomez, R., Quero, J.L., 2012. It is getting hotter in here: determining and projecting the impacts of global environmental change on drylands Introduction. Philos. Trans. R. Soc. B-Biol. Sci., 367(1606), 3062-3075.

McKee, E.D., Bigarella, J.J., 1979. Sedimentary structures in dunes. In: E.D. McKee (Ed.), A Study of Global Sand Seas. U.S. Geological Survey Professional Paper 1052, pp. 83-134.

Millennium Ecosystem Assessment, 2005. Ecosystems and Human Well-being: Desertification Synthesis. World Resources Institute, Washington, DC.

Muckersie, C., Shepherd, M.J., 1995. Dune phases as time-transgressive phenomena, Manawatu, New Zealand. Quaternary International, 26, 61-67.

Muhs, D.R., Maat, P.B., 1993. The potential response of eolian sands to greenhouse warming and precipitation reduction on the Great Plains of the U.S.A. Journal of Arid Environments, 25(4), 351-361.

Muhs, D.R., Stafford, T.W., Cowherd, S.D., Mahan, S.A., Kihl, R., Maat, P.B., Bush, C.A., Nehring, J., 1996. Origin of the late Quaternary dune fields of northeastern Colorado. Geomorphology, 17(1-3), 129-149.

Reitz, M.D., Jerolmack, D.J., Ewing, R.C., Martin, R.L., 2010. Barchan-parabolic dune pattern transition from vegetation stability threshold. Geophysical Research Letters, 37.

Rietkerk, M., Dekker, S.C., de Ruiter, P.C., van de Koppel, J., 2004. Self-Organized Patchiness and Catastrophic Shifts in Ecosystems. Science, 305(5692), 1926-1929.

Scherr, S.J., Yadav, S., 1996. Land degradation in the developing world: implications for food, agriculture and the environment to 2020. IFPRI, Food, Agric. and the Environment Discussion Paper 14, Washington, DC.

Sole, R., 2007. Ecology: Scaling laws in the drier. Nature, 449(7159), 151-153.

Stetler, L.D., Gaylord, D.R., 1996. Evaluating eolian-climatic interactions using a regional climate model from Hanford, Washington (USA). Geomorphology, 17(1–3), 99-113.

Thomas, D.S.G., Knight, M., Wiggs, G.F.S., 2005. Remobilization of southern African desert dune systems by twenty-first century global warming. Nature, 435(7046), 1218-1221.

Thomas, D.S.G., Leason, H.C., 2005. Dunefield activity response to climate variability in the southwest Kalahari. Geomorphology, 64(1–2), 117-132.

Tsoar, H., Blumberg, D.G., 2002. Formation of parabolic dunes from barchan and transverse dunes along Israel's Mediterranean coast. Earth Surface Processes and Landforms, 27(11), 1147-1161.

Tsoar, H., Levin, N., Porat, N., Maia, L.P., Herrmann, H.J., Tatumi, S.H., Claudino-Sales, V., 2009. The effect of climate change on the mobility and stability of coastal sand dunes in Ceará State (NE Brazil). Quaternary Research, 71(2), 217-226.

Wolfe, S.A., Hugenholtz, C.H., 2009. Barchan dunes stabilized under recent climate warming on the northern Great Plains. Geology, 37(11), 1039-1042.

Yizhaq, H., Ashkenazy, Y., Tsoar, H., 2007. Why Do Active and Stabilized Dunes Coexist under the Same Climatic Conditions? Physical Review Letters, 98(18), 188001.

Yizhaq, H., Ashkenazy, Y., Tsoar, H., 2009. Sand dune dynamics and climate change: A modeling approach. Journal of Geophysical Research: Earth Surface, 114(F1), F01023.

Chapter 2

Background and Rationale

This chapter:

- Reviews past research on morphology, development, and migration of parabolic dunes;
- Compiles a comprehensive global inventory of studied parabolic dunefields across a variety of climatic zones;
- Explores mechanisms of parabolic dune related transformations (both stabilisation and activation) and their implications of dunefield mobility and land management practices in the context of climatic changes.

This chapter provides the background and rationale of the dune stabilisation from highly mobile barchan dunes into vegetated parabolic dunes as well as the dune activation from parabolic dunes into highly mobile non-parabolic dunes, and explores the possible mechanisms and physical processes underlying both dune transformations. Based on the knowledge, the hypothesis and objectives of this research are then proposed in Chapter 3.

2.1 Morphology, Development, and Migration of Parabolic Dunes

Simple parabolic dunes are U- or V-shaped dunes in plan with two trailing arms pointing upwind, a deflation basin contained within arms, and a depositional lobe at the downwind end (Hesp and Walker, 2013; Pye and Tsoar, 1990). Vegetation, usually shrubs or trees, surrounding the parabolic dunes can resist widening of the deflation basins, whilst plants on the trailing arms can bind sand and maintain the parabolic shape of dunes. Many parabolic dunes have a slip face, and some large ones may have multiple crests and slip faces. As the airflow approaches towards the dune crest, flow is compressed by the stoss slope, resulting in the increases in shear stress and sediment transport. Beyond the crest, flow expands and may create a separation zone within which positive

pressure causes reversal of flow back up the lee slope, forming 'back-eddies' (Delgado-Fernandez et al., 2013; Walker and Nickling, 2002). In the zones of flow separation, flow deceleration causes grainfall deposition which forms grainfall lamination on slip faces (Hunter, 1977). As deposition continues, avalanching occurs where the slope angle reaches the critical angle of repose. The resulting grainflow and sand flowage change pre-existing stratification and form cross-strata (Hugenholtz et al., 2007; Hunter, 1977).

Parabolic dunes can exhibit variable morphologies (Cooke et al., 1993; Kilibarda and Blockland, 2011) (Figure 2-1), governed by wind regime, sediment supply and local vegetation characteristics (Baas, 2007; Hack, 1941; Hugenholtz, 2010; Pye, 1990; Rubin and Hunter, 1987; Wasson and Hyde, 1983).

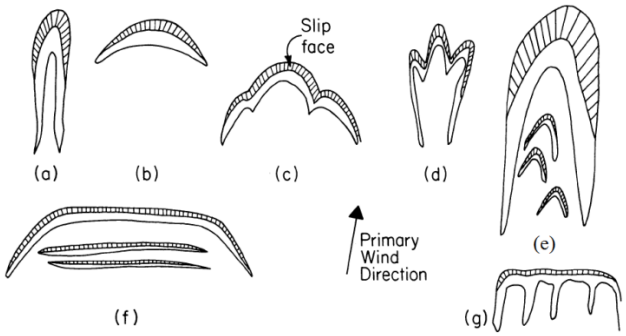

Figure 2-1. Diagram from Pye and Tsoar (1990) showing the following seven morphologies of parabolic dunes: (a) hairpin; (b) lunate; (c) hemicyclic; (d) digitate; (e) nested; (f) long-walled transgressive ridge with secondary transverse dunes; and (g) rake-like en-echelon dunes.

Elongated parabolic dunes with long-walled arms, also referred to as hairpin- or U-shaped dunes, develop in a strong unidirectional wind regime, whereas a greater directional variability results in much shorter trailing arms and imbricate dune forms (Gaylord and Dawson, 1987; Hesp and Walker, 2013; Pye, 1982; Pye, 1983c; Tinley, 1985). Cross-winds that blow oblique to the prevailing wind may lead to left- or right-handed asymmetry in dune morphology. Where multiple discrete wind directions dominate at different times, hemicyclic- or digitate-shaped parabolic dunes may form (Filion and Morisset, 1983; Pye and Tsoar, 1990). The seasonal variations of winds also significantly influence airflow patterns and sediment transport over dunes (Byrne, 1997; Hansen et al., 2009).

Relatively abundant sediment supply is crucial for dunes to maintain their mobility and grow in height. The availability of external sediment supply from sandy beaches and foredunes largely controls the size of coastal dunefields (Aren et al. 2004). As dunes move forward, they can also grow in height by incorporating sand from their substrata underneath (Livingstone and Warren, 1996). If dunes move onto a non-sandy substratum in the absence of an external sediment supply, the depositional lobes may flatten gradually due to continuous sand loss.

The ecological conditions and characteristics of the regional vegetation are the other essential factors determining the morphology of parabolic dunes. Digitate parabolic dunes are usually associated with the presence of a forest cover, as trees force dunes to move in divergent directions and facilitate the formation of high depositional lobes with steep windward and lee slopes (Buynevich et al., 2010; Filion and Morisset, 1983; Levin, 2011). If a regeneration of the tree population is interrupted (by wildfires, for example), digitate parabolic dunes can further transform to hemicyclic dunes (Filion and Morisset, 1983). Long-lived perennial shrubs may also play an important role in trapping sediment, developing into nebkhas, and maintaining the shape of parabolic dunes (Hesp, 2008; Tsoar and Blumberg, 2002). Ephemeral annual plants, however, can only anchor dune surfaces temporarily and suffer abrupt changes under external pressures (e.g., precipitation, temperature and grazing intensities), and therefore exert minimal impacts.

Migration of parabolic dunes is principally controlled by the interplay between sand drift potential imparted by wind regime, moisture content and vegetation cover (Ash and Wasson, 1983; Bagnold, 1941; Fryberger, 1979; Lancaster, 1997; Lancaster and Baas, 1998).

The orientation of coastal parabolic dunes is largely determined by wind regime (Jennings, 1957; Landsberg, 1956), which is usually defined in terms of sand drift potential, reflecting the capacity of winds to transport sediment, as an index of regional wind energy (Arens et al., 2004; Fryberger, 1979; Levin, 2011; Levin et al., 2006; Tsoar, 2005; Wasson and Hyde, 1983).

Moisture content, which is largely controlled by precipitation and evapotranspiration, is another crucial factor for modifying sand transport and the associated dune migration (Lancaster, 1997; Tsoar, 2005). The spatial heterogeneity of soil moisture resulting from differences of local micro-environments (e.g., slope) can lead to spatial variations in sedimentation balance (Ritsema and Dekker, 1994; Stout, 2004). A greater moisture content of sand increases the critical shear

velocity needed for the initiation of particle movement and inhibits sediment transport (Belly, 1964; Cornelis and Gabriels, 2003; Davidson-Arnott et al., 2008; Hugenholtz et al., 2009; Jackson and Nordstrom, 1998; Namikas and Sherman, 1995; Wiggs et al., 2004). Precipitation can, therefore, reduce the migration rates of parabolic dunes significantly (Arens et al., 2004). For example, at the Great Sand Dunes National Park and Preserve (Colorado, USA), some parabolic dunes were mobilised six times faster during drought periods than (preceding or subsequent) wet periods (Marín et al., 2005).

Unpredictable rainfall events in semi-arid regions, moreover, encourage the growth of vegetation characterised by a 'pulse-activity' response (Noy-Meir, 1973; Wand et al., 1999), and further increase surface roughness (Wolfe and Nickling, 1996). In the more humid coastal dune areas, however, precipitation variations can also significantly influence the local water table and subsequently change the sand availability, vegetation cover and dunefield mobility (Luna et al., 2012; Miot da Silva and Hesp, 2013). The spatial distribution and temporal variations of vegetation then alter the airflow dynamics over the surface, and influence the spatial heterogeneity in the migration rate of a single dune and of a dunefield as a whole (Kuriyama et al., 2005; Lancaster and Baas, 1998; Wasson and Nanninga, 1986; Wiggs et al., 1995).

Migration rates of parabolic dunes reported in the literature (Table 2-1) naturally vary because of different local environmental settings but also depend on the measuring methods used. Typical measurement approaches, from short to long time scales, include ground surveys by setting transects and/or pins (Arens et al., 2004; Cooper, 1958; Ranwell, 1958; Wolfe and Lemmen, 1999), interpretation of multi-time aerial photographs and topographic maps (Anthonsen et al., 1996; Arens et al., 2004; Bailey and Bristow, 2004; Hesp, 2001; Hugenholtz et al., 2008; Marín et al., 2005; Pye, 1982; Siljeström and Clemente, 1990; Stetler and Gaylord, 1996; Tsoar and Blumberg, 2002), and chronological dating such as tree-ring dating and optical dating (Cooper, 1958; David et al., 1999; Wiles et al., 2003).

Table 2-1. Research on migration rates of parabolic dunes.

Reference	Study Region	Average Migration Rate (m yr^{-1})	Data	Measuring Period (yr)	Method
		Australia			
Pye, 1982	Cape Bedform, Queensland	4.8	1 dune	18	aerial photographic interpretation
	Mt. Mitchell dune, Cape Flattery, Queensland	5.6	1 dune	19	aerial photographic interpretation
Story, 1982	Northern Australia	0.05	2 dunes	32	aerial photographic interpretation
Pye, 1983a	Northern Cape York Peninsula dunefield, Queensland	<6	-	-	description
Pye, 1983b	Temple Bay, Northern Cape York Peninsula	3-4	-	-	field surveys
		Brazil			
Bigarella et al., 2005	Lagoa dune field, Santa Catarina Island	2.49	1 dune	29	aerial photographic interpretation and topographic measurements of dune nose crest advance
Barbosa and Dominguez, 2004	São Francisco River Strandplain	24	-	33	aerial photographic interpretation and field measurements of spacing between ridges
		Canada			
Hugenholtz et al., 2008	Bigstick Sand Hills, Saskatchewan	3.4	3 dunes	56	aerial photographic interpretation
Wolfe and Lemmen, 1999	Great Sand Hills, Saskatchewan	2.6	7 dunes	3	measurements of slip face advance
David et al., 1999	Seward Sand Hills, Saskatchewan	2.2	7 dunes	60	optical dating chronology and aerial photographic interpretation
		Denmark			
Anthonsen et al., 1996	Råbjerg Mile, Skagen Odde	12.2	1 dune	53	digital terrain models from topographic maps
		Israel			
Tsoar and Blumberg, 2002	South-eastern Mediterranean coast	2.8	15 dunes	46	aerial photographic interpretation
		Netherlands			
Arens et al., 2004	Kennemerland, Netherlands	3	1 dune	2	aerial photographic interpretation and erosion pin measurements
		New Zealand			
Brothers, 1954	Auckland	2.7	-	44	literature records
Hesp, 2001	Manawatu	5 - 80	-	various	aerial photographic interpretation
Muckersie and Shepherd, 1995	Manawatu	5	-	-	estimated from previous studies
Hart et al., 2012	Mason Bay	24 / 0.79	1 dune	20 / 13	aerial photographic interpretation and field surveys by a total station
		Spain			
García-Novo et al., 1976	Doñana National Park	5	-	-	aerial photographic interpretation
Arteaga et al., 2008	Liencres dune system, Cantabria	8.5	1 dune, 11 profiles	1.4	photogrammetric techniques and topographic surveys by a total station
		United Kingdom			
Ranwell, 1958	Anglesey, Wales	1.5-6.7	6 transects, 2 dunes	3	transects across dune ridges along dune migrating direction
Bailey and Bristow, 2004	Anglesey, Wales	1	4 dune ridges	53	Linear-fit method calculated from aerial photographs
	Anglesey, Wales	1.3	4 dune ridges	53	Crest-to-crest method calculated from aerial photographs
		United States			
Forman et al., 2008	Cape Cod National Seashore, Massachusetts	4 / 1	12 dunes	39 / 16	aerial photographic interpretation
Marín et al., 2005	Great Sand Dunes, Colorado	7.9	13 dunes	63	remote sensing imagery (Landsat ETM) interpretation
Stetler and Gaylord, 1996	Hanford, Washington	1.8	-	39	stereo aerial photographic interpretation
Yurk et al., 2002	Holland, eastern shore of Lake Michigan	1.45	1 dune	61	aerial photographic interpretation
Wiles et al., 2003	Northern Chugach Mountains, Alaska	1 - 3	2 transects	200	tree-ring dating
Cooper, 1958	Oregon	1.6	-	6	measurements of slip face advance

	Oregon	<2.11	-	51	tree-ring dating
Girardi and Davis, 2010	Walking Dunes, New York	<5	1 dune	74	geo-referenced maps and aerial photographic interpretation

In contrast to barchan dunes that move forward as coherent entities, parabolic dunes continuously change in form as they elongate downwind. Whilst the arms of parabolic dunes are largely fixed in place by vegetation, the dune depositional lobes migrate at various rates. A wide morphological variety reinforces a great spatial heterogeneity in dune mobility. Precisely determining migration rates of parabolic dunes is thus a challenge (Bailey and Bristow, 2004; Girardi and Davis, 2010). Some studies have measured the advance of slip faces (Cooper, 1958; Forman et al., 2008; Wolfe and Lemmen, 1999), whereas others have used a linear-fit method or a crest-to-crest method (Bailey and Bristow, 2004). One study, furthermore, proposed a calculus method aided with GIS technology to determine the average migration rates of lobes (Levin and Ben-Dor, 2004; Levin, 2011). Meanwhile, as a migration rate measured is an average over a certain time period and usually also an average of a number of dunes in an area, measuring frequency and duration (in addition to the spatial scope of study sites) are also key factors for determining the migration rate.

Because of climatic instability, a dune migration rate should be evaluated on a sensible spatiotemporal scale (Lockwood, 2001). A migration rate based on a short period of field experiments (usually a few events or years) can hardly be scaled up to provide an adequate understanding of long-term dune behaviour (on a temporal scale of decades or centuries). Likewise, chronological dating elucidates long-term historical trajectories (e.g., centuries) of dunefield development, but is insufficient to assist in a detailed understanding of shorter-term variations (e.g., seasons or decades) (Aagaard et al., 2004; Sherman, 1995).

Changes in migration rates of parabolic dunes may be caused by external forces such as environmental controls and human activities (Forman et al., 2008), but also by internal or autocyclic adjustments of a geomorphological system (Brunsden, 2001). Some large parabolic dunes may migrate faster than smaller ones because of ample sand supply for wind entrainment and less vegetation impeding saltation (Marín et al., 2005). Relatively small surface roughness creates less turbulence, thereby increasing the sand transport efficiency and the dune migration rate. When a dune moves onto a thicker sandy substratum, the dune migrates slower because the substratum provides more abundant sand supply to the dune. Similarly, in a sand-starving

environment, as the lobe of a parabolic dune shrinks over time the dune migrates at an increasing rate. Collectively, a dune migration rate is a poor indicator of mobility of a larger dune system.

In order to estimate impacts of physical and anthropogenic variables on the development of aeolian dunes and to anticipate potential changes in dunefield mobility in the context of environmental fluctuations and climatic changes, it is necessary to choose an appropriate time scale. Because dune dynamics involve time-lags and hysteresis effects between climate and dune mobility, an appropriate time scale should ensure that geomorphological components of an aeolian system have had sufficient response time to adjust themselves to external conditions such as temperature and precipitation (Hugenholtz and Wolfe, 2005; Knight et al., 2004; Levin, 2011; Yizhaq et al., 2009). The response time of dunes, however, differs depending on the characteristics of different geomorphological components (e.g., the flora) (Overpeck et al., 1992), as well as on the spatial scale (e.g., local, regional or global) of climatic changes to which the dunes are responding (Huggett, 1991). Moreover, a sensible spatial scale is needed to differentiate the spatial variability of individual dune mobility from entire dunefield mobility, a variability that arises from the specific history of single dunes, for instance related to localised anthropogenic impacts.

2.2 Distribution of Parabolic Dunes

A global distribution of parabolic dunefields was collected from a comprehensive literature review of approximately 250 publications, and all sites mentioned in the literature sources were examined from Google Earth imagery. Presently discernible parabolic dunefields were compiled and mapped as shown in Figure 2-2. Some parabolic dunefields reported in literature have been reshaped by human activities (e.g., agriculture, recreation and urbanisation), and in some regions have been largely destroyed (e.g., in Portugal, Hungary, Poland and Brazil). In China, in particular, few coastal parabolic dunefields have survived the large-scale urbanisation and industrialisation. Some other dunefields could not be identified because of insufficient image resolution and/or because they had become covered with dense vegetation. An undocumented active parabolic dunefield has also been found on the southwest coasts of Madagascar.

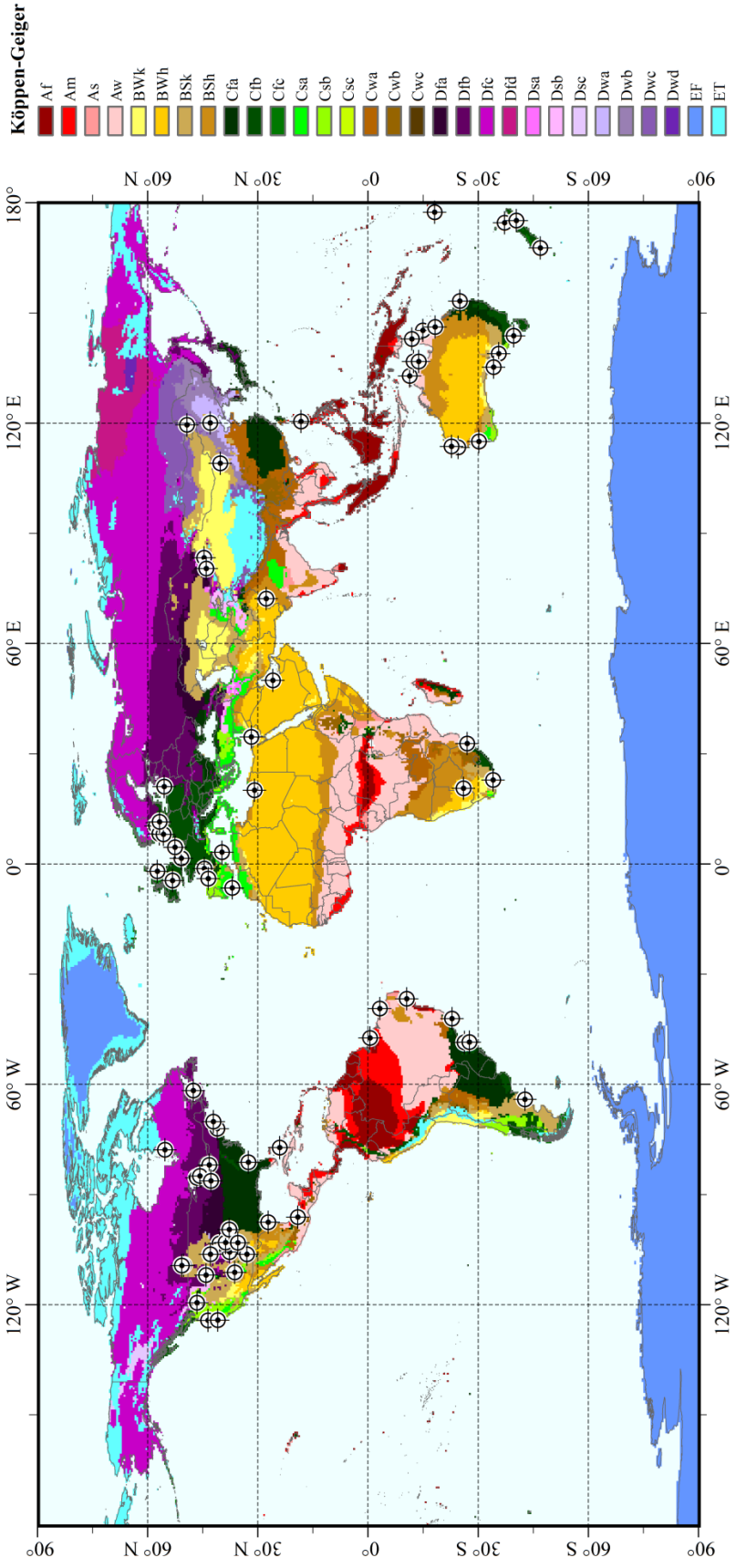

Figure 2-2. Global distribution of parabolic dunes. Köppen-Geiger climate zone is adapted from Kottek et al., (2006).

Research on parabolic dunes started in the first half of the 20th century in the United States (Cooper, 1958; Hack, 1941; Melton, 1940), Australia (Jennings, 1957), New Zealand (Brothers, 1954) and Europe (Lefevre, 1931; Landsberg, 1956; Paul, 1944). Early research was mainly limited to qualitative description of dune morphology and local distribution, an attempt at morphology-based classification, and associated conjectures regarding dune origins and formative processes. The crucial role of wind regime on the development and morphology of parabolic dunes has been well-recognised (Bagnold, 1941; Fryberger, 1979; Jennings, 1957), but only a number of studies quantitatively measured dune morphology and migration rates (Brothers, 1954; Cooper, 1958; Ranwell, 1958).

The importance of parabolic dunes did not gain much attention until the 1980s, when research gradually expanded to a number of different regions including India (Wasson et al., 1983), Australia (Pye, 1982; Story, 1982), Fiji (Kirkpatrick and Hassall, 1981), South Africa (Eriksson et al., 1989) and Saudi Arabia (Anton and Vincent, 1986). During this period, research focused on field measurements and understandings of physical processes (flow dynamics and sand transport) and controlling factors (wind regime, sediment supply and vegetation cover). Different dune transformations have been noted in various regions, yet detailed investigation has been absent. Increasingly wide use of advanced technology such as aerial photographs, nevertheless, expanded research on a much larger spatial and longer temporal scale, which facilitated the systematic exploration and comparison of parabolic dunes in various environments and also facilitated the development of schematic models regarding dune formation and classification (David et al., 1999; Pye, 1982; Wolfe and David, 1997).

From 1995 onwards, more research on parabolic dunes has been conducted across different climatic regions both on the coast and inland. In particular, the use of computer modelling and simulation, expanded from the Werner Model (Werner, 1995), has enabled exploration of fundamental principles underlying the dynamics of dune patterns and testing of possible assumptions based on real-world observations and investigations. Parabolic dunes with trailing arms developing from blowouts have been successfully simulated by the Discrete Eco-geomorphic Aeolian Landscape (DECAL) model (Baas, 2002; Nield and Baas, 2008), whilst a dune transformation from the barchan to the parabolic form has been simulated with a continuous model (Duran et al., 2008). GIS technology, advances in remote sensing (e.g., LiDAR), and advances in luminescence dating techniques have further expanded the capability and scope of

investigations (Anthonsen et al., 1996; Levin and Ben-Dor, 2004; Tsoar and Blumberg, 2002; Swezey et al., 2013; Wolfe and Hugenholtz, 2009).

Presently, with progressive concerns about the potential impacts of climatic changes on aeolian dune environments and associated impacts of human behaviour, parabolic dunes are receiving increased attention because of their sensitivity to changes in environmental conditions. Research on potential activation of currently stabilised parabolic dunefields imparted by climatic variations has been conducted in a few regions such as the Canadian Prairies (Hugenholtz and Wolfe, 2005; Wolfe, 1997) and Israel (Tsoar, 2005), and will likely continue to be an important topic.

As indicated in Figure 2-2 and Table 2-2, parabolic dunes are widely spread across a large range of climatic gradients from hot equatorial savannah (Fernandez et al., 2009; Hesp et al., 2010; Hesp, 2008; Porat and Botha, 2008; Pye, 1982; Shulmeister and Lees, 1992) to warm climates (Anthonsen et al., 1996; Arens et al., 2004; Clemmensen et al., 2007; Hart et al., 2012; Morkunaite et al., 2011; Tsoar and Blumberg, 2002; Zular et al., 2013) to cold climates (Bélanger and Filion, 1991; Bhiry et al., 2011; Eyles and Meulendyk, 2012; McKee, 1966), and from humid climates (Bailey and Bristow, 2004; Bigarella et al., 2006; Levin, 2011; Ranwell, 1958; Wakes et al., 2010) to arid climates (Hack, 1941; Hugenholtz et al., 2010; Hugenholtz et al., 2008; Reitz et al., 2010; Wolfe and Lemmen, 1999; Yan et al., 2010) to hyper-arid desert climates (Anton and Vincent, 1986; Carter et al., 1990; Eriksson et al., 1989; Kar et al., 1998; Nichol and Brooke, 2011). In contrast to highly mobile barchan dunes and transverse dunes that may be distributed extensively across a large region, parabolic dunes are usually restricted to relatively small areas, mostly arranged in belts in coastal settings, or along inland river valleys and lake shores.

Table 2-2. Global distribution of parabolic dunes.

Region	Representative Literature	Köppen-Geiger Climate Zone & Main Climate	Mean Annual Precipitation (mm)	Mean Annual Temperature (˚C)	Location
		Argentina			
Valdes Peninsula, Northeastern Patagonia	del Valle et al., 2010	BSk: arid steppe climate	steppe 231	cold arid 13	coastal
		Australia			
Cape Bedford and Cape Flattery, Queensland	Pye, 1982; 1984	Aw: equatorial savannah with dry winter	winter dry 1784	hot 27	coastal
Cervantes-Dongara coast	Shepherd and Eliot, 1995	Csa: warm temperate climate with dry summer	summer dry 534	hot summer 20	coastal
Eyre Peninsula	Dutkiewicz and Prescott, 1997	Csb: warm temperate climate with dry summer	summer dry 383	warm summer 18	coastal
Fraser Island	Ward, 2006; Levin, 2011	Cfa: warm temperate climate	fully humid 1200	hot summer 22	coastal
Groote Eylandt	Shulmeister and Lees, 1992	Aw: equatorial savannah with dry winter	winter dry 1350	hot 26	coastal
King Island, Tasmania	Jennings, 1957	Csb: warm temperate climate with dry summer	summer dry 811	warm summer 13	coastal
north of Carnarvon	Carter et al., 1990	BWh: desert climate	desert 241	hot arid 31	coastal
Northern Cape York Peninsula, Queensland	Pye, 1983b; 1984	Aw: equatorial savannah with dry winter	winter dry 1745	hot 26	coastal
Northern Territory coast	Story, 1982	Aw: equatorial savannah with dry winter	winter dry 1200	hot 27	coastal
Point Cloates, Carnarvon shelf	Nichol and Brooke, 2011	BWh: desert climate	desert 226	hot arid 22	coastal
Ramsay Bay, Hinchinbrook Island, Queensland	Pye, 1983a; 1984; Pye and Mazzullo, 1994	Am: equatorial monsoon	monsoonal 2143	hot 25	coastal
River Murray mouth region	Murray-Wallace et al., 2010	Csb: warm temperate Mediterranean climate with dry summer	summer dry 400	warm summer 16	coastal
		Brazil			
Atalaia Beach, Pará State	Buynevich et al., 2010	Am: equatorial monsoon	monsoonal 2500	hot 25	coastal
Fortaleza, Ceará	Duran et al., 2008	As: equatorial savannah with dry summer	summer dry 1642	hot 27	coastal
Lagoa dunefield, Santa Catarina Island	Bigarella et al., 2005; 2006	Cfa: warm temperate subtropical climate	fully humid 1521	hot summer 21	coastal
Rio de Janeiro coast	Fernandez et al., 2009	Aw: equatorial savannah with dry winter	winter dry 771	hot 24	coastal
São Francisco do Sul coastal barrier	Zular et al., 2013	Cfa: warm temperate subtropical climate	fully humid 1250	hot summer 18	coastal
São Francisco River Strand Plain	Barbosa and Dominguez, 2004	As: equatorial savannah with dry summer	summer dry 1700	hot 24	coastal
		Canada			
Bigstick Sand Hills, Saskatchewan	Hugenholtz et al., 2007; Hugenholtz, 2010	BSk: continental steppe climate	steppe 380	cold arid 3	inland, river bank
Eastern coast of Hudson Bay, Northern Québec	Filion and Morisset, 1983; Bélanger and Filion, 1991; Bhiry et al., 2011	Dfc: snow climate	fully humid 637	cool summer -4	coastal
Îles de la Madeleine, Quebec	Giles and McCann, 1997	Dfb: snow climate	fully humid 795	warm summer 5	coastal
Lake Huron coast, Ontario	Byrne, 1997; Eyles and Meulendyk, 2012	Dfb: snow climate	fully humid 847	warm summer 8	inland, lake shore
Northern Great Plains, Saskatchewan	Wolfe and Hugenholtz, 2009	BSk: continental steppe climate	steppe 380	cold arid 3	inland, river bank
		China			
Ebinur Lake district, Xinjiang	Jia et al., 2012	BWk: arid desert climate	desert 91	cold arid 8	inland, lake shore
Hobq Desert, Ordos, Inner	Yan, 2010; Zhang et al.,	BSk: arid steppe climate	steppe 312	cold arid 7	inland,

Mongolia	2011				river bank
Horqin Desert, Inner Mongolia	Yan, 2010	BSk: arid steppe climate	steppe 360	cold arid 5	inland, river bank
Hulunbuir Grasslands, Inner Mongolia	Zhuang and Hasi, 2005; Yan, 2010	Dwb: snow climate with dry winter	winter dry 354	warm summer -1	inland, river bank
Take Ermu Ku'er Desert, Xinjiang	Zeng, 2008	BSk: arid desert climate	steppe 178	cold arid 10	inland, river bank
Denmark					
Anholt, Kattegat	Clemmensen et al., 2007	Cfb: warm temperate climate	fully humid 478	warm summer 9	coastal
Lodbjerg, northwest coast of Jutland	Clemmensen et al., 2001	Cfb: warm temperate climate	fully humid 359	warm summer 9	coastal
Råbjerg Mile, Skagen Odde	Anthonsen et al., 1996	Cfb: warm temperate climate	fully humid 706	warm summer 7	coastal
Vejers, west coast of Jutland	Clemmensen et al., 1996	Cfb: warm temperate climate	fully humid 355	warm summer 9	coastal
Fiji					
Sigatoka sand dunes, Viti Levu	Kirkpatrick and Hassall, 1981	Af: equatorial rainforest	fully humid 1862	hot 30	coastal
France					
Northern shore	Meurisse et al., 2005	Cfb: warm temperate climate	fully humid 592	warm summer 11	coastal
Southwestern coast	Bertran et al. 2011	Cfb: warm temperate climate	fully humid 823	warm summer 11	coastal
India & Pakistan					
Thar Desert	Wasson et al., 1983; Goossens et al., 1993; Kar et al., 1998	BWh: tropical desert climate	desert 172	hot arid 27	inland, river bank
Israel					
Southeastern Mediterranean Coast	Tsoar and Blumberg, 2002; Ardon et al., 2009	Csa: warm temperate Mediterranean climate with dry summer	summer dry 500	hot summer 20	coastal
Libya					
Adjabiya coast	Goudie 2011	BWh: desert climate	desert 143	hot arid 21	coastal
Lithuania					
Curonian Spit, southeastern Baltic Sea Coast	Morkunaite et al., 2011	Cfb: warm temperate climate, intermediate between marine and continental	fully humid 660	warm summer 7	coastal
Mexico					
El Farallon-La Mancha Dunefield	Hesp et al., 2010	Aw: equatorial savannah with dry winter	winter dry 1200	hot 24	coastal
Netherlands					
Castricum	Jungerius and Riksen, 2010	Cfb: warm temperate climate	fully humid 847	warm summer 10	coastal
Kennemerland	Arens et al., 2004	Cfb: warm temperate climate	fully humid 847	warm summer 10	coastal
New Zealand					
Manawatu coastal plain	Hesp, 2001; Clement et al., 2010	Cfb: warm temperate maritime climate	fully humid 900	warm summer 13	coastal
Mason Bay, Stewart Island	Wakes et al., 2010; Hart et al., 2012	Cfb: warm temperate maritime climate	fully humid 1324	warm summer 10	coastal
Western coast of Auckland	Brothers, 1954	Cfb: warm temperate maritime climate	fully humid 1240	warm summer 15	coastal
Philippines					
Ilocos Norte	Hesp, 2008	Aw: equatorial savannah with dry winter	winter dry 2067	hot 27	coastal
Saudi Arabia					
Jafurah Desert, Eastern Province	Anton and Vincent, 1986	BWh: desert climate, Indian Ocean Monsoonal	desert 88	hot arid 27	coastal
South Africa					

Maputaland coastal plain	Porat and Botha, 2008	Aw: equatorial savannah with dry winter	winter dry 1100	hot 22	coastal
Southern Kalahari Desert	Eriksson et al., 1989	BWh: arid to semi-arid desert climate	desert 237	hot arid 18	inland, river bank
Wilderness Dune Cordons	Hellström, 1996; Illenberger, 1996	Cfb: warm temperate climate	fully humid 681	warm summer 17	coastal
		Spain			
Doñana National Park	Siljeström and Clemente, 1990	Csa: warm temperate Mediterranean climate with dry summer	summer dry 542	hot summer 17	coastal
Liencres dune system, Cantabria	Arteaga et al., 2008	Cfb: warm temperate climate	fully humid 1150	warm summer 14	coastal
Mallorca	Servera et al., 2009	Csa: warm temperate Mediterranean climate with dry summer	summer dry 427	hot summer 18	island
		United Kingdom			
Anglesey, north Wales	Bailey and Bristow, 2004	Cfb: warm temperate maritime climate	fully humid 1434	warm summer 11	coastal
Sands of Forvie, Scotland	Robertson-Rintoul, 1990; Ritchie, 2000	Cfb: warm temperate maritime climate	fully humid 750	warm summer 9	coastal
		United States			
Cape Cod National Seashore, Massachusetts	Forman et al., 2008	Cfa: warm temperate climate	fully humid 1065	hot summer 10	coastal
Casper, Wyoming	Halfen et al., 2010	BSk: semi-arid steppe climate	steppe 300	cold arid 7	inland, river bank
Eastern Colorado	Madole, 1995	BSk: semi-arid steppe climate	steppe 380	cold arid 10	inland, river bank
eastern Upper Michigan	Loope et al., 2010	Dfb: snow continental climate	fully humid 3500	warm summer 6	inland, lake shore
Great Bend Sand Prairies, Kansas	Arbogast, 1996	Cfa: warm temperate continental climate, semi-arid to sub-humid	fully humid 678	hot summer 14	inland, river bank
Great Sand Dunes National Park and Preserve, Colorado	Marín et al., 2005; Forman et al., 2006	BSk: semi-arid steppe climate	steppe 933	cold arid 7	inland, river bank
Hanford, Washington	Stetler and Gaylord, 1996	BSk: arid steppe climate	steppe 160	cold arid 12	inland, river bank
High Plains of Colorado	Forman et al., 1992; Muhs et al., 1996	BSk: semi-arid steppe climate	steppe 912	cold arid 10	inland, river bank
Holland, eastern shore of Lake Michigan	Arbogast et al., 2002; Timmons et al., 2007; Hansen et al., 2009, 2010	Dfb: snow continental climate	fully humid 2738	warm summer 9	inland, lake shore
Lanphere Dunes, Northern California	Craig, 2000	Csb: warm temperate climate with dry summer	summer dry 969	warm summer 12	coastal
Navajo County, Arizona	Hack, 1941	BSk: steppe climate, true desert to humid mountain climate	steppe 210	cold arid 12	inland, river bank
Northwestern Bahamas	Kindler and Strasser, 2000	Aw: equatorial savannah with dry winter	winter dry 1120	Hot 24	coastal
Oregon coast	Cooper, 1958	Csb: warm temperate climate with dry summer	summer dry 1794	warm summer 12	coastal
Petoskey State Park, Michigan	Lepczyk and Arbogast, 2005	Dfb: snow continental climate	fully humid 813	warm summer 7	inland, lake shore
Savannah River valley, South Carolina	Swezey et al., 2013	Cfa: warm temperate climate	fully humid 1298	hot summer 18	inland, river bank
St. Anthony, Idaho	Chadwick and Dalke, 1965	BSk: semi-arid steppe climate	steppe 340	cold arid 13	inland, river bank
south Texas	Forman et al., 2009	Cfa: warm temperate subtropical climate	fully humid 806	hot summer 22	coastal
Southern High Plains of Texas and New Mexico	Holliday, 2001	BSk: semi-arid steppe climate	steppe 409	cold arid 8	inland, river bank
Walking Dunefield, Napeague, New York	Girardi and Davis, 2010	Cfa: warm temperate climate	fully humid 1217	hot summer 11	coastal

White Sands Dunefield, New Mexico	McKee, 1966; Reitz et al., 2010	BSk: arid steppe climate	steppe 264	cold arid 16	inland, river bank
Wilderness State Park, northern lower Michigan	Lichter, 1995	Dfb: snow continental climate	fully humid 767	warm summer 5	inland, lake shore

Parabolic dunes in coastal settings are strongly influenced by the geometrical alignment of the coastline relative to onshore winds (Jennings, 1957). Unidirectional onshore winds are preferable for the development of parabolic dunes, and such dunes are often associated with the initiation of blowouts on previously vegetated foredunes. Blowouts develop when vegetation cover is breached by either natural processes such as increased wind erosion during periods of drought or storminess or human activities such as excessive grazing (Hesp, 2002). Sand exposed in a blowout is transported and deposited in the leeward margin, developing into a bare lobe. A parabolic dune forms as the bare lobe migrates inland (*cf.* Section 2.3.3). These coastal parabolic dunes are widely seen in humid, sub-humid, and semi-arid regions, usually in conjunction with coastal foredunes in such areas as the west coast of Manawatu, New Zealand (Hesp, 2001), the Oregon coasts of the United States (Cooper, 1958), and the west and northeast coasts of Australia (Carter et al., 1990; Nichol and Brooke, 2011; Pye, 1982; Shepherd and Eliot, 1995).

Elongated parabolic dunes occur in coastal settings where relatively abundant sand supply continuously supplements sand loss from mobile lobes, without which dunes would otherwise be stabilised by vegetation. Elongated parabolic dunes are usually present in an equatorial or warm climate with ample annual precipitation interspersed with periodic dry seasons. These areas are generally dissipative systems and well-covered by dense forests or scrubs. Seasonal dry periods accompanied by strong onshore winds expose abundant sediment previously inundated by inter-dune lakes, which enables dune lobes to maintain mobility whereas vegetation on arms remains intact, forming long-walled arms. An alternation between wet and dry periods and strong onshore winds occurring in dry seasons are crucial in the elongation of parabolic dunes such as those on the east coasts of Australia, South America and Africa (Barbosa and Dominguez, 2004; Porat and Botha, 2008; Pye, 1982).

Digitate and hemicyclic parabolic dunes may develop on coasts that are exposed to multidirectional onshore winds. Presence of a woodland cover is of particular importance in forcing bare lobes moving inland in divergent directions, as can be seen on the northern coast of

Brazil (Buynevich et al., 2010), and the east coasts of Fraser Island (Levin, 2011) and Queensland (Pye, 1982) in Australia.

Other important controls on the development of coastal parabolic dunes include wave power, beach morphology, storm surge, and sea level change. High wave energy dissipative and intermediate beaches have a wide and flat/gently-sloping sloping backshore. Without considerable flow disturbance, onshore winds can maintain high velocities and have a great potential for continuously landward sand transport, thereby providing an abundant sediment supply for dune development (Short and Hesp, 1982). Strong storms may cause powerful wave action that removes vegetation and scars foredunes, and initiate blowouts (Hesp, 2002). The frequency and magnitude of storms, therefore, contribute significantly to shoreline destruction and coastal dune development. Sea level rise induces the near-shore profile to keep adjusting itself to a new level, which is likely to increase dynamics in sediment exchange and potentially to provide a greater sediment supply for aeolian sand transport (Carter, 1991; Hesp and Thom, 1990; Psuty and Silveira, 2010).

Coastal parabolic dunes are also usually found adjacent to river mouths or estuaries, where sediment from rivers provides an abundant sand supply for wind transport, as can be seen in the areas at the mouth of the Sigatoka River in Fiji (Kirkpatrick and Hassall, 1981), on the south coast of Wilderness Dune Cordons in South Africa (Illenberger and Rust, 1988), on the Oregon coast in the United States (Cooper, 1958), and on the São Francisco River Strand Plain and northeast coast of Brazil (Barbosa and Dominguez, 2004; Duran et al., 2008).

In contrast to the relatively extensive research on coastal parabolic dunes - across eighteen countries - inland parabolic dunes have been investigated in only five countries. Inland parabolic dunes are usually found in arid and semi-arid regions adjacent to river valleys and along lake margins. Their formation and development are strongly governed by regional controls: the orographic conditions and the distance to rivers or lakes.

Many of the inland parabolic dunes in western North America are derived from river sediment. In this setting, mountain ridges alter the regional climate regime and the local bio-geomorphic interactions, as is the case for the widespread dunefields on the Great Plains along the eastern side of the Rocky Mountains (Forman et al., 1992; Halfen et al., 2010; Holliday, 2001; Hugenholtz, 2010; Madole, 1995; Muhs et al., 1996). The Rocky Mountains block moisture from the Pacific Ocean in the west, casting areas in the east in rain shadow (Hugenholtz et al., 2010).

Most parabolic dunes in this region are stabilised under prevailing climate conditions, and LiDAR images reveal that they have been transformed from barchans under recent climate warming (Wolfe and Hugenholtz, 2009). Stabilised parabolic dunes derived from fluvial sediment are also found in the south-eastern United States such as in the Savannah River valley in Jasper County of South Carolina (Swezey et al., 2013) and on the Coastal Plain of Georgia (Ivester and Leigh, 2003).

Inland parabolic dunes can also be derived from lake sediment. The White Sands, for example, consist of gypsum sediment that precipitated as a saline lake evaporated (Kocurek et al., 2007; Langford, 2003; Scheidt et al., 2010). A small area of parabolic dunes on the eastern shore of Lake Michigan is associated with the development of blowouts (Arbogast et al., 2002; Hansen et al., 2009; Hansen et al., 2010). On the eastern shore of Hudson Bay, imbricate parabolic dunes have developed under multidirectional winds (Filion and Morisset, 1983).

In contrast to coastal parabolic dunes that usually develop either from expansion and activation of blowouts or from stabilisation of transgressive dunefields (Hesp, 2013), inland parabolic dunes usually develop from barchan or transverse dunes. When barchans move into an environment with more abundant vegetation (e.g., closer to a river or a higher water table), their horns are invaded and anchored by grasses and shrubs first. The remaining bare lobes then move forward, leaving behind the stabilised horns (*cf.* Section 2.3.2). Ample sand availability from mobile dunefields upwind may enable such parabolic dunes to maintain high mobility. Examples of such parabolic dunes are widely found on the eastern margins of White Sands in New Mexico (McKee, 1966; Reitz et al., 2010), in the west of Fremont County and on the eastern Snake River Plain in Idaho (Chadwick and Dalke, 1965; Forman et al., 2003), and in the east of the Horqin Desert in Inner Mongolia (Yan, 2010).

Arms of inland parabolic dunes usually have relatively low relief compared with the arms of coastal parabolic dunes because grasses and shrubs rather than trees dominate these inland regions. As dune arms are frequently overridden or cut through by following dunes, elongated parabolic dunes are not commonly seen inland (Halfen et al., 2010; Marín et al., 2005), with the exception of those in the Thar Desert of India and Pakistan (Wasson et al., 1983). Although trees hardly survive in an arid desert environment, patches of stunted trees have been shown to initiate the development of small parabolic dunes in the Kalahari Desert, South Africa (Eriksson et al., 1989).

As discussed above, the development and morphology of parabolic dunes both on the coast and inland are controlled by various localised factors interactive with their general climate settings, although there is no direct correlation between the presence and morphology of parabolic dunes and climate zones.

2.2.1 Coastal Parabolic Dunes

Coastal parabolic dunes are extensively developed in Australia. Hairpin-, hemicyclic-, and digitate-shaped parabolic dunes are found on the northeast coast (Figure 2-3a), and some of these dunes overlap with or are nested within others, developing a compound dune form (Levin, 2011; Pye, 1982; Pye, 1983a; Pye, 1983c; Pye, 1984; Pye and Mazzullo, 1994; Shulmeister and Lees, 1992; Ward, 2006). These parabolic dunes have been mostly stabilised by vegetation except some in the Cape Bedford – Cape Flattery dunefields and on the east coast of Northern Cape York Peninsula. This region is controlled by an equatorial savannah climate or an equatorial monsoon climate with a strong seasonal variation of humidity in the north, to a fully humid climate down to the south. In comparison to the very elongated parabolic dunes on the east coast of Australia, parabolic dunes on the west coast (Figure 2-3b) are more mobile and somewhat less elongated (Carter et al., 1990; Nichol and Brooke, 2011; Shepherd and Eliot, 1995). The climate there is hot and arid, with a desert climate in the northwest to a seasonal humid climate (dry summers) in the southeast. In the Carnarvon dunefield, for example, the mean annual precipitation is only ~200 mm. Parabolic dunes are also present on King Island (Jennings, 1957) and on the south coast of South Australia (Dutkiewicz and Prescott, 1997; Murray-Wallace et al., 2010), but on a relatively smaller scale, governed by a temperate climate with dry summers (Figure 2-3c).

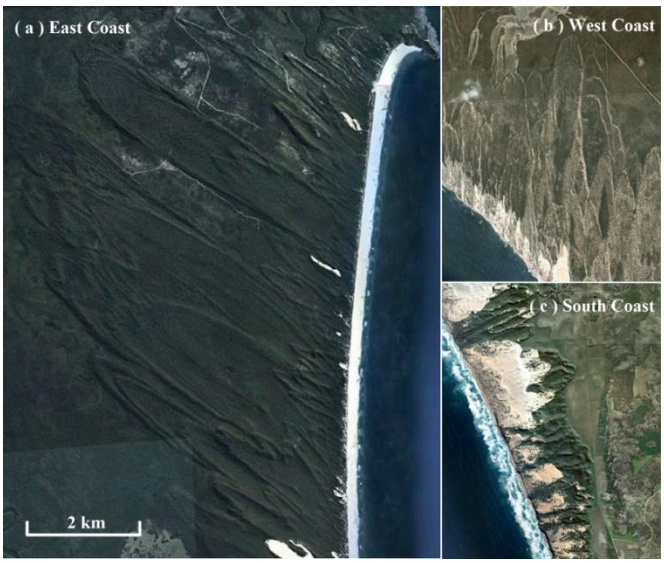

Figure 2-3. Coastal parabolic dunes in Australia, at the same scale.

Hairpin-shaped parabolic dunes are present along the west coast of Auckland in New Zealand (Brothers, 1954), along the west coast of Maputaland Plain and south coast of Wilderness Dune Cordons in South Africa (Hellström, 1996; Illenberger, 1996; Porat and Botha, 2008), and at the mouth of the Sigatoka River in Fiji (Kirkpatrick and Hassall, 1981). In these coastal regions, most of the parabolic dunes are fully vegetated with minor aeolian sediment transport. In some of these locations, the movement of parabolic dunes is impeded by a forest canopy, and the dunes have developed digitate-shaped lobes. On the coasts of Mason Bay and Manawatu Plain in New Zealand, however, parabolic dunes are highly mobile and they move inland continuously (Figure 2-4), even though the climate is fully humid with a mean annual precipitation of ~900 mm (Clement et al., 2010; Hesp, 2001; Hart et al., 2012; Wakes et al., 2010).

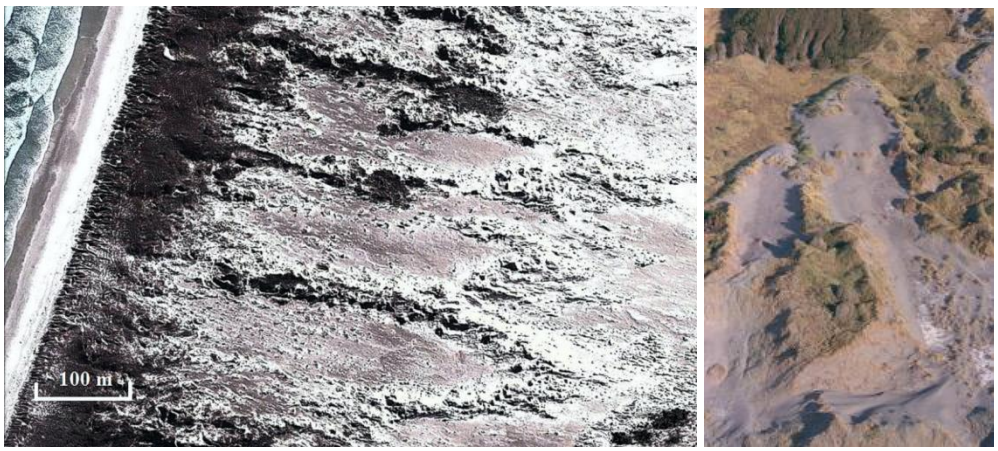

Figure 2-4. Coastal parabolic dunes on the lower west coast (Manawatu region) of the North Island, New Zealand (Photo courtesy of Patrick Hesp ©).

In Brazil, active parabolic dunefields are primarily concentrated on the equatorial coast (in an equatorial savannah climate with dry summers) in particular on the São Francisco River Strand Plain (Barbosa and Dominguez, 2004) and Fortaleza coast (Duran et al., 2008). In these areas, the parabolic dunes display a long-walled transgressive ridge/lobe with relatively thin and short trailing arms (Figure 2-5). Parabolic dunes at the São Francisco do Sul coastal barrier, however, are influenced by a humid subtropical climate and have been fully stabilised by a forest canopy only with minor development of blowouts (Zular et al., 2013). Due to the impacts of human activity, few active parabolic dunes survive on the Atalaia Beach in Pará State (Buynevich et al., 2010; Miot da Silva and Hesp, 2010) and the coast of Rio de Janeiro (Fernandez et al., 2009).

Figure 2-5. Coastal parabolic dunes on the São Francisco River Strand Plain in Brazil.

Lunate parabolic dunes are present in Oregon on the west coast of the United States (Cooper, 1958), and on the Mediterranean coast of Israel (Ardon et al., 2009; Tsoar and Blumberg, 2002). The Israeli coastal dunefield described in the literature, however, may also be interpreted as vegetated transverse dunes, and only a few have developed into somewhat parabolic shape, although this dunefield forms the basis for the parabolic dune stabilisation mechanism proposed by Tsoar and Blumberg (2002), see Section 2.3.2. These parabolic dunes have lunate-shaped lobes yet lack well-defined trailing arms (Figure 2-6). A temperate climate with dry summers dominates these regions, and aeolian activity alternates with periods of stabilisation by vegetation cover. Small active parabolic dunefields also occur on the east coast of the United States, such as Cape Cod National Seashore in Massachusetts (Forman et al., 2008; Winkler, 1992) and Walking Dunefield in New York (Girardi and Davis, 2010), both of which are in a temperate climate with an annual precipitation greater than 1000 mm. Presently partial-submerged parabolic dunes are also found in the north-western Bahamas (Kindler and Strasser, 2000).

Figure 2-6. Coastal parabolic dunes in Israel. The dune outlined in the red rectangle has been investigated as a parabolic dune in Ardon et al., (2009).

In Canada, coastal parabolic dunes are characterised by niveo-aeolian deposits that formed in a continental setting where winds transported snow and sand coincidently during the winter (Bélanger and Filion, 1991; Bhiry et al., 2011; Filion and Morisset, 1983; Giles and

McCann, 1997). The cold and dry climatic conditions during winter facilitate niveo-aeolian activity compared with cool and humid conditions during summer.

In Europe, coastal parabolic dunes are usually stabilised by vegetation and are relic features that formed under different climatic conditions, and the dunes are hence not easily identified because of their complex forms, full coverage by vegetation, and/or destruction by human activities. Stabilised parabolic dunes can be identified in northern Denmark (Clemmensen et al., 2001), the Netherlands (Jungerius and Riksen, 2010), and Scotland in the United Kingdom (Ritchie, 2000; Robertson-Rintoul, 1990), whereas active parabolic dunes can be discernible on the coasts of France (Meurisse et al., 2005), Doñana National Park and Cantabrian Coast in Spain (Arteaga et al., 2008; Siljeström and Clemente, 1990), Curonian Spit in Lithuania (Morkunaite et al., 2011), Wales in the United Kingdom (Bailey and Bristow, 2004), and Vejers in Denmark (Clemmensen et al., 1996).

A large coastal parabolic dunefield is present along the edge of the Jafurah Desert in Saudi Arabia (Figure 2-7), and this dunefield extends from the inland area to the coast (Anton and Vincent, 1986). Although the Jafurah Desert has a mean annual precipitation less than 100 mm, the ubiquitous presence of shallow groundwater enables the survival of sparse desert scrubs that cause local erosion that forms parabolic dunes.

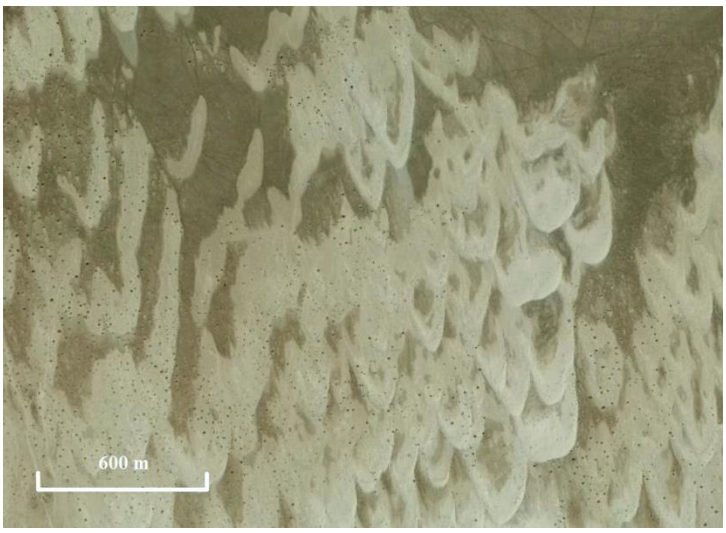

Figure 2-7. Coastal parabolic dunes in the Jafurah Desert, Saudi Arabia.

2.2.2 Inland Parabolic Dunes

Inland parabolic dunes are located in many areas of western North America, both in the United States and Canada. On the Great Plains of western North America, large-scale aeolian sediment mobilisation is attributed to orographic impacts by the Rocky Mountains (Odynsky, 1958; Smith, 1952). Parabolic dunes are scattered widely across the Canadian Prairies, where the climate is arid continental steppe with a mean annual precipitation of ~400 mm (Hugenholtz et al., 2010; Wolfe and Hugenholtz, 2009). Most parabolic dunes here have been fully stabilised by vegetation (Figure 2-8), although a highly active parabolic dune with development of blowouts has been studied in detail in the Bigstick Sand Hills of Saskatchewan (Hugenholtz, 2010; Hugenholtz et al., 2008; Hugenholtz et al., 2009).

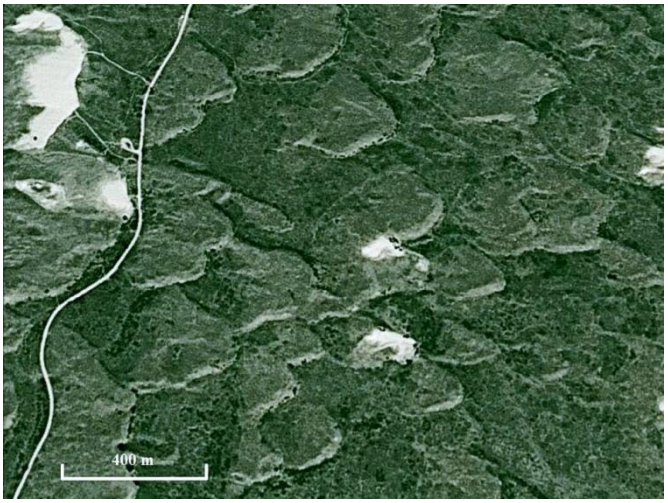

Figure 2-8. Inland parabolic dunes in the Canadian Prairies.

Compared with those on the Canadian Prairies, parabolic dunes on the United States Prairies exhibit greater mobility. This region is governed by a semi-arid steppe climate with varying precipitation depending on altitude and orography. Hairpin-shaped parabolic dunes occur in the Casper Dune Field in Wyoming (Figure 2-9) (Gaylord, 1982; Halfen et al., 2010), in the Great Sand Dunes National Park and Preserve in Colorado (Forman et al., 2006; Marín et al., 2005), and in various parts of eastern Colorado (Madole, 1995). These parabolic dunes are fully- or semi-stabilised by vegetation with trailing arms anchored by grasses and shrubs. Small active compound parabolic dunes are widespread on the High Plains of north-eastern Colorado (Figure

2-10), Texas and New Mexico (Forman et al., 1992; Holliday, 2001; Muhs et al., 1996), and on the Great Bend Sand Prairies in Kansas (Arbogast, 1996).

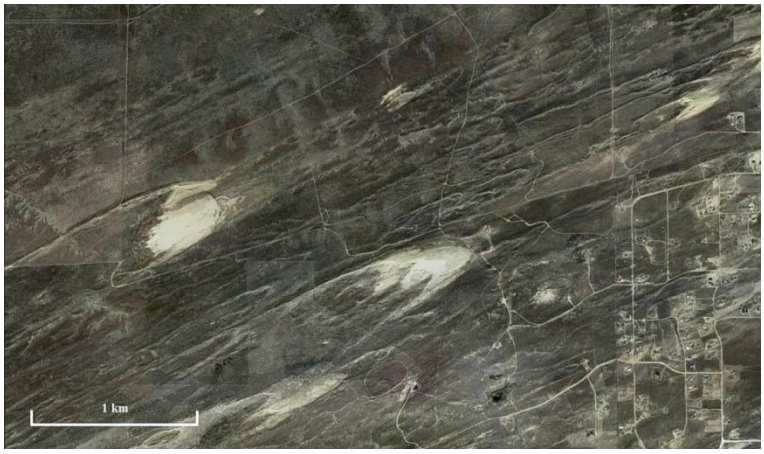

Figure 2-9. Inland parabolic dunes in the Casper Dune Field, Wyoming.

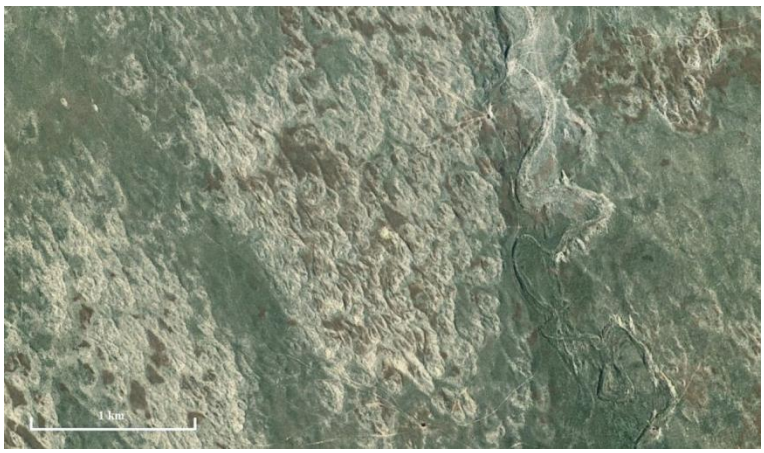

Figure 2-10. Inland compound parabolic dunes in north-eastern Colorado.

In the United States west of the Great Plains, parabolic dunes are found on the eastern margin of White Sands in New Mexico (Figure 2-11) (McKee, 1966; Reitz et al., 2010), in the Navajo County in Arizona (Hack, 1941), and in the Hanford dunefield in eastern Washington (Stetler and Gaylord, 1996). These parabolic dunes, on average, have greater mobility with evident bare lobes, compared with those on the High Plains (Figure 2-12).

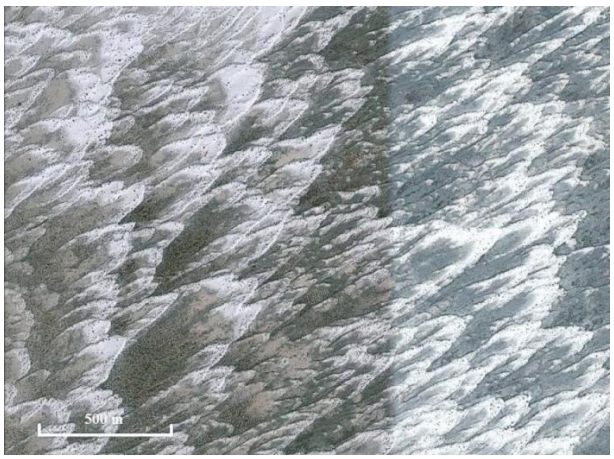

Figure 2-11. Inland parabolic dunes at White Sands, New Mexico.

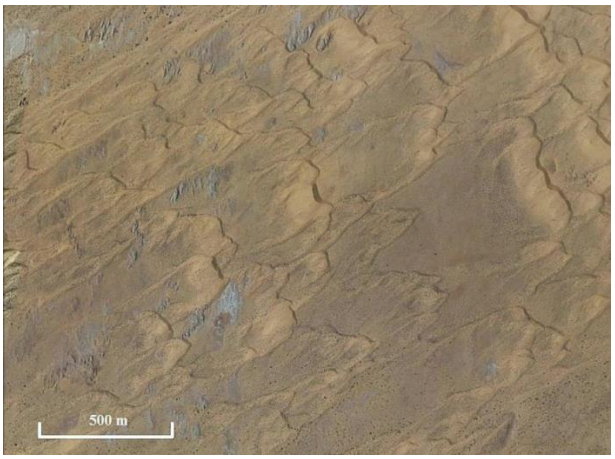

Figure 2-12. Inland parabolic dunes in the Navajo County, Arizona.

Inland parabolic dunes are present along some of the shores of the Great Lakes of North America. For example, parabolic dunes are well-developed along the east shore of Lake Michigan and along the south shore of Lake Huron (Arbogast et al., 2002; Byrne, 1997; Eyles and Meulendyk, 2012; Hansen et al., 2009; Hansen et al., 2010; Lepczyk and Arbogast, 2005; Lichter, 1995; Timmons et al., 2007). Under the influence of a fully humid continental climate, most of these parabolic dunes are fully vegetated. Only a few that arise from blowouts are active at present.

In the Thar Desert of India and Pakistan, inland parabolic dunes link and override each other, presenting a clustered ‘rake-like’ appearance (Wasson et al., 1983). The irregular and asymmetric noses of parabolic dunes have developed during the process of dune overriding, in which one side of a parabolic dune is cut off when another parabolic dune moves across the nose.

This process also causes the dune clusters to be irregular. The clustered parabolic dunes near Shergarh in Pakistan possess rounded noses and exhibit U-shaped dune morphology (Figure 2-13), whereas those between Barmer and Jaisalmer in India display V-shaped dune morphology and have exceedingly elongated arms (Figure 2-14).

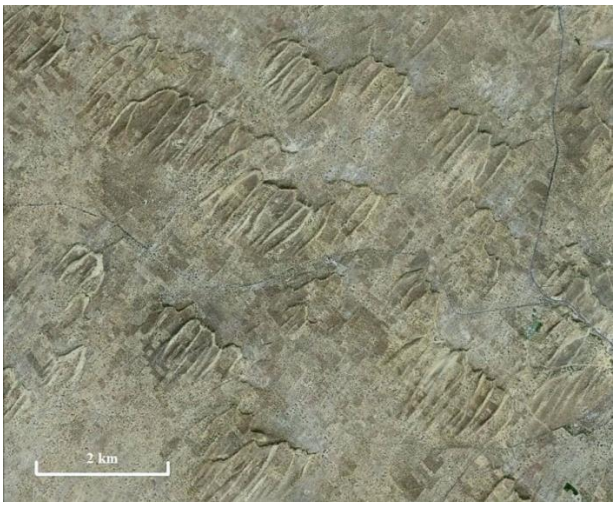

Figure 2-13. U-shaped parabolic dunes near Shergarh in the Thar Desert. These parabolic dunes are clustered forming individual dune groups.

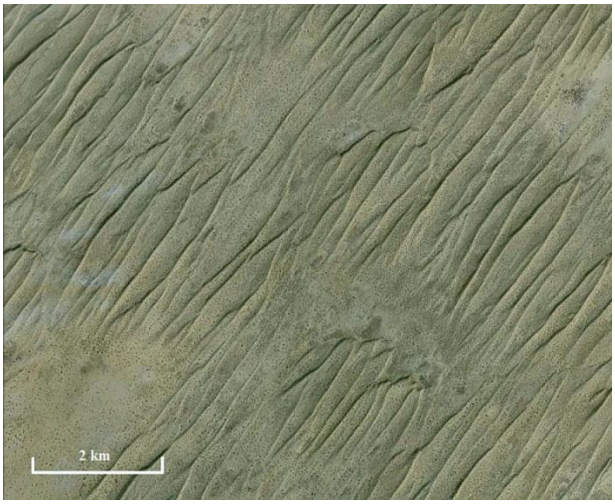

Figure 2-14. V-shaped parabolic dunes between Barmer and Jaisalmer in the Thar Desert. These parabolic dunes are imbricated to various degrees, and have very elongated arms.

Inland parabolic dunes in the Kalahari Desert in South Africa (Figure 2-15) have developed in patches under a hot and arid climate. Eriksson et al. (1989) suggested that the formation of these parabolic dunes is associated with the presence of stunted trees. Winds may continuously erode the base of the stunted trees, eventually forming blowouts and small parabolic dunes behind these blowouts.

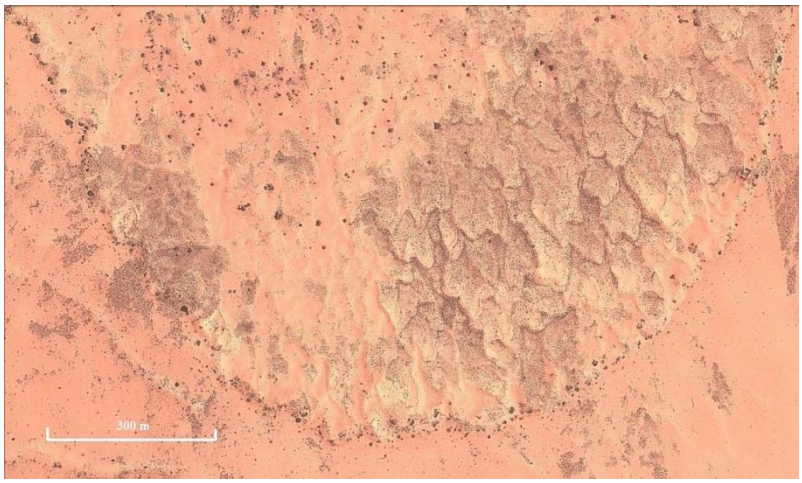

Figure 2-15. Inland parabolic dunes in the Kalahari Desert, South Africa.

There is a variety of parabolic dunes in northern China (Yan, 2010; Yan et al., 2010). Parabolic dunes developed from blowouts are concentrated on the Hulunbuir grasslands (Zhuang and Hasi, 2005), where extensive human activity, in particular grazing and off-road driving, breaches the vegetated surface, exposes sand underneath, and initiates aeolian sand transport. The spatial arrangement of parabolic dunes in this area is hence highly controlled by local socio-economic activities, especially the related transportation networks and grazing behaviour. The Horqin Desert is located on the southeast of mountains governed by an arid steppe climate, and exhibits a transition from transverse dunes in the west to parabolic dunes in the east in similarity with White Sands in New Mexico. Highly active parabolic dunes occur extensively between the Xilamulun River and the Laoha River along the north bank of the Laoha River (Figure 2-16). In contrast, parabolic dunes in the Hobq Desert are fully- or partially-stabilised by shrubs (Figure 2-17), and these dunes are mostly located along the east bank of the Xuhaitu River (Yan, 2010; Zhang et al., 2011). This region is characterised by strong seasonality of both precipitation and

wind regime, resulting in dunes migrating periodically. Parabolic dunes are also found in the Ebinur Lake District (Jia et al., 2012) and the Take Ermu Ku'er Desert (Zeng, 2008) of Xinjiang.

Figure 2-16. Inland parabolic dunes in the Horqin Desert, north-eastern China.

Figure 2-17. Inland parabolic dunes in the Hobq Desert, northern China.

2.3 Parabolic Dune Related Transformations

Parabolic dunes play a significant role in dune transformations. Parabolic dunes, can not only develop from highly mobile barchan dunes, transverse dunes, and coastal transgressive dunes (McKee, 1966; Reitz et al., 2010; Stetler and Gaylord, 1996; Tsoar and Blumberg, 2002; Wolfe

and Hugenholtz, 2009; Hesp and Walker, 2013), but also from blowouts (Baas and Nield, 2007; Girardi and Davis, 2010; Hesp, 2001), and stabilised transverse dunes and coastal foredunes (Carter et al., 1990; Hesp, 2002; Klijn, 1990; Muckersie and Shepherd, 1995; Nield and Baas, 2008). Well-vegetated parabolic dunes, on the other hand, can also be activated and transformed into more mobile barchan dunes and transverse dunes mediated by external pressures of both environmental changes and anthropogenic disturbances (Anton and Vincent, 1986; Hack, 1941; Hesp, 2001). In order to understand the different dune transformation mechanisms and their indications in the context of global climate change, the following sections first examine how vegetation plays a significant role in shaping aeolian dune morphology, and then explore how eco-geomorphic interactions lead to different dune transformations.

2.3.1 Eco-geomorphic Interactions with Aeolian Dunes

The development of a vegetated dunefield depends on the ability of vegetation to limit sand movement on the one hand, and on the ability of aeolian sand transport to limit the growth of vegetation on the other (Ashkenazy et al., 2012; Baas and Nield, 2010; Hack, 1941). Vegetation shapes local aeolian dune landscapes through processes of physical and biochemical interactions (Figure 2-18).

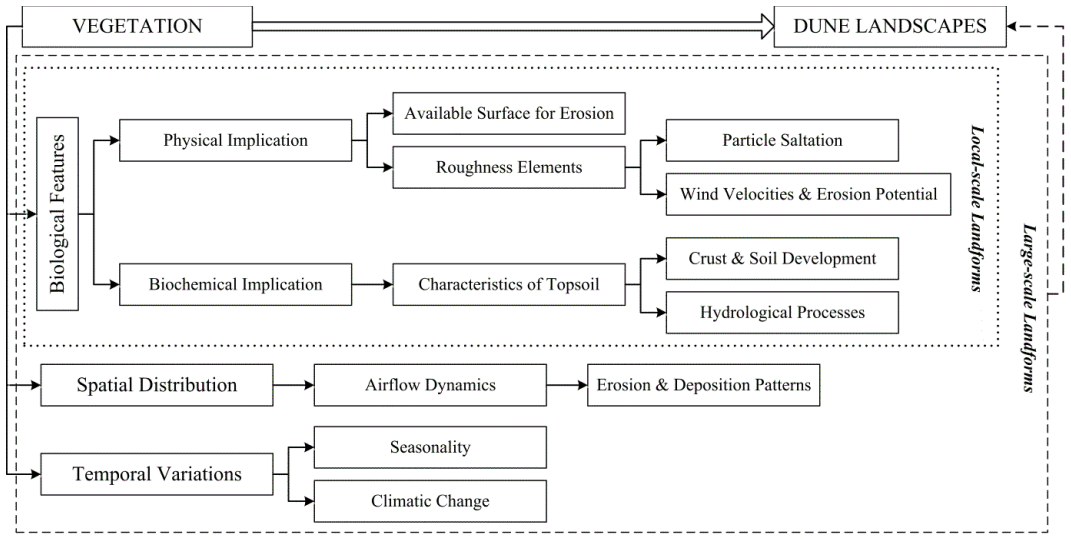

Figure 2-18. Schematic diagram of vegetation influences on aeolian dune landscapes.

Almost all aeolian sand transport happens within 50 cm above the surface (McEwan and Willetts, 1993; Sherman et al., 1998). Physically, vegetation may shelter an erodible surface and decrease the available surface area for wind erosion. Comprising the primary roughness elements in aeolian dune environments, vegetation partitions shear stresses and hence decreases particle saltation and erosion potential, because only finer grains with lower threshold shear velocities can be dislodged and transported by winds (Ash and Wasson, 1983; Gillies et al., 2007; Gillies et al., 2010; Levin et al., 2008; Musick and Gillette, 1990; Nordstrom et al., 2007; Raupach, 1992; Raupach et al., 1993; Turpin et al., 2010; Wiggs et al., 1995; Wolfe and Nickling, 1993; Wolfe and Nickling, 1996). Sand transport is effectively ceased when vegetation ground cover reaches ~20% (Kuriyama et al., 2005; Lancaster and Baas, 1998; Wiggs et al., 1995), although it is recognised that the threshold very much depends on the plant species, plant geometry and structure, and spatial distribution (Buckley, 1987). The roughness density or lateral cover, defined as the ratio of the total frontal-silhouette areas (perpendicular face that is vertical to the wind direction) of roughness elements to the total surface area (Marshall, 1971), is commonly used to evaluate the degree to which vegetation protects surfaces against wind erosion (Burri et al., 2011; Musick and Gillette, 1990; Raupach, 1992; Raupach, 1994; Raupach et al., 1993).

Whilst vegetation limits the capacity of winds to transport sand, vegetation promotes considerably its potential for trapping blown sand. This process can have profound biochemical implications for the micro-environment. By continuously trapping finer grains carried by winds, plants alter the particle-size distribution of sediment in their vicinity, in addition to altering soil texture and structure (Jungerius et al., 1995; Shields and Drouet, 1962). A relatively stable surface, a better water-retaining soil structure, and a greater nutrient content (from plant roots and litter) promote the formation and development of crusts underneath the plants (Johansen, 1993). Biological soil crusts (usually arising from cyanobacteria, mosses, and lichens) further increase soil stability and resistance to wind erosion by binding surface particles, and contribute nutrients to plants by fixing atmospheric nitrogen (Abed et al., 2013; Belnap, 2002; Belnap and Gillette, 1997; Belnap and Gillette, 1998; Delgado-Baquerizo et al., 2013; Drahorad et al., 2013; Eldridge and Leys, 2003; Johnson et al., 2007; Pluis, 1994; Shields et al., 1957; Thiet et al., 2005). Biological soil crusts, moreover, can resist long periods of drought and desiccation, and can recover biological activity quickly as long as sufficient water is available from dew or precipitation, for instance (Veste et al., 2001; West, 1990). The formation of Calcretes and gypcretes can also play

an important role in reducing aeolian sediment transport and stabilising mobile dunes (Amit, 1995; Chen, 1997; Dijkmans et al., 1986; Galloway et al., 1992; Pye, 1980; Swezey, 2003; Warren, 1983). Aeolian dunes in southern Tunisia, for example, are stabilised by 0.1 to 0.5 m thick gypcretes (Swezey, 2003).

Changes in the characteristics of topsoil significantly alter hydrological regimes of aeolian dune environments, in particular water distribution and budget. In aeolian dune environments, precipitation can easily be lost due to the low moisture tension and high hydraulic conductivity pertaining to sand (Tsoar and Blumberg, 2002). Plant canopies and plant litter increase interception, lower soil bulk density, and act as a buffer protecting water from rapid loss (West, 1990). Biological crusts also modify infiltration, percolation, moisture retention, overland flow, and water redistribution (Belnap, 2006; Chamizo et al., 2012; Johansen, 1993; Rodríguez-Caballero et al., 2013; Tsoar and Moller, 1986; Verrecchia et al., 1995; West, 1990; Yair, 1990).

The complex mosaic pattern of vegetation in aeolian dune environments is responsible for spatial differences in flow dynamics over the surface and the associated patterns of sediment erosion and deposition (Ranwell, 1958; Willis and Yemm, 1961). Plants act as obstacles that cause sand to accumulate in their vicinity, thereby modifying the topography of dunes that they inhabit (Raupach, 1992; Wolfe and Nickling, 1993). Resulting sand accretion in and behind plants can lead to the formation of nebkhas (Tengberg, 1995; Tengberg and Chen, 1998) and shadow dunes (Gunatilaka, 1989; Hesp, 1981), respectively. Changes in the micro-topography further alter airflow patterns over surfaces and shape dune landforms on a larger spatial scale (Frank and Kocurek, 1996a; Frank and Kocurek, 1996b). Nevertheless, vegetation, sand transport, and dune development are interactive within the context of climatological background that is subject to a variety of environmental fluctuations caused by seasonal or year-to-year variations in wind regime, temperature, precipitation, water table, and salinity. During drought or windy periods, for example, intense aeolian sediment transport can reshape dune landscapes significantly (Anderson and Walker, 2006; Byrne, 1997).

In order to survive in aeolian dune environments, plants employ both avoidance and tolerance strategies to cope with environmental stresses such as high wind velocities, sand blasting, sand accretion, wind erosion, unstable substratum, high soil temperature, and nutrient deficiency (Hesp, 1991; Maun, 1994; Maun, 1998). Seedling recruitment, for instance, usually happens

during periods of low wind energy and high moisture availability (Maun, 1994). Survival on an eroding surface is usually a challenge for most plants. They likely die of desiccation when their roots are exposed to the air by constant erosion (Lee and Ignaciuk, 1985; Maun, 1981).

Many plants, however, have various capabilities of withstanding sand burial. According to the tolerance to sand accretion, Maun (1998) classified plant species in aeolian dune communities into the following three categories: non-tolerant, sand-tolerant, and sand-dependent. In his model (Figure 2-19), an individual plant may show the following different responses as sand burial increases: (I) a negative response that causes the plant to die soon; (II) no response and the plant grows normally within a certain level of sand accretion; and (III) a stimulation of plant growth within a certain level of sand accretion. Despite a broad spectrum of the maximum tolerance to sand burial, every plant species will show a negative response beyond a certain limit (Dech and Maun, 2005; Gilbert and Ripley, 2010; Ievinsh, 2006; Kent et al., 2001; Maun, 1998; Maun and Lapierre, 1984; Wagner, 1964; Zhang and Maun, 1994).

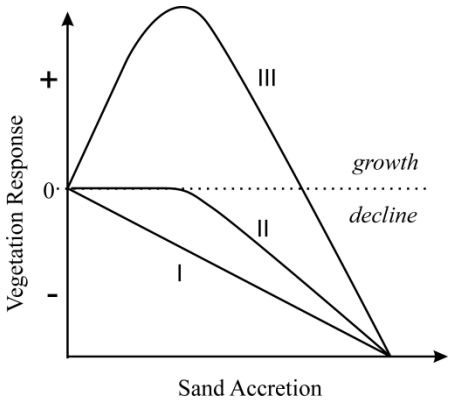

Figure 2-19. A model of interaction between vegetation response and increasing levels of sand accretion in aeolian dune environments (adapted from Maun, 1998). I. negative vegetation response; II. no vegetation response within a limited level of sand accretion; and III. a stimulation of vegetation growth within a certain level of sand accretion.

Burial acts as a strong selective force by eliminating sensitive plant species, decreasing the abundance of less tolerant species, and increasing the abundance of sand-tolerant and sand-dependent species (Dech and Maun, 2005; Eldred and Maun, 1982; Martinez et al., 2001; Maun, 1994; Maun, 1998; Maun and Perumal, 1999; Moreno-Casasola, 1986). Many studies have indicated that some plant species are well-adapted to dynamic and recurrent burial, and that some

plant species even require a certain amount of regular burial in order to maintain their high vigour (Bendali et al., 1990; Harris and Davy, 1987; Maun, 1998; Olson, 1958).

2.3.2 Transformations from Transverse/Barchan Dunes to Parabolic Dunes

In contrast to parabolic dunes with two trailing arms pointing upwind, typical barchan dunes are crescent-shaped with two horns extending downwind and a slip face in their interiors. Barchan dunes develop under conditions of a high-energy unidirectional wind, a low sediment supply and a sparse vegetation cover (Hack, 1941; Rubin and Hunter, 1987; Wasson and Hyde, 1983). As sand supply increases, barchan dunes merge laterally into crescentic dunes with continuously sinuous ridges (Lancaster, 1995; Reitz et al., 2010). If sand supply is ample, then transverse dunes emerge with tall and continuous slip faces.

An increase in vegetation cover may lead to a transformation from barchan dunes or transverse dunes to parabolic dunes. This phenomenon has been studied in many countries including Israel (Tsoar and Blumberg, 2002), Brazil (Duran et al., 2008), Denmark (Anthonsen et al., 1996; Landsberg, 1956), the United Kingdom (Landsberg, 1956), New Zealand (Hesp, 2001), Canada (Wolfe and Hugenholtz, 2009) and the United States (Hack, 1941; McKee, 1966; Stetler and Gaylord, 1996) (Table 2-3). Most of these studies attribute the transformation to a progressive increase in vegetation cover caused by either climatic changes or human disturbances. In many of these studies, however, the exact transformation process and the underlying mechanism remain unclear.

Table 2-3. Studies on transformations from barchan or transverse dunes to parabolic dunes.

Reference	Study Region	Method	Transformation Cause
Hack, 1941	Navajo Country, Arizona, US	Field surveys and photo-engravings	Aggressive plants survive sand burial
Landsberg, 1956	UK and Denmark	Field observation	Wetter climate
McKee, 1966	White Sands, New Mexico, US	Analysis of cross-stratification	Dune arms are anchored by vegetation
Muckersie and Shepherd, 1995	New Zealand	Radiocarbon dating	El Niño-Southern Oscillation
Anthonsen et al., 1996	Rabjerg Mile, Skagen Odde, Denmark	Topographical maps and aerial photographic interpretation	Climatic changes (wind regime and vegetation cover)
Stetler and Gaylord, 1996	Hanford, Washington, US	A regional climate model	Increase in precipitation
Hesp, 2001	Manawatu, New Zealand	Aerial photographic interpretation	Human activity (vegetated by farmers and less grazing pressure)
Tsoar and Blumberg, 2002	Southeastern Mediterranean Coast, Israel	Aerial photographic interpretation	Decrease in human pressure (cessation of agricultural land-use and reduction in grazing activity)
Duran et al., 2008	Ceara, Brazil	Field surveys, QuickBird panchromatic satellite imagery interpretation and continuum modelling	Low ratio of dune surface erosion and deposition rate to vegetation growth rate
Ardon et al., 2009	Southern coastal plain of Israel	Field surveys and aerial photographic interpretation	Land use change and emergence of shrubs on dune crests
Wolfe and Hugenholtz, 2009	Northern Great Plains, Canada	LiDAR imagery interpretation and optical stimulation luminescence dating	Climate warming
Reitz et al., 2010	White Sands, New Mexico, US	LIDAR imagery and aerial photographic interpretation	Dune surface erosion or deposition rate decreases below the threshold of half vegetation growth rate
Barchyn and Hugenholtz, 2012a	-	CA modelling	Climate shift
Barchyn and Hugenholtz, 2012b	-	process-based hypothesis	Slipface deposition rate is smaller than peak deposition tolerance of vegetation
Hart et al., 2012	Mason Bay, New Zealand	field surveys and aerial photographic interpretation	Marram grass invasion

Some studies have suggested that the transformation is rooted in the anchor-like function of vegetation on the horns of barchan dunes (Livingstone and Warren, 1996; Muckersie and Shepherd, 1995; Reitz et al., 2010; Robertson-Rintoul, 1990; Stetler and Gaylord, 1996; Wolfe and Hugenholtz, 2009). Vegetation retards movement of horns, acting as anchors, whilst the dune apex continues to migrate downwind. As vegetation cover extends from dune horns to the apex, the advancing apex leaves behind the protected trailing ridges, and the dune is gradually transformed from the barchan to the parabolic shape in plan. Duran and Hermann (2006) simulated this process using a continuum model starting with a single barchan dune on a non-erodible bed. Barchyn and Hugenholtz (2012a) simulated a barchan-to-parabolic dunefield transformation imposed by a climate shift using a cellular automaton (CA) model (Baas and Nield, 2010; Nield and Baas, 2008). A few studies have suggested that this transformation happens when the sand erosion or deposition rate decreases below a certain threshold related to the vegetation growth rate (Barchyn and Hugenholtz, 2012b; Duran and Herrmann, 2006; Reitz et al., 2010).

The ‘horns-anchoring’ mechanism described above is likely to happen on the following three conditions: (1) barchan dunes are surrounded by well-vegetated land; (2) vegetation species are sufficiently aggressive to withstand a certain amount of sand burial; and (3) sediment availability is relatively limited. The first prerequisite can be fulfilled when a barchan dune is moving onto an area with a greater vegetation cover (Reitz et al., 2010). As an alternative, the interdune areas of barchan dunefields may be re-vegetated because of changes in environmental factors, such as increased precipitation (Landsberg, 1956; Stetler and Gaylord, 1996), reduced wind strength (Anthonsen et al., 1996), and climate warming (Wolfe and Hugenholtz, 2009), or because of changes in anthropogenic pressure on the environment, such as reduced grazing activity or artificial vegetation restoration (Hesp, 2001). The second condition depends on the characteristics of local plant communities, in particular the dominant species, and is also closely related to the regional climate parameters of wind regime, temperature, and precipitation. The third condition is determined by sand sources, specifically a limited external sand supply and a thin sandy substratum.

Tsoar and Blumberg (2002) proposed another potential mechanism driving the transformation from barchan dunes or transverse dunes to parabolic dunes, specifying that the establishment of vegetation on the crests of barchan dunes or transverse dunes initiates the transformation. Their argument is that the vegetation preferentially grows and recovers on the crest of a barchan/transverse dune where the erosion/deposition balance is neutral. The establishment of vegetation on the crest then changes the airflow and sediment transport dynamics over the stoss slope. Sand eroded from the stoss slope is partly trapped by clumps of plants forming isolated nebkhas, and the associated abrupt reduction in sediment supply encourages plants to take root on the lee slopes and slip faces. The accumulation of sand on the crest by nebkhas, meanwhile, gradually changes the profile of the stoss slope from convex to concave. The subsequent funnelling effect of the wind over the concave stoss slope can undercut the nebkhas and expose plant roots on the central apex, but plants on dune sides remain intact and are left behind by the mobile dune apex, developing into trailing arms eventually. Hugenholtz et al. (2008) confirmed the important role of vegetation on the dune crest in trapping sand transported from the stoss slope and in changing the dune profile.

In contrast to the previous mechanism in which vegetation is established close to the groundwater table in interdune areas and on the horns of barchan dunes, in the mechanism

proposed by Tsoar and Blumberg (2002) vegetation starts to germinate and grow on the crests of dunes where erosion and deposition balance each other. Some studies have shown that a small amount of sand burial may prevent atmospheric desiccation, increase relative humidity around seeds, and anchor seedlings into soil; therefore, a small amount of sand burial may be vital to ensure successful seed germination and plant growth (Maun, 1998). Maun and Lapierre (1986) suggested that a maximum germination rate occurs at a burial depth of 2-4 cm across all four studied dune species. A study on seven dune species by Zhang and Maun (1994) has shown that the majority of seeds germinate at a depth of 5-10 cm, and that deeper burial greater than 15 cm significantly inhibits seed germination. These results are consistent with the findings from Lee and Ignaciuk (1985). A relatively stable surface with a slight amount of net deposition is clearly crucial for seeds to take root.

This 'nebkhas-initiation' mechanism proposed by Tsoar and Blumberg (2002) involves the following steps/prerequisites: (1) seeds germinate successfully on dune crests during a less windy season; (2) sufficient precipitation and minor aeolian sediment mobilisation allow seedlings on the crests to thrive such that they can prepare themselves adequately for strong wind energy during the following windy season; and (3) plants develop tap roots that allow them to use relatively sustainable groundwater during a dry and windy season, ensuring that the plants are able to keep vitality, trap sand continually, and develop into nebkhas that can subsequently alter the profile of stoss slopes in shape. These three prerequisites are intimately connected with each other and fundamentally provide an opportunity for vegetation to survive on the crests of dunes, arising from some combination of increased precipitation, reduced windiness, and/or rise of local groundwater table. These variables, in turn, respond to seasonal fluctuations, climatic changes, and/or human pressures. To act as initial traps and further develop into nebkhas that initiate this transformation process, the vegetation involved should be perennial and needs not only to grow up in height quickly, but also to display a branching growth pattern in order to achieve a high sand-trapping efficiency (Livingstone and Warren, 1996). Isolated plants that have lost their lower branches and leaves are much less efficient in decreasing wind velocity and sand transport, because almost all sand transport happens close to the ground. Extensive roots are necessary for vegetation survival on dune crests where soils have particularly low fertility and low capacity for retaining the precipitation.

The interaction between vegetation and sand transport as well as the related mechanism of the transformation from barchan/transverse dunes to parabolic dunes is likely to vary depending on vegetation species and the limiting factors that control vegetation germination and growth. Annual grasses such as Agriophyllum squarrosum are short-lived with shallow roots, are unlikely to access groundwater, and hence only survive on precipitation. They usually germinate and grow rapidly after episodic rainfall events, but die of drought shortly afterwards. The impacts of annuals on dune morphology are, therefore, generally highly limited. Perennial vegetation, on the other hand, develops deep and/or widespread roots, and can exert different impacts depending on their growth forms. For perennial grasses that grow uniformly over the surface, the degree to which such grasses reduce sand transport is primarily determined by an overall coverage of a grass assembly. Perennial vegetation in need of a large water supply is usually distributed relatively sparsely as discrete clumps and shrubs. Such perennial vegetation influences the local wind regime more as individual entities through their outstanding canopies.

The 'horns-anchoring' transformation mechanism tends to occur in an environment where water deficiency is the limiting factor for vegetation growth, whereas the 'nebkhas-initiation' mechanism tends to occur where wind erosion is the predominant limiting factor. In comparison with the 'horns-anchoring' mechanism in which any perennial species can play the anchoring role as long as it can withstand a small degree of wind erosion and sand burial (Reitz et al., 2010; Wolfe and Hugenholtz, 2009), perennial vegetation in the 'nebkhas-initiation' mechanism needs to develop tap roots in order to access groundwater from dune crests and at the same time has the capability of withstanding substantial amounts of sand burial as the nebkhas form (Tsoar and Blumberg, 2002). The 'nebkhas-initiation' mechanism demands more specialised plant species and is hence less common. Parabolic dunes formed by the 'nebkhas-initiation' mechanism, furthermore, are much less elongated compared with that of the 'horns-anchoring' mechanism in which bare lobes can move forward unimpeded over a long period.

2.3.3 Transformations from Blowouts to Parabolic Dunes

The evolution of blowouts can result in the formation of parabolic dunes, specifically on vegetated sandy surfaces (Gutierrezelorza et al., 2005; Landsberg, 1956; Pye, 1982). Coastal examples have been documented in Australia (Pye, 1982; Pye, 1983b), New Zealand (Brothers, 1954; Hesp,

2001), the United Kingdom (Ranwell, 1958), the Netherlands (Klijn, 1990), Spain (Gutierrezelorza et al., 2005), Brazil (Duran et al., 2008), and the United States (Girardi and Davis, 2010; Hansen et al., 2009), whereas inland examples have been documented in the southern Kalahari Desert in south Africa (Eriksson et al., 1989) and the Jafurah Desert in Saudi Arabia (Anton and Vincent, 1986) (Table 2-4). Some early studies refer to parabolic dunes developed from blowouts as "blowout dunes" (Brothers, 1954; Cooper, 1958; Eriksson et al., 1989; Melton, 1940).

Table 2-4. Studies on transformations from blowouts to parabolic dunes.

Reference	Study Region	Method	Transformation Cause
Melton, 1940	Southern High Plains, US	Aerial photographic interpretation	More arid climate and lowered water table
Hack, 1941	Navajo Country, Arizona, US	Field surveys and photo-engravings	Periglacial winds and sparsely vegetated sandy surface
Brothers, 1954	Auckland, New Zealand	Field observation	Burning-off, animal tracks and topographic difference
Cooper, 1958	Oregon, US	Description	Windward slope stabilisation of saucer blowouts
Ranwell, 1958	Anglesey, Wales, UK	Field surveys	Natural forces
Pye, 1982	Cape Bedform and Cape Flattery, Queensland, Australia	Aerial photographic interpretation	Natural forces (fire, cyclones and lightning strikes) and local difference in vegetation cover or topography
Pye, 1983b	Northern Cape York Peninsula, Queensland, Australia	Field surveys, aerial photograph interpretation and sediment analyses	Increase in windiness or reduction in rainfall
Anton and Vincent, 1986	Jafurah Desert, Eastern Province, Saudi Arabia	Field surveys and aerial photographic interpretation	Preferable deflation of sand sheet areas
Eriksson et al., 1989	Southern Kalahari Desert, South Africa	Field surveys and aerial photographic interpretation	Deflation of bare patches shaded by trees, assisted by biological processes
Carter et al., 1990	West coast, Australia	Description	Trough blowout depressions evolve into parabolic dunes
Klijn, 1990	Younger Dunes, Netherlands	^{14}C and historical dating	Climatic changes (sea level rise and increases in storm frequency and storm surges)
Hesp, 2001	Manawatu, New Zealand	Aerial photographic interpretation	Natural forces aided by human recreational activity
Hesp, 2002	-	Description	High wind energy coasts
Gutierrezelorza et al., 2005	Tierra de Pinares, Spain	Field observation	Climatic changes
Baas and Nield, 2007	-	DECAL model	Dynamic interplay between sedimentation balance and vegetation effectiveness
Duran et al., 2008	Ceara, Brazil	Field surveys, QuickBird panchromatic satellite imagery interpretation and continuum modelling	Low ratio of dune surface erosion or deposition rate to vegetation growth rate
Hansen et al. 2009	Green Mountain Beach dune, Holland, southeast shore of Lake Michigan, US	Field surveys	Steering of winds in deflation areas
Girardi and Davis, 2010	Walking Dunes, New York, US	Aerial photographic interpretation and previous literature	Dune-vegetation interactions

Blowouts are saucer-, bowl-, cup-, or trough-shaped depressions that usually develop by wind erosion on a pre-existing sand deposit (Hesp et al., 2011; Hesp, 2002; Hesp and Hyde, 1996).

The initiation of blowouts may be associated with both natural and anthropogenic disturbances to a vegetation cover such as wildfires, increased windiness, rises in sea level, increased frequency of drought, large volcanic eruptions, storms, overgrazing, trampling, and diseases (Gutierrezelorza et al., 2005; Muckersie and Shepherd, 1995; Pye and Tsoar, 1990; Watt, 1937). These agents locally exterminate vegetation, breach surface crusts, and create discrete bare patches that develop into hollows as erosion continues. These hollows may become enlarged, and turbulent eddies may form and further accelerate the expansion of the hollows (Hesp, 2002). The deepening of the hollows also encourages the funnelling of winds, which in turn can result in more intense erosion (Smyth et al., 2014). Continued wind scour widens blowouts by steepening side walls and inducing side wall failure (Carter et al., 1990). Sand eroded from a deflation hollow is transported by winds and accumulates in the leeward margin, forming a depositional lobe, which is regarded as part of a blowout by some researchers (Hesp and Hyde, 1996; Robertson-Rintoul, 1990).

Cooper (1958) defined two primary types of blowouts: saucer blowouts and trough blowouts. Despite a wide range of variability in different aeolian environments, most blowouts can be classified as either of these two types (Hesp, 2002). Saucer blowouts are shallow, and semicircular- or saucer-shaped. Trough blowouts are deeper, and more elongated with longer lateral walls (Carter et al., 1990; Cooper, 1958; Hesp, 2002; Hesp and Hyde, 1996). Compared with a short, wide, radial depositional lobe found in the leeward margin of a saucer blowout, a trough blowout develops a tall, parabolic-shaped depositional lobe. In a trough blowout, corkscrew airflows may develop in the deflation basin. These airflows are then compressed and accelerated towards the crest of the depositional lobe, and subsequently decelerate rapidly due to flow expansion upon the existing trough, leading to the development of a parabolic lobe (Hesp, 2002).

If a trough blowout and its lobe overcome the surrounding vegetation, they continue to migrate and develop downwind, enlarging over time and evolving into a fully developed parabolic dune (Carter et al., 1990; Hesp and Hyde, 1996; Livingstone and Warren, 1996). The parabolic dune may continue to increase in size if the blowout provides a continuous sediment supply by down-wearing its deflation basin. The dune may cease to increase in size if the funnelling effect is lessened by progressive widening of the openings, if a groundwater table or resistant stratum is exposed (such as a caliche bed or a clay bed), or if reinvigorated growth of vegetation impedes further erosion (Cooper, 1958; Livingstone and Warren, 1996; Melton, 1940). Baas and Nield (2007) simulated the development of blowouts using a Discrete ECo-geomorphic Aeolian

Landscape model (DECAL), and showed the significant role of the interplay between vegetation growth and sand transport in the transformation from blowouts to elongated parabolic dunes. Baas and Nield (2010) further showed that blowouts can also expand laterally, incorporate progressively increased sand, and develop into more mobile transgressive and transverse ridges. The initiation of blowouts by disturbances and their potential impacts on overall dunefield activation have been conceptualised by Barchyn and Hugenholtz (2013) in the context of vegetation resilience and sediment transport activity. They also showed that depth-limited blowouts can migrate and elongate at a high rate, and are hence more difficult to be stabilised by vegetation. In addition to cellular automaton models, Duran et al. (2008) applied a continuum model to simulate the development of a parabolic dune in north-eastern Brazil.

The formation of parabolic dunes from blowouts requires the following three conditions: (1) a generally stabilised surface that enables concentration of winds at isolated points of weakness; (2) an underlying sandy substratum that provides sufficient sediment supply for forming a parabolic-shaped depositional lobe and that must avoid the coalescence of adjacent blowouts; and (3) predominantly unidirectional winds (Cooper, 1958; Eriksson et al., 1989; Pye, 1983b). Blowouts developed on coastal dunes are in some instances regarded as a symptom of a negative sand budget (Livingstone and Warren, 1996; Psuty, 1988). A decrease in sand supply from a beach means that onshore winds have larger capacity to erode foredunes. The higher parts of the dunes are usually more vulnerable to desiccation and disturbance, and therefore more susceptible to the initiation of a blowout. Blowouts are, however, present widely on the coasts of Manawatu Plain in New Zealand where beaches are progradational (Hesp, 2002). Sufficient sand supply and strong unidirectional winds are essential for the further transformation of blowouts into parabolic dunes, and may be secured by climatic changes such as a stronger wind regime, a more arid climate, and a lowered groundwater table, or by land degradation induced by anthropogenic perturbations such as grazing and human recreational activities.

2.3.4 Transformations from Parabolic Dunes to Other Dune Morphologies

Under certain conditions, parabolic dunes may be transformed into other dune morphologies. Parabolic dunes are commonly developed in well-vegetated landscapes and under conditions of a restricted sediment supply (Hack, 1941; Lancaster, 1995). If a new sediment supply becomes

available or if vegetation cover decreases below a certain level, parabolic dunes may be transformed into more mobile dunes (Livingstone and Warren, 1996; McKee, 1966). Some studies have indicated that parabolic dunes can lose vegetation, and are activated and transformed into transverse dunes (Anton and Vincent, 1986; Hack, 1941; Hesp, 2001). Some regions exhibit a downwind transition continuum from parabolic dunes to barchan dunes and transverse dunes (Pye and Tsoar, 1990). Studies on these transformations are, nevertheless, few and often limited to anecdotal descriptions (Table 2-5). The eco-geomorphic interactions and physical processes underlying the activation of parabolic dunes and their transformations into highly mobile barchan dunes or transverse dunes have not been investigated in detail, whereas these transformations may have significant implications for local land management and social-economic development. Parabolic dunes may also develop into other dune forms such as dome dunes (Anton and Vincent, 1986).

Table 2-5. Studies on transformations from parabolic dunes to other types of dunes

Transformation Type	Reference	Study Region	Method	Transformation Cause
parabolic to transverse and barchan	Hack, 1941	Navajo Country, Arizona, US	Field surveys and photo-engravings	Vegetation destruction caused by external sand supply from blowouts
	Anton and Vincent, 1986	Jafurah Desert, Eastern Province, Saudi Arabia	Field surveys and aerial photographic interpretation	Decline in vegetation density possibly caused by lowed water table, natural vegetation succession and over-grazing
	Shulmeister and Lees, 1992	Groote Eylandt, Australia	Thermo-luminescence dating	Decline in vegetation cover caused by decreased precipitation and/or increased aboriginal burning
	Hesp, 2001	Manawatu, New Zealand	Aerial photographic interpretation	Human activity (burning, grazing, introduction of exotic species and wetland modification)
	García-Hidalgo et al., 2002	Duero Basin, Spain	Aerial photographic interpretation	Noses of parabolic dunes are stopped by water and dune arms continue to move forward
parabolic to dome	Anton and Vincent, 1986	Jafurah Desert, Eastern Province, Saudi Arabia	Field surveys and aerial photographic interpretation	Vegetation colonisation in deflation hollows with relatively low groundwater salinity
parabolic to longitudinal	Meurisse et al., 2005	Northern shore, France	Stratigraphy, ^{14}C dating and sedimentology	Climatic modifications, agricultural practices and sea level rise

2.4 Summary

The development of parabolic aeolian dunes and related transformations to and from other dune morphologies are very sensitive to vegetation characteristics and environmental variations arising from both natural and anthropogenic disturbances. This chapter reviews the literature on parabolic dunes and their related transformations on a global scale to provide a comprehensive inventory. Coastal and inland parabolic dunes differ on environmental controls, transformation processes, and morphologies. Coastal parabolic dunes are controlled by geometrical alignment of the coastline,

tidal range, wave power, and sea level change. Coastal parabolic dunes are often associated with the initiation of blowouts on previously vegetated foredunes by either natural forces such as storms or human disturbances such as grazing. In contrast, inland parabolic dunes are governed by orographic conditions and groundwater availability related to nearby rivers or lakes. Inland parabolic dunes are largely transformed from transverse dunes or barchan dunes, and are usually found in arid and semi-arid regions. In relatively humid areas, coastal parabolic dunes can migrate over trees and form arms of relatively high relief, whereas inland parabolic dunes usually have arms of relatively low relief because grasses and shrubs dominate those areas. Elongated parabolic dunes are often found on coasts where wet periods alternate with dry periods accompanied by strong onshore winds (usually in an equatorial or warm climate), but such elongated dunes are not commonly seen inland because the dune arms are frequently overridden or cut though by following dunes.

The transformation process from barchan dunes to parabolic dunes varies depending on vegetation species as well as the limiting factors of their germination and growth. The 'horns-anchoring' transformation mechanism is likely to happen when water deficiency is the limiting factor, whereas the 'nebkhas-initiation' transformation mechanism is likely to occur when vegetation growth is threatened primarily by wind erosion. Of the two mechanisms, the 'nebkhas-initiation' mechanism is less common because it requires more specialised species that can develop extensive roots utilizing groundwater, while being able to withstand severe sand burial.

Parabolic dunes are widely distributed around the world across a broad climatic gradient. A number of studies have explored the transformation from barchan dunes and blowouts to parabolic dunes. But detailed processes and mechanisms involved in the barchan-to-parabolic dune transformations remain unclear. The transformation of parabolic dunes into highly mobile barchan dunes driven by vegetation deterioration caused by environmental changes and human activities, meanwhile, has not drawn sufficient attention. Furthermore, a dune transformation usually takes a relatively long period of time, and direct observation and investigation in the field are arduous. As thus, this thesis applies computer modelling techniques in combination with field measurements and remote sensing techniques to explore the controlling mechanisms and physical processes involved in the stabilisation and transformations from barchan dunes into parabolic dunes, as well as the reactivation and transformations from parabolic dunes into highly mobile barchan dunes. The hypothesis and specific research objectives and questions are discussed in detail in Chapter 3.

References

Aagaard, T., Davidson-Arnott, R., Greenwood, B., Nielsen, J., 2004. Sediment supply from shoreface to dunes: linking sediment transport measurements and long-term morphological evolution. Geomorphology, 60(1–2), 205-224.

Abed, R.M.M., Al-Sadi, A.M., Al-Shehi, M., Al-Hinai, S., Robinson, M.D., 2013. Diversity of free-living and lichenized fungal communities in biological soil crusts of the Sultanate of Oman and their role in improving soil properties. Soil Biology and Biochemistry, 57(0), 695-705.

Amit, R., and Harrison, J.B.J., 1995, Biogenic calcic horizon development under extremely arid conditions, Nizzana sand dunes, Israel: Advances in Geoecology, v. 28, p. 65-88.

Anderson, J., Walker, I., 2006. Airflow and sand transport variations within a backshore–parabolic dune plain complex: NE Graham Island, British Columbia, Canada. Geomorphology, 77(1-2), 17-34.

Anthonsen, K.L., Clemmensen, L.B., Jensen, J.H., 1996. Evolution of a dune from crescentic to parabolic form in response to short-term climatic changes: Rabjerg mile, Skagen Odde, Denmark. Geomorphology, 17(1-3), 63-77.

Anton, D., Vincent, P., 1986. Parabolic dunes of the Jafurah Desert, Eastern Province, Saudi Arabia. Journal of Arid Environments, 11(3), 187-198.

Arbogast, A.F., 1996. Stratigraphic evidence for late-Holocene aeolian sand mobilization and soil formation in south-central Kansas, USA. Journal of Arid Environments, 34(4), 403-414.

Arbogast, A.F., Hansen, E.C., Van Oort, M.D., 2002. Reconstructing the geomorphic evolution of large coastal dunes along the southeastern shore of Lake Michigan. Geomorphology, 46(3-4), 241-255.

Ardon, K., Tsoar, H., Blumberg, D.G., 2009. Dynamics of nebkhas superimposed on a parabolic dune and their effect on the dune dynamics. Journal of Arid Environments, 73(11), 1014-1022.

Arens, S.M., Slings, Q., de Vries, C.N., 2004. Mobility of a remobilised parabolic dune in Kennemerland, The Netherlands. Geomorphology, 59(1-4), 175-188.

Arteaga, C., Juan de Sanjosé, J., Serrano, E., 2008. Terrestrial photogrammetric techniques applied to the control of a parabolic dune in the Liencres dune system, Cantabria (Spain). Earth Surface Processes and Landforms, 33(14), 2201-2210.

Ash, J.E., Wasson, R.J., 1983. Vegetation and sand mobility in the Australian desert dunefield. Zeitschrift fur Geomorphologie Supplementband, 45, 7-25.

Ashkenazy, Y., Yizhaq, H., Tsoar, H., 2012. Sand dune mobility under climate change in the Kalahari and Australian deserts. Climatic Change, 112(3-4), 901-923.

Baas, A.C.W., 2002. Chaos, fractals and self-organization in coastal geomorphology: simulating dune landscapes in vegetated environments. Geomorphology, 48(1-3), 309-328.

Baas, A.C.W., 2007. Complex systems in aeolian geomorphology. Geomorphology, 91(3-4), 311-331.

Baas, A.C.W., Nield, J.M., 2007. Modelling vegetated dune landscapes. Geophysical Research Letters, 34(6).

Baas, A.C.W., Nield, J.M., 2010. Ecogeomorphic state variables and phase-space construction for quantifying the evolution of vegetated aeolian landscapes. Earth Surface Processes and Landforms, 717-731.

Bagnold, R.A., 1941. The physics of blown sand and desert dunes. Methuen & Co. Ltd, London.

Bailey, S.D., Bristow, C.S., 2004. Migration of parabolic dunes at Aberffraw, Anglesey, north Wales. Geomorphology, 59(1-4), 165-174.

Barbosa, L.M., Dominguez, J.M.L., 2004. Coastal dune fields at the São Francisco River strandplain, northeastern Brazil: morphology and environmental controls. Earth Surface Processes and Landforms, 29(4), 443-456.

Barchyn, T.E., Hugenholtz, C.H., 2012a. Aeolian dune field geomorphology modulates the stabilization rate imposed by climate. Journal of Geophysical Research, 117(F2).

Barchyn, T.E., Hugenholtz, C.H., 2012b. A process-based hypothesis for the barchan-parabolic transformation and implications for dune activity modelling. Earth Surface Processes and Landforms, 37(13), 1456-1462.

Barchyn, T.E., Hugenholtz, C.H., 2013. Reactivation of supply-limited dune fields from blowouts: A conceptual framework for state characterization. Geomorphology, 201(0), 172-182.

Bélanger, S., Filion, L., 1991. Niveo-aeolian sand deposition in subarctic dunes, eastern coast of Hudson Bay, Québec, Canada. J. Quat. Sci., 6(1), 27-37.

Belly, P.Y., 1964. Sand movement by wind. U.S. Army Coastal Engineering Research Center. Technical Memorandum No. 1, 1-38.

Belnap, J., 2002. Nitrogen fixation in biological soil crusts from southeast Utah, USA. Biol Fertil Soils, 35(2), 128-135.

Belnap, J., 2006. The potential roles of biological soil crusts in dryland hydrologic cycles. Hydrological Processes, 20(15), 3159-3178.

Belnap, J., Gillette, D.A., 1997. Disturbance of biological soil crusts: Impacts on potential wind erodibility of sandy desert soils in southeastern Utah. Land Degradation & Development, 8(4), 355-362.

Belnap, J., Gillette, D.A., 1998. Vulnerability of desert biological soil crusts to wind erosion: the influences of crust development, soil texture, and disturbance. Journal of Arid Environments, 39(2), 133-142.

Bendali, F., Floret, C., Le Floc'h, E., Pontanier, R., 1990. The dynamics of vegetation and sand mobility in arid regions of Tunisia, 18. Elsevier, Kidlington, ROYAUME-UNI.

Bertran P., Bateman M.D., Hernandez M., Mercier N., Millet D., Sitzia L. and Tastet J.P., 2011. Inland aeolian deposits of south-west France: facies, stratigraphy and chronology, J. Quat. Sci. 26 (4), 374–388.

Bhiry, N., Delwaide, A., Allard, M., Begin, Y., Filion, L., Lavoie, M., Nozais, C., Payette, S., Pienitz, R., Saulnier-Talbot, E., Vincent, W.F., 2011. Environmental change in the Great Whale River region, Hudson Bay: Five decades of multidisciplinary research by Centre d'etudes nordiques (CEN). Ecoscience, 18(3), 182-203.

Bigarella, J.J., Klein, A.H.D., Menezes, J.T., Vintem, G., 2005. Sub-tropical coastal dunes: Examples from southern Brazil. Journal of Coastal Research, 113-137.

Bigarella, J.J., Klein, A.H.D., Menezes, J.T., Vintem, G., 2006. Southern Brazilian coastal dunes: Movement and structures. Journal of Coastal Research, 1-15.

Brothers, R.N., 1954. A physiographic study of Recent sand dunes on the Auckland west coast. New Zealand Geographer, 10, 47-59.

Brunsden, D., 2001. A critical assessment of the sensitivity concept in geomorphology. Catena, 42(2–4), 99-123.

Buckley, R., 1987. The effect of sparse vegetation on the transport of dune sand by wind. Nature, 325(29), 426-428.

Burri, K., Gromke, C., Lehning, M., Graf, F., 2011. Aeolian sediment transport over vegetation canopies: A wind tunnel study with live plants. Aeolian Research, 3(2), 205-213.

Buynevich, I.V., Filho, P.W.M.S., Asp, N.E., 2010. Dune advance into a coastal forest, equatorial Brazil: A subsurface perspective. Aeolian Research, 2(1), 27-32.

Byrne, M.L., 1997. Seasonal sand transport through a trough blowout at Pinery Provincial Park, Ontario. Can. J. Earth Sci., 34(11), 1460-1466.
Carter, R.W.G., 1991. Near-future sea level impacts on coastal dune landscapes. Landscape Ecology, 6(1-2), 29-39.
Carter, R.W.G., Hesp, P.A., Nordstrom, K.F., 1990. Erosional landforms in coastal dunes. In: K.F. Nordstrom, N.P. Psuty, R.W.G. Carter (Eds.), Coastal Dunes: Form and Process. John Wiley & Sons Ltd., Chichester.
Chadwick, H.W., Dalke, P.D., 1965. Plant Succession on Dune Sands in Fremont County, Idaho. Ecology, 46(6), 766-780.
Chamizo, S., Cantón, Y., Rodríguez-Caballero, E., Domingo, F., Escudero, A., 2012. Runoff at contrasting scales in a semiarid ecosystem: A complex balance between biological soil crust features and rainfall characteristics. Journal of Hydrology, 452–453(0), 130-138.
Chen, X.Y., 1997. Pedogenic gypcrete formation in arid central Australia. Geoderma, 77(1), 39-61.
Clement, A.J.H., Sloss, C.R., Fuller, I.C., 2010. Late Quaternary geomorphology of the Manawatu coastal plain, North Island, New Zealand. Quaternary International, 221(1–2), 36-45.
Clemmensen, L.B., Andreasen, F., Nielsen, S.T., Sten, E., 1996. The late Holocene coastal dunefield at Vejers, Denmark: Characteristics, sand budget and depositional dynamics. Geomorphology, 17(1-3), 79-98.
Clemmensen, L.B., Bjornsen, M., Murray, A., Pedersen, K., 2007. Formation of aeolian dunes on Anholt, Denmark since AD 1560: A record of deforestation and increased storminess. Sedimentary Geology, 199(3-4), 171-187.
Clemmensen, L.B., Pye, K., Murray, A., Heinemeier, J., 2001. Sedimentology, stratigraphy and landscape evolution of a Holocene coastal dune system, Lodbjerg, NW Jutland, Denmark. Sedimentology, 48(1), 3-27.
Cooke, R., Warren, A., Goudie, A., 1993. Desert geomorphology. UCL Press Limited, London.
Cooper, W.S., 1958. Coastal dunes of Oregon and Washington. Geological Society of America Memoir 72, New York.
Cornelis, W.M., Gabriels, D., 2003. The effect of surface moisture on the entrainment of dune sand by wind: an evaluation of selected models. Sedimentology, 50(4), 771-790.
Craig, M.S., 2000. Aeolian sand transport at the Lanphere Dunes, northern California. Earth Surface Processes and Landforms, 25(3), 239-253.
David, P.P., Wolfe, S.A., Huntley, D.J., Lemmen, D.S., 1999. Activity cycle of parabolic dunes based on morphology and chronology from Seward sand hills, Saskatchewan, Holocene Climate and Environmental Change in the Palliser Triangle: a Geoscientific Context for Evaluating the Impacts of Climate Change on the Southern Canadian Prairies. Geological Survey of Canada Bulletin 534, pp. 223-238.
Davidson-Arnott, R.G.D., Yang, Y., Ollerhead, J., Hesp, P.A., Walker, I.J., 2008. The effects of surface moisture on aeolian sediment transport threshold and mass flux on a beach. Earth Surface Processes and Landforms, 33(1), 55-74.
Dech, J.P., Maun, M.A., 2005. Zonation of vegetation along a burial gradient on the leeward slopes of Lake Huron sand dunes. Can. J. Bot.-Rev. Can. Bot., 83(2), 227-236.
Delgado-Fernandez, I., Jackson, D.W.T., Cooper, J.A.G., Baas, A.C.W., Beyers, J.H.M., Lynch, K., 2013. Field characterization of three-dimensional lee-side airflow patterns under offshore winds at a beach-dune system. Journal of Geophysical Research: Earth Surface, 118(2), 706-721.
del Valle, H.F., Blanco, P.D., Metternicht, G.I., Zinck, J.A., 2010. Radar remote sensing of wind-driven land degradation processes in Northeastern Patagonia. J. Environ. Qual., 39(1), 62-75.
Delgado-Baquerizo, M., Maestre, F., Gallardo, A., 2013. Biological soil crusts increase the resistance of soil nitrogen dynamics to changes in temperatures in a semi-arid ecosystem. Plant and Soil, 366(1-2), 35-47.
Dijkmans, J.W.A., Koster, E.A., Galloway, J.P., Mook, W.G., 1986. Characteristics and Origin of Calcretes in a Subarctic Environment, Great Kobuk Sand Dunes, Northwestern Alaska, U.S.A. Arctic and Alpine Research, 18(4), 377-387.
Drahorad, S., Felix-Henningsen, P., Eckhardt, K.U., Leinweber, P., 2013. Spatial carbon and nitrogen distribution and organic matter characteristics of biological soil crusts in the Negev desert (Israel) along a rainfall gradient. Journal of Arid Environments, 94(0), 18-26.
Duran, O., Herrmann, H.J., 2006. Vegetation against dune mobility. Physical Review Letters, 97(18), 188001/188001-188004.
Duran, O., Silva, M.V.N., Bezerra, L.J.C., Herrmann, H.J., Maia, L.P., 2008. Measurements and numerical simulations of the degree of activity and vegetation cover on parabolic dunes in north-eastern Brazil. Geomorphology, 102(3-4), 460-471.
Dutkiewicz, A., Prescott, J.R., 1997. Thermoluminescence ages and Palaeoclimate from the Lake Malata Lake Greenly complex, Eyre peninsula, south Australia. Quaternary Science Reviews, 16(3-5), 367-385.
Eldred, R.A., Maun, M.A., 1982. A multivariate approach to the problem of decline in vigor of Ammophila. Can. J. Bot.-Rev. Can. Bot., 60(8), 1371-1380.
Eldridge, D.J., Leys, J.F., 2003. Exploring some relationships between biological soil crusts, soil aggregation and wind erosion. Journal of Arid Environments, 53(4), 457-466.
Eriksson, P.G., Nixon, N., Snyman, C.P., Bothma, J.D., 1989. Ellipsoidal parabolic-dune patches in the southern Kalahari desert. Journal of Arid Environments, 16(2), 111-124.
Eyles, N., Meulendyk, T., 2012. Ground-penetrating radar stratigraphy and depositional model for evolving Late Holocene aeolian dunes on the Lake Huron coast, Ontario. Journal of Great Lakes Research, 38(4), 708-719.
Fernandez, G.B., Pereira, T.G., da Rocha, T.B., 2009. Coastal Dunes along Rio de Janeiro Coast: Evolution and Management. Journal of Coastal Research, 307-311.
Filion, L., Morisset, P., 1983. Eolian landforms along the eastern coast of Hudson Bay, Northern Quebec. Nordicana, 47, 73-94.
Forman, S.L., Goetz, A.F.H., Yuhas, R.H., 1992. Large-scale stabilized dunes on the High Plains of Colorado: Understanding the landscape response to Holocene climates with the aid of images from space. Geology, 20(2), 145-148.
Forman, S.L., Nordt, L., Gomez, J., Pierson, J., 2009. Late Holocene dune migration on the south Texas sand sheet. Geomorphology, 108(3–4), 159-170.
Forman, S.L., Pierson, J., 2003. Formation of linear and parabolic dunes on the eastern Snake River Plain, Idaho in the nineteenth century. Geomorphology, 56(1–2), 189-200.
Forman, S.L., Sagintayev, Z., Sultan, M., Smith, S., Becker, R., Kendall, M., Marin, L., 2008. The twentieth-century migration of parabolic dunes and wetland formation at Cape Cod National Sea Shore, Massachusetts, USA: landscape response to a legacy of environmental disturbance. Holocene, 18(5), 765-774.
Forman, S.L., Spaeth, M., Marín, L., Pierson, J., Gómez, J., Bunch, F., Valdez, A., 2006. Episodic Late Holocene dune movements on the sand-sheet area, Great Sand Dunes National Park and Preserve, San Luis Valley, Colorado, USA. Quaternary Research, 66(1), 97-108.

Frank, A., Kocurek, G., 1996a. Toward a model for airflow on the lee side of aeolian dunes. Sedimentology, 43(3), 451-458.
Frank, A.J., Kocurek, G., 1996b. Airflow up the stoss slope of sand dunes: limitations of current understanding. Geomorphology, 17(1–3), 47-54.
Fryberger, S.G., 1979. Dune forms and wind regime. In: E.D. McKee (Ed.), A study of global sand seas. US Geological Survey Professional Paper, Washington, pp. 137-169.
Galloway, J.P. et al., 1992, Early Holocene calcretes from the subarctic active Nogahabara sand dune field, northern Alaska: U.S. Geological Survey Bulletin, p. 100-111.
García-Hidalgo, J.F., Temiño, J., Segura, M., 2002. Holocene eolian sediments on the southern border of the Duero basin (Spain): Origin and development of an eolian system in a temperate zone. Journal of Sedimentary Research, 72(1), 30-39.
García-Novo, F., Torres-Martínez, A., Ramírez-Díaz, L., 1976. El sistema de dunas de Doñana. Naturalia Hispanica 5. ICONA, Madrid.
Gaylord, D.R., 1982. Geologic history of the Ferris Dune Field, south-central Wyoming. Geological Society of America Special Papers, 192, 65-82.
Gaylord, D.R., Dawson, P.J., 1987. Airflow-terrain interactions through a mountain gap, with an example of eolian activity beneath an atmospheric hydraulic jump. Geology, 15, 789-792.
Gilbert, M.E., Ripley, B.S., 2010. Resolving the differences in plant burial responses. Austral Ecology, 35(1), 53-59.
Giles, P.T., McCann, S.B., 1997. Foredune development on Iles de la Madeleine (Quebec), Atlantis Canada. Can. J. Earth Sci., 34(11), 1467-1476.
Gillies, J., Nickling, W., King, J., 2007. Shear stress partitioning in large patches of roughness in the atmospheric inertial sublayer. Boundary-Layer Meteorology, 122(2), 367-396.
Gillies, J.A., Nickling, W.G., King, J., Lancaster, N., 2010. Modeling aeolian sediment transport thresholds on physically rough Martian surfaces: A shear stress partitioning approach. Geomorphology, 121(1-2), 15-21.
Girardi, J.D., Davis, D.M., 2010. Parabolic dune reactivation and migration at Napeague, NY, USA: Insights from aerial and GPR imagery. Geomorphology, 114(4), 530-541.
Goossens, E.M.C., de Roover, B.P., Goossens, R.E.A., 1993. A digital approach to the separation of parabolic sand dune areas from interdunal areas using Landsat MSS data. Journal of Arid Environments, 25(1), 131-140.
Goudie, A., 2011. Parabolic Dunes: Distribution, Form, Morphology and Change. Ann. Arid. Zone, 50(3&4), 1-7.
Gunatilaka, A., Mwango, S.B., 1989. Flow separation and the internal structure of shadow dunes. Sedimentary Geology, 61(1–2), 125-134.
Gutierrezelorza, M., Desir, G., Gutierrezsantolalla, F., Marin, C., 2005. Origin and evolution of playas and blowouts in the semiarid zone of Tierra de Pinares (Duero Basin, Spain). Geomorphology, 72(1-4), 177-192.
Hack, J.T., 1941. Dunes of the Western Navajo Country. Geogr. Rev., 31(2), 240-263.
Halfen, A.F., Fredlund, G.G., Mahan, S.A., 2010. Holocene stratigraphy and chronology of the Casper Dune Field, Casper, Wyoming, USA. Holocene, 20(5), 773-783.
Hansen, E., DeVries-Zimmerman, S., van Dijk, D., Yurk, B., 2009. Patterns of wind flow and aeolian deposition on a parabolic dune on the southeastern shore of Lake Michigan. Geomorphology, 105(1-2), 147-157.
Hansen, E.C., Fisher, T.G., Arbogast, A.F., Bateman, M.D., 2010. Geomorphic history of low-perched, transgressive dune complexes along the southeastern shore of Lake Michigan. Aeolian Research, 1(3-4), 111-127.
Harris, D., Davy, A.J., 1987. Seedling growth in elymus-farctus after episodes of burial with sand. Ann. Bot., 60(5), 587-593.
Hart, A.T., Hilton, M.J., Wakes, S.J., Dickinson, K.J.M., 2012. The Impact of Ammophila arenaria Foredune Development on Downwind Aerodynamics and Parabolic Dune Development. Journal of Coastal Research, 112-122.
Hellström, G.B., 1996. Preliminary investigations into recent changes of the Goukamma Nature Reserve frontal dune system, South Africa - With management implications. Landscape and Urban Planning, 34(3-4), 225-235.
Hesp, P., Martinez, M., da Silva, G.M., Rodriguez-Revelo, N., Gutierrez, E., Humanes, A., Lainez, D., Montano, I., Palacios, V., Quesada, A., Storero, L., Trilla, G.G., Trochine, C., 2011. Transgressive dunefield landforms and vegetation associations, Dona Juana, Veracruz, Mexico. Earth Surface Processes and Landforms, 36(3), 285-295.
Hesp, P., Schmutz, P., Martinez, M.L., Driskell, L., Orgera, R., Renken, K., Revelo, N.A.R., Orocio, O.A.J., 2010. The effect on coastal vegetation of trampling on a parabolic dune. Aeolian Research, 2(2-3), 105-111.
Hesp, P.A., 1981. The formation of shadow dunes. Journal of Sedimentary Petrology, 51(1), 101-112.
Hesp, P.A., 1991. Ecological processes and plant adapatations on coastal dunes. Journal of Arid Environments, 21(2), 165-191.
Hesp, P.A., 2001. The Manawatu Dunefield: Environmental Change and Human Impacts. New Zealand Geographer, 57(2), 33-40.
Hesp, P.A., 2002. Foredunes and blowouts: initiation, geomorphology and dynamics. Geomorphology, 48(1-3), 245-268.
Hesp, P.A., 2008. Coastal dunes in the tropics and temperate regions: Location, formation, morphology and vegetation processes. In: M.L. Martinez, N.P. Psuty (Eds.), Ecological Studies. Ecological Studies : Analysis and Synthesis. Springer, 233 Spring Street, New York, Ny 10013, United States, pp. 29-49.
Hesp, P., 2013. Conceptual models of the evolution of transgressive dune field systems. Geomorphology, 199(0), 138-149.
Hesp, P.A., Hyde, R., 1996. Flow dynamics and geomorphology of a trough blowout. Sedimentology, 43(3), 505-525.
Hesp, P.A., Thom, B.G., 1990. Geomorphology and evolution of active transgressive dunefields. In: K.F. Nordstrom, N. Psuty, B. Carter (Eds.), Coastal dunes: form and process. John Wiley & Sons, Chichester, pp. 253-288.
Hesp, P.A., Walker, I.J., 2013. Aeolian environments: coastal dunes. In: Shroder, J., Lancaster, N., Sherman, D.J., Baas, A.C.W. (Eds.), Aeolian Geomorphology. Treatise on Geomorphology, vol. 11. Academic Press, San Diego, CA, pp. 328–355.
Holliday, V.T., 2001. Stratigraphy and geochronology of upper quaternary eolian sand on the Southern High Plains of Texas and New Mexico, United States. Geological Society of America Bulletin, 113(1), 88-108.
Hugenholtz, C.H., 2010. Topographic changes of a supply-limited inland parabolic sand dune during the incipient phase of stabilization. Earth Surface Processes and Landforms, 35(14), 1674-1681.
Hugenholtz, C.H., Bender, D., Wolfe, S.A., 2010. Declining sand dune activity in the southern Canadian prairies: Historical context, controls and ecosystem implications. Aeolian Research, 2(2-3), 71-82.
Hugenholtz, C.H., Moorman, B.J., Wolfe, S.A., 2007. Ground penetrating radar (GPR) imaging of the internal structure of an active parabolic sand dune. The Geological Society of America Special Paper 432.
Hugenholtz, C.H., Wolfe, S.A., 2005. Biogeomorphic model of dunefield activation and stabilization on the northern Great Plains. Geomorphology, 70(1-2), 53-70.

Hugenholtz, C.H., Wolfe, S.A., Moorman, B.J., 2007. Sand-water flows on cold-climate eolian dunes: Environmental analogs for the eolian rock record and martian sand dunes. Journal of Sedimentary Research, 77(7-8), 607-614.
Hugenholtz, C.H., Wolfe, S.A., Moorman, B.J., 2008. Effects of sand supply on the morphodynamics and stratigraphy of active parabolic dunes, Bigstick Sand Hills, southwestern Saskatchewan. Can. J. Earth Sci., 45(3), 321-335.
Hugenholtz, C.H., Wolfe, S.A., Walker, I.J., Moorman, B.J., 2009. Spatial and temporal patterns of aeolian sediment transport on an inland parabolic dune, Bigstick Sand Hills, Saskatchewan, Canada. Geomorphology, 105(1-2), 158-170.
Huggett, R.J., 1991. Climate, Earth Processes and Earth History. Springer, Berlin.
Hunter, R.E., 1977. Basic types of stratification in small eolian dunes. Sedimentology, 24(3), 361-387.
Ievinsh, G., 2006. Biological basis of biological diversity: physiological adaptations of plants to heterogeneous habitats along a sea coast. Acta Universitatis Latviensis (Biology), 710, 53-79.
Illenberger, W.K., 1996. The geomorphologic evolution of the Wilderness dune cordons, South Africa. Quaternary International, 33, 11-20.
Illenberger, W.K., Rust, I.C., 1988. A sand budget for the Alexandria coastal dunefield, South Africa. Sedimentology, 35(3), 513-521.
IPCC, 2013. Climate change 2013: the physical science basis. Contribution of working group I to the fifth assessment report of the intergovernmental panel on climate change. Cambridge University Press, Cambridge.
Ivester A.H. and Leigh D.S., 2003. Riverine dunes on the Coastal Plain of Georgia, USA, Geomorphology, 51(4), 289–311.
Jackson, N.L., Nordstrom, K.F., 1998. Aeolian transport of sediment on a beach during and after rainfall, Wildwood, NJ, USA. Geomorphology, 22(2), 151-157.
Jennings, J.N., 1957. On the orientation of parabolic or U-dunes. Geographical Journal, 123(4), 474-480.
Jia, C.R., Wu, S.L., Ma, J., 2012. Spatial distribution of parabolic dunes in Ebinur Lake Basin of Xinjiang, China, 2012 Annual Meeting of the Geographic Society of China. Geographical Society of China & Henan Institute of Science and Technology, Kaifeng, pp. 45-45.
Johansen, J.R., 1993. Cryptogamic crusts of semiarid and arid lands of North America. Journal of Phycology, 29(2), 140-147.
Johnson, S.L., Neuer, S., Garcia-Pichel, F., 2007. Export of nitrogenous compounds due to incomplete cycling within biological soil crusts of arid lands. Environmental Microbiology, 9(3), 680-689.
Jungerius, P.D., Koehler, H., Kooijman, A.M., Mücher, H.J., Graefe, U., 1995. Response of vegetation and soil ecosystem to mowing and sod removal in the coastal dunes 'Zwanenwater', the Netherlands. Journal of Coastal Conservation, 1(1), 3-16.
Jungerius, P.D., Riksen, M., 2010. Contribution of laser altimetry images to the geomorphology of the Late Holocene inland drift sands of the European Sand Belt. Baltica, 23(1), 59-70.
Kar, A., Tsunekawa, A., Miyazaki, T., 1998. Potentiality of global positioning system in sand dune measurement: A case study from the Thar desert, India. Quaternary Deserts and Climatic Change. A a Balkema Publishers, Leiden.
Kent, M., Owen, N.W., Dale, P., Newnham, R.M., Giles, T.M., 2001. Studies of vegetation burial: a focus for biogeography and biogeomorphology? Progress in Physical Geography, 25(4), 455-482.
Kilibarda, Z., Blockland, J., 2011. Morphology and origin of the Fair Oaks Dunes in NW Indiana, USA. Geomorphology, 125(2), 305-318.
Kindler, P., Strasser, A., 2000. Palaeoclimatic significance of co-occurring wind- and water-induced sedimentary structures in the last-interglacial coastal deposits from Bermuda and the Bahamas. Sedimentary Geology, 131(1–2), 1-7.
Kirkpatrick, J.B., Hassall, D.C., 1981. Vegetation of the Sigatoka sand dunes, Fiji. N. Z. J. Bot., 19(3), 285-297.
Klijn, J.A., 1990. The younger dunes in the Netherlands: chronology and causation. In: T.W.M. Bakker, P.D. Jungerius, J.A. Klijn (Eds.), Dunes of the European coasts, Catena Supplement 18, pp. 89-100.
Knight, M., Thomas, D.S.G., Wiggs, G.F.S., 2004. Challenges of calculating dunefield mobility over the 21st century. Geomorphology, 59(1–4), 197-213.
Kocurek, G., Carr, M., Ewing, R., Havholm, K.G., Nagar, Y.C., Singhvi, A.K., 2007. White Sands Dune Field, New Mexico: Age, dune dynamics and recent accumulations. Sedimentary Geology, 197(3–4), 313-331.
Kottek M., Grieser J., Beck C., Rudolf B. and Rubel F., 2006. World Map of the Koppen-Geiger climate classification updated, Meteorol. Z. 15 (3), 259–263.
Kuriyama, Y., Mochizuki, N., Nakashima, T., 2005. Influence of vegetation on aeolian sand transport rate from a backshore to a foredune at Hasaki, Japan. Sedimentology, 52(5), 1123-1132.
Lal, R., 2001. Potential of Desertification Control to Sequester Carbon and Mitigate the Greenhouse Effect. Climatic Change, 51(1), 35-72.
Lancaster, N., 1995. Geomorphology of Desert Dunes. Routledge, London.
Lancaster, N., 1997. Response of eolian geomorphic systems to minor climate change: Examples from the southern Californian deserts. Geomorphology, 19(3-4), 333-347.
Lancaster, N., Baas, A.C.W., 1998. Influence of vegetation cover on sand transport by wind: Field studies at Owens Lake, California. Earth Surface Processes and Landforms, 23(1), 69-82.
Landsberg, S.Y., 1956. The orientation of dunes in Britain and Denmark in relation to wind. Geographical Journal, 122(2), 176-189.
Langford, R.P., 2003. The Holocene history of the White Sands dune field and influences on eolian deflation and playa lakes. Quaternary International, 104(1), 31-39.
Lavee, H., Imeson, A.C., Sarah, P., 1998. The impact of climate change on geomorphology and desertification along a Mediterranean-arid transect. Land Degradation & Development, 9(5), 407-422.
Le Houérou, H.N., 1996. Climate change, drought and desertification. Journal of Arid Environments, 34(2), 133-185.
Lee, J.A., Ignaciuk, R., 1985. The physiological ecology of strandline plants. Plant Ecol., 62(1), 319-326.
Lefevre, M.A., 1931, Morphologie eolienne littorale entre Nieuport et la frontier francaise: Bulletin de la Societe Belge d'Etudes Geographiques, t. 1, pp. 36-60.
Lepczyk, X.C., Arbogast, A.F., 2005. Geomorphic history of dunes at Petoskey State Park, Petoskey, Michigan. Journal of Coastal Research, 21(2), 231-241.
Levin, N., 2011. Climate-driven changes in tropical cyclone intensity shape dune activity on Earth's largest sand island. Geomorphology, 125(1), 239-252.
Levin, N., Ben-Dor, E., 2004. Monitoring sand dune stabilization along the coastal dunes of Ashdod-Nizanim, Israel, 1945–1999. Journal of Arid Environments, 58(3), 335-355.
Levin, N., Ben-Dor, E., Kidron, G.J., Yaakov, Y., 2008. Estimation of surface roughness (z0) over a stabilizing coastal dune field based on vegetation and topography. Earth Surface Processes and Landforms, 33(10), 1520-1541.

Levin, N., Kidron, G.J., Ben-Dor, E., 2006. The spatial and temporal variability of sand erosion across a stabilizing coastal dune field. Sedimentology, 53(4), 697-715.
Lichter, J., 1995. Lake Michigan beach-ridge and dune development, lake level, and variability in regional water balance. Quaternary Research, 44(2), 181-189.
Livingstone, I., Warren, A., 1996. Aeolian Geomorphology: An Introduction. Longman, Harlow.
Lockwood, J.G., 2001. Abrupt and sudden climatic transitions and fluctuations: a review. International Journal of Climatology, 21(9), 1153-1179.
Loope, H.M., Loope, W.L., Goble, R.J., Fisher, T.G., Jol, H.M., Seong, J.C., 2010. Early Holocene dune activity linked with final destruction of Glacial Lake Minong, eastern Upper Michigan, USA. Quaternary Research, 74(1), 73-81.
Luna, M.C.M.d.M., Parteli, E.J.R., Herrmann, H.J., 2012. Model for a dune field with an exposed water table. Geomorphology, 159–160(0), 169-177.
Madole, R.F., 1995. Spatial and temporal patterns of late quaternary eolian deposition, Eastern Colorado, U.S.A. Quaternary Science Reviews, 14(2), 155-177.
Maestre, F.T., Salguero-Gomez, R., Quero, J.L., 2012. It is getting hotter in here: determining and projecting the impacts of global environmental change on drylands Introduction. Philos. Trans. R. Soc. B-Biol. Sci., 367(1606), 3062-3075.
Marín, L., Forman, S.L., Valdez, A., Bunch, F., 2005. Twentieth century dune migration at the Great Sand Dunes National Park and Preserve, Colorado, relation to drought variability. Geomorphology, 70(1–2), 163-183.
Marshall, J.K., 1971. Drag measurements in roughness arrays of varying density and distribution. Agricultural Meteorology, 8(0), 269-292.
Martinez, M.L., Vazquez, G., Sanchez Colon, S., 2001. Spatial and temporal variability during primary succession on tropical coastal sand dunes. J. Veg. Sci., 12(3), 361-372.
Maun, M.A., 1981. Seed-germination and seedling establishment of calamovilfa-longifolia on Lake Huron sand dunes. Can. J. Bot.-Rev. Can. Bot., 59(4), 460-469.
Maun, M.A., 1994. Adaptations enhancing survival and establishment of seedlings on coastal dune systems. Plant Ecol., 111(1), 59-70.
Maun, M.A., 1998. Adaptations of plants to burial in coastal sand dunes. Can. J. Bot.-Rev. Can. Bot., 76(5), 713-738.
Maun, M.A., Lapierre, J., 1984. The effects of burial by sand on Ammophila breviligulata. Journal of Ecology, 72(3), 827-839.
Maun, M.A., Lapierre, J., 1986. Effects of burial by sand on seed germination and seedling emergence of four dune species. American Journal of Botany, 73(3), 450-455.
Maun, M.A., Perumal, J., 1999. Zonation of vegetation on lacustrine coastal dunes: effects of burial by sand. Ecol. Lett., 2(1), 14-18.
McEwan, I.K., Willetts, B.B., 1993. Adaptation of the near-surface wind to the development of sand transport. Journal of Fluid Mechanics, 252, 99-115.
McKee, E.D., 1966. Structures of dunes at white sands national monument, New Mexico. Sedimentology, 7(1), 3-69.
McKee E.D. and Bigarella J.J., 1979. Sedimentary structures in dunes. In: E.D. McKee (Ed.), A Study of Global Sand Seas, U.S. Geol. Surv Prof Pap. 1052, 83–134.
Melton, F.A., 1940. A tentative classification of sand dunes its application to dune history in the southern high plains. Journal of Geology, 48(2), 113-U117.
Meurisse, M., Van Vliet-Lanoe, B., Talon, B., Recourt, P., 2005. Holocene dune and peat complexes along the shore of northern France. C. R. Geosci., 337(7), 675-684.
Millennium Ecosystem Assessment, 2005. Ecosystems and Human Well-being: Desertification Synthesis. World Resources Institute, Washington, DC.
Miot da Silva, G., Hesp, P., 2010. Coastline orientation, aeolian sediment transport and foredune and dunefield dynamics of Moçambique Beach, Southern Brazil. Geomorphology, 120(3–4), 258-278.
Miot da Silva, G.M., Martinho, C.T., Hesp, P., Keim, B.D., Ferligoj, Y., 2013. Changes in dunefield geomorphology and vegetation cover as a response to local and regional climate variations. Journal of Coastal Research, 1307-1312.
Moreno-Casasola, P., 1986. Sand movement as a factor in the distribution of plant communities in a coastal dune system. Vegetatio, 65(2), 67-76.
Morkunaite, R., Bauziene, I., Cesnulevicius, A., 2011. Parabolic dunes and soils of the Curonian Spit, south-eastern Baltic Sea coast. Baltica, 24(2), 95-106.
Muckersie, C., Shepherd, M.J., 1995. Dune phases as time-transgressive phenomena, Manawatu, New Zealand. Quaternary International, 26, 61-67.
Muhs, D.R., Maat, P.B., 1993. The potential response of eolian sands to greenhouse warming and precipitation reduction on the Great Plains of the U.S.A. Journal of Arid Environments, 25(4), 351-361.
Muhs, D.R., Stafford, T.W., Cowherd, S.D., Mahan, S.A., Kihl, R., Maat, P.B., Bush, C.A., Nehring, J., 1996. Origin of the late Quaternary dune fields of northeastern Colorado. Geomorphology, 17(1-3), 129-149.
Murray-Wallace, C.V., Bourman, R.P., Prescott, J.R., Williams, F., Price, D.M., Belperio, A.P., 2010. Aminostratigraphy and thermoluminescence dating of coastal aeolianites and the later Quaternary history of a failed delta: The River Murray mouth region, South Australia. Quaternary Geochronology, 5(1), 28-49.
Musick, H.B., Gillette, D.A., 1990. Field evaluation of relationships between a vegetation structural parameter and sheltering against wind erosion. Land Degradation & Development, 2(2), 87-94.
Namikas, S.L., Sherman, D.J., 1995. A review of the effects of surface moisture content on aeolian sand transport. In: V.P. Tchakerian (Ed.), Desert Aeolian Processes. Chapman & Hall, London, pp. 269-293.
Nichol, S.L., Brooke, B.P., 2011. Shelf habitat distribution as a legacy of Late Quaternary marine transgressions: A case study from a tropical carbonate province. Continental Shelf Research, 31(17), 1845-1857.
Nield, J.M., Baas, A.C.W., 2008. Investigating parabolic and nebkha dune formation using a cellular automaton modelling approach. Earth Surface Processes and Landforms, 33(5), 724-740.
Nordstrom, K.F., Jackson, N.L., Hartman, J.M., Wong, M., 2007. Aeolian sediment transport on a human-altered foredune. Earth Surface Processes and Landforms, 32(1), 102-115.
Noy-Meir, I., 1973. Desert Ecosystems: Environment and Producers. Annual Review of Ecology and Systematics, 4(ArticleType: research-article / Full publication date: 1973 / Copyright © 1973 Annual Reviews), 25-51.
Odynsky, W., 1958. U-SHAPED DUNES AND EFFECTIVE WIND DIRECTIONS IN ALBERTA. Canadian Journal of Soil Science, 38(1), 56-66.
Olson, J.S., 1958. Rates of Succession and Soil Changes on Southern Lake Michigan Sand Dunes. Botanical Gazette, 119(3), 125-170.

Overpeck, J.T., Webb, R.S., Webb, T., 1992. Mapping eastern North American vegetation change of the past 18 ka: No-analogs and the future. Geology, 20(12), 1071-1074.
Paul, K., 1944. Morphologie und vegetation der Kurische Nehrung. Nova Acta Leopoldina Carol. NF 13, 217–378.
Phillips, J.D., 1995. Biogeomorphology and landscape evolution: The problem of scale. Geomorphology, 13(1–4), 337-347.
Pluis, J.L.A., 1994. Algal Crust Formation in the Inland Dune Area, Laarder Wasmeer, the Netherlands. Vegetatio, 113(1), 41-51.
Porat, N., Botha, G., 2008. The luminescence chronology of dune development on the Maputaland coastal plain, southeast Africa. Quaternary Science Reviews, 27(9-10), 1024-1046.
Psuty, N.P., 1988. Sediment budget and beach/dune interaction, in: N.P. Psuty (Ed), Dune/Beach Interaction. J. Coastal Research Special Issue No. 3: 1-4.
Psuty, N. P., Silveira, T. M., 2010. Global climate change: an opportunity for coastal dunes?? Journal of Coastal Conservation, 14(2), 153-160.
Pye, K., 1980. Beach salcrete and eolian sand transport; evidence from North Queensland. Journal of Sedimentary Research, 50(1), 257-261.
Pye, K., 1982. Morphological development of coastal dunes in a humid tropical environment, Cape Bedford and Cape Flattery, North Queensland. Geografiska Annaler Series a-Physical Geography, 64(3-4), 213-227.
Pye, K., 1983a. The coastal dune formations of northern Cape York Peninsula, Queensland. Proceedings of the Royal Society of Queensland, 94, 33-39.
Pye, K., 1983b. Coastal dunes. Progress in Physical Geography, 7(4), 531-557.
Pye, K., 1983c. Dune formation on the humid tropical sector of the North Queensland Coast, Australia. Earth Surface Processes and Landforms, 8(4), 371-381.
Pye, K., 1984. Models of transgressive coastal dune building episodes and their relationship to Quaternary sea level changes: a discussion with reference to evidence from eastern Australia. In: M.W. Clark (Ed.), Coastal Research: UK Perspectives. Geo Books, Norwich, pp. 81-104.
Pye, K., 1990. Physical and human influences on coastal dune development between the Ribble and Mersey estuaries, northwest England. In: K.F. Nordstrom, N.P. Psuty, R.W.G. Carter (Eds.), Coastal Dunes: Form and Process. Wiley, Chichester, pp. 339-359.
Pye, K., Mazzullo, J., 1994. Effects of tropical weathering on quartz grain shape; an example from northeastern Australia. Journal of Sedimentary Research, 64(3a), 500-507.
Pye, K., Tsoar, H., 1990. Aeolian sand and sand dunes. Unwin Hyman Ltd, London.
Ranwell, D., 1958. Movement of vegetated sand dunes at Newborough Warren, Anglesey. Journal of Ecology, 46(1), 83-100.
Raupach, M.R., 1992. Drag and drag partition on rough surfaces. Boundary-Layer Meteorology, 60(4), 375-395.
Raupach, M.R., 1994. Simplified expressions for vegetation roughness length and zero-plane displacement as functions of canopy height and area index. Boundary-Layer Meteorology, 71(1-2), 211-216.
Raupach, M.R., Gillette, D.A., Leys, J.F., 1993. The effect of roughness elements on wind erosion threshold. Journal of Geophysical Research, 98(D2), 3023-3029.
Reitz, M.D., Jerolmack, D.J., Ewing, R.C., Martin, R.L., 2010. Barchan-parabolic dune pattern transition from vegetation stability threshold. Geophysical Research Letters, 37.
Rietkerk, M., Dekker, S.C., de Ruiter, P.C., van de Koppel, J., 2004. Self-Organized Patchiness and Catastrophic Shifts in Ecosystems. Science, 305(5692), 1926-1929.
Ritchie, W., 2000. The Sands of Forvie (Scotland): A case study in geomorphology and conservational management. Journal of Coastal Conservation, 6(2), 207-218.
Ritsema, C.J., Dekker, L.W., 1994. Soil moisture and dry bulk density patterns in bare dune sands. Journal of Hydrology, 154(1–4), 107-131.
Robertson-Rintoul, M.J., 1990. A quantitative analysis of the near-surface wind flow pattern over coastal parabolic dunes. In: K.F. Nordstrom, N.P. Psuty, R.W.G. Carter (Eds.), Coastal Dunes Form And Processes. John Wiley & Sons Ltd., Chichester, pp. 57-78.
Rodríguez-Caballero, E., Cantón, Y., Chamizo, S., Lázaro, R., Escudero, A., 2013. Soil Loss and Runoff in Semiarid Ecosystems: A Complex Interaction Between Biological Soil Crusts, Micro-topography, and Hydrological Drivers. Ecosystems, 16(4), 529-546.
Rubin, D.M., Hunter, R.E., 1987. Bedform alignment in directionally varying flows. Science, 237(4812), 276-278.
Scherr, S.J., Yadav, S., 1996. Land degradation in the developing world: implications for food, agriculture and the environment to 2020. IFPRI, Food, Agric. and the Environment Discussion Paper 14, Washington, DC.
Scheidt S., Ramsey M. and Lancaster N., 2010. Determining soil moisture and sediment availability at White Sands Dune Field, New Mexico, from apparent thermal inertia data, J. Geophys.Res. Earth Surf. 115 (F2), F02019.
Servera, J., Gelabert, B., Rodriguez-Perea, A., 2009. Development and setting of the Alcudia Bay beach-dune system (Mallorca, Spain). Geomorphology, 110(3-4), 172-181.
Shepherd, M.J., Eliot, I.G., 1995. Major phases of coastal erosion ca. 6700-6000 and ca. 3000-2000 BP between Cervantes and Dongara, western Australia. Quaternary International, 26(0), 125-130.
Sherman, D.J., 1995. Problems of scale in the modeling and interpretation of coastal dunes. Marine Geology, 124(1-4), 339-349.
Sherman, D.J., Jackson, D.W.T., Namikas, S.L., Wang, J., 1998. Wind-blown sand on beaches: an evaluation of models. Geomorphology, 22(2), 113-133.
Shields, L.M., Drouet, F., 1962. Distribution of Terrestrial Algae within the Nevada Test Site. American Journal of Botany, 49(6), 547-554.
Shields, L.M., Mitchell, C., Drouet, F., 1957. Alga- and Lichen-Stabilized Surface Crusts as Soil Nitrogen Sources. American Journal of Botany, 44(6), 489-498.
Short, A.D., Hesp, P.A., 1982. Wave, beach and dune interactions in southeastern Australia. Marine Geology, 48(3–4), 259-284.
Shulmeister, J., Lees, B.G., 1992. Morphology and chronostratigraphy of a coastal dunefield; Groote Eylandt, northern Australia. Geomorphology, 5(6), 521-534.
Siljeström, P.A., Clemente, L.E., 1990. Geomorphology and soil evolution of a moving dune system in south-west Spain (Doñana National Park). Journal of Arid Environments, 150, 139-150.
Smith, H.T.U., 1952. Map of the Pleistocene eolian deposits of the United States, Alaska and parts of Canada. I :250 000. Geological Society of America.
Smyth, T.A.G., Jackson, D., Cooper, A., 2014. Airflow and aeolian sediment transport patterns within a coastal trough blowout during lateral wind conditions. Earth Surface Processes and Landforms, DOI: 10.1002/esp.3572.

Sole, R., 2007. Ecology: Scaling laws in the drier. Nature, 449(7159), 151-153.
Stetler, L.D., Gaylord, D.R., 1996. Evaluating eolian-climatic interactions using a regional climate model from Hanford, Washington (USA). Geomorphology, 17(1–3), 99-113.
Story, R., 1982. Notes on parabolic dunes, winds and vegetation in Northern Australia. CSIRO Australian Division of Water and Land Resources, 43, 1-33.
Stout, J.E., 2004. A method for establishing the critical threshold for aeolian transport in the field. Earth Surface Processes and Landforms, 29(10), 1195-1207.
Swezey, C.S., 2003. The role of climate in the creation and destruction of continental stratigraphic records: An example from the northern margin of the Sahara Desert. In: C.B. Cecil, N.T. Edgar (Eds.), Climate Controls on Stratigraphy. SEPM Special Publication 77, pp. 207-225.
Swezey, C.S., Schultz, A.P., González, W.A., Bernhardt, C.E., Doar Iii, W.R., Garrity, C.P., Mahan, S.A., McGeehin, J.P., 2013. Quaternary eolian dunes in the Savannah River valley, Jasper County, South Carolina, USA. Quaternary Research, 80(2), 250-264.
Tengberg, A., 1995. Nebkha dunes as indicators of wind erosion and land degradation in the Sahel zone of Burkina Faso. Journal of Arid Environments, 30(3), 265-282.
Tengberg, A., Chen, D.L., 1998. A comparative analysis of nebkhas in central Tunisia and northern Burkina Faso. Geomorphology, 22(2), 181-192.
Thiet, R.K., Boerner, R.E.J., Nagy, M., Jardine, R., 2005. The effect of biological soil crusts on throughput of rainwater and N into Lake Michigan sand dune soils. Plant and Soil, 278(1-2), 235-251.
Thomas, D.S.G., Knight, M., Wiggs, G.F.S., 2005. Remobilization of southern African desert dune systems by twenty-first century global warming. Nature, 435(7046), 1218-1221.
Thomas, D.S.G., Leason, H.C., 2005. Dunefield activity response to climate variability in the southwest Kalahari. Geomorphology, 64(1–2), 117-132.
Timmons, E.A., Fisher, T.G., Hansen, E.C., Eisaman, E., Daly, T., Kashgarian, M., 2007. Elucidating aeolian dune history from lacustrine sand records in the Lake Michigan Coastal Zone, USA. Holocene, 17(6), 789-801.
Tinley, K.L., 1985. Coastal dunes of South Africa. South African National Scientific Prog. Report No. 109. FRD CSIR, Pretoria, South Africa.
Tsoar, H., 2005. Sand dunes mobility and stability in relation to climate. Physica A, 357(1), 50-56.
Tsoar, H., Blumberg, D.G., 2002. Formation of parabolic dunes from barchan and transverse dunes along Israel's Mediterranean coast. Earth Surface Processes and Landforms, 27(11), 1147-1161.
Tsoar, H., Levin, N., Porat, N., Maia, L.P., Herrmann, H.J., Tatumi, S.H., Claudino-Sales, V., 2009. The effect of climate change on the mobility and stability of coastal sand dunes in Ceará State (NE Brazil). Quaternary Research, 71(2), 217-226.
Tsoar, H., Moller, J.T., 1986. The role of vegetation in the formation of linear sand dunes. In: W.G. Nickling (Ed.), Aeolian geomorphology. Allen & Unwin, Boston, pp. 75-95.
Turpin, C., Badr, T., Harion, J.L., 2010. Numerical modelling of aeolian erosion over rough surfaces. Earth Surface Processes and Landforms, 35(12), 1418-1429.
Verrecchia, E., Yair, A., Kidron, G.J., Verrecchia, K., 1995. Physical properties of the psammophile cryptogamic crust and their consequences to the water regime of sandy soils, north-western Negev Desert, Israel. Journal of Arid Environments, 29(4), 427-437.
Veste, M., Littmann, T., Friedrich, H., Breckle, S.W., 2001. Microclimatic boundary conditions for activity of soil lichen crusts in sand dunes of the north-western Negev desert, Israel. Flora, 196(6), 465-474.
Viles, H.A., Goudie, A.S., 2003. Interannual, decadal and multidecadal scale climatic variability and geomorphology. Earth-Science Reviews, 61(1–2), 105-131.
Wagner, R.H., 1964. The ecology of Uniola paniculata L. in the dune-strand habitat of North Carolina. Ecol. Monogr., 34(1), 79-96.
Wakes, S.J., Maegli, T., Dickinson, K.J., Hilton, M.J., 2010. Numerical modelling of wind flow over a complex topography. Environmental Modelling & Software, 25(2), 237-247.
Walker, I.J., Nickling, W.G., 2002. Dynamics of secondary airflow and sediment transport over and in the lee of transverse dunes. Progress in Physical Geography, 26(1), 47-75.
Wand, S.J.E., Esler, K.J., Rundel, P.W., Sherwin, H.W., 1999. A preliminary study of the responsiveness to seasonal atmospheric and rainfall patterns of wash woodland species in the arid Richtersveld. Plant Ecol., 142(1-2), 149-160.
Ward, W.T., 2006. Coastal dunes and strandplains in southeast Queensland: sequence and chronology. Aust. J. Earth Sci., 53(2), 363-373.
Warren, J.K., 1983. Pedogenic calcrete as it occurs in Quaternary calcareous dunes in coastal South Australia. Journal of Sedimentary Research, 53(3), 787-796.
Wasson, R.J., Hyde, R., 1983. Factors determining desert dune type. Nature, 304(5924), 337-339.
Wasson, R.J., Nanninga, P.M., 1986. Estimating wind transport of sand on vegetated surfaces. Earth Surface Processes and Landforms, 11(5), 505-514.
Wasson, R.J., Rajaguru, S.N., Misra, V.N., Agrawal, D.P., Dhir, R.P., Singhvi, A.K., Rao, K.K., 1983. Geomorphology, late Quaternary stratigraphy and palaeoclimatology of the Thar dunefield. Zeitschrift fuer Geomorphologie. Neue Folge, (Suppl.)45, 117-151.
Watt, A.S., 1937. Studies in the Ecology of Breckland. Journal of Ecology, 25(1), 91-112.
Werner, B.T., 1995. Eolian dunes: Computer simulations and attractor interpretation. Geology, 23(12), 1107-1110.
West, N.E., 1990. Structure and function of Microphytic soil crusts in wildland ecosystems of arid to semi-arid regions. Advances in Ecological Research, 20, 179-223.
Wiggs, G.F.S., Baird, A.J., Atherton, R.J., 2004. The dynamic effects of moisture on the entrainment and transport of sand by wind. Geomorphology, 59(1-4), 13-30.
Wiggs, G.F.S., Thomas, D.S.G., Bullard, J.E., Livingstone, I., 1995. Dune mobility and vegetation cover in the Southwest Kalahari desert. Earth Surface Processes and Landforms, 20(6), 515-529.
Wiles, G.C., McAllister, R.P., Davi, N.K., Jacoby, G.C., 2003. Eolian response to Little Ice Age climate change, Tana dunes, Chugach Mountains, Alaska, USA. Arctic Antarctic and Alpine Research, 35(1), 67-73.
Willis, A.J., Yemm, E.W., 1961. Braunton burrows: Mineral nutrient status of the dune soils. Journal of Ecology, 49(2), 377-390.
Winkler, M.G., 1992. Development of parabolic dunes and interdunal wetlands in the Provincelands, Cape Cod National Seashore. In: C.H. Fletcher, III, J.F. Wehmiller (Eds.), Sepm. SEPM (Society for Sedimentary Geology) Special Publication. SEPM {a}, Tulsa, Oklahoma, USA, pp. 57-64.

Wolfe, S.A., 1997. Impact of increased aridity on sand dune activity in the Canadian Prairies. Journal of Arid Environments, 36(3), 421-432.
Wolfe, S.A., David, P.P., 1997. Parabolic dunes: examples from the Great Sand Hills, southwestern Saskatchewan. Canadian Geographer / Le Géographe canadien, 41(2), 207-213.
Wolfe, S.A., Hugenholtz, C.H., 2009. Barchan dunes stabilized under recent climate warming on the northern Great Plains. Geology, 37(11), 1039-1042.
Wolfe, S.A., Lemmen, D.S., 1999. Monitoring of dune activity in the Great Sand Hills region, Saskatchewan. In: D.S. Lemmen, R.E. Vance (Eds.), Holocene Climate and Environmental Change in the Palliser Triangle: a Geoscientific Context for Evaluating the Impacts of Climate Change on the Southern Canadian Prairies. Geological Survey of Canada Bulletin 534, pp. 199-210.
Wolfe, S.A., Nickling, W.G., 1993. The protective role of sparse vegetation in wind erosion. Progress in Physical Geography, 17(1), 50-68.
Wolfe, S.A., Nickling, W.G., 1996. Shear stress partitioning in sparsely vegetated desert canopies. Earth Surface Processes and Landforms, 21(7), 607-619.
Yair, A., 1990. Runoff generation in a sandy area—the nizzana sands, Western Negev, Israel. Earth Surface Processes and Landforms, 15(7), 597-609.
Yan, N., 2010. Surface process and morphological evolution of parabolic dunes. Msc., Beijing Normal University, Beijing, 42 pp.
Yan, N., Hasi, E., Liu, H.Q., Li, S.Q., 2010. Research progress in morphology and evolution of the parabolic dunes. Journal of Desert Research, 30(4), 801-807.
Yizhaq, H., Ashkenazy, Y., Tsoar, H., 2007. Why Do Active and Stabilized Dunes Coexist under the Same Climatic Conditions? Physical Review Letters, 98(18), 188001.
Yizhaq, H., Ashkenazy, Y., Tsoar, H., 2009. Sand dune dynamics and climate change: A modeling approach. Journal of Geophysical Research: Earth Surface, 114(F1), F01023.
Yurk, B.P., Hansen, E.C., Sherron, K.A., Johnson, B.G., Arbogast, A.F., 2002. Migration history of Green Mountain Beach parabolic dune, southeastern shore of Lake Michigan, Geological Society of America, 2002 Annual Meeting. Abstract with Programs, Denver.
Zeng, Y.J., 2008. A study on the morphologic characteristics and causes of parabolic dunes in Takeermohuer Desert in Yili by DEM. Msc., Xinjiang Normal University, Xinjiang, 36 pp.
Zhang, J.H., Maun, M.A., 1994. Potential for seed bank formation in seven great lakes sand dune species. American Journal of Botany, 81(4), 387-394.
Zhang, P., Hasi, E., Du, H.S., Wu, X., Yang, Y., 2011. Dynamic relationship between parabolic dunes and Artemisia ordosica (in Chinese with English abstract). Chinese Science Bulletion, 56(35), 3003-3010.
Zhuang, Y.M., Hasi, E., 2005. Progress of the study on shapes and dynamical process of blowouts on dunes. Arid Land Geography, 28(5), 632-637.
Zular, A., Sawakuchi, A.O., Guedes, C.C.F., Mendes, V.R., Nascimento Jr, D.R., Giannini, P.C.F., Aguiar, V.A.P., DeWitt, R., 2013. Late Holocene intensification of colds fronts in southern Brazil as indicated by dune development and provenance changes in the São Francisco do Sul coastal barrier. Marine Geology, 335(0), 64-77.

Chapter 3

Hypothesis and Research Framework

After reviewing background and rationale regarding eco-geomorphic interactions and dune transformations in aeolian environments, this chapter presents a hypothesis, followed by objectives and a research framework comprised of four primary components.

3.1 Hypothesis

This thesis aims to understand how changes in environmental variables and anthropogenic activities can lead to a dune transformation from barchan to parabolic dunes (a process of dune stabilisation) as well as a dune transformation from parabolic to barchan dunes (a process of dune reactivation). A hypothesis was inspired by field observations during my quest for a MSc (Yan, 2010).

The hypothesis presents four phases that are involved in a sequence of a barchan-to-parabolic dune stabilisation and a parabolic-to-barchan dune reactivation, as shown in Figure 3-1. When a barchan is moving into a shrub field, its two horns may start to be stabilised by shrubs from the horns due to lower sedimentation transport thereof. As the lobe moves forward, the dune changes gradually in shape and is transformed into a parabolic dune with two trailing arms (from phase 1 to 2). For a barchan dune with relatively high mobility, the dune is likely to move forward over a long distance, forming elongated trailing arms. The deflation basin between two trailing arms can be re-vegetated, developing a zonation along the migration direction of the dune. Under the same stable climate, the parabolic dune is likely to be fully-stabilised eventually. A periodic drought period or increased grazing pressure, however, may prohibit this dune-stabilisation process, or even reactivate already stabilised parabolic dunes. Relatively sparse vegetation on and near the lobe often suffers more severe deterioration, and the lobe regains great mobility (from phase 2-3). Sand trapped on the arms, at the same time, may be exposed to transport again to a different degree and deposited on the lee slope. As the lobe moves forward, it may break from its better-vegetated arms and transform into a barchan dune (from phase 3-4).

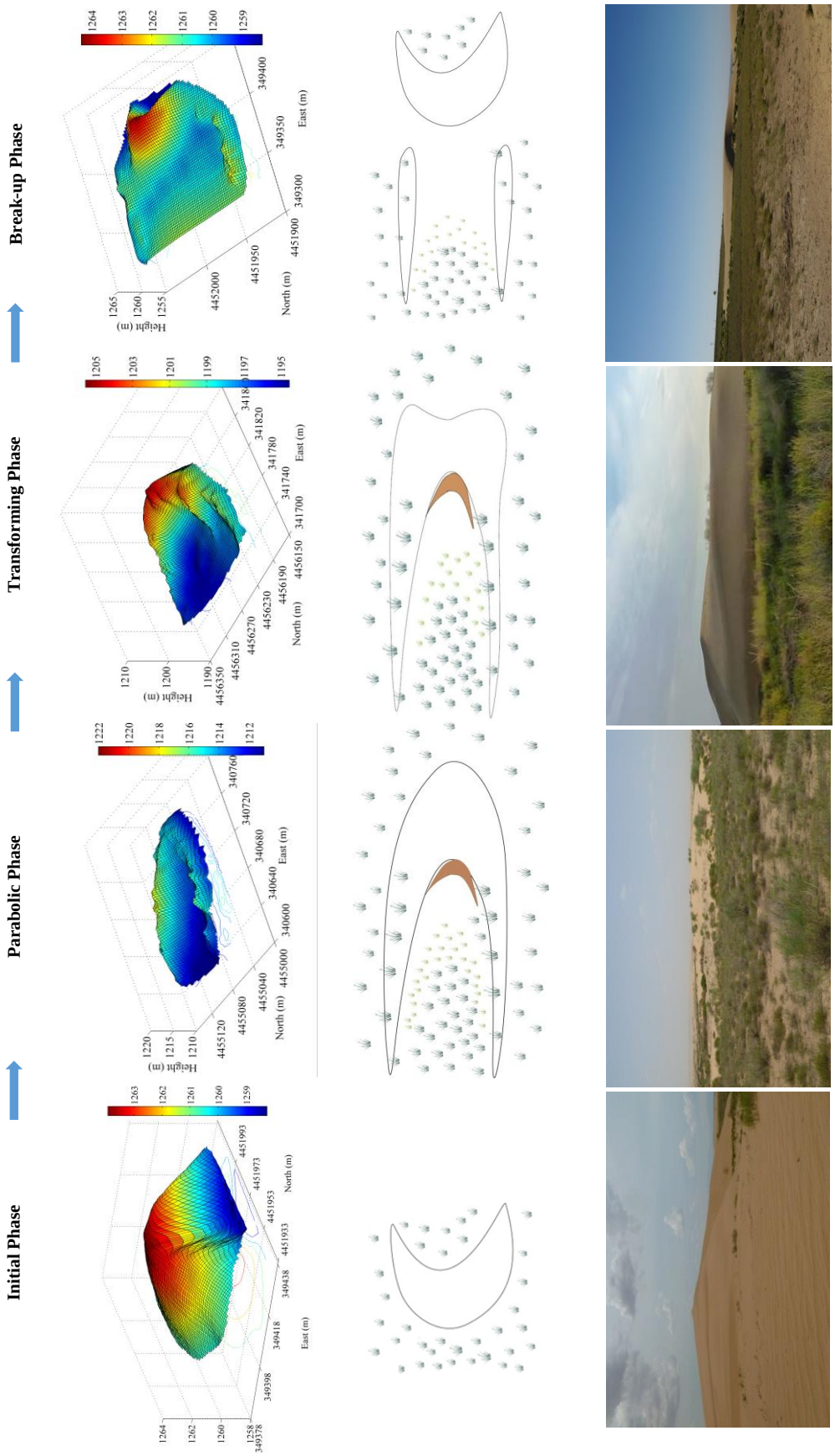

Figure 3-1. Hypothesis of transformations from barchan to parabolic dunes (initial phase - parabolic phase), and from parabolic to barchan dunes (parabolic shape - transforming phase - break-up phase). The DEMs are measurements by a D-GPS from field surveys, showing examples of different dune phases abstracted in the cartoons. Photos show the associated field sites.

The barchan-to-parabolic dune transformations have been studied actively in the aeolian research community, but research on reactivation of parabolic dunes into highly mobile barchan dunes has been nearly absent (*cf.* Section 2.3.1 & Section 2.3.4). The reactivation of vegetated dunes may have significant implications for land management, local economy and human activities. The Hobq Desert provides an arena for examining and exploring both dune transformations (*cf.* Chapter 4). A small barchan dune with two trailing arms left behind has been found in a field site in 2009 (Figure 3-2). However, because the dune was located beside a road and a new railway was under construction nearby, the barchan had been stabilised by artificial straw checkerboards by 2010 (Figure 3-3).

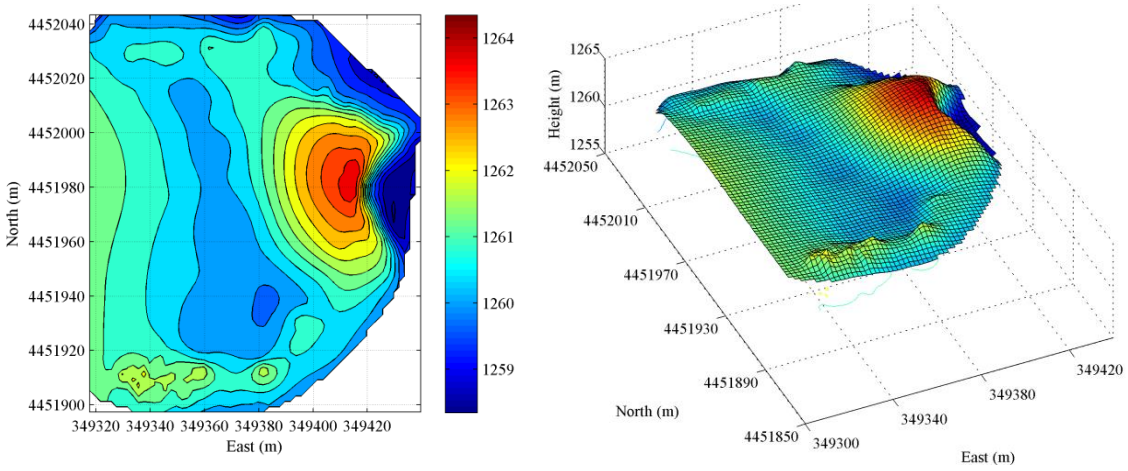

Figure 3-2. View of a barchan dune with two trailing arms left behind, investigated in May 2009. The contour interval is 0.4 m and the colour bar shows height in meter.

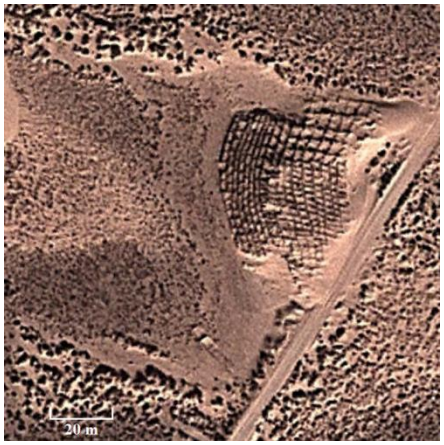

Figure 3-3. Google Earth Image of the barchan dune in 2012.

Both the barchan-to-parabolic and the parabolic-to-barchan dune transformations have been observed in the field. However, the fundamental mechanisms underlying these transformations, their environmental controls, and the stability of an aeolian system remain inadequately understood. In order to address these questions, the objectives and research framework of this thesis are presented in the next section.

3.2 Objectives and Research Framework

The aim of this thesis is to investigate (1) how different environmental controls influence the eco-geomorphic interactions and the processes of a barchan-to-parabolic dune transformation, and (2) how environmental changes can lead to the reactivation of stabilising parabolic dunes into highly mobile barchan dunes.

Specific objectives include:

(1) Explore how a CA model can be used to simulate interactions between different vegetation species and environmental conditions, in particular perennial grasses/shrubs that have relatively long life spans and strong seasonal growth patterns.

(2) Explore how to utilise field investigations and remote sensing techniques to help parameterise the model and predict potential dunefield evolutions under climatic changes.

(3) Investigate sensitivity of a barchan-to-parabolic dune transformation to changes in the sand availability (sandy substratum thickness and the size of barchan dunes), the wind regime, and the characteristics of vegetation species (the capability of withstanding wind erosion and sand burial).

(4) Understand the fundamental eco-geomorphic processes during a barchan-to-parabolic dune transformation.

(5) Explore how environmental parameters in a dune system interact and compromise with each other and fundamentally determine the processes of a barchan-to-parabolic dune transformation.

(6) Investigate the processes and possibilities of the parabolic-to-barchan dune transformations under potential increases in drought stress and wind strength.

(7) Understand the eco-geomorphic interactions that fundamentally govern the dune reactivation and parabolic-to-barchan dune transformations.

(8) Primarily explore the influence of periodic drought events and grazing activities on both dune stabilisation and reactivation.

(9) Explore the applicability of the Extended-DECAL in different aeolian systems.

The detailed research framework of the thesis is shown in Figure 3-4. By combining empirical field data from an inland shrub dunefield, remote sensing image interpretation, and secondary data with the DECAL model, the Extended-DECAL includes dynamic growth functions and climatic and anthropogenic impacts, and can be used to explore eco-geomorphic interactions in the mutual transformations between barchan and parabolic dunes, to investigate significance and sensitivity of boundary conditions and environmental controls, and to predict the potential likelihood of dunefield reactivation under environmental and anthropogenic forces.

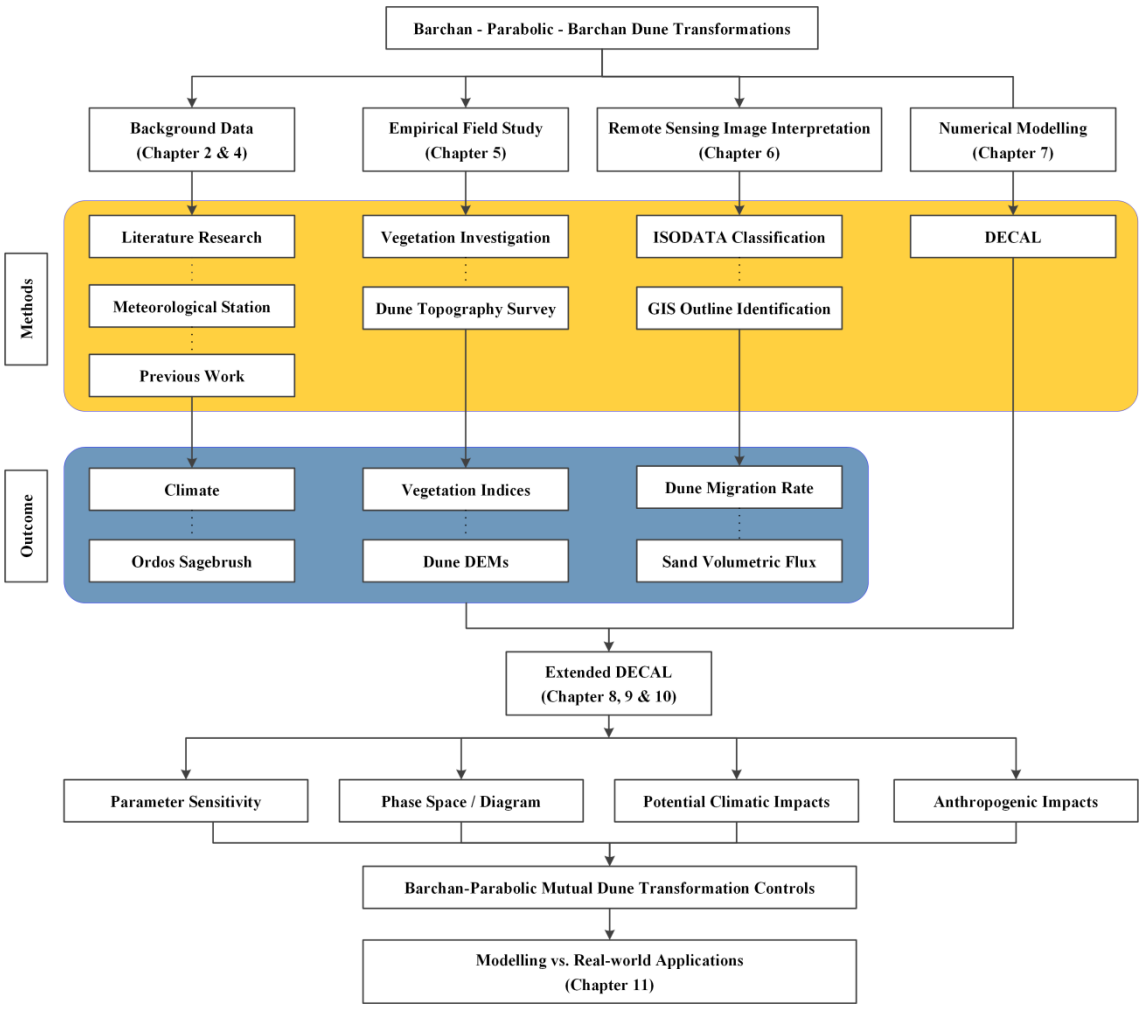

Figure 3-4. Research framework.

References

Yan, N., 2010. Surface process and morphological evolution of parabolic dunes. Msc., Beijing Normal University, Beijing, 42 pp.

Chapter 4

Study Region

This chapter provides a detailed background of the study region in four respects: 1) the geographic setting of the study region and dune sites, 2) the historical context regarding regional desertification, 3) the climatic context, and 4) the ecological context. The geographic setting of the study region and specific dune sites is introduced in the first section. As this region is closely linked with and influenced by historical human migration and reclamation activities, a brief historical background that caused desertification is then presented in the second section to assist in understanding the formative context of current dune landscapes. The third section provides the climatic context based on analyses of historical records from a local meteorological station regarding temperature, precipitation, and wind velocities. Sand drift potentials, meanwhile, are calculated using the Fryberger method. Ecological context is presented in the last section, in particular, the characteristics of the dominant species, Ordos Sagebrush, which plays a key role in the formation, development, and transformations of dune landforms in the study region.

4.1 Geographic Setting

The study region is located in the North of Ordos Plateau, Inner Mongolia, China (40°14' N, 109°08' E, Figure 4-1). The Ordos plateau is a farming-pastoral ecotone, with an arid continental temperate climate in the northwest and a semi-arid monsoonal climate in the southeast (Li et al., 2009; Zheng et al., 2005b). The Ordos plateau also experiences a transition between the Gobi deserts in the west to the Loess plateau in the east. The soil primarily originates from Cretaceous and Jurassic deposits, and is dominantly composed of sand, thereby being easily transported by winds when surface protection by vegetation is absent (Zhu et al., 1980). The elevation in the study region decreases from the south to the north. The south part is an earth-rocky mountainous area belonging to the Ordos abraded tableland with elevations between 1300 and 1500 m; the middle part is the Hobq Desert with elevations between 1000 and 1300 m; and the north part is the alluvial plain of the Yellow River with elevations between 1000 and 1100 m.

Most seasonal rivers originating from the Ordos tableland flow through the study region from the south towards the north.

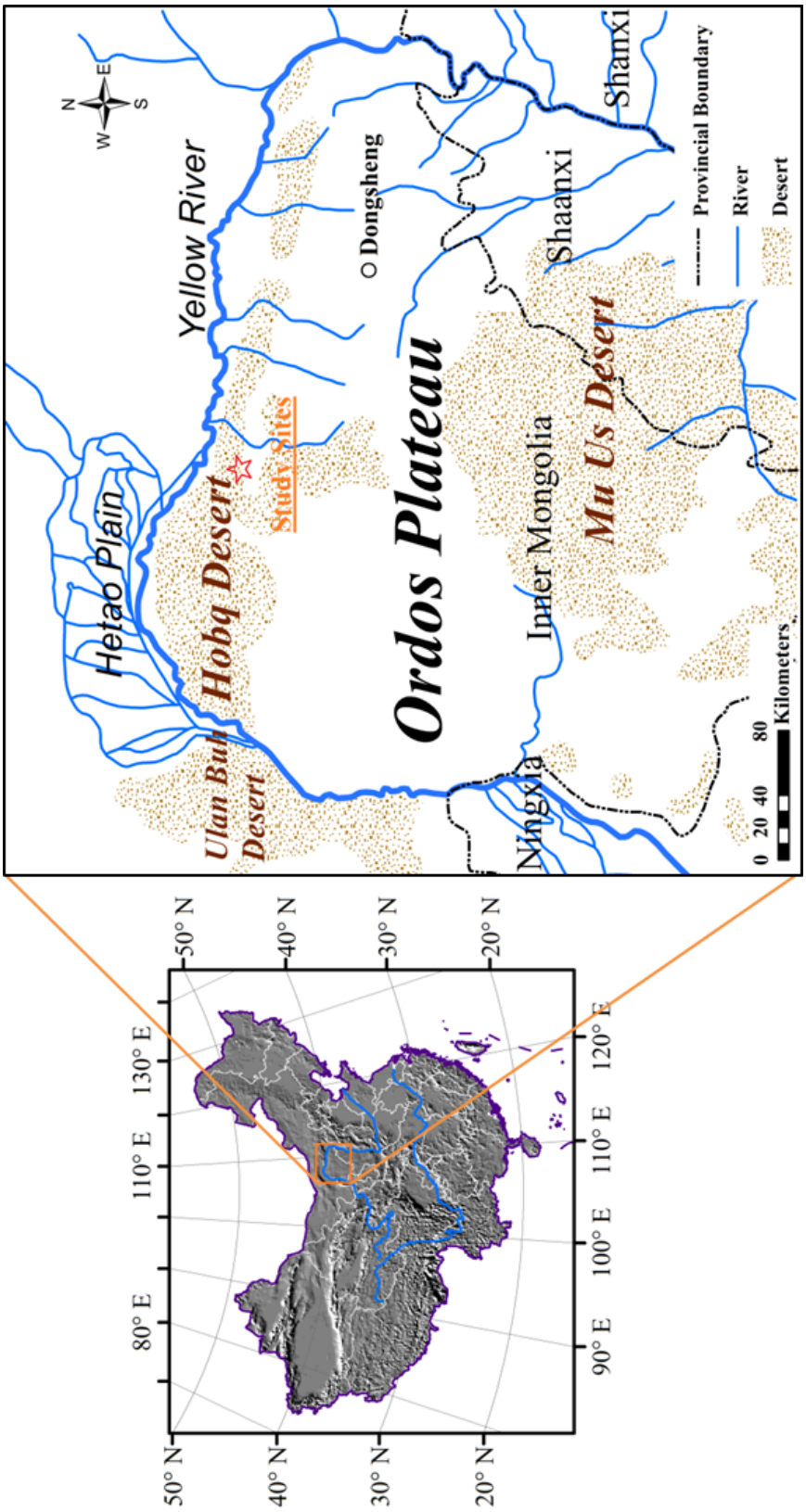

Figure 4-1. Location of study region and sites.

The field sites are located in the Hobq Desert, between two seasonal rivers. Barchan and crescent dunes are distributed in the north; semi-vegetated parabolic dunes are in the middle; and sand sheets are in the south. The parabolic dunes investigated in the field are shown in Figure 4-2. Five parabolic dunes were investigated during the first field trip in 2011, which were selected to represent three types of parabolic dunes observed in the study region that were in different mobility and formed under different local environments. (1) The D1 and D2 are semi-mobile parabolic dunes with bare lobes and tall slip faces. They may be either in a phase between the initial phase and the parabolic phase in Figure 3-1, or in a phase between the transforming phase and the break-up phase. (2) The D3 and D4 have been stabilised by vegetation and do not have slip faces, and are hence in the parabolic phase in Figure 3-1. All of these four dunes are in the absence of external sand supply because they are surrounded by well-vegetated interdune shrub lands. (3) In contrast, the D5 is located right on the strand of a seasonal river and may receive external sand supply in winter when strong winds can transport dry sand from the nearby river. The frontal edge of the D5 has extended more than 100 meter away from its dune crest. The D5 is likely to be in a phase between the initial phase and the parabolic phase in Figure 3-1. Based on the overall understanding of different types of parabolic dunes in the study region, more detailed investigation was employed in 2012, but only semi-mobile parabolic dunes (D1 & D2) were surveyed because the second field trip aimed at measuring a change in dune morphology over the one year period.

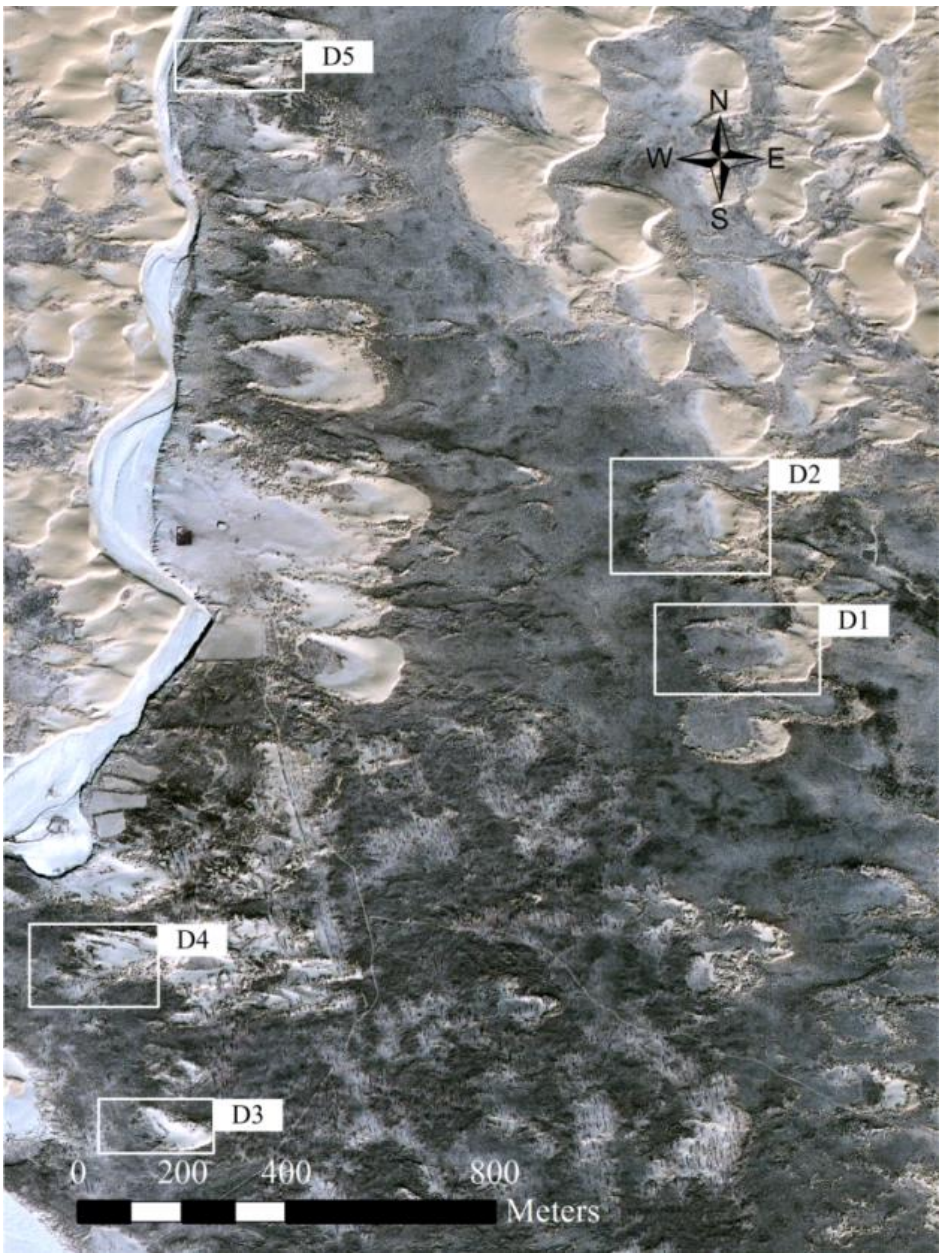

Figure 4-2. Field sites and parabolic dunes investigated. Dunes (D1-D5) are labelled on a Quickbird image in 2007.

4.2 Historic Context

The desertification and encroaching of sand has been an outstanding problem on the Ordos Plateau (Zha and Gao, 1997), although the Ordos in the past was known for its rich pastures and grasslands (Li and Zheng, 2002). Aboriginal inhabitants are nomadic minorities including Huns and Mongolians. Historical records show that cultivation activity has been present in the Warring States and the Qin Dynasty by the Hans, but large scales of migration of Han people and the associated reclamation activity did not begin until the Qing Dynasty in the 19th century and continued to escalate over the Minguo period when

extensive reclamation and crop rotation farming had extended to the Yellow River's elbow plain (Jiang et al., 1995; Zhu, 1986). Reclamation activity during this period was principally responsible for the environmental deterioration and desertification in the region. From the late 1950s to the 1970s, desertification spread rapidly and the area of the Hobq Desert expanded approximately 500 km^2 (Yang et al., 1991). The Hobq Desert became one of the largest deserts and dust sources in northern China. Dusts originated from Hobq Desert in spring can reach Beijing within a couple of hours.

In order to control dust sources and restore vegetation, the Chinese government launched the 'Three-North Shelterbelt' project in 1978 and since then trees have been widely planted in the north, northwest and northeast of China. Although some positive impacts have been achieved, serious challenges remain outstanding. Overgrazing and drought significantly intensified desertification (Chen et al., 2008). Coal mining, undertaken extensively only lately with the discovery of the Dongsheng coal field (one of the largest high quality coal bases in China), and the associated road constructions further exacerbated desertification and has given rise to severe environmental issues (Zheng et al., 2005b). Another notable problem contributing to desertification was excessive collection of firewood and medicinal plants. The potential climatic changes, in particular progressively increased mean temperature, may have significant implications for the fragile ecosystem of the Ordos Plateau (Li and Zheng, 2002). More frequent extreme disasters such as long-lasting droughts may significantly impact vegetation establishment and growth, as well as the associated ecological restoration of deserts (State Forestry Administration, 2011).

4.3 Climatic Context

Meteorological data from Dongsheng station (Figure 4-1), the meteorological station nearest to the study sites on the Ordos Plateau (a distance of ~150 km), were acquired from the China Meteorological Administration. Primary data include daily average temperature and daily precipitation from 1956 to 2011, and wind velocities per 6 hours from 1957 to 2003. The study region is generally governed by a typical temperate continental semi-arid monsoon climate with strong seasonality. Winters are cold, dry and windy, whilst summers are hot, rainy and windless.

4.3.1 Temperature and Precipitation

As shown in Figure 4-3, annual mean temperature is ~6 ^{o}C, and the lowest and highest temperatures occur in January and July respectively with average temperatures of -11 ^{o}C and 21 ^{o}C. The average temperature in each month is relatively stable with a small standard deviation ranging from 1 ^{o}C to 3 ^{o}C. Compared with summer, the temperature in winter fluctuates more substantially.

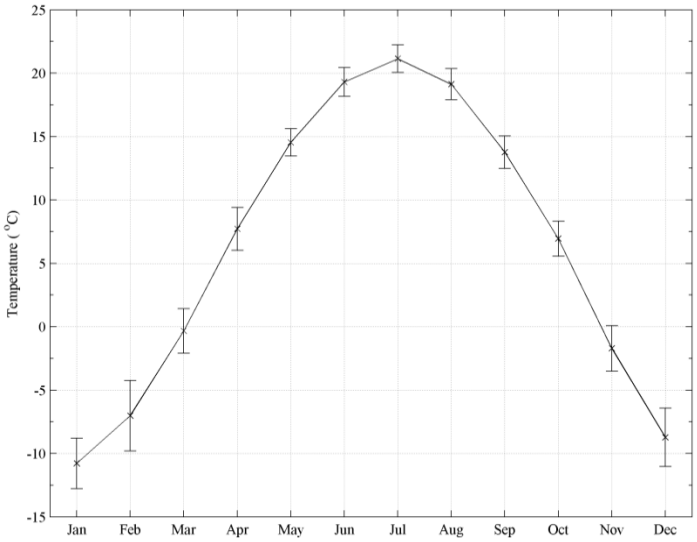

Figure 4-3. Monthly temperature (data from 1956 – 2011, whiskers denote the standard deviation).

The mean annual precipitation is ~370 mm (Figure 4-4) and the period between June and September receives approximately 78 % of annual rainfall (Figure 4-5). Precipitation primarily happens in summer but fluctuates considerably with a largest standard deviation of 58.02 mm in August, which may have significant implications for vegetation growth and the associated change in sand transport of the study region.

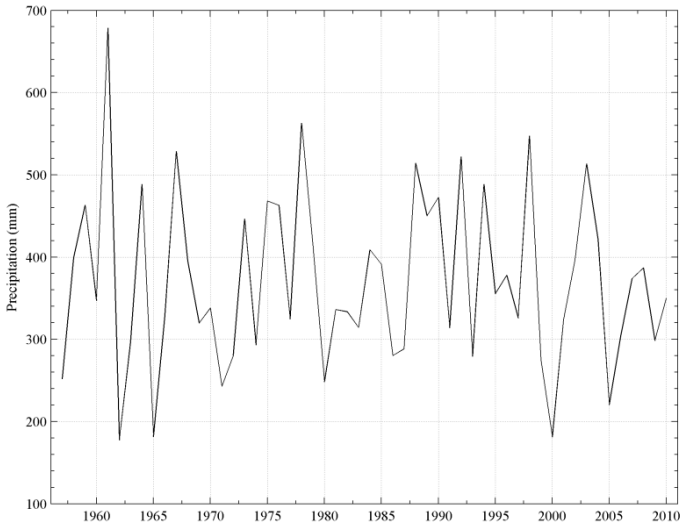

Figure 4-4. Annual precipitation (data from 1956 – 2011).

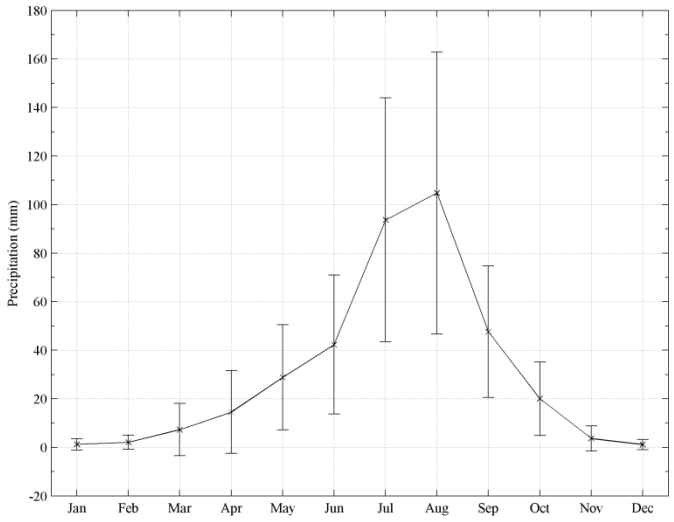

Figure 4-5. Monthly precipitation (data from 1956 – 2011, whiskers denote the standard deviation).

4.3.2 Wind Regime

The data of wind velocities, collected at a height of 10.4 m above the surface at the Dongsheng meteorological station, are shown in Figure 4-6 and Figure 4-7. Annual average wind speed is ~3 m s^{-1} with an average standard deviation of 2 m s^{-1} in each month. Two peaks occur in April and November with average wind speeds of 4 m s^{-1} and 3 m s^{-1} respectively. The region is governed by northwesterly and southwesterly winds throughout the year.

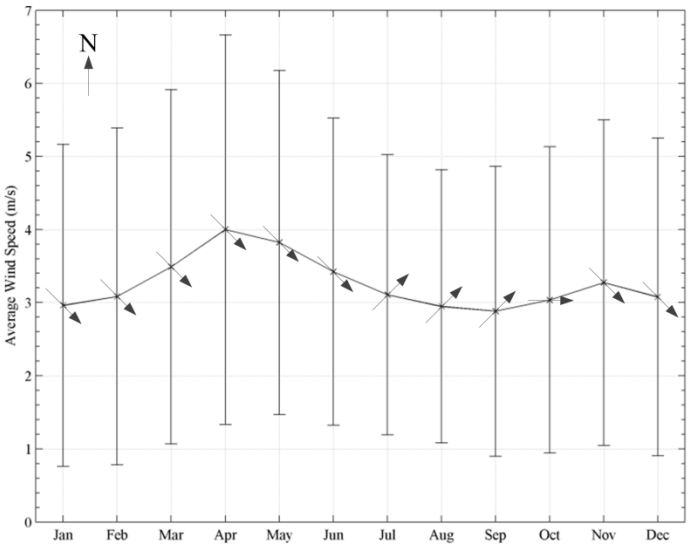

Figure 4-6. Monthly wind speed and direction (data from 1953-2003, whiskers denote the standard deviation and arrows denote wind direction).

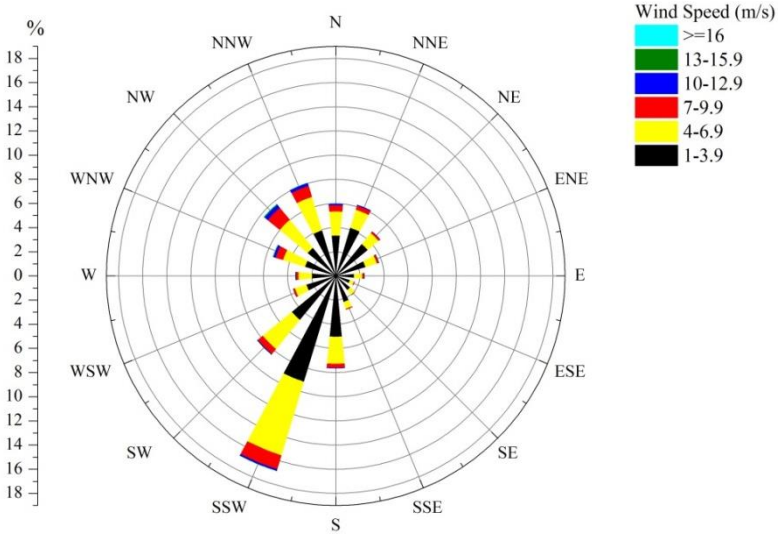

Figure 4-7. Wind speed rose (data from 1953-2003).

Regional wind regime was also analysed using the Fryberger method (Fryberger, 1979), in which sand drift potentials were estimated for winds above the threshold wind velocity at a given height. Estimating the threshold wind velocity accurately at the height of meteorological station where the historical data of wind velocities were collected is therefore of particular importance. In order to achieve this, three steps were involved. First, the average particle size of sand grains in the study region was acquired by analysing the distributions of particle sizes of soil samples collected in a previous study in

2009. Second, the threshold value of shear velocity was then calculated using the Bagnold equation (1941). Finally, the threshold velocity at the height of 10.4 m, the height of the cup anemometers at the meteorological station, was acquired with the method of the Law of the Wall.

4.3.2.1 Average Particle Size of Sand Grains

Wind profiles, dune topography, and soil samples (within 3 cm depth) were collected in 2009 in the Hobq Desert, supported by my previous supervisor Professor Hasi Eerdun at Beijing Normal University. Sampling transects were set up along three cross sections across arms and three radial sections on the lobe of a parabolic dune (Figure 4-8). The distributions of particle sizes were tested by a Mastersizer2000 laser particle sizer with a measuring range of 0.5 to 2000 μm.

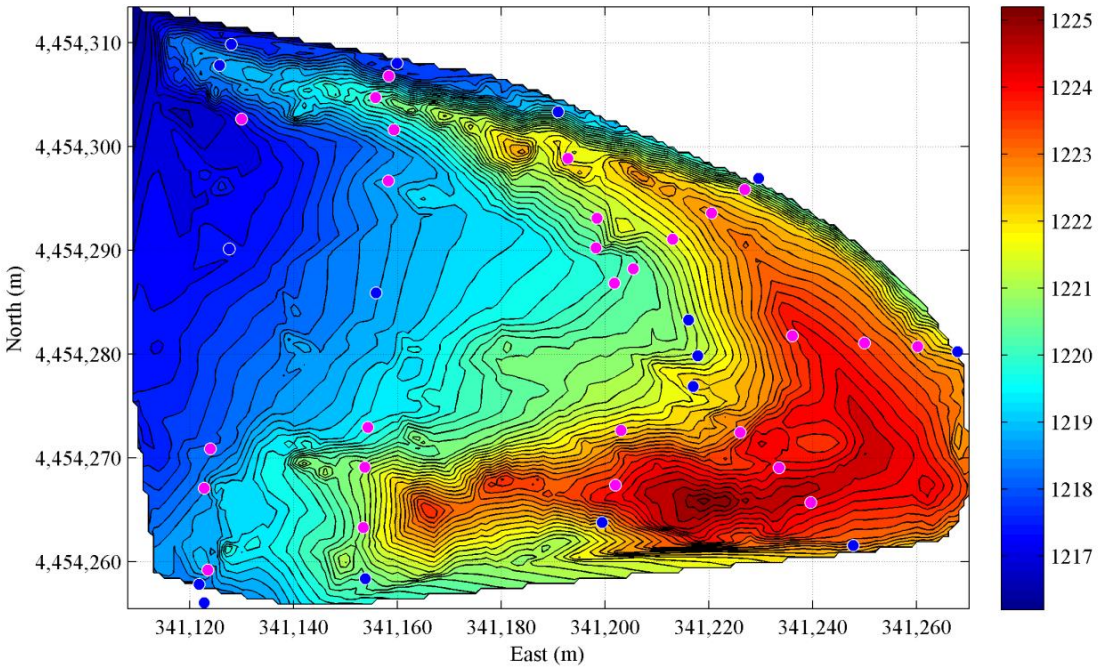

Figure 4-8. Distribution of soil samples on a parabolic dune. The colour bar denotes the height in meter. Magenta dots were used in the calculation of average diameter of sand grains, whilst blue dots were excluded.

Sampling points between the two trailing arms as well as those on the foot of slopes of the outside boundary of the parabolic dune were excluded from the average particle size calculation, because the surfaces have been well-vegetated and covered with soil and silt and sand transport is unlikely to happen. Meanwhile, sampling points upwind of the windward slope where an ancient fossil soil layer had

been exposed by intensive wind erosion were also excluded. As a result, the average particle sizes of samples vary between 190 μm and 465 μm, with an average value of 272 μm.

4.3.2.2 Threshold Value of Shear Velocity on the Ground Surface

The threshold value of shear velocity [U_{*t}, m s^{-1}] on the ground surface was calculated by an expression from Bagnold (1941):

$$U_{*t} = A\sqrt{\frac{\sigma-\rho_a}{\rho_a}gd} \tag{4-1}$$

where σ is the density of quartz sand grains, [2643 kg m^{-3}]; ρ_a is the density of air, [1.2 kg m^{-3}]; g is the gravitational constant, [9.8 m s^{-2}]; d is the diameter of quartz grains, [m]; and A is a constant determined by the grain diameter. A is usually replaced with 0.085 for grains larger than 0.1 mm (Chepil, 1945) and with 0.080 when grains are larger than 0.25 mm (Bagnold, 1941). Thus, by substituting d = 272 μm and A = 0.08, the threshold value of shear velocity over the ground surface was determined, as 0.19 m s^{-1}.

4.3.2.3 Threshold Velocity at the Height of 10.4 m

The threshold velocity at the height of 10.4 m where cup anemometers were set up at the Dongsheng meteorological station can be estimated by substituting the threshold value of shear velocity (u_{*t}) for the shear velocity (u_*) using the Law of the Wall (Equation 4-2), if the roughness length of the surface (z_0) is known:

$$u = \frac{u_*}{\kappa}\ln(\frac{z}{z_0}) \tag{4-2}$$

where u is the velocity at the height z; and κ is von Karman's constant [~0.4].

The roughness length of the surface (z_0) was obtained by analysing wind profiles with the Law of the Wall. Wind profiles were measured by a tower of cup anemometers at nine different heights in 2009, specifically 0.1 m, 0.3 m, 0.6 m, 1 m, 1.2 m, 1.5 m, 2 m, 3 m and 4 m above the surface. Wind speeds at each height were recorded for twenty minutes, and average wind speeds within one minute were used. In order to minimise the influence of local surface environments, vegetation for example, only the seven heights larger than 0.6 m were used to extrapolate the roughness length of bare sand surface by fitting mean wind speed data per minute with optimised least-squares linear regression to the Law of the

Wall (Bauer et al., 1992; Oke, 1987), because even sparse vegetation on the ground surface may cause turbulence that disturbs the near-surface environment and changes the airflow to be thermally un-neutral (Wolfe and Nickling, 1993). Wind profiles were further strictly filtered based on the goodness of fit to the Law of the Wall (Ellis et al., 2009). Fitted equations with R^2 larger than 0.98 were only included to the calculation of the average surface roughness length, which comes out to 1.39 mm (Figure 4-9 and Table 4-1). By substituting z_0 = 1.39 mm and u_* = 0.19 m s^{-1}, the threshold velocity at the height of 10.4 m was then calculated by using the Law of the Wall, which is 4.32 m s^{-1}.

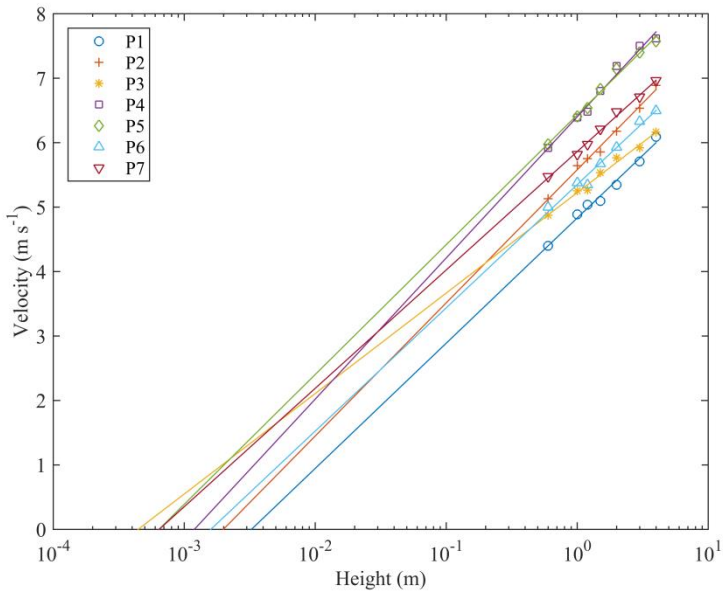

Figure 4-9. Wind profiles used to calculate average roughness length of bare sand surface.

Table 4-1. Parameters of wind profiles

	R^2	Slope	Roughness length (m)
P1	0.985	0.84	0.0033
P2	0.992	0.90	0.0020
P3	0.986	0.68	0.0004
P4	0.983	0.95	0.0012
P5	0.989	0.87	0.0006
P6	0.981	0.83	0.0016
P7	0.994	0.80	0.0006

4.3.2.4 Sand Drift Potentials

Average 6-hourly wind velocities from 1957 to 2003 were acquired from the meteorological station in Dongsheng, Inner Mongolia. Wind directions were recorded in 16 directions. Sand drift potentials (*DP*), which reflect the relative amount of potential sand drift for a certain period of time, were evaluated by the Fryberger method (Fryberger, 1979):

$$DP = u^2(u - u_t)t \tag{4-3}$$

where *DP* is drift potential expressed in vector units, [VU], for a specific wind direction; u is wind velocity, [m s^{-1}]; u_t is threshold wind velocity, 4.32 m s^{-1}; and t is the frequency probability of wind velocities larger than the threshold wind velocity. Resultant drift potential (*RDP*) and ratios of resultant drift potential to drift potential (*RDP/DP*) were also calculated. Results are shown in Figure 4-10 and Figure 4-11.

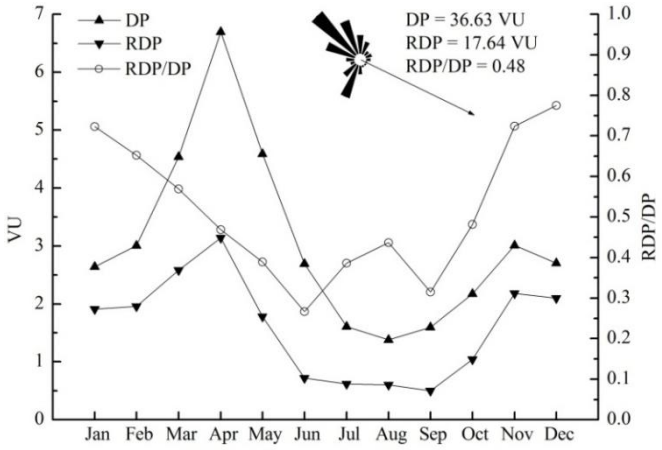

Figure 4-10. Sand drift potential in different months.

The study region, in general, represents a medium-energy wind environment with sand drift potentials varying moderately. Annual sand drift potential is 36.63 VU with a *RDP/DP* of 0.48. Sand drift potential presents a noticeably seasonal change throughout the year. The prevailing wind direction for sand transport is around 315 ˚ and a relatively minor prevailing wind direction is around 202.5 ˚. The wind regime in the study area is dominated by the northwest and the southwest winds with strongest winds occurring in April and May when weather is cold and vegetation starts to grow but has yet to reach its maximum. Winds are relatively weak in summer especially over the period from June to October. In

summary, the strongest winds generally occur in spring and winter, and NW and SW winds dominate the study region.

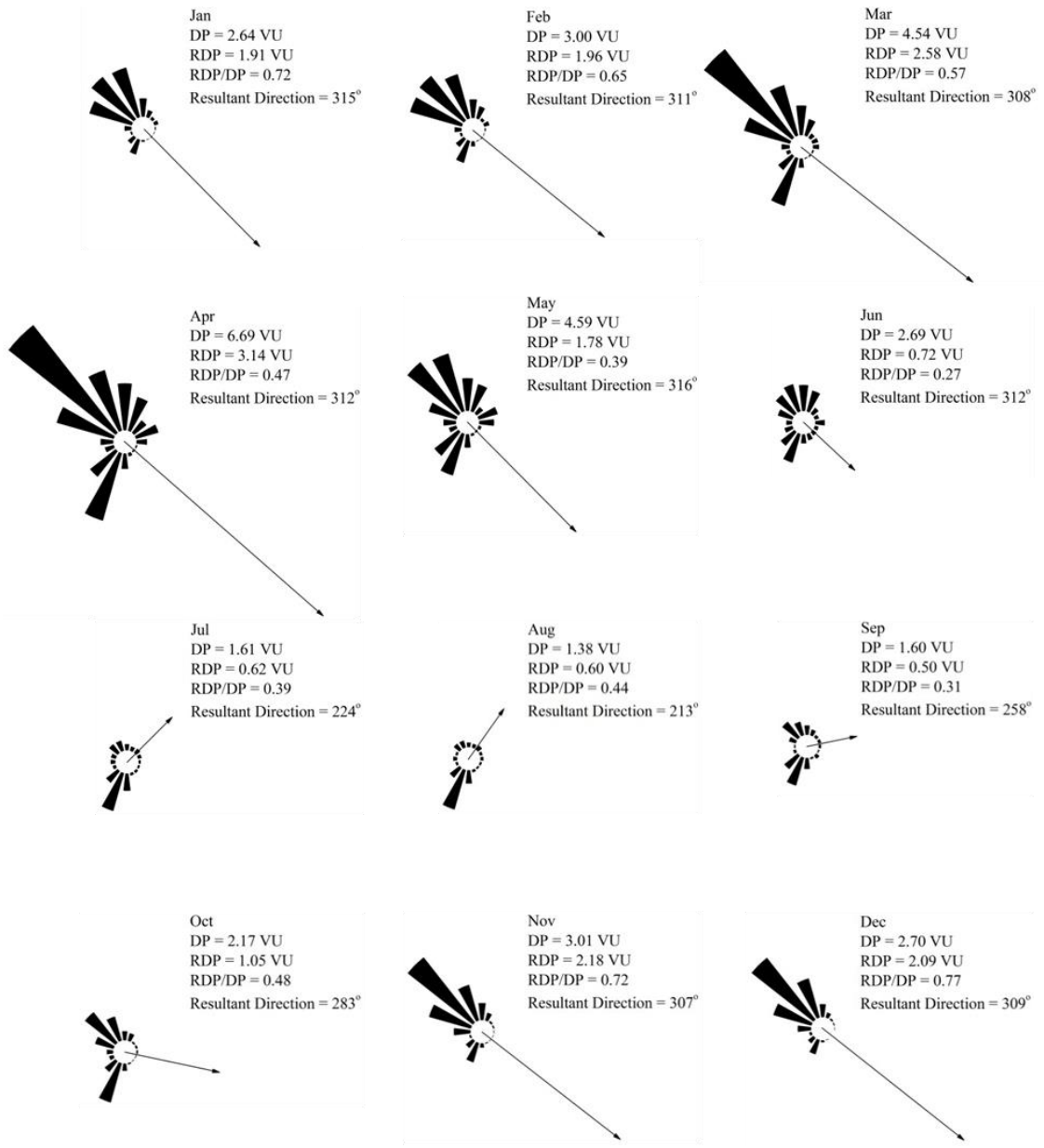

Figure 4-11. Rose diagrams of sand drift potential in each month.

4.4 Ecological Context

Vegetation in the study region is dominated by Ordos Sagebrush (*Artemisia ordosica*, Figure 4-12), and other species include Mongolian Sweetvetch (*Hedysarum mongolicum*, Figure 4-13), Sand Rice (*Agriophyllum squarrosum*, Figure 4-14), Broom Sweetvetch (*Hedysarum scoparium*), and Littleleaf

Peashrub (*Caragana microphylia*). The Ordos Sagebrush often out-competes other species significantly and presents a generally exclusive colonisation.

Figure 4-12. Ordos Sagebrush in the Kubq Desert on the Ordos Plateau.

Figure 4-13. Mongolian Sweetvetch in the Kubq Desert on the Ordos Plateau.

Figure 4-14. Sand Rice in the Kubq Desert on the Ordos Plateau.

The Ordos Sagebrush is a native, deciduous, and psammophytic semi-shrub species (species grows in sandy areas and is capable of tolerating sand burial) on the Ordos Plateau, adapted to the inland arid and semi-arid environments with relatively strong capability of resisting drought and cold. The height of the Ordos Sagebrush is 0.5 - 1.0 m with the maximum canopy coverage of approximately 1.0 m^2 (Li et al., 2010; Yang et al., 2008; Zhang et al., 2008). The Ordos Sagebrush has been used to stabilise mobile dunes and recover local ecosystems. The Ordos Sagebrush also serves as important forage for livestock (Zhang, 1994).

Natural propagation is primarily from seeds, although occasionally plants can propagate themselves from clonal branches (Wang et al., 2002). The mucilaginous coat of seeds can absorb considerable amounts of water after precipitation and provide precious moisture for germination in an arid environment. The mucilaginous coat, meanwhile, facilitates seeds to be anchored on the shifting dune surfaces more easily (Zheng et al., 2005a). Sand burial, on one hand, can protect seeds from high temperature and rapid loss of moisture from evaporation. On the other hand, deeper burial may hinder the germination because of insufficient light (Tobe et al., 2006; Woolley and Stoller, 1978). A shallow depth is, therefore, preferable for seed germination, where moisture is higher than ground surfaces but sunlight is able to penetrate the buried sand layer.

In northern China, temperature falls below 0 ˚C in winter, inhibiting seed germination significantly. Strong aeolian activity and lack of precipitation in winter further suppress seed germination. Because optimal temperature for seed germination of the Ordos Sagebrush is ~20 ˚C, the seeds usually germinate in spring on the Ordos Plateau (Yang et al., 2004).

The Ordos Sagebrush has a large number of adventitious roots and an extensive root system. Seedlings of the Ordos Sagebrush usually can grow rapidly and endure partial burial as long as sand burial does not reach their terminal buds, but they hardly survive from complete burial. Relative growth rates, nonetheless, are significantly reduced when sand burial is as little as 10 cm (Ohte et al., 2003). Similarly, relatively deep roots enable seedlings to survive from a certain depth of denudation, but severe denudation impairs plant growth significantly and may cause plants to die of desiccation (Li et al., 2010).

Precipitation is the main water source of the Ordos Sagebrush, as their roots are distributed primarily within 1 m below the ground surface although some may reach more than 2 m (Bao et al., 2009; Li et al., 2004; Wang et al., 2007; Zhang et al., 2011; Zhang et al., 2008). The below (root) to over-ground biomass ratio of vegetation is varying dependent on the mobility of dunes. The below to over-ground

biomass ratio is the largest on mobile dunes and the smallest on stabilised dunes (Li and Xiao, 2007). Bigger shrubs on the crest of parabolic dunes may result from a greater infiltration depth and better water availability. The depth of infiltration in the deflation plain between trailing arms of parabolic dunes, covered by macrobiotic crusts, is usually shallower than over the shifting lobes (Wang et al., 1997). Bigger shrubs, meanwhile, have more extensive root systems and are capable of withstanding stronger aeolian activity, which further benefits their growth and increases their chance to survive in a water-stressed environment. Hydraulic lift and stomata control, by which water in the deep soil layer is absorbed and transported by roots to the upper soil layer where roots are concentrated, also enable shrubs to withstand a certain period of drought (Ohte et al., 2003; Xu et al., 2007).

The growth of the Ordos Sagebrush has a high degree of seasonality. The Ordos Sagebrush usually germinates and starts to grow leaves in March, produces shoots in June, and reaches their prime from July to September (Wang et al., 2002). Capitula (a type of flower head with the bracts under the basis) are formed in late July, blossom in August, and produce seeds in September. From late October to early November, leaves gradually turn yellow and are shed eventually. The Ordos Sagebrush has two types of branches: foliage branches and reproductive branches. Foliage branches can form dormant buds and continue to grow in the next year, whilst reproductive branches only grow in the current year and die after the winter. The Ordos Sagebrush can live many years, some may even live more than 10 years (Zhang et al., 2011).

The Ordos Sagebrush, as discussed above, plays a significant role in the development of parabolic dunes in the study region. Many other species that have similar characteristics have also proven to be of particular importance in stabilising mobile dunes and forming parabolic-shaped dune morphologies. For example, marram grass (*Ammophila arenaria* and *Ammophila breviligulata*) grows as clumps (shrub-like form) and has been widely found on migrating parabolic dunes, including those in Wilderness Dune Cordons of South Africa (Hellström, 1996), Îles de la Madeleine of Quebec (Giles and McCann, 1997), Mason Bay and Manawatu coastal plain of New Zealand (Clement et al., 2010; Hart et al., 2012; Hesp, 2001), Mediterranean Coast of Israel (Tsoar and Blumberg, 2002), some places in the United States including the Oregon coast (Cooper, 1958), the Walking Dunes of New York (Girardi and Davis, 2010), and eastern shore of Lake Michigan (Hansen et al., 2009), as well as various places in Europe such as Anholt of Denmark (Clemmensen et al., 2007), Kennemerland of Netherlands (Arens et al., 2004), Mallorca of Spain (Servera et al., 2009), and Wales of the United Kingdom (Bailey and Bristow, 2004). Other species, like sagebrush (*Artemisia filifolia* and *Artemisia abyssinica*), have also

contributed significantly to the stabilisation of mobile dunes and their transformations into parabolic dunes, as those areas in the Navajo Country of Arizona (Hack, 1941), High Plains of Colorado (Forman et al., 1992; Muhs et al., 1996), and the Jafurah Desert of Saudi Arabia (Anton and Vincent, 1986). The impacts of the Ordos Sagebrush on sand transport processes are also likely to be comparable to *Spinifex* species (such as *Spinifex hirsutus* and *Spinifex sericeus*), which are widely found on active parabolic dunes in Queensland of Australia (Levin, 2011; Pye, 1982; Pye and Mazzullo, 1994), as well as shrubs like Skunkbrush (*Rhus trilobata*) and Mintbush (*Poliomintha incana*), which anchor barchan and transverse dunes into parabolic dunes at White Sands in New Mexico (McKee, 1963).

.

References

Anton, D., Vincent, P., 1986. Parabolic dunes of the Jafurah Desert, Eastern Province, Saudi Arabia. Journal of Arid Environments, 11(3), 187-198.

Arens, S.M., Slings, Q., de Vries, C.N., 2004. Mobility of a remobilised parabolic dune in Kennemerland, The Netherlands. Geomorphology, 59(1-4), 175-188.

Bagnold, R.A., 1941. The physics of blown sand and desert dunes. Methuen & Co. Ltd, London.

Bailey, S.D., Bristow, C.S., 2004. Migration of parabolic dunes at Aberffraw, Anglesey, north Wales. Geomorphology, 59(1-4), 165-174.

Bao, H.L., He, X., Zhao, H.Y., Liu, J., Yu, H.T., 2009. Fine roots distribution characteristics and the relationship with the soil moisture of Artemisia ordosica Krasch. community in Mu Us sandy land (in Chinese with English abstract). Journal of Arid Land Resources and Environment, 23(4), 175-178.

Bauer, B.O., Sherman, D.J., Wolcott, J.F., 1992. Sources of uncertainty in shear stress and roughness length estimates derived from velocity profiles. Prof. Geogr., 44(4), 453-464.

Chen, Y.L., L., C.X., Cui, B.L., Song, Y.H., 2008. Dynamics Analysis on Development of Desertification in Hobq Desert (in Chinese with English abstract). Journal of Desert Research, 28(1), 27-34.

Chepil, W.S., 1945. Dynamics of wind erosion .2. Initiation of soil movement. Soil Sci., 60(5), 397-411.

Clement, A.J.H., Sloss, C.R., Fuller, I.C., 2010. Late Quaternary geomorphology of the Manawatu coastal plain, North Island, New Zealand. Quaternary International, 221(1–2), 36-45.

Clemmensen, L.B., Bjornsen, M., Murray, A., Pedersen, K., 2007. Formation of aeolian dunes on Anholt, Denmark since AD 1560: A record of deforestation and increased storminess. Sedimentary Geology, 199(3-4), 171-187.

Cooper, W.S., 1958. Coastal dunes of Oregon and Washington. Geological Society of America Memoir 72, New York.

Ellis, J.T., Li, B., Farrell, E.J., Sherman, D.J., 2009. Protocols for characterizing aeolian mass-flux profiles. Aeolian Research, 1(1–2), 19-26.

Forman, S.L., Goetz, A.F.H., Yuhas, R.H., 1992. Large-scale stabilized dunes on the High Plains of Colorado: Understanding the landscape response to Holocene climates with the aid of images from space. Geology, 20(2), 145-148.

Fryberger, S.G., 1979. Dune forms and wind regime. In: E.D. McKee (Ed.), A study of global sand seas. US Geological Survey Professional Paper, Washington, pp. 137-169.

Giles, P.T., McCann, S.B., 1997. Foredune development on Iles de la Madeleine (Quebec), Atlantis Canada. Can. J. Earth Sci., 34(11), 1467-1476.

Girardi, J.D., Davis, D.M., 2010. Parabolic dune reactivation and migration at Napeague, NY, USA: Insights from aerial and GPR imagery. Geomorphology, 114(4), 530-541.

Hack, J.T., 1941. Dunes of the Western Navajo Country. Geogr. Rev., 31(2), 240-263.

Hansen, E., DeVries-Zimmerman, S., van Dijk, D., Yurk, B., 2009. Patterns of wind flow and aeolian deposition on a parabolic dune on the southeastern shore of Lake Michigan. Geomorphology, 105(1-2), 147-157.

Hart, A.T., Hilton, M.J., Wakes, S.J., Dickinson, K.J.M., 2012. The Impact of Ammophila arenaria Foredune Development on Downwind Aerodynamics and Parabolic Dune Development. Journal of Coastal Research, 112-122.

Hellström, G.B., 1996. Preliminary investigations into recent changes of the Goukamma Nature Reserve frontal dune system, South Africa - With management implications. Landscape and Urban Planning, 34(3-4), 225-235.

Hesp, P.A., 2001. The Manawatu Dunefield: Environmental Change and Human Impacts. New Zealand Geographer, 57(2), 33-40.

Jiang, H., Zhang, P.Y., Zheng, D., Wang, F.H., 1995. The Ordos Plateau of China. In: J.X. Kasperson, R.E. Kasperson, B.L. Turner II (Eds.), Regions at risk: comparisons of threatened environments. The United Nations University, Tokyo.

Levin, N., 2011. Climate-driven changes in tropical cyclone intensity shape dune activity on Earth's largest sand island. Geomorphology, 125(1), 239-252.

Li, C.P., Xiao, C.W., 2007. Above- and belowground biomass of Artemisia ordosica communities in three contrasting habitats of the Mu Us desert, northern China. Journal of Arid Environments, 70(2), 195-207.

Li, G.Q., Zheng, Y.R., 2002. Characteristics of regional climate change and pattern analysis on Ordos Plateau. Journal of Environmental Sciences, 14(4), 568-576.

Li, Q.S., Zhang, C., Wang, F., Lai, L.M., Zhang, L., Li, W.T., Bai, H., Zheng, Y.R., 2009. Response of spatial distribution pattern of Artemisia ordosica population to the precipitation gradient on Ordos Plateau (in Chinese with English abstract). Chinese Journal of Applied Ecology, 20(9), 2105-2110.

Li, S.-L., Werger, M.J.A., Zuidema, P.A., Yu, F.-H., Dong, M., 2010. Seedlings of the semi-shrub Artemisia ordosica are resistant to moderate wind denudation and sand burial in Mu Us sandland, China. Trees, 24(3), 515-521.

Li, X.R., Ma, F.Y., Xiao, H.L., Wang, X.P., Kim, K.C., 2004. Long-term effects of revegetation on soil water content of sand dunes in arid region of Northern China. Journal of Arid Environments, 57(1), 1-16.

McKee, E., 1963. Origin of the Nubian and similar sandstones. Geol Rundsch, 52(2), 551-587.

Muhs, D.R., Stafford, T.W., Cowherd, S.D., Mahan, S.A., Kihl, R., Maat, P.B., Bush, C.A., Nehring, J., 1996. Origin of the late Quaternary dune fields of northeastern Colorado. Geomorphology, 17(1-3), 129-149.

Ohte, N., Koba, K., Yoshikawa, K., Sugimoto, A., Matsuo, N., 2003. Water utilization of natural and planted trees in the semiarid desert of Inner Mongolia, China. Ecological Applications, 13(2), 337-351.

Oke, T.R., 1987. Boundary Layer Climates. Routledge, London.

Pye, K., 1982. Morphological development of coastal dunes in a humid tropical environment, Cape Bedford and Cape Flattery, North Queensland. Geografiska Annaler Series a-Physical Geography, 64(3-4), 213-227.

Pye, K., Mazzullo, J., 1994. Effects of tropical weathering on quartz grain shape; an example from northeastern Australia. Journal of Sedimentary Research, 64(3a), 500-507.

Servera, J., Gelabert, B., Rodriguez-Perea, A., 2009. Development and setting of the Alcudia Bay beach-dune system (Mallorca, Spain). Geomorphology, 110(3-4), 172-181.

State Forestry Administration, 2011. A bulletin of status quo of desertification and sandification in China, Beijing.

Tobe, K., Zhang, L., Omasa, K., 2006. Seed germination and seedling emergence of three Artemisia species (Asteraceae) inhabiting desert sand dunes in China. Seed Science Research, 16(1), 61-69.

Tsoar, H., Blumberg, D.G., 2002. Formation of parabolic dunes from barchan and transverse dunes along Israel's Mediterranean coast. Earth Surface Processes and Landforms, 27(11), 1147-1161.

Wang, L.Q., Chen, S.H., Hao, L.Z., 2002. The study of ecological biological characters and geological distribution law of Artemisia ordosica Krasch. (in Chinese with English abstract). Journal of Arid Land Resources and Environment, 16(4), 95-98.

Wang, Q.S., Dong, X.J., Chen, X.D., Yang, B.Z., 1997. Study on some features of Artemisia ordosica community at the different successional stages (in Chinese with English abstract). Acta Phytoecologica Sinica, 21(6), 531-538.

Wang, X.-P., Li, X.-R., Xiao, H.-L., Berndtsson, R., Pan, Y.-X., 2007. Effects of surface characteristics on infiltration patterns in an arid shrub desert. Hydrological Processes, 21(1), 72-79.

Wolfe, S.A., Nickling, W.G., 1993. The protective role of sparse vegetation in wind erosion. Progress in Physical Geography, 17(1), 50-68.
Woolley, J.T., Stoller, E.W., 1978. Light penetration and light-induced seed germination in soil. Plant Physiology, 61(4), 597-600.
Xu, D.H., Li, J.h., Fang, X.W., Wang, G., 2007. Changes in soil water content in the rhizosphere of Artemisia ordosica: Evidence for hydraulic lift. Journal of Arid Environments, 69(4), 545-553.
Yang, G.S., Di, Z.M., Huang, Z.H., 1991. Integrated improvement of land desertification in the sandy area north of the loess plateau (in Chinese). Science Press, Beijing.
Yang, H.X., Zhang, J.T., Li, Z.D., Wu, B., Zhang, Z.S., Wang, Y., 2008. Comparative study on spatial patterns of Artemisia ordosica populations in the Mu Us sandy land (in Chinese with English abstract). Acta Ecologica Sinica, 28(5), 1901-1910.
Yang, H.X., Zhang, J.T., Wu, B., Wang, Y., Li, X.S., Xu, B., 2004. Adaptation of Artemisia ordosica to temperate arid sandy land and its roles in habitat shift (in Chinese with English abstract). Journal of Beijing Normal University (Natural Science), 40(5), 684-690.
Zha, Y., Gao, J., 1997. Characteristics of desertification and its rehabilitation in China. Journal of Arid Environments, 37(3), 419-432.
Zhang, J.H., Wu, B., Lei, Y.K., Li, X.M., He, J., Gao, D.X., 2011. Analysis of Artemisia ordosica plant morphology and structure Characteristics in Mu Us Sandland (in Chinese with English abstract). Journal of Southwest Forestry University, 31(5), 6-9.
Zhang, X.S., 1994. The ecological background of the Maowusu sandland the principles and optimal models for grass land management (in Chinese with English abstract). Acta Phytoecologica Sinica, 18, 1-6.
Zhang, Z.-S., Li, X.-R., Wang, T., Wang, X.-P., Xue, Q.-W., Liu, L.-C., 2008. Distribution and Seasonal Dynamics of Roots in a Revegetated Stand ofArtemisia ordosicaKracsh. in the Tengger Desert (North China). Arid Land Research and Management, 22(3), 195-211.
Zheng, Y., Rimmington, G.M., Gao, Y., Jiang, L., Xing, X., An, P., El-Sidding, K., Shimizu, H., 2005a. Germination characteristics ofArtemisia ordosica(Asteraceae) in relation to ecological restoration in northern China. Canadian Journal of Botany, 83(8), 1021-1028.
Zheng, Y., Xie, Z., Jiang, L., Shimizu, H., Rimmington, G.M., Zhou, G., 2005b. Vegetation responses along environmental gradients on the Ordos plateau, China. Ecological Research, 21(3), 396-404.
Zhu, S.G., 1986. Comments on the discussion of the formation and change of the Mu Us sandy land. History and Geography of Northwest China, 4, 17-27.
Zhu, Z.D., Wu, Z., Liu, S., Di, X., 1980. Introduction to Chinese deserts (in Chinese). Science Press, Beijing.

Chapter 5

Empirical Field Study

This chapter reports on a detailed field investigation in terms of two respects: vegetation characteristics and dune morphology. Five typical parabolic dunes with varying mobility were investigated in the pilot study in 2011, of which the three semi-mobile parabolic dunes (D1, D2, and D5 in Figure 4-2) were selected in a more detailed exploration in 2012. Vegetation quadrats combined with individual shrub measurements were employed to investigate vegetation characteristics over different parabolic dunes. Dune topography was surveyed using a RTK Differential-GPS. The results and findings regarding the changes in vegetation characteristics (such as canopy coverage) and dune morphology provide a guide for constructing a computer modelling algorithm in Chapter 7, and provide real-world data for parameterising the model (Chapter 8). The model is then used to explore potential impacts of environmental fluctuations, climatic changes, and anthropogenic forces on dune transformations (Chapter 9 & Chapter 10).

5.1 Methodology

5.1.1 Vegetation Survey

Five parabolic dunes with varying mobility were investigated in July 2011 and three of them were re-investigated in Sep 2012 (Table 5-1). For the pilot study in 2011, sampling transects were established along longitudinal sections, cross sections and lee slopes of individual dunes (Figure 5-1a). Plant distributions over dunes were mapped and surveyed using 5×5 m^2 quadrats (Figure 5-1b). Within each quadrat, the characteristics of individual plants were examined including the species, plant height, length and width of a plant canopy, height of the sand mount trapped by a plant, and plant vitality. In specific, as shown in Figure 5-2, the length of a plant (L) is the longest distance of the cross section of its canopy; the width of a plant (W) is the distance perpendicular to the length of its canopy; the height of a plant (H) is the highest distance from the plant base; and the height of the sand mount (H_s) trapped by a plant is the distance from the base of the plant to the lowest depression point around the plant. The coordinates of the central points of each quadrat were also recorded by a D-GPS.

Table 5-1. Summary of field investigations.

	Year	D-GPS points	Quadrats	Plants measured within quadrats	Big individual shrubs	Dune mobility
D1	2011	499	20	346	-	semi-mobile, inland
	2012	897	7	279	134	
D2	2011	399	24	480	-	semi-mobile, inland
	2012	1388	7	279	216	
D3	2011	597	47	718	-	stabilised
D4	2011	503	27	561	-	stabilised
D5	2011	636	27	376	-	semi-mobile
	2012	370	16	225	111	

(a) (b)

Figure 5-1. Vegetation survey in 2011. (a). Sampling transects (the red rope is the longitudinal section and the white tape is a cross section) of a parabolic dune; (b). View of a 5×5 m^2 survey quadrat.

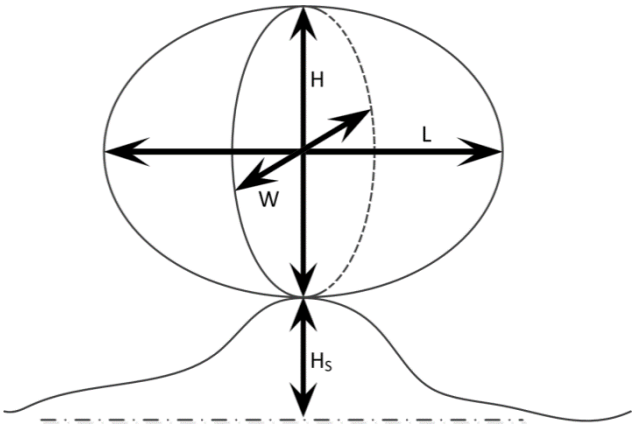

Figure 5-2. Schematic drawing of morphological parameters of a shrub.

For the second field trip in 2012, a more flexible survey strategy was used based on the experience, observation and data analyses from the previous pilot study. In flat depressions between trailing arms of parabolic dunes, vegetation was distributed uniformly, generally showing a distinctive zonation along the longitudinal axis of parabolic dunes; therefore, several representative quadrats were set up in each vegetation zone. For vegetation zones dominated by plants of relatively small sizes, 5×5 m^2 quadrats were employed, whilst 10×10 m^2 quadrats were used to survey areas comprised of relatively large plants (Figure 5-3). All shrubs on the lobes and representative sections of arms were measured individually (Figure 5-4a). Meanwhile, the coordinates of four corners of quadrats as well as the coordinates of individual plants measured on dunes were recorded by a D-GPS (Figure 5-4b).

(a) (b)

Figure 5-3. Vegetation survey in 2012. (a) View of a 10×10 m^2 survey quadrat for big shrubs. (b) View of a 5×5 m^2 survey quadrat for small shrubs.

(a) (b)

Figure 5-4. (a) Shrubs on the lobe of a parabolic dune. (b) A flag to mark the location of a quadrat.

5.1.2 High-resolution Dune Morphology Measurement

Three-dimensional topography of selected parabolic dunes was collected using a RTK (Real Time Kinematic)-Differential GPS system with a horizontal accuracy of 1 cm and a vertical accuracy of 2 cm respectively. The RTK system consists of a single base station receiver (stationary receiver) and a mobile receiver. The base station was set at a known surveyed point, providing a benchmark. For each measurement, both stations receive radar signals from satellites synchronously. At the same time, the base station uses the coordinates of the benchmark to calculate the timing discrepancy arising from errors in its clock and a delay by atmosphere, and transmits the calculated correction to the mobile receiver which can then adjust its measurement based on the correction. As the radar signals received by both base and mobile stations travel through the same slice of atmosphere, measurements from both stations should hence have the same errors. This technique ensures measurements with great accuracy.

The aim of the pilot study in 2011 was to capture the whole picture of different types of parabolic dunes in the study region. Both stabilised parabolic dunes that the dune lobe is well-covered by vegetation and semi-mobile parabolic dunes that the dune lobe is largely bare and has great mobility were selected. Control points of dune morphology were chosen according to the fluctuation of local topography. Nebkhas on the arms and crests of dunes were surveyed at a minimum of four points, i.e., the top point of sedimentary mounds and three points at the foot. In 2012 for the second field trip, only the three semi-mobile parabolic dunes (D1, D2 and D5 in Figure 4-2) were chosen for more detailed investigation. D5 is located right on the bank of a seasonal river which is a small branch of Yellow River, whilst D1 and D2 lie more than 1 km away from the river and they are separated by well-vegetated inter-dune areas and dune relics. Therefore, D1 and D2, as typical representatives of semi-mobile parabolic dunes in the inland arid dune systems, were focused in this field investigation. Furthermore, relic sand heaps and nebkhas were also found upwind (to the west) of D1 and D2, and seemed to partly connect with the trailing arms of the parabolic dunes. In order to examine the spatial relationship between these relics and the parabolic dunes, more extensive surveys were conducted as compared with the pilot study. The morphological parameters of parabolic dunes investigated are summarised in Table 5-2.

Table 5-2. Morphological parameters of investigated parabolic dunes.

	Lobe length (m)	**Lobe width (m)**	**Dune height (m)**
D1	90	100	4
D2	69	146	8
D3	117	88	3
D4	110	94	4
D5	150	52	2

The topographic maps of five parabolic dunes in 2011 are shown in Figure 5-5. Magenta circles represent points surveyed by the D-GPS, and white lines and green squares denote sampling transects and locations of 5 × 5 m^2 survey quadrats. The topographic maps of three semi-mobile parabolic dunes in 2012 are shown in

Figure 5-6. Magenta circles denote points collected by the D-GPS, but green squares were obtained by connecting coordinates of four corners of quadrats. Big and small squares denote 10 × 10 m^2 and 5 × 5 m^2 quadrats respectively. White triangles denote the locations of individual plants measured on the lobes and arms of the parabolic dunes. To facilitate the comparisons of different parabolic dunes, all maps are on the same scale with the same height range of 11 m. These DEMs were acquired by interpolating measured UTM coordinates with the method of Minimum Curvature. Dune profiles along longitudinal sections of dunes were then extracted from the interpolated DEMs.

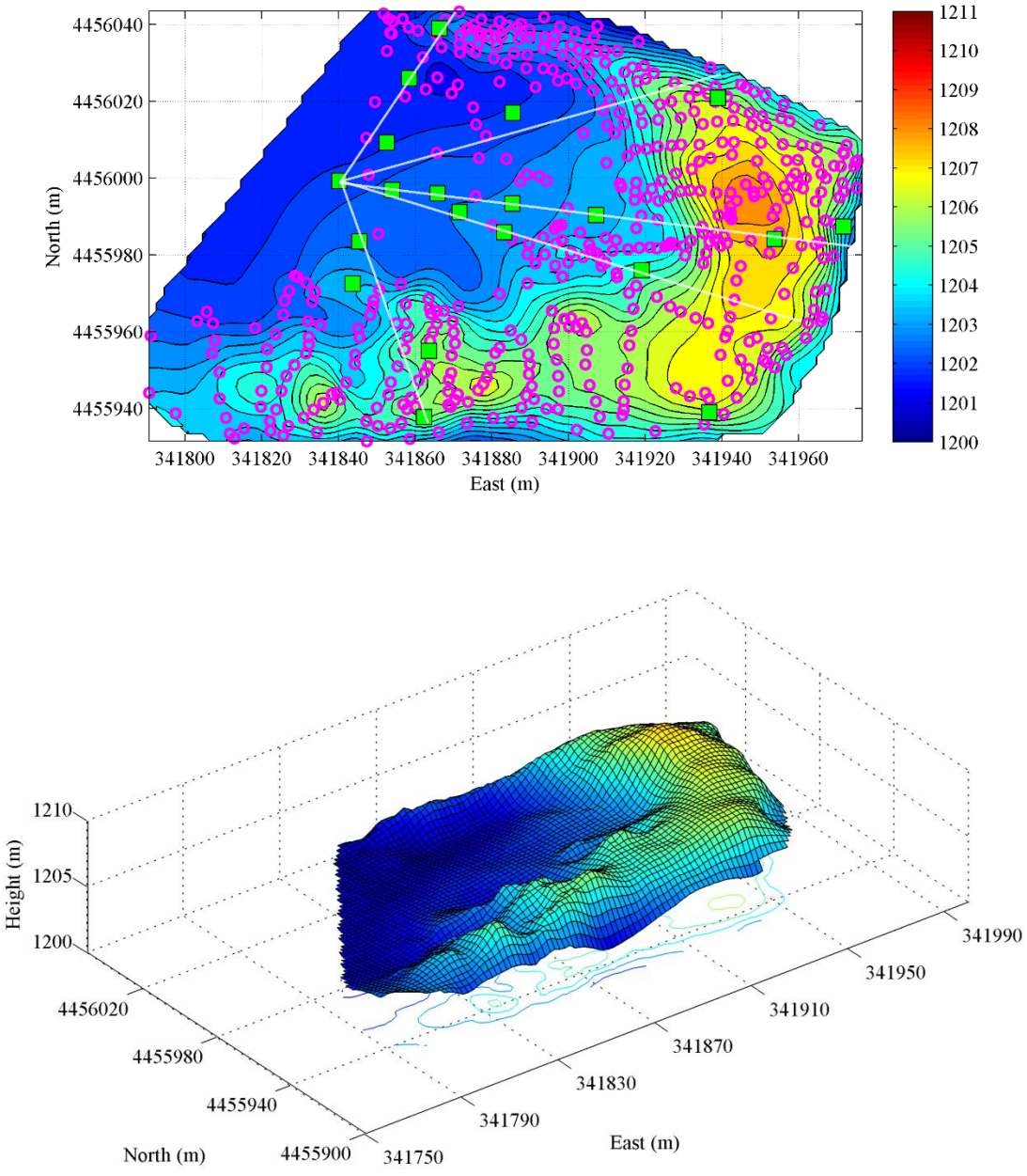

(a) Semi-mobile parabolic dune D1

Figure 5-5. (*to be continued*) Contour and DEM maps of parabolic dunes investigated in 2011 (UTM coordinates). White lines are sampling transects, whilst magenta dots and green squares denote the points recorded by D-GPS and the locations of quadrats respectively. The colour bar denotes height in meter, and the contour interval is 0.4 m.

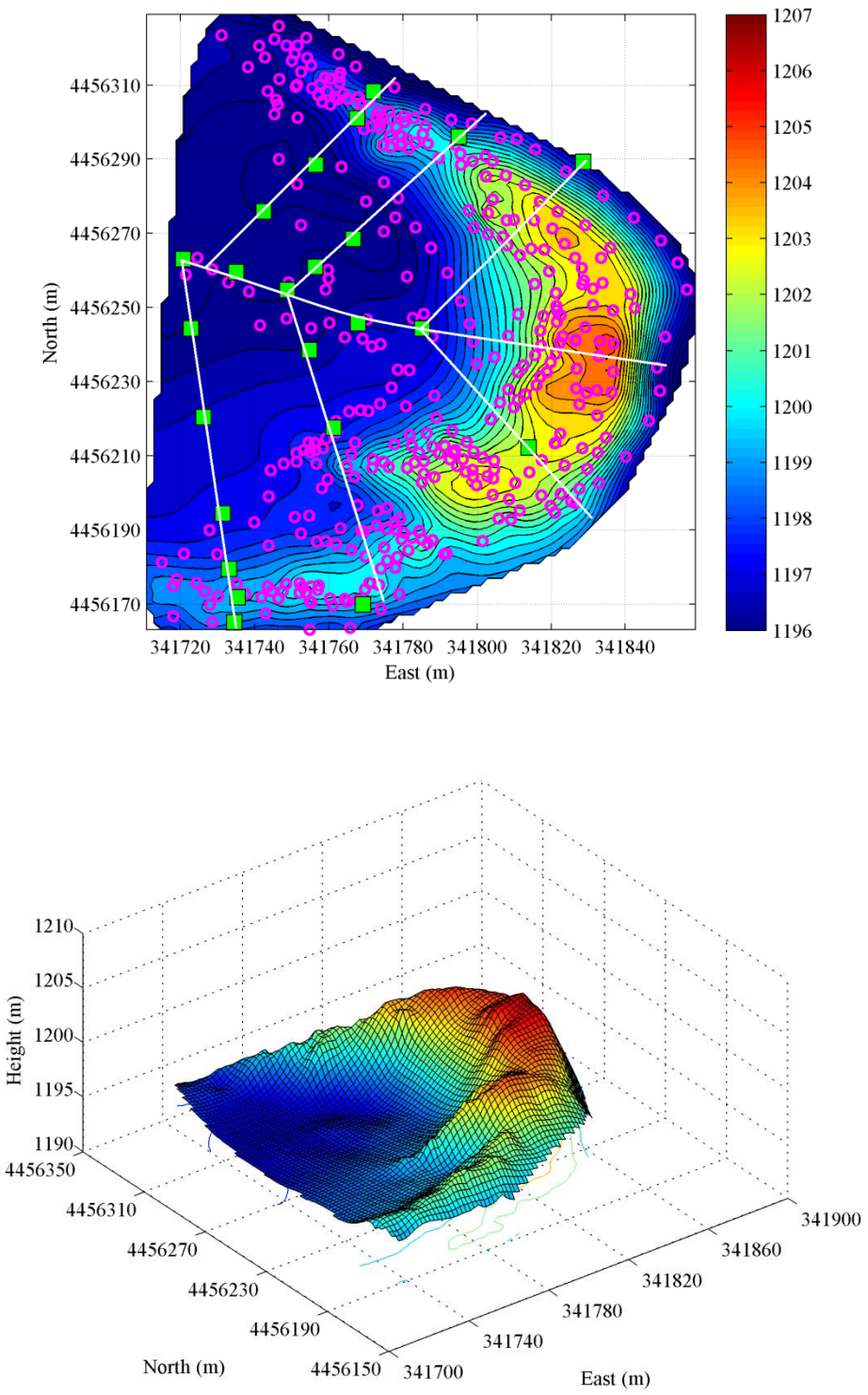

(b) Semi-mobile parabolic dune D2

Figure 5-5. (*continued*) Contour and DEM maps of parabolic dunes investigated in 2011 (UTM coordinates). White lines are sampling transects, whilst magenta dots and green squares denote the points recorded by D-GPS and the locations of quadrats respectively. The colour bar denotes height in meter, and the contour interval is 0.4 m.

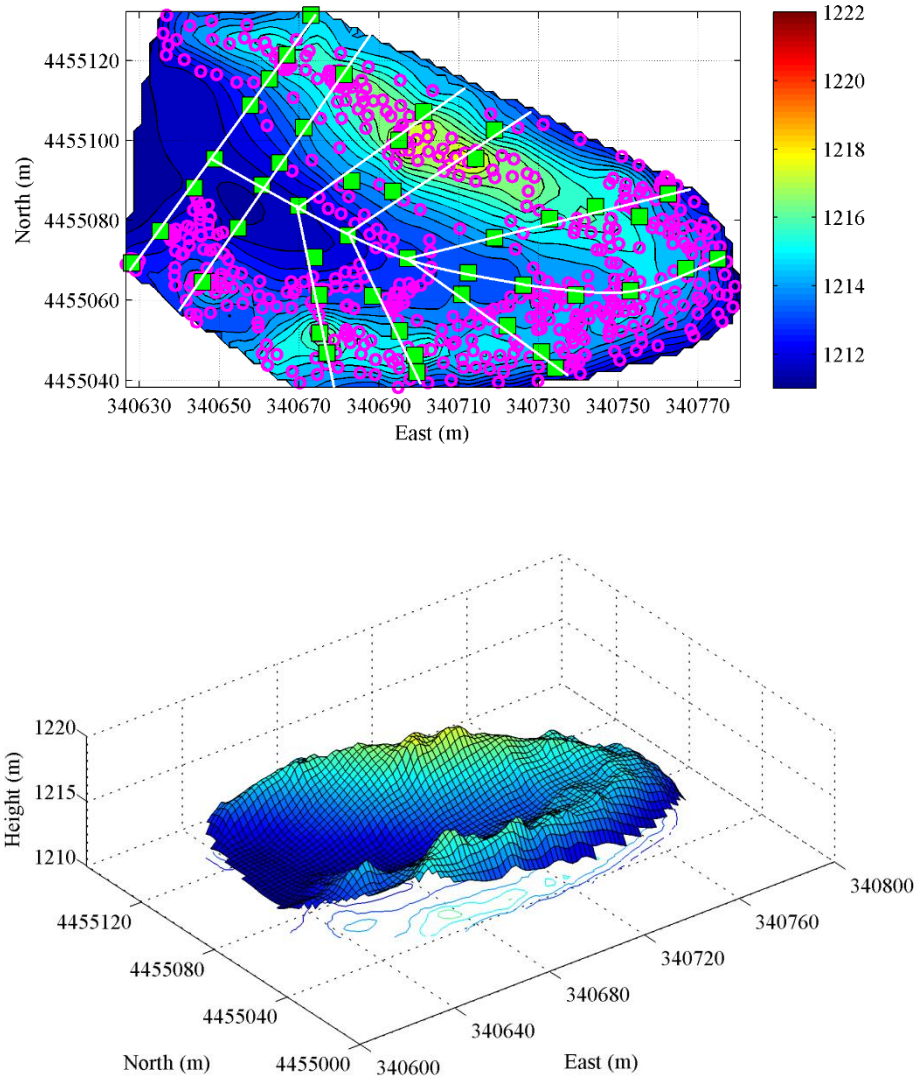

(c) Stabilised parabolic dune D3

Figure 5-5. (*continued*) Contour and DEM maps of parabolic dunes investigated in 2011 (UTM coordinates). White lines are sampling transects, whilst magenta dots and green squares denote the points recorded by D-GPS and the locations of quadrats respectively. The colour bar denotes height in meter, and the contour interval is 0.4 m.

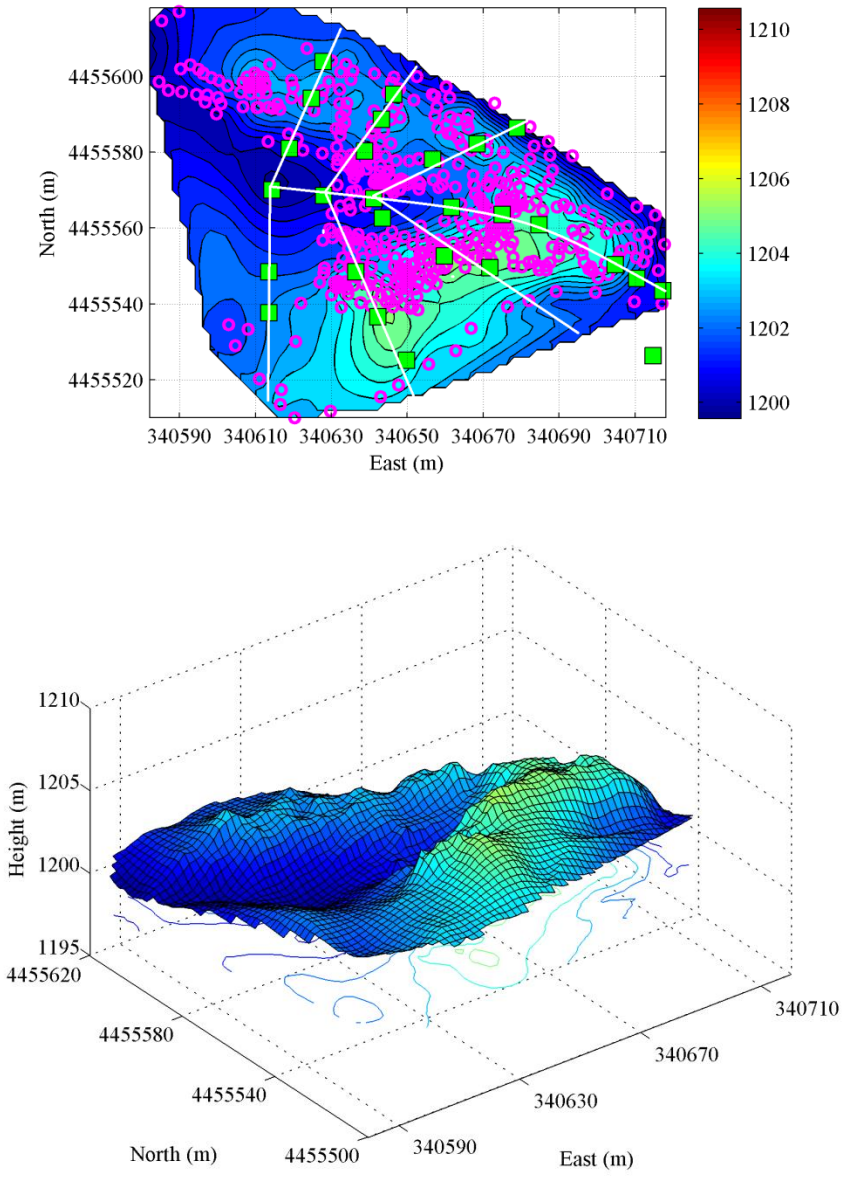

(d) Stabilised parabolic dune D4

Figure 5-5. (*continued*) Contour and DEM maps of parabolic dunes investigated in 2011 (UTM coordinates). White lines are sampling transects, whilst magenta dots and green squares denote the points recorded by D-GPS and the locations of quadrats respectively. The colour bar denotes height in meter, and the contour interval is 0.4 m.

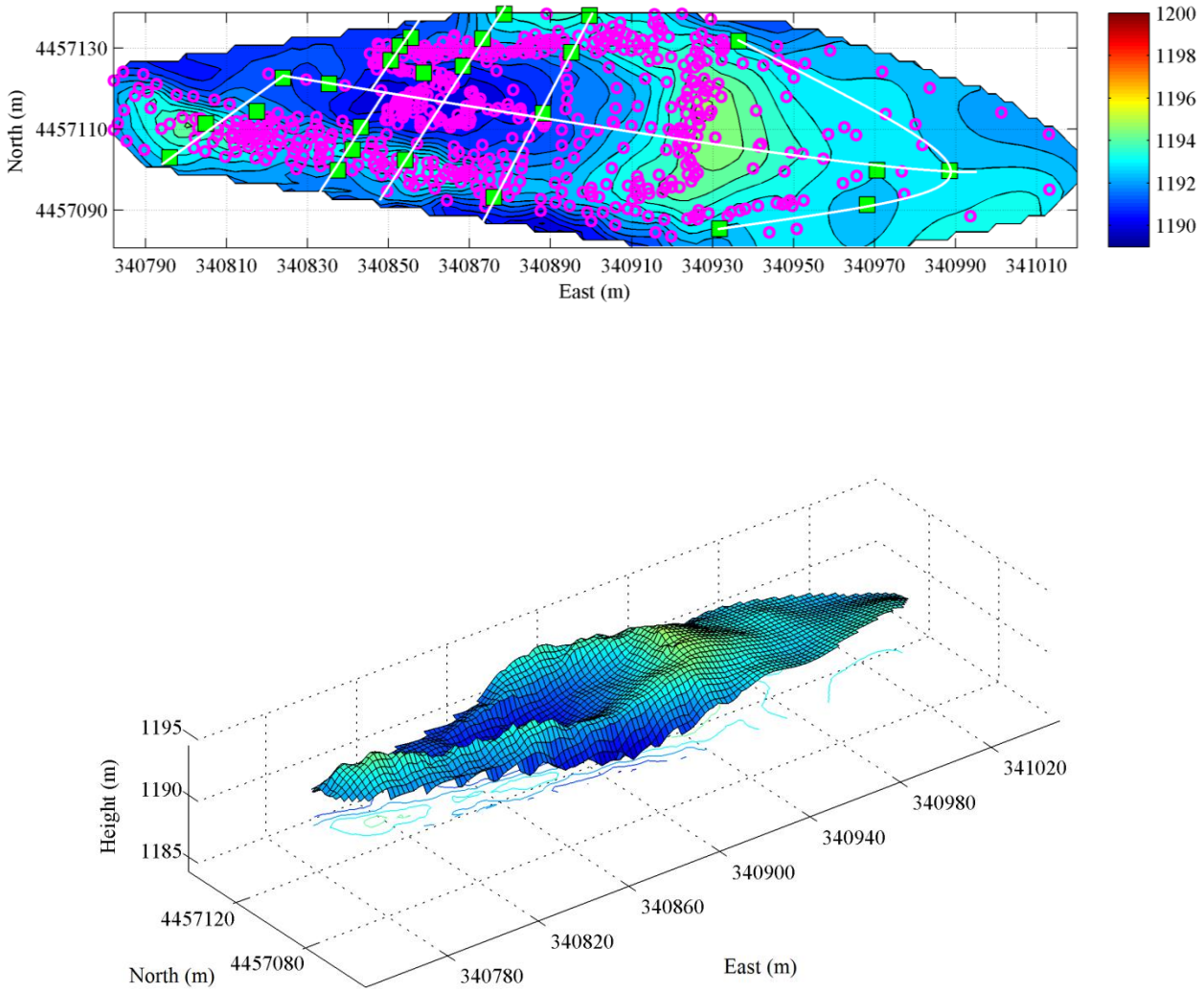

(e) Semi-mobile parabolic dune D5

Figure 5-5. (*continued*) Contour and DEM maps of parabolic dunes investigated in 2011 (UTM coordinates). White lines are sampling transects, whilst magenta dots and green squares denote the points recorded by D-GPS and the locations of quadrats respectively. The colour bar denotes height in meter, and the contour interval is 0.4 m.

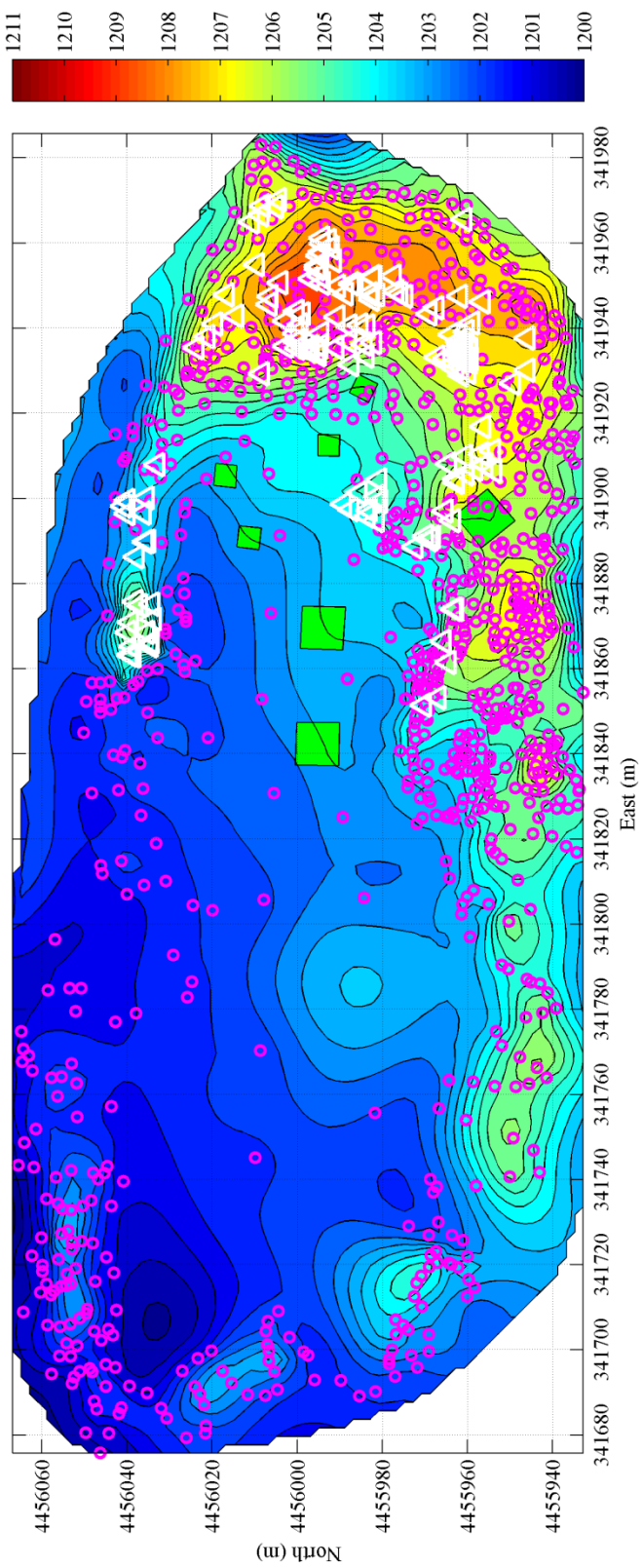

(a1) Semi-mobile parabolic dune D1

Figure 5-6. (*to be continued*) Contour and DEM maps of parabolic dunes investigated in 2012 (UTM coordinates). Magenta circles and green squares denote the points recorded by the D-GPS and the locations of quadrats respectively. The while triangles are the locations of individual plants measured. The colour bar denotes height in meter, and the contour interval is 0.4 m.

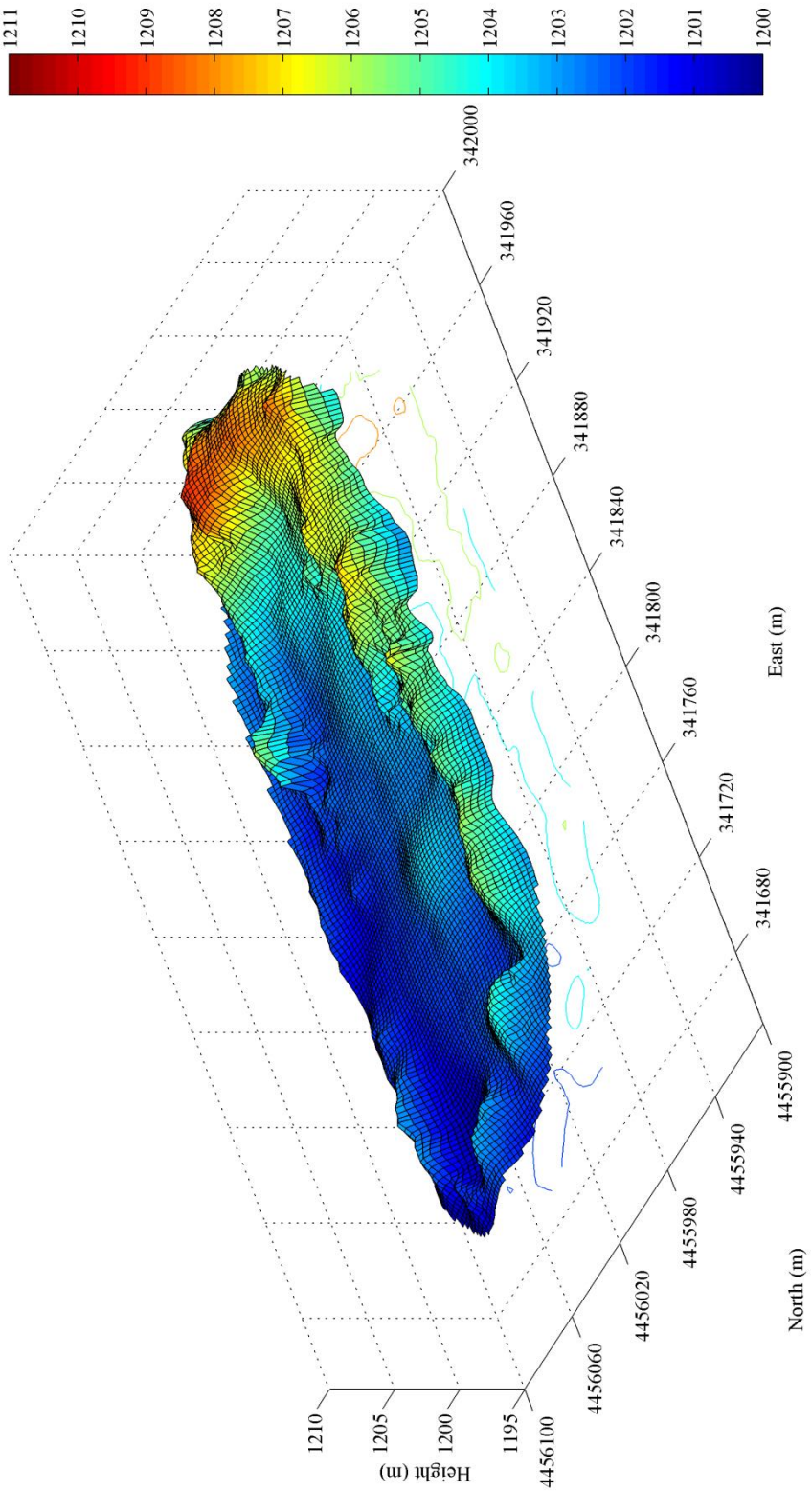

(a2) Semi-mobile parabolic dune D1

Figure 5-6. (*continued*) Contour and DEM maps of parabolic dunes investigated in 2012 (UTM coordinates). Magenta circles and green squares denote the points recorded by the D-GPS and the locations of quadrats respectively. The while triangles are the locations of individual plants measured. The colour bar denotes height in meter, and the contour interval is 0.4 m.

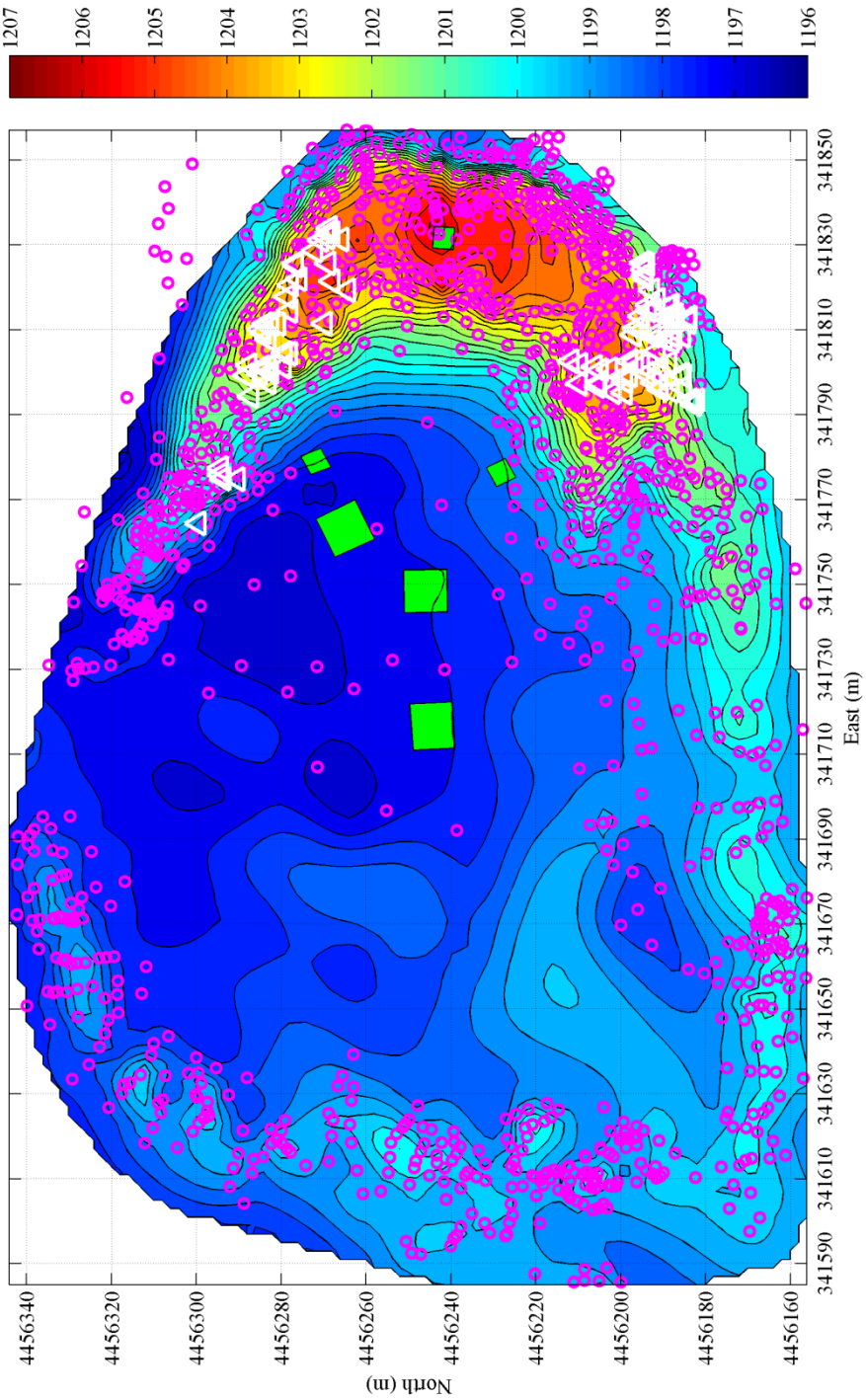

(b1) Semi-mobile parabolic dune D2

Figure 5-6. (*continued*) Contour and DEM maps of parabolic dunes investigated in 2012 (UTM coordinates). Magenta circles and green squares denote the points recorded by the D-GPS and the locations of quadrats respectively. The while triangles are the locations of individual plants measured. The colour bar denotes height in meter, and the contour interval is 0.4 m.

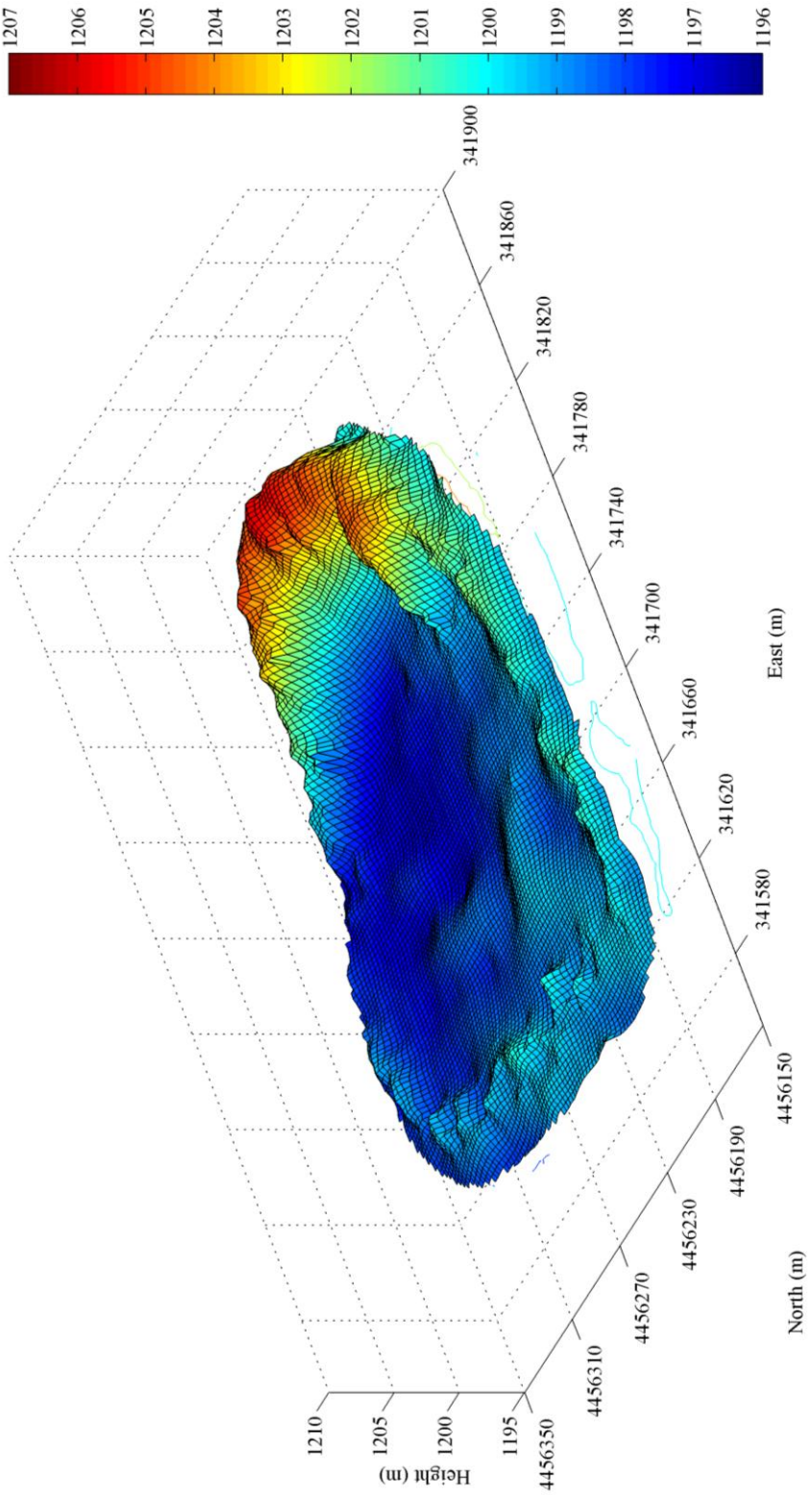

(b2) Semi-mobile parabolic dune D2

Figure 5-6. (*continued*) Contour and DEM maps of parabolic dunes investigated in 2012 (UTM coordinates). Magenta circles and green squares denote the points recorded by the D-GPS and the locations of quadrats respectively. The while triangles are the locations of individual plants measured. The colour bar denotes height in meter, and the contour interval is 0.4 m.

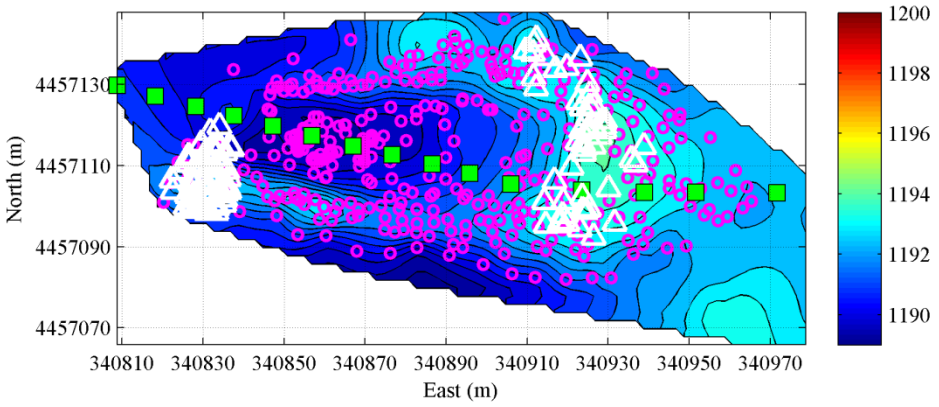

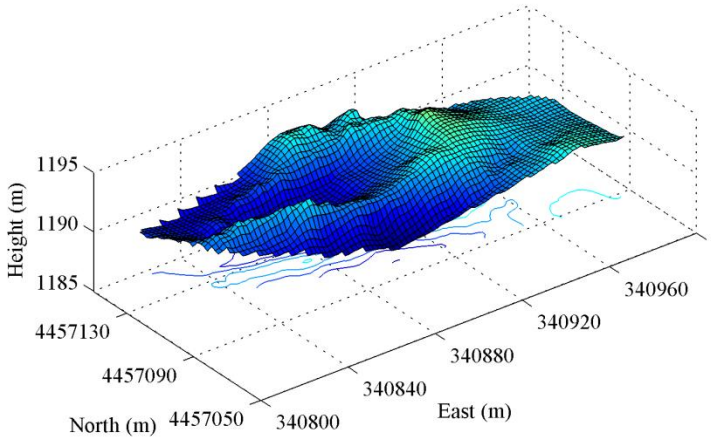

(c) Semi-mobile parabolic dune D5

Figure 5-6. (*continued*) Contour and DEM maps of parabolic dunes investigated in 2012 (UTM coordinates). Magenta circles and green squares denote the points recorded by the D-GPS and the locations of quadrats respectively. The while triangles are the locations of individual plants measured. The colour bar denotes height in meter, and the contour interval is 0.4 m.

5.2 Data Analyses

The areal number density [D, m^{-2}] for each species in a quadrat was calculated by:

$$D = \frac{N}{S} \tag{5-1}$$

where: S is the sampled area (i.e., the area of a quadrat); and N is the number of individual plants within the sampled area.

Assuming plan-view canopies of plants are ellipsoid in shape, the canopy cover area [S_c, m^2] of each plant was calculated by:

$$S_c = \frac{1}{4}\pi LW \tag{5-2}$$

where: L and W are the length and the width of a plant canopy respectively, [m] (Figure 5-2). Then, the fractional canopy coverage [C, -] was obtained by the sum of canopy cover area of plants in a sampled quadrat divided by the area of the quadrat:

$$C = \frac{\sum S_c}{S} \tag{5-3}$$

The canopy cover refers to the area of the ground surface covered by the vertical projection of the outmost perimeter of a plant canopy, and thus includes spaces between plant leaves. The fractional canopy coverage of a quadrat can, therefore, be larger than 1 if plant canopies overlap each other substantially.

The canopy volume [V, m^3] of individual shrubs was estimated using a formula suggested by Thorne et al. (2002):

$$V = \frac{2}{3}HS_c \tag{5-4}$$

where: H is the height of a plant, [m] (Figure 5-2). The canopy volume index [I_v, -] of a quadrat was then calculated by dividing the sum of the canopy volume of plants in a quadrat by the quadrat area as shown below:

$$I_v = \frac{\sum V}{S} \tag{5-5}$$

At the same time, the average frontal area [F_s, m^2] of each plant was evaluated by:

$$F_s = \frac{1}{2}\left(\frac{\pi}{4}HL + \frac{\pi}{4}HW\right) \tag{5-6}$$

Roughness density [λ, m^2 m^{-2}] or frontal area index, [FAI, m^2 m^{-2}] was determined by Raupach et al., (1993):

$$\lambda = \frac{\sum F_s}{S} \tag{5-7}$$

Combining high resolution DEMs of parabolic dunes with vegetation parameters calculated, vegetation characteristics on parabolic dunes with different mobility were analysed. The nebkha sizes and the roughness densities along the arms of a stabilised parabolic dune (D1) were examined, because nebkhas on the arms of semi-mobile parabolic dunes were relatively sparse, random, and difficult to quantify by quadrats. Meanwhile, the distribution of nebkhas and large shrubs were examined considering their more significant impacts on the processes of trapping sand and maintaining the parabolic shape of dunes as compared with smaller plants without outstanding canopies. To eliminate the influence brought about by small shrubs, the average nebkha size in each quadrat was calculated as the mean value of the cubic volume of shrubs with $L > 0.5$ m.

5.3 Results

5.3.1 Sediment Supply and Dune Mobility

The shape of dune profiles is closely related to sand availability and dune mobility (Hugenholtz et al., 2008). Profiles of five typical parabolic dunes with varying mobility (surveyed in 2011) were compared. As shown in Figure 5-5 and Figure 5-7, the lobes of semi-mobile parabolic dunes D1 and D2 are largely bare and relatively tall, and have evident slip faces, in comparison with the stabilised parabolic dunes D3 and D4 whose lee slopes have been well-vegetated and exhibit a convex shape, reflecting a sand-starved environment. In contrast with D1 and D2, the semi-mobile dune D5 possesses a much lower, yet more extensive tongue-shaped depositional lobe protruding as far as 100 meter away from its crest. This morphological difference between semi-mobile parabolic dunes may be explained by their different locations and the associated sand availability. The dune D5 is right on the bank of a seasonal river and highly mobile crescentic dune fields are in its upwind direction (west). As a result, a relatively large sand influx is likely to occur for D5. In contrast, the D1 and D2 are located away from the river and are surrounded by well-vegetated shrub fields and dune relics (Figure 5-8). In such a closed dune environment without external sand supply, the movement of parabolic dunes only occurs when the sand on the windward slopes, arms, and deflation plains between arms is eroded, transported by winds, and deposited on their lee slopes.

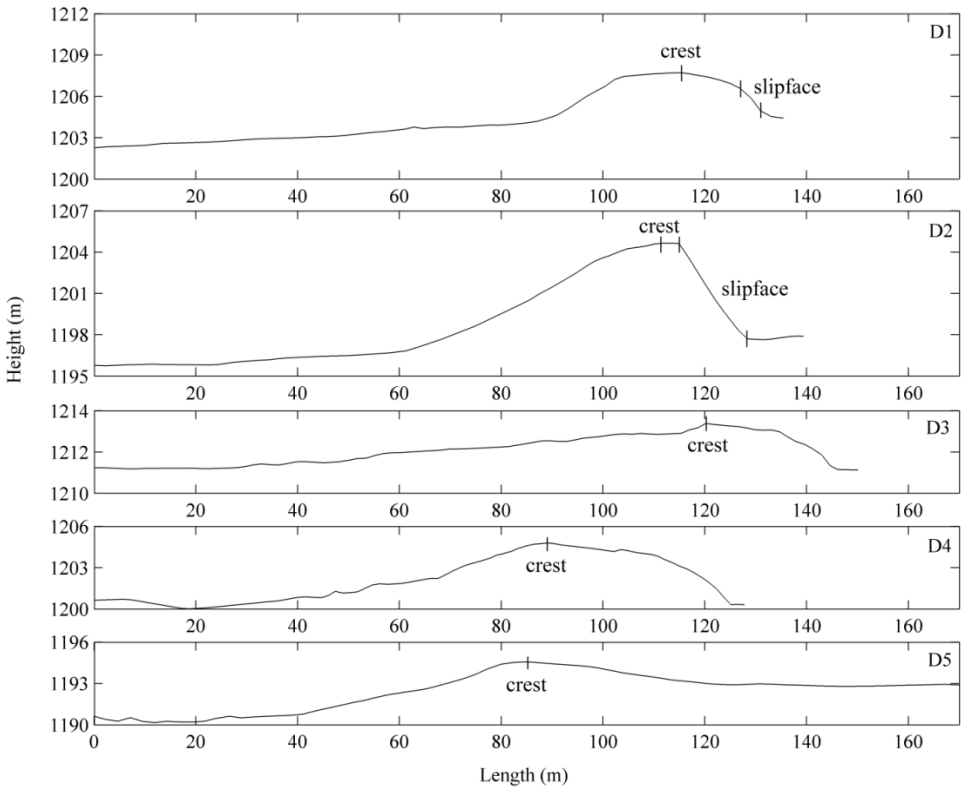

Figure 5-7. Topographic profiles of parabolic dunes in 2011. The dominant wind direction is from the left to the right.

Figure 5-8. A side view of the parabolic dune D1 in 2011, from the south.

5.3.2 Dune Movement

Figure 5-9 shows dune topographic maps of three semi-mobile parabolic dunes in 2011 and 2012. The morphology of all three dunes did not show substantial change over this year. The heights of D1 and D2 as well as some parts on arms increased slightly. Sand movement on both sides of the lobes of D1 and D2 seemed to occur more strongly than the middle of the lobes, as shown in red dotted circles. For D5, slight

sand loss occurred on the dune crest and arms, whereas sand accumulated on the lee side of its tongue-shaped lobe.

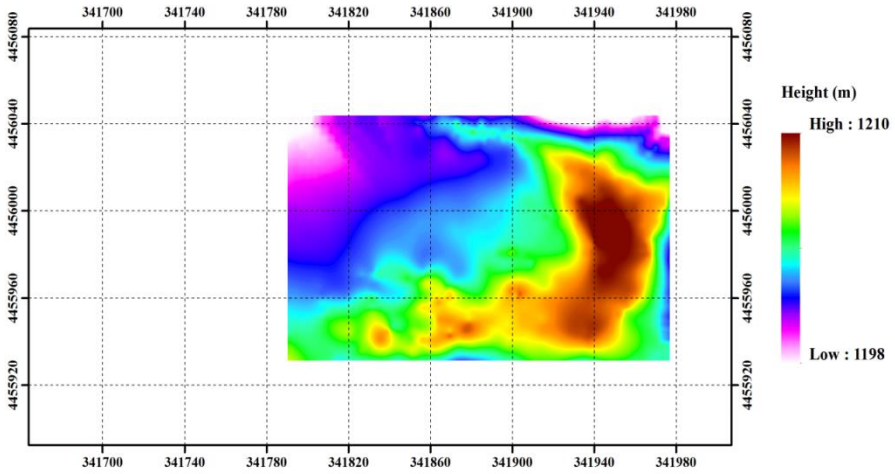

(D1) 2011

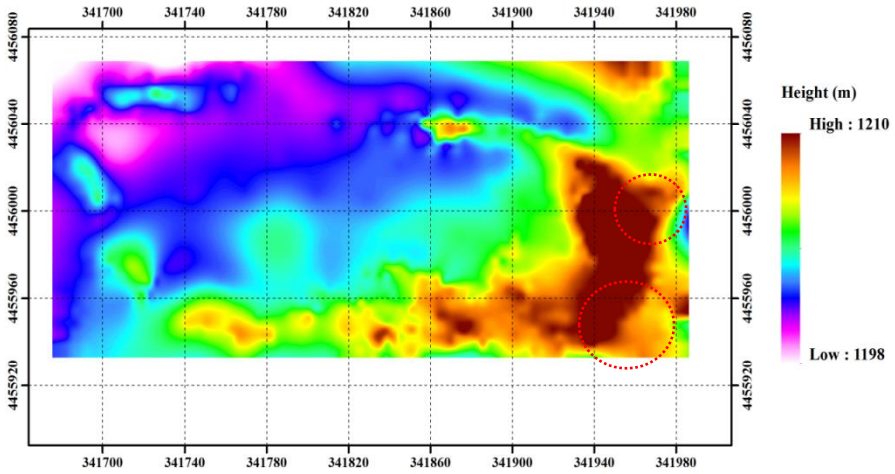

(D1) 2012

Figure 5-9. (*to be continued*) Dune topography of semi-stabilised parabolic dunes in 2011 and 2012. Red circles show where sand deposition has occurred more greatly.

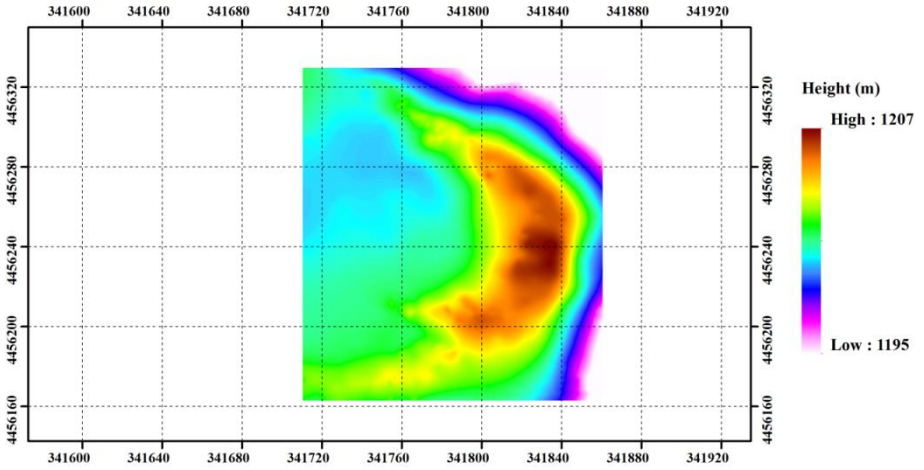

(D2) 2011

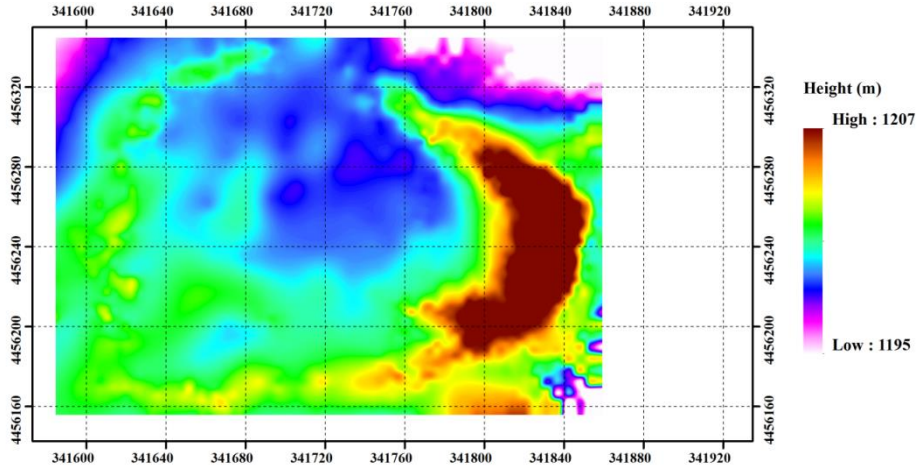

(D2) 2012

Figure 5-9. (*continued*) Dune topography of semi-stabilised parabolic dunes in 2011 and 2012.

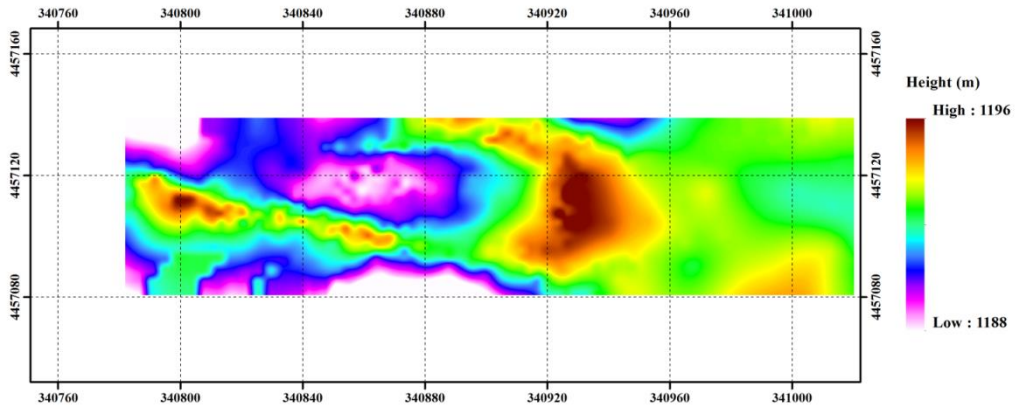

(D5) 2011

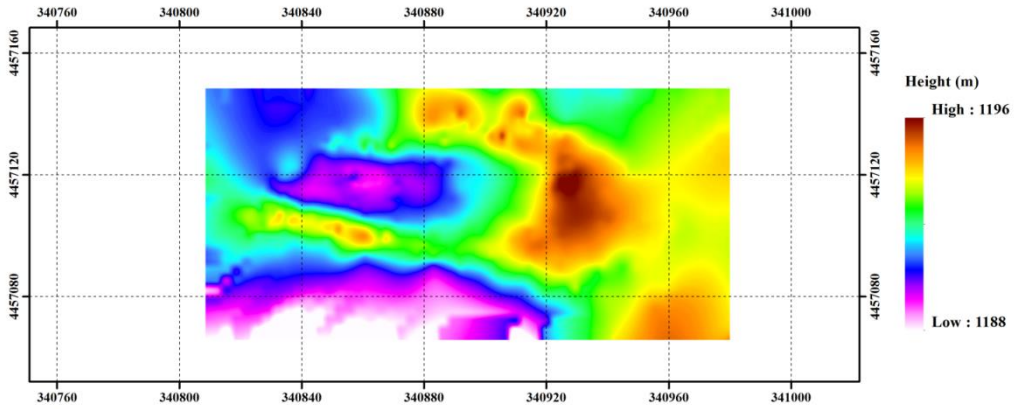

(D5) 2011

Figure 5-9. (*continued*) Dune topography of semi-stabilised parabolic dunes in 2011 and 2012.

5.3.3 Distribution of Vegetation

Figure 5-10 shows the histogram and cumulative percentage of canopy cover area of individual Ordos Sagebrush measured in the field, which includes plants on all of the parabolic dunes regardless of where plants are exactly located. The canopy cover area within 1 m^2 accounts for more than 70 % of the population. This result agrees with the maximum canopy coverage of ~1.0 m^2 described in the literature (Li et al., 2010; Yang et al., 2008; Zhang et al., 2008). The larger shrubs measured are usually ones on the crest of dunes where they have formed nebkhas due to continuously sand-trapping, or ones that are aggregated together and cannot be differentiated from one another because their branching bases have been deeply buried by sand.

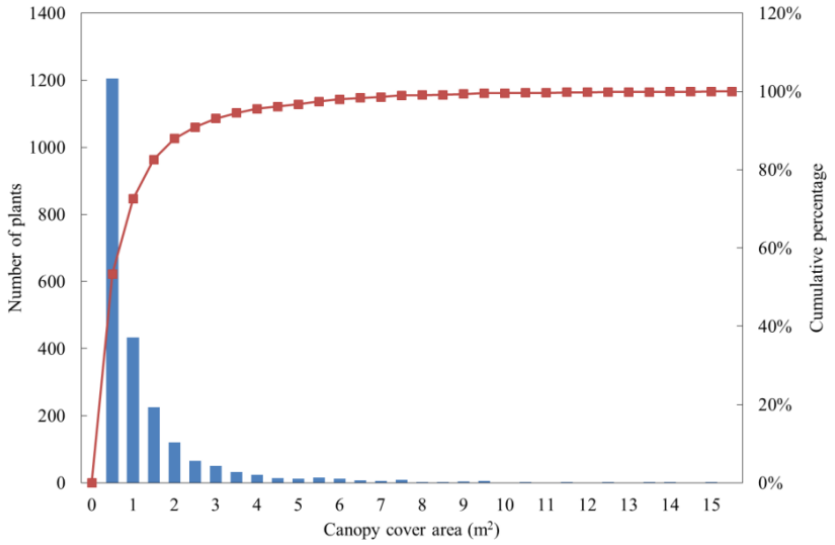

Figure 5-10. Histogram and cumulative percentage of canopy cover area of Ordos Sagebrush measured in the field.

Figure 5-11 to Figure 5-21 show the vegetation parameters of quadrats including the canopy coverage [C, -], the canopy volume index [I_v, -] and the frontal area index [FAI, m^2 m^{-2}], as well as the vegetation parameters of individual plants including the canopy cover area [S_c, m^2], the canopy volume [V, m^3] and the frontal area index over different dunes.

In general, vegetation cover in 2012 was greater in comparison with that of 2011. In particular, the deflation plains close to the windward slopes of D1 and D2 that were almost bare in 2011 were covered by shoots and seedlings of shrubs and annual grasses in 2012 (Figure 5-12, 5-13, 5-15, 5-16, and 5-22). On the crests of D1 and D2, vegetation cover increased significantly in 2012 compared with the sparsely speckled vegetation in 2011 (Figure 5-14, 5-17, and 5-23). Meanwhile, the Mongolian Sweetvetch only seldom seen on the deflation plains between the trailing arms of D1 and D2 in 2011 could be easily found on the dune arms and the crests in 2012. Similarly, for D5, the bare deflation plain with prominent residual piers formed by severe wind erosion in 2011 was vegetated to various degrees in 2012 (Figure 5-20, 5-21, and 5-24). In particular, its windward slope was well-vegetated with a coverage larger than 1. Vegetation cover on the tongue-shaped depositional lobe also increased significantly. The better vegetation cover in 2012 may result from 1) better water availability because of greater precipitation (a recent flood) in the Yellow River before the field trip in 2012, and 2) relieved grazing pressure due to the departure of landowners in the summer of 2011.

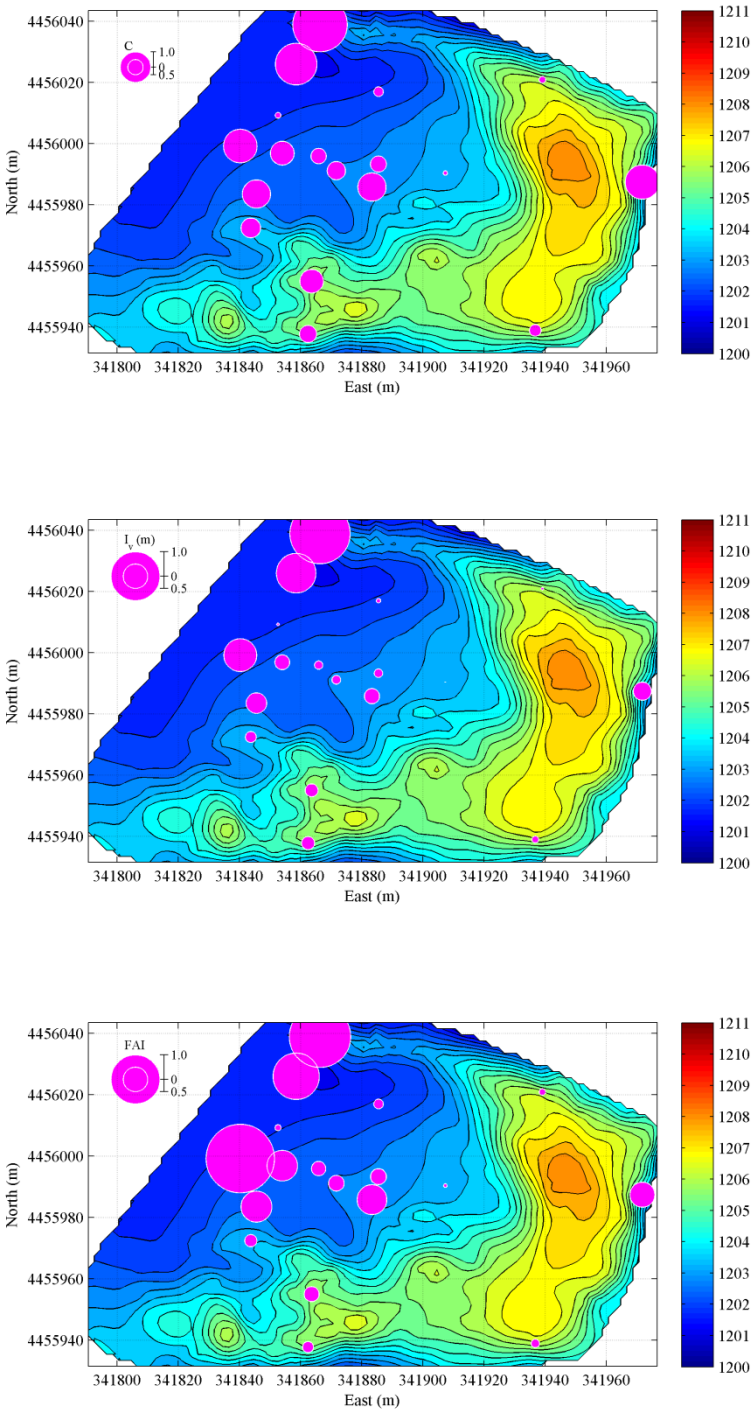

Figure 5-11. Vegetation parameters over D1 surveyed by quadrats in 2011.

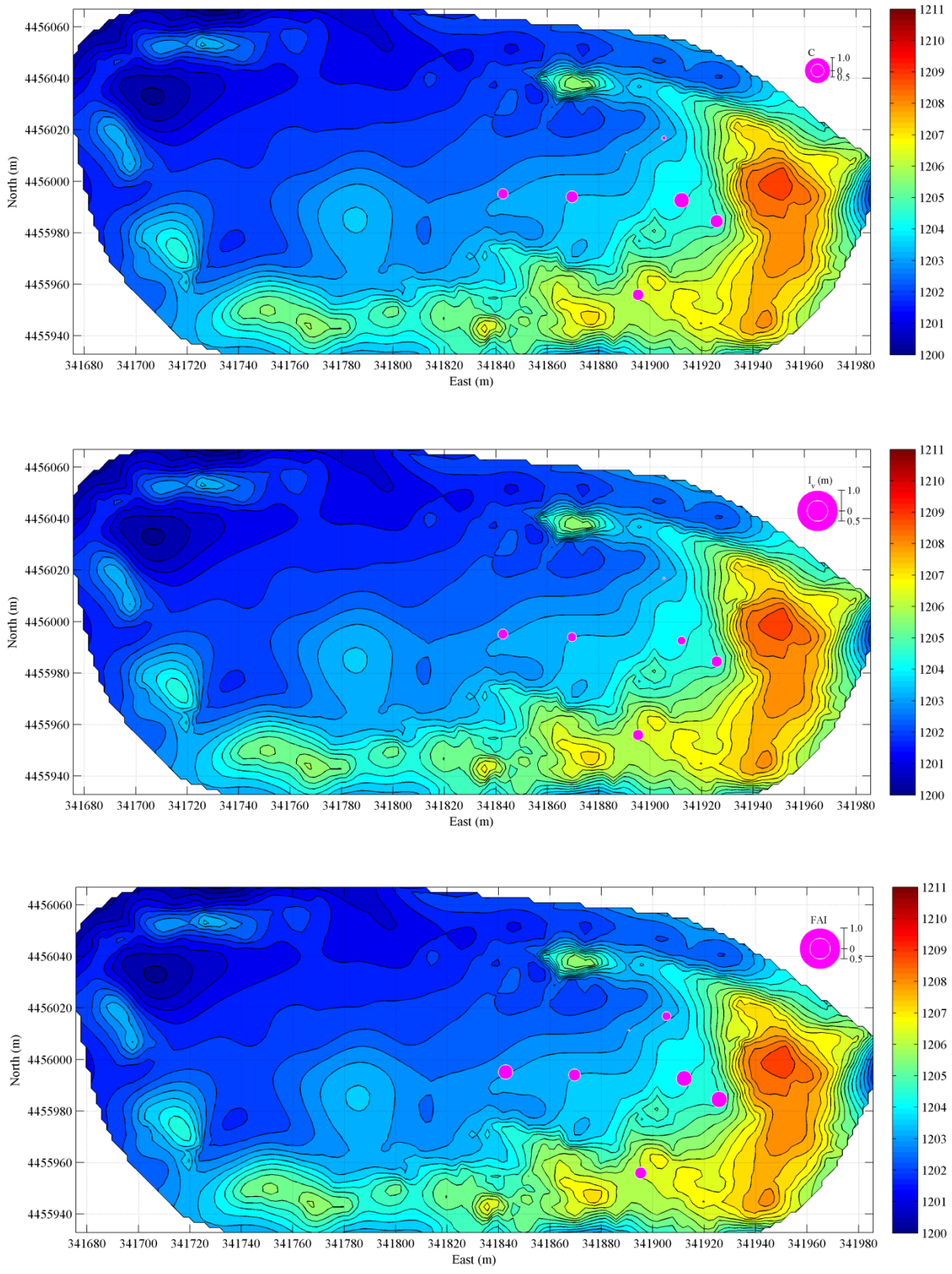

Figure 5-12. Vegetation parameters over D1 surveyed by quadrats in 2012.

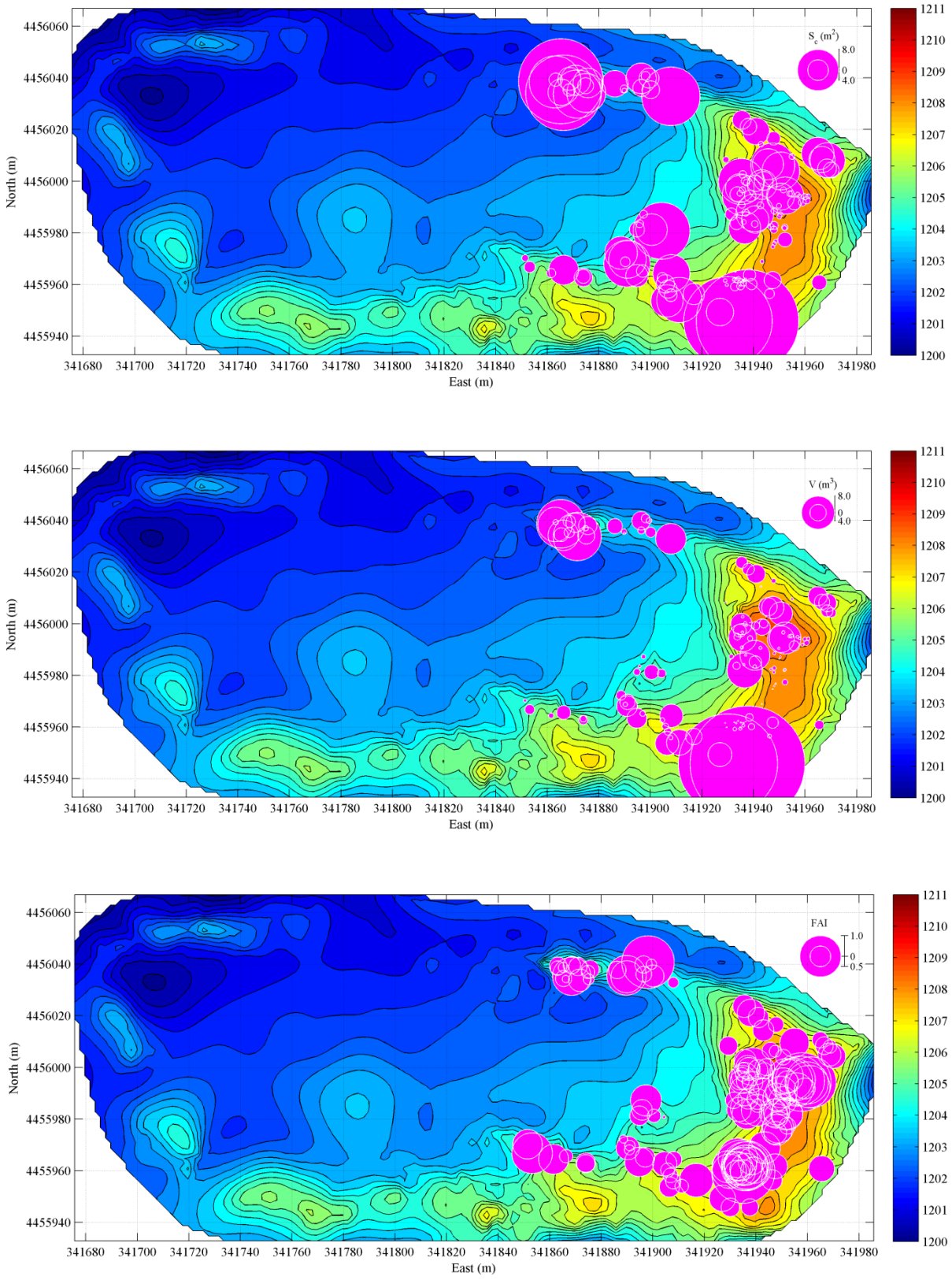

Figure 5-13. Vegetation parameters of individual plants on the lobe and arms of D1 surveyed in 2012.

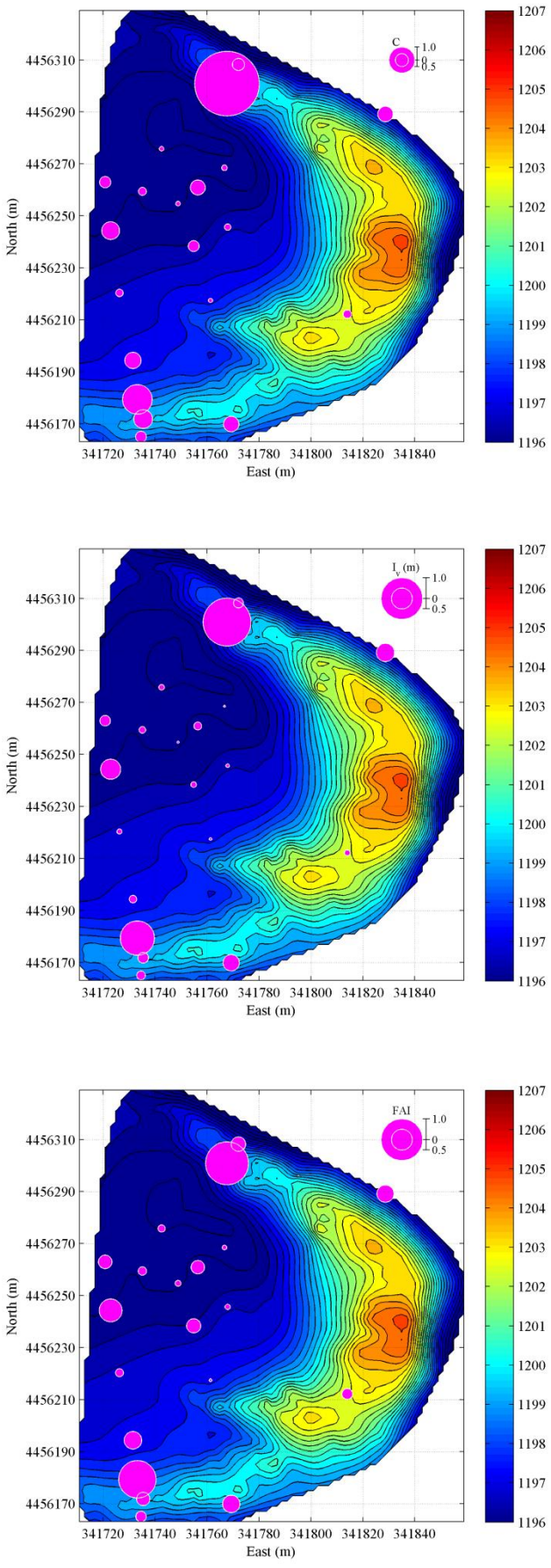

Figure 5-14. Vegetation parameters over D2 surveyed by quadrats in 2011.

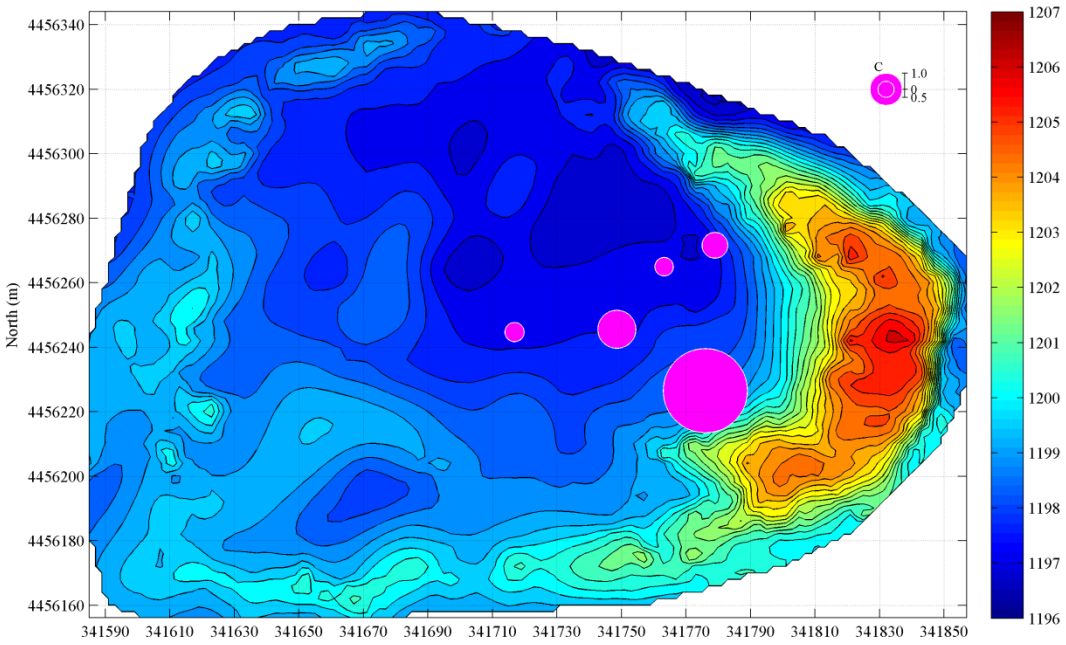

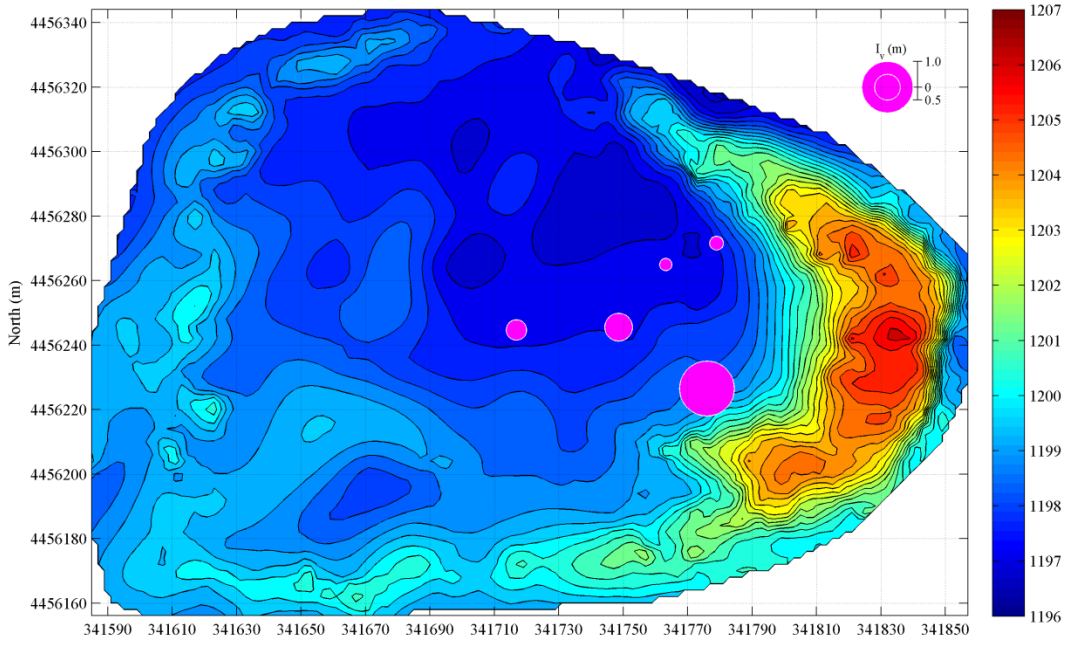

Figure 5-15. (*to be continued*) Vegetation parameters over D2 surveyed by quadrats in 2012.

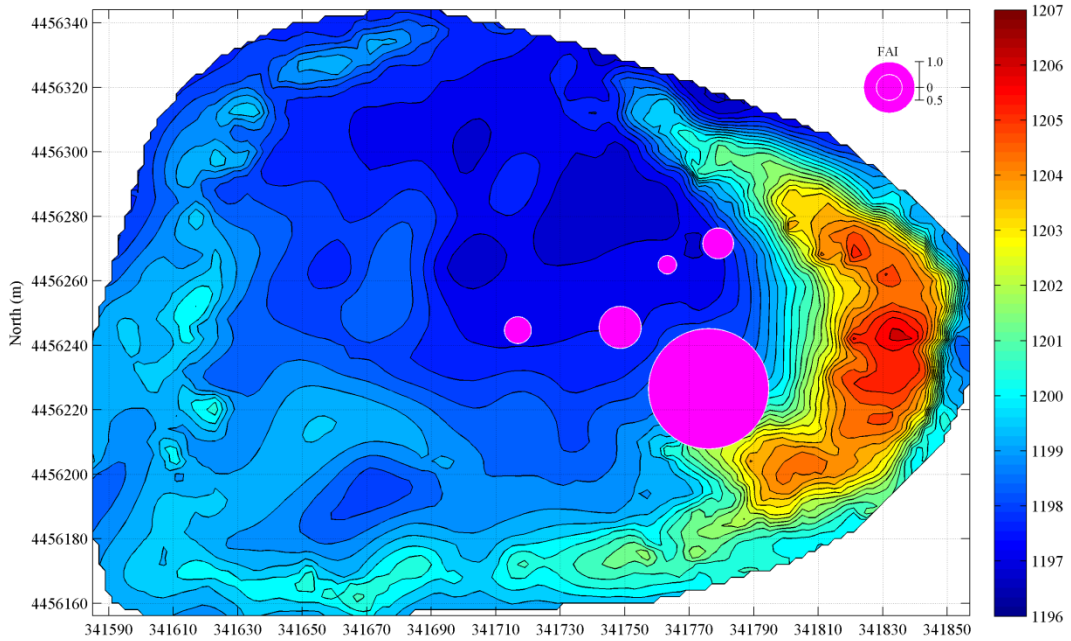

Figure 5-15. (*Continued*) Vegetation parameters over D2 surveyed by quadrats in 2012.

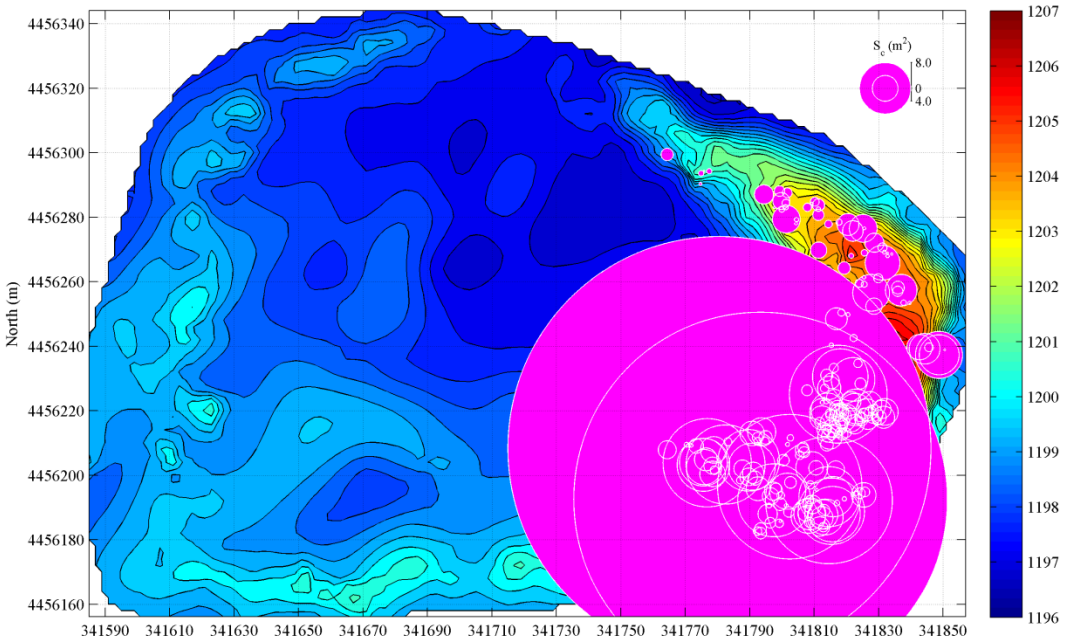

Figure 5-16. (*to be continued*) Vegetation parameters of individual plants on the lobe and arms of D2 surveyed in 2012.

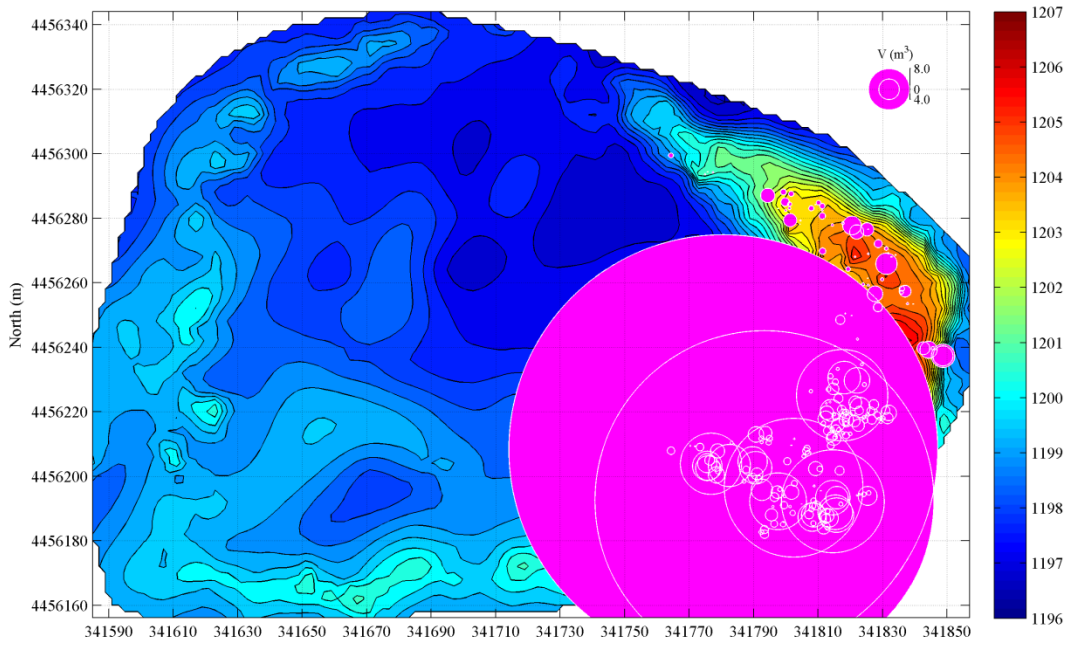

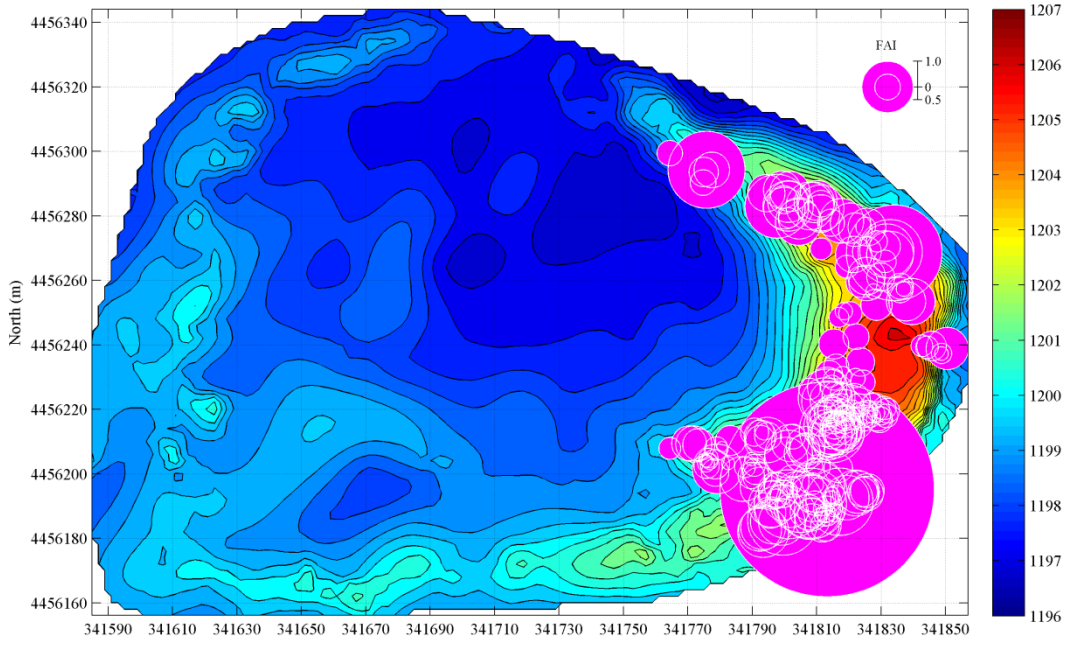

Figure 5-16. (*continued*) Vegetation parameters of individual plants on the lobe and arms of D2 surveyed in 2012.

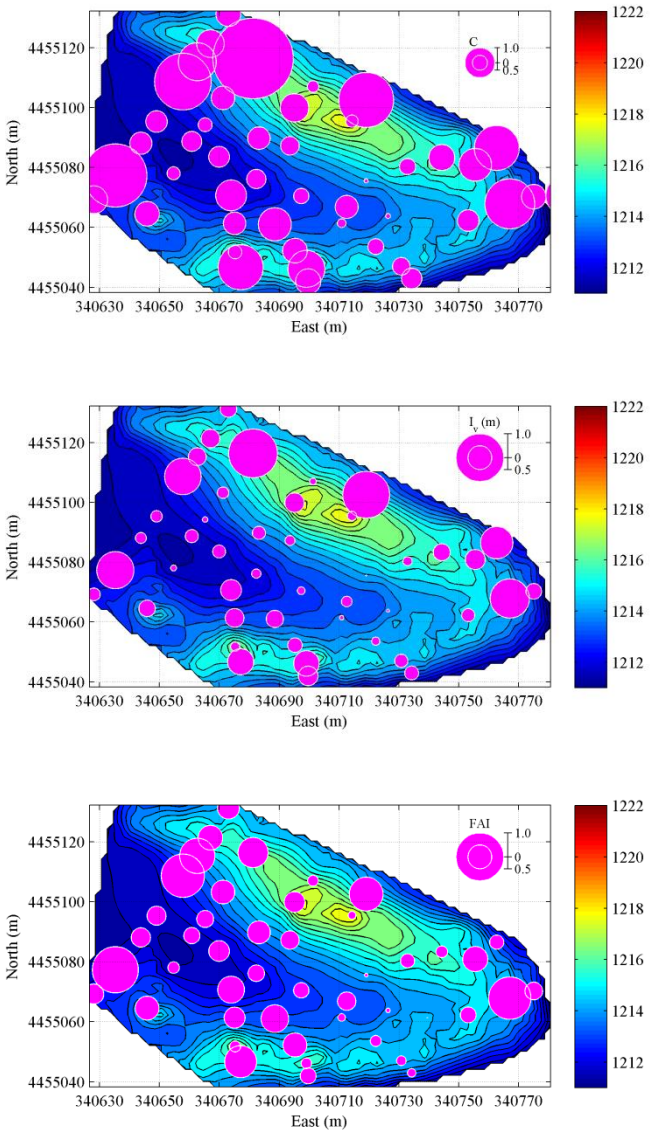

Figure 5-17. Vegetation parameters over D3 surveyed by quadrats in 2011.

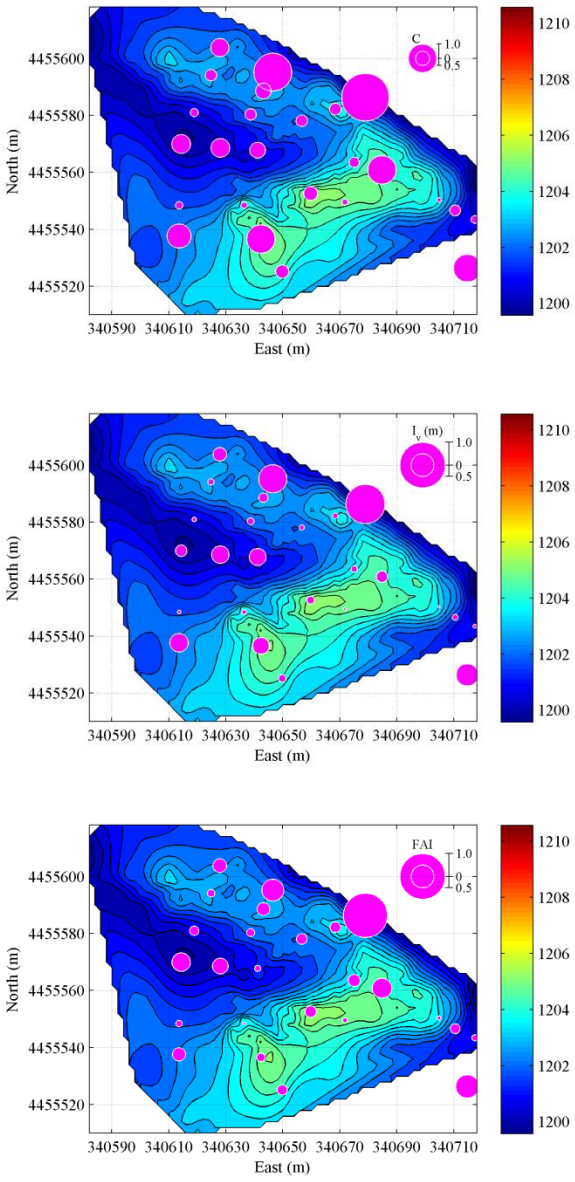

Figure 5-18. Vegetation parameters over D4 surveyed by quadrats in 2011.

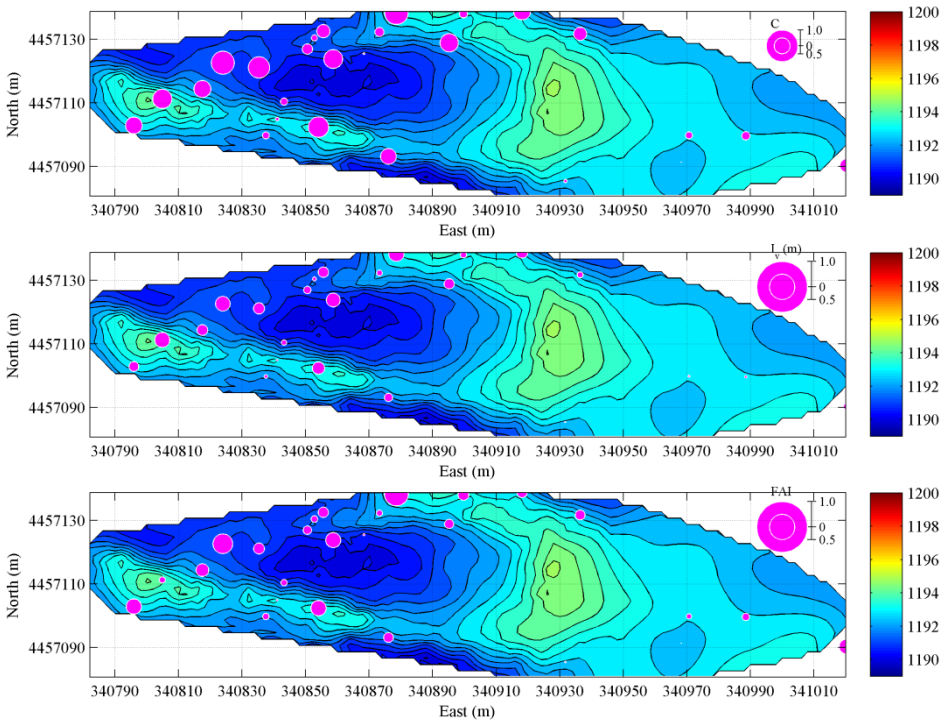

Figure 5-19. Vegetation parameters over D5 surveyed by quadrats in 2011.

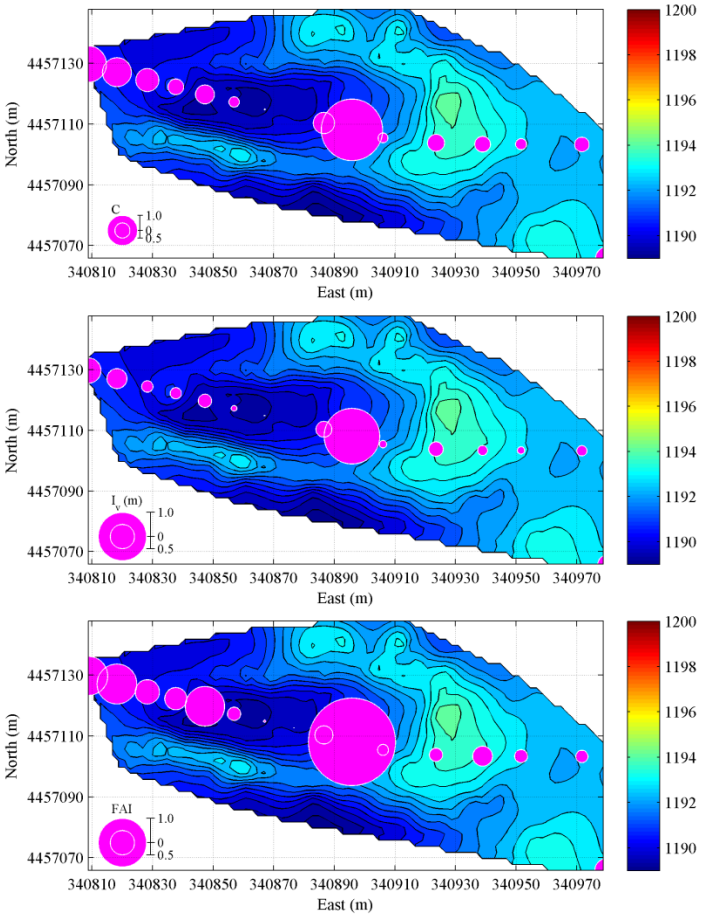

Figure 5-20. Vegetation parameters over D5 surveyed by quadrats in 2012.

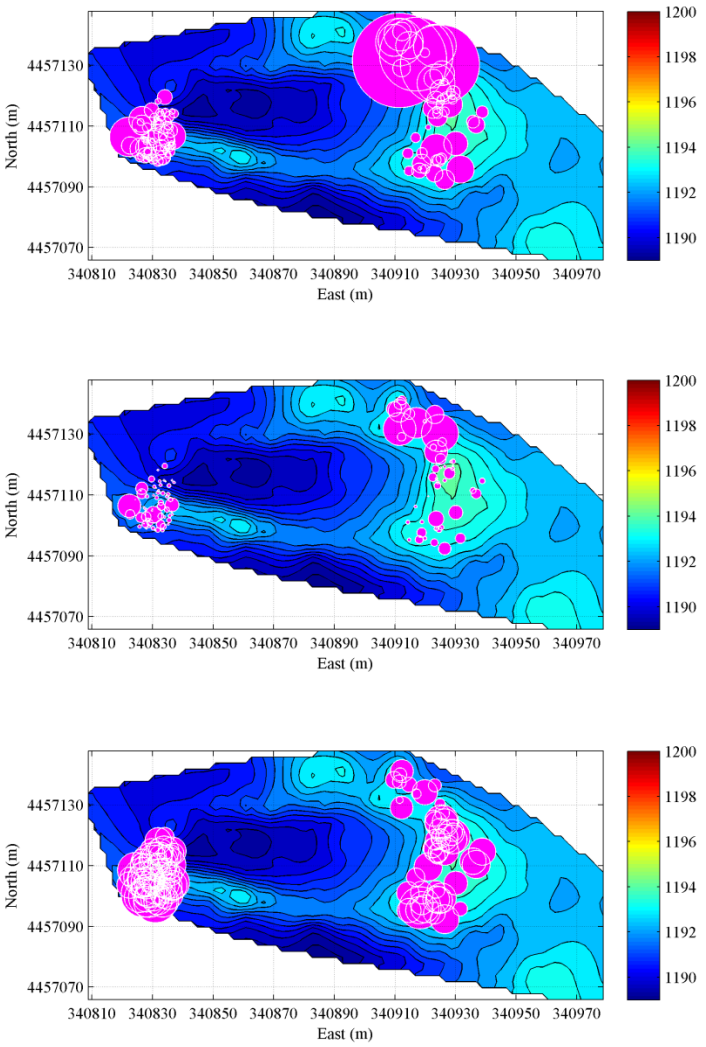

Figure 5-21. Vegetation parameters of individual plants on the lobe and arms of D5 surveyed in 2012.

Figure 5-22. The comparison of vegetation on the deflation plain between trailing arms of D2 in 2011 (left) and 2012 (right).

Figure 5-23. The comparison of vegetation on the lobe crest of D2 in 2011 (left) and 2012 (right).

Figure 5-24. The comparison of vegetation on the deflation plain between trailing arms of D5 in 2011 (left) and 2012 (right).

The roughness densities along longitudinal sections of two semi-mobile (D1, D2) and two fixed parabolic dunes (D3, D4) investigated in 2011 are shown in Figure 5-26. It can be seen that the roughness density along the longitudinal axis of parabolic dunes displays a characteristic of zonation. Within each zone, the roughness density does not show a significant change; nonetheless, it principally decreases towards the crests of parabolic dunes (Figure 5-12, 5-15, 5-18, 5-19, and 5-25). The roughness density and average shrub volume of big shrubs with lengths larger than 0.5 m of D3 in 2011 are shown in Figure 5-27 and Figure 5-28 respectively. The roughness density of big shrubs is decreasing along arms towards the head of the parabolic dune, whereas the shrub volume exhibits an increase trend. Therefore, it can be concluded that the density of nebkhas is declining while their sizes are growing along arms towards the dune head. In conclusion, shrubs are distributed continuously in the depression zones between arms, but the characteristics such as the size, the age and the coverage show a zonation along longitudinal sections of parabolic dunes. The big shrubs/nebkhas along arms are distributed sparsely but essential for

maintaining the parabolic shape of dunes.

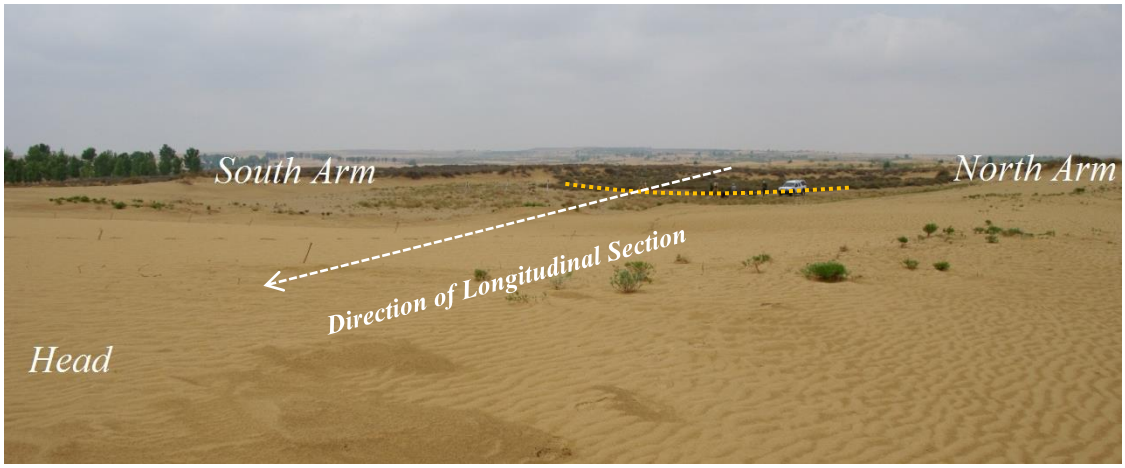

Figure 5-25. Vegetation zonation in the deflation plain of a parabolic dune. The yellow dotted line denotes the boundary between two vegetation zones.

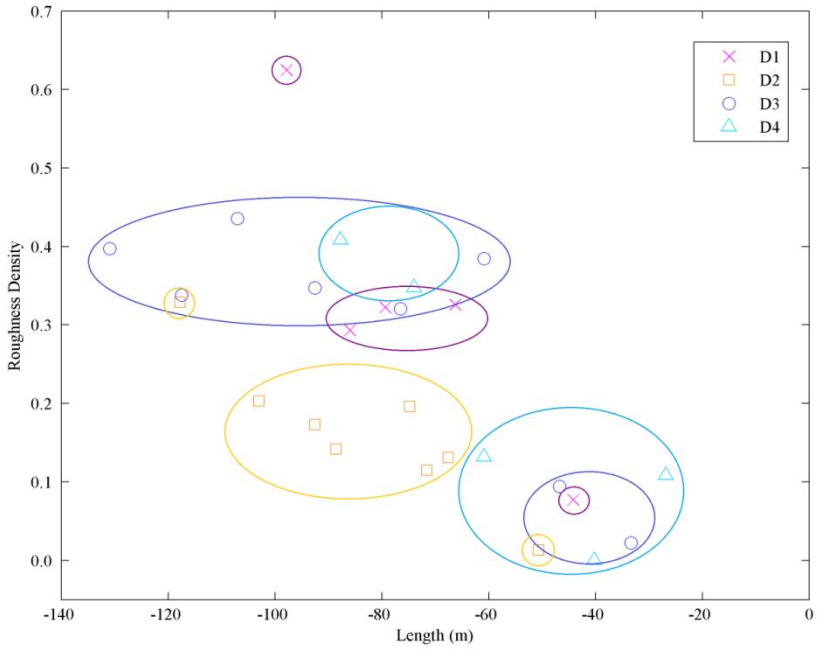

Figure 5-26. The roughness density along longitudinal sections of parabolic dunes in 2011. Zero point on x-axis denotes the location of crests, and circles denote vegetation zones.

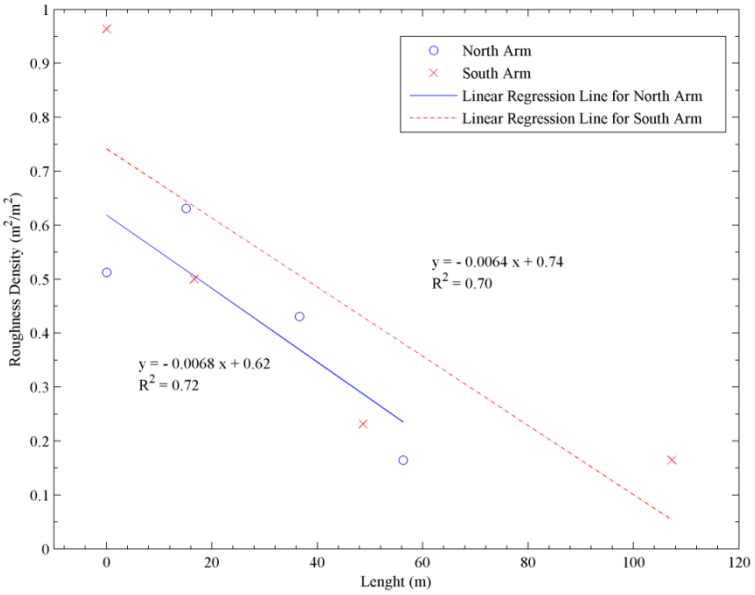

Figure 5-27. Roughness densities of plants with $L > 0.5$ m in the quadrats along arms of D3 in 2011.

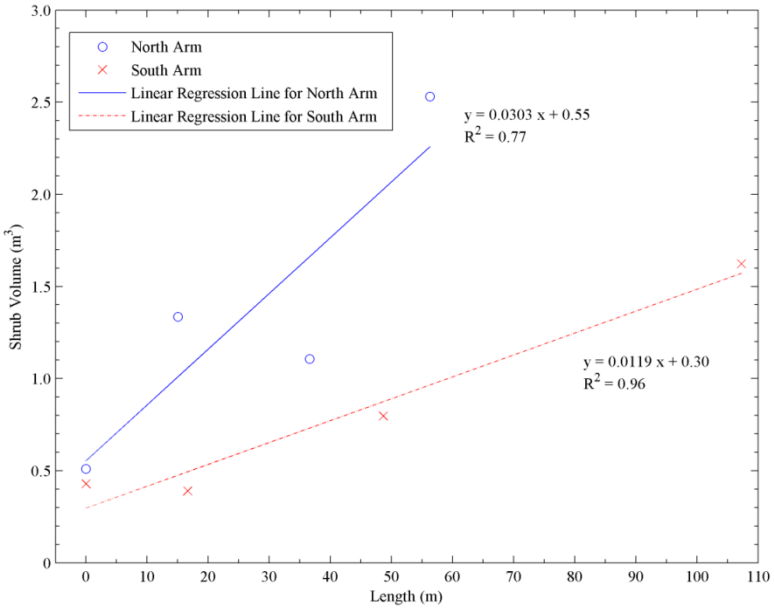

Figure 5-28. Average shrub volumes with $L > 0.5$ m in the quadrats along arms of D3 in 2011.

5.4 Discussion

The three types of parabolic dunes that have been identified in the study region (Chapter 4) are different in dune morphology and stability, which can be abstracted into representative cartoon models based on field measurements. The first type including most active semi-mobile parabolic dunes in this region

possesses a relatively large bare lobe with evident slip faces (D1 and D2), as shown in Figure 5-29 and Figure 5-30. These parabolic dunes exhibit a gently digitate shape.

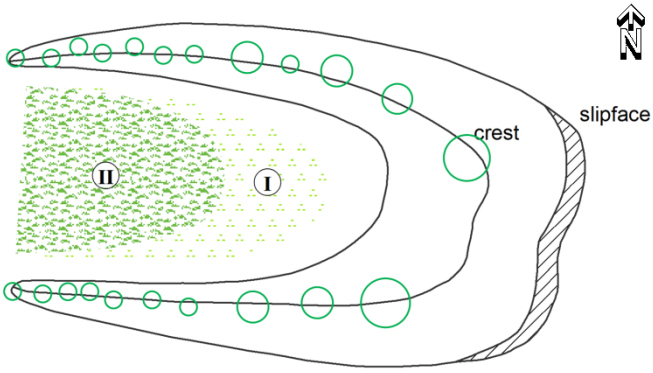

Figure 5-29. Schematic drawing of the first type of parabolic dunes. Region I and II are distinctive zones for younger shrubs and older shrubs respectively. Green circles denote canopies of nebkhas.

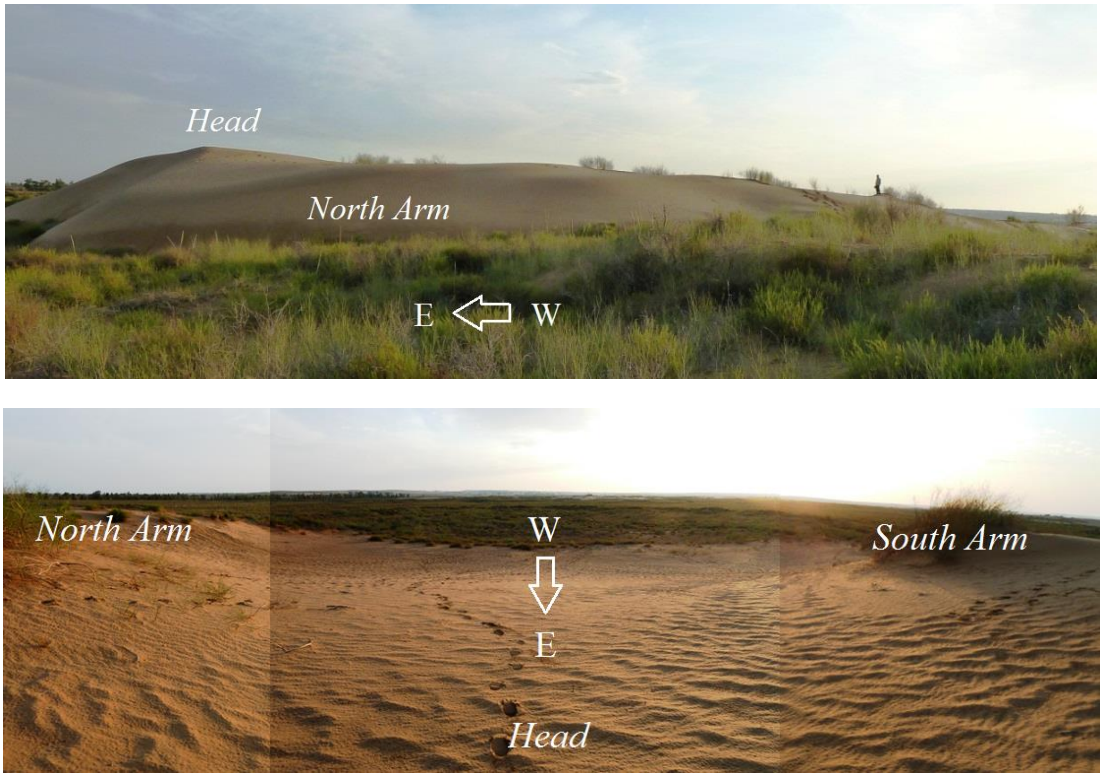

Figure 5-30. View of the parabolic dune D2 in 2011.

Vegetation exerts a significant impact on the geomorphic characteristics of dunes. The ephemeral annual Sand Rice grows rapidly on bare sand surfaces after a rainfall event; nevertheless, the shallow roots of the Sand Rice make it vulnerable to wind erosion, high surface temperature, and rapid loss of water induced by strong evapotranspiration. The Sand Rice can only thrive for a short period and die quickly, and hence contributes insignificantly to the development of dune morphology. In contrast, the perennial shrub Ordos Sagebrush plays a crucial role in shaping dune morphology because of its strong capability of withstanding sand burial and low temperature, in particular, during the winter.

Two to three distinctive vegetation zones usually have formed along the longitudinal axis of the flat deflation plain enclosed by two trailing arms of parabolic dunes. The zonation of vegetation is closely related with yearly recurrent sand burial events. In the winter and spring, strong westerly winds dominate the study region. As the lobes of parabolic dunes move forward and encroach on vegetated areas, the erosion of windward slopes leaves behind a strip of fresh surface incorporated into its deflation plain for subsequent revegetation. In the summer and autumn, given sufficient precipitation, vegetation can germinate and grow in this area (region I in Figure 5-29), whilst vegetation that used to be buried earlier and has got through previous harsh winter (region II in Figure 5-29) continues to grow. Consequently, vegetation on the deflation plain between the trailing arms exhibits a zonation regarding the age and the associated vegetation parameters such as the vegetation coverage and the frontal area index.

In addition to the important role of the Ordos Sagebrush in the zonation of vegetation on the deflation plain, it also plays an essential role in maintaining the parabolic shape of dunes, in particular, by forming nebkhas on the trailing arms. While the roughness density of vegetation is decreasing along arms towards the lobe of a parabolic dune, the size of individual nebkhas shows an increasing trend (Figure 5-26 and 5-27). This may be explained in three respects. First, larger shrubs need a relatively larger water supply area, which may result in a more severe intraspecific competition for water and the associated sparse distribution. Second, greater sediment supply towards the lobe enables the development of larger nebkhas. Finally, intensive erosion of the windward slope of nebkhas nearer to the lobe can expose roots of plants and then lead to their death due to desiccation. As a result, few plants survive from severe wind erosion, in particular, on the transitional areas connecting trailing arms with the lobe of a parabolic dune where intensive erosion occurs owing to the prevailing westerly winds.

The second type of parabolic dunes shown in Figure 5-31 and Figure 5-32 has been fully-stabilised by vegetation without slip faces (D3 and D4). Compared with the first type of parabolic dunes

with a digitate-shaped lobe, the lobe of this type of parabolic dunes is much lower and smaller on which vegetation has invaded and colonised. Vegetation on the deflation basin shows a similar zonation as the first type of parabolic dunes, but usually has more, although less-distinctive, zones (> 3) in terms of vegetation parameters such as the vegetation coverage and the roughness density. Nebkhas on the crest along the trailing arms also display a similar trend in their density and size, but the size of individual nebkhas on and close to the lobes is smaller than that of the first type of parabolic dunes possibly because of a lower sediment supply.

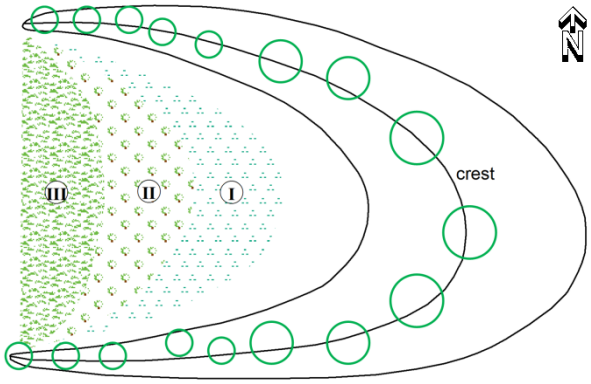

Figure 5-31. Schematic drawing of the second type of parabolic dunes. Region I, II and III are distinctive zones from younger shrubs to older shrubs. Green circles denote canopies of nebkhas.

Figure 5-32. View of the parabolic dune D3 in 2011.

In contrast to both the first and second types of parabolic dunes which have developed in a closed system surrounded by well-vegetated shrub fields with limited sediment supply, the third type of parabolic dunes (Figure 5-33 & Figure 5-34) is located right on the bank of an ephemeral river, and highly mobile crescentic dune fields are situated at its upwind direction. Therefore, it may receive relatively ample sediment supply. This type of parabolic dunes develops a low (around 5 m), yet very

extensive, tongue-shaped lobe reaching as far as 100 m away from its crest (Figure 5-9: D5). Vegetation on the deflation plain shows a similar trend as that of the above two types of parabolic dunes. But the vegetated area is relatively limited, and a large bare area is present close to the windward slope where ancient hard soil layers have exposed by severe erosion. Nebkhas on trailing arms also exhibit a similar trend as that of the previous two types.

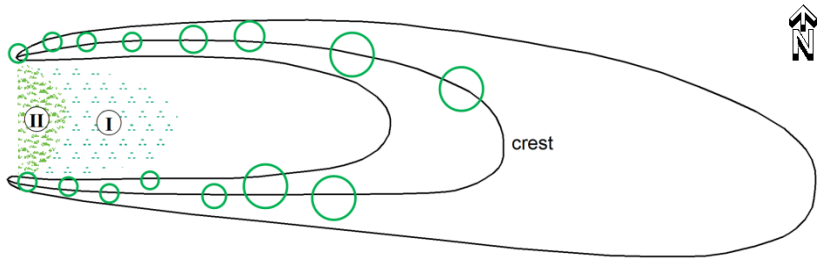

Figure 5-33. Schematic drawing of the third type of parabolic dunes. Region I and II are distinctive zones for younger shrubs and older shrubs respectively. Green circles denote canopies of nebkhas.

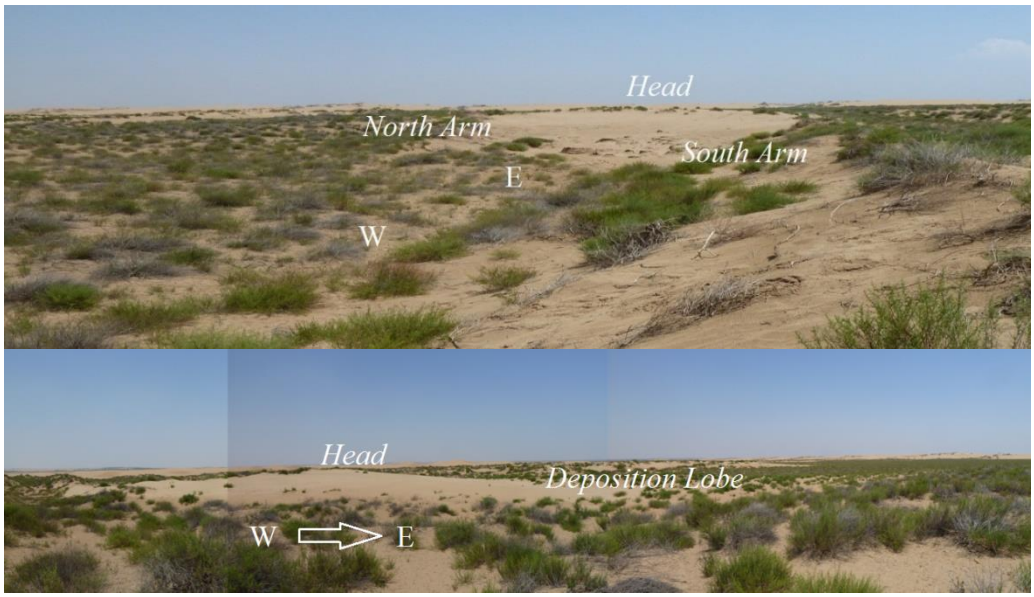

Figure 5-34. View of the parabolic dune D5.

In conclusion, the Ordos Sagebrush which is widely distributed in the study region predominantly determines the morphology and movement of parabolic dunes, combined with prevailing westerly winds and sand availability. This native species is capable of withstanding sand burial, low

temperature and seasonal drought, thereby continuously growing for years. The Ordos Sagebrush provides a relatively continuous cover on the deflation plain of parabolic dunes, whereas it is usually absent or patchy on the lobes and slip faces of active parabolic dunes because of strong recurrent sand burial events. The compact branch structure of Ordos Sagebrush, meanwhile, enables them to trap sediment effectively and form nebkhas, which is partly responsible for maintaining the parabolic shape of dunes.

To explore the past and the future of parabolic dunes as well as the roles of environmental fluctuations, climatic changes and anthropogenic stresses in the processes of parabolic dune-related dune transformations, computer modelling is used to bridge the gap between the limited empirical field study and the need for long-term understanding. This chapter complemented with next chapter serves as the foundation to construct modelling algorithm, inform modelling parameters, and impose boundary conditions.

References

Hugenholtz, C.H., Wolfe, S.A., Moorman, B.J., 2008. Effects of sand supply on the morphodynamics and stratigraphy of active parabolic dunes, Bigstick Sand Hills, southwestern Saskatchewan. Can. J. Earth Sci., 45(3), 321-335.

Li, S.-L., Werger, M.J.A., Zuidema, P.A., Yu, F.-H., Dong, M., 2010. Seedlings of the semi-shrub Artemisia ordosica are resistant to moderate wind denudation and sand burial in Mu Us sandland, China. Trees, 24(3), 515-521.

Raupach, M.R., Gillette, D.A., Leys, J.F., 1993. The effect of roughness elements on wind erosion threshold. J. Geophys. Res.-Atmos., 98(D2), 3023-3029.

Thorne, M.S., Skinner, Q.D., Smith, M.A., Rodgers, J.D., Laycock, W.A., Cerekci, S.A., 2002. Evaluation of a technique for measuring canopy volume of shrubs. Journal of Range Management, 55(3), 235-241.

Yang, H.X., Zhang, J.T., Li, Z.D., Wu, B., Zhang, Z.S., Wang, Y., 2008. Comparative study on spatial patterns of Artemisia ordosica populations in the Mu Us sandy land (in Chinese with English abstract). Acta Ecologica Sinica, 28(5), 1901-1910.

Zhang, Z.-S., Li, X.-R., Wang, T., Wang, X.-P., Xue, Q.-W., Liu, L.-C., 2008. Distribution and Seasonal Dynamics of Roots in a Revegetated Stand ofArtemisia ordosicaKracsh. in the Tengger Desert (North China). Arid Land Research and Management, 22(3), 195-211.

Chapter 6

Remote Sensing Image Interpretation

The migration rates of dunes are regarded as an important proxy of aeolian activity. To unveil the historical trajectories of dune mobility and morphologic changes, four sets of remote sensing (RS) satellite imagery in 2005, 2007, 2010, and 2012 were used to calculate the migration rates of two typical semi-mobile parabolic dunes. By combining RS analysis with fieldwork study, the maximum volumetric flux in the study region was then determined, and it serves as an import parameter of a cellular automaton model (Chapter 8) to explore the history and possible future sceneries of parabolic dunes under environmental changes (Chapter 9 & 10).

6.1 Introduction

Remote sensing imagery has been progressively used in broad subjects, in particular, cartography, environmental science, archaeology, geology, and geomorphology. In aeolian dune research, early applications of RS imagery focus on dune taxonomy and mapping, starting from as early as the 1940s (Melton, 1940). The first orbital satellite, *Sputnik I*, was launched in 1957 by the Soviet Union (Jensen, 2007). Broad non-military applications of orbital photographs, however, were not started until the 1970s when the first Landsat satellite was launched in 1972. Orbital satellite imagery enables researchers to investigate dune patterns on large temporal and spatial scales, and to explore aeolian landforms on outer planets such as Venus, Titan, and Mars (Bishop, 2007). Digital Elevation Models (DEMs) produced by stereo aerial photographs, Interferometric Synthetic Aperture Radar (InSAR), and Light Detection And Ranging (LiDAR) further propel research to a revolutionary stage and offer great advantages by providing high resolution three dimensional data that tremendously facilitate our understanding of 3D dune morph-dynamics (Blumberg, 2006; Gaylord and Stetler, 1994; Hugenholtz et al., 2010), facilitate our understanding of contributing factors shaping large-scale dune patterns (Vermeesch and Drake, 2008), and facilitate our understanding of effects arising from changes in system boundary conditions such as

environmental variations (Marín et al., 2005), and anthropogenic stresses such as grazing activities (Tsoar and Blumberg, 2002).

Compared with a paucity of empirical field data, RS imagery extends temporal baselines and is widely used in examination of dune migration rates and dunefield mobility. Al-Dabi et al. (1997) mapped the Al-Kuwaimiliyah dunefield and monitored the change of dune patterns in Kuwait between 1989 and 1992 using 4 sets of multi-temporal Landsat Thematic Mapper (TM) images. Bailey and Bristow (2004) compared migration rates of parabolic dunes at Aberffraw, north Wales from 1940 to 1993 using three sets of aerial photographs by a linear-fit method as opposed to a crest-to-crest method. Levin and Ben-Dor (2004) proposed to determine the average dune migration rates of bare lobes using a calculus method aided with GIS (Levin, 2011). Marín et al. (2005) used aerial photographs and Landsat ETM images to quantify migration rates of parabolic and barchan dunes from 1936 to 1999 by the changes in their front edges at the Great Sand Dunes national park and Preserve, Colorado. Representative studies on migration rates of parabolic dunes are shown in Table 6-1.

Table 6-1. Research on migration rates of parabolic dunes using RS imagery.

Reference	Study Region
García-Novo et al., 1976	Doñana National Park, Spain
Pye, 1982	Queensland, Australia
Story, 1982	Northern Australia
Stetler and Gaylord, 1996	Hanford, Washington, US
David et al., 1999	Seward Sand Hills, Saskatchewan, Canada
Hesp, 2001	Manawatu, New Zealand
Tsoar and Blumberg, 2002	South-eastern Mediterranean coast, Israel
Yurk et al., 2002	Holland, eastern shore of Lake Michigan, US
Arens et al., 2004	Kennemerland, Netherlands
Bailey and Bristow, 2004	Anglesey, Wales, UK
Barbosa and Dominguez, 2004	São Francisco River Strandplain, Brazil
Bigarella et al., 2005	Lagoa dune field, Santa Catarina Island, Brazil
Marín et al., 2005*	Great Sand Dunes, Colorado
Forman et al., 2008	Cape Cod National Seashore, Massachusetts, US
Hugenholtz et al., 2008	Bigstick Sand Hills, Saskatchewan, Canada
Girardi and Davis, 2010	Walking Dunes, New York, US
Hart et al., 2012	Mason Bay, New Zealand

*: QuickBird; others: aerial photographs.

Continuous improvement of spectral and spatial resolutions of RS imagery diverts research from the examination of morphology-based dune mobility to the exploration of dune morpho-dynamics and the associated controlling factors after 1995. Impacts of climatic changes and anthropogenic pressure on aeolian dune systems, meanwhile, have drawn an increasing public attention. Anthonsen et al. (1996) compared digitised contour maps and aeolian photographs of Råbjerg Mile Dune over past 100 years, and suggested a decrease in wind energy associated with an increase in vegetation cover after 1924 was responsible for the transformation from crescentic dunes to parabolic dunes thereof. Tsoar and Blumberg (2002) interpreted dune migration rates from 1944 to 1995 using 12 sets of aerial photographs, and contributed the transformation from barchan to parabolic dunes to a decrease in agricultural and pastoral activities. Marín et al. (2005) concluded an increase in drought severity and a concomitant decrease in vegetation cover accelerated dune migrations at the Great Sand Dunes between 1936 and 1999. Wolfe and Hugenholtz (2009) used LiDAR imagery (with vertical accuracy of 0.20 m and horizontal accuracy of 0.3 m) to discover residual dune ridges left behind parabolic dunes on the Canadian prairies, and demonstrated that these parabolic dunes were transformed from barchan dunes around 200 years ago under the influence of recent climate warming. Reitz et al. (2010) extracted the DEM from LiDAR imagery of White Sands and suggested that a barchan to parabolic dune transformation takes place when the dune surface erosion or deposition rate decreases below a vegetation growth threshold. Levin (2011) found dune activity on Fraser Island, Australia, was closely related with the tropical cyclone intensity by analysing aeolian photographs and a SPOT satellite image from 1943 to 2005. Representative research on dune morpho-dynamics using RS imagery is shown in Table 6-2.

Self-organisation and emergent behaviour of dune landscapes stimulate new interests in exploring spatial patterns, dune transformations, and interactions among environmental controls using numerical modelling (Werner, 1995). RS imagery plays an essential role in supplementing limited empirical field data and validating numerical models. Nield and Baas (2008) developed a Discrete Eco-geomorphic Aeolian landscape (DECAL) cellular automation model and simulated hairpin-shaped parabolic dunes at White Sands by using two types of abstract vegetation species. Duran et al. (2008) simulated a barchan to parabolic dune transformation using a continuum model. Pelletier et al. (2009) used LiDAR and aerial photographs, and simulated dunefield evolution under the changes in interdune vegetation. In sum, multi-temporal and high resolution RS imagery expands temporal and spatial scales, presents important evidence of dune morphological changes, and provides qualitative and quantitative parameters used in numerical models.

Table 6-2. Research on dune morpho-dynamics using RS imagery.

Reference	Study Region
Melton, 1940	southern High Plains, US
Pye, 1982	Cape Bedform and Cape Flattery, Queensland, Australia
Pye, 1983b	Northern Cape York Peninsula, Queensland, Australia
Anton and Vincent, 1986	Jafurah Desert, Eastern Province, Saudi Arabia
Eriksson et al., 1989	southern Kalahari Desert, South Africa
Anthonsen et al., 1996	Rabjerg Mile, Skagen Odde, Denmark
Hesp, 2001	Manawatu, New Zealand
García-Hidalgo et al., 2002	Duero Basin, Spain
Tsoar and Blumberg, 2002	Southeastern Mediterranean Coast, Israel
Duran et al., 2008*	Ceara, Brazil
Ardon et al., 2009	southern coastal plain of Israel
Wolfe and Hugenholtz, 2009**	Northern Great Plains, Canada
Girardi and Davis, 2010	Walking Dunes, New York
Reitz et al., 2010**	White Sands, New Mexico, US
Hart et al., 2012	Mason Bay, New Zealand

*: QuickBird; **: LiDAR; others: aerial photographs.

6.2 Methodology

To unveil the historical trajectories of dune migration and morphological changes, four sets of satellite imagery from 2005 to 2012 were compared. Three images in 2005, 2010 and 2012 were acquired from Google Earth, and geo-rectified and co-registered with a high resolution Quick Bird panchromatic image (a resolution of 0.6 m) in 2007, resulting in an average RMS error of 1.14 pixel or 0.68 m. To accurately calculate migration rates of parabolic dunes, the Universal Transverse Mercator (UTM) geographic coordinate system was used. The image in 2013 was available from Google Earth, but the quality was unsatisfactory. Bare dune lobes in the image in 2012 exhibited an odd dark colour in the image in 2013, possibly due to a vegetation cover of annual plants or high surface moisture after a rainfall event. It was difficult to make reasonable judgement without a field investigation. The image in 2013 was, therefore, excluded from analysis and comparison.

Recall that three semi-mobile and two stabilised parabolic dunes were investigated in the fieldwork in 2011 and 2012. D3 and D4 had been stabilised by 2005 and no discernible migration and morphological change occurred since then. Semi-mobile parabolic dune D5 was situated on the bank of a seasonal river and is hence not a good representative of semi-mobile parabolic dunes in a closed system in which dunes are surrounded by well-vegetated shrub fields. D1 and D2 were semi-mobile parabolic dunes

with active sand transport in a typical closed environment without external sediment supply and are the main focus of this study.

6.2.1 Dune Migration Rate

The dune migration rate between two successive times was determined with the method proposed by Levin and Ben-Dor (2004). An example is shown in Figure 6-1. Dune frontal edges (the outer boundaries of a lobe) at different times were identified from two successive aerial images. The migration rate [R_i, m yr^{-1}] at point i is the migration distance [D_i, m] over the time period between the two aerial images [Δt, yr]:

$$R_i = \frac{D_i}{\Delta t} \tag{6-1}$$

The migration rate at a different point, however, may be different, such as the point $i+1$. The mean migration rate (R) can then be calculated by averaging migration rates at sampled points over the frontal edge:

$$R = \frac{\sum_{i=1}^{n} R_i}{n} = \frac{\sum_{i=1}^{n} D_i}{n\Delta t} \tag{6-2}$$

where: n is the number of sampled points. The larger n is, the more accurate the result is. When n increases to the infinity ($n \to \infty$), the average distance between two frontal edges is approximately equal to the area enclosed by the two successive frontal edge lines [S, m^2] divided by the length of the middle line between them [L_m, m], as shown below:

$$R = \frac{S}{L_m \Delta t} \tag{6-3}$$

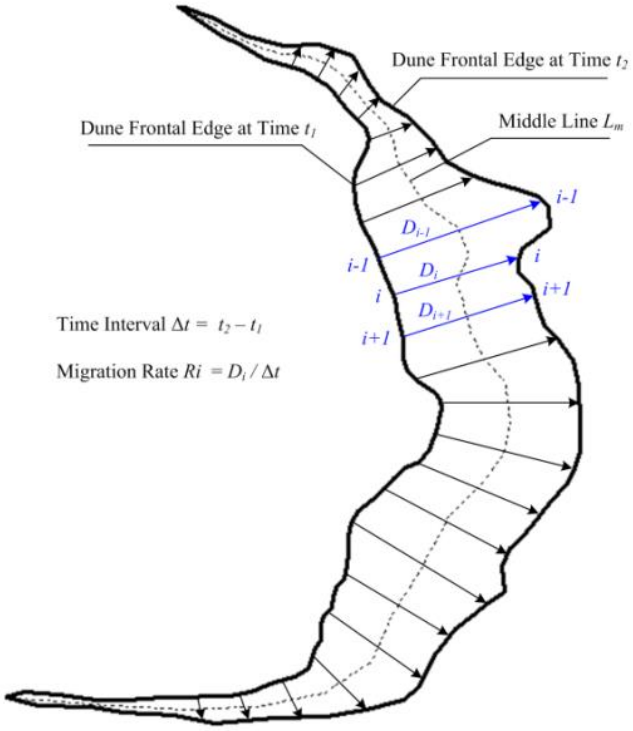

Figure 6-1. Schematic drawing of the method for calculating the average migration rate.

6.2.2 ISODATA Classification and Dune Outline Identification

The migration rates of both the erosion boundaries (the toe of windward slope) and the deposition boundaries (the frontal edge of dune lobe) were calculated. The erosion and deposition boundaries of semi-mobile parabolic dunes D1 and D2 were firstly identified in four aerial images assisted with unsupervised ISO data classification by ENVI. The ISO data classification, based on iterative procedures, is one of the simplest and most widely-used clustering algorithms (Dunn, 1973). In the classification, arbitrary initial cluster vectors (such as RGB of pixels) are assigned at the start. Each pixel is then classified to the cluster at the shortest distance, and the new mean vectors of pixels in the same clusters are calculated. This process is repeated until the number of pixels moving among clusters between two successive iterations is small enough or the maximum number of iterations is reached. In the study sites, surface types are relatively simple and distinguishable. The spectral analysis of a typical transect along a longitudinal section of the parabolic dune D1 is shown in Figure 6-2. It can be seen that the RGB values of pixels denoting bare sand surfaces are significantly higher than that of vegetated surfaces. The study sites with different vegetated conditions can hence be effectively classified based on the RGB values of pixels. Because aerial images of different years were taken in different seasons, comparisons of vegetation in different years are intractable. Spatial change of vegetation over dunes, nonetheless, was

possible. Three clusters were identified including the bare sand area, the sparse vegetated area, and dense vegetated area. In aid of the resulting classification maps, outlines of dunes could be drawn reasonably objectively.

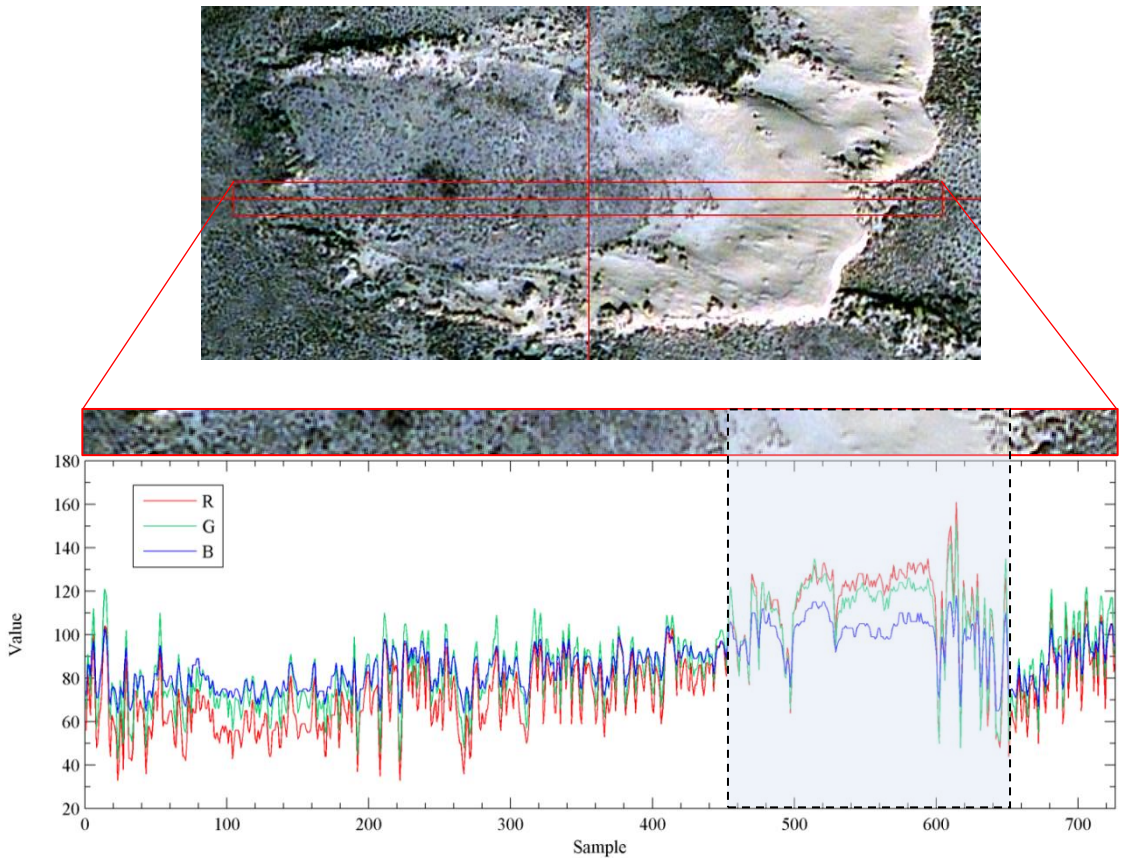

Figure 6-2. Spectral analysis of a typical transect along a longitudinal section of the parabolic dune D1. The light blue area was the bare sand area of the slice of the dune lobe.

Dune outlines and vegetation classification maps in 2005, 2007, 2010, and 2012 are shown in Figure 6-3. Parabolic dune D1 had an easily identifiable lobe, of which different parts were moving relatively steadily. In contrast, the crest/lobe of D2 exhibited an outstanding shift from 2005 to 2007, although the overall outer boundary of the dune did not change notably as shown in the red dotted line (the red dotted lines in all images of different years are the same, denoting the outer boundary of D2 in 2005 to facilitate comparisons). In 2005, it can be seen that the area between the deposition boundary of the lobe (orange line) and the outer boundary of the dune (red dotted line) was speckled by big shrubs. However, these shrubs in 2007 were buried to a large extent. Sand continued to accumulate in this area in 2010, forming slip faces, although the whole lobe did not seem to move forward appreciatively. Hence,

the deposition boundaries of the lobe of D2 in 2005 and 2007 were necessarily differentiated from the outer boundaries of the overall dune (orange line). No such differentiation was needed for D2 in 2010 and 2012, and for D1.

As the sand deposits on the lee slopes and the frontal edges of dune lobes were moving forward, the windward slopes of dunes were experiencing erosion and moving forward along at the same time. Therefore, both migrations rates of windward slope edges (erosion boundaries) [R_{inner}, m yr^{-1}] and migration rates of frontal edges (deposition boundaries) [R_{outer}, m yr^{-1}] were calculated with the method introduced in the previous section. The areas between outlines identified from two successive images were acquired using ArcGIS by creating polygons. Meanwhile, middle points of intersecting lines perpendicular to the successive lines were identified. The length of a middle line was then secured by calculating the overall length of lines connecting these middle points.

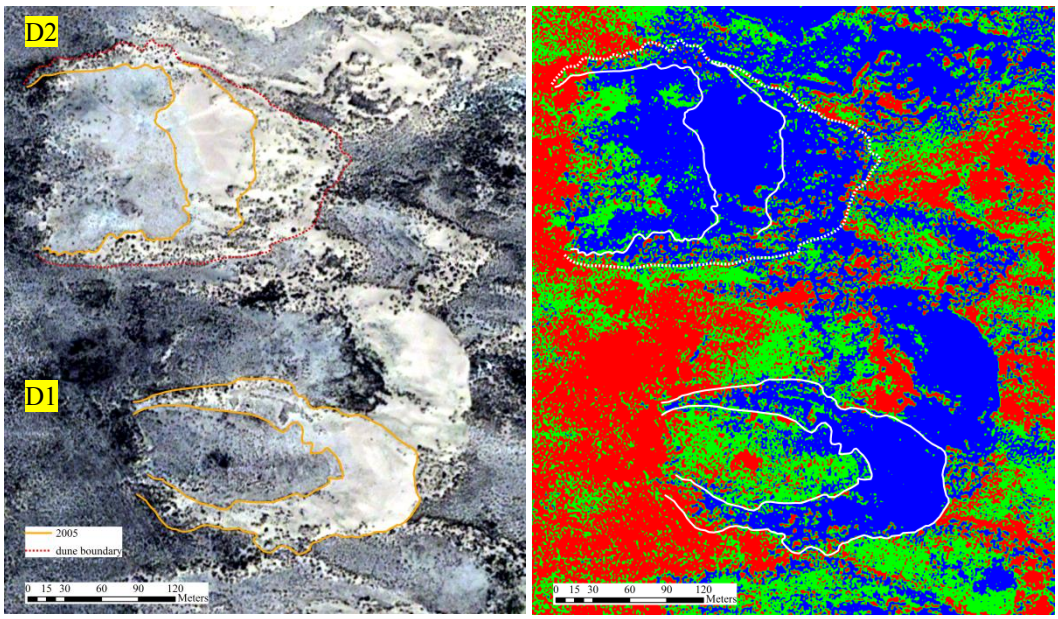

17 Aug. 2005

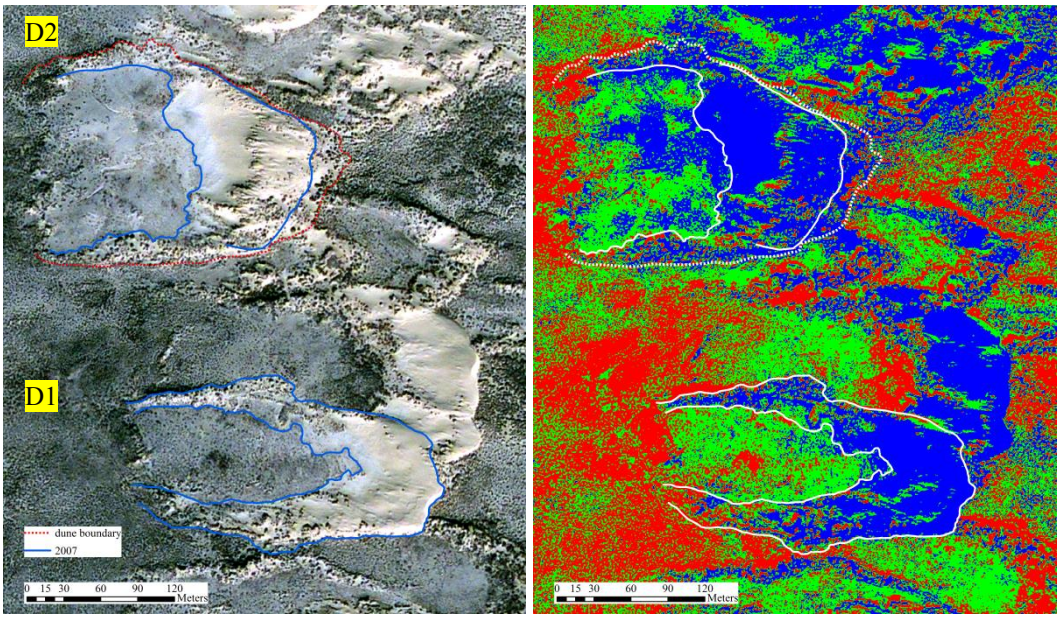

29 Jan. 2007

Figure 6-3. Vegetation classification with the method of ISODATA. The red, green and blue areas denote the areas with dense vegetation, sparse vegetation and bare sand respectively. White lines are outlines of dunes.

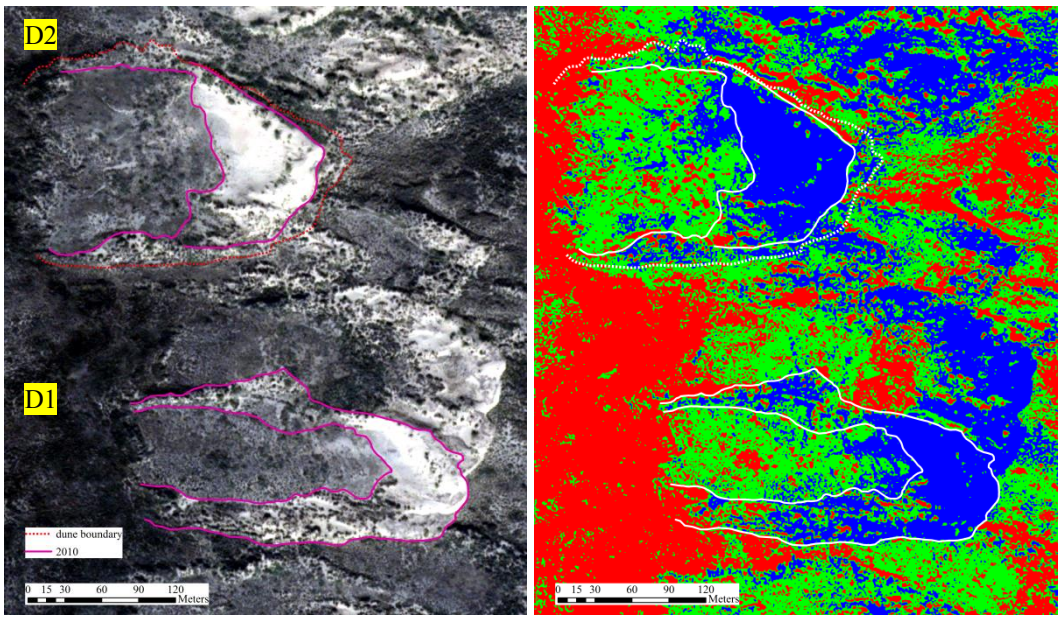

30. Oct. 2010

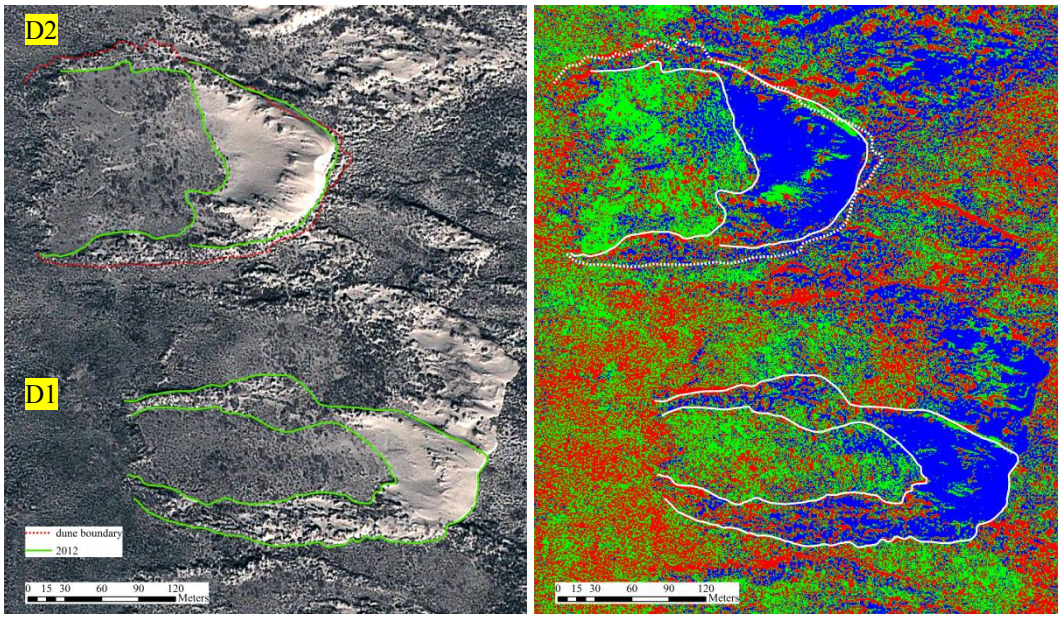

21. Jan. 2012

Figure 6-3. (Continued) Vegetation classification with the method of ISODATA. The red, green and blue areas denote the areas with dense vegetation, sparse vegetation and bare sand respectively. White lines are outlines of dunes.

6.2.3 Sand Volumetric Flux

The sand volumetric flux [q_v, m^3 m^{-1} yr^{-1}] is the volume of sand [V, m^3] transported by winds passing through a vertical section per unit width [w, m] per unit time [t, yr], as shown below:

$$q_v = \frac{V}{wt} \tag{6-4}$$

For a longitudinal section of a dune, the sand volumetric flux is dependent on the profile of the section and the migration rate [R, m yr^{-1}] along the wind direction (Figure 6-4):

$$q_v = \frac{S_p}{L_b} R = \overline{H} R \tag{6-5}$$

where: S_p is the area of a longitudinal section of a dune, [m^2]; L_b is the length of the section base, [m]; and $\overline{H}$ is the average height of the section, [m]. This equation is only applicable when external sand influx is minimal and the average height changes insignificantly.

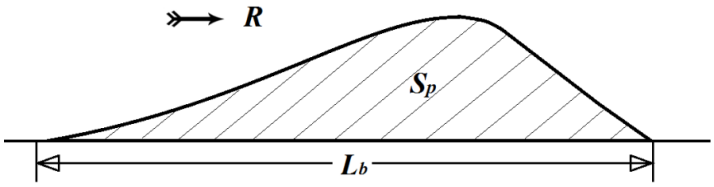

Figure 6-4. An example of a longitudinal section of a dune: parabolic dune in this case.

The migration of parabolic dunes is generally complicated. Unlike a barchan dune which moves forward more like a single entity and keeps its shape for relatively long period of time, the movement of a parabolic dune is usually accompanied by a constant change in dune morphology. As the lobe of a parabolic dune migrates downwind, dune arms are elongating and may be gradually stabilised by vegetation. Migration rates of different parts of a parabolic dune are hence varying to a large degree alongside sand volumetric fluxes. Meanwhile, the movement of parabolic dunes is closely interactive with changes in vegetation characteristics due to environmental fluctuations or anthropogenic pressure. In consequence, a uniform sand volumetric flux is unrealistic for parabolic dunes. The maximum volumetric flux is, however, useful to indicate the local wind region and the associated sand transport potential. The maximum volumetric flux [q_{vMax}, m^3 m^{-1} yr^{-1}] is defined as the equation below:

$$q_{vMax} = H_{crest} R \tag{6-6}$$

where: H_{crest} is the lobe height of a parabolic dune [m] relative to the foot of slip faces, estimated from the topography survey in the field (Figure 5-9): 4 m for D1 and 7 m for D2 respectively; and R is the average migration rate [m yr^{-1}], acquired from remote sensing image interpretations.

6.3 Results

6.3.1 Dune Migration Rate

In the study region, mobile dunes migrate forward periodically in the winter and the spring when winds are strong and shrubs are in their non-growing season, leaving behind the discernible vestiges that mark the previous locations of the toe of a dune, as yellow dash lines shown in Figure 6-5. The migration rates including both the erosion and the deposition boundaries of dune lobes were examined (Figure 6-6 & Table 6-3). The toes (windward edges) of both D1 and D2 experienced noticeable movement by wind erosion from 2005 to 2007, and to 2010, with an average migration rate of 6.54 m y^{-1} and 6.46 m y^{-1} respectively, yet experienced insignificant change from 2010 to 2012. Meanwhile, sand deposition of D1 and D2 showed different behaviour. Slip faces of D1 were encroaching on a vegetated shrub field continuously during the period of 2005-2012 with varying speeds (3 - 7 m yr^{-1}), whilst its trailing arms were gradually elongating. In contrast to the relatively steady migration of D1, the lobe/crest of D2 exhibited a pronounced shift between 2005 and 2010, although the dune boundaries (red dotted line) did not show significant change. In 2005, the area between the deposition boundary and the dune boundary was partially buried and shrubs could be easily identified. As sand continued to accumulate in this area, these shrubs had been almost completely buried by 2007. In 2010, the lobe of the dune has displayed a typical parabolic shape and slip faces have formed.

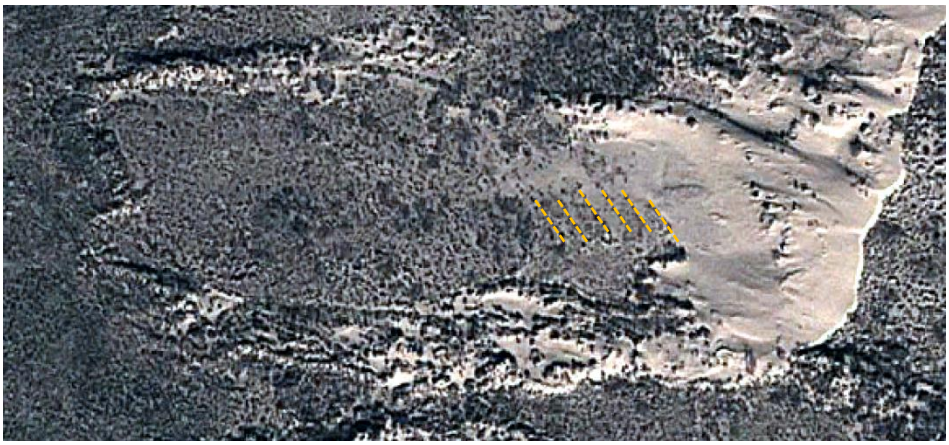

Figure 6-5. Satellite image of D1 in 2012. Yellow dash lines denote vestiges of previous locations of the toe of the dune lobe.

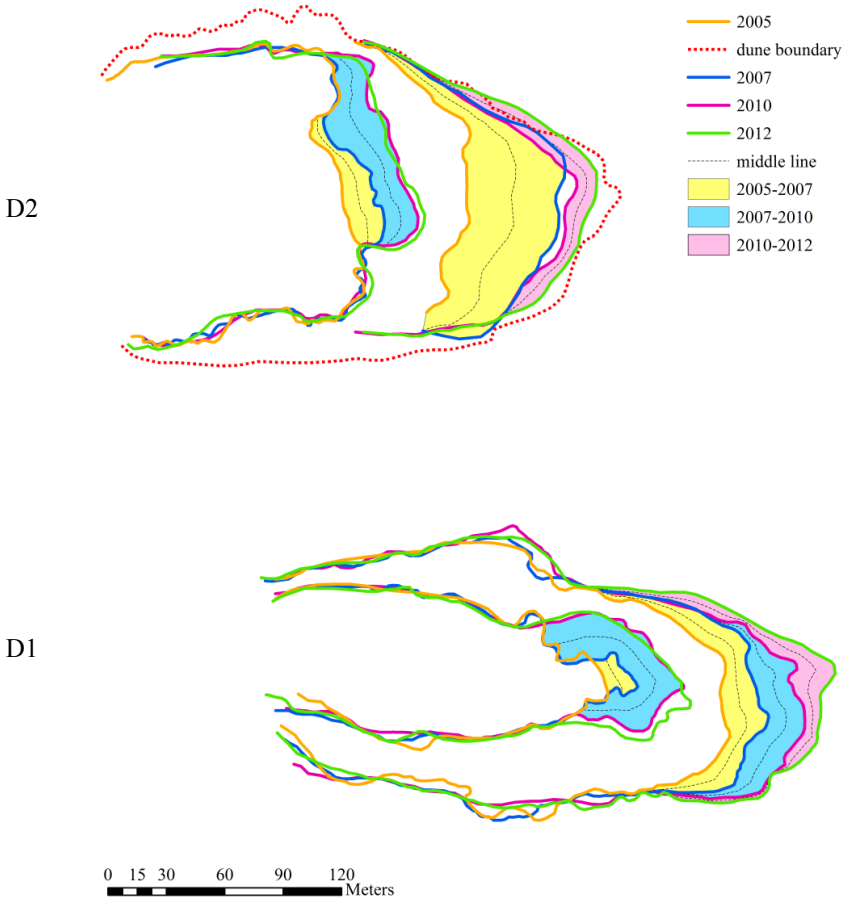

Figure 6-6. Identification of boundaries and calculation of migration rates. Orange, blue, purple, and green lines denote boundaries of dune lobes in 2005, 2007, 2010 and 2012 respectively. The yellow, cyan, and purple areas were migration areas between 2005-2007, 2007-2010, and 2010-1012 respectively. The red dotted line is the dune boundaries of D2 in 2005. The black dotted lines are the middle lines between two successive lines.

Table 6-3. Migration rates of two semi-mobile parabolic dunes from 2005 to 2012

		Date (from - to)	Δt (days)	S (m^2)	L_m (m)	R (m y^{-1})
D1	Erosion	17.08.05-29.01.07	530	246.11	20.54	8.26
		29.01.07-30.10.10	1370	2014.92	111.38	4.82
		30.10.10-21.01.12	448	-	-	-
	Deposition	17.08.05-29.01.07	530	1929.66	189.71	7.01
		29.01.07-30.10.10	1370	1760.84	167.64	2.80
		30.10.10-21.01.12	448	1493.30	252.72	4.82
D2	Erosion	17.08.05-29.01.07	530	915.08	75.85	8.31
		29.01.07-30.10.10	1370	1968.61	114.16	4.60
		30.10.10-21.01.12	448	-	-	-
	Deposition	17.08.05-29.01.07	530	5365.89	204.52	18.08
		29.01.07-30.10.10	1370	-	-	-
		30.10.10-21.01.12	448	1564.36	214.98	5.93

6.3.2 Sand Volumetric Flux

Due to lack of information regarding dune topography from RS image interpretations, accurate sand volumetric fluxes could not be determined. The maximum volumetric fluxes, nevertheless, could be roughly estimated by using the dune heights measured in the field in 2011. The average migration rates of D1 and D2 from 2005 to 2012 were 5 m yr^{-1} and 6 m yr^{-1} respectively. In comparison to D2 whose lobe showed an abrupt shift between 2005 and 2010, the movement of D1 was relatively smooth and the dune lobe displayed a typical parabolic shape; therefore, the D1 was chosen as the representative of typical parabolic dunes in the study region and was used to calculate the maximum volumetric flux. As the average migration rate and the dune height were 5 m yr^{-1} and 4 m respectively, the maximum volumetric flux was obtained as 20 m^3 m^{-1} yr^{-1}, which is used as the standard potential sand transport rate in the study region for computer modelling (details in Chapter 8).

6.4 Discussion

The migration of parabolic dunes is governed by sediment availability, vegetation cover, and wind regime collectively, although no simple interrelationships exist. As shown in Figure 6-2, semi-mobile parabolic dunes D1 and D2 were partially vegetated and surrounded by well-vegetated shrub fields. Without external sediment supply, sand on the arms and beneath the dunes is the only resource for transport by winds. Sand is eroded from the deflation plain between trailing arms as well as windward slopes, and transported to the crest by progressively compressed and accelerated wind flows that are formed by the concave profile of parabolic dunes (Tsoar and Blumberg, 2002). Parabolic dunes can continue to move forward only if a continuous sediment supply is available to their lobes. As dunes are moving forward on a sandy substratum, the size of parabolic dunes may be maintained or even increased by incorporating newly exposed sand beneath the dunes. However, if dunes are moving over a non-sandy substratum or a sandy substratum with a limited thickness, sand may be gradually lost. Meanwhile, dunes may be stabilised when they migrate into an area with a higher water table, which reduces sand supply beneath dunes and increases water availability for vegetation growth.

The migration of parabolic dunes is closely related to the change of vegetation characteristics over dunes. Whereas bare lobes of dunes are moving forward, the existence of vegetation on trailing arms, in particular, big shrubs and nebkhas, stabilises loose sand and is essential to maintain the parabolic shape

of the dunes. The surrounding vegetation of dunes limits the expansion of the deflation plain between the arms, and further confines the shape of the dunes. As shown in Figure 6-2, from 2005 to 2012, big shrubs on the arms could be easily identified, although vegetation coverage was varying because the RS images were taken in different seasons. Sand on the arms of dunes was gradually lost during this period (ref. to images in Jan. 2007 and Jan. 2012). Big shrubs also existed sparsely on the crest of dunes, probably because only big shrubs with extensive root systems can survive strong wind erosion and sand burial activity. In the study region, wind erosion and sand burial events happen recurrently in the winter when winds are strong whilst precipitation is low and vegetation coverage is sparse. As a result, vegetation in the deflation plain between trailing arms shows a zonation along longitudinal sections of parabolic dunes as bare lobes are moving forward leaving behind fresh spaces for further colonisation by vegetation in a better environmental condition.

The technology of RS imagery offers the advantages of continuously monitoring changes of landscapes on a long-term scale. This chapter used four RS images to explore the changes in dune morphologies, migration rates, and sand volumetric fluxes over seven years, which serve as foundations for determining important parameters in the computer modelling (Chapter 8) and then examining the impacts of potential environmental changes on dunefield stabilisation and reactivation (Chapter 9 & 10).

References

Al-Dabi, H., Koch, M., Al-Sarawi, M., El-Baz, F., 1997. Evolution of sand dune patterns in space and time in north-western Kuwait using Landsat images. Journal of Arid Environments, 36(1), 15-24.

Anthonsen, K.L., Clemmensen, L.B., Jensen, J.H., 1996. Evolution of a dune from crescentic to parabolic form in response to short-term climatic changes: Rabjerg mile, Skagen Odde, Denmark. Geomorphology, 17(1-3), 63-77.

Bailey, S.D., Bristow, C.S., 2004. Migration of parabolic dunes at Aberffraw, Anglesey, north Wales. Geomorphology, 59(1-4), 165-174.

Bishop, M.A., 2007. Point pattern analysis of north polar crescentic dunes, Mars: A geography of dune self-organization. Icarus, 191(1), 151-157.

Blumberg, D.G., 2006. Analysis of large aeolian (wind-blown) bedforms using the Shuttle Radar Topography Mission (SRTM) digital elevation data. Remote Sensing of Environment, 100(2), 179-189.

Dunn, J.C., 1973. A fuzzy relative of the ISODATA process and its use in detecting compact well-separated clusters. J. Cybern., 3(3), 32-5757.

Duran, O., Silva, M.V.N., Bezerra, L.J.C., Herrmann, H.J., Maia, L.P., 2008. Measurements and numerical simulations of the degree of activity and vegetation cover on parabolic dunes in north-eastern Brazil. Geomorphology, 102(3-4), 460-471.

Gaylord, D.R., Stetler, L.D., 1994. Aeolian-climatic thresholds and sand dunes at the Hanford site, south-central Washington, U.S.A. Journal of Arid Environments, 28(2), 95-116.

Hugenholtz, C.H., Bender, D., Wolfe, S.A., 2010. Declining sand dune activity in the southern Canadian prairies: Historical context, controls and ecosystem implications. Aeolian Research, 2(2-3), 71-82.

Jensen, J.R., 2007. Remote sensing of the environment: an earth resource perspective (2nd ed.). Pearson Education Ltd., London.

Levin, N., 2011. Climate-driven changes in tropical cyclone intensity shape dune activity on Earth's largest sand island. Geomorphology, 125(1), 239-252.

Levin, N., Ben-Dor, E., 2004. Monitoring sand dune stabilization along the coastal dunes of Ashdod-Nizanim, Israel, 1945–1999. Journal of Arid Environments, 58(3), 335-355.

Marín, L., Forman, S.L., Valdez, A., Bunch, F., 2005. Twentieth century dune migration at the Great Sand Dunes National Park and Preserve, Colorado, relation to drought variability. Geomorphology, 70(1–2), 163-183.

Melton, F.A., 1940. A tentative classification of sand dunes its application to dune history in the southern high plains. Journal of Geology, 48(2), 113-U117.

Nield, J.M., Baas, A.C.W., 2008. The influence of different environmental and climatic conditions on vegetated aeolian dune landscape development and response. Global and Planetary Change, 64(1–2), 76-92.

Pelletier, J.D., Mitasova, H., Harmon, R.S., Overton, M., 2009. The effects of interdune vegetation changes on eolian dune field evolution: a numerical-modeling case study at Jockey's Ridge, North Carolina, USA. Earth Surface Processes and Landforms, 34(9), 1245-1254.

Reitz, M.D., Jerolmack, D.J., Ewing, R.C., Martin, R.L., 2010. Barchan-parabolic dune pattern transition from vegetation stability threshold. Geophysical Research Letters, 37.

Tsoar, H., Blumberg, D.G., 2002. Formation of parabolic dunes from barchan and transverse dunes along Israel's Mediterranean coast. Earth Surface Processes and Landforms, 27(11), 1147-1161.

Vermeesch, P., Drake, N., 2008. Remotely sensed dune celerity and sand flux measurements of the world's fastest barchans (Bodélé, Chad). Geophysical Research Letters, 35(24), L24404.

Werner, B.T., 1995. Eolian dunes: Computer simulations and attractor interpretation. Geology, 23(12), 1107-1110.

Wolfe, S.A., Hugenholtz, C.H., 2009. Barchan dunes stabilized under recent climate warming on the northern Great Plains. Geology, 37(11), 1039-1042.

Chapter 7

Numerical Dune Modelling

This chapter:

- Reviews research on numerical modelling in aeolian systems;
- Introduces the basic algorithm of the Discrete ECo-geomorphic Aeolian Landscape (DECAL) model;
- Introduces new functionality and algorithm of the Extended DECAL;
- Differentiates modelling strategies between short-lived grasses and long-lived shrubs in dune systems;
- Shows how to incorporate real-world fieldwork data into the Extended DECAL to mimic a realistic interaction between Ordos Sagebrush and sand transport in the study region.

Quantifiably modelling dunefield dynamics driven by complex eco-geomorphic interactions remains a constant challenge to aeolian researchers. This chapter, based on empirical field study and the available literature, attempts to provide a possible approach to deal with this challenge, and serves as the foundation for examining the underlying mechanisms of vegetation-driven dune transformations in the following chapters.

7.1 Modelling Aeolian Dune Landscapes

Computer modelling of aeolian landscapes and sand transport processes has been in wide use over the past few decades due to its capability of bridging the gap between different temporal and spatial scales. Numerical simulations serve as an important tool to interpret field data and phenomena observed, to investigate theoretical foundations underlying distinctive landscape patterns, to elucidate possible landscape evolutions and threshold sensitivities, to explore responses to perturbations arising from both

natural and anthropogenic impacts, and to assist in understanding complex system behaviour and planning land management practices.

7.1.1 Background

Landscapes in aeolian systems exhibit complex nonlinear interactions and self-organisation with properties of attractors and emergent behaviour (Baas, 2002; Werner, 1995; Werner, 1999). Two approaches are usually utilised to model behaviour of a complex self-organising system. One traditional approach, representative by continuum models, is to use a set of nonlinear differential equations to represent physical processes involved in the internal dynamics of a system. A system is broken apart into small components representing the underlying fundamental processes that are thought to be crucial in explaining the phenomena observed. The complex behaviour of the system is reduced entirely to variables of these components, which may pose a risk for fully understanding the system behaviour as a whole, because the resulting behaviour of the whole system may not be easily explained by adding together the behaviour of its components. The interactions between components on varying temporal scales are usually constrained by the imposition of artificial boundaries. Some processes, meanwhile, have to be decoupled in order to solve differential equations involved in a model. Limited and incomplete knowledge makes difficult the determination of system components and the prediction of emergent properties underlying a system.

Cellular Automaton (CA) modelling is the other approach. From the 1970s, deterministic chaos and cellular automaton (CA) modelling have been progressively accepted and used in broad scientific disciplines. In a chaotic system, slight differences in initial conditions may result in a completely distinctive end state. This unpredictability of the chaotic systems is determined by the nonlinear interactions between multiple elements. Complex and highly structured phenomena of a chaotic system may be produced by a number of relatively simple local rules. By iteratively applying these rules locally over a certain amount of time, the whole system could manifest higher-level emergent behaviour and exhibit ordered structures. This self-organisation behaviour is the hallmark of a thermodynamically open or dissipative system, in which external continuous flows of matter and energy drive the internal dynamics of the system and keep the system away from the state of thermodynamic equilibrium. Self-organising systems have been proved to be prevalent in the natural world (Baas, 2002).

CA models discretise continuous space into cells on a grid of specified shape: square, triangular or hexagonal. A set of rules and relationships involved in the model are deployed iteratively on individual cells over a number of discrete time steps, and the rules often occur locally between adjacent or neighbouring cells without reference to the global pattern. By repeating the local rules, self-organising systems can present structured patterns on the cellular grid. The CA approach deploys repetitions of a set of simple rules and interactions on a local scale to induce higher-level complex patterns of a self-organising system, avoiding a drawback of artificial boundaries between system components and constraints of conceptual structure imposed by the traditional approach. Despite a great simplicity in algorithms, CA models are capable of reproducing realistic patterns and dynamics on a range of spatial scales, although lacking detailed characteristics on a relatively small scale sometimes (Fonstad, 2006).

7.1.2 Continuum Modelling

Continuum modelling of sand dunes performs numerical solutions of a set of differential equations that describe basic physical mechanisms. Barchans have been widely simulated because of a relatively simple mechanism and stable morphology (Andreotti et al., 2002a; Andreotti et al., 2002b; Duran et al., 2010; Sauermann et al., 2001b; Tsoar, 1989). In these continuum models, different physical processes of aeolian sand transport (e.g., saltation, creep, and collision of individual grains on the sand bed) are distinguished and described by a set of equations on the basis of physical mechanisms or empirical evidence from field or laboratory (e.g. wind tunnel experiment). The trajectory of a saltating grain is simplified to be a ballistic shape. The logarithmic velocity profile is used according to the Law of the Wall in a turbulent boundary layer. The erosion/deposition rate and morphologic change are derived from the mass conservation. External forces on the saltation layer are evaluated from the momentum conservation. In order to keep the morphologic feature of a barchan and mimic flow separation behind slip faces, a heuristic recirculation bubble is introduced to exclude it from the calculation domain along a bounding surface envelope (Andreotti et al., 2002a; Sauermann et al., 2001a; Tsoar, 1989).

Earlier continuum models are restricted to a two-dimensional description of a slice of dunes aligned with unidirectional winds, and neglect the lateral sand transport arising from diffusion and gravity (Andreotti et al., 2002b; Andreotti et al., 2002c; Kroy et al., 2002; Sauermann et al., 2001a). Three dimensional barchans are then simulated by cutting a dune into longitudinal two dimensional slices. The performance of the whole dune is a sum of the contributions from all of these two dimensional slices. A

more fully three-dimensional continuum model is introduced by Hersen (2004), who incorporated the lateral reptation flux to couple barchan slices. Schwämmle and Hermann (2005) employed a similar approach , but included the lateral shear stress that represents the diffusion in the saltation transport rather than reptation flux. They found that the lateral shear stress plays an important role in the manifestation of specific properties of barchan dunes, in particular, the position of slip faces. Duran et al. (2010) further validated the model by comparing simulated barchans with empirical data, reproduced intrinsic instability of barchan fields, and examined the formation of barchans under variable wind strength and different boundary conditions.

The homogeneous corridors of barchans with similar size and spacing have received much attention. Lima et al. (2002) incorporated a lateral movement of sand at horns to simulate inter-dune sand flux, and reproduced the distribution patterns of barchans staying confined within a stripe by assuming that dunes can maintain their stability by adapting themselves to sand exchange. Hersen et al. (2004), however, demonstrated that there are intrinsic instabilities of barchans in response to wind variations and collisions, and proposed that additional mechanisms should be incorporated which regulate and select the size of dunes to form homogeneous barchan corridors (Hersen and Douady, 2005). The formation of this dune pattern is attributed to surface waves caused by the instabilities of barchans by Elbelrhiti et al. (2005). They suggested that the surface waves can break horns into elementary barchans such that the size of dunes can be kept in check and dune patterns are hence maintained. Specific mechanisms controlling the equilibrium and selective dune sizes, nevertheless, remain unclear (Elbelrhiti et al., 2005). Durán et al. (2011) also incorporated sand exchange and collisions of barchans into their model, and are able to reproduce the size distribution of barchans in a Moroccan dunefield, but they failed to reproduce the homogeneity of barchan corridors.

In addition to wide use of modelling approach in understanding evolution of barchan dunes and dunefields, bare sand dune modelling has also been applied to transverse dunes (Schwämmle and Herrmann, 2004) and dunes on Mars and Venus (Claudin and Andreotti, 2006; Parteli and Herrmann, 2007). More recently, Herrmann et al. (2008) have reproduced various shape of dunes observed on Mars, and suggested that induration is another key factor controlling morphologies of Martian dunes.

The continuum model has also been extended to simulate vegetated dunes, in particular, parabolic dunes transformed from barchans. Duran and Herrmann (2006) included a set of differential equations of motion that describe the competition between sand transport and vegetation growth. In the

model, the absorbed shear stress is proportional to the vegetation frontal area density. The vegetation only grows where vegetation growth rate is larger than the change in surface elevation. Vegetation growth rate, meanwhile, has a negative linear relationship with the height of plant. They initiated simulations from a bare barchan surrounded by non-erodible surfaces, and found that vegetation growth on the areas with low sedimentation balance are of particular importance in the transformation from a barchan to a parabolic dune. They further proposed a dimensionless fixation index θ determined by the initial barchan volume, wind strength, and vegetation growth rate, and they suggested that a barchan can only be transformed into a parabolic dune when θ is smaller than 0.5, a threshold that has also been found by (Reitz et al., 2010). Duran et al. (2008) parameterised the model by using field measurements and remote sensing analysis in Brazil, and simulated a parabolic dune developed from a blowout under influence of herbaceous plants, which is, however, only comparable with one in the field in general morphology. The discrepancy might be due to the lack of algorithms that regulate a seasonal change in both wind regime and precipitation. Seasonality is likely to exert a significant impact on vegetation growth and shear stress partitioning in their study region. Furthermore, the same amounts of wind erosion and sand burial have the same influence on the vegetation growth, which may not be realistic for some vegetation species.

Continuum modelling has also been applied to understand the morphology and evolution of coastal dunes. de M. Luna et al.(2011) investigated evolution of dunes which merge from a sand strip upwind and move over vegetated terrain under the controls of unidirectional wind and constant sand flux – a scenario that is analogous to a coastal dune field, and they found dune morphologies are fundamentally determined by wind shear velocity and vegetation growth rate. Duran and Moore (2013) extended the model to include the minimum distance from the shoreline that vegetation is able to build a mature foredune, and found that plant zonation determines the maximum size of foredunes and sand supply determines the timescale of foredune formation.

Despite of a substantial improvement of continuum modelling in the simulations of behaviour in aeolian systems, several drawbacks are substantial. First, these models are usually limited to simulate isolated dunes or interactions between two dunes, and are unable to mimic various patterns in a large landscape because of a lack of sufficient lateral interactions. Second, the scaling between simulated dunes in the model and real dunes in the field is still a challenge, because of inconsistencies in scaling laws employed by different parameters. Third, these models are usually limited to ideal scenarios governed by unidirectional winds, but complex wind regimes with variations of wind direction and intensity are important and more common in the field. Fourth, seasonal variations of wind regime, precipitation, and

groundwater may play an important role in the formation of vegetated dunes, yet have not been included. Finally, because of uniform solutions implemented in a continuum model, some emergent behaviour resulting from complex interactions between multilevel scales or from intrinsic randomness of a system cannot be replicated. For example, these models are not able to generate dunes from a perfectly flat or even sandy surface; instead, they simulate barchans from Gaussian sand piles, and simulate transverse dunes and coastal dunes from a strip of sand with a Gaussian transect. This is due to the fact that the system needs at least a small fluctuation in order to initiate dune growth processes.

7.1.3 Cellular Automaton Modelling

Aeolian sand transport is both nonlinear and dissipative with properties of attractors and emergent behaviour. Werner (1995) employed a set of simple rules that control the sand erosion and deposition locally, and his model is capable of simulating various bare sand dune landforms including barchan, crescentic, transverse, linear, and star dunes (*cf.* details in Section 7.2). He found that systems with different starting conditions may converge over time to an attractor which possesses similar characteristics of dune morphologies. Nishimori and Ouchi (1993) and Nishimori et al. (1998) used a similar CA approach, but explicitly considered two fundamental processes of sand movement: saltation and creep. Saltation is controlled by a slope-effect that changes the transport length based on the local topography, and creep is determined by the convexity of the sandy surface. Their model is also able to replicate realistic barchans, transverse dunes, linear dunes, seif dunes, and network dunes, but not star dunes. Katsuki et al. (2011) applied the model to simulate collisions between migrating barchans, and they found that an additional algorithm of stronger erosion at the reattachment point of the separation flow enables the model to replicate four basic collision patterns (i.e., coalescence, ejection, split, and reorganisation) of aqueous barchans observed in a water tank experiment.

Werner's model (described in more detail further below) is the seminal model of dune landscape CA models because of its great simplicity and capability of replicating realistic dune morphodynamics, based on which new algorithms and improvements are continuously introduced by a number of other researchers. Momiji et al. (2000) incorporated wind acceleration over the stoss slope of transverse dunes via a height-dependent transport length, and acquired more realistic cross-sectional profiles in comparison with the symmetrical cross-sections in Werner's model. They also found that incorporating a non-linear increase in the transport length on the stoss slope can result in a lower dune height and a near-equilibrium

dunefield state (Momiji and Bishop, 2002; Momiji and Warren, 2000). Bishop et al. (2002a) modified Werner's model by taking into account of realistic temporal and spatial scales, and replicated the Wasson and Hyde (1983) phase diagram for bare dune types under different wind regime and sand availability. Pelletier (2009) coupled Werner's model with a model for boundary layer flow over complex topography (Jackson and Hunt, 1975), and demonstrated the roughness length likely controls the height and spacing of ripples and transverse dunes in a steady-state condition. Eastwood et al. (2011) extended Werner's model with various geometries of the sediment source area to investigate the influence of sediment supply and transport capacity on the evolution of dune-field patterns in an open domain (Baas, 2002).

In contrast to classical CA models which use separated sand slabs to mimic sediment transport, Narteau et al. (2005) developed a Boltzmann lattice-gas CA model in which a fluid velocity field and a continuity equation were incorporated within a CA lattice. The dune topography changes through transitions of cells among several basic states pertaining to a grain, transitions that are determined by states of its Von Neumann neighbourhoods. Narteau et al. (2009) determined the length and time scales by comparing simulated superimposed bed forms on barchan and transverse dunes with the characteristic size of those dunes in the real world, and further established a linkage between the characteristic length scale for the formation of dunes in their model and the saturation length in continuum models (Claudin and Andreotti, 2006). The secondary recirculating airflow in the lee of dunes can also be simulated (Zhang et al., 2010). Compared with the traditional CA models, their model can reproduce more realistic barchan, transverse, and star dunes, yet with much more complicated algorithms and computational demand (Zhang et al., 2010; Zhang et al., 2012).

Based on Werner's model for bare dunes, several researchers incorporated an interaction between vegetation and sand transport to reproduce vegetated dunefields. Baas (1996; 2002) introduced vegetation effects into Werner's model and developed the Discrete ECo-geomorphic Aeolian Landscape (DECAL) model. In this model, the interaction between vegetation growth and sand transport is controlled by a growth function (*cf*. details in Section 7.2). The DECAL model has been able to replicate realistic vegetated dune landforms on different spatio-temporal scales. Baas and Nield (2007) and Nield and Baas (2008b) simulated the development of nebkhas under various sediment supply and transport flux using a mesquite-like growth function, and replicated parabolic dunes with typical trailing arms evolved from blowouts using two types of plant species. Nield and Baas (2008a), meanwhile, explored impacts of the peak annual growth of these two types of species on dune development from initially bare, flat surface under different environmental conditions, and compared outputs with real-world dunefields.

Phase spaces and phase diagrams for vegetated dune landscapes were further fully scrutinised by Baas and Nield (2010).

De Castro (1995) simulated the dynamics of a partly-vegetated coastal dune system by including feedback of vegetation growth on an arbitrarily predefined water table. Vegetation only grows where wind erodes surface sufficiently such that vegetation can access groundwater. Any sand deposition would eliminate local vegetation completely. In spite of simplicity, this model can generate a banded pattern of dunes similar to the transverse dunes of the Doñana National Park. Nishimori and Tanaka (2001) adapted the bare dune CA model by Nishimori et al. (1998) to simulate the development of parabolic dunes by incorporating the effect of vegetation in supressing saltation and creep on the one hand and the effect of sedimentation balance on vegetation growth on the other, similar to the approaches in DECAL. Pelletier et al. (2009) modified Werner's model to examine the influence of changes in interdune vegetation on dune height and dune area in North Carolina. The probability of sand entrainment is determined by the local elevation, which indirectly links to vegetation density or surface roughness. The local deposition tolerance, however, is not influenced by vegetation and remains constant. Vegetation growth, meanwhile, would not be directly influenced by sedimentation balance (erosion or deposition), but only through the absolute change in local elevation. Barchyn and Hugenholtz (2012a; 2012b) used a similar approach as Baas and Nield (2007), and simulated the influence of climatic shifts on the stabilisation of highly mobile dune landscapes by introducing vegetation after a predefined dune developing time into the domain initiated from a flat surface. They suggested that the barchan-to-parabolic dune transformation happens when the deposition tolerance of vegetation is larger than the slipface deposition rate of a barchan (Barchyn and Hugenholtz, 2012c).

The CA modelling selects the most fundamental processes and interactions that control the development and evolution of bedform patterns, and can replicate realistic results in the most simplistic manner (Kocurek et al., 2010; Werner, 1999). The CA models hence require much less computational demand as opposed to traditional continuum models, and serve as a useful tool to explore the self-organising dune patterns and dune interactions on large temporal and spatial scales. Among these models, the DECAL model has been well-recognised due to its robust capability to reproduce a variety of realistic looking vegetated dunefields and elucidate eco-geomorphic dynamics over a range of spatio-temporal scales (Baas, 1996; Baas, 2002; Baas and Nield, 2007; Baas and Nield, 2010; Nield and Baas, 2008a; Nield and Baas, 2008b). Herein, the DECAL model is expanded to incorporate various other functionalities to simulate processes of dune stabilisation and reactivation based on real-world data from

dunefields and remote sensing imagery. The following sections first review the basic Werner's algorithm, followed by the DECAL algorithm, based on which the Extended-DECAL algorithm is presented.

7.2 Werner's Algorithm

In Werner's model, topography is simulated by stacks of discrete sand slabs on a Von Neumann neighbourhood cellular lattice with periodic boundaries, which means that sand slabs transported outside of the boundary are brought back into the modelling domain on the opposite side of the lattice (Figure 7-1). A grid cell is randomly picked and the sand slab on top of a sand stack is moved (analogous with wind erosion) over a specified number of lattice sites (l) in the transport direction (analogous with wind direction). At the destination site, whether the sand slab is deposited or not is controlled by a probability of deposition dependent on whether there are existing sand slabs present or not (p_s or p_{ns} respectively). This differentiation arises from a greater likelihood of rebound for saltating grains on a hard rock surface than on a sandy surface (Bagnold, 1941). If the slab is not deposited, it moves another l sites in the transport direction until a deposition occurs. This procedure is repeated a certain number of times to yield the time iterations. The time of iteration is defined as the period during which the number of sand slabs that have been picked to move is equal to the overall number of cells in a domain grid. A polling method with replacement was used, which means a cell is selected randomly each time in the whole grid domain. As a consequence, within an iteration period, some cells may be selected multiple times, whilst some others may not be chosen at all.

Two additional constrains are enforced in the algorithm: shadow zones and the angle of repose. Shadow zones are areas in the leeside of relief where wind flows are decelerated significantly thereby inhibiting further sand transport. A shadow zone is usually defined as an angle of 15˚ from horizontal corresponding to the attachment point downwind estimated as 4 times as long as dune heights (Delgado-Fernandez et al., 2011; Walker and Nickling, 2002). In shadow zones, the probability of deposition is 1 and no erosion takes place. The angle of repose is the steepest angle of slope relative to horizontal plane when loose, dry sand on the slope face is on the verge of sliding, which is approximately 30°. If a slope angle is greater than the angle of repose, sand slabs are moved down the steepest gradient until compliance is achieved.

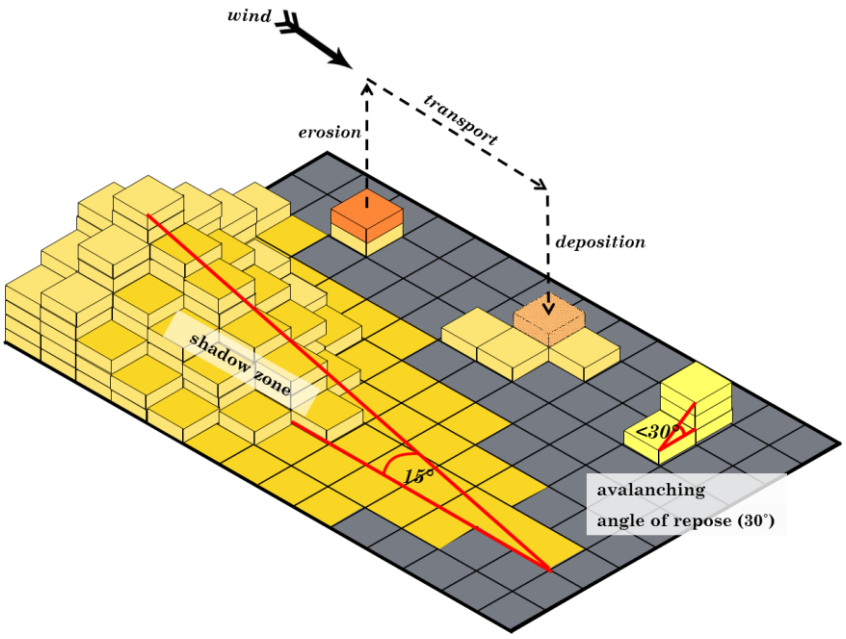

Figure 7-1. Schematic representation of the slab-covered grid, sand transport process and shadow zones in the algorithm. Shaded cells are located in shadow zones. (Baas, 2002)

7.3 DECAL Algorithm

To mimic the interaction between vegetation growth and sediment transport, a vegetation growth function was introduced to represent a dynamic relationship between sedimentation balance and a change in vegetation effectiveness. Vegetation effectiveness (ρ) was loosely conceptualised as the frontal area index or the vegetation coverage, thereby exerting a negative impact on sediment transport (i.e., decreased surface erosion or increased sediment deposition). In DECAL, local erosion probability (p_e) and deposition probability (p_d) in a grid cell are modified linearly as a function of the local vegetation effectiveness (ρ):

$$p_{e(veg)} = p_e - \rho \tag{7-1}$$

$$p_{d(veg)} = p_d + \rho\,(1 - p_d) \tag{7-2}$$

where: $p_{e(veg)}$ and p_e are the erosion probabilities on a surface with and without vegetation respectively, and $p_{d(veg)}$ and p_d are the deposition probabilities on a surface with and without vegetation respectively. If multiple types of vegetation are contained in a cell, their combined influence on erosion and deposition probabilities is obtained by adding up individual ρ values. p_e and p_d are predefined parameters controlled by wind regime and characteristics of sand grains.

Vegetation effectiveness ρ of a certain species is constrained within its physiological range. Pioneer grass species, such as Marram grass, have a short life cycle, and a physiological range of [0, 1] was assigned. In contrast, successional shrub species are more resilient to external forces (e.g., environmental changes), and therefore had a wider physiological range of [-0.5, 1.5]. For all simulations, vegetation effectiveness on non-vegetated surfaces was started with 0. According to Equation 7-1 and 7-2, sand transport is completely shut off when vegetation effectiveness reaches 1. Permitting the vegetation effectiveness to exceed 1 enables plants in a cell to grow to its peak biomass, beyond its maximum influence on sand transport, as nearly all sand transport occurs within 30 cm above ground surface. Vegetation effectiveness between -0.5 and 0 mimics a situation of soil depletion after a shrub dies, and provides a buffer period for revegetation. Furthermore, the angle of repose is increased to 40˚ when ρ is larger than 0.3, which enables a steeper slope to form on vegetated surfaces.

The vegetation effectiveness (ρ) of each species in a cell was updated every modelling year based on the local sedimentation balance, defined by its growth function that reflects its capability of withstanding erosion and sand burial. Examples of vegetation growth functions representing typical grass species and shrub species are shown in Figure 7-2. Pioneer grass species, as shown in the green line, usually have strong capability of withstanding sand burial. In effect, they often need a small amount of sand burial in order to maintain their optimal growth (sedimentation balance is positive when the change in ρ is 0). Erosion, however, is lethal to their growth (change in ρ is negative when sedimentation balance is negative). Shrub species, in contrast, as shown in the red line, can tolerate a certain degree of both erosion and sand burial, and the optimal growth in this example happens where sedimentation balance is neutral. Nonetheless, no plant species can survive from severe erosion and sedimentation burial.

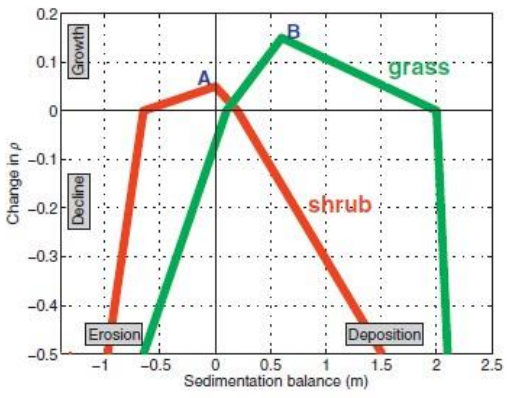

Figure 7-2. Growth functions of two typical vegetation species used in DECAL (Baas and Nield, 2010).

In addition to the primary improvement regarding the incorporation of the interactions between vegetation and sand transport, several other important adjustments were involved in the DECAL in comparison with other CA models. Firstly, the transport length (l) was enforced to one cell width, which ensures a moving sand slab cannot pass through intervening local influence such as vegetation. Secondly, a polling method without replacement was introduced, and every grid cell is polled exactly once per iteration in a random cell sequence. This avoids un-proportional selection of sand slabs that happens in the Werner's Model. Thirdly, a circular domain was used when rotating and resampling a domain, enabling multiple wind directions at any angle. Furthermore, sediment was conserved, although edge effects were still substantial, in particular, during long-run simulation scenarios (Bishop et al., 2002b; Narteau et al., 2005; Nield and Baas, 2008b).

The DECAL model has been widely recognised due to its capability of modelling morphogenesis and dynamics of complex systems efficiently with a simple algorithm, large diversity, and less computational demand; nevertheless, some problems remain. The scaling of the model is not strictly defined such that the comparison between modelling results and observations in the field is difficult and mostly limited to qualitative analogy. Vegetation effectiveness cannot be directly connected to field measurements, and the vegetation growth function is somewhat conceptual. Quantifiably comparing modelling results with the natural reality has been an on-going challenge.

7.4 Extended-DECAL Algorithm

To mimic the eco-geomorphic interactions in different aeolian systems, several issues are addressed in the Extended-DECAL. A seed germination process is introduced to address different impacts of the same sedimentation balance on seed germination and plant growth. Then, different modelling strategies of annual grasses and perennial shrubs are compared and discussed, based on which seasonality and a dynamic growth function of clump-like perennials is proposed and elucidated. Furthermore, approaches of evaluating possible impacts arising from both environmental changes and anthropogenic pressures are presented.

7.4.1 New Perspective of Growth Function and Seed Germination

In the original DECAL, the range of vegetation effectiveness that can exert impacts on sand transport is a subset of its physiological range. To simulate the growth of clump-like perennials, the Extended-DECAL employs a similar approach, but adopts a different perspective. The physiological range of a certain type of vegetation species denotes a gradient between seed germination to peak biomass. Vegetation effectiveness on bare surface is initialised with the physiological minimum. Plants in a grid cell germinate, grow, and do not influence sand transport until the vegetation effectiveness in the cell reaches over 0. A negative ρ denotes a state when vegetation has grown on the surface, yet is not sufficient to impede sand transport. This is an analogue of the growth trajectory of perennial species especially shrubs in reality, in which a shrub may have germinated and grown some twigs but cannot effectively influence the process of sand transport until it grows to a certain minimal size.

A typical simplified growth function is shown in Figure 7-3. In this example, vegetation in a cell is able to grow within a scope of certain amount of erosion and sand burial (a, b). Vegetation also starts to germinate in this range on bare dune surfaces, but may not yet be able to influence sand transport. Vegetation grows best (m, maximum positive change in ρ) when the sedimentation balance is neutral. The sedimentation balance can be regarded as a representative of the average mobility of the dune surface within an updating interval (i.e., a modelling year in the original DECAL). A smaller absolute sedimentation balance denotes a relatively stable surface on which seeds can germinate more easily. A small amount of sand burial sometimes may stimulate the growth of vegetation in an aeolian environment.

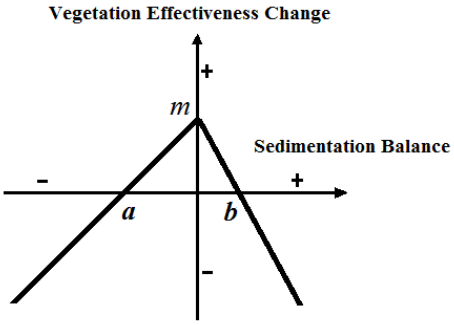

Figure 7-3. Schematic graph of a simplified growth function.

The seed germination range for some plant species may not necessarily be the same as the positive feedback range (a, b). The same amounts of sedimentation balance often have significantly

different impacts on the growth of mature plants as opposed to the germination of seeds. An additional germination algorithm may be of particular importance in the vegetation-sand transport interaction. A germination range of sedimentation balance is hence specified in the algorithm. Seeds can only germinate on bare dune surfaces where sedimentation balance is within this range. A vegetation growth function only applies to the grid cells in which seeds have germinated. When vegetation in a cell is eradicated due to either erosion or sand burial (i.e., ρ decreases to its physiological minimum), vegetation cannot grow again in the cell until its germination condition is met. If more than one type of vegetation is used in the model, different species may require different germination conditions.

7.4.2 Impacts on Sand Transport: Annual Grasses vs. Clump-like Perennials

The interaction between vegetation and sand transport is to a large extent determined by the characteristics of plant species. Annual grasses and clump-like perennials (e.g., shrubs) are commonly found in both coastal and inland dune systems and can be regarded as two basic categories in each of which different species share some crucial and fundamental features.

Annual grasses are short-lived with shallow roots and unlikely to access groundwater, and hence only survive on precipitation. They usually germinate and grow rapidly after an episodic rainfall event, but die of drought shortly afterwards. Some pioneer grass species can tolerate substantial sand burial. Some species even require a small amount of sand burial in order to maintain their optimal growth. These grasses are distributed relatively uniformly and spread over the surface; consequently, their ability to reduce sand transport is primarily determined by an overall coverage rather than the canopy of a single grass element. A surface cover of ~15% has been found to completely cease any sand transport (Lancaster and Baas, 1998; Wiggs et al., 1995). Accordingly, the vegetation effectiveness of these grass species in a cell (assuming 1 by 1 m^2) reflects the overall coverage of the grass assembly (Figure 7-4).

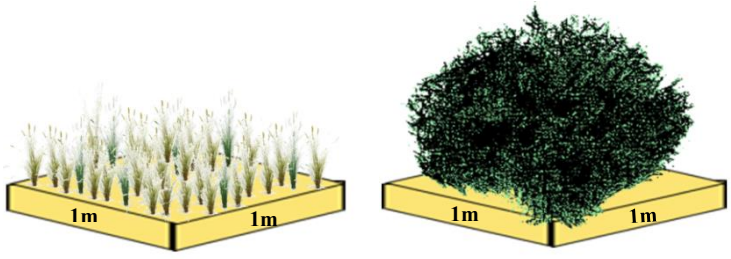

(a) (b)

Figure 7-4. Schematic graphs of different growth forms of vegetation: (a) uniform grass vs. (b) shrub.

In contrast to annual grasses, clump-like perennials such as shrubs are long-lived with spread roots. In dune systems, they are usually distributed relatively sparsely and have outstanding canopies, thereby exerting impacts on sand transport as individual entities. Individual shrubs can significantly modify the wind velocity profile near the surface and create zones of accelerated- and decelerated-airflows. As shown in Figure 7-5, a wake region usually develops downwind of a roughness element (a single plant) in which wind flows are separated from the surrounding air mass and are decelerated (Wolfe and Nickling, 1993). As the airflow is compressed and forced to move around of the roughness element, horseshoe vortices may develop by the accelerated airflow on both sides. Shrubs retard sand particles and the associated sand accumulation in and behind plants can lead to the formation of nebkhas (Ranwell, 1972; Tengberg, 1995) and sand shadows (Hesp, 1981) respectively. Spatial distribution of shrubs hence significantly influences erosion and deposition patterns and the associated large-scale dune landscapes (Figure 7-6).

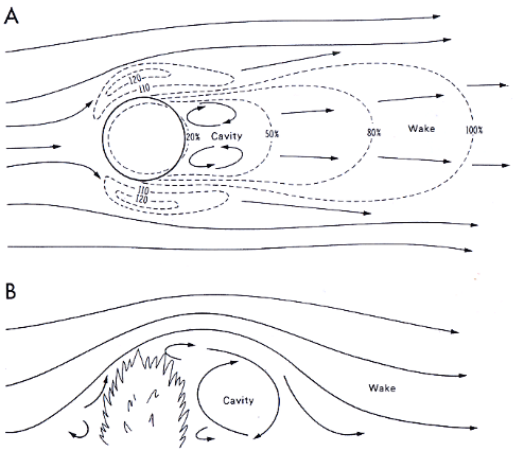

Figure 7-5. (A) Percentage wind speed and streamlines (in plan) around a bush. (B) Streamlines and separation (in section) around a bush (Ash and Wasson, 1983).

Figure 7-6. Airflow acceleration between two shrubs and deceleration behind.

In the study region, the average coverage of an individual Ordos Sagebrush is at the magnitude of 1 by 1 meters according to fieldwork investigations. The model hence uses a spatial resolution of 1 × 1 m^2 as the default resolution, and assumes only one shrub can exist within each grid cell (Figure 7-4). Unlike annual grasses which grow rapidly in a few days and spread over the surface, a shrub in a grid cell needs relatively longer time (on a monthly basis) to germinate and grow to a certain size before being able to reduce erosion and trap sand. During this period, a shrub seedling, meanwhile, may die of severe erosion. The vegetation effectiveness of shrub species in a cell is directly related to the size or coverage of an individual shrub (*cf.* Section 7.4.6).

7.4.3 Dynamic Growth Functions

The growth of the Ordos Sagebrush, the dominant species in the study region, is strongly controlled by a regional climatic seasonality, as discussed in section 4.4. The Ordos Sagebrush germinates and starts to grow leaves in April, produces shoots in June, and reaches its prime in September (Lin, 1991). Then, its leaves turn yellow and are shed gradually. There are two types of branches for the Ordos Sagebrush: foliage branches and reproductive branches. Foliage branches can form dormant buds and continue to grow in the next year, whilst reproductive branches only grow in the current year and die in the winter. Like the Ordos Sagebrush, many species have a similar seasonal growth throughout a year, which can be simplified into two types of distinctive periods: growing seasons and non-growing seasons. Meanwhile, the perennial species are characterized by a continuous growth over a few years. The Ordos Sagebrush in the study region, for example, may live even more than ten years.

In the Extended-DECAL, the influence of seasonality on vegetation growth is included. A simplified example regarding a change in vegetation effectiveness throughout a year is shown in Figure 7-7. In the black line, a positive growth rate α, denoting an increasing influence on sediment transport, occurs in the growing season (from April to September). The positive growth rate α reflects the peak growth of vegetation in its typical climate when sedimentation balance is neutral (*cf.* point *m* in Figure 7-3). A negative 'growth' rate β, representing a decreasing impact on sand transport such as leaves-shedding, is present in the non-growing season (from October to March). Nevertheless, vegetation may not grow and influence sand transport in such a linear way as the black line; instead, it may show a behavior like the red curve for example, in which case the growth rate α is progressively increasing through a growing season. Both 'growth' rates α and β denote vegetation effective change in a typical

environment without the influence of sedimentation transport, and may be varying dependent on the size or age of individual plants (*cf.* Section 7.4.6). An updating interval of three months is used to simulate the evolution of dune landforms in the study region (4 updates per year). This is different from the original DECAL in which vegetation is assumed to grow throughout the whole year and the updating of vegetation effectiveness only occurs at the end of each modeling year.

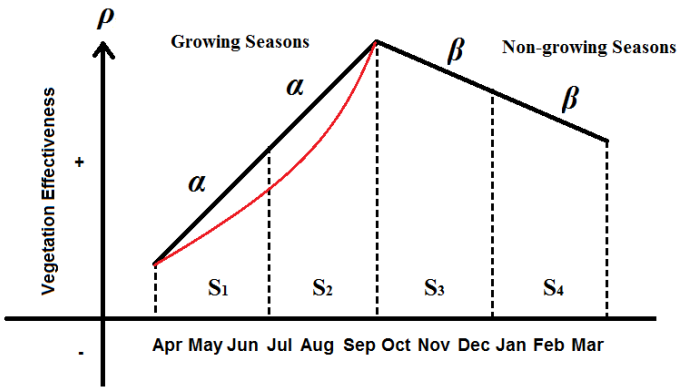

Figure 7-7. A simplified example of vegetation natural growth throughout a year for a situation when sedimentation balance is neutral. α and β are the 'growth' rate of vegetation in growing seasons and non-growing seasons respectively. S1, S2, S3 and S4 denote four different seasons. The red curve shows an example in which vegetation growth rate is nonlinear.

In comparison with the original DECAL in which fixed growth fuctions are employed throughout a year, the Extended DECAL employs 'dynamic' growth functions that are governed by seasonality. Different growth functions are used in the growing seasons and non-growing seasons. Examples of growth functions (vegetation effectiveness change vs. sedimentation balance) in both growing seasons and non-growing seasons are shown in Figure 7-8. The red line is a vegetation growth function in the growing seasons. Within the sedimentation balance range (a, b), vegetation maintains its ability to keep growing. Outside of this range, vegetation suffers negative impacts and even dies when erosion or sand burial is larger than its maximum erosion or burial tolerance respectively. In the non-growing seasons, a plant stops growing and starts to shed leaves, resulting in a decrease of vegetation effectiveness at a natural 'growth' rate of β (negative) and an attenuated impact on sediment transport. Both erosion and sand burial, meanwhile, are likely to exacerbate the decline of a plant in the non-growing seasons as the growth function shown in the blue line.

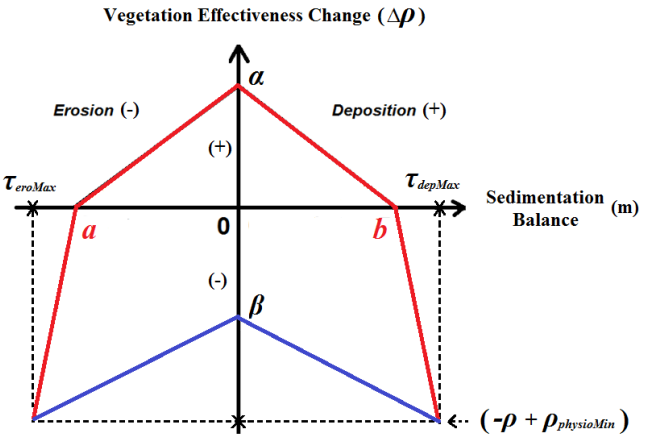

Figure 7-8. Examples of growth functions in both growing seasons (red lines) and non-growing seasons (blue lines). Maximum negative change of vegetation effectiveness is $(-\rho + \rho_{physioMin})$ to ensure that vegetation can (only) be reduced to $\rho_{physioMin}$.

Not only does the 'growth' rate of vegation depend on seasons and the age or size of individual plants, growth functions are 'dynamic' also because the maximum erosion tolerance (τ_{eroMax}) and the maximum depsoition tolerance (τ_{depMax}) are not fixed, but instead are also determined by vegetation effectiveness (ρ) before an updating. This mimics a reality that vegetation has a different capability of withstanding erosion and sand burial dependent on which stage of its life cycle a plant is in. Compared with small seedlings, bigger, mature plants (in particular perennial shrub species) usually have greater resilience to changes in environmental forces (e.g., erosion and sand burial in this case). A taller plant can endure more severe sand burial. Some species can even survive as long as plants are not completely submerged by sand. Bigger, mature plants also have extensive roots, helping anchor plants on the ground, keeping sand in check, and resisting wind erosion.

In the model, the capabilities of a plant to withstand wind erosion [τ_{eroMax}, m] and sand burial [τ_{depMax}, m] within which the plant can survive are linearly scaled with its present vegetation effectiveness (ρ) that relates closely to its state or size:

$$\tau_{eroMax} = \frac{\rho - \rho_{physioMin}}{\rho_{physioMax} - \rho_{physioMin}} \tau_{E\_physioMax} \quad (7\text{-}3)$$

$$\tau_{depMax} = \frac{\rho - \rho_{physioMin}}{\rho_{physioMax} - \rho_{physioMin}} \tau_{D\_physioMax} \quad (7\text{-}4)$$

where: $\tau_{E\_physioMax}$ and $\tau_{D\_physioMax}$ are erosion tolerance and deposition tolerance when vegetation is at $\rho_{physioMax}$, [m season^{-1}].

The 'a' and 'b' in Figure 7-7 are assumed to be a percentage (φ) of its maximum erosion tolerance (τ_{eroMax}) and maximum deposition tolerance (τ_{depMax}) respectively for simplification, as shown below:

$$a = \varphi\tau_{eroMax} \tag{7-5}$$

$$b = \varphi\tau_{depMax} \tag{7-6}$$

The growth function in the growing seasons denoted by the red line is comprised of 4 piecewise functions. Vegetation effectiveness change ($\Delta\rho$) is obtained by substituting sedimentation balance within an updating interval [$\Delta\rho$, m] to one of the four piecewise functions accordingly:

$$\Delta\rho = f(\Delta h) = \begin{cases} -\frac{\rho - \rho_{physioMin}}{(1-\varphi)\tau_{eroMax}}\Delta h + (\frac{\varphi}{1-\varphi})(\rho - \rho_{physioMin}), & \Delta h \le a \\ -\frac{\alpha}{\varphi\tau_{eroMax}}\Delta h + \alpha, & a < \Delta h \le 0 \\ -\frac{\alpha}{\varphi\tau_{depMax}}\Delta h + \alpha, & 0 < \Delta h \le b \\ -\frac{\rho - \rho_{physioMin}}{(1-\varphi)\tau_{depMax}}\Delta h + (\frac{\varphi}{1-\varphi})(\rho - \rho_{physioMin}), & \Delta h > b \end{cases} \tag{7-7}$$

The growth function in the non-growing seasons denoted by the blue line is comprised of 2 piecewise functions, as shown below:

$$\Delta\rho = f(\Delta h) = \begin{cases} -\frac{\rho - \rho_{physioMin} + \beta}{\tau_{eroMax}}\Delta h + \beta, & \Delta h < 0 \\ -\frac{\rho - \rho_{physioMin} + \beta}{\tau_{depMax}}\Delta h + \beta, & \Delta h \ge 0 \end{cases} \tag{7-8}$$

7.4.4 Climatic Impacts

As mentioned in the previous sections, α is the growth rate of an individual plant in the growing seasons under its typical climatic environment in the absence of sedimentation effects. Any change of climatic factors leading to the change of water availability may significantly influence the vitality and the growth rate of local plant species. Water availability is particularly crucial to plants in their growing seasons, whereas it is likely to exert a minimal impact on plants in the non-growing seasons. Therefore, climatic impacts on the vegetation growth are incorporated in the model through an influence on plant natural growth rate (α) in the growing seasons.

Perennials like shrubs at different stages of their life cycles usually have different stress-resilience to external forces. Different plant species, meanwhile, may have different sensitivities to

respond to the same climatic change and have different capabilities of maintaining its optimal growth. The more sensitive a vegetation species is, the more intensively the vegetation responds to the same climatic change. The change of natural growth rate arising from a climatic impact ($\Delta\alpha_{climate}$) is hence simplified as the equation below:

$$\Delta\alpha_{climate} = I_{climate}\, S_{veg}\alpha^{i} \tag{7-9}$$

where: $I_{climate}$ denotes the climatic impact arising from periodic environmental fluctuations or long-trend climatic change; S_{veg} denotes the sensitivity of a specific plant species to respond to the climatic impact, [0, 1]; and i is a curve factor dependent on plant species and environmental forces. A positive climatic impact promotes the growth of vegetation; and vice versa, a negative climatic impact discourages the growth of vegetation.

7.4.5 Grazing Pressure

Overgrazing is one of the most significant pressures on vegetation in dune systems brought about by human beings (Ravi et al., 2010). Here the model simulates a situation in which animals are roaming around and eating a small portion of plant at each stop or time until their demands are satisfied. Forage demand per year (δ), defined by vegetation effectiveness in the model, is primarily controlled by the number of livestock, the amount of forage needed per capita per foraging time, and the grazing frequency. Forage demand per iteration (ε) can be expressed as:

$$\varepsilon = \frac{\delta}{\sum_{1}^{n} I_i} \tag{7-10}$$

where: n is the number of growing seasons per year; and I_i is the number of iterations at the i^{th} growing season.

Every grid cell in the modelling domain is assumed to have an equal probability to offer forage to animals. Once a grid cell is randomly selected, it will provide animals with a certain amount of vegetation ($\Delta\rho_g$) that is proportional to its available vegetation as the equation below:

$$\Delta\rho_g = \gamma(\rho - \rho_{physioMin}) \tag{7-11}$$

where: γ is the predefined rate of a plant to be consumed by animals each time, 0.05 by default. This process is repeated until the overall vegetation assumed by animals meets the forage demand per iteration (ε).

If multiple vegetation species exist in a model, a relative preference degree of each species can be assigned within a range of [0, 1]. Preference degrees of multiple species should add up to 1. For example, if two type of vegetation (*vegA* and *vegB*) are used in a model, relative preference degrees of 0.8 for *vegA* and 0.2 for *vegB* denote that *vegA* is much more preferable by animals in comparison to *vegB*. A relative preference degree of 0 represents an inedible species. Forage demand per iteration for different species (ε_v) can hence be expressed as:

$$\varepsilon_v = \varepsilon P_v \tag{7-12}$$

where: P_v is the preference degree of a plant species.

7.4.6 Customising the Growth Function to the Dominant Species: Ordos Sagebrush

Most perennial species, in particular, shrubs like the Ordos Sagebrush, have different capability of growing and responding to the same amount of sedimentation balance at different stages of their life cycles. Although occasionally the Ordos Sagebrush can propagate themselves from clonal branches, its natural propagation is predominately from seeds. Like most species, the growth of the Ordos Sagebrush is not a liner process over its entire life cycle. A plant germinates and grows rapidly first in the vertical direction without a significant augmentation of its canopy. After reaching a certain height, the plant grows largely in the horizontal direction with an outstanding expansion of the canopy, and the vertical development dwindles to a minimum. The dimension or size of a plant, therefore, can be used as a simple indicator to estimate its age. This assumption can be expressed as:

$$age \propto \sqrt[3]{V} \tag{7-13}$$

where: V is the canopy volume, [m^3]. The vegetation effectiveness (ρ) in a grid cell is assumed to be linearly correlated to the canopy cover area (S_c in Equation 5-2). The relationship between the vegetation effectiveness and the plant age can then be deduced by acquiring the relationship between the canopy cover area (S_c) and the canopy dimension ($V^{1/3}$).

A spatial resolution of 1 × 1 m^2 was chosen to mimic the growth of individual shrubs, as field measurements shows that 73 % of measured plants have a canopy cover area within 1 m^2 (*cf.* Section 5.3.3. & Figure 5-10) in agreement with the pervious findings from the literature suggesting that the maximum canopy coverage of the Ordos Sagebrush can achieve at the magnitude of 1.0 m^2 (*cf.* Section 4.4). Those larger shrubs measured are usually nebkhas or the aggregation of several shrubs and thus not good representatives of natural vegetation growth in the absence of sand transport. The growth curve of shrubs within a grid cell (1 × 1 m^2) is of particular importance also because it determines the extent to which sand transport is reduced, whereas larger shrubs can completely eliminate any sand transport regardless of their exact sizes. Plants with a canopy cover area below 1 m^2 are hence focused in the model. Figure 7-9 shows the relationship between the canopy cover area (up to 1 m^2) and the canopy dimension of the Ordos Sagebrush, as determined from the field measurements. Each point represents a shrub measured in the field (*cf.* Section 5.3.3). A spectrum of 2 was used as the physiological range. The canopy cover of each shrub with a range of [0, 1] m^2 in Figure 7-9 was then linearly scaled as vegetation effectiveness with a range of [0, 2]. The canopy dimension corresponding to the canopy cover area of 1 m^2 was determined from the regression function acquired from Figure 7-9, which is 0.91 m. According to field observations and literature research (*cf.* Section 4.4), it takes approximately 3 years for the Ordos Sagebrush in the study region to develop a canopy cover of 1 m^2. Hence, the dimension of each shrub in the range of [0, 0.91] m was scaled as the shrub age with the range of [0, 3] yr. The resulting relationship between vegetation effectiveness and shrub age is shown in Figure 7-10.

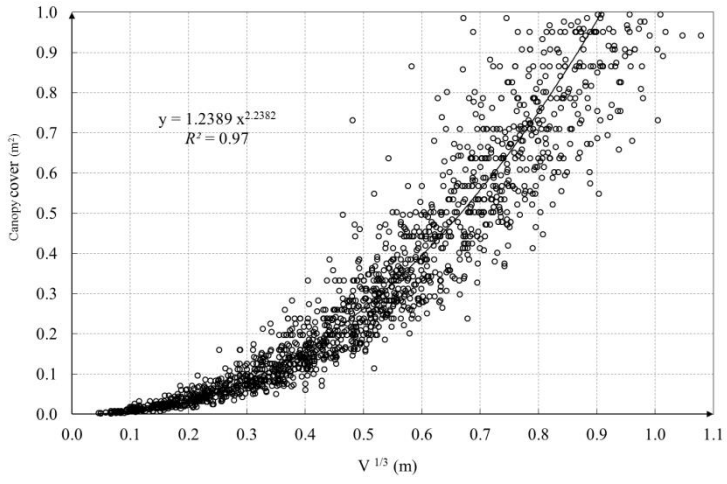

Figure 7-9. Relationship between plant dimension and canopy cover of Ordos Sagebrush measured in the field.

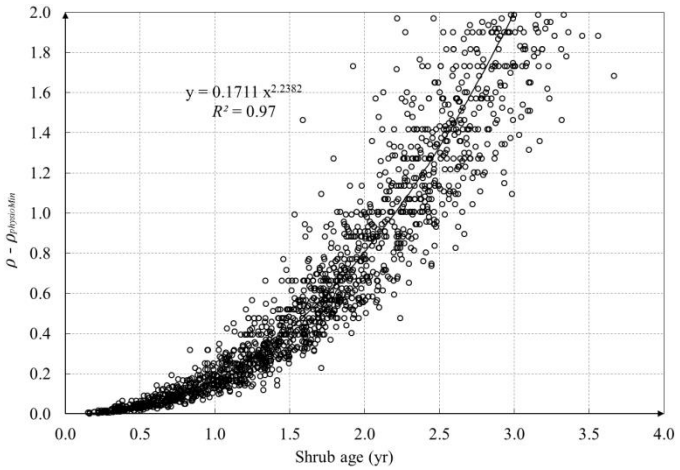

Figure 7-10. Relationship between shrub age and vegetation effectiveness of Ordos Sagebrush used in the model.

The yearly growth rate of a plant (v) at different ages can then be obtained from the derivative of the regression function in Figure 7-10:

$$v = \frac{\partial \rho}{\partial t_{age}} = 0.3830 {t_{age}}^{1.2382} \tag{7-14}$$

Given the vegetation effectiveness, the age of a plant (t_{age}) can be deduced:

$$t_{age} = \sqrt[2.2382]{\frac{\rho - \rho_{physioMin}}{0.1711}} \tag{7-15}$$

As an updating interval of 3 month was used, there are two growing seasons and two non-growing seasons in a year. Vegetation natural growth only occurs in the growing seasons. Hence, vegetation natural growth rate (α) is half of the yearly growth rate (v):

$$\alpha = 0.5v = 0.1915 \left(\frac{\rho - \rho_{physioMin}}{0.1711}\right)^{0.5532} \tag{7-16}$$

As can be seen from the equation above, natural growth rate in the model algorithm is determined by existing vegetation effectiveness that indirectly reflects the vegetation size or age. The 'growth' rate of vegetation in the non-growing seasons (β), meanwhile, is simply assumed to be proportional to its existing vegetation effectiveness:

$$\beta = \eta(\rho - \rho_{physioMin}) \tag{7-17}$$

where: η is the decline coefficient of vegetation in the non-growing seasons, within a range of [0, 1]. Examples of dynamic growth functions are shown in Figure 7-9.

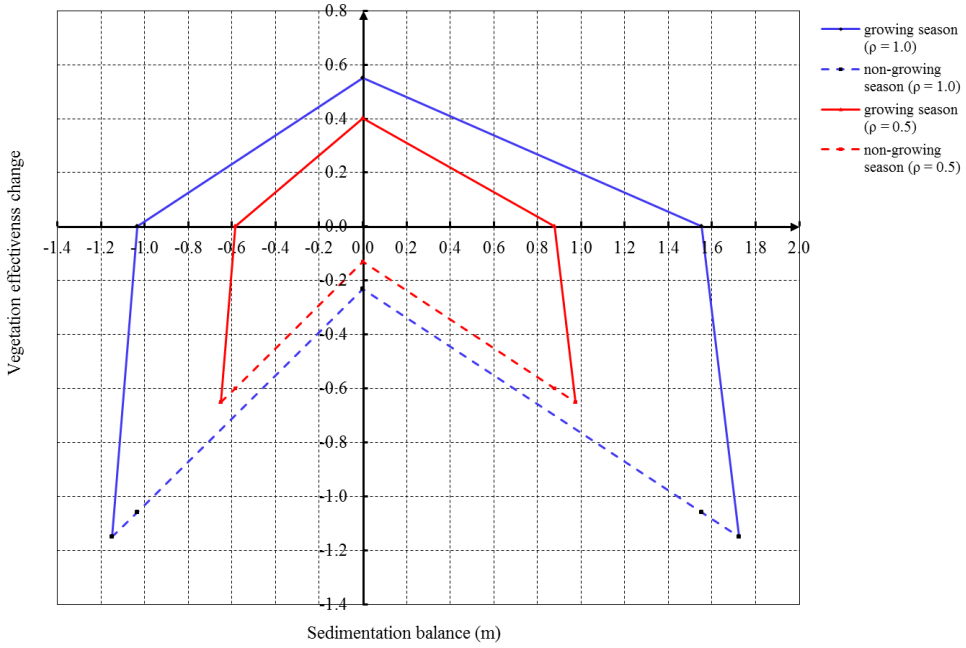

Figure 7-11. Examples of dynamic growth functions in the growing seasons and non-growing seasons when ρ is 1.0 and 0.5 respectively. φ is 0.9 in these cases.

According to the literature and field observation, a shrub germinates and starts to influence sand transport near the end of the first year when vegetation effectiveness is ~0.15 (calculated from the regression equation in Figure 7-10). This leads to a canopy cover of 0.08 m^2, which seems realistic as the threshold for a plant to start exerting an impact on sand transport. The physiological range of the vegetation effectiveness is accordingly defined as [-0.15, 1.85] in absolute terms.

Summary:

This chapter reviewed numerical models to simulate aeolian dune landscapes, discussed the original DECAL algorithm, and introduced the new algorithm of the Extended DECAL including seasonality, dynamic growth functions, climatic impacts (water availability), and anthropogenic pressures (grazing). Meanwhile, based on field work study and the literature, the model was customised to adapt to the dominant species, the Ordos Sagebrush, in the study region. The process provides a good example to show how to transfer data investigated in the field to parameters in the model. The following three chapters will fully explore transformations between barchan and parabolic dunes, examine their fundamental controls, and predict potential dunefield reactivation under the impacts of climatic changes and human disturbances.

To sum up, parameters to fully define the characteristics of a vegetation species in the model include:

a) seed germination range;

b) vegetation physiological range: $\rho_{physioMax}$ and $\rho_{physioMax}$;

b) vegetation maximum erosion and deposition tolerances: $\tau_{E\_physioMax}$ and $\tau_{D\_physioMax}$;

c) the shape factor of vegetation growth function: φ;

d) the sensitivity of vegetation species to respond to the climatic impact: S_{veg};

e) the consumption rate per visit by animals: γ;

f) the decline coefficient of vegetation in the non-growing seasons: η; and

g) the coefficients in the regression equation $\rho = f(t_{age})$.

References

Andreotti, B., Claudin, P., Douady, S., 2002a. Selection of dune shapes and velocities Part 2: A two-dimensional modelling. The European Physical Journal B - Condensed Matter and Complex Systems, 28(3), 341-352.

Andreotti, B., Claudin, P., Douady, S., 2002b. Selection of dune shapes and velocities. Part 1: Dynamics of sand, wind and barchans. Eur. Phys. J. B, 28(3), 321-339.

Andreotti, B., Claudin, P., Douady, S., 2002c. Selection of dune shapes and velocities. Part 2: A two-dimensional modelling. The European Physical Journal B - Condensed Matter and Complex Systems, 28(3), 341-352.

Ash, J.E., Wasson, R.J., 1983. Vegetation and sand mobility in the Australian desert dunefield. Zeitschrift fur Geomorphologie Supplementband, 45, 7-25.

Baas, A.C.W., 1996. Stochastic Dune Model for the Simulation of Dune Landscapes under Desert and Coastal Conditions. MSc. thesis, University of Amsterdam, Amsterdam, 47 pp.

Baas, A.C.W., 2002. Chaos, fractals and self-organization in coastal geomorphology: simulating dune landscapes in vegetated environments. Geomorphology, 48(1-3), 309-328.

Baas, A.C.W., Nield, J.M., 2007. Modelling vegetated dune landscapes. Geophysical Research Letters, 34(6).

Baas, A.C.W., Nield, J.M., 2010. Ecogeomorphic state variables and phase-space construction for quantifying the evolution of vegetated aeolian landscapes. Earth Surface Processes and Landforms, 717-731.

Bagnold, R.A., 1941. The physics of blown sand and desert dunes. Methuen & Co. Ltd, London.

Barchyn, T.E., Hugenholtz, C.H., 2012a. Aeolian dune field geomorphology modulates the stabilization rate imposed by climate. Journal of Geophysical Research, 117(F2).

Barchyn, T.E., Hugenholtz, C.H., 2012b. Predicting vegetation-stabilized dune field morphology. Geophysical Research Letters, 39.

Barchyn, T.E., Hugenholtz, C.H., 2012c. A process-based hypothesis for the barchan-parabolic transformation and implications for dune activity modelling. Earth Surface Processes and Landforms, 37(13), 1456-1462.

Bishop, S.R., Momiji, H., Carretero-Gonzalez, R., Warren, A., 2002a. Modelling desert dune fields based on discrete dynamics. Discrete Dynamics in Nature and Society, 7(1), 7-17.

Bishop, S.R., Momiji, H., Carretero, G., x000E, lez, R., Warren, A., 2002b. Modelling desert dune fields based on discrete dynamics. Discrete Dynamics in Nature and Society, 7(1), 7-17.

Claudin, P., Andreotti, B., 2006. A scaling law for aeolian dunes on Mars, Venus, Earth, and for subaqueous ripples. Earth and Planetary Science Letters, 252(1–2), 30-44.

De Castro, F., 1995. Computer simulation of the dynamics of a dune system. Ecological Modelling, 78(3), 205-217.

de M. Luna, M.C.M., Parteli, E.J.R., Durán, O., Herrmann, H.J., 2011. Model for the genesis of coastal dune fields with vegetation. Geomorphology, 129(3-4), 215-224.

Delgado-Fernandez, I., Jackson, D.W.T., Cooper, J.A.G., Baas, A.C.W., Lynch, K., Beyers, J.H.M., 2011. Re-attachment zone characterisation under offshore winds blowing over complex foredune topography. Journal of Coastal Research, 273-277.

Duran, O., Herrmann, H.J., 2006. Vegetation against dune mobility. Physical Review Letters, 97(18), 188001/188001-188004.

Duran, O., Moore, L.J., 2013. Vegetation controls on the maximum size of coastal dunes. Proceedings of the National Academy of Sciences of the United States of America, 110(43), 17217-17222.

Duran, O., Parteli, E.J.R., Herrmann, H.J., 2010. A continuous model for sand dunes: Review, new developments and application to barchan dunes and barchan dune fields. Earth Surface Processes and Landforms, 35(13), 1591-1600.

Durán, O., Schwämmle, V., Lind, P.G., Herrmann, H.J., 2011. Size distribution and structure of Barchan dune fields. Nonlin. Processes Geophys., 18(4), 455-467.

Duran, O., Silva, M.V.N., Bezerra, L.J.C., Herrmann, H.J., Maia, L.P., 2008. Measurements and numerical simulations of the degree of activity and vegetation cover on parabolic dunes in north-eastern Brazil. Geomorphology, 102(3-4), 460-471.

Eastwood, E., Nield, J., Baas, A., Kocurek, G., 2011. Modelling controls on aeolian dune-field pattern evolution. Sedimentology, 58(6), 1391-1406.

Elbelrhiti, H., Claudin, P., Andreotti, B., 2005. Field evidence for surface-wave-induced instability of sand dunes. Nature, 437(7059), 720-723.

Fonstad, M.A., 2006. Cellular automata as analysis and synthesis engines at the geomorphology–ecology interface. Geomorphology, 77(3–4), 217-234.

Herrmann, H.J., Durán, O., Parteli, E.J.R., Schatz, V., 2008. Vegetation and induration as sand dunes stabilizators. Journal of Coastal Research, 1357-1368.

Hersen, P., 2004. On the crescentic shape of barchan dunes. The European Physical Journal B - Condensed Matter, 37(4), 507-514.

Hersen, P., Andersen, K.H., Elbelrhiti, H., Andreotti, B., Claudin, P., Douady, S., 2004. Corridors of barchan dunes: Stability and size selection. Physical Review E, 69(1), 011304.

Hersen, P., Douady, S., 2005. Collision of barchan dunes as a mechanism of size regulation. Geophysical Research Letters, 32(21), L21403.

Hesp, P.A., 1981. The formation of shadow dunes. Journal of Sedimentary Petrology, 51(1), 101-112.

Jackson, P.S., Hunt, J.C.R., 1975. Turbulent wind flow over a low hill. Quarterly Journal of the Royal Meteorological Society, 101(430), 929-955.

Katsuki, A., Kikuchi, M., Nishimori, H., Endo, N., Taniguchi, K., 2011. Cellular model for sand dunes with saltation, avalanche and strong erosion: collisional simulation of barchans. Earth Surface Processes and Landforms, 36(3), 372-382.

Kocurek, G., Ewing, R.C., Mohrig, D., 2010. How do bedform patterns arise? New views on the role of bedform interactions within a set of boundary conditions. Earth Surface Processes and Landforms, 35(1), 51-63.

Kroy, K., Sauermann, G., Herrmann, H.J., 2002. Minimal Model for Sand Dunes. Physical Review Letters, 88(5), 054301.

Lancaster, N., Baas, A.C.W., 1998. Influence of vegetation cover on sand transport by wind: Field studies at Owens Lake, California. Earth Surface Processes and Landforms, 23(1), 69-82.

Lima, A.R., Sauermann, G., Herrmann, H.J., Kroy, K., 2002. Modelling a dune field. Physica A: Statistical Mechanics and its Applications, 310(3–4), 487-500.

Lin, Y.Z., 1991. Flora of China, 76(2). Science Press, Beijing.

Momiji, H., Bishop, S.R., 2002. Estimating the windward slope profile of a barchan dune. Sedimentology, 49(3), 467-481.

Momiji, H., Carretero-González, R., Bishop, S.R., Warren, A., 2000. Simulation of the effect of wind speedup in the formation of transverse dune fields. Earth Surface Processes and Landforms, 25(8), 905-918.

Momiji, H., Warren, A., 2000. Relations of sand trapping efficiency and migration speed of transverse dunes to wind velocity. Earth Surface Processes and Landforms, 25(10), 1069-1084.

Narteau, C., Lajeunesse, E., Metivier, F., Rozier, O., 2005. Modelling of dune patterns by short range interactions, River, Coastal and Estuarine Morphodynamics, pp. 1035-1046.

Narteau, C., Zhang, D., Rozier, O., Claudin, P., 2009. Setting the length and time scales of a cellular automaton dune model from the analysis of superimposed bed forms. Journal of Geophysical Research: Earth Surface, 114(F3), F03006.

Nield, J.M., Baas, A.C.W., 2008a. The influence of different environmental and climatic conditions on vegetated aeolian dune landscape development and response. Global and Planetary Change, 64(1–2), 76-92.
Nield, J.M., Baas, A.C.W., 2008b. Investigating parabolic and nebkha dune formation using a cellular automaton modelling approach. Earth Surface Processes and Landforms, 33(5), 724-740.
Nishimori, H., Ouchi, N., 1993. Formation of ripple patterns and dunes by wind-blown sand. Physical Review Letters, 71(1), 197-200.
Nishimori, H., Tanaka, H., 2001. A simple model for the formation of vegetated dunes. Earth Surface Processes and Landforms, 26(10), 1143-1150.
Nishimori, H., Yamasaki, M., Andersen, K.H., 1998. A simple model for the various pattern dynamics of dunes. International Journal of Modern Physics B, 12(3), 257-272.
Parteli, E.J.R., Herrmann, H.J., 2007. Dune formation on the present Mars. Physical Review E, 76(4), 041307.
Pelletier, J.D., 2009. Controls on the height and spacing of eolian ripples and transverse dunes: A numerical modeling investigation. Geomorphology, 105(3-4), 322-333.
Pelletier, J.D., Mitasova, H., Harmon, R.S., Overton, M., 2009. The effects of interdune vegetation changes on eolian dune field evolution: a numerical-modeling case study at Jockey's Ridge, North Carolina, USA. Earth Surface Processes and Landforms, 34(9), 1245-1254.
Ranwell, D., 1972. Ecology of salt marshes and sand dunes. Chapman and Hall, London.
Ravi, S., Breshears, D.D., Huxman, T.E., D'Odorico, P., 2010. Land degradation in drylands: Interactions among hydrologic–aeolian erosion and vegetation dynamics. Geomorphology, 116(3–4), 236-245.
Reitz, M.D., Jerolmack, D.J., Ewing, R.C., Martin, R.L., 2010. Barchan-parabolic dune pattern transition from vegetation stability threshold. Geophysical Research Letters, 37.
Sauermann, G., Kroy, K., Herrmann, H.J., 2001a. Continuum saltation model for sand dunes. Physical Review E, 64(3), 031305.
Sauermann, G., Kroy, K., Herrmann, H.J., 2001b. Continuum saltation model for sand dunes. Physical review. E, Statistical, nonlinear, and soft matter physics, 64(3 Pt 1), 031305.
Schwämmle, V., Herrmann, H., 2004. Modelling transverse dunes. Earth Surface Processes and Landforms, 29(6), 769-784.
Schwämmle, V., Herrmann, H.J., 2005. A model of Barchan dunes including lateral shear stress. The European Physical Journal E: Soft Matter and Biological Physics, 16(1), 57-65.
Tengberg, A., 1995. Nebkha dunes as indicators of wind erosion and land degradation in the Sahel zone of Burkina-faso. Journal of Arid Environments, 30(3), 265-282.
Tsoar, H., 1989. Linear dunes - forms and formation. Progress in Physical Geography, 13(4), 507-528.
Walker, I.J., Nickling, W.G., 2002. Dynamics of secondary airflow and sediment transport over and in the lee of transverse dunes. Progress in Physical Geography, 26(1), 47-75.
Wasson, R.J., Hyde, R., 1983. Factors determining desert dune type. Nature, 304(5924), 337-339.
Werner, B.T., 1995. Eolian dunes: Computer simulations and attractor interpretation. Geology, 23(12), 1107-1110.
Werner, B.T., 1999. Complexity in Natural Landform Patterns. Science, 284(5411), 102-104.
Wiggs, G.F.S., Thomas, D.S.G., Bullard, J.E., Livingstone, I., 1995. Dune mobility and vegetation cover in the Southwest Kalahari desert. Earth Surface Processes and Landforms, 20(6), 515-529.
Wolfe, S.A., Nickling, W.G., 1993. The protective role of sparse vegetation in wind erosion. Progress in Physical Geography, 17(1), 50-68.
Zhang, D., Narteau, C., Rozier, O., 2010. Morphodynamics of barchan and transverse dunes using a cellular automaton model. Journal of Geophysical Research, 115(F3).
Zhang, D., Narteau, C., Rozier, O., Courrech du Pont, S., 2012. Morphology and dynamics of star dunes from numerical modelling. Nature Geosci, 5(7), 463-467.

Chapter 8

Simulation and Analysis Approach

This chapter:

- Presents default settings in terms of system parameters, boundary conditions, and sand transport regime, those of which are kept constant in the simulations in Chapter 9 and Chapter 10 if not otherwise specified;
- Shows representative simulations which illustrate both the processes of a barchan-to-parabolic dune transformation arising from vegetation colonisation as well as the processes of a parabolic-to-barchan dune transformation under an increase in environmental stresses;
- Defines and explains terminology involved in the analysis of modelling results.

This chapter provides the methodological basis for exploring the impacts of boundary conditions, parameter controls, and external forces of a dune system resembling the study region on the processes of dune stabilisation (the barchan-to-parabolic dune transformations) and dune reactivation (the parabolic-to-barchan dune transformations) in Chapter 9 and Chapter 10 respectively.

8.1 Default Settings

Default settings in this section refer to standard values of system parameters, boundary conditions, and wind regime that are kept constant for all the simulations explored in this thesis.

8.1.1 System Parameters

The study region is located in an inland environment with a limited sand supply. Dunes are surrounded by well-vegetated shrub lands. To mimic this closed aeolian environment devoid of external sediment sources, initial vegetation effectiveness of shrub lands is set to the physiological maximum (i.e., 1.85) and

no sand transport occurs. Vegetation effectiveness on bare dune surfaces, on the other hand, is assigned with the physiological minimum (i.e., -0.15). A spatial resolution of 1 by 1 m^2 is chosen to mimic the growth of individual shrubs (*cf.* Section 7.4.6). The slab height is set to one tenth of the spatial resolution (i.e., 0.1 m), as is also the default value in the majority of previous DECAL simulations (Nield and Baas, 2008b). In addition, a Moore neighbourhood is used, meaning that sand avalanching conditions of a cell are evaluated by examining the slopes with all eight surrounding neighbourhood cells instead of only the four perpendicular ones in a Von Neumann neighbourhood.

An updating interval (the temporal resolution) in the model, meanwhile, is critical to ensure that plants can change realistically. On the one hand, as plants are to a varying degree resilient to external forces and there is a time-lag for vegetation to respond to environmental changes, the updating interval should be long enough to ensure sufficient time for vegetation to adjust to sedimentation balance that is able to represent a realistic, average mobility during that time period. On the other hand, the updating interval should be short enough to catch sand transport fluctuations between erosion and deposition in a grid cell over time. Nonetheless, in vegetated dune landscapes it is unlikely that extreme sedimentation episodes happen and a relatively long temporal scale can be used as compared to bare dune surfaces. Therefore, a vegetation updating interval of 3 months is used to differentiate the shrub growth between the growing and the non-growing seasons (resulting in two consecutive growing seasons and two consecutive non-growing seasons for each year - an alternation between 6 month growth and 6 month non-growth).

Based on the characteristics of the dominant species Ordos Sagebrush in the study region, plant seeds in the model can only germinate on bare surfaces where minimal sand burial happens ($\leq$ 0.1 m per season). Seeds are not allowed to germinate on eroded surfaces. The maximum erosion tolerance ($\tau_{E\_physioMax}$) and the maximum deposition tolerance ($\tau_{D\_physioMax}$) of the plant are explored in the range of [-1.5, -2.5] m and [2.5, 3.5] m respectively. The yearly growth rate of vegetation in the growing seasons (α) follows the growth curve of the Ordos Sagebrush deduced from the field measurements shown in Equation 7-16, and the yearly 'growth' rate of vegetation in the non-growing seasons (β) applies the expression in Equation 7-17 in which the decline rate (η) is -0.2. The shape factor of the vegetation growth function (φ) is 0.9 (*cf.* Figure 7-8). Two parameters that relate to external forces are the sensitivity of vegetation species to respond to a climatic impact (S_{veg}) and the fodder consumption rate per visit by animals (γ), which are assumed to be 1 and 0.05 respectively.

8.1.2 Boundary Conditions

The sandy substratum beneath the shrub lands in the study region is relatively thin and lying over hard fluvial deposits comprised of gravel, sand, silt, and clay, according to fieldwork investigations (Figure 8-1). A range of substratum thickness of 0 - 1.5 m with 0.3 m steps is selected to cover the possible differences caused by spatial heterogeneity. For simplification and consistency, representative barchans used as the initial dunes of explorations are acquired by the model itself. At the start of this process, a barchan dunefield emerged from an initially flat bare surface devoid of vegetation under the control of unidirectional winds. A standard symmetrical barchan was then chosen from the resulting barchan dunefield as the prototype. It was then scaled in three-dimensions to generate five barchans at different heights: 5.2 m, 6.2 m, 7.2 m, 8.2 m and 9.2 m. The dimensions of these barchans are shown in Figure 8-2 and Table 8-1. The shape of these dunes follows the same morphometric relationship between the height and the width of barchans found from statistical analysis of dune measurements in different fields (Hesp and Hastings, 1998; Sauermann et al., 2000), and is thus comparable and analogous to that of real-world barchans.

Figure 8-1. Soil profile of the study region.

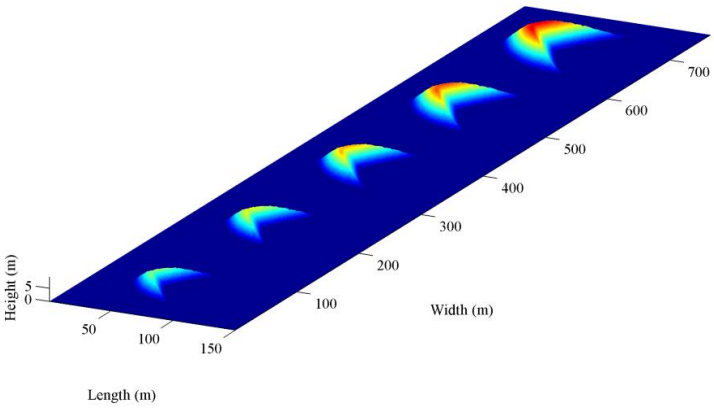

Figure 8-2. Five initial barchans of simulations.

Table 8-1. Dimensions of five initial barchans.

Barchan	Height (m)	Width (m)	Length (m)	Sand volume (m^3)
a	5.2	72	45	3448
b	6.2	80	53	5241
c	7.2	86	59	7528
d	8.2	94	66	10359
e	9.2	100	73	13780

8.1.3 Sand Transport Regime

The study region is controlled by westerly winds with an average potential sand transport rate of 20 $m^3\ m^{-1}\ yr^{-1}$ (*cf.* Section 6.3.2). The temporal scale in the model can be determined using the equation developed by Nield and Baas (2008b):

$$q = \frac{h_s l}{p_d I} \tag{8-1}$$

where: q is the potential sand transport rate, 20 $m^3\ m^{-1}\ yr^{-1}$; h_s is the slab height, 0.1 m; l is the transport length, 1 m; p_d is the deposition probability of non-vegetated surfaces, 0.6; and I is the modelling time represented by 1 iteration. Given all other variables, I can be calculated accordingly, equal to 1/120 yr. Hence, 120 iterations in the model represent a timescale of 1 year. Although Figure 4-11 suggests north-westerly winds dominate the region, satellite imagery and field observations show that parabolic dunes and barchans in the study sites are clearly orientated from the west to the east. As the meteorological station is 150 km away from the study sites, only the magnitudes of the measured drift potentials are used in the simulations, whilst the dominant wind direction is assumed from the west to the east according to satellite imagery and field observations. The number of iterations for each season was then allocated based on the proportion of its resultant drift potential to the yearly sum (*RDP*, *cf.* Section 4.3.2). Modelling parameters representing the typical wind regime in the study region are shown in Table 8-2 in which p_d, p_{dn}, and l are fixed for simplification in consistency with the values used by previous studies (Baas and Nield, 2010; Nield and Baas, 2008a; Nield and Baas, 2008b).

Table 8-2. Sand transport regime in the study region.

Season	p_e	p_d	p_{dn}	l **(m)**	***RDP* (%)**	**Iterations**
Apr-Jun	1	0.6	0.4	1	30	35
Jul-Sep	1	0.6	0.4	1	12	15
Oct-Dec	1	0.6	0.4	1	25	30
Jan-Mar	1	0.6	0.4	1	33	40
Sum					100	120

8.2 Dune Transformations

Typical examples of both a barchan-to-parabolic dune transformation and a parabolic-to-barchan dune transformation are presented in this section, and then the associated terminology in terms of dune morphology and movement is detailed in the next section.

8.2.1 Barchan-to-parabolic Dune Transformations

Figure 8-3 shows an example of the barchan-to-parabolic dune transformations. Dune topography is shown in a grey scheme (on the left-hand side) and the deflation plain between arms in white shows a hard substratum where sand has been completely eroded by the wind. Vegetation, meanwhile, is shown in a jet colour scheme on top of dune topography (on the right-hand side). The (fully-grown) vegetation on the surrounding plain of the dune is not shown such that the stabilised arms and frontal edges of the dune can stand out and be easily identified and compared. The simulation is initiated from a 9.2 m high barchan with completely bare surface (ρ = -0.15), and the barchan is surrounded by a fully-vegetated shrub field (ρ = 1.85). The sandy substratum beneath the barchan is 0.6 m thick. The vegetation can tolerate more sand burial than wind erosion with $\tau_{E\_physioMax}$ of -2.2 m season^{-1} and $\tau_{D\_physioMax}$ of 3.0 m season^{-1}.

It can be seen from the simulation that the initial barchan is moving forward and gradually transforming into a parabolic dune, leaving behind two elongated trailing arms. Vegetation first encroaches on the barchan from both horns and slows down the migration of dune edges, whereas the barchanoid lobe in the middle continues to move forward at a high rate. The position or height of lee slopes where vegetation can reach is of particular importance in the transformation. The boundary between parabolic arms and the barchanoid lobe is related to where the vegetation starts to encroach higher up the slip-face towards arms. As this boundary moves to the middle, the barchanoid lobe (with the toe of the original barchan) disappears and a barchan-to-parabolic dune transition completes. Vegetation subsequently colonises the windward slopes and the dune is fully-stabilised by vegetation quickly.

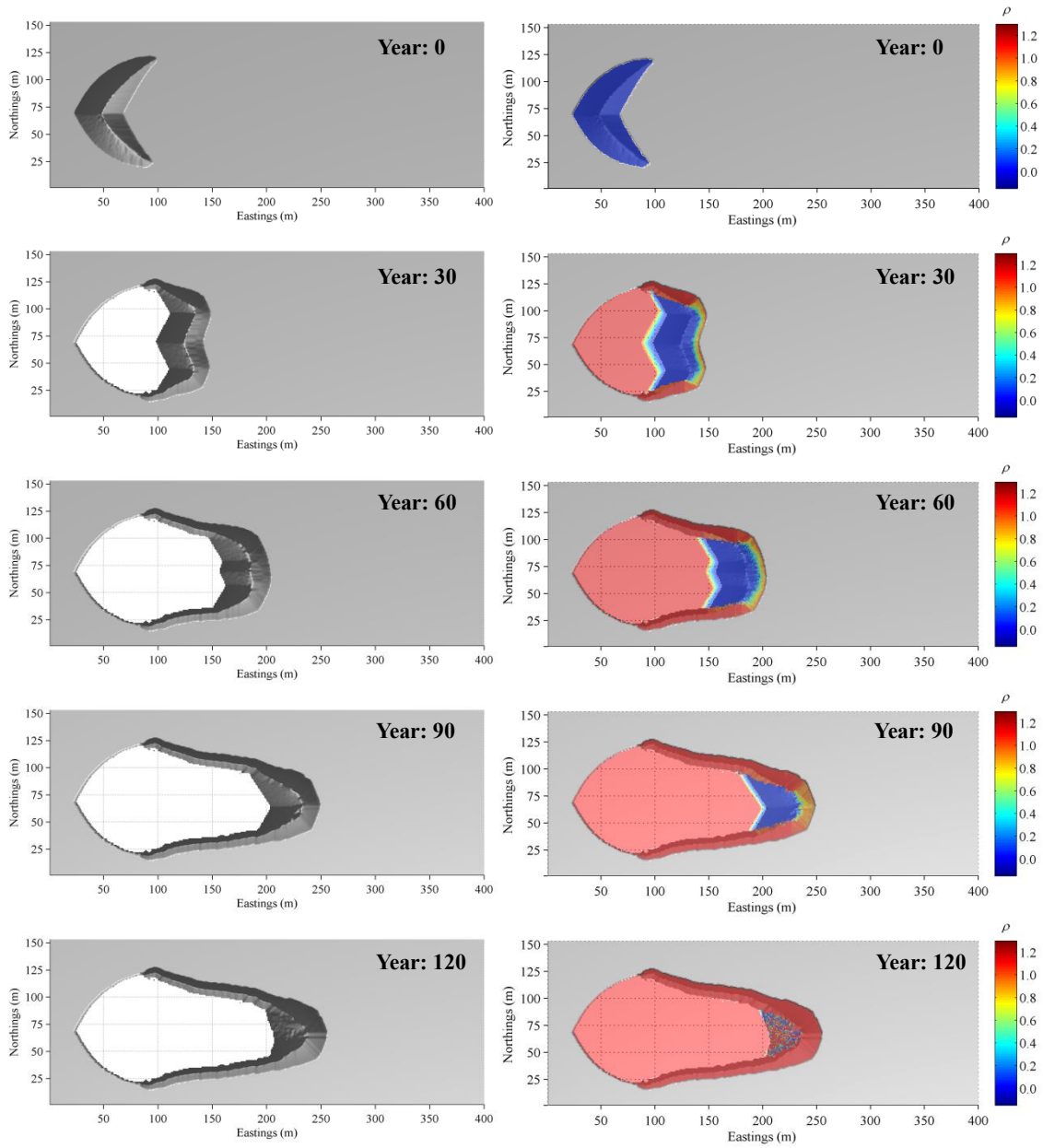

Figure 8-3. An example of the barchan-to-parabolic dune transformations with an interval of 30 years between two pairs of snapshots. q = 20 m^3 m^{-1} yr^{-1}, H_0 = 9.2 m, D_0 = 0.6 m, $\tau_{E\_physioMax}$ = -2.3 m $season^{-1}$, and $\tau_{D\_physioMax}$ = 3.0 m $season^{-1}$.

8.2.2 Parabolic-to-barchan Dune Transformations

An example in Figure 8-4 illustrates how a negative climatic impact can reactivate and transform a parabolic dune into a highly mobile barchan. The initial topography is from the simulation in Figure 8-3 at 80 yr. A negative climatic impact of -0.3 was imposed into the model continuously from that point onwards, which is analogous to a decrease in water availability arising from climatic changes such as drought. The $\tau_{E\_physioMax}$ and $\tau_{D\_physioMax}$ of vegetation are -2.1 and 2.9 m $season^{-1}$ respectively.

As the arms of the parabolic dune have been fully-stabilised by vegetation, the less stabilised lobe in the middle is more easily reactivated. Vegetation on the lee slopes declines first, which, in turn, increases sand transport. Because a negative climatic impact decreases the capability of vegetation to grow and withstand erosion and sand burial, the mobile lobe can move forward unimpeded. The edges of the dune, nonetheless, can still be stabilised by vegetation due to lower deposition rates therein. As the lobe moves forward, it is gradually separated from the original arms of the parabolic dune and transforms into a barchan. As the resulting barchan is encroaching over the shrub lands, continuous incorporation of sand from the sandy substratum underneath and the associated lateral avalanching expand the mobile frontal area and increase the dune size progressively.

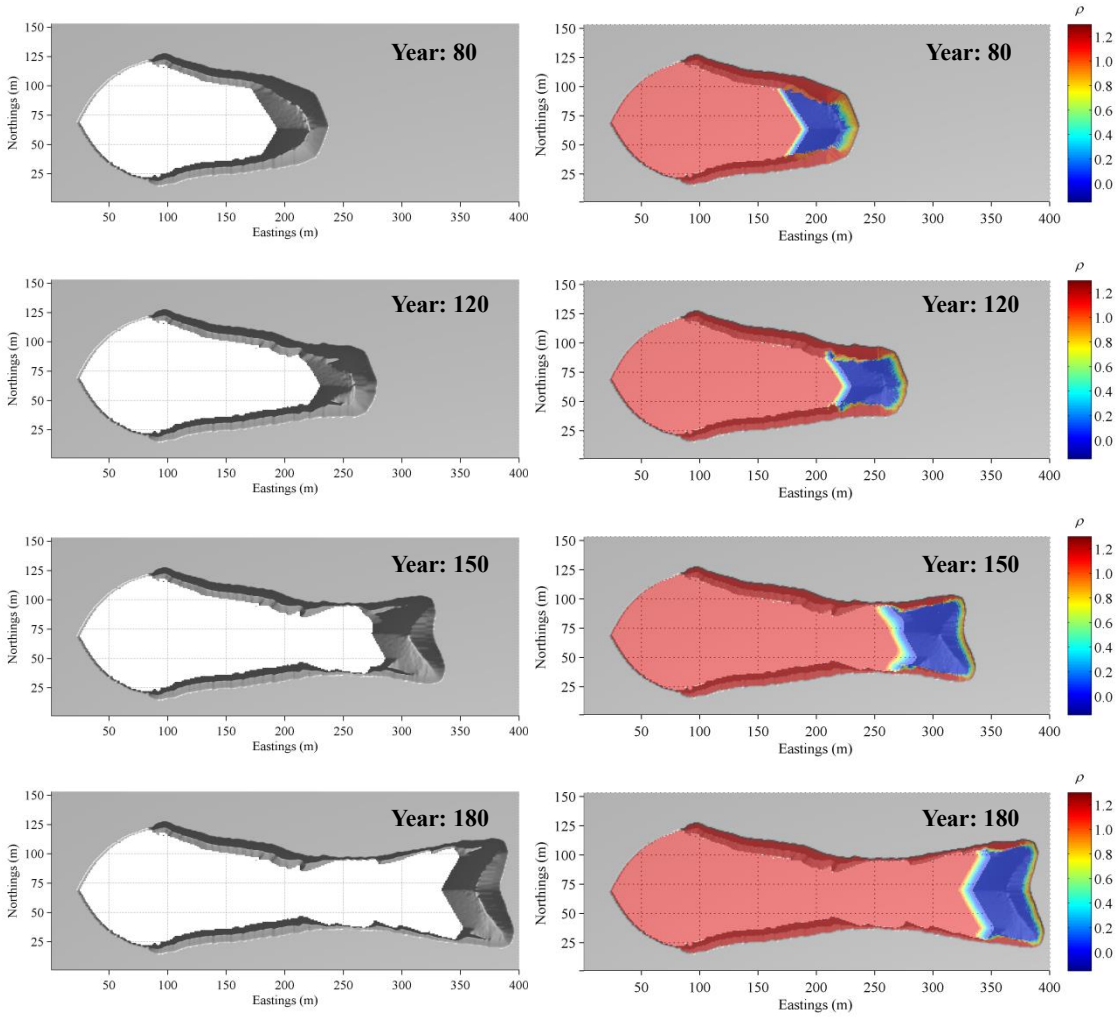

Figure 8-4. An example of the parabolic-to-barchan dune transformations with an interval of 30 years between two pairs of snapshots. The initial parabolic dune is the parabolic dune at 80 yr in Figure 8-3, and a climatic impact of -0.14 was imposed into the model since then. q = 20 m^3 m^{-1} yr^{-1}, $\tau_{E\_physioMax}$ = -2.3 m $season^{-1}$, and $\tau_{D\_physioMax}$ = 3.0 m $season^{-1}$.

8.3 Terminology

This section defines and explains the terminology and definitions to analyse modelling results of the barchan-to-parabolic dune transformations and the parabolic-to-barchan dune transformations, in terms of dune morphology indices that describe static morphology of a dune at a particular time, and dune movement indices that reflect the mobility of a dune and its potential for stabilisation or activation. The top of the sandy substratum layer is referred to as the **zero-plane**. The surrounding area of a dune that is fully-vegetated is referred to as the **surrounding plain**, whereas the eroded area between trailing arms of a parabolic dune below the zero-plane is referred to as the **deflation plain**. Sand volume in all simulations is conserved, which means that no sand escapes from a simulation domain.

8.3.1 Dune Morphology Indices

8.3.1.1 Barchan Dunes

The morphology of a typical barchan dune is shown in Figure 8-5.

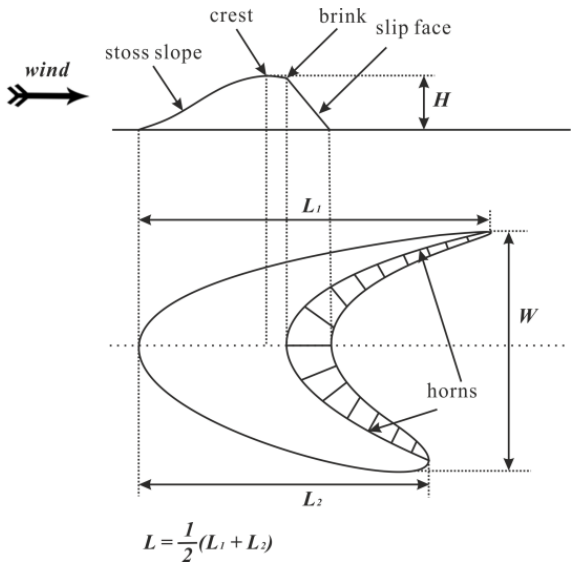

Figure 8-5. The morphology of a typical barchan.

- **Dune Height [*H*, m]:** the height of the dune crest (the highest point) above the zero-plane.
- **Dune Length [*L*, m]:** the average distance between the toe of the stoss slope and the two tips of the horns along the longitudinal section of the dune.

- **Dune Width [*W*, m]:** the distance between the two tips of the horns perpendicular to the longitudinal section of the dune.

- **Trailing Ridges:** low ridges left behind of a barchan, which are formed when tips of horns are stabilised by vegetation, whereas the main body maintains the crescentic shape and migrates forward at a high speed.

8.3.1.2 Parabolic Dunes

The morphology of a typical parabolic dune is shown in Figure 8-6.

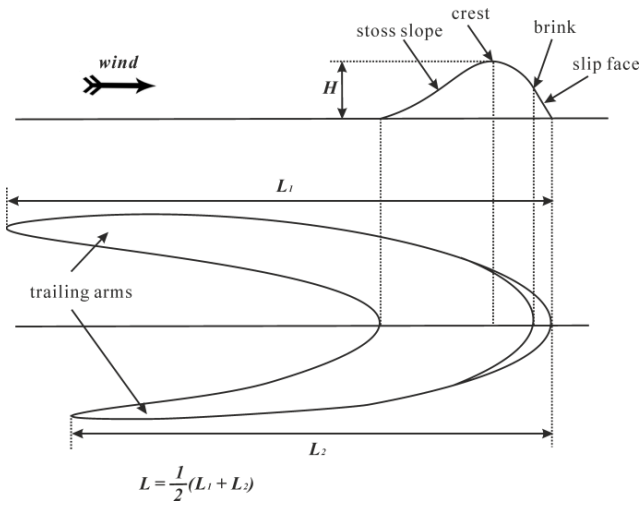

Figure 8-6. The morphology of a typical parabolic dune.

- **Dune Height [*H*, m]:** the height of the dune crest (the highest point) above the zero-plane.

- **Dune Length [*L*, m]:** the average distance between the frontal edge of the lobe and the two tips of trailing arms along the longitudinal section of the dune.

- **Trailing Arms:** the transverse boundary between an arm and the lobe is identified as where the topography starts to significantly increase beyond the average or trend of the arm height. The algorithm to distinguish arms from a lobe is shown by an example in Figure 8-7. Firstly, the whole domain is divided into two halves (the top and the bottom) along the longitudinal section in the middle of a dune. Secondly, the height of barchanoid stoss slopes in each half domain (the area within the

white squares) is assigned with 0, eliminating the potential influence on the determination of the crest location along arms. Thirdly, the highest point of each column along the longitudinal section of the dune is identified respectively for each half domain. The maximum height along the north arm is shown in the example. The column with a maximum height of H_0 is then selected as the start point, from which the maximum height is compared with that of the neighbouring point upwind. If the maximum height of the neighbouring point upwind is smaller than that of the point, the comparing pair moves upwind one step further (1 m in this case, determined by the spatial resolution of domain). This process repeats until the maximum height of a neighbouring point upwind is found to be larger than that of the point downwind. This turning point is regarded as the breaking point between the arm and the lobe. $H_0 = factor H_{max}$, where: H_{max} is the maximum height along an arm; and *factor* is a scaling constant within the range of [0.3, 0.45] determined by the simulation time. The *factor* is scaled with the time range of [100, 200] yr. Beyond the range, 0.3 and 0.45 are assigned to *factor* when the simulation time is below 100 year and above 200 year respectively. This algorithm is validated by comparing the results of ~100 simulations with that of the visual identification. The difference between these two methods is within 3 points (3 m), which is minimal compared to the length of an arm.

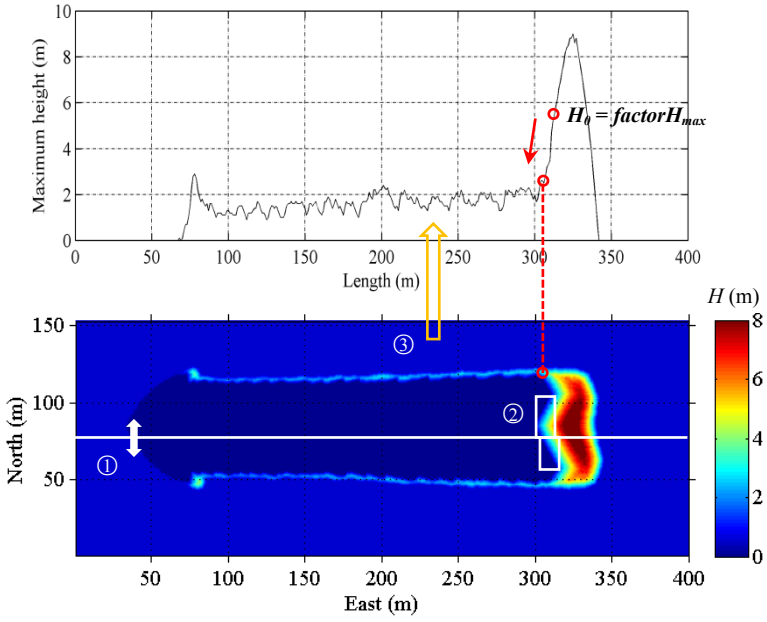

Figure 8-7. The algorithm to distinguish arms from a dune lobe (details in the text).

- **Lobe Width:** the transverse distance between two arm-lobe boundaries, perpendicular to the longitudinal section of a dune.

- **Lobe Length:** the longitudinal length of the dune lobe.

- **Average Dune Width:** the average width between the two arms along the longitudinal section of a dune.

- **Elongation Ratio**: the ratio of dune length to average dune width.

- **Sand Volume of a Dune:** sand volume of a dune above the zero-plane. For the purpose of calculation, the zero-plane is chosen as the base of a dune, although there is a slight underestimation due to the fact that the inside boundary of a (barchanoid-) parabolic dune is slightly lower on the deflation plain as compared with the outside surrounding plain.

- **Sand Volume of Arms:** sand volume of two arms above the zero-plane.

- **Sand Volume of a Lobe:** sand volume of a dune lobe excluding two trailing arms of a parabolic dune.

- **Sand Volume of the Lobe per Width (*V'*):** the ratio of sand volume of the lobe to the lobe width.

- **Sand Volume of the Arms per Distance:** the ratio of sand volume of the arms to the average length of arms.

8.3.2 Dune Movement Indices

8.3.2.1 Barchan-to-parabolic Dune Transformations

- **Migration Distance:** the distance of the dune crest along the wind direction at a certain time relative to the original crest location of the initial barchan at the start of a simulation.

- **Cell Mobility:** the probability of sand in a cell to be eroded by winds, expressed as:

$$M_c = f(\rho) = \begin{cases} 1, & \rho \le 0 \\ 1-\rho, & 0 < \rho \le 1 \\ 0, & \rho > 1 \end{cases} \quad (8\text{-}2)$$

  If no sand exists in a cell, the cell mobility is 0 no matter whether vegetation exists or not.

- **Dune Surface Erodibility (*DSE*):** the average cell mobility of the dune above the zero-plane.

- **Transition Time (t_{tran}):** the time when an initial barchan is completely transformed into a parabolic dune - the toe of the original barchanoid lobe disappears completely and the inner boundary of the windward slope exhibits a smooth parabolic-shaped curve.

- **Transition Duration**: the duration needed for an initial barchan to be transformed into a complete parabolic dune (at the transition time).

- **Arms-initiation Time:** the time when the trailing arms of a parabolic dune emerge.

- **Stabilisation Time (t_{stab}):** the time when the resulting parabolic dune is fully stabilised by vegetation, and there is no difference between vegetation on the dune and vegetation on the surrounding plain.

- **Stabilisation Duration:** the duration needed for an initial barchan to be transformed into a fully-stabilised parabolic dune (at the stabilisation time).

- **Average Migration Rate:** the ratio of the migration distance to the stabilisation duration.

- **Arms-elongating Duration:** the duration between the initiation of arms (arms-initiation time) and the stabilisation of a parabolic dune (stabilisation time).

- **Arms-elongating Rate:** the ratio of the average arm length to the arms-elongating duration.

- **Dune-elongating Ratio:** the ratio of the dune length to the stabilisation duration.

- **Average Dune Migration Rate:** the ratio of the migration distance to the stabilisation duration.

- **Arms-developing Angle (θ_{arms}):** the angle between two trailing arms. The coordinates of points on the crest along the arms are first extracted when a parabolic dune is fully stabilised. For each arm, a regression line is then fitted linearly using the coordinates of these points (R^2 > 95%). The angle between these two regression lines can then be obtained. A positive angle (e.g., α in Figure 8-8) denotes a parabolic dune with two arms developing towards each other in the downwind direction and the lobe shrinking progressively, whilst a negative angle (e.g., β in Figure 8-8) indicates that two arms of a parabolic dune are propagating away from each other and the dune lobe is expanding laterally.

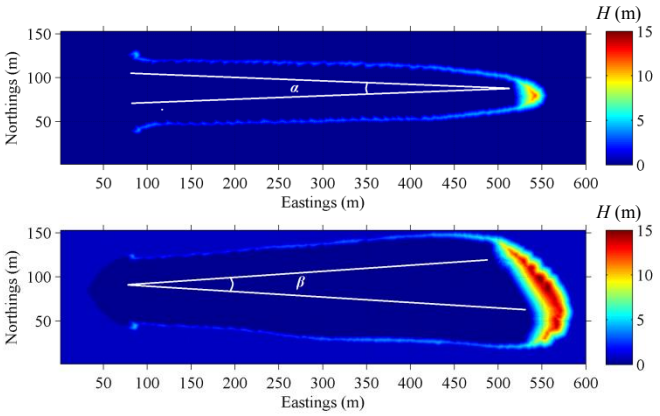

Figure 8-8. Examples of the arms-developing angle of parabolic dunes. The α and β denote a positive angle and a negative angle respectively.

- **Sand Volume Gained on the Dune Lobe:** the increase in sand volume on the dune lobe between two consecutive years.
- **Sand Volume Gained on the Arms:** the increase in sand volume on the arms between two consecutive years.
- **Sand Volume Lost from the Substratum:** the decrease in sand volume in the sandy substratum below the zero-plane between two consecutive years.

8.3.2.2 Parabolic-to-barchan Dune Transformations

- **Transition Time (t_{tran}):** the time when an initial parabolic dune is completely transformed into a barchan dune - a crescentic lobe with a clearly identifiable toe and slip faces. The determining algorithm is shown in Figure 8-9. S_0 is the representative plane shape of the windward boundary of a parabolic dune (i.e., the foot of windward slopes). The temporal point when S_0 first appears is defined as the transition time from a barchan to a parabolic dune. The time needed to develop S_0 from an initial barchan is regarded as the transformation duration. S_1, S_2, S_3, and S_4 are other possible scenarios during the processes of the transformation, happening before the transition time. S_0 can thus be identified if all the other scenarios prove to be not present at the time. In the algorithm, the horizontal location (west to east, column number C_0) of the dune crest is firstly identified. Then, the profile of vertical cross sections (north to south) is checked upwind (to the west) until a profile as column C_j in S_1, S_2, S_3 is found, which exhibits three peaks separating the inner section between arms into two parts.

The profile of the column C_{j+1}, at the same time, displays two peaks as the ones in S_1 and S_3, or only one peak as the one in S_2. If C_j is not found in the domain, S_4 is then further examined. S_4 occurs when a barchan-to-parabolic dune transformation is nearly completed. The profiles of vertical cross sections on the lobe upwind of the most inner foot of the windward slopes all exhibit two peaks similar to those in S_0. Nevertheless, a small part close to the middle of the dune remains highly mobile and the windward boundary is not completely changed to a smooth parabolic curve (C_j in S_3). To identify this scenario, the vertical distance between points on the windward boundary of the dune from two columns next to each other is calculated (such as $|R_{i-1}\text{-}R_i|$ or $|R_i\text{-}R_{i+1}|$). S_3 is confirmed if the vertical distance between the two points from neighbouring columns is larger than 3 vertical points (3 m, determined by the spatial resolution). The process repeats until either S_3 is found or the examined pairs reach the breaking point between an arm and the lobe. A dune is classified into S_0 if any of the scenarios like S_1, S_2, S_3, and S_4 is not found.

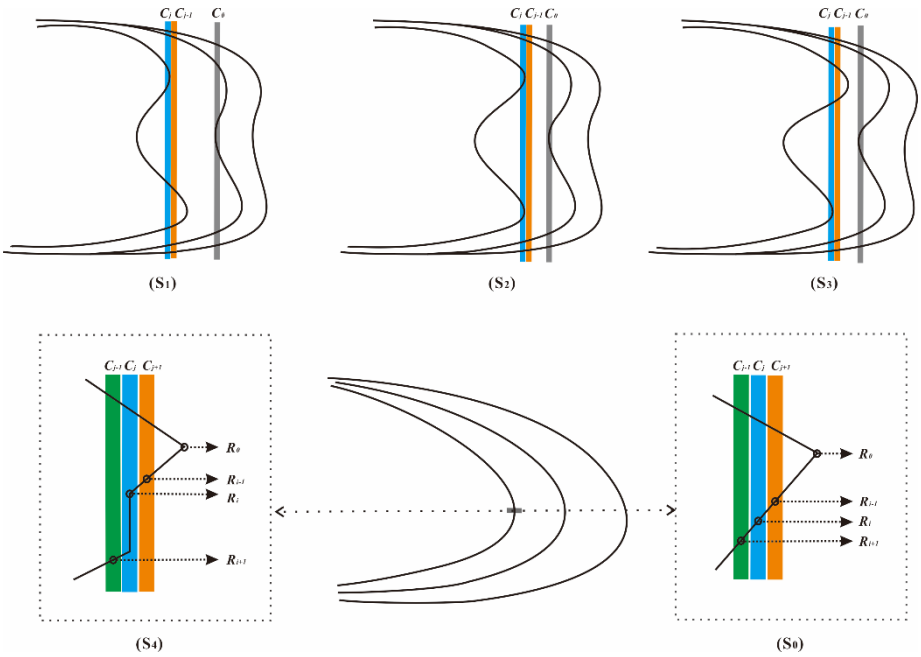

Figure 8-9. The algorithm to determine the transformation point of a barchan into a parabolic dune. C_j and R_i denote the column j and row i respectively. The column number increases from the left to the right and the row number increases from the top to the bottom. C_0 represents the column where the crest of a dune is located. R_0 represents the row where the most inner foot of the windward boundary of a dune is located. The typical windward boundary of a parabolic dune is shown as S_0 which can be deduced by excluding the scenarios of S_1, S_2, S_3, and S_4.

- **Transformation Duration:** the duration needed for an initial parabolic dune to be transformed into a barchan dune (at the transition time).

- **Reactivation Angle:** a parabolic dune can be reactivated by either external natural forces or human disturbances, and develops into a barchan or multiple barchans, as the less-vegetated dune lobe gains momentum and moves forward breaking up with its arms eventually. As the lobe continuously buries vegetation on its way and incorporates sand underneath, low ridges are left behind on both edges of the mobile lobe or traveling track because vegetation can survive minimal sand burial therein. The angle between the two low ridges or the edges of the deflation plain is defined as the reactivation angle and can be derived by linearly fitting two regression lines of both edges of the track with R^2 > 95%. The negative angle denotes the two low ridges are propagating away from each other, and the resulting dune keeps expanding laterally, as examples shown in Figure 8-10.

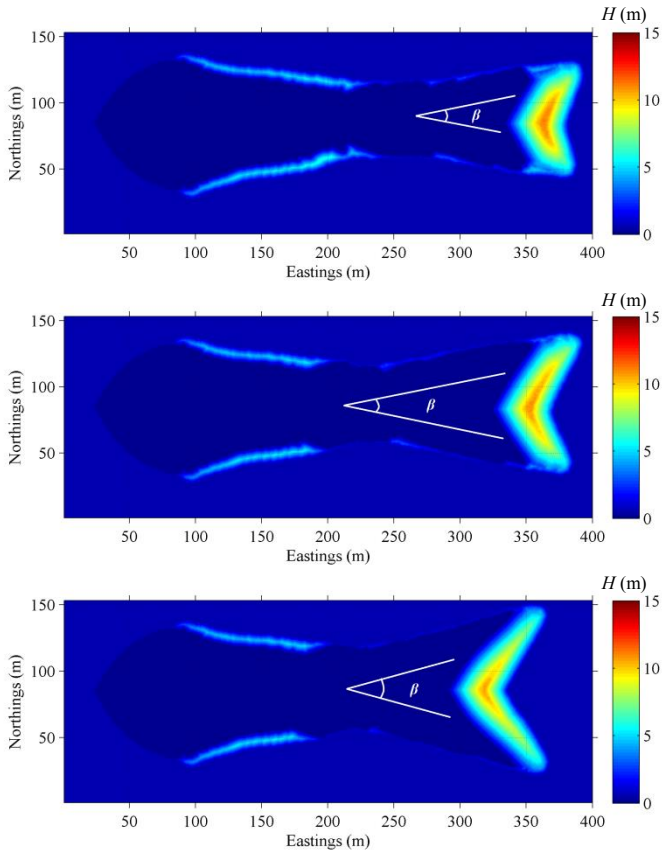

Figure 8-10. Examples of different reactivation angles.

References

Baas, A.C.W., Nield, J.M., 2010. Ecogeomorphic state variables and phase-space construction for quantifying the evolution of vegetated aeolian landscapes. Earth Surface Processes and Landforms, 717-731.

Hesp, P.A., Hastings, K., 1998. Width, height and slope relationships and aerodynamic maintenance of barchans. Geomorphology, 22(2), 193-204.

Nield, J.M., Baas, A.C.W., 2008a. The influence of different environmental and climatic conditions on vegetated aeolian dune landscape development and response. Global and Planetary Change, 64(1–2), 76-92.

Nield, J.M., Baas, A.C.W., 2008b. Investigating parabolic and nebkha dune formation using a cellular automaton modelling approach. Earth Surface Processes and Landforms, 33(5), 724-740.

Sauermann, G., Rognon, P., Poliakov, A., Herrmann, H.J., 2000. The shape of the barchan dunes of Southern Morocco. Geomorphology, 36(1–2), 47-62.

Chapter 9

Dune Stabilisation and Barchan-to-parabolic Dune Transformations

---

This chapter:

- Classifies the resulting parabolic dunes transformed from an initial barchan under the influence of vegetation colonisation;
- Explores how vegetation characteristics, boundary conditions, and wind regime control the processes of barchan-to-parabolic dune transformations and the morphologies of the resulting parabolic dunes;
- Analyses how key parameters described above interact and compromise with each other, determining the barchan-to-parabolic dune transformations;
- Proposes a universal non-dimensional number, the 'dune stabilising index', and shows how it can assist in reconstructing paleo-environments and monitoring impacts of climatic changes on a stabilising system;
- Discusses the fundamental mechanism that governs a barchan-to-parabolic dune transformation.

9.1 Exploring Framework

The influence of five key environmental parameters on barchan-to-parabolic dune transformations is explored in detail by four batches of simulations, as shown in Figure 9-1. The maximum erosion tolerance ($\tau_{E\_physioMax}$) and the maximum deposition tolerance ($\tau_{D\_physioMax}$) of a vegetation species are erosion and deposition tolerances when vegetation effectiveness (ρ) is at its maximum physiological state ($\rho_{physioMax}$)

when a plant has reached its mature stage. Both are the most important characteristics of vegetation that determine whether or not plants can survive in an aeolian system.

The first batch aims at a fundamental understanding of how changes in vegetation characteristics (i.e., $\tau_{E\_physioMax}$ and $\tau_{D\_physioMax}$) lead to the development of different dune morphologies and the associated physical processes involved. Parameter values selected are shown on the light blue line. $\tau_{E\_physioMax}$ is in a realistic range of -1.5 to -2.5 m season^{-1} (the negative sign denotes erosion), whilst $\tau_{D\_physioMax}$ varies in a range of 2.5 to 3.5 m season^{-1}. Both ranges are explored with a resolution of 0.1 m season^{-1} steps.

The second batch is to explore how the height of the initial barchan (H_0) contributes to a barchan-to-parabolic dune transformation (on the yellow line). The initial barchan of simulations varies in height from 5.2 to 9.2 m with 1 m gradations.

The third batch is to examine how the sandy substratum thickness beneath dunes (D_0) interacts with those three parameters mentioned, complementary to each other, controlling barchan-to-parabolic dune transformation processes (on the purple line). D_0 varies in a range of 0.3 to 1.5 m with 0.3 m gradations. $\tau_{E\_physioMax}$ and $\tau_{D\_physioMax}$ are explored in a subset of the original range in which the barchan-to parabolic dune transformations are more likely to happen.

The final batch incorporates changes in the potential sand transport rate (q) with an attempt to fully examine interactions between all the above parameters and analyse their particular contributions in a barchan-to-parabolic dune transformation. Each of the parameter settings has been simulated at least twice, and replicates yield very similar dune morphologies. Therefore, only one simulation from each of 1775 scenario settings is included in the following analyses.

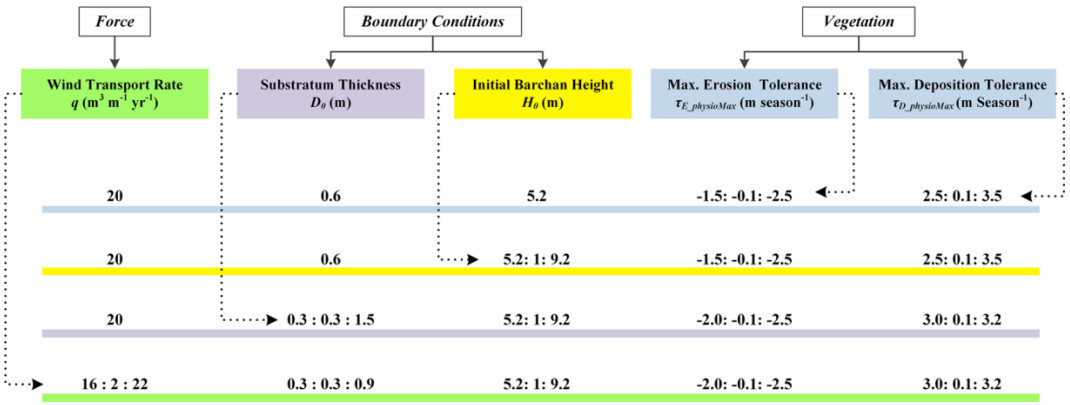

Figure 9-1. Exploring framework of key environmental parameters. The numbers (# : # : #) indicate the minimum value : the increment step : the maximum value of each batch of simulations respectively.

9.2 The Classification of Resulting Dunes from an Initial Barchan

Resulting dunes that are developed from an initial barchan surrounded by well-vegetated shrub lands under unidirectional wind regime can be classified into three main categories: parabolic, barchanoid, and barchanoid-parabolic dunes, according to the morphology (planar shape) of their lobes (Figure 9-2 & Figure 9-3). The parabolic dunes are further subdivided into chevron, lunate, typical, and elongated parabolic dunes, based on whether or not trailing arms are in existence as well as the magnitude of the normalised dune length. The normalised dune length is the degree to which arms of dunes are elongated in comparison to the average width of a dune: the ratio of dune length to average dune width. This ratio is a good indicator to differentiate parabolic dunes with the same width of the opening and the same dune length, yet having a different size (length and width) of dune lobes. Examples of the eight resulting dune types are shown in Figure 9-3. The colour codes of the eight basic dune types are consistently used in the figures of the following sections.

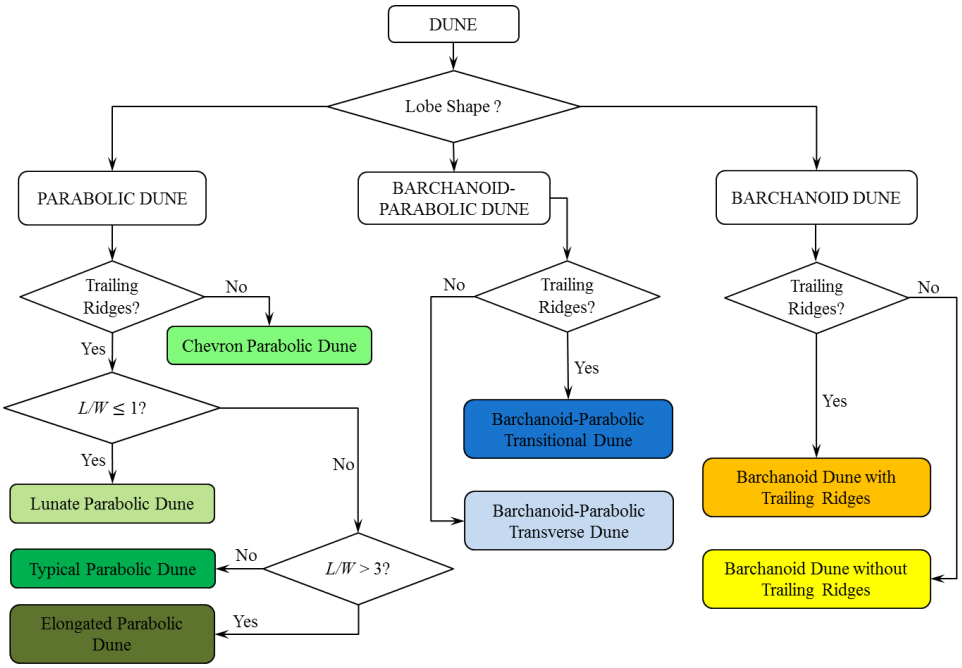

Figure 9-2. The classification of the resulting dunes developed from an initial barchan surrounded by well-vegetated shrub lands, based on the modelling outcome.

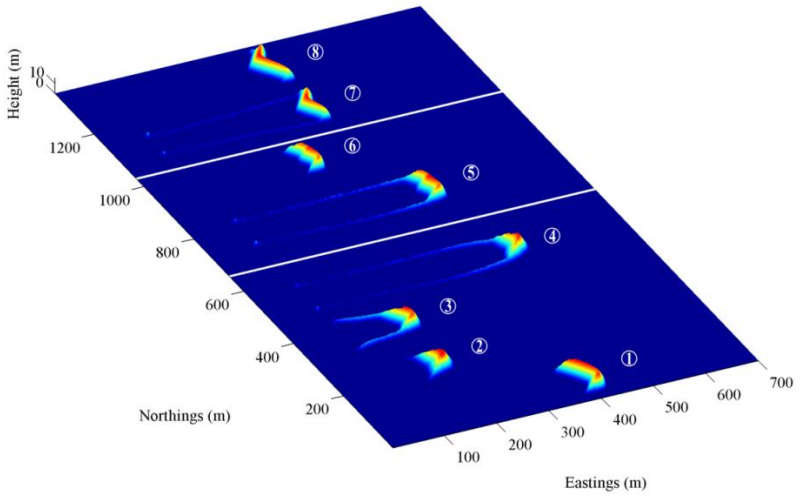

Figure 9-3. Examples of the eight resulting dune types: (1) chevron parabolic dune; (2) lunate parabolic dune; (3) typical parabolic dune; (4) elongated parabolic dune; (5) barchanoid-parabolic transitional dune; (6) barchanoid-parabolic transverse dune; (7) barchanoid dune with trailing ridges; and (8) barchanoid dune without trailing ridges.

The chevron parabolic dunes have v-shaped lobes without trailing arms. Their longitudinal cross sections are generally the same across the whole dune width. The lunate parabolic dunes, compared to the chevron parabolic dunes, exhibit more rounded crescentic shape with very short arms. The typical parabolic dunes have well-defined trailing arms, with a dune length to width ratio larger than 1.5 up to 3. The elongated parabolic dunes, also referred to as the hairpin-shaped parabolic dunes, have long-walled trailing arms with a length to width ratio larger than 3 (Pye, 1982). The barchanoid-parabolic transitional and transverse dunes are intermediate stages between the barchan and the parabolic shapes, whose lobes present a batwing shape in a horizontal plane. These dunes have a crescentic-shaped toe and parabolic-shaped dune edges. Given enough time, both types of barchanoid-parabolic dunes often develop into parabolic dunes eventually in such an environment where bare dunes are surrounded by well-vegetated fields.

9.3 Influence of Vegetation Characteristics

9.3.1 Dune Shape

The simulations presented in Section 9.3 start from an initial barchan at the height of 5.2 m with a sandy substratum thickness of 0.6 m under the standard wind regime (q = 20 m^3 m^{-1} yr^{-1}). Phase diagrams in

Figure 9-4 show the morphological types of resulting dunes at the transition time (t_{tran}) and the stabilisation time (t_{stab}). The deposition tolerance of vegetation primarily determines the basic types of the resulting dunes, whilst the erosion tolerance of vegetation contributes to the formation of trailing arms or ridges. Chevron parabolic dunes temporarily emerge at relatively low erosion tolerances, and they further develop into lunate or typical parabolic dunes as trailing arms form and elongate afterwards. In contrast to the developing processes of all other three types of parabolic dunes in which arms have formed before t_{tran}, chevron parabolic dunes do not have trailing arms. This suggests that the formation of trailing arms is not necessarily a prerequisite for a barchan-parabolic dune transformation. The phase diagrams show that simulations with $\tau_{D\_physioMax}$ smaller than 3.0 m season^{-1} do not lead to parabolic-type dunes within the explored simulation time of 300 years. All subsequent analyses thus focus on the transformations from barchan to parabolic dunes under $\tau_{D\_physioMax}$ of 3.0 to 3.5 m season^{-1}.

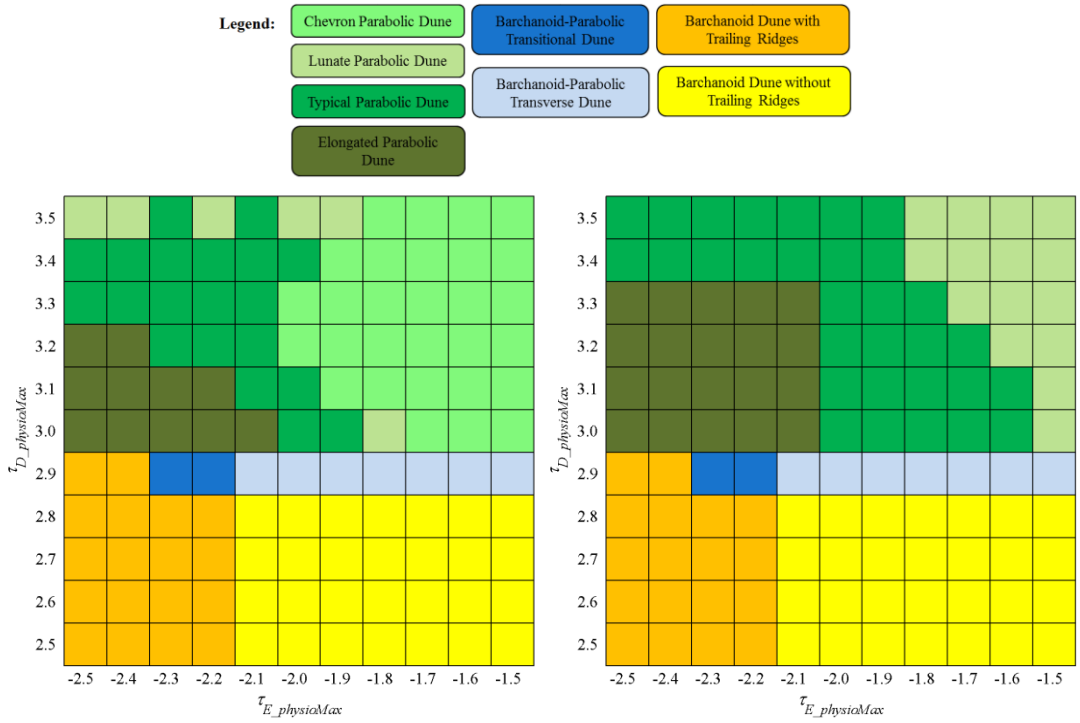

Figure 9-4. Dune types at (a) t_{tran} and (b) t_{stab}. Colour codes are consistent with that of Figure 9-2.

Figure 9-5 shows that the dune length increases as either the deposition tolerance decreases or the erosion tolerance increases. A larger erosion tolerance exerts a stronger positive impact on the dune length at a smaller deposition tolerance. The average dune width, as shown in Figure 9-6, also increases as the deposition tolerance decreases; however, it shows a slightly decreasing trend as the erosion tolerance increases. Lower erosion and deposition tolerances generally contribute to a wider eroded plain

between arms of a parabolic dune. It can be seen from Figure 9-7 that the dune-elongating ratio increases as the deposition tolerance decreases at a relatively large erosion tolerance (>2.0 m season^{-1}), but it exhibits insignificant difference at a relatively small erosion tolerance. The deposition tolerance is responsible for a greater increase in the dune-elongating ratio at a larger erosion tolerance. However, Figure 9-8 indicates that although the deposition tolerance does not significantly contribute to the dune-elongating ratio of resulting parabolic dunes at a low erosion tolerance, it impacts both the lobe length and the lobe width. The height of parabolic dunes at t_{tran} increases at a smaller deposition tolerance, but no significant difference arises from the erosion tolerance (Figure 9-9). The height at t_{stab}, nevertheless, exhibits an increasing trend with a decrease in the deposition tolerance or the erosion tolerance. Collectively, at a relatively low erosion tolerance (<2.0 m season^{-1}), a lower deposition tolerance encourages the development of larger lobes despite the fact that there is minimal difference in terms of the dune-elongating ratio. A lower deposition tolerance significantly promotes the development of long-walled trailing arms, in particular, to a larger extent at a higher erosion tolerance.

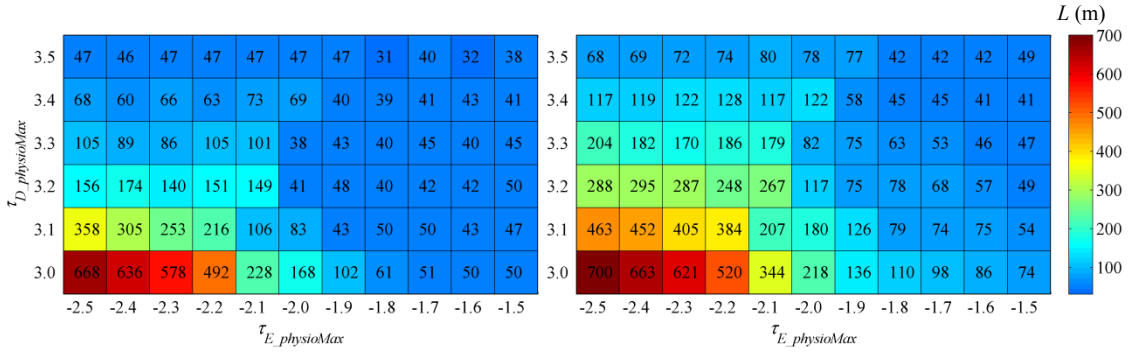

(a) (b)

Figure 9-5. The length of the resulting parabolic dunes at (a) t_{tran} and (b) t_{stab}.

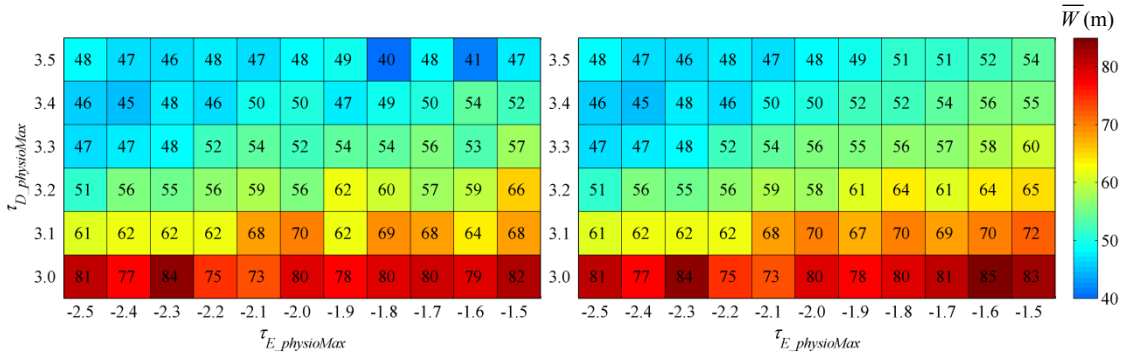

(a) (b)

Figure 9-6. The average dune width of the resulting parabolic dunes at (a) t_{tran} and (b) t_{stab}.

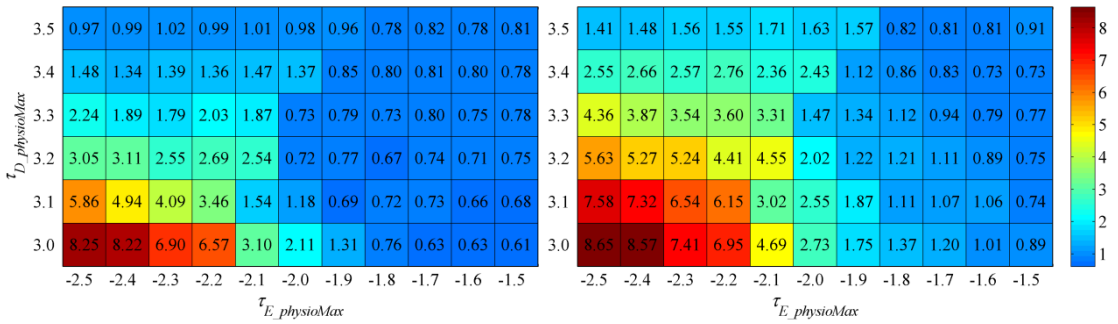

(a) (b)

Figure 9-7. The dune-elongating ratio of the resulting parabolic dunes at (a) t_{tran} and (b) t_{stab}.

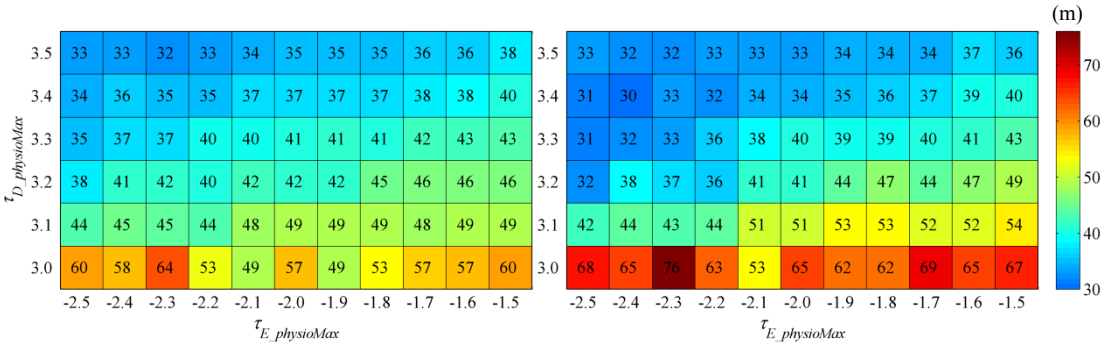

(a) (b)

Figure 9-8. The (a) lobe length and (b) lobe width of the resulting parabolic dunes at t_{stab}.

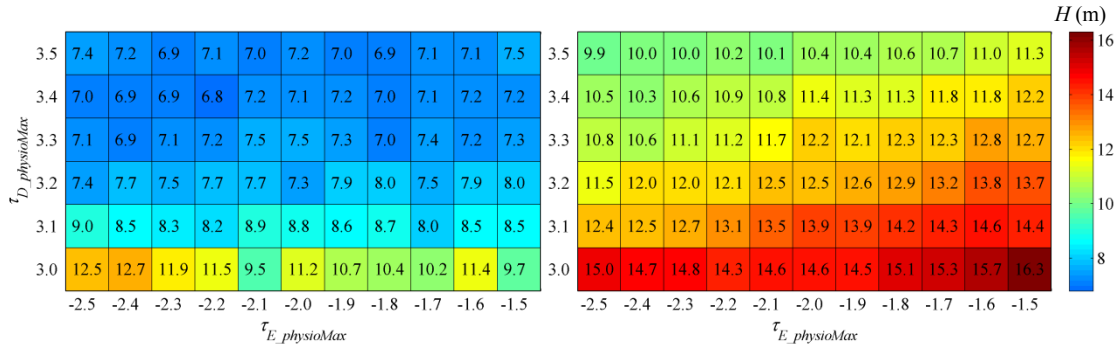

(a) (b)

Figure 9-9. The height of the resulting parabolic dunes at (a) t_{tran} and (b) t_{stab}.

9.3.2 Transition and Stabilisation Times

The transition time and the stabilisation time are of particular importance in a barchan-to-parabolic dune transformation, because the transition time captures the birth of a parabolic dune, whilst the stabilisation time signifies the cessation of sand transport. Figure 9-10 shows that both t_{tran} and t_{stab} of a barchan-to-parabolic dune transformation increase exponentially as the deposition tolerance decreases. The decrease in the deposition tolerance exerts a more considerable impact on series governed by relatively large

erosion tolerances. Fitted trend-lines suggest that for a deposition tolerance of 2.9 m season^{-1}, the time needed for the completion of a barchan-to-parabolic dune transformation extrapolates dramatically up to ~600 years. Detailed comparisons and analyses regarding the deposition tolerance in the following sections are hence constrained within the representative range of 3.0 to 3.5 m season^{-1}.

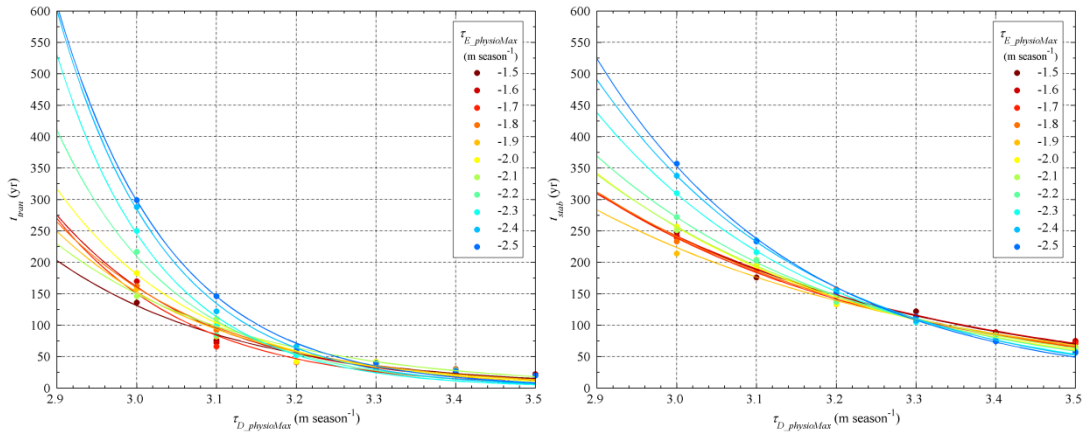

(a) (b)

Figure 9-10. The relationships (a) between the erosion and deposition tolerances and t_{tran}, and (b) between the erosion and deposition tolerances and t_{stab}. Varying colours of dots represent different vegetation erosion tolerances as shown in the legends, and the associated lines denote exponential curves fitted with the method of least squares. (a) $R^2 > 0.94$, and (b) $R^2 > 0.97$.

The influence of the vegetation erosion tolerance on t_{tran} and t_{stab} during a barchan-to-parabolic dune transformation is dependent on the magnitude of the deposition tolerance. A larger erosion tolerance yields longer t_{tran} and t_{stab} when the deposition tolerance is larger than 3.3 m season^{-1}, whereas below which the erosion tolerance exerts a minimal impact.

9.3.3 Dune Migration

The average dune migration rate is greater at lower deposition tolerances and higher erosion tolerances (Figure 9-11). Examples of the migration rate over time in Figure 9-12 show that the erosion tolerance and the deposition tolerance influence the dune migration rate in different manners. A higher deposition tolerance slows down the dune migration rate almost immediately from the beginning of a simulation, and it encourages a faster barchan-to-parabolic dune transformation and stabilisation. In contrast, the erosion

tolerance does not lead to a significant difference at the beginning but can influence t_{stab} significantly particularly at a relatively low deposition tolerance.

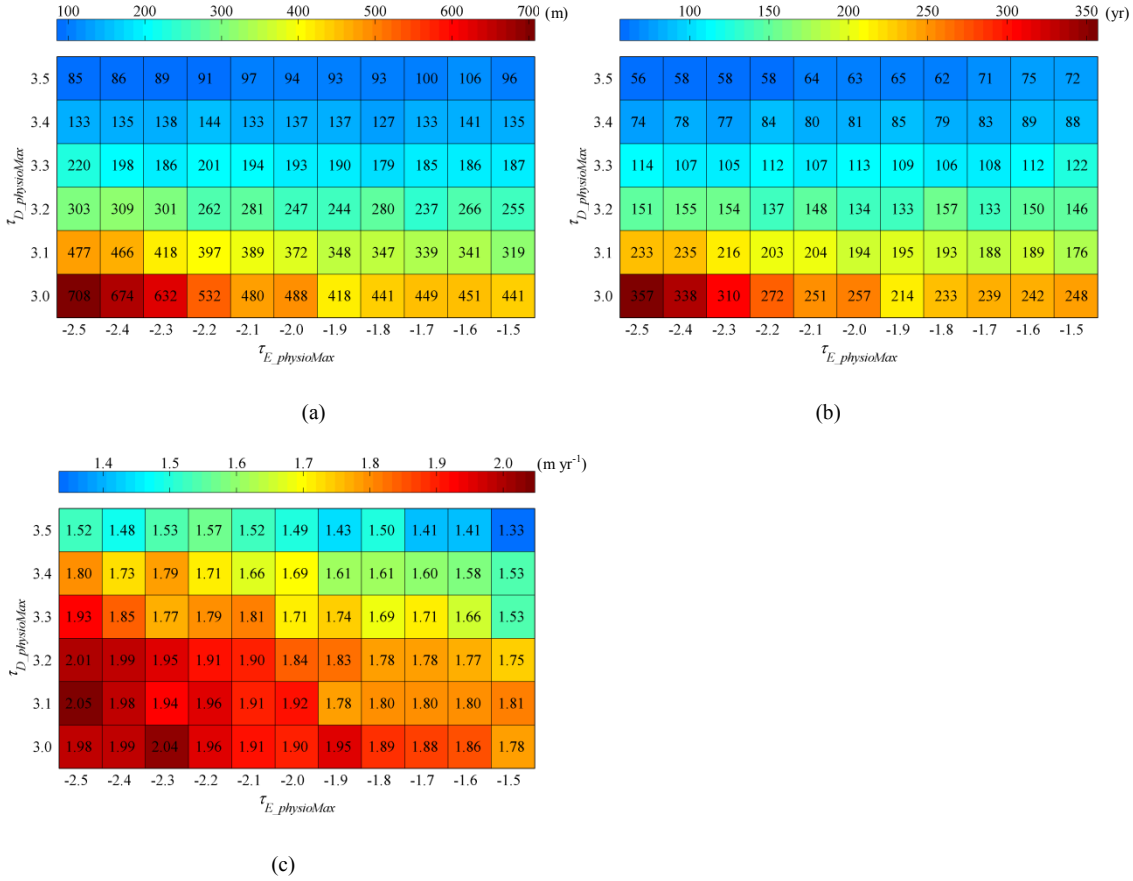

Figure 9-11. (a) the migration distance; (b) the stabilisation duration; and (c) the average migration rate.

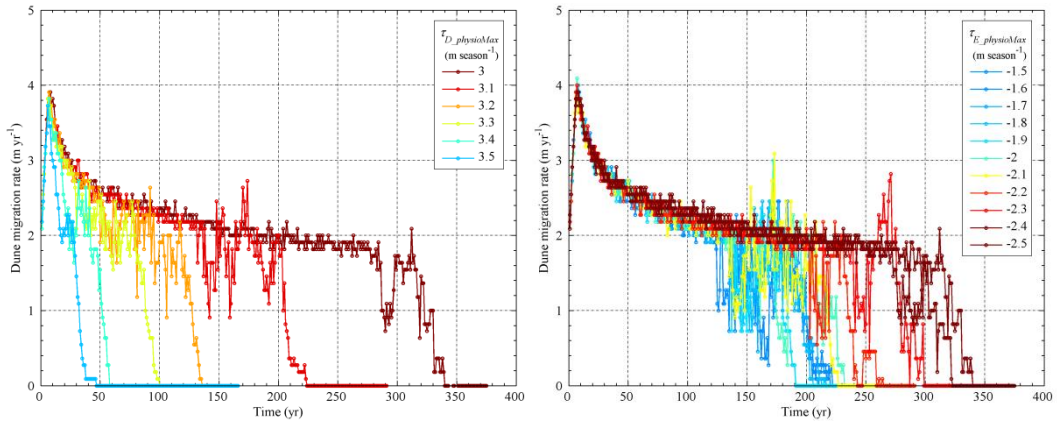

Figure 9-12. Change in the dune migration rate over time, using a smoothing-window of 11 years. (a) $\tau_{E\_physioMax}$ = -2.5 m season^{-1}. (b) $\tau_{D\_physioMax}$ = 3.0 m season^{-1}.

9.3.4 Trailing Arms

Low erosion and deposition tolerances generally lead to a later initiation of trailing arms (Figure 9-13a). A high deposition tolerance encourages a quick initiation of trailing arms at a relatively low erosion tolerance. Arms persist over the whole history of a simulation at a relatively high erosion tolerance. As the erosion tolerance decreases, trailing arms are initiated later, whereas the arms-elongating duration shortens (Figure 9-13b), which means dunes are stabilised more quickly after the initiation of arms. The average arms-elongating rate generally increases at a lower deposition tolerance but at a higher erosion tolerance (Figure 9-13c).

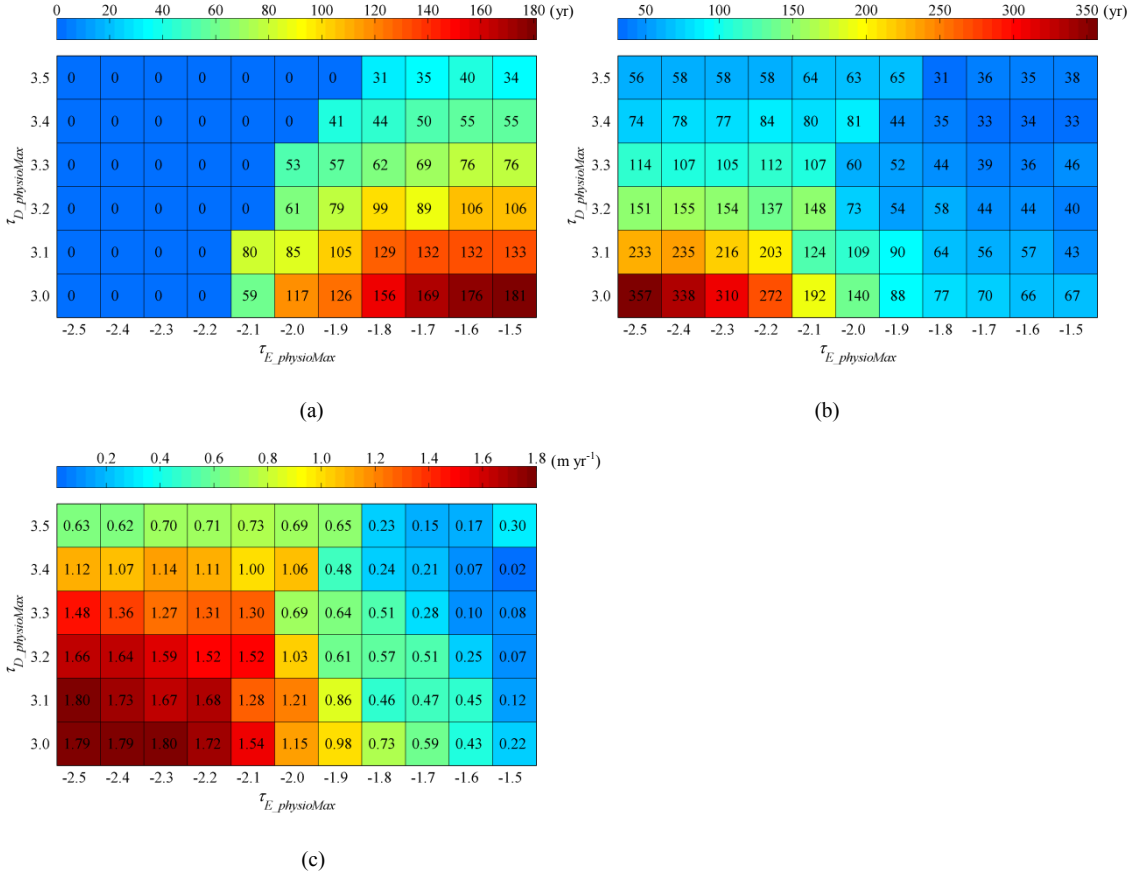

Figure 9-13. (a) the arms-initiation time; (b) the arms-elongating duration; and (c) the arms-elongating rate.

At a relatively low erosion tolerance, as the deposition tolerance decreases, the arms-initiation time and the arms-elongating rate increase. The dune-elongating ratio, however, does not show significant difference, and there is a strong similarity in the shape of resulting parabolic dunes (Figure 9-7b). This suggests that the deposition tolerance to a large extent determines the travel distance of a dune before the initiation of arms. At a high erosion tolerance (> 2.1 m season^{-1}), whilst the change in the deposition

tolerance does not create a difference regarding the arms-initiation time, it does play a crucial role in determining the arms-elongating rate as well as the dune-elongating ratio of resulting parabolic dunes.

9.3.5 Sand Volume Dynamics

The sand volume of dune lobes increases at a lower erosion tolerance, resulting in a higher sand volume of the dune lobe per width (V') at t_{stab} (Figure 9-14), which is associated with a shorter stabilisation duration (Figure 9-10) and a slower dune migration rate (Figure 9-11c). As most elongated parabolic dunes develop at a relatively low deposition but high erosion tolerances (Figure 9-7b), it can be deduced that even though elongated parabolic dunes move downwind a relatively long distance before finally being stabilised and more sand in the substratum is exposed, eroded, and incorporated into the dune, there is a more significant sand loss from the lobe to its arms in comparison to parabolic dunes developed under a lower erosion tolerance. Figure 9-15 also shows the sand volume from arms takes a larger percentage in the sand volume of the whole dune with an increase in the erosion tolerance. As the erosion tolerance increases, less sand is gained on the dune lobe, whereas more sand is gained on arms.

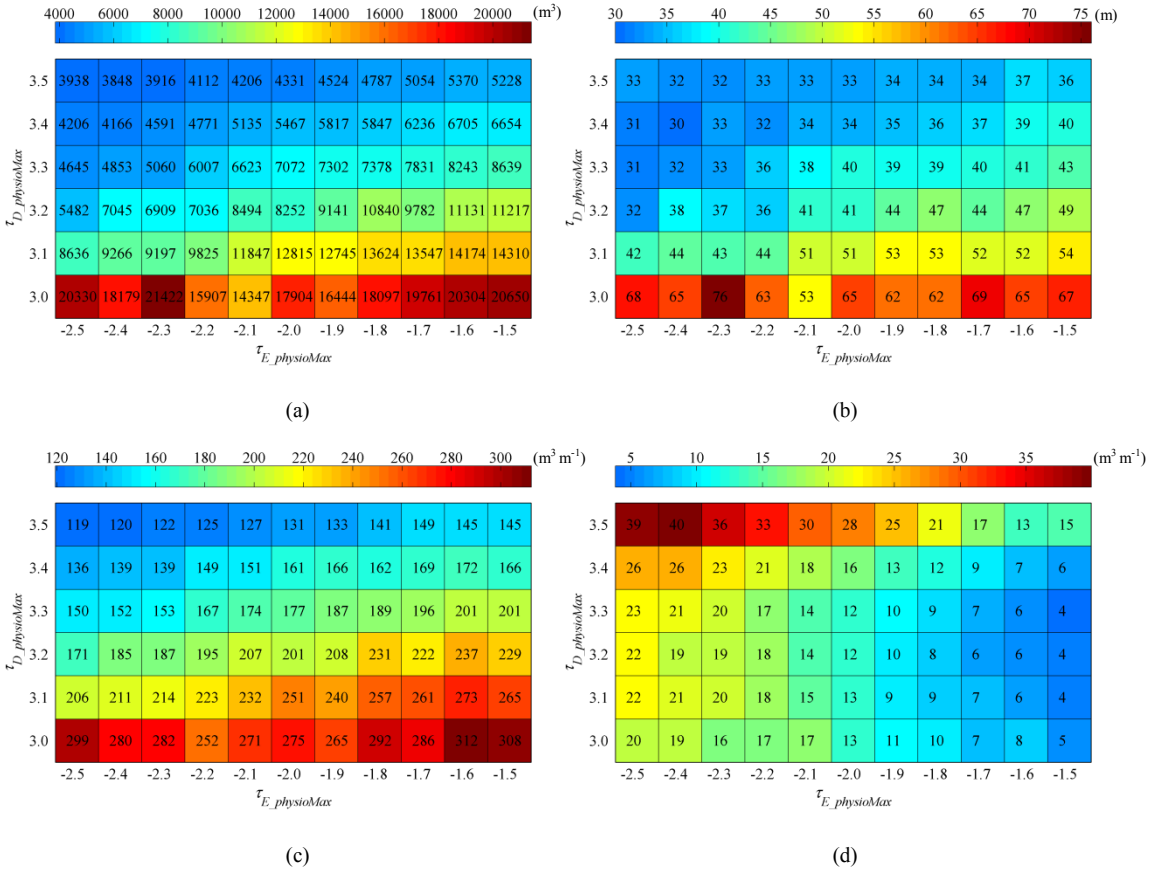

Figure 9-14. (a) the sand volume of the dune lobe, (b) the lobe width, (c) the sand volume of the dune lobe per width, and (d) the sand volume of the arms per distance, at t_{stab}.

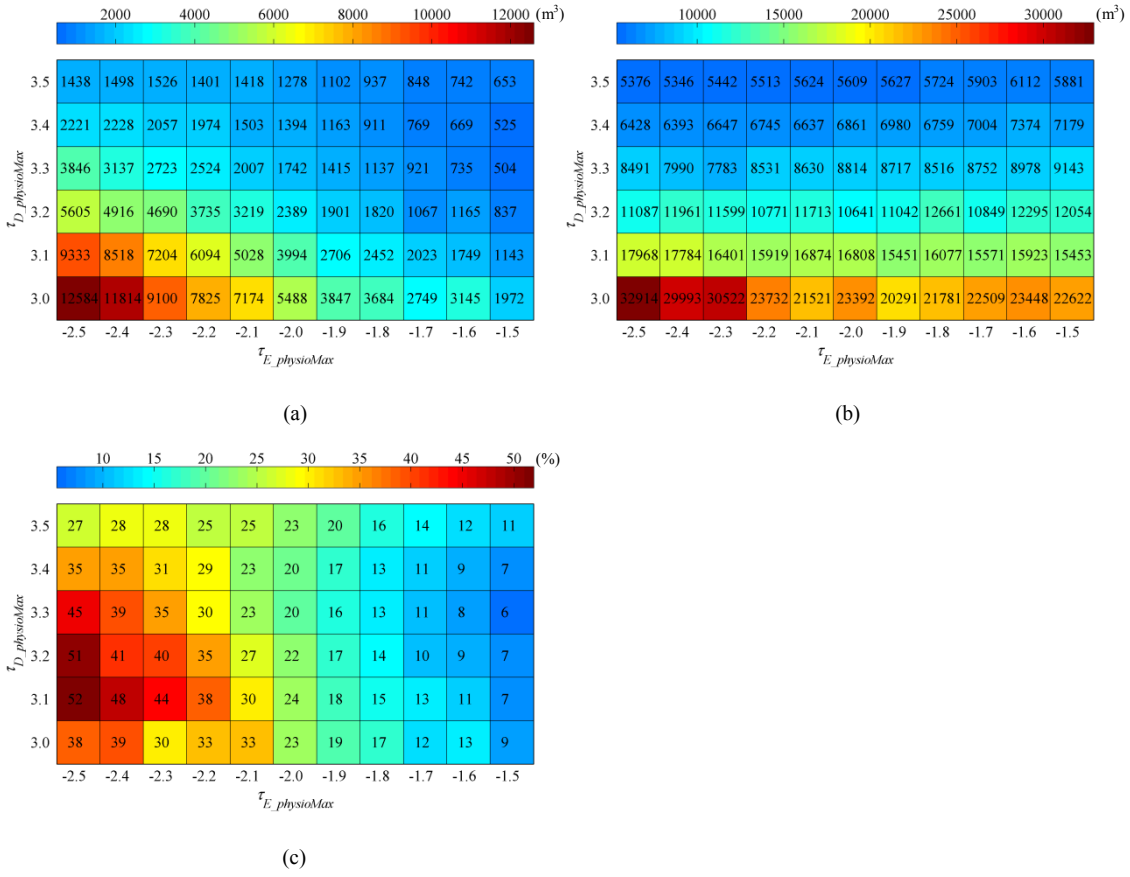

Figure 9-15. (a) the sand volume of the arms, (b) the sand volume of the dune, and (c) the percentage of sand volume from arms on a dune, at t_{stab}.

The simplified schematic graph of V' change over time is shown in Figure 9-16. The solid and dashed lines in the same colour outline the upper and the lower boundaries of a group of simulations at the same deposition tolerance (representing situations at the lowest and the highest erosion tolerances within the group respectively), within which the erosion tolerance increases gradually (not shown in the graph for simplification). It can be seen that the deposition tolerance plays a dominant role in determining the general level of V'. Given that the erosion tolerance is the same, as the deposition tolerance increases, V' increases in a larger rate and levels off more quickly, resulting in a smaller final value. This indicates that the lobe of dunes at a smaller deposition tolerance grows slower and travels longer. Within each group, a larger erosion tolerance leads to an increase in V' at a lower rate and dune stabilisation at a smaller value. This suggests that as the erosion tolerance increases, the lobe of dunes grows slower. However, the impact of the erosion tolerance on the travel time of a dune before being stabilised is dependent on the magnitude of the deposition tolerance. The t_{low} and t_{high} represent the dune stabilisation times at the smallest and the highest erosion tolerances in each group respectively when the deposition tolerance is the same. The time difference between t_{low} and t_{high} shortens gradually as the deposition

tolerance increases. The erosion tolerance exerts a strong negative impact on the dune stabilisation at a low deposition tolerance, and a larger erosion tolerance increases the dune stabilisation time significantly (t_{high} is ahead of t_{low} further). Nevertheless, as the deposition tolerance continues to increase, a shift between t_{low} and t_{high} occurs and t_{high} moves ahead of t_{low} slightly. A larger erosion tolerance starts to encourage the stabilisation of a dune to a minor degree. When the deposition tolerance is very high, dunes are stabilised quickly and the time difference arising from the erosion tolerance is indiscernible.

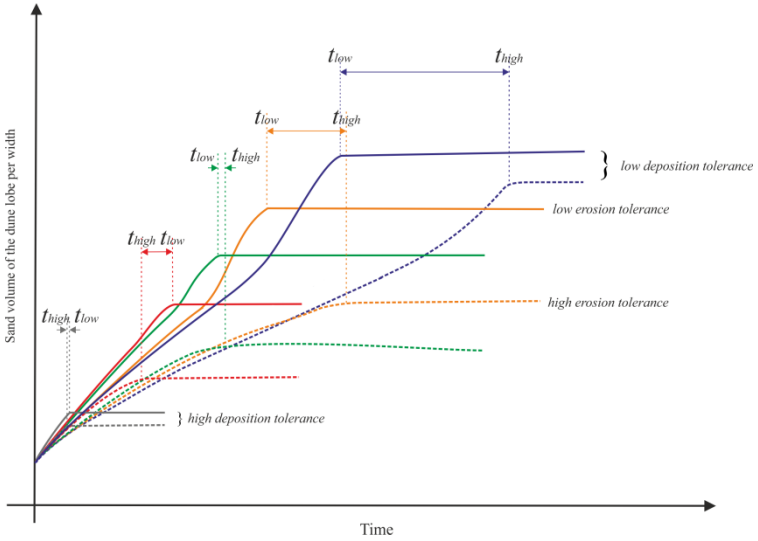

Figure 9-16. The schematic graph of sand volume on the dune lobe per width change over time according to the results of 66 simulations. Each colour represents a group of simulations with the same deposition tolerance. Solid and dashed lines are representatives of the lowest and highest erosion tolerances for each group with the same deposition tolerance respectively. Simulations between these two representatives of erosion tolerances in each group are not presented here for simplification. t_{low} and t_{hight} denote the dune stabilisation times at the lowest and the highest erosion tolerances in each deposition tolerance group respectively.

9.3.6 Arms-developing Angles

The arms-developing angle (θ_{arms}) is governed by the deposition tolerance, but is largely independent of the erosion tolerance, as shown in Figure 9-17. Results from Kruskal-Wallis testing show there are significant differences ($p < 0.001$) between groups of simulations with the same deposition tolerance but differnet erosion tolerances. As the deposition tolerance increases, θ_{arms} increases significantly with a larger variablity. The larger variability may be due to the fact that the dunes at a higher deposition

tolerance are stablised more quickly and therefore a smaller number of points are available to define the crests of arms. As a result, the varability of θ_{arms} grows as the deposition tolerance increases.

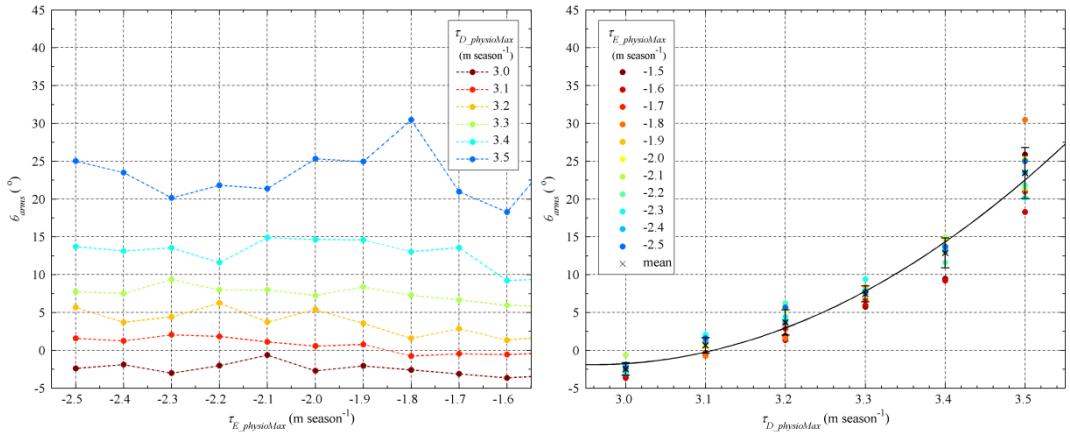

(a) (b)

Figure 9-17. The arms-developing angle under different erosion and deposition tolerances. The cross and the whisker in (b) denote the mean and the associated standard deviation of the simulations at the same deposition tolerance but different erosion tolerances, and the black line is the best-fitted 2nd order polynomial regression curve of means (R^2 = 0.99).

As the deposition tolerance decreases, θ_{arms} becomes smaller and the two arms are more parallel with each other, which is associated with the formation of more elongated parabolic dunes. When the deposition tolerance decreases to 3.0 m season^{-1}, two trailing arms can even form a negative angle, which means that the arms are separating away from each other and the dune lobe is expanding gradually. A negative θ_{arms} is rare due to the fact that the barchan-to-parabolic dune transformations in these cases usually take very long time and an initial barchan can maintain its crescentic shape and migrate forward over a very long distance before being transformed into a parabolic dune, although the shape of a lobe can flip quickly at the final stage. At an even lower deposition tolerance, an initial barchan migrates outside of a simulation domain without changing its shape. Meanwhile, a very high deposition tolerance (e.g., 4 m seaon^{-1}) can cause an immediate stabilisation of dunes and no parabolic shape can develop.

9.4 Influence of the Boundary Condition: Initial Barchan Height

9.4.1 Dune Shape

Phase diagrams in Figure 9-18 show the types of resulting parabolic dunes at both t_{tran} and t_{stab} under the impacts of vegetation with different erosion and deposition tolerances. The initial barchan varies in height from 5.2 m, 6.2 m, 7.2 m, 8.2 m, to 9.2 m. The chevron parabolic dunes can only be found at low erosion and deposition tolerances at t_{tran}. As H_0 increases, the boundaries of erosion and deposition tolerances developing chevron parabolic dunes move to a smaller region. When H_0 reaches 9.2 m, chevron parabolic dunes cannot form any more. After transformations from barchans, chevron parabolic dunes can continue to develop into lunate and typical parabolic dunes before being stabilised completely. Elongated parabolic dunes develop at low deposition tolerances but high erosion tolerances. With an increase in H_0, there is no significant change in the lower boundary of erosion tolerances, whereas the upper boundary of deposition tolerances moves towards a much lower value and at an extreme even beyond the selected minimal deposition tolerance of 3.0 m season^{-1} when H_0 is 9.2 m. Lunate parabolic dunes, however, extend their realm significantly to a much lower deposition tolerance as H_0 increases. For typical parabolic dunes, whilst the upper boundary of deposition tolerances is pushed towards a lower value by the replacement of lunate parabolic dunes, the lower boundary of deposition tolerances also drops significantly. Collectively, the resulting parabolic dunes become less elongated as the height of the initial barchans increases.

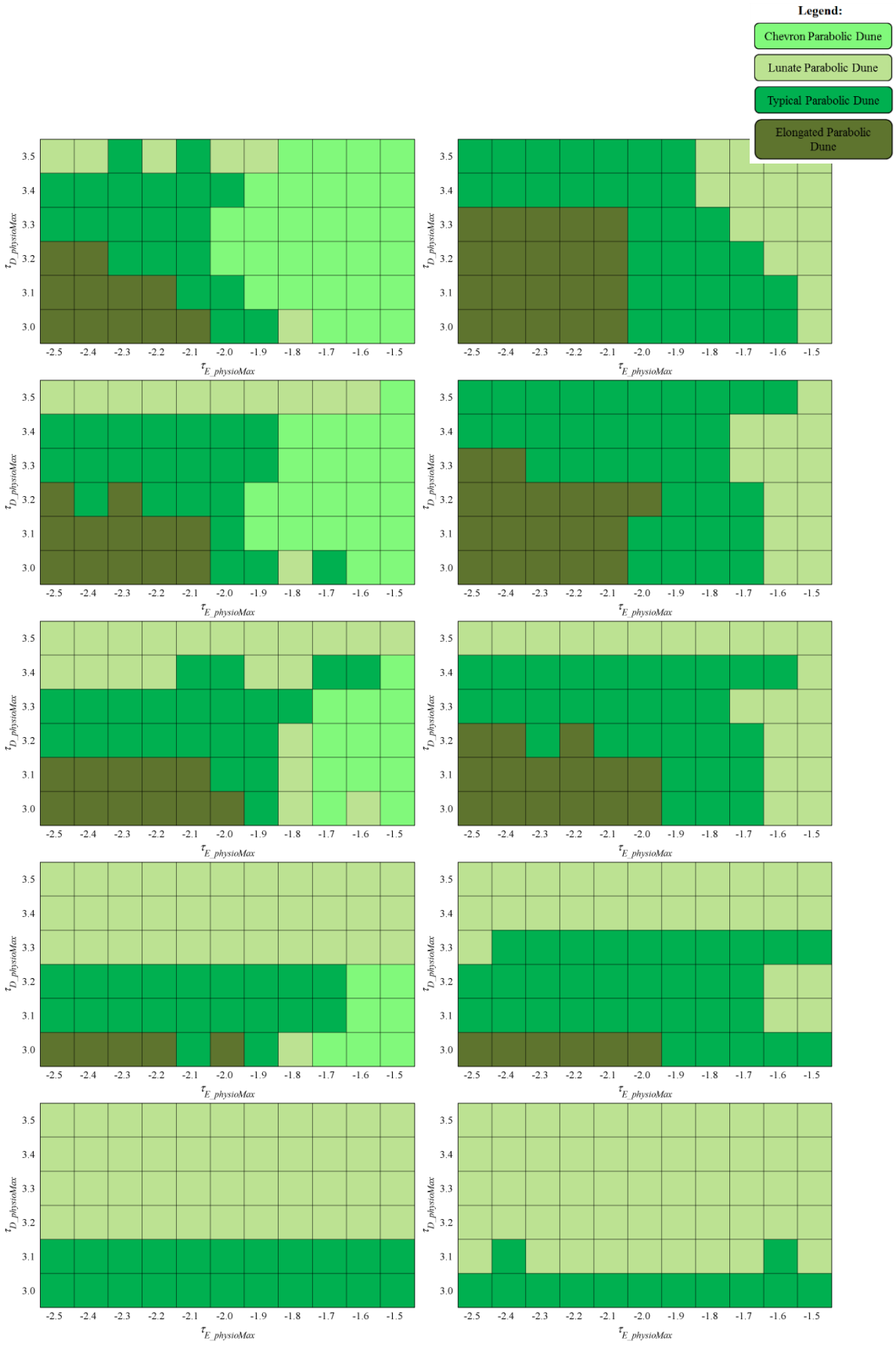

Figure 9-18. The resulting dune types at t_{tran} (left) and t_{stab} (rigth). H_0 from the top to the bottom is 5.2 m, 6.2 m, 7.2 m, 8.2 m, and 9.2 m in sequence.

Figure 9-19 presents the average dune width and length of parabolic dunes at t_{stab}. The associated dune-elongating ratio is shown in Figure 9-20. As H_0 increases, the influence of erosion tolerances on the length, average width, and dune-elongating ratio becomes much less significant. A relatively low initial barchan encourages the development of long-walled trailing arms and elongated parabolic dunes. The change in H_0 exerts strong impacts on the shape of the resulting parabolic dunes at relatively high erosion but low deposition tolerances. The outstanding difference in the dune-elongating ratio arising from a high erosion or low deposition tolerance can thus be compromised by a larger H_0. A barchan-to-parabolic transformation from a smaller H_0 is more sensitive to the erosion and deposition tolerances of vegetation species.

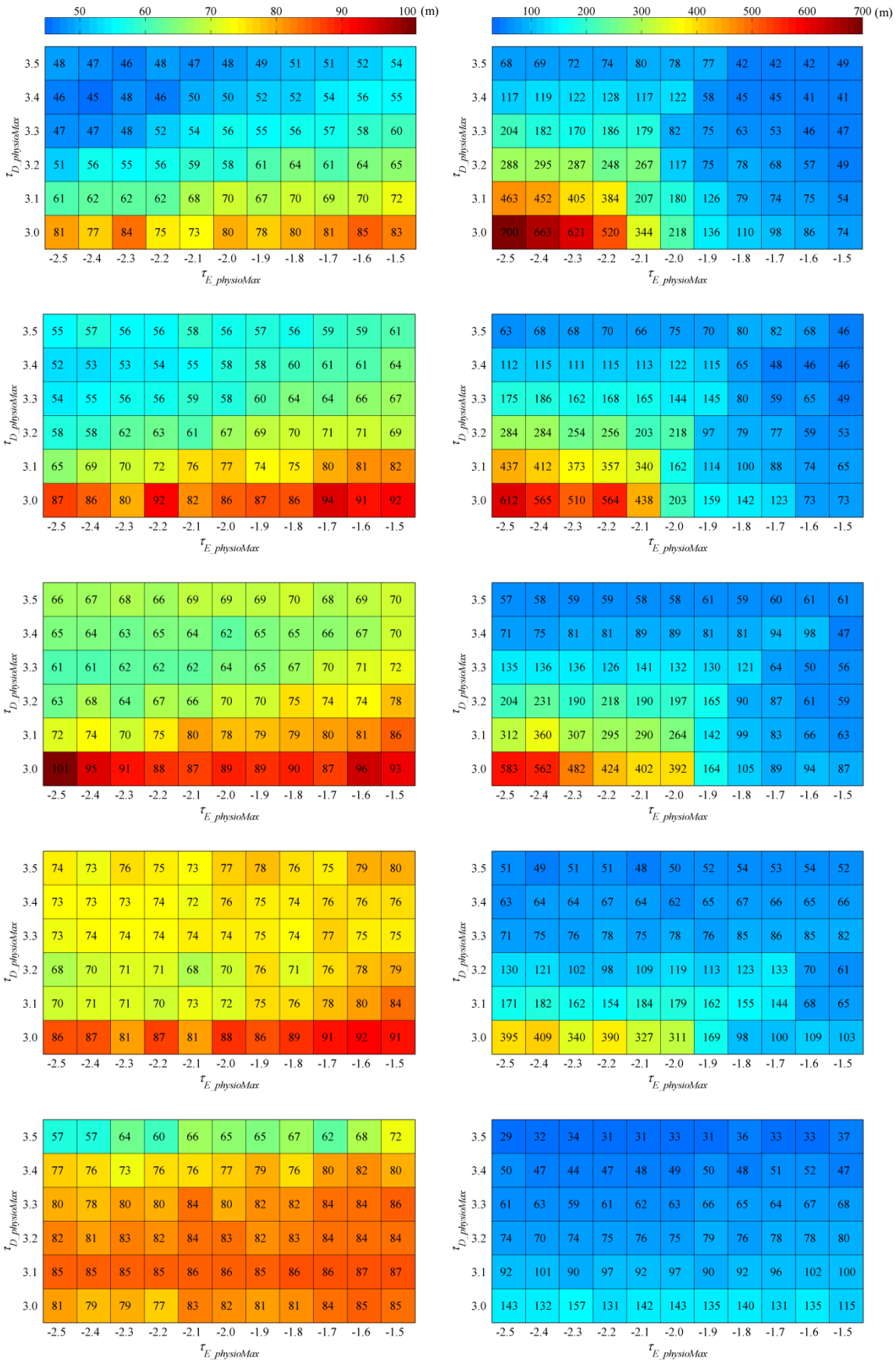

Figure 9-19. The average dune width (left) and dune length (right) of parabolic dunes at t_{stab}. H_0 from the top to the bottom is 5.2 m, 6.2 m, 7.2 m, 8.2 m, and 9.2 m in sequence.

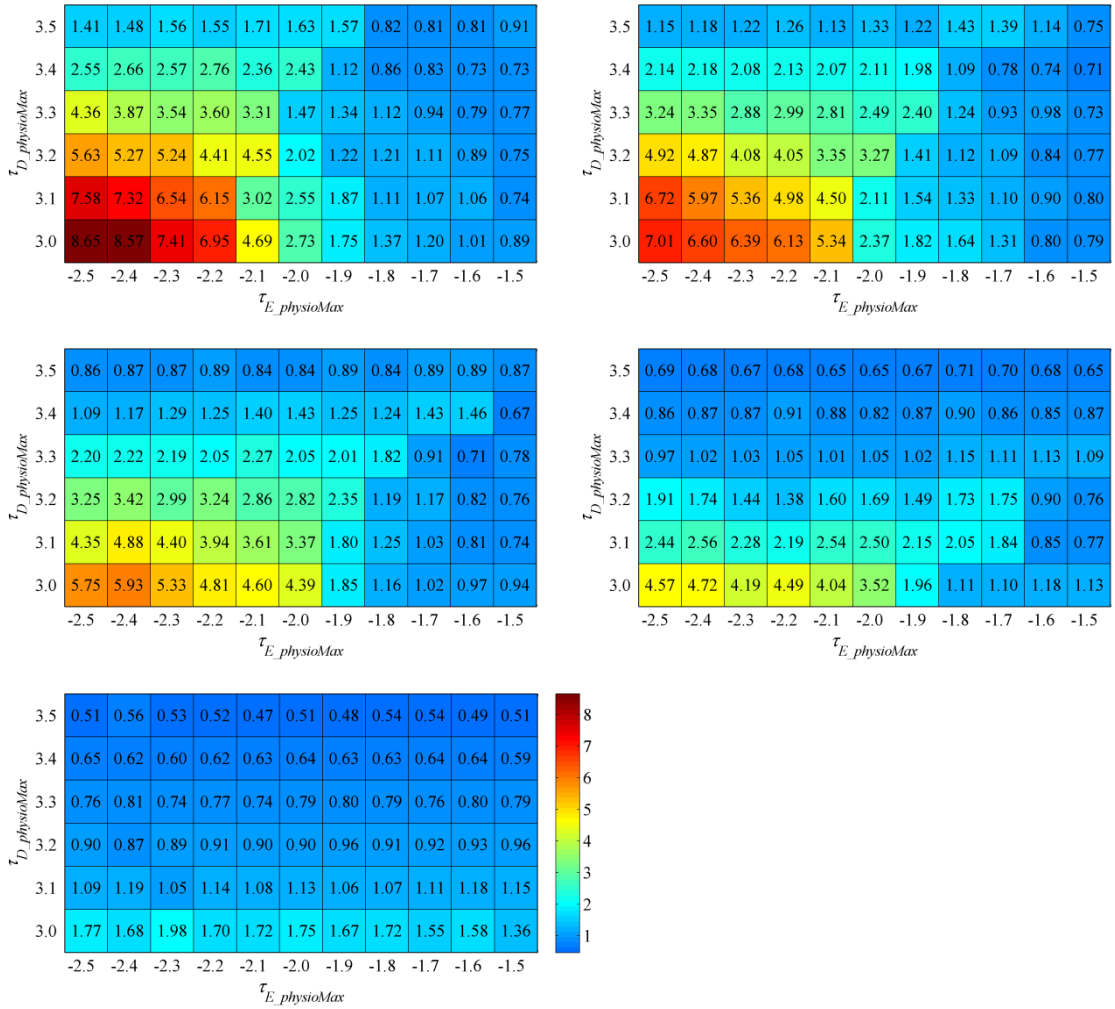

Figure 9-20. The dune-elongating ratio of resulting parabolic dunes at t_{stab}. H_0 is 5.2 m, 6.2 m, 7.2 m, 8.2 m, and 9.2 m in sequence.

9.4.2 Transition and Stabilisation Times

A large H_0 of initial barchans generally results in a relatively quick dune transition and stabilisation, to a larger extent when a deposition tolerance is relatively low (Figure 9-21 and Figure 9-22). Compared with the deposition tolerance which is essential to control the dune transition and stabilisation, the erosion tolerance seems to play a limited role, effective only when an initial barchan is relatively small as well as the deposition tolerance is relatively low.

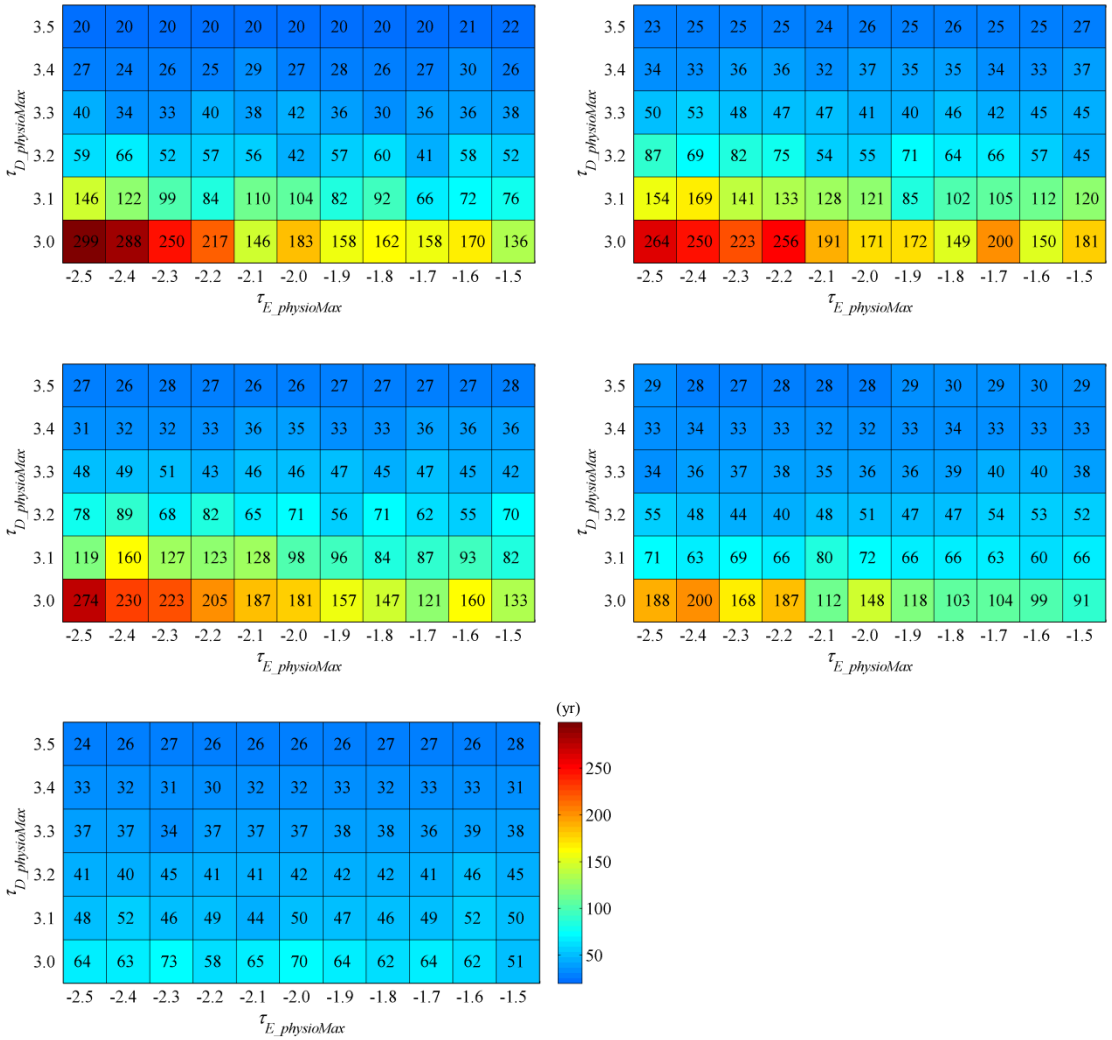

Figure 9-21. The t_{tran} of the barchan-to-parabolic dune transformations. H_0 is 5.2 m, 6.2 m, 7.2 m, 8.2 m, and 9.2 m in sequence.

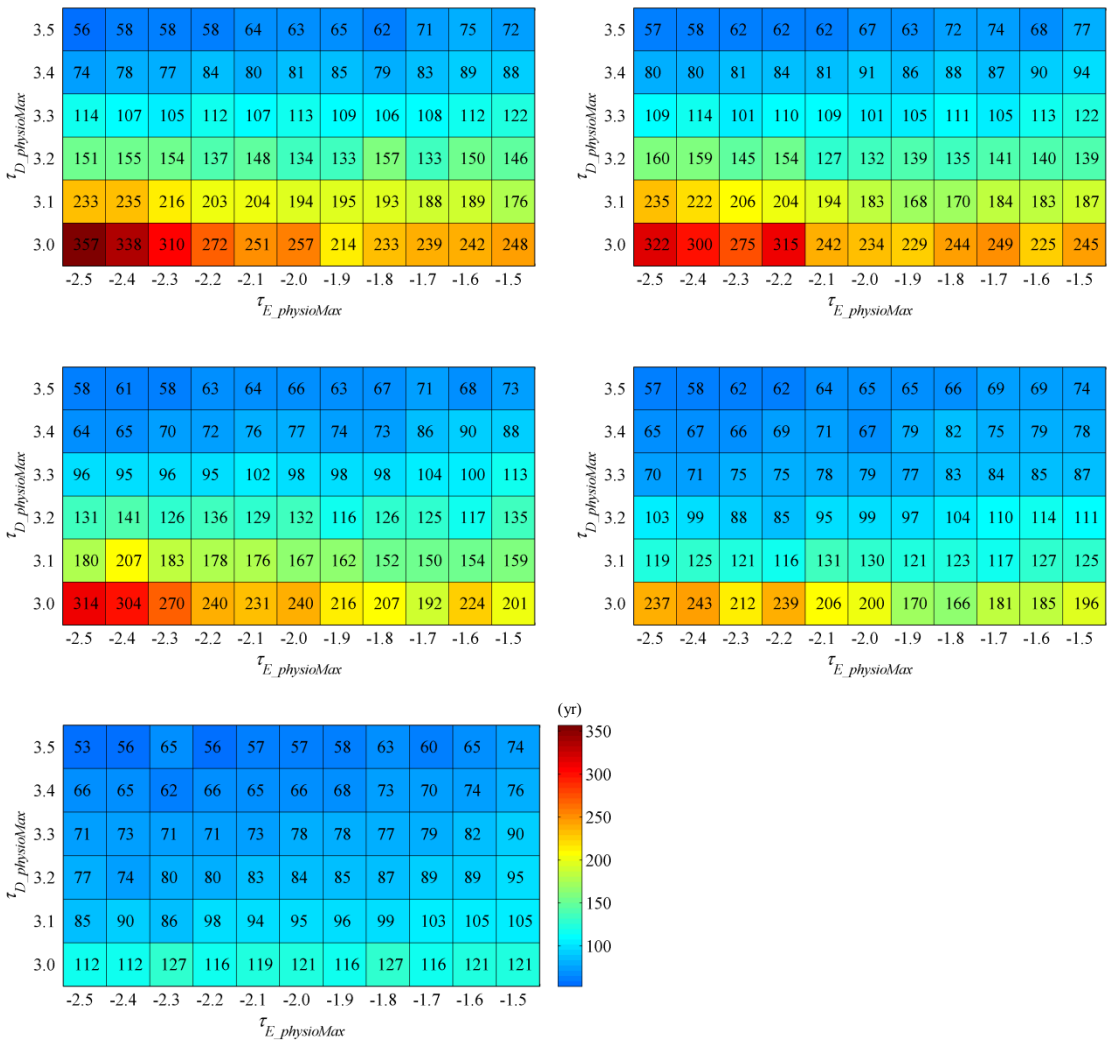

Figure 9-22. The t_{stab} of the barchan-to-parabolic dune transformations. H_0 is 5.2 m, 6.2 m, 7.2 m, 8.2 m, and 9.2 m in sequence.

9.4.3 Dune Migration and Trailing Arms

Figure 9-23 presents the average migration rate of resulting parabolic dunes. As H_0 increases, the average migration rate decreases considerably. A high erosion tolerance or a low deposition tolerance accelerates dune migration rate more significantly for a smaller H_0. As H_0 increases, dunes migrate at a lower rate and are stabilised more quickly, resulting in a smaller dune-elongating ratio (Figure 9-20).

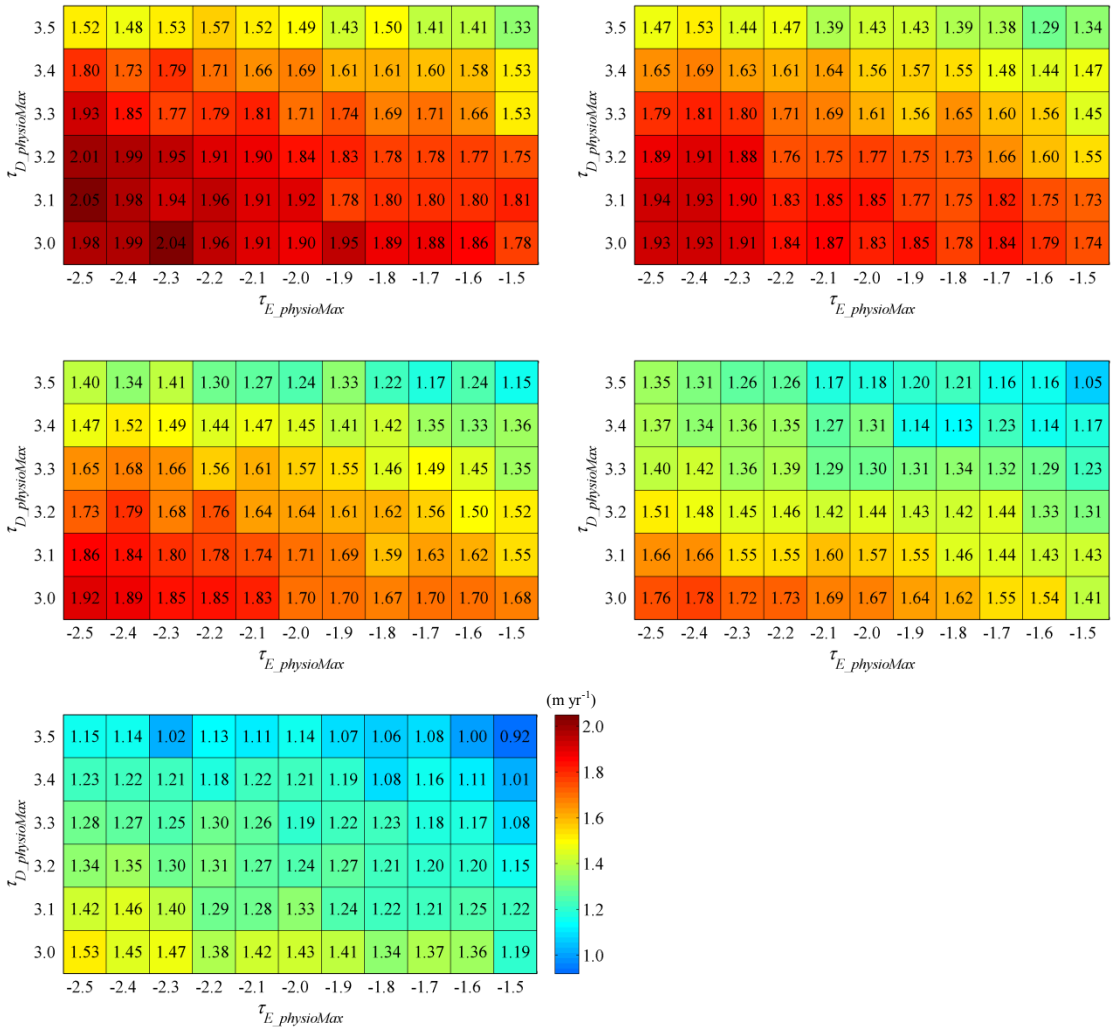

Figure 9-23. The average dune migration rate of resulting parabolic dunes. H_0 is 5.2 m, 6.2 m, 7.2 m, 8.2 m, and 9.2 m in sequence.

The arms-initiation time, meanwhile, decreases substantially at low erosion and deposition tolerances as H_0 increases (Figure 9-24). A larger initial barchan encourages the development of trailing arms more immediately, which is associated with a smaller average migration rate. The impacts of erosion and deposition tolerances on delaying arms-initiation are repressed and even eliminated at high initial barchans.

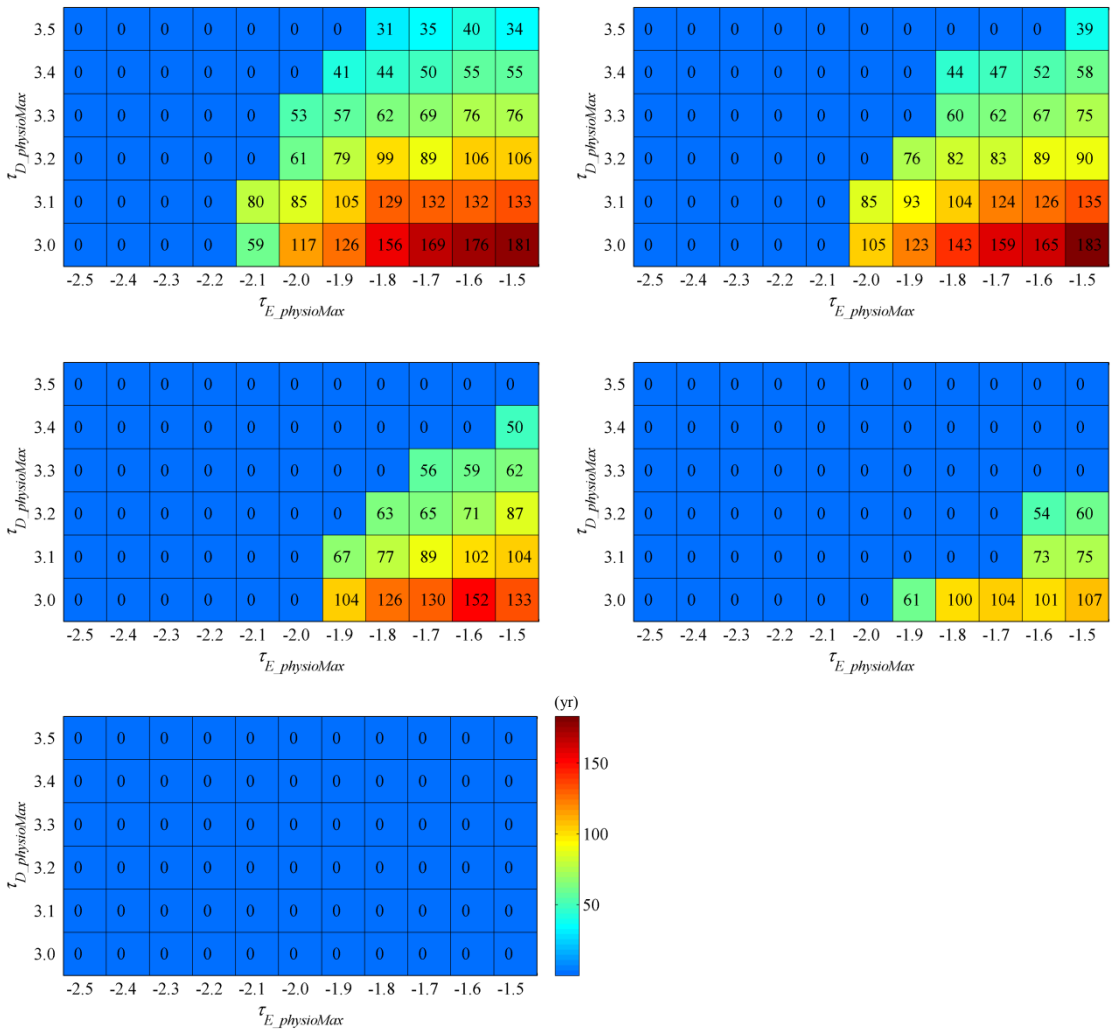

Figure 9-24. The arms-initiation time of resulting parabolic dunes. H_0 is 5.2 m, 6.2 m, 7.2 m, 8.2 m, and 9.2 m in sequence.

9.4.4 Sand Volume Dynamics

The height and the sand volume of dune lobes at t_{stab} are shown in Figure 9-25. Starting with a larger H_0, a barchan is expected to transform into a taller parabolic dune, which is however only the case when the deposition tolerance is relatively high. There is no significant increase in both the height and the sand volume of lobes at a relatively low deposition tolerance as H_0 increases. In particular, for simulations with a deposition tolerance of 3.0 m season^{-1}, the size of lobes even decreases slightly when H_0 increases larger than 7.2 m. The changes in the height of resulting parabolic dunes relative to the initial barchans, shown in Figure 9-26, indicate that a smaller initial barchan increases in height more significantly than a larger initial barchan. Low erosion and deposition tolerances generally encourage the development of a higher lobe, but the erosion tolerance becomes less important as the height of an initial barchan increases. When a deposition tolerance is relatively low, dunes at a higher erosion tolerance migrate forward at a higher

rate over a longer period of time (Figure 9-22 and Figure 9-23) but counter-intuitively grow less in height than those at a lower erosion tolerance, which indicates that a more significant sand loss occurs by forming trailing arms.

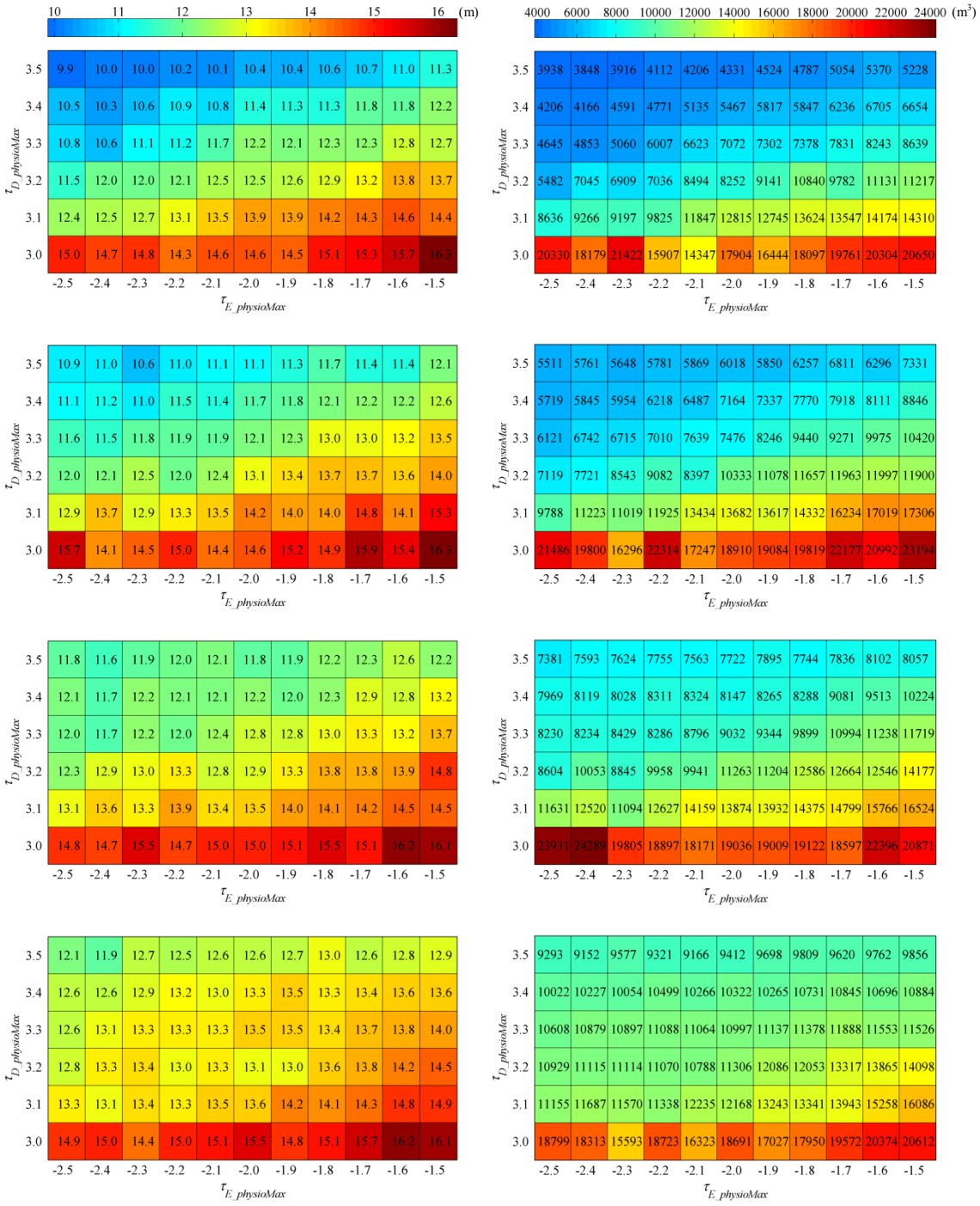

Figure 9-25. The dune lobe height (left) and the lobe volume (right) at t_{stab}. H_0 from the top to the bottom is 5.2 m, 6.2 m, 7.2 m, 8.2 m, and 9.2 m in sequence.

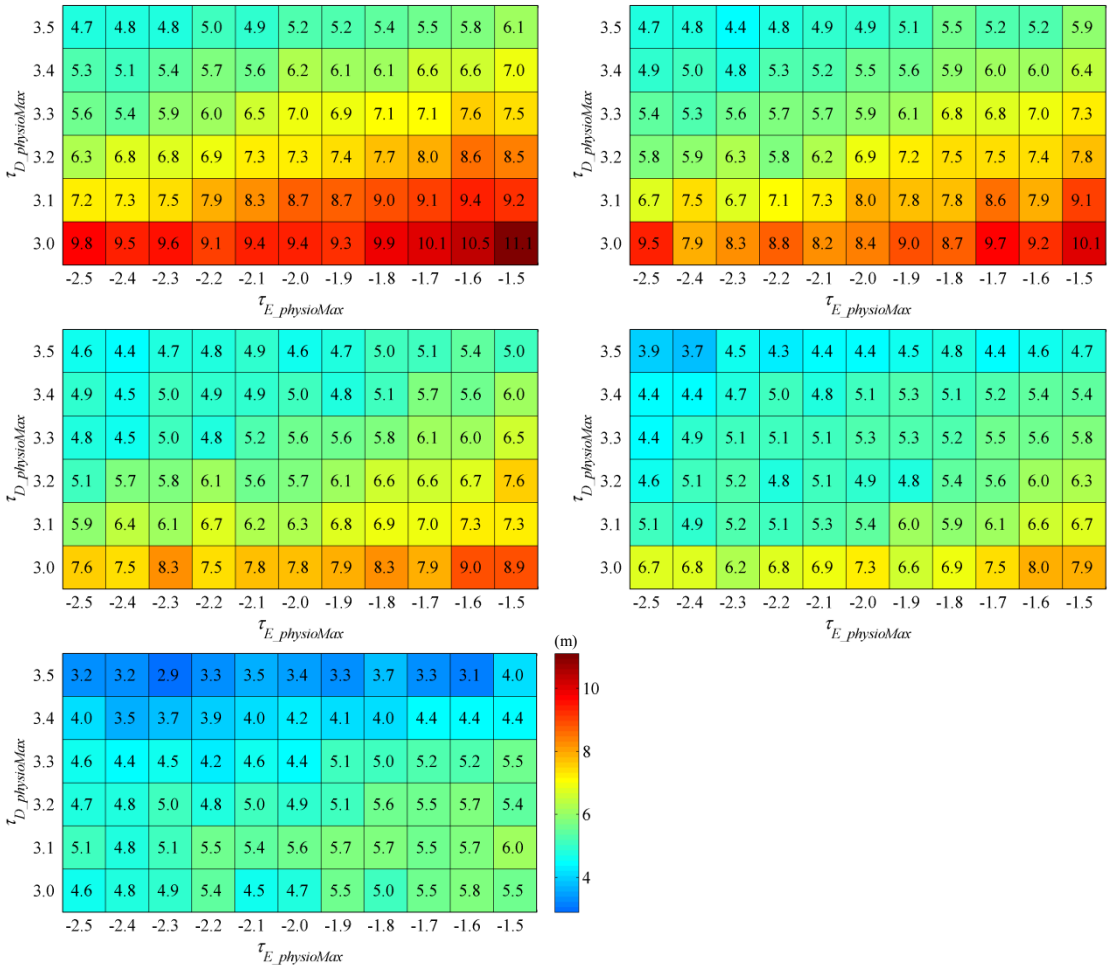

Figure 9-26. The change in dune height relative to H_0 at t_{stab}. H_0 is 5.2 m, 6.2 m, 7.2 m, 8.2 m, and 9.2 m in sequence.

9.4.5 Arms-developing Angles

The arms-developing angle (θ_{arms}) of parabolic dunes appears to be independent of the erosion tolerance and governed solely by the deposition tolerance, as has been previously discussed in Section 9.3.4. Figure 9-27 presents the relationships between θ_{arms} and the transition and the stabilisation times, showing the similar results. The t_{tran} and t_{stab} are largely controlled by the deposition tolerance, but they seem to be minimally influenced by H_0. As the deposition tolerance decreases, both t_{tran} and t_{stab} increase generally. For the same θ_{arms}, a larger initial barchan needs a longer time to be transformed into a parabolic dune and fully-stabilised by vegetation. When θ_{arms} is smaller than 10˚, t_{tran} and t_{stab} increase exponentially. Nonetheless, for the same θ_{arms}, a higher erosion tolerance is associated with a higher dune migration rate, irrespective of the deposition tolerance and H_0 (Figure 9-28).

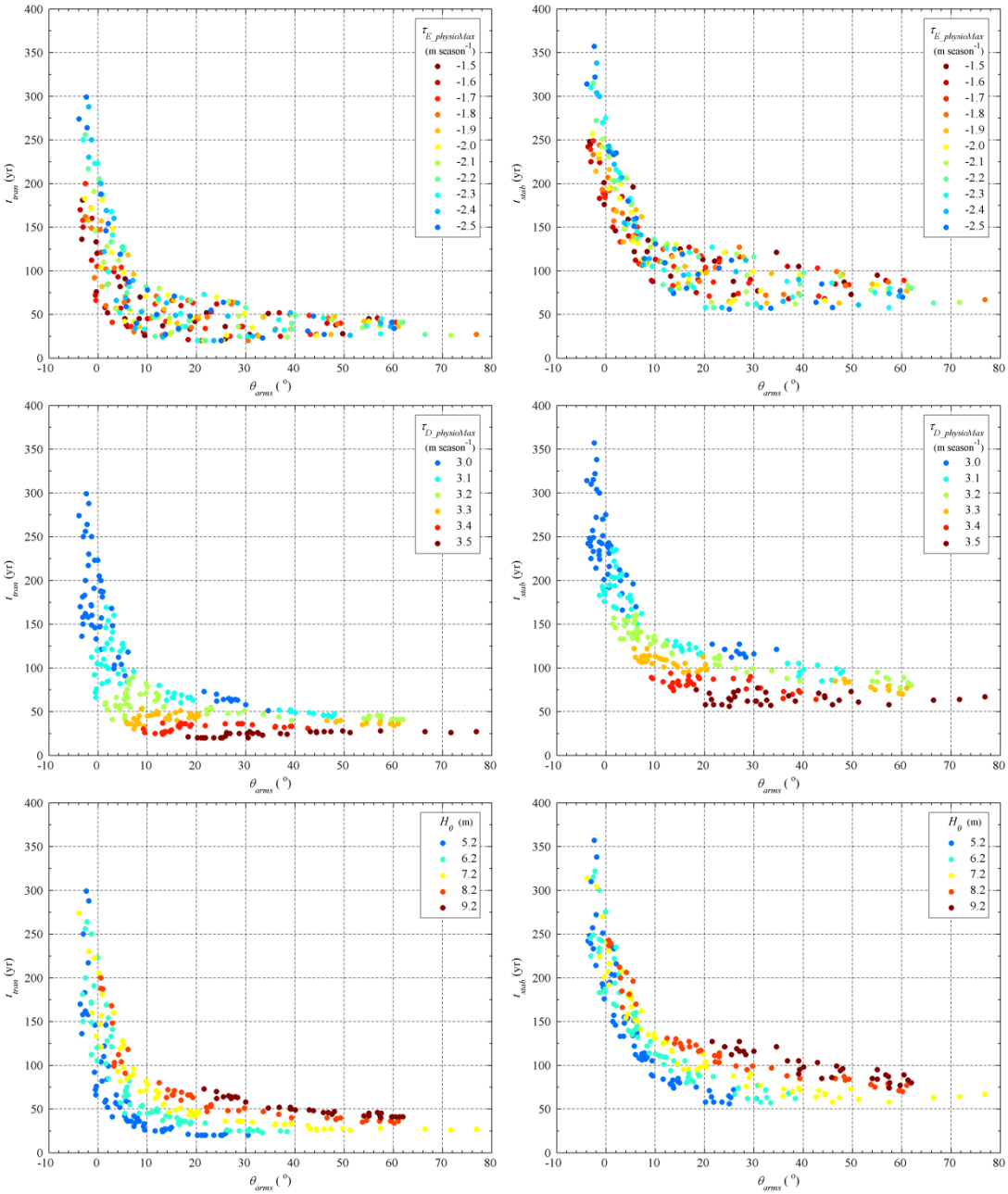

Figure 9-27. The relationships between θ_{arms} and t_{tran} (left) and between θ_{arms} and t_{stab} (right) of the barchan to parabolic dune transformations, as a function of three different simulation parameters: the erosion tolerance, the deposition tolerance, and the initial barchan height.

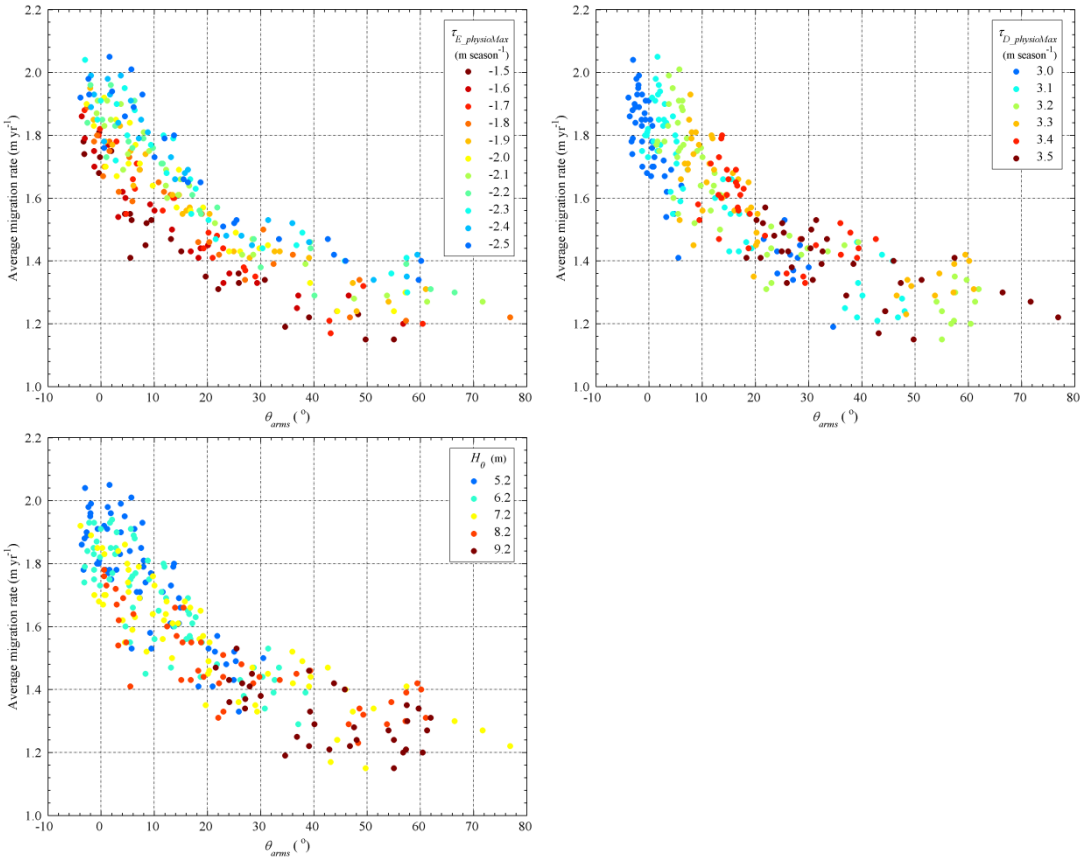

Figure 9-28. The relationships between the arms-developing angle and the average dune migration rate as a function of three different simulation parameters: the erosion tolerance, the deposition tolerance, and the initial barchan height.

9.5 Influence of the Boundary Condition: Sandy Substratum Thickness

9.5.1 Dune Shape

Figure 9-29 and Figure 9-30 show the dune type and the dune-elongating ratio of resulting parabolic dunes at t_{stab} respectively. As the sandy substratum thickness (D_0) increases, the resulting parabolic dunes become less elongated. A smaller initial barchan, however, encourages the formation of more elongated parabolic dunes. A higher deposition tolerance encourages dune stabilisation and the development of less elongated dune morphologies, whereas the erosion tolerance only exerts a limited impact on a relatively small initial barchan migrating over a relatively thin substratum. Generally, a barchan-to-parabolic dune transformation happens more quickly where a large initial barchan on a thick sandy substratum interacts with a vegetation species with a strong capability of withstanding sand burial.

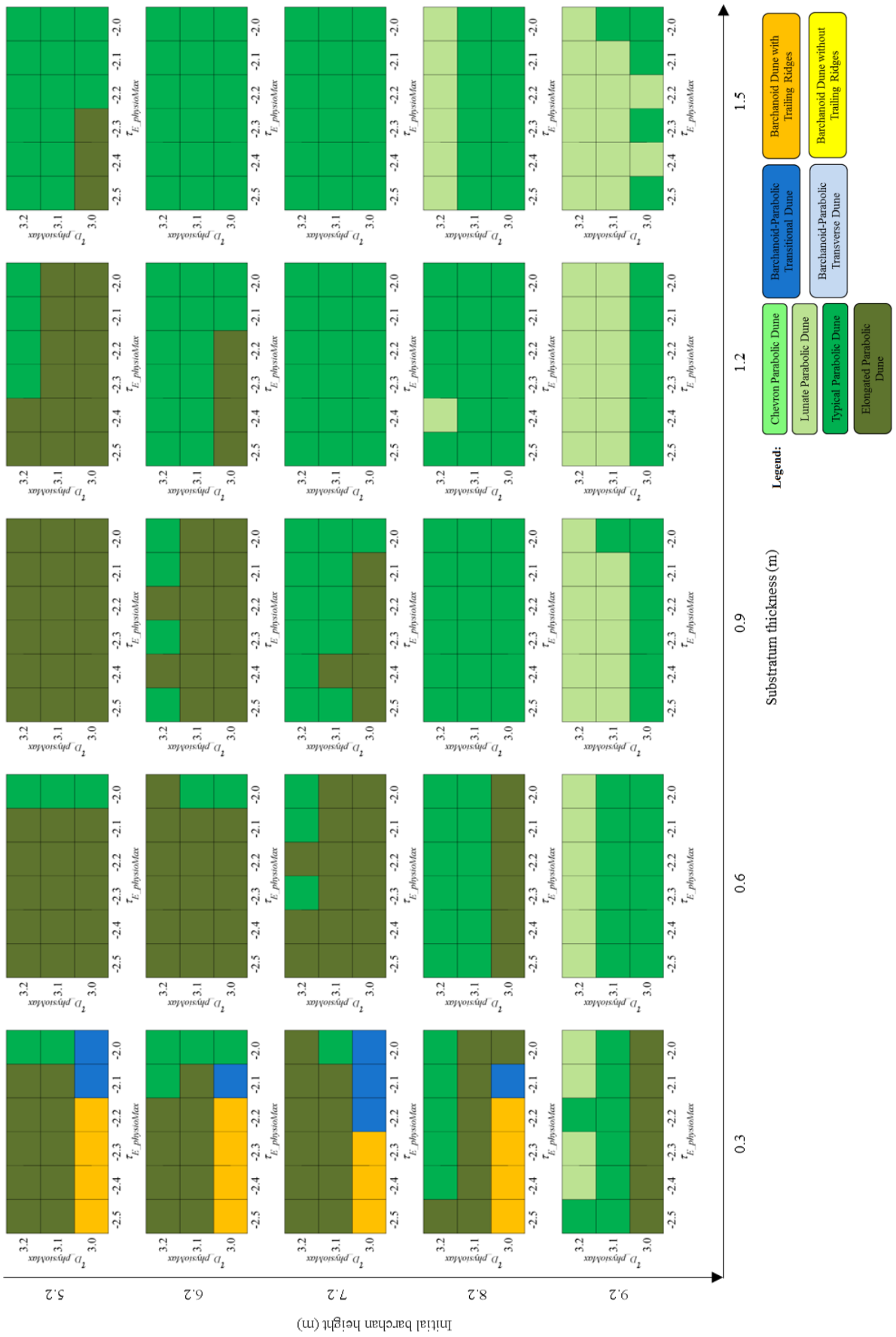

Figure 9-29. Resulting dune types from an initial barchan at different heights on a substratum of different thicknesses.

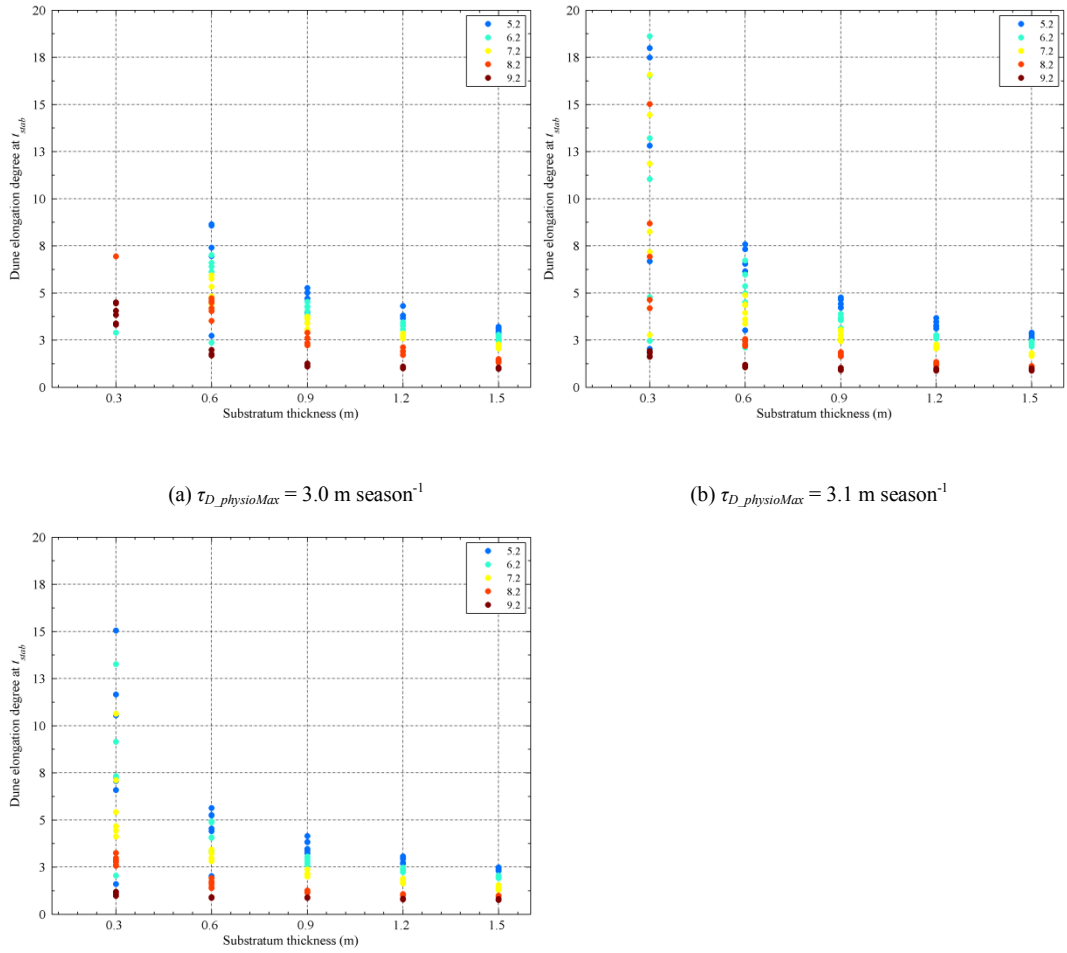

(a) $\tau_{D\_physioMax}$ = 3.0 m season^{-1}

(b) $\tau_{D\_physioMax}$ = 3.1 m season^{-1}

(c) $\tau_{D\_physioMax}$ = 3.2 m season^{-1}

Figure 9-30. The dune-elongating ratio of resulting parabolic dunes at t_{stab}. Different colours represent different heights of the initial barchans as shown in the legends. Multiple dots of the same colour denote simulations with different erosion tolerances but with the same deposition tolerance, initial barchan height, and substratum thickness.

The normalised width and height of resulting parabolic dunes (normalised by the width and height of the initial barchan respectively) are shown in Figure 9-31. The height of an initial barchan exerts a stronger impact on the normalised width of resulting parabolic dunes over a thinner substratum. For example, at a deposition tolerance of 3.0 m season^{-1}, the normalised width decreases significantly for an initial barchan at the height of 9.2 m as the substratum thickness decreases, whereas the normalised width increases considerably when an initial barchan is smaller even for an initial barchan at the height of 8.2 m. As the substratum thickness increases, the impact of the initial barchan height on the width of parabolic dunes is less profound. Interestingly, at a deposition tolerance of 3.0 m season^{-1}, a smaller initial barchan develops a wider normalised width of parabolic dunes; however, at a deposition tolerance of 3.2 m season^{-1}, a larger initial barchan forms a wider normalised width. There is hence a gradually reversing

trend for the impact of initial barchan height on the width of resulting parabolic dunes as the deposition tolerance increases. This is likely to indicate that sand sources change from external-dominant (from a sandy substratum) to internal-dominant (from the dune itself) as the deposition tolerance increases. Meanwhile, a smaller initial barchan leads to a greater increase in the normalised height of resulting parabolic dunes. The influence of the substratum thickness, however, is not significant. As the deposition tolerance increases, the normalised height of resulting parabolic dunes decreases slightly for a small initial barchan (5.2 – 7.2 m), but it does not show discernible change for a large initial barchan (8.2 – 9.2 m).

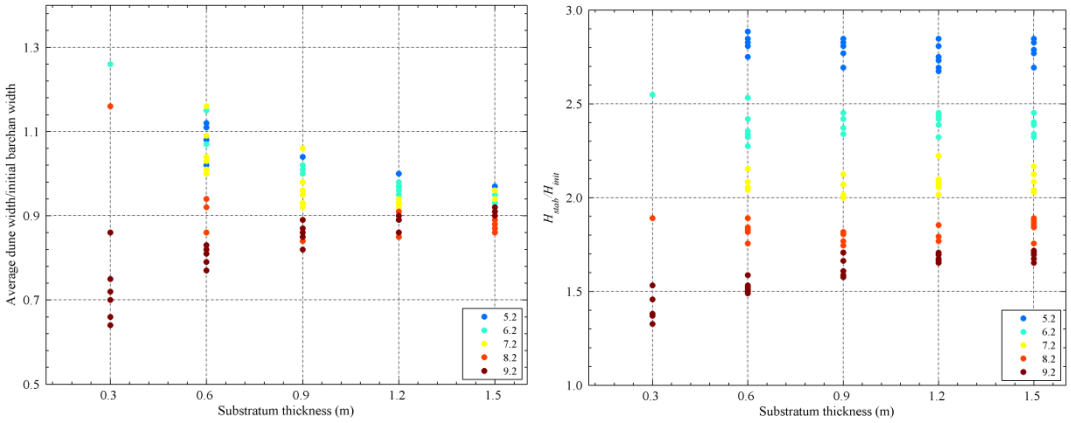

(a) $\tau_{D\_physioMax}$ = 3.0 m season^{-1}

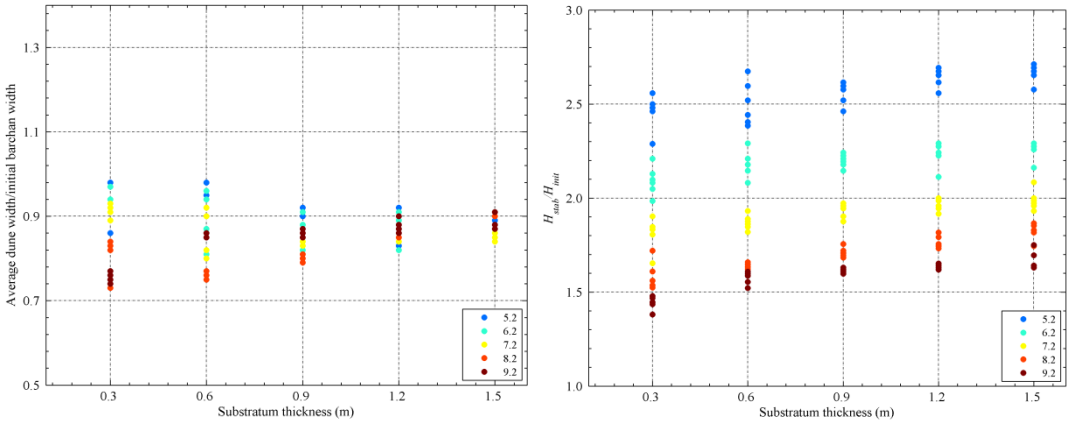

(b) $\tau_{D\_physioMax}$ = 3.1 m season^{-1}

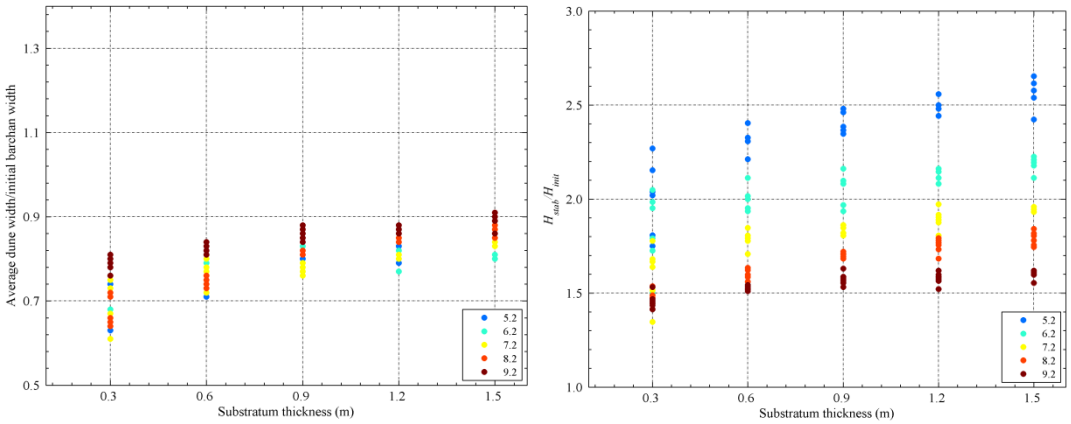

(c) $\tau_{D\_physioMax}$ = 3.2 m season^{-1}

Figure 9-31. The ratio of the average dune width to the initial barchan width as well as the ratio of the stabilised dune height to the initial barchan height. Different colours represent different heights of the initial barchans as shown in the legends. Multiple dots of the same colour denote simulations with different erosion tolerances but with the same deposition tolerance, initial barchan height, and substratum thickness.

9.5.2 Transition and Stabilisation Times

The transition and the stabilisation times are significantly influenced by the substratum thickness especially for a smaller initial barchan and for a vegetation species less tolerant of sand burial (Figure 9-32). An increase in D_0 shortens both t_{tran} and t_{stab} substantially. A smaller initial barchan requires a longer time to be transformed into parabolic dunes and stabilised by vegetation eventually. A higher deposition tolerance encourages more significantly the dune transition and the stabilisation of a smaller initial barchan. The transformation from a smaller initial barchan into a parabolic dune is thus more sensitive to changes in both the substratum thickness and the deposition tolerance.

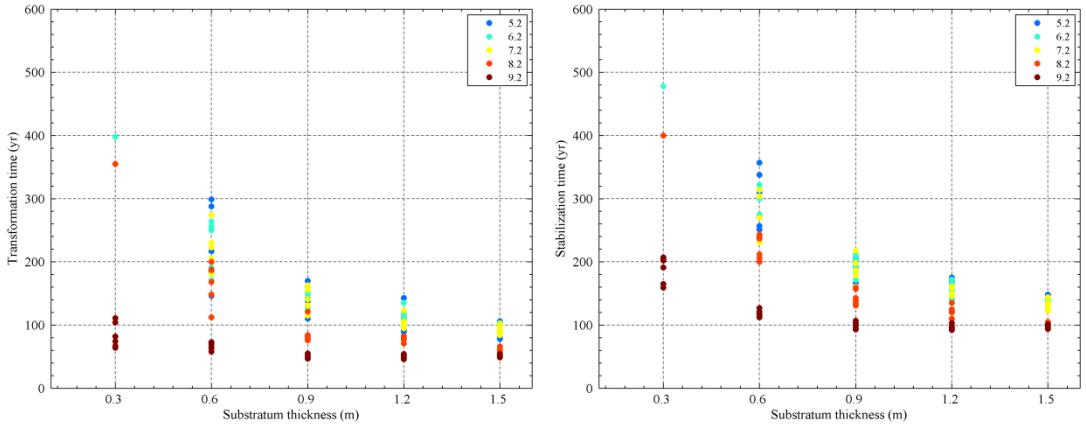

(a) $\tau_{D\_physioMax}$ = 3.0 m season^{-1}

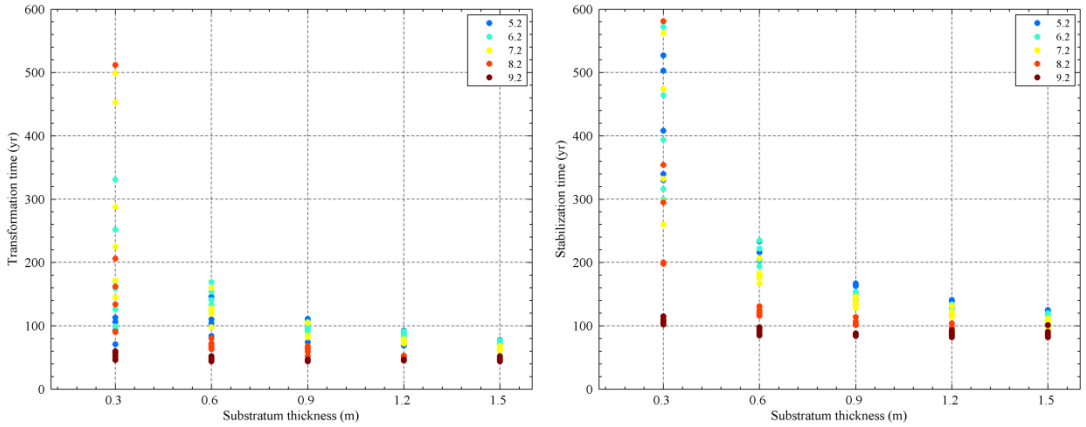

(b) $\tau_{D\_physioMax}$ = 3.1 m season^{-1}

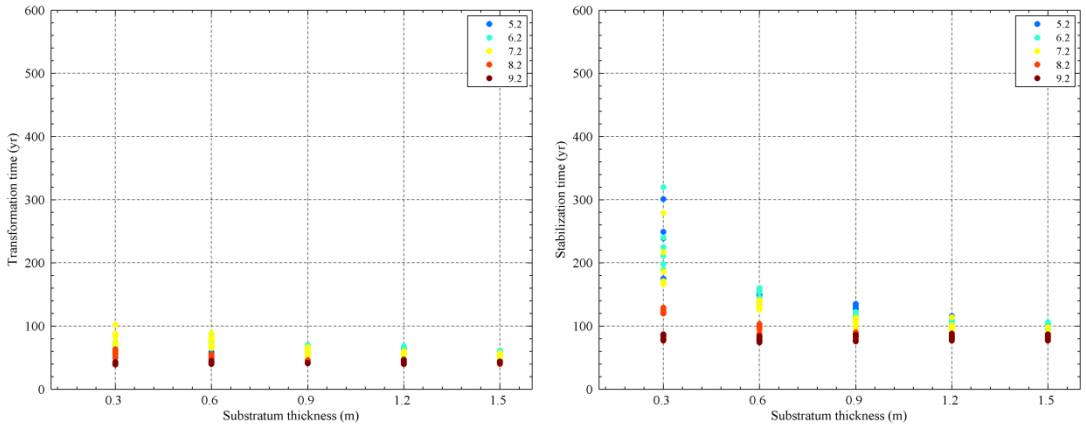

(c) $\tau_{D\_physioMax}$ = 3.2 m season^{-1}

Figure 9-32. The t_{tran} and t_{stab} of the barchan-to-parabolic dune transformations. Different colours represent different heights of the initial barchans as shown in the legends. Multiple dots of the same colour denote simulations with different erosion tolerances but with the same deposition tolerance, initial barchan height, and substratum thickness.

9.5.3 Dune Migration

As shown in Figure 9-33, a dune generally migrates at a higher rate and travels further before being stabilised by vegetation as a sandy substratum decreases. A smaller initial dune maintains a higher rate for a longer period of time (Figure 9-32), which can be undermined by a higher deposition tolerance provided that a sandy substratum is relatively thin. As the sandy substratum thickness increases, the influence of the deposition tolerance on the dune migration rate is lessened and even inconsequential when D_0 increases up to 0.9 m.

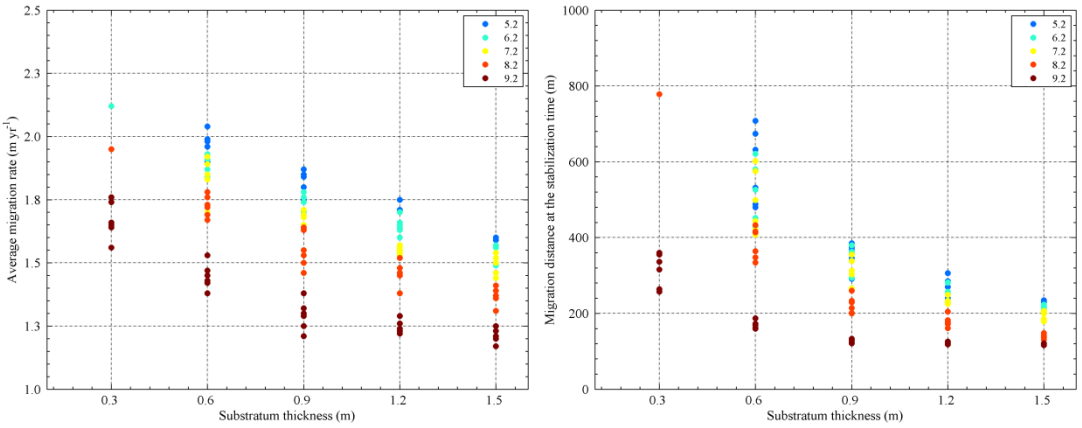

(a) $\tau_{D\_physioMax}$ = 3.0 m season^{-1}

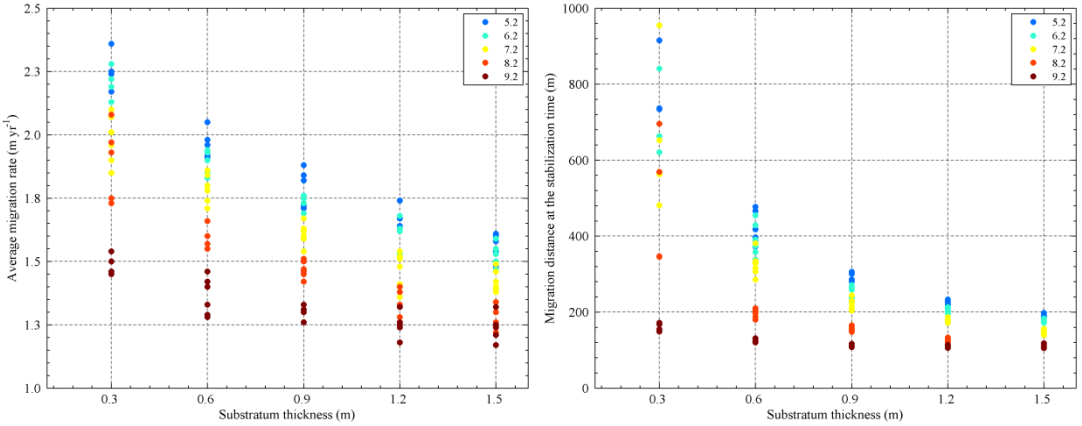

(b) $\tau_{D\_physioMax}$ = 3.1 m season^{-1}

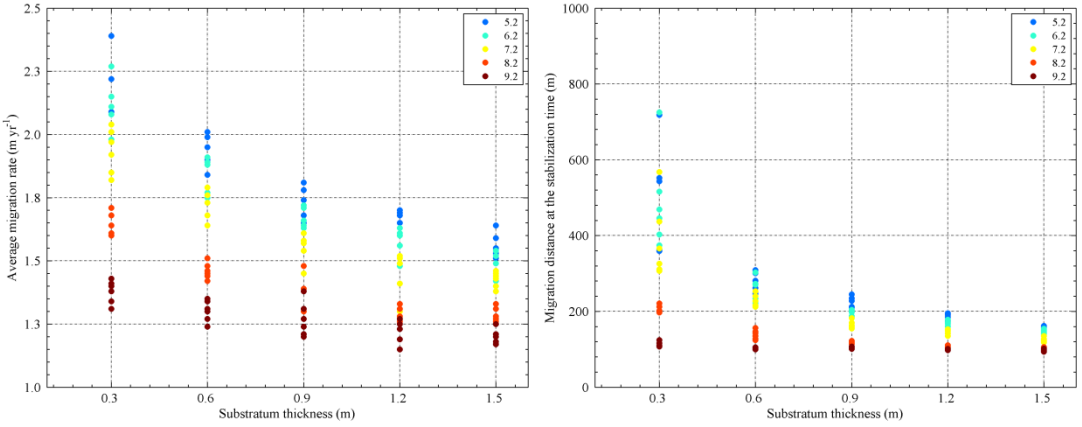

(c) $\tau_{D\_physioMax}$ = 3.2 m season^{-1}

Figure 9-33. The average migration rate and the migration distance before a dune is fully stabilised. Different colours represent different heights of the initial barchans as shown in the legends. Multiple dots of the same colour denote simulations with different erosion tolerances but with the same deposition tolerance, initial barchan height, and substratum thickness.

9.5.4 Sand Volume Dynamics

Figure 9-34 shows the sand volume gained from a sandy substratum during the processes of dune stabilisation and barchan-to-parabolic dune transformations. Generally, a smaller initial barchan gains more sand from its substratum, and a higher deposition tolerance encourages a quicker stabilisation and hence reduces the amount of sand that a dune gains from its substratum. The influence of the substratum thickness on the sand volume of resulting parabolic dunes, nonetheless, varies depending on the height of the initial barchan as well as the deposition tolerance of the vegetation species. When a deposition tolerance is 3.0 m, as a substratum thickness increases, the sand gained from the substratum also increases for a relatively large initial barchan (9.2 m), but it decreases for smaller initial barchans (5.2 to 8.2 m). However, a thicker substratum leads to a slight increase in the sand volume of resulting parabolic dunes when the deposition tolerance increases to 3.2 m, regardless of the height of initial barchans. A relatively large deposition tolerance, therefore, significantly limits small initial barchans gaining sand from a relatively thin substratum. It is likely that there is a trade-off between the advantages deriving from a thicker substratum that provides more local sand and the disadvantages resulting from a decrease in the dune migration rate and the associated limitation imposed to shorten its travel track.

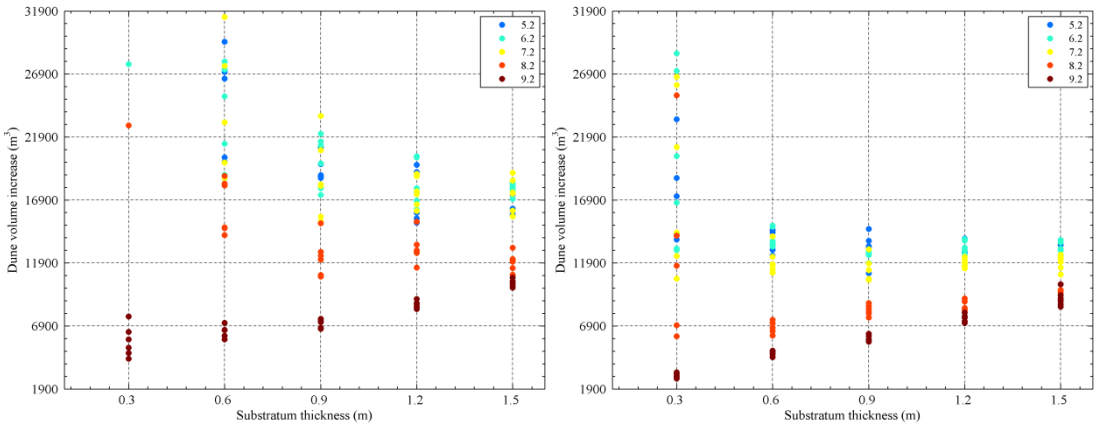

(a) $\tau_{D\_physioMax}$ = 3.0 m season^{-1}

(b) $\tau_{D\_physioMax}$ = 3.1 m season^{-1}

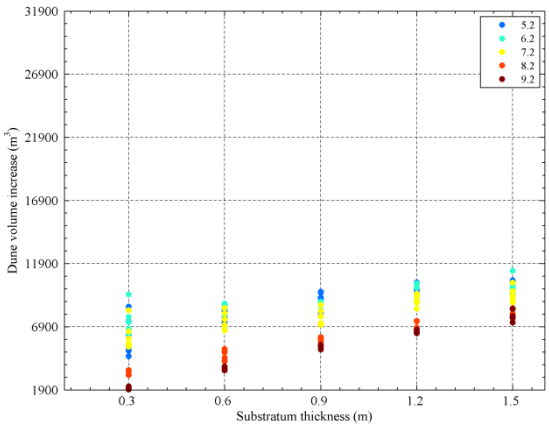

(c) $\tau_{D\_physioMax}$ = 3.2 m season^{-1}

Figure 9-34. The dune volume increase at t_{stab}. Different colours represent different heights of the initial barchans as shown in the legends. Multiple dots of the same colour denote simulations with different erosion tolerances but with the same deposition tolerance, initial barchan height, and substratum thickness.

9.5.5 Arms-developing Angles

The arms-developing angle is significantly influenced by the substratum thicknesses (Figure 9-35). Negative arms-developing angles indicate that dune lobes are gradually expanding and widening laterally, whilst positive arms-developing angles suggest the horns of initial barchans are anchored by vegetation and dune lobes are shrinking gradually. A thicker substratum thickness results in a larger arms-developing angle of resulting parabolic dunes. As the deposition tolerance increases, the arms-developing angle increases to a larger degree for dunes migrating on a thinner substratum.

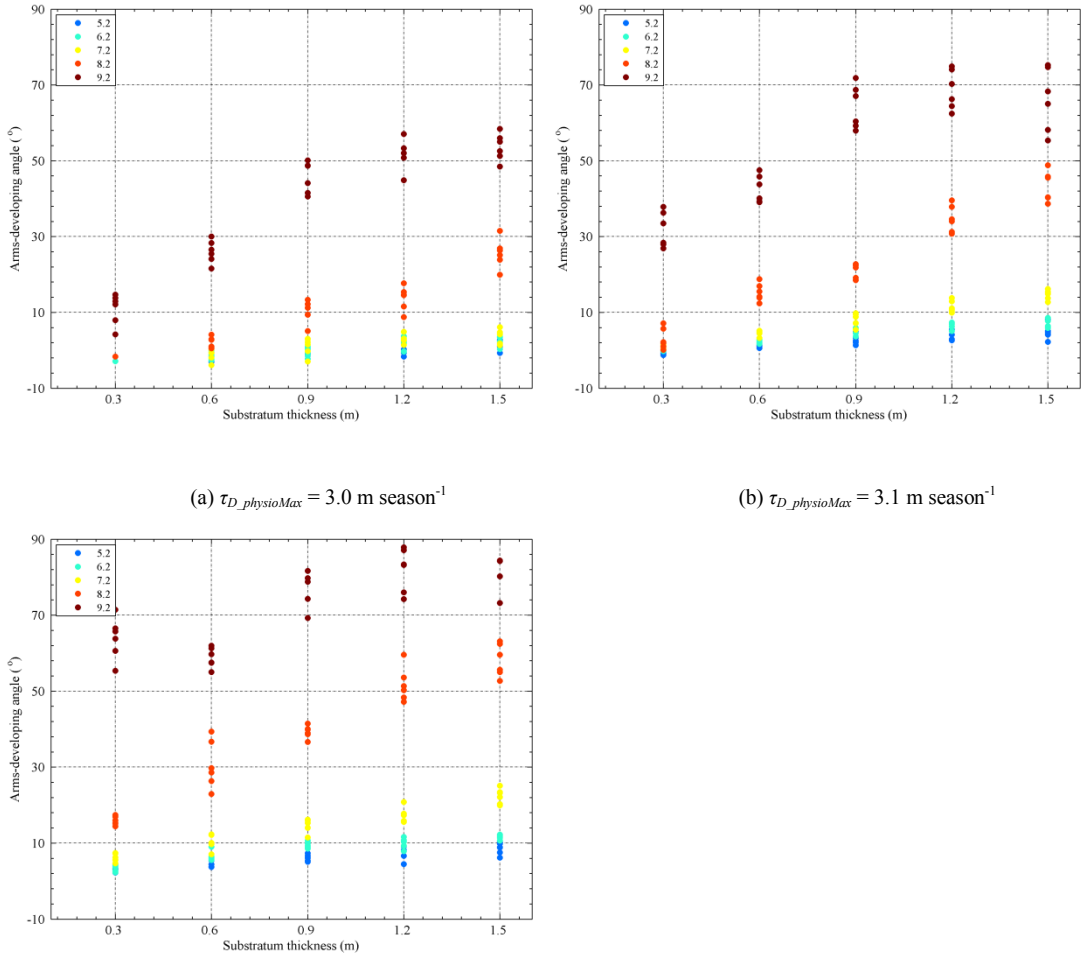

(a) $\tau_{D\_physioMax}$ = 3.0 m season^{-1}

(b) $\tau_{D\_physioMax}$ = 3.1 m season^{-1}

(c) $\tau_{D\_physioMax}$ = 3.2 m season^{-1}

Figure 9-35. The arms-developing angle of resulting parabolic dunes. Different colours represent different heights of the initial barchans as shown in the legends. Multiple dots of the same colour denote simulations with different erosion tolerances but with the same deposition tolerance, initial barchan height, and substratum thickness.

The relationships between the arms-developing angle of resulting parabolic dunes and the transformation and the stabilisation times are shown in Figure 9-36. Negative arms-developing angles only develop at relatively low deposition tolerances (i.e., 3.0 and 3.1 m season^{-1}), whereas large positive arms-developing angles occur when an initial barchan is sufficiently large (i.e., 8.2 and 9.2 m) regardless of the deposition tolerance and the substratum thickness (Figure 9-23c). A thicker substratum, meanwhile, encourages more rapid dune transformation and stabilisation (Figure 9-23d). A relatively small arms-developing angle is generally associated with longer transformation and stabilisation times. In particular, significant increases in both the transformation and the stabilisation times occur when the arms-developing angle narrows below 10˚.

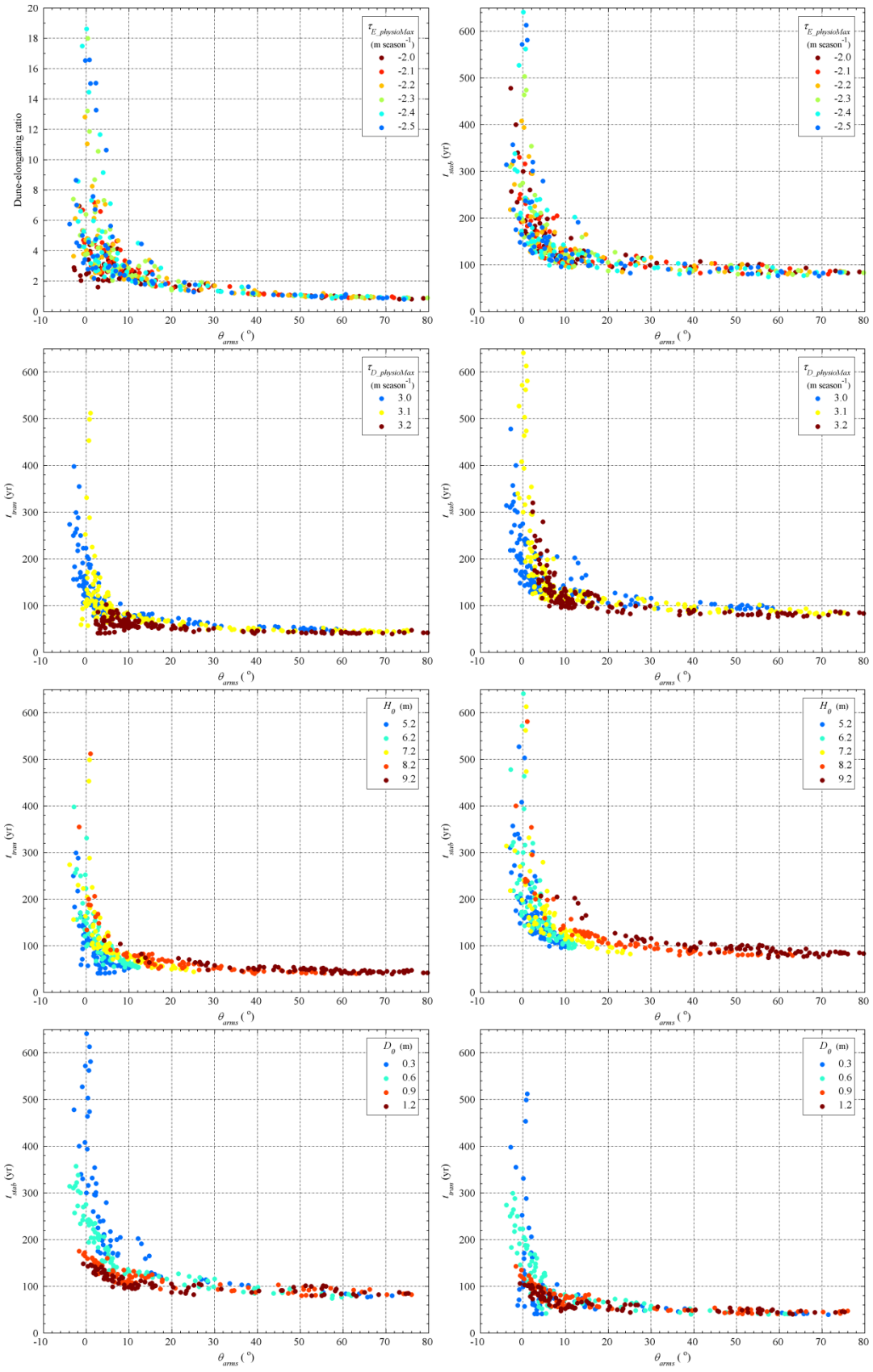

Figure 9-36. The relationships between θ_{arms} and t_{tran},, and between θ_{arms} and t_{stab}.

A large average migration rate is associated with a small arms-developing angle (Figure 9-37). It appears that the deposition tolerance determines the minimal boundary of arms-developing angles for barchan-to-parabolic dune transformations (Figure 9-37b). A tall initial barchan is essential to form a large arms-developing angle (Figure 9-37c). For the same arms-developing angle, dunes on a thinner substratum migrate at higher rates (Figure 9-37d).

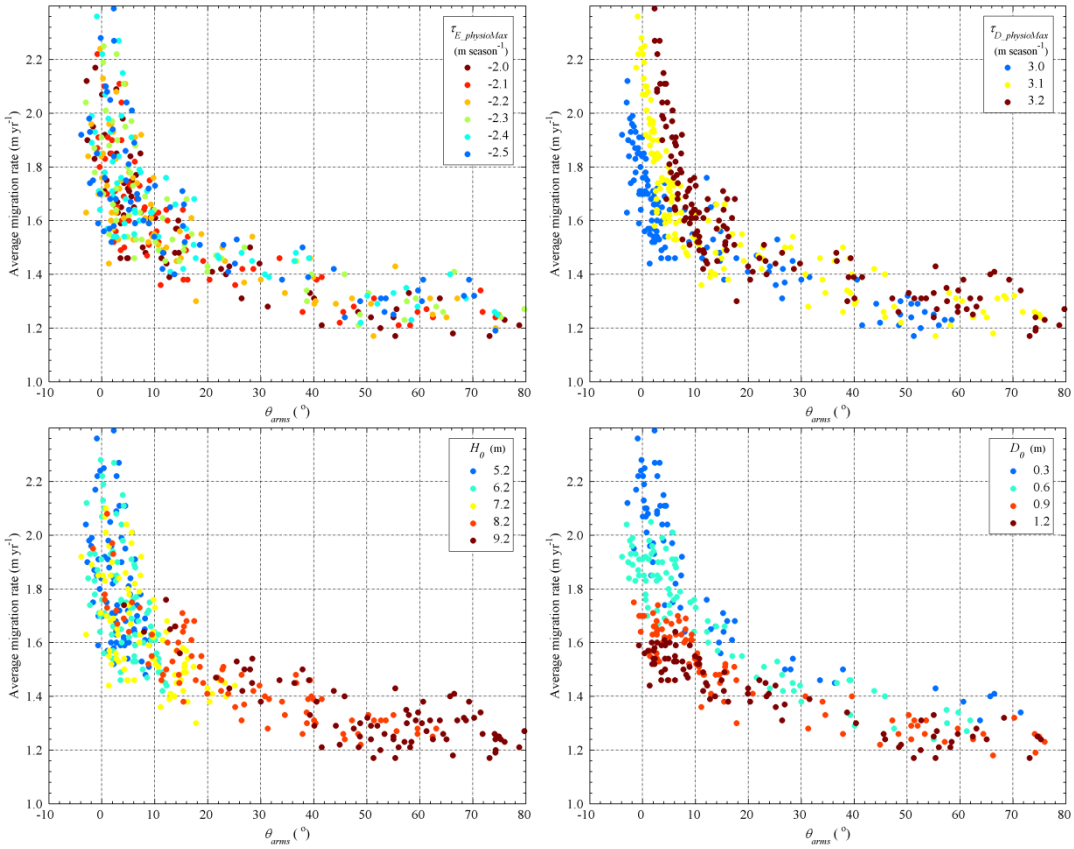

Figure 9-37. The average migration rate of the barchans-to-parabolic dune transformations.

The elongation ratio of resulting parabolic dunes exhibits a similar trend as the average migration rate (Figure 9-38). A high deposition tolerance and a large initial dune height encourage a dune being transformed into a parabolic dune and becoming stabilised to develop rounded trailing arms. Dunes on a thin substratum migrate at greater rates, forming long-walled trailing arms in parallel with each other.

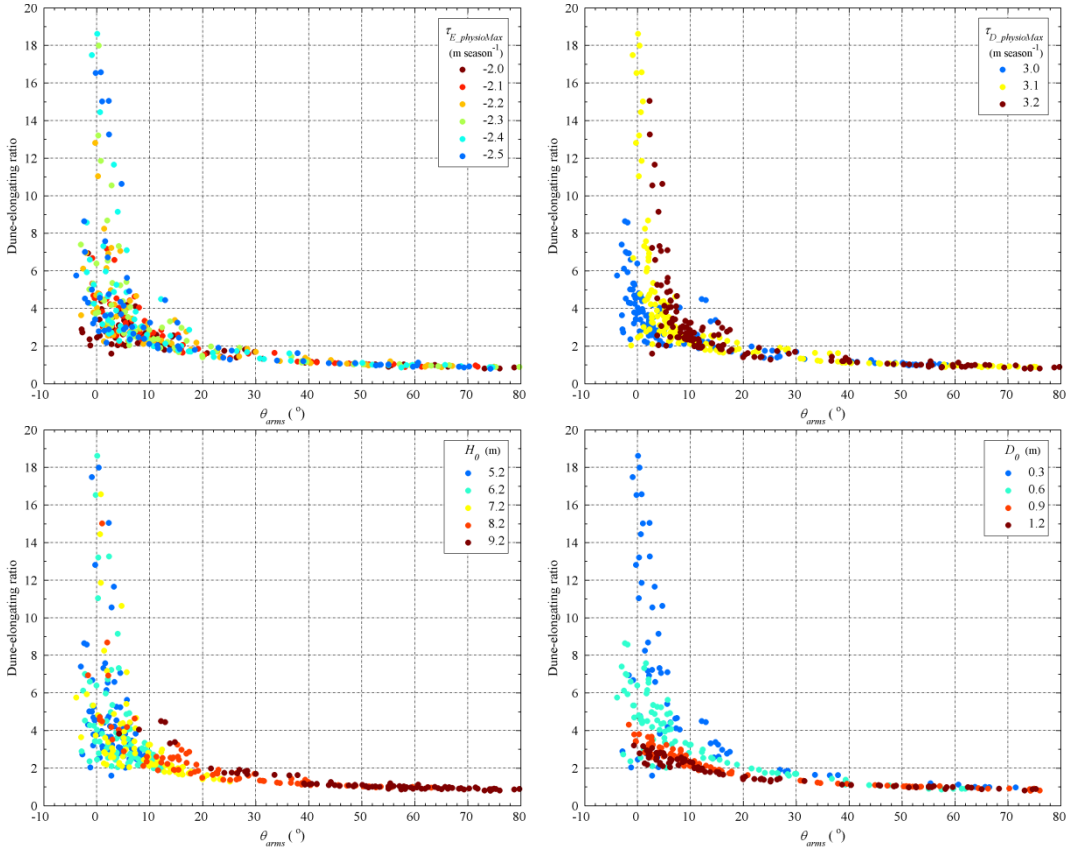

Figure 9-38. The dune-elongating ratio of resulting parabolic dunes.

9.6 Influence of Wind Regime: Sand Transport Potential

9.6.1 Dune Shape

The resulting dune types from 1080 simulations under changes of five key parameters are shown in Figure 9-39. An increase in the sand transport rate encourages the development of more elongated parabolic dunes at a relatively large deposition tolerance and/or a relatively thick sandy substratum. A low deposition tolerance and/or a thin substratum can transform initial barchans into elongated parabolic dunes at a low transport rate, but initial dunes maintain a barchanoid shape when the sand transport rate is relatively high. The deposition tolerance is more crucial in determining the resulting dune types in comparison with the erosion tolerance. A large initial barchan at a low transport rate is quickly stabilised, developing into lunate and sometimes typical parabolic dunes. The sand transport rate significantly influences the types of resulting dunes developed from a larger initial barchan on a thinner substratum.

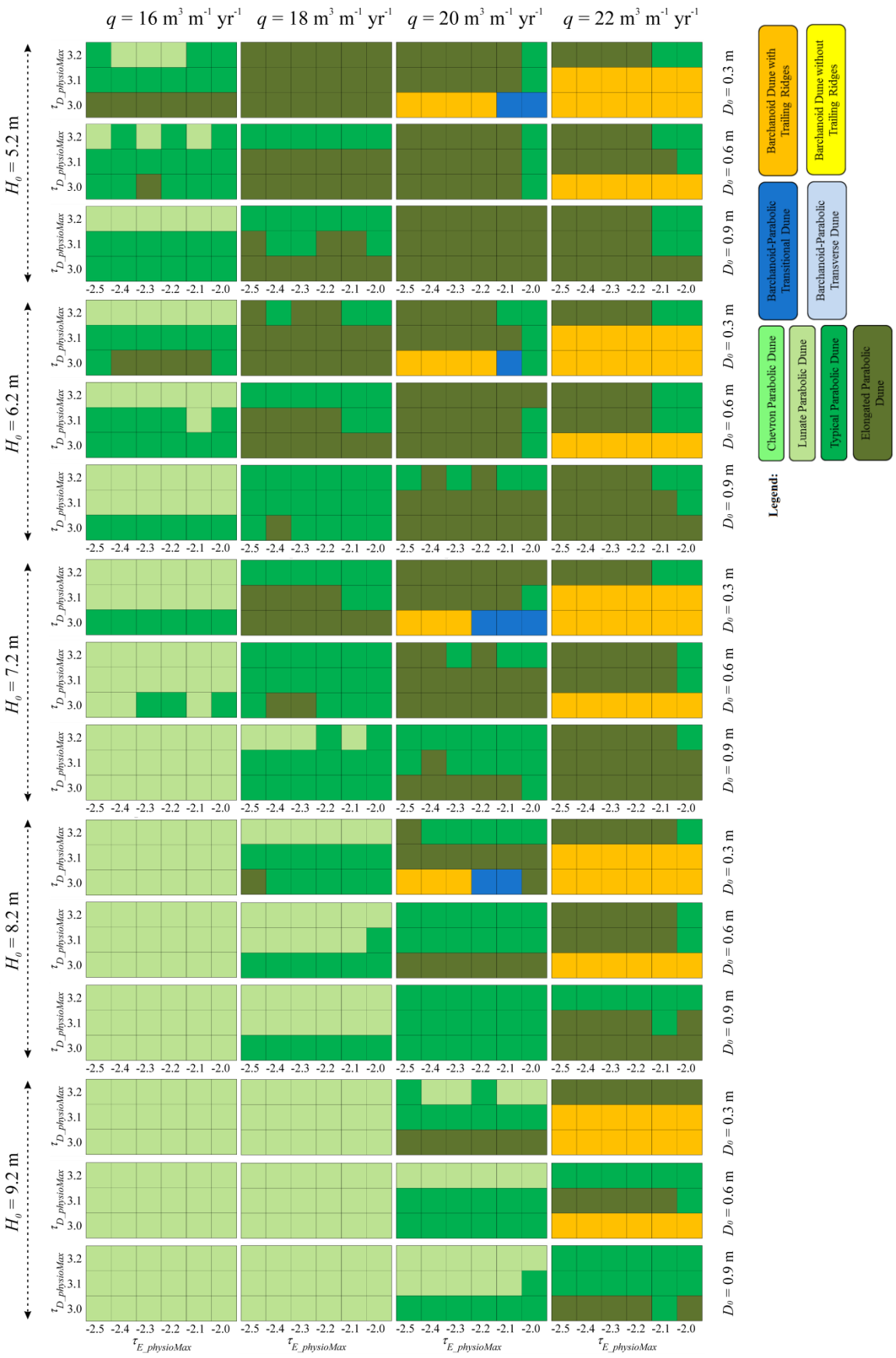

Figure 9-39. The resulting dune types at different erosion and deposition tolerances, initial barchan heights, substratum thicknesses, and wind transport potentials.

An increase in the sand transport rate promotes the development of elongated parabolic dunes (Figure 9-40). A high erosion tolerance develops dunes with a more elongated parabolic form only when q is relatively large, yet exerts a minimal impact when q decreases to 16 m^3 m^{-1} yr^{-1}. The impact of the deposition tolerance, however, is significant regardless of the sand transport rate. Relatively small initial barchans (5.2 m and 6.2 m) are more sensitive to the change in q, whereas there is no significant difference for larger barchans (8.2 m and 9.2 m) until q increases to 22 m^3 m^{-1} yr^{-1}. The sand transport rate plays a more considerable role in dune transformations where dunes migrate on a thinner substratum. In particular, a great surge occurs at a substratum thickness of 0.3 m.

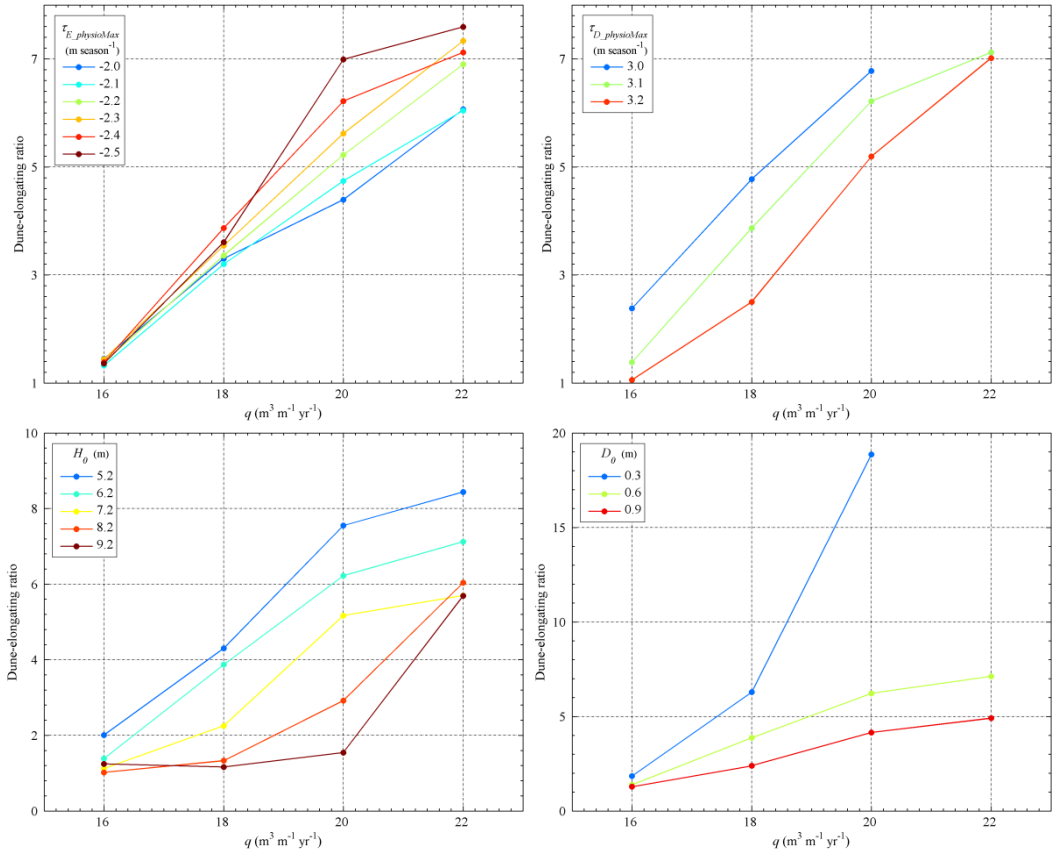

Figure 9-40. The relationships between the dune-elongating ratio and the sand transport rate. (a) H_0 = 6.2 m, D_0 = 0.6 m, and $\tau_{D\_physioMax}$ = 3.1 m season^{-1}; (b) H_0 = 6.2 m, D_0 = 0.6 m, and $\tau_{E\_physioMax}$ = -2.4 m season^{-1}; (c) D_0 = 0.6 m, $\tau_{D\_physioMax}$ = 3.1 m season^{-1}, and $\tau_{E\_physioMax}$ = -2.4 m season^{-1}; and (d) H_0 = 6.2 m, $\tau_{D\_physioMax}$ = 3.1 m season^{-1}, and $\tau_{E\_physioMax}$ = -2.4 m season^{-1}.

The average width of resulting parabolic dunes relative to the width of initial barchans generally increases with q (Figure 9-41). The similar trend also occurs for the dune height at t_{stab} relative to H_0 (Figure 9-42). A high erosion tolerance or a low deposition tolerance significantly increases both the

width and the height of resulting parabolic dunes at a high sand transport rate, whereas no significant difference arises when q is lower than 18 m^3 m^{-1} yr^{-1}. A smaller initial barchan increases the width and the height to a larger degree, which suggests that relatively severe sand accumulation on a lobe happens during its transforming process. A thicker sandy substratum leads to the development of parabolic dunes with less increase in both the width and the height at a high sand transport, but it increases the width and the height slightly at a low sand transport. This may suggest a transition from internal-dominant sand resource (the dune itself) to external-dominant sand resource (the sandy substratum) as the sand transport rate increases.

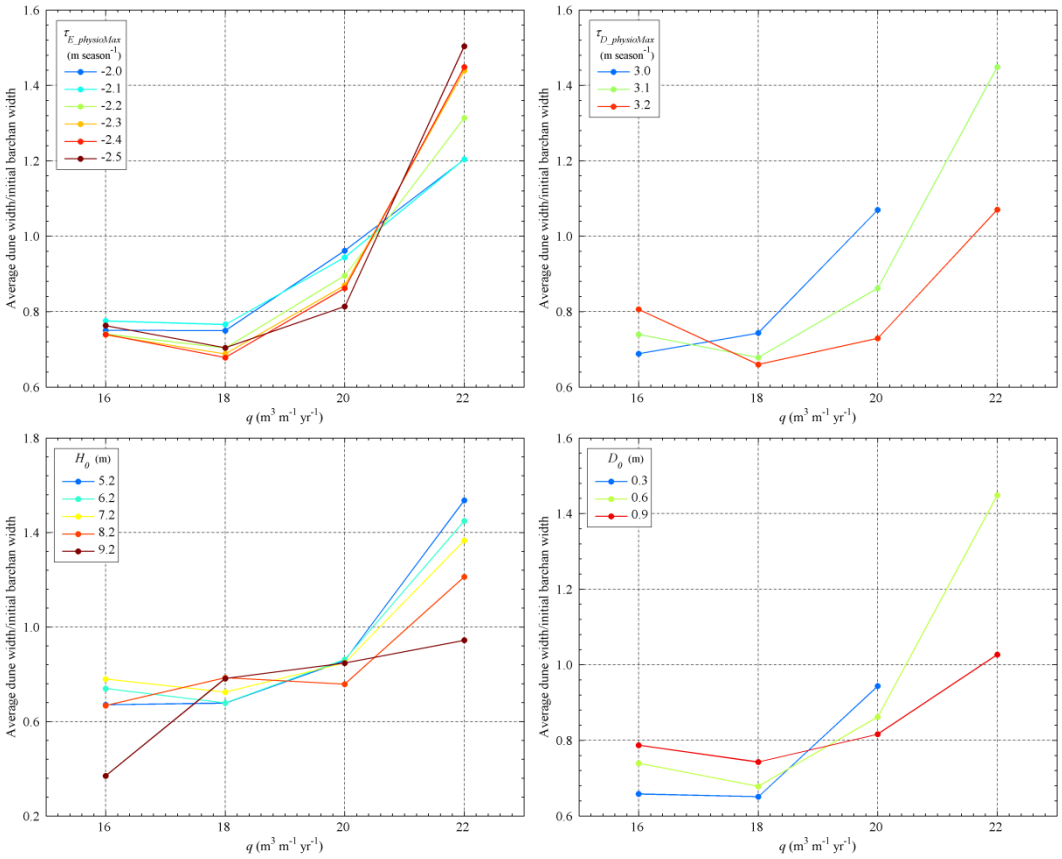

Figure 9-41. The relationships between the sand transport rate and the ratio of average dune width to initial barchan width. (a) H_0 = 6.2 m, D_0 = 0.6 m, and $\tau_{D\_physioMax}$ = 3.1 m season^{-1}; (b) H_0 = 6.2 m, D_0 = 0.6 m, and $\tau_{E\_physioMax}$ = -2.4 m season^{-1}; (c) D_0 = 0.6 m, $\tau_{D\_physioMax}$ = 3.1 m season^{-1}, and $\tau_{E\_physioMax}$ = -2.4 m season^{-1}; and (d) H_0 = 6.2 m, $\tau_{D\_physioMax}$ = 3.1 m season^{-1}, and $\tau_{E\_physioMax}$ = -2.4 m season^{-1}.

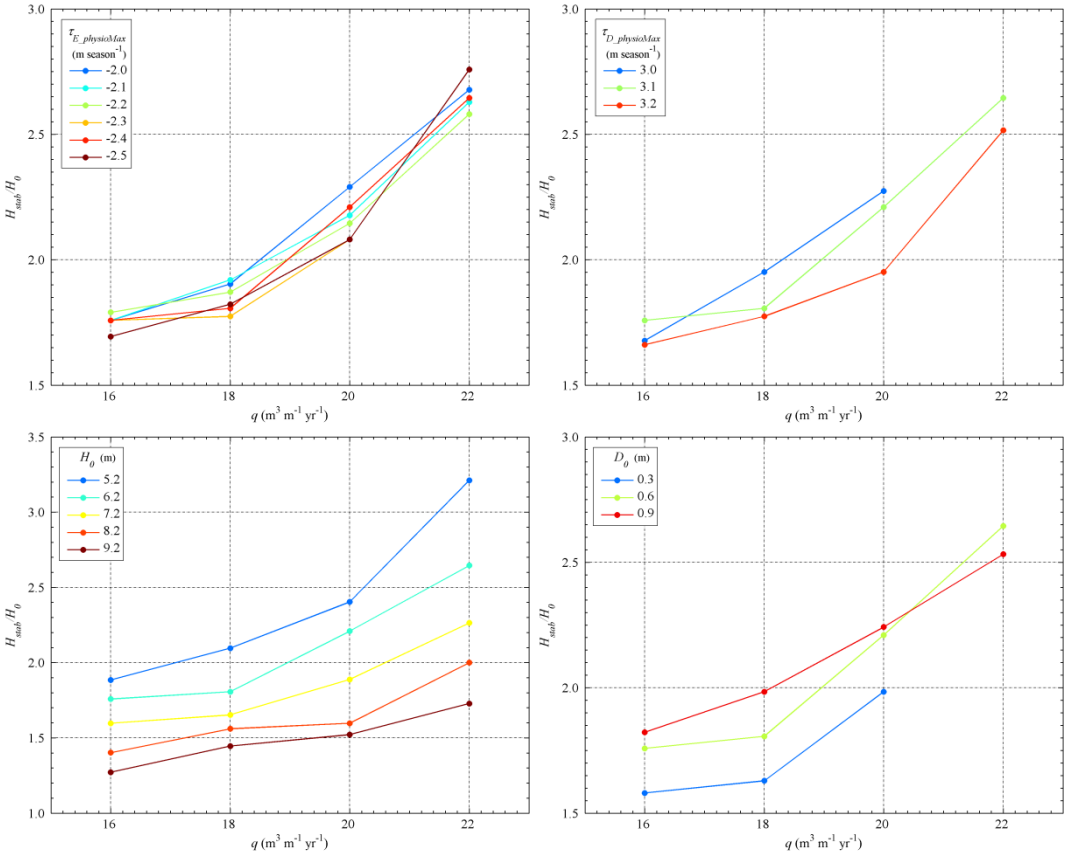

Figure 9-42. The relationships between the sand transport rate and the ratio of dune height at t_{stab} to initial barchan height. (a) H_0 = 6.2 m, D_0 = 0.6 m, and $\tau_{D\_physioMax}$ = 3.1 m season^{-1}; (b) H_0 = 6.2 m, D_0 = 0.6 m, and $\tau_{E\_physioMax}$ = -2.4 m season^{-1}; (c) D_0 = 0.6 m, $\tau_{D\_physioMax}$ = 3.1 m season^{-1}, and $\tau_{E\_physioMax}$ = -2.4 m season^{-1}; and (d) H_0 = 6.2 m, $\tau_{D\_physioMax}$ = 3.1 m season^{-1}, and $\tau_{E\_physioMax}$ = -2.4 m season^{-1}.

9.6.2 Transition and Stabilisation Times

As the sand transport rate increases, both the transition and the stabilisation times increase exponentially (Figure 9-43 and Figure 9-44). A high sand transport rate enlarges the differences of t_{tran} and t_{stab} arising from the other controls (H_0, D_0, $\tau_{E\_physioMax}$ and $\tau_{D\_physioMax}$). A high erosion tolerance increases t_{tran} and t_{stab} more significantly at a relatively high sand transport rate, whilst a high deposition tolerance shortens both t_{tran} and t_{stab}. Similarly, a smaller H_0 or D_0 increases t_{tran} and t_{stab} to a larger degree at a higher sand transport rate.

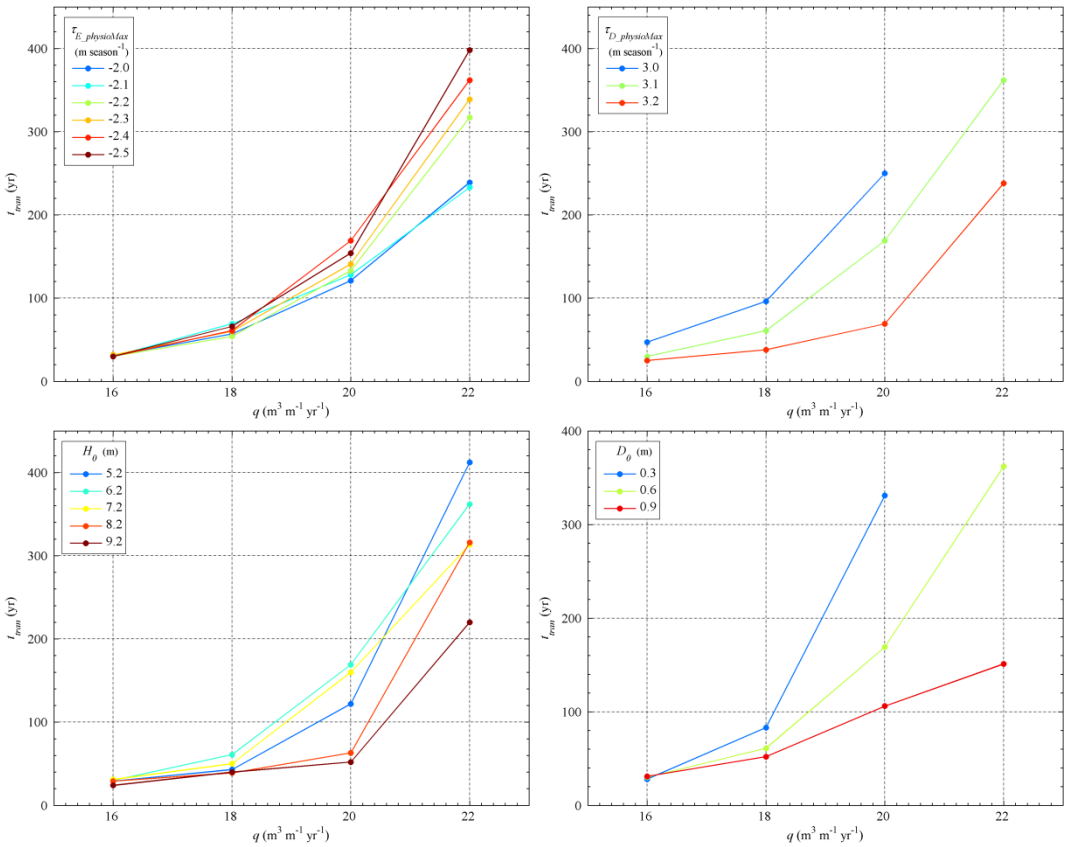

Figure 9-43. The relationship between t_{tran} and q. (a) H_0 = 6.2 m, D_0 = 0.6 m, and $\tau_{D\_physioMax}$ = 3.1 m season^{-1}; (b) H_0 = 6.2 m, D_0 = 0.6 m, and $\tau_{E\_physioMax}$ = -2.4 m season^{-1}; (c) D_0 = 0.6 m, $\tau_{D\_physioMax}$ = 3.1 m season^{-1}, and $\tau_{E\_physioMax}$ = -2.4 m season^{-1}; and (d) H_0 = 6.2 m, $\tau_{D\_physioMax}$ = 3.1 m season^{-1}, and $\tau_{E\_physioMax}$ = -2.4 m season^{-1}.

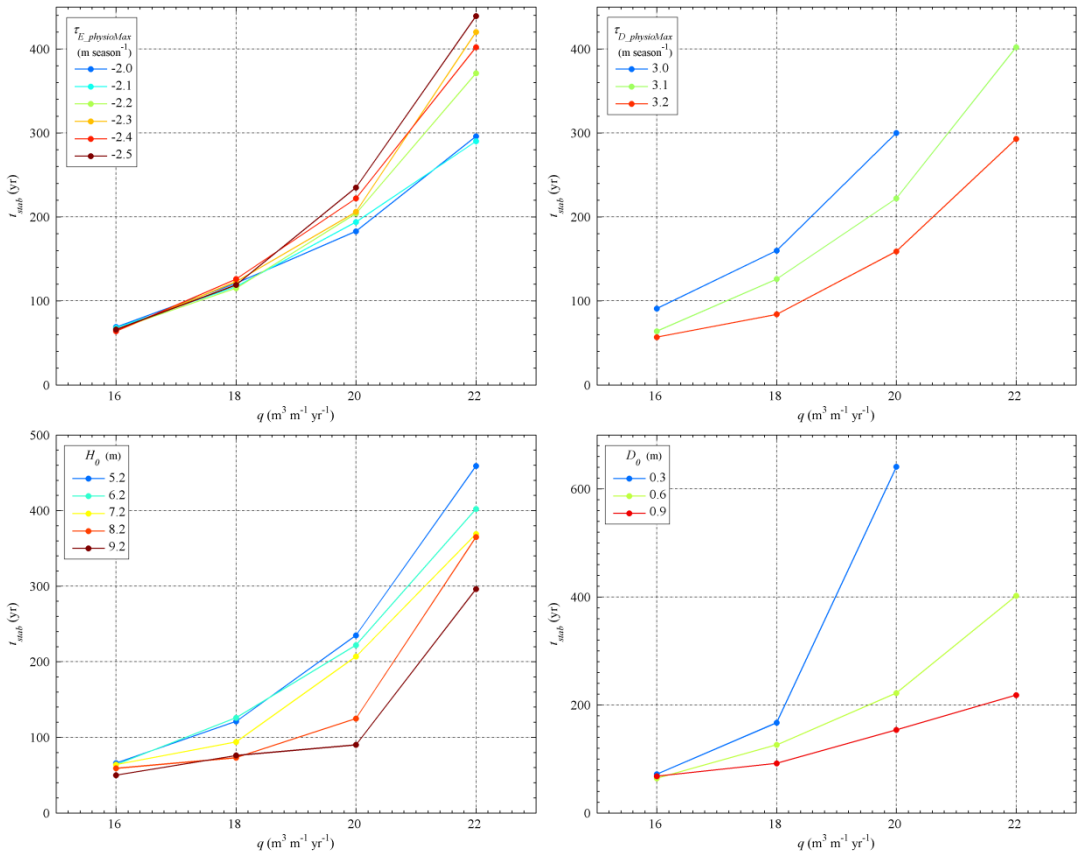

Figure 9-44. The relationship between t_{stab} and q. (a) H_0 = 6.2 m, D_0 = 0.6 m, and $\tau_{D\_physioMax}$ = 3.1 m season^{-1}; (b) H_0 = 6.2 m, D_0 = 0.6 m, and $\tau_{E\_physioMax}$ = -2.4 m season^{-1}; (c) D_0 = 0.6 m, $\tau_{D\_physioMax}$ = 3.1 m season^{-1}, and $\tau_{E\_physioMax}$ = -2.4 m season^{-1}; and (d) H_0 = 6.2 m, $\tau_{D\_physioMax}$ = 3.1 m season^{-1}, and $\tau_{E\_physioMax}$ = -2.4 m season^{-1}.

9.6.3 Dune Migration

An increase in the sand transport rate enables a dune to travel a longer distance at a higher migration rate before being stabilised completely (Figure 9-45 & Figure 9-46). A high erosion tolerance encourages a dune to migrate further and faster at a high sand transport rate. When q is relatively low, the influence of the erosion tolerance on the average migration rate is random as there is no significant different in the migration distance and t_{stab} under a change in the erosion tolerance (Figure 9-44). A high deposition tolerance decreases the dune migration distance significantly; however, its influence on the average migration rate lessens as q increases. A larger initial barchan on a thicker sandy substratum migrates at a smaller rate and is stabilised by vegetation more quickly.

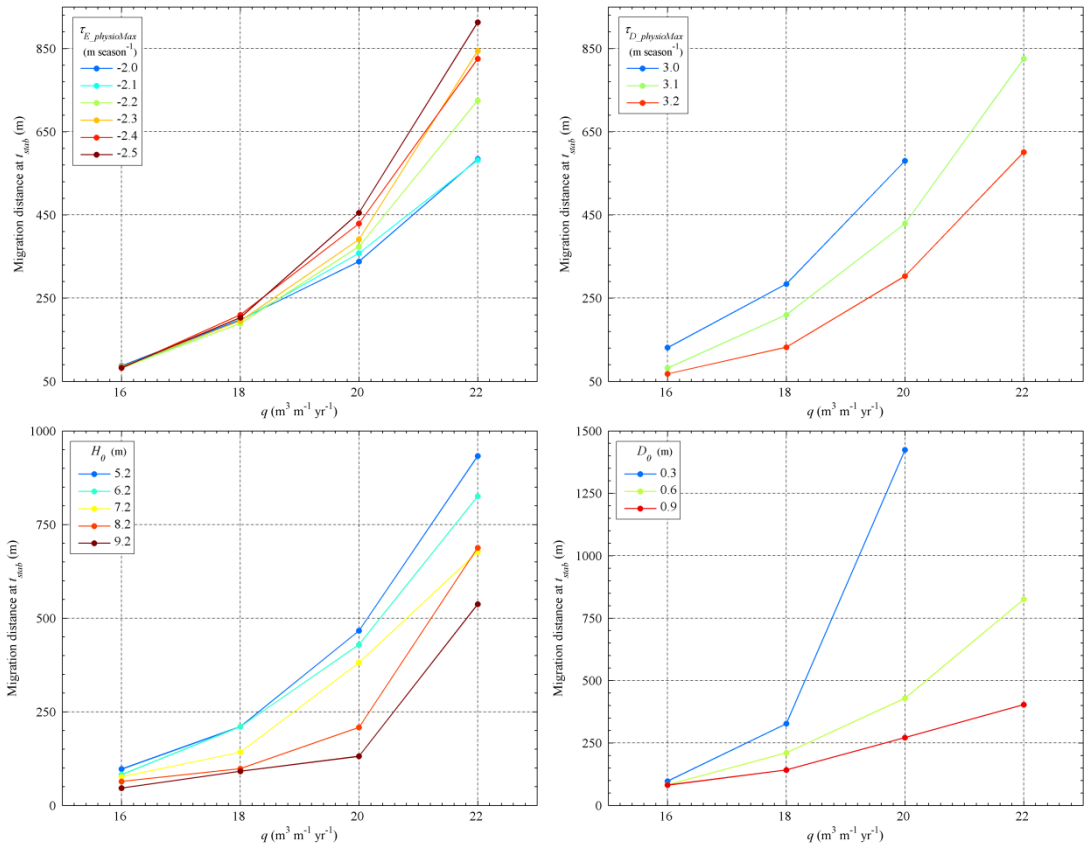

Figure 9-45. The relationship between q and the migration distance at t_{stab}. (a) H_0 = 6.2 m, D_0 = 0.6 m, and $\tau_{D\_physioMax}$ = 3.1 m season^{-1}; (b) H_0 = 6.2 m, D_0 = 0.6 m, and $\tau_{E\_physioMax}$ = -2.4 m season^{-1}; (c) D_0 = 0.6 m, $\tau_{D\_physioMax}$ = 3.1 m season^{-1}, and $\tau_{E\_physioMax}$ = -2.4 m season^{-1}; and (d) H_0 = 6.2 m, $\tau_{D\_physioMax}$ = 3.1 m season^{-1}, and $\tau_{E\_physioMax}$ = -2.4 m season^{-1}.

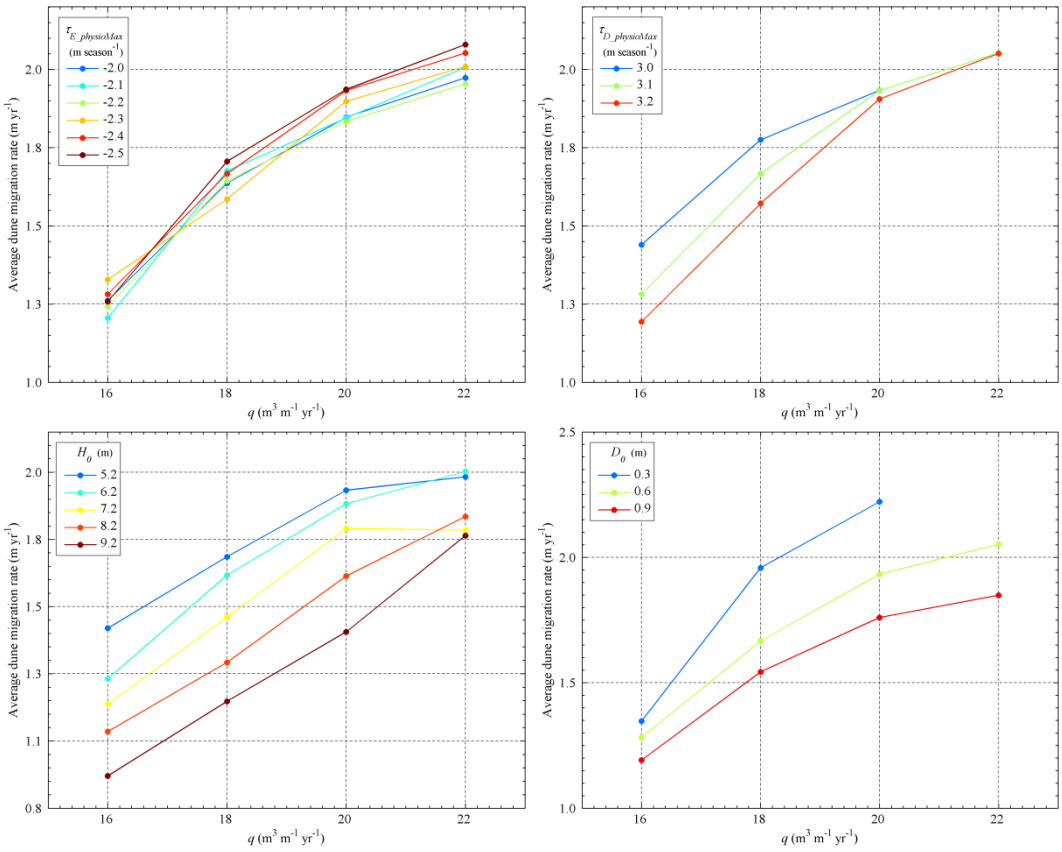

Figure 9-46. The relationship between q and the average migration rate. (a) H_0 = 6.2 m, D_0 = 0.6 m, and $\tau_{D\_physioMax}$ = 3.1 m season^{-1}; (b) H_0 = 6.2 m, D_0 = 0.6 m, and $\tau_{E\_physioMax}$ = -2.4 m season^{-1}; (c) D_0 = 0.6 m, $\tau_{D\_physioMax}$ = 3.1 m season^{-1}, and $\tau_{E\_physioMax}$ = -2.4 m season^{-1}; and (d) H_0 = 6.2 m, $\tau_{D\_physioMax}$ = 3.1 m season^{-1}, and $\tau_{E\_physioMax}$ = -2.4 m season^{-1}.

9.6.4 Sand Volume Dynamics

The dune volume increases progressively with the sand transport rate (Figure 9-47). A higher erosion tolerance or a lower deposition tolerance increases the dune volume more significantly at a higher sand transport rate. The fact that a larger initial barchan increases the dune volume to a smaller degree during a barchan-to-parabolic dune transformation indicates that its substratum provides less sand in comparison to a smaller initial barchan. A dune on a thinner substratum counterintuitively incorporates more sand, suggesting that the migration distance and rate play more significant roles in the growth of a dune lobe.

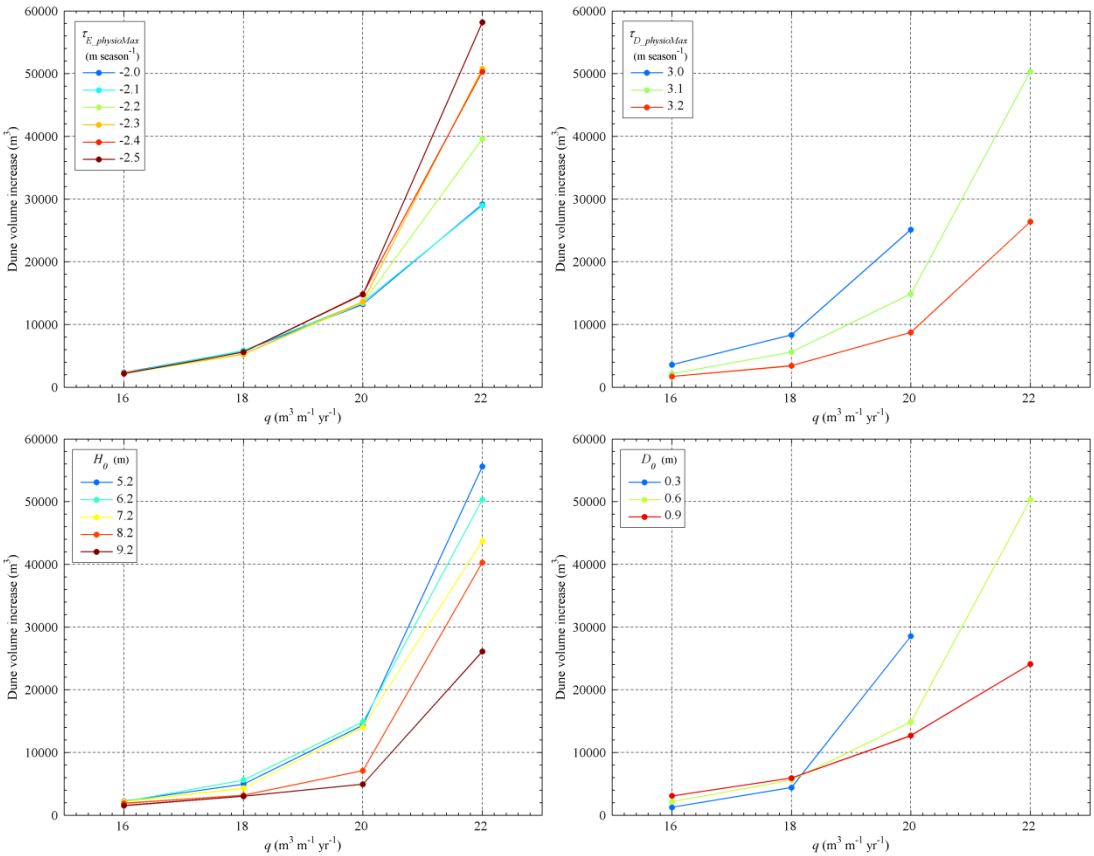

Figure 9-47. The relationship between q and the sand gained from a substratum. (a) H_0 = 6.2 m, D_0 = 0.6 m, and $\tau_{D\_physioMax}$ = 3.1 m season^{-1}; (b) H_0 = 6.2 m, D_0 = 0.6 m, and $\tau_{E\_physioMax}$ = -2.4 m season^{-1}; (c) D_0 = 0.6 m, $\tau_{D\_physioMax}$ = 3.1 m season^{-1}, and $\tau_{E\_physioMax}$ = -2.4 m season^{-1}; and (d) H_0 = 6.2 m, $\tau_{D\_physioMax}$ = 3.1 m season^{-1}, and $\tau_{E\_physioMax}$ = -2.4 m season^{-1}.

9.6.5 Arms-developing Angles

A higher sand transport rate develops a parabolic dune with a smaller, even negative, arms-developing angle (Figure 9-48). An increase in the deposition tolerance results in a more rapid shrinking of the lobe, leading to a relatively large arms-developing angle, whereas a change in erosion tolerance seems to play an insignificant role in altering an arms-developing angle. A larger initial barchan contributes to the formation of a larger arms-developing angle, to a more significant degree as q decreases. A thicker substratum also encourages the development of a larger arms-developing angle.

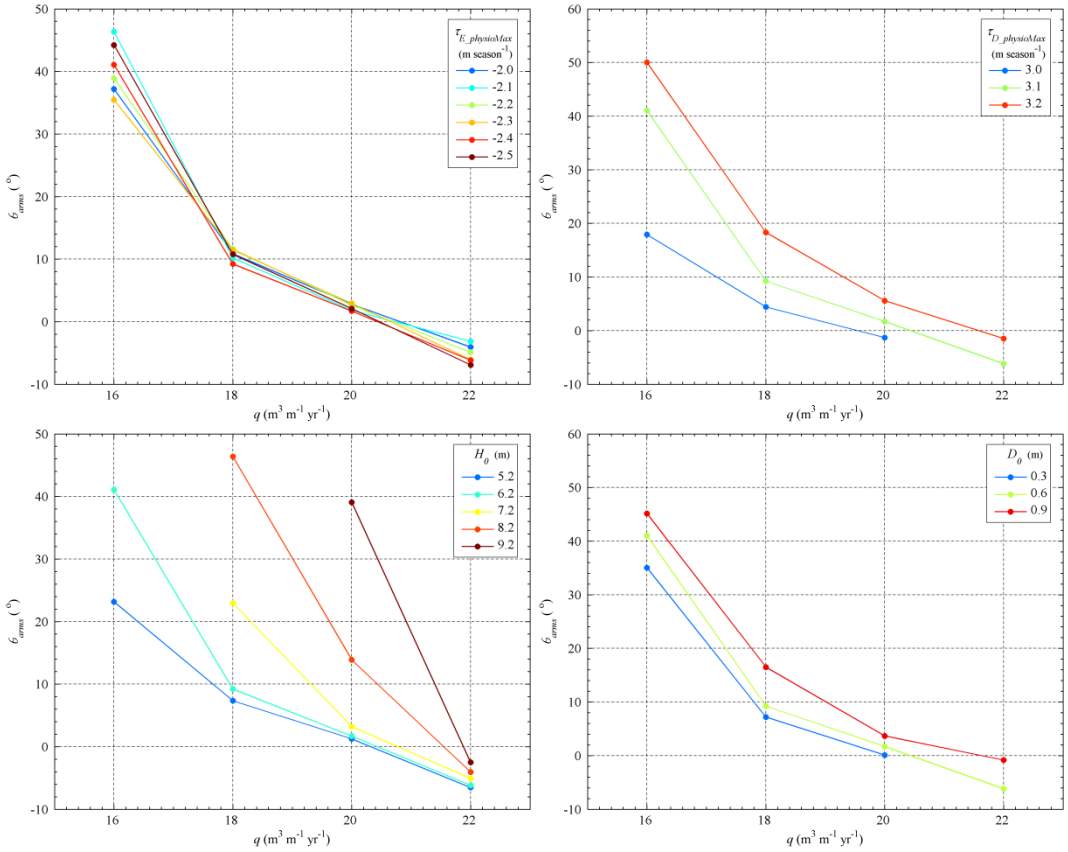

Figure 9-48. The relationship between θ_{arms} and q. (a) H_0 = 6.2 m, D_0 = 0.6 m, and $\tau_{D\_physioMax}$ = 3.1 m season^{-1}; (b) H_0 = 6.2 m, D_0 = 0.6 m, and $\tau_{E\_physioMax}$ = -2.4 m season^{-1}; (c) D_0 = 0.6 m, $\tau_{D\_physioMax}$ = 3.1 m season^{-1}, and $\tau_{E\_physioMax}$ = -2.4 m season^{-1}; and (d) H_0 = 6.2 m, $\tau_{D\_physioMax}$ = 3.1 m season^{-1}, and $\tau_{E\_physioMax}$ = -2.4 m season^{-1}.

The arms-developing angle is linked to the transformation and the stabilisation times of a barchan-to-parabolic dune transformation (Figure 9-49). A smaller arms-developing angle is associated with longer transition and stabilisation times; in particular, when an arms-developing angle decreases to 0˚, both the transition and the stabilisation times increase substantially. A large negative arms-developing angle requires a high sand transport rate. It is likely that the sand transport rate determines the minimal boundary of arms-developing angles of the barchan-to-parabolic dune transformations. For the same arms-developing angle, a larger sand transport rate indicates that a dune needs longer time to be transformed into a parabolic dune and stabilised finally.

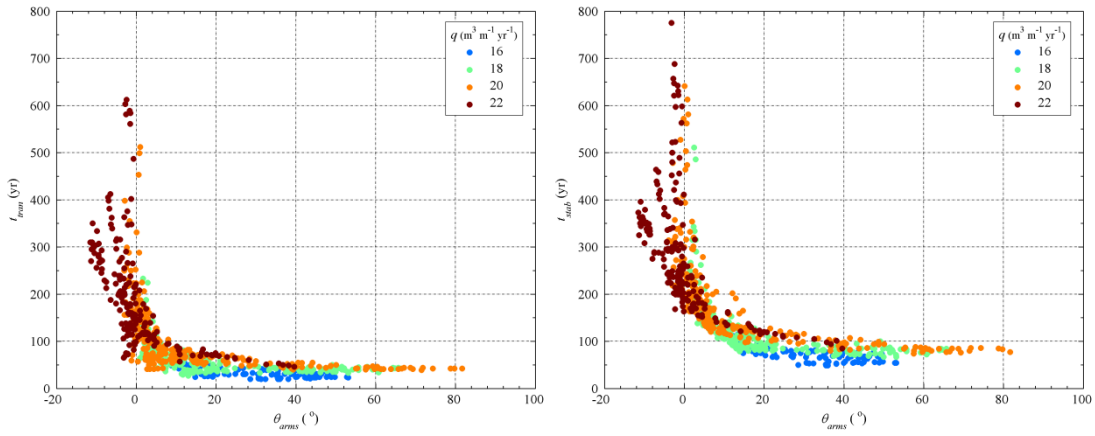

Figure 9-49. The relationships between θ_{arms} and t_{tran}, and between θ_{arms} and t_{stab}, with the other parameter settings undifferentiated.

9.7 Summary of Modelling Outcomes

Before moving forward to analyse physical processes and mechanism that control the barchan-to-parabolic dune transformations, the main outcomes of modelling simulations are summarised in the Table 9-1. The table follows the same structure as the exploring framework in Figure 9-1, and comprises the outcomes of four batches of modelling simulations, consistent with the presenting sequence in this chapter.

Table 9-1. Summary of modelling outcomes.

Batch #1 (Section 9.3): Influence of Vegetation Characteristics	
Modelling Measurements	**Vegetation Characteristics**
Dune Length	Highest (high *ET*, low *DT*) - Lowest (low *ET*, high *DT*)
Avg. Dune Width	Highest (low *ET*, low *DT*) - Lowest (high *ET*, high *DT*)
Dune Height	Highest (low *ET*, low *DT*) - Lowest (high *ET*, high *DT*)
Dune-elongation Ratio	Highest (high *ET*, low *DT*) - Lowest (low *ET*, high *DT*)
Stabilisation Time	Highest (high *ET*, low *DT*) - Lowest (low *ET*, high *DT*)
Lobe Length	Highest (low *ET*, low *DT*) - Lowest (high *ET*, high *DT*)
Lobe Width	Highest (low *ET*, low *DT*) - Lowest (high *ET*, high *DT*)
Avg. Migration Rate	Highest (high *ET*, low *DT*) - Lowest (low *ET*, high *DT*)
Arms-initiation Time	Highest (low *ET*, low *DT*) - Lowest (high *ET*, high *DT*)
Arms-elongating Duration	Highest (high *ET*, low *DT*) - Lowest (low *ET*, high *DT*)
Arms-elongating Rate	Highest (high *ET*, low *DT*) - Lowest (low *ET*, high *DT*)
Sand Volume of Dune Lobe per Width	Highest (low *ET*, low *DT*) - Lowest (high *ET*, high *DT*)
Sand Volume of Arms per Distance	Highest (high *ET*, high *DT*) - Lowest (low *ET*, low *DT*)
Sand Volume Ratio of Arms to Dune	Highest (high *ET*, low *DT*) - Lowest (low *ET*, high *DT*)

Batch #2 (Section 9.4): Influence of the Boundary Condition: Initial Barchan Height

Modelling Measurements	**High *ET* & Low *DT***	**High *ET* & High *DT***	**Low *ET* & Low *DT***	**Low *ET* & High *DT***
Dune Length	Highest (low H_0) - Lowest (high H_0)	Highest (low H_0) - Lowest (high H_0)	Highest (high H_0) - Lowest (low H_0)	Highest (middle H_0) - Lowest (high H_0)
Avg. Dune Width	Highest (middle H_0) - Lowest (high & low H_0)	Highest (middle H_0) - Lowest (low H_0)	Highest (middle H_0) - Lowest (low H_0)	Highest (high H_0) - Lowest (low H_0)
Dune-elongation Ratio	Highest (low H_0) - Lowest (high H_0)	Highest (low H_0) - Lowest (high H_0)	Highest (high H_0) - Lowest (low H_0)	Highest (low H_0) - Lowest (high H_0)
Stabilisation Time	Highest (low H_0) - Lowest (high H_0)	no significant change	Highest (low H_0) - Lowest (high H_0)	no significant change
Avg. Migration Rate	Highest (low H_0) - Lowest (high H_0)	Highest (low H_0) - Lowest (high H_0)	Highest (low H_0) - Lowest (high H_0)	Highest (low H_0) - Lowest (high H_0)
Arms-initiation Time	no significant change	no significant change	Highest (low H_0) - Lowest (high H_0)	Highest (low H_0) - Lowest (high H_0)
Dune Height	Highest (middle H_0) - Lowest (high H_0)	Highest (high H_0) - Lowest (low H_0)	Highest (low H_0) - Lowest (high H_0)	Highest (high H_0) - Lowest (low H_0)
Dune Height Change	Highest (low H_0) - Lowest (high H_0)	Highest (low H_0) - Lowest (high H_0)	Highest (low H_0) - Lowest (high H_0)	Highest (low H_0) - Lowest (high H_0)
Sand Volume of Dune Lobe	Highest (middle H_0) - Lowest (high H_0)	Highest (high H_0) - Lowest (low H_0)	Highest (middle H_0) - Lowest (high H_0)	Highest (high H_0) - Lowest (low H_0)

Batch #3 (Section 9.5): Influence of the Boundary Condition: Sandy Substratum Thickness

Modelling Measurements	**High H_0 & Low *DT***	**High H_0 & High *DT***	**Low H_0 & Low *DT***	**Low H_0 & High *DT***
Dune-elongation Ratio	Highest (low D_0) - Lowest (high D_0)	no significant change	Highest (low D_0) - Lowest (high D_0)	Highest (low D_0) - Lowest (high D_0)
Ratio of Dune Height to H_0	Highest (high D_0) - Lowest (low D_0)	Highest (high D_0) - Lowest (low D_0)	Highest (high D_0) - Lowest (low D_0)	Highest (high D0) - Lowest (low D0)
Stabilisation Time	Highest (low D_0) - Lowest (high D_0)	no significant change	Highest (low D_0) - Lowest (high D_0)	Highest (low D_0) - Lowest (high D_0)
Avg. Migration Rate	Highest (low D_0) - Lowest (high D_0)	Highest (low D_0) - Lowest (high D_0)	Highest (low D_0) - Lowest (high D_0)	Highest (low D_0) - Lowest (high D_0)
Migration Distance	Highest (low D_0) - Lowest (high D_0)	no significant change	Highest (low D_0) - Lowest (high D_0)	Highest (low D_0) - Lowest (high D_0)
Dune Volume Increase	Highest (high D_0) - Lowest (low D_0)	Highest (high D_0) - Lowest (low D_0)	Highest (low D_0) - Lowest (high D_0)	Highest (high D_0) - Lowest (low D_0)

Batch #4 (Section 9.6): Influence of Wind Regime

Modelling Measurements	**High *q***	**Low *q***
Dune-elongation Ratio	Highest (high *ET*, low *DT*, low H_0, low D_0) - Lowest (low *ET*, high *DT*, high H_0, high D_0)	Highest (low *DT*, low H_0) - Lowest (high *DT*, high H_0)
Ratio of Dune Height to H_0	Highest (high *ET*, low *DT*, low H_0, low D_0) - Lowest (low *ET*, high *DT*, high H_0, high D_0)	Highest (low *ET*, low *DT*, low H_0, high D_0) - Lowest (high *ET*, high *DT*, high H_0, low D_0)
Stabilisation Time	Highest (high *ET*, low *DT*, low H_0, low D_0) - Lowest (low *ET*, high *DT*, high H_0, high D_0)	Highest (low *DT*) - Lowest (high *DT*)
Avg. Migration Rate	Highest (high *ET*, low H_0, low D_0) - Lowest (low *ET*, high H0, high D_0)	Highest (high *ET*, low *DT*, low H_0, low D_0) - Lowest (low *ET*, high *DT*, high H_0, high D_0)
Migration Distance	Highest (high *ET*, low *DT*, low H_0, low D_0) - Lowest (low *ET*, high *DT*, high H_0, high D_0)	Highest (low *DT*, low H_0) - Lowest (high *DT*, high H_0)
Dune Volume Increase	Highest (high *ET*, low *DT*, low H_0, low D_0) - Lowest (low *ET*, high *DT*, high H_0, high D_0)	Highest (low *DT*, high D_0) - Lowest (high *DT*, low D_0)

Note: ET = $\tau_{E\_physioMax}$; and DT = $\tau_{D\_physioMax}$.

9.8 Barchan-to-parabolic dune transformations under various conditions

As discussed in the previous sections, a barchan-to-parabolic dune transformation is primarily controlled by the sand transport rate, initial barchan height, substratum thickness, and characteristics of vegetation species, in particular, their capabilities of withstanding erosion and sand burial. These key parameters interact with each other, controlling the processes involved and the morphology of resulting parabolic dunes. Dimensional analysis and nondimensionalisation, Buckingham's Π-theorem for example, have been widely used in extracting the fundamental physical processes governed by key parameters, independent of the magnitude of base units involved, such that the role of each parameter and interactions between parameters can be easily identified and the same phenomenon can be compared across different systems. This section presents a fundamental relationship between system controls expressed by a non-dimensional number termed the 'dune stabilising index (S_*)', and the plan-view morphology of resulting parabolic dunes, expressed by a normalised migration distance (L_t'), as the key relationship that controls the barchan-to-parabolic dune transformation. Then, based on analyses of four batches of simulations, physical processes-based explanations are formulated to show how each parameter influences a barchan-to-parabolic dune transformation that leads to various dune morphology from the perspective of a fundamental physical mechanism. Examples to show how to use the non-dimensional equation to assist in understanding the past and the future of a barchan-to-parabolic dune transformation and the associated implications are discussed in the last section.

9.8.1 Nondimensionlisation

Dimensional analysis, combined with the trends and relationships observed in the previous sections, suggests a non-dimensional dune stabilising index [S_*], defined by system parameters and stabilising time [t, yr]:

$$S_* = -\frac{\tau_{E\_physioMax}{}^{q}}{H_0 D_0 \tau_{D\_physioMax}} t \tag{9-1}$$

where: t is the time that has elapsed since a barchan has moved into a well-vegetated field or when interdune areas were re-vegetated in an ameliorated water condition such that bare barchans are surrounded by vegetation and no external sand supply is available for sand transport (i.e., the starting point of the simulation scenarios); H_0 is the height of an initial barchan when the processes of a barchan-

to-parabolic dune transformation and stabilisation start, [m]; D_0 is the sandy substratum thickness beneath a barchan, [m]; q is the potential sand transport rate determined by wind regime, [m^3 m^{-1} yr^{-1}]; and $\tau_{E\_physioMax}$ and $\tau_{D\_physioMax}$ are the maximum erosion and deposition tolerances of dominant vegetation species in a region, [m $season^{-1}$].

The normalised migration distance [L_t', -] is the ratio of the migration distance of the dune crest along the windward direction [L_t, m] to the average width between trailing ridges/arms of barchanoid, barchanoid-parabolic, and parabolic dunes [$\overline{W}$, m] during the process of a barchan-to-parabolic dune transformation:

$$L_t' = L_t / \overline{W} \tag{9-2}$$

Figure 9-50(a) shows the normalised migration distance as a function of stabilising time for 1097 simulations, with 1-year time-steps, resulting in 80241 points. The best-fit curve indicates that there is a good power-law relation between S_* and L_t' (with an R^2 of 0.90):

$$L_t' = 0.07\ S_*^{0.64} \tag{9-3}$$

Power-law relations have been found to underlie a wide variety of natural and anthropogenic phenomena such as the Gutenberg–Richter law for earthquake sizes, self-similarity of fractals, and Pareto's law of income distribution (Baas, 2002; Bak and Tang, 1989; Bouchaud, 2001; Mandelbrot, 1960). The relatively tight clustering around the power-law indicates that the non-dimensional dune stabilising index encapsulates the fundamental physical processes governing a barchan-to-parabolic dune transformation, the mechanism of which is discussed in detail in Section 9.7.2. The nondimensionalisation performs well compared with Figure 9-50(b) in which the normalised migration distance is plotted as a function only of the simple absolute time, showing a much wider spread amongst the various parameter values of the 1097 scenario simulations. Incorporating the five key parameters into the dune stabilising index of Equation 9-1 collapses the simulations onto the much narrower strip of similarities and overlaps of Figure 9-50(a).

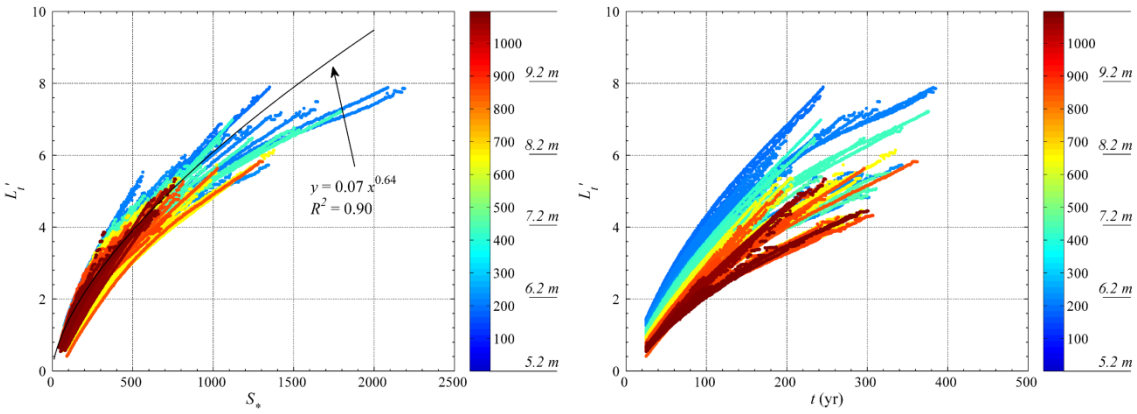

(a) (b)

Figure 9-50. Relations (a) between S_* and L_t' and (b) between t and L_t'. Simulations are ordered by H_0 first, then q, and D_0. The Jet stream colour scheme is used in which colour changes gradually from dark blue to dark red; blue, cyan, yellow, orange, and red are roughly in accordance with simulations starting from a barchan at 5.2 m, 6.2 m, 7.2 m, 8.2 m, and 9.2 m respectively, although each simulation is in effect represented by a different colour according to its ordered relative position on the list. The black line shows the best-fit curve by using 1097 simulations and 80241 points (1-year steps), excluding simulations with a substratum thickness of 0.3 m because of a great magnitude of randomness (see text in detail).

It can be deduced from Equations 9-2 and 9-3 that L_t increases with $\overline{W}$, if S_* is the same. To evaluate this, simulations with the same S_* of 400 are examined. Details of representative simulations with different combinations of parameter settings are shown in Table 9-2; the DEMs of the resulting dunes from these simulations at their specified stabilising times are presented in Figure 9-51. Despite the fact that the dunes in these simulations are in different stages of transforming into parabolic dunes, and their lobes display various shapes (ranging from barchanoid, barchanoid-parabolic, to parabolic shapes), the normalised migration distance is highly linearly-correlated with the average width between trailing ridges or arms (Figure 9-52).

Table 9-2. Representative simulations at their specified stabilising times with the same S_* of 400.

	H_0 (m)	D_0 (m)	$\tau_{E\_physioMax}$ (m season^{-1})	$\tau_{D\_physioMax}$ (m season^{-1})	q (m^3 m^{-1} yr^{-1})	t (yr)	L_t (m)	$\overline{W}$ (m)
a	5.2	0.6	-2.4	3.0	20	78	223	67
b	6.2	0.6	-2.3	3.2	22	94	263	79
c	7.2	0.6	-1.8	3.0	20	144	314	91
d	8.2	0.6	-2.2	3.2	22	130	294	87
e	9.2	0.9	-2.4	3.1	22	188	376	113

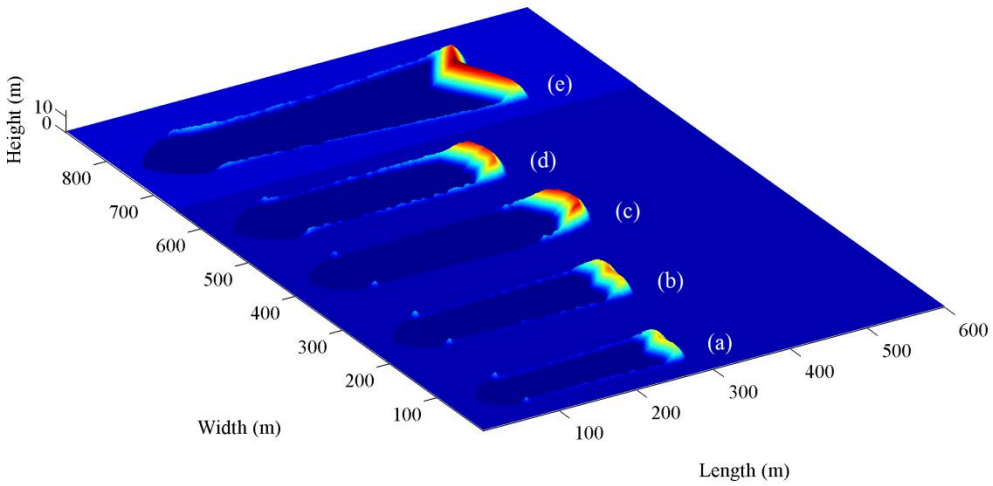

Figure 9-51. DEMs of dunes with the same S_* of 400, from representative simulations at their specified stabilising times.

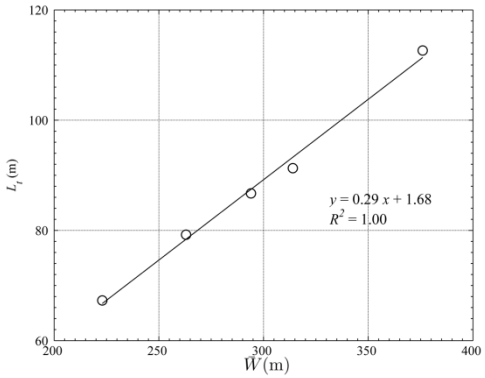

Figure 9-52. The relationship between the average dune width and the migration distance from representative simulations at their specified stabilising times.

The relationship expressed in Equation 9-1, however, fails when a substratum thickness is very thin, at D_0 of 0.3 m. This is due to the fact that dunes migrate at a fast rate and sand is lost very quickly to the arms. As a consequence, a relatively small lobe is more likely to be influenced by the survival of individual plants by sheer chance, and the stochastic nature of the simulations overwhelms any trends in behaviours and parameter relationships. For example, the survival of a few plants on the lee slope can sometimes break a lobe into smaller sections, resulting in a fast stabilisation of a dune (Figure 9-53). In contrast, without this lobe-breaking process, a dune can maintain its high mobility for a much longer time.

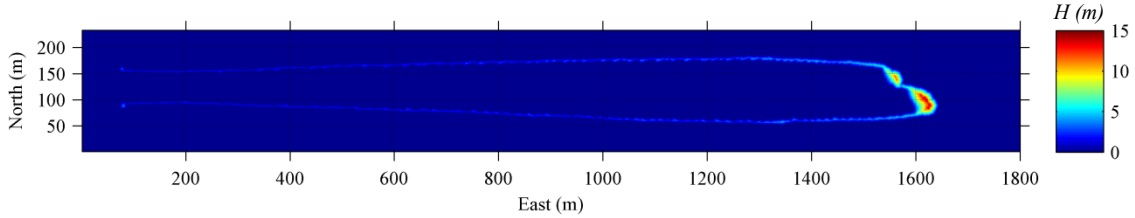

Figure 9-53. The dune lobe is broken into much smaller lobes by survived individual plants. D_0 = 0.3 m, H_0 = 5.2 m, q = 22 m^3 m^{-1} yr^{-1}, $\tau_{E\_physioMax}$ = -2.4 m season^{-1}, and $\tau_{D\_physioMax}$ = 3.2 m season^{-1}.

9.8.2 Processes and Mechanisms

This section considers the fundamental physical processes and mechanisms, partially reflected by the nondimensionalisation in the previous section, and how changes in key parameters influence the processes of a barchan-to-parabolic dune transformation and stabilisation as well as the morphological variations of resulting parabolic dunes.

9.8.2.1 Migration of a Barchan on Hard Surfaces

Dune longitudinal profiles of a barchan migrating over a hard non-vegetated surface, without external sand input, are found to experience one of the three representative changes over time as the schematic drawing in Figure 9-54.

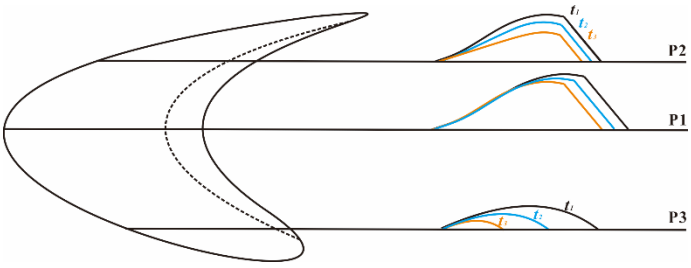

Figure 9-54. A schematic drawing of the changes in longitudinal profiles of a barchan.

(a) Dune slices close to the middle of a barchan (P1) are relatively high, and sand eroded from the windward slope primarily deposits on its lee side. Meanwhile, some sand is also partially lost due to lateral avalanching, leading to a gradual decrease in height over time, provided that no external sand

resources are available to supplement the sand loss. Both the windward and the lee slopes, nevertheless, maintain their shapes/slopes in general.

(b) Dune slices close to the horns of a barchan (P3) are much lower. As the depositional slope is below the shadow zone (~15 ˚), both the windward and the lee sides suffer escalated sand loss because the crest height of a dune slice is not sufficient to protect the lee slope against wind erosion (Figure 9-55).

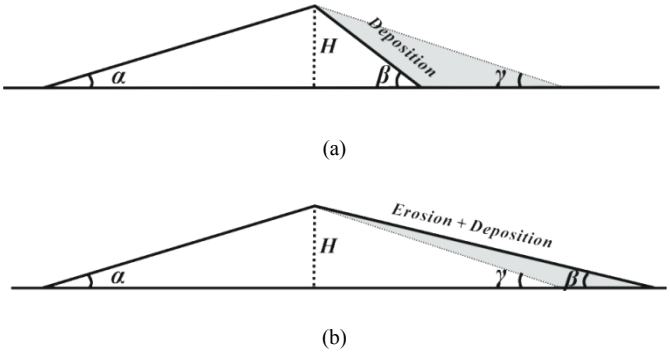

Figure 9-55. Schematic cross profiles of a barchan dune. α is the windward slope; β is the leeward slope; γ is the slope of a shadow zone; and H is the height of the dune slice. (a) When $\beta > \gamma$, only deposition occurs in the grey zone. (b) When $\beta < \gamma$, both erosion and deposition occur in the grey zone.

(c) A dune profile as P2 is an intermediate form between P1 and P3. It has a distinct slip face and a shadow zone. However, compared to P1, it suffers more severe sand loss, resulting in a progressive decrease in its windward slope.

Under the same potential sand transport rate, a dune slice with a larger cross-sectional area moves at a smaller rate (Figure 9-56). A barchan on a hard substratum disappears eventually because of a continuous sand loss from its horns (Figure 9-57). The annual sand volume loss, expressed as a fraction (the ratio of sand volume loss within a year to sand volume before the year), correlates strongly with the dune height at any time, irrespective of the size of an initial barchan (Figure 9-58). A smaller dune loses sand more significantly than a larger one. The annual sand volume loss, meanwhile, has a strong linear correlation with the dune migration rate. It therefore follows that a dune that migrates faster (and is smaller) has a higher annual sand volume loss.

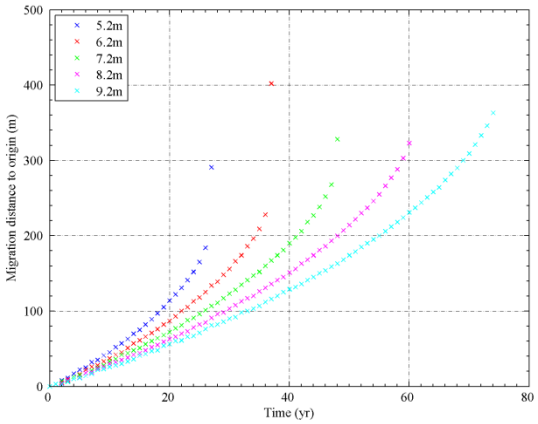

Figure 9-56. The migration distance of barchans on a hard substratum. Different colours denote initial heights of barchans, as shown in the legend.

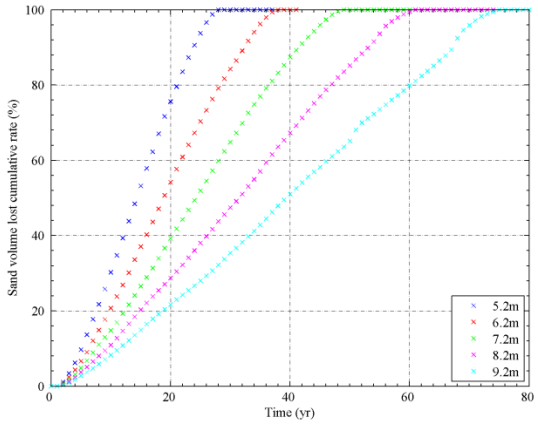

Figure 9-57. The cumulative annual sand volume loss on a hard substratum. Different colours denote initial heights of barchans, as shown in the legend.

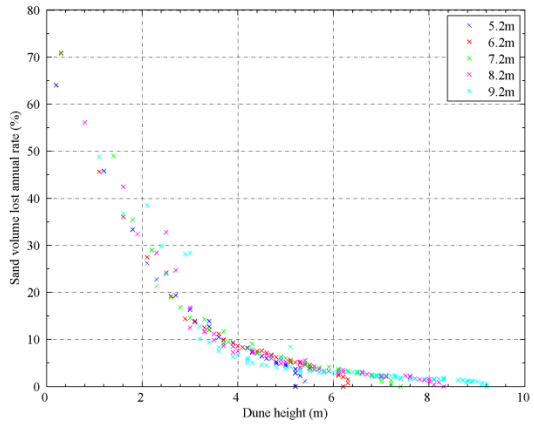

Figure 9-58. The relationship between annual sand volume loss and dune height. Different colours denote initial heights of barchans, as shown in the legend.

9.8.2.2 *Migration of a Barchan on Well-vegetated Surfaces*

The movement of a barchan and its interaction with vegetation is a complex balance between local sand burial and deposition tolerance, local erosion and erosion tolerance, and the sequencing of burial and erosion events as the horn passes over a location. When a barchan migrates over a vegetated surface, sand cannot escape from its horns, but it is trapped and stabilised by vegetation (Figure 9-59). Sand on the windward slope near the horns is eroded and deposited on the lee slope; this small amount of sand, however, is insufficient to completely remove vegetation and the plants on the lee slope maintain capability of trapping sand. As the horn migrates downwind, this vegetation then finds itself on the windward side. The previous burial will have increased the local surface erodibility, and so the subsequent survival of vegetation when it is located on the windward slope is then determined by its capability of withstanding erosion. Under the same horn-migration and sand budget scenario, plants with a higher deposition tolerance can endure more severe subsequent erosion on the windward slope because of their higher vitality. A high erosion tolerance, meanwhile, allows vegetation to survive more severe erosion and facilitates the development of trailing ridges or arms as a lobe moves forward. In contrast, vegetation with a low erosion tolerance is likely to be eliminated by even gentle erosion on the windward slope; as a result, trapped sand is re-exposed to transport, eroded, and moved further downwind - a process that prevents trailing arms from developing. This is the reason why the erosion tolerance of vegetation significantly impacts the arms-initiation time as well as the height of trailing arms. Arms can only be initiated when sand burial of plants on the lee slope is not sufficient to increase surface erodibility significantly once these plants find themselves on the windward slope, or if a smaller dune migration rate enables vegetation to survive the erosion. Meanwhile, a higher erosion tolerance encourages accelerated dune migration by trapping sand, forming outstanding arms, leading to a smaller and faster migrating lobe.

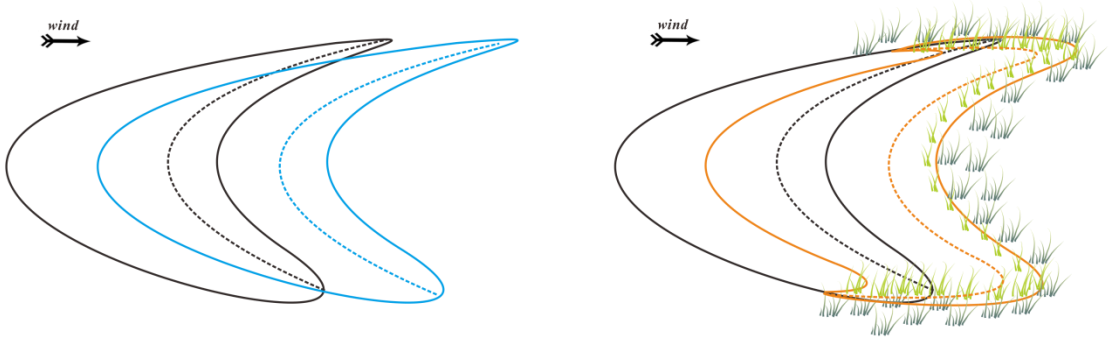

(a) (b)

Figure 9-59. Comparison of a barchan migration on (a) non-vegetated and (b) well-vegetated surfaces.

As sand availability increases from the horns towards the middle of a lobe, vegetation can no longer survive the significant sand burial and high dune cross-sections migrate forward unimpeded. A thicker substratum provides relatively abundant sand and encourages dune growth in height, resulting in a decreased migration rate. Therefore, vegetation can establish on a lobe more easily and a barchan is transformed into a parabolic dune more quickly. A barchan is transformed into a barchanoid-parabolic shape as its horns are stabilised by vegetation, whilst the middle part of the lobe continues to move downwind at a relatively constant rate. A thicker substratum decelerates the dune migration rate (Figure 9-33), and hence allows vegetation to survive more easily, developing into trailing arms. A high sand transport rate, meanwhile, increases both sand burial and wind erosion, preventing trailing arms from developing more effectively.

9.8.2.3 Formation of Parabolic-shaped Lobes and Trailing Arms

Figure 9-60 illustrates the slow-down effect arising from the specified parabolic sections of a lobe through which stabilised arms connect with the mobile barchanoid section. As the middle section of a lobe maintains a barchanoid shape, W_{ero} (the width of a lobe section perpendicular to winds on the windward slope) and W_{dep} (the associated width of the lobe section for deposition of sand from the W_{ero}) are similar in magnitude, which enables the barchanoid section to move forward at a relatively constant rate. Where the parabolic sections of the lobe link the arms with the barchanoid section, W_{dep} is larger than W_{ero} because of the lateral avalanching of deposited sand, leading to a gradual decrease in the migration rate. As the parabolic sections experience progressive deceleration, vegetation gradually encroaches on the lobe from the edges; as a consequence, the lobe transforms into a completed parabolic shape.

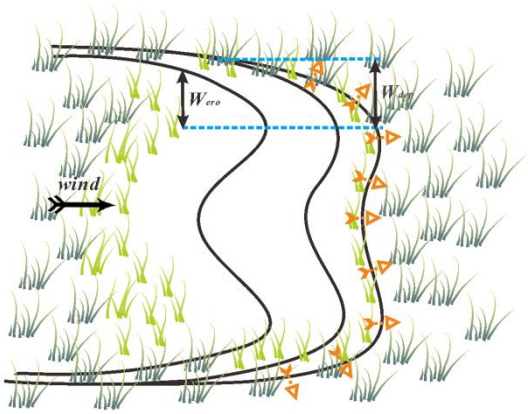

Figure 9-60. Schematic illustration of the slow-down effect of lobe edges due to sand avalanching on the depositional slopes. W_{ero} and W_{dep} are the effective erosion width and the associated deposition width respectively. Orange arrows denote sand avalanching directions on the lee slopes.

Given that W_{ero} is the same, a lower deposition tolerance enables the frontal edges of a lobe to migrate further, resulting in a larger associated W_{dep} (illustrated in Figure 9-61). As a result, a lower deposition tolerance develops trailing arms with a smaller (even negative) arms-elongating angle compared with that of a higher deposition tolerance. A smaller arms-developing angle, in particular, a negative one, exposes a larger surface area of substratum sediment (a wider deflation plane between the arms), thereby providing more sand for transport and decreasing subsequently the migration rate of lobe edges. However, if the deposition tolerance of vegetation is too small such that vegetation cannot survive even a small amount of burial, a dune would not transform into a parabolic shape at all, but develop into a larger barchan by incorporating more sand from its substratum. Nevertheless, the formation of a large barchan and the associated decrease in the migration rate is likely to lead to a faster transformation into a parabolic dune as soon as outstanding arms/ridges are initiated. A higher transport rate encourages the frontal edges of a lobe migrating further to form a smaller positive or a larger negative arms-developing angle (Figure 9-62). Although a thicker substratum provides more sand for transport and the frontal edges of a lobe migrate further, a significant decrease in the migration rate enables vegetation to colonise the whole lobe quickly forming a larger arms-developing angle (Figure 9-63).

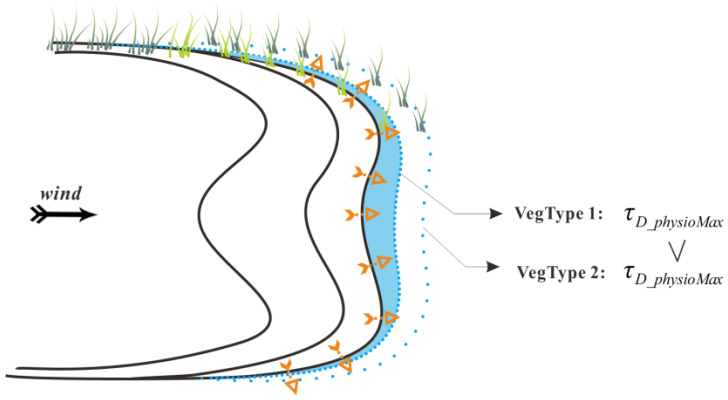

Figure 9-61. Schematic illustration of how the vegetation deposition tolerance determines the arms-developing angle. Orange arrows denote sand avalanching directions on the lee slopes.

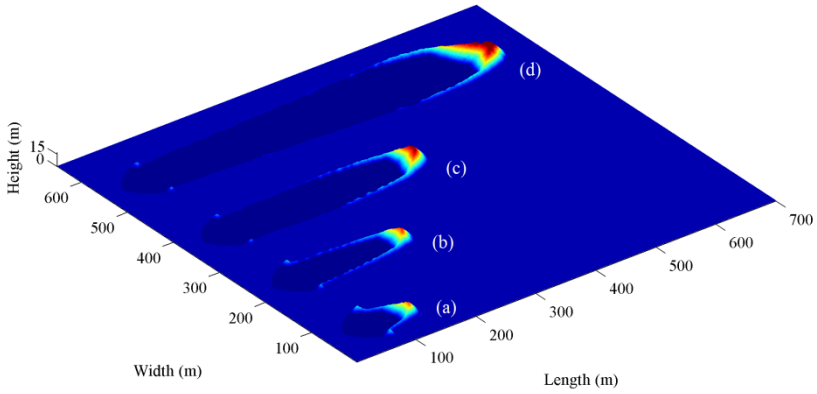

Figure 9-62. Influence of the sand transport rate on the arms-developing angle. D_0 = 0.6 m, H_0 = 6.2 m, $\tau_{E\_physioMax}$ = -2.0 m season^{-1}, and $\tau_{D\_physioMax}$ = 3.1 m season^{-1}. From (a) to (d), q increases gradually, from 16, 18, 20 to 22 m^3 m^{-1} yr^{-1} in sequence, resulting in an arms-developing angle of 38˚, 11˚, 3˚, and - 4˚ respectively.

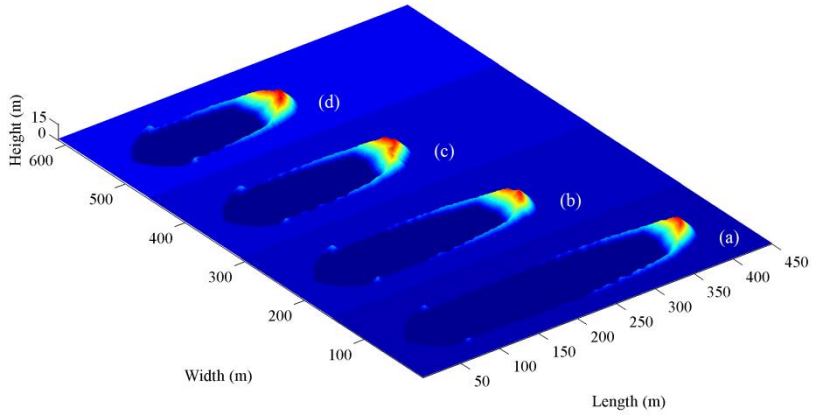

Figure 9-63. Influence of the substratum thickness on the arm-developing angle. q = 20 m^3 m^{-1} yr^{-1}, H_0 = 6.2 m, $\tau_{E\_physioMax}$ = -2.0 m season^{-1}, and $\tau_{D\_physioMax}$ = 3.1 m season^{-1}. From (a) to (d), D_0 increases gradually, from 0.6, 0.9, 1.2 to 1.5 m in sequence, resulting in an arms-developing angle of 3˚, 6˚, 7˚ and 8˚ respectively.

9.8.2.4 Dune Profile Change and Vegetation Growth

The interrelationship between dune profile changes and vegetation growth varies dependent on sand availability. When sand eroded from the windward slope of a dune slice is sufficient to exert a severely negative impact on vegetation growth on the lee side, the maximum height on the lee slope where vegetation can survive is constant as well as the migration rate of the dune slice (Figure 9-64). A higher sand transport rate can erode more sand from the windward slope and the dune slice migrates at a larger rate, but the maximum height where vegetation on the lee slope can survive maintains the same as long as the deposition tolerance of vegetation is the same. In a similar manner, a thicker substratum thickness increases the height of a lobe slice and slows down the dune migration rate, but the maximum position that vegetation on the lee slope can reach is the same dependent solely on the deposition tolerance of vegetation species. As shown in Figure 9-65, given that the sand transport rate keeps constant, from t_0 to t_3, as the sandy substratum experiences downward erosion and the transported sand is deposited on the lee slope, the toe of the windward slope stays at the same location, whilst the height increases gradually, resulting in a slightly decreasing migration rate. When the deepening of the deflation by wind erosion stops by a hard substratum, the windward slope begins to move forward by erosion, and the whole dune slice migrates at a relatively constant rate (from t_3 onwards). A dune with a thicker sandy substratum develops a higher lobe before reaching a non-erodible hard stratum, and thus migrates at a lower rate.

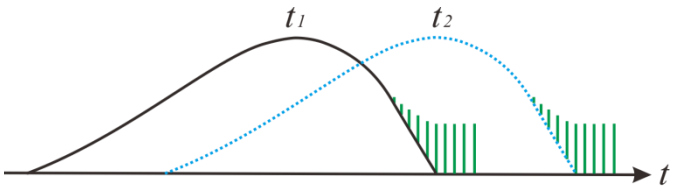

Figure 9-64. The interrelationship between dune profile and vegetation growth when sand is sufficient to kill surviving vegetation on the lee slope.

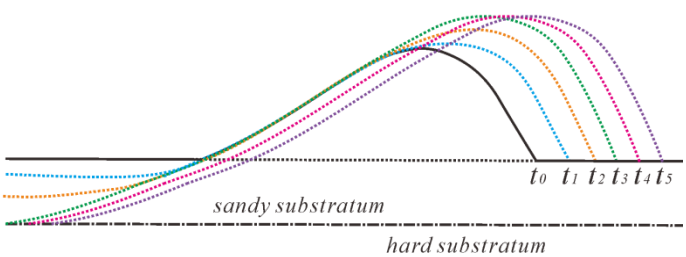

Figure 9-65. Influence of a sandy substratum on the dune migration rate.

When sand is insufficient to eliminate partial vegetation on its lee slope because of sand loss to arms by lateral avalanching and/or because of a decrease in migration rate allowing vegetation to maintain its vitality, sand eroded from the windward slope then deposits and accumulates on the bare surface of the upper lee slope (from t_1 to t_2 in Figure 9-66). This is because sand is inadequate to supress the presence of newly-grown vegetation, which enables a steeper slope than a bare surface. The upwind toe of the dune slice, meanwhile, stops migrating and vegetation continues to grow. As vegetation is able to reach up to a higher vertical position, less sand is available for wind erosion. Once sand erosion decreases below the vegetation erosion tolerance, the whole dune slice is fully-stabilised instantly (from t_2 to t_3 in Figure 9-66). The barchan-to-parabolic dune transformation is complete when all dune slices change from the state in Figure 9-64 to the state in Figure 9-66.

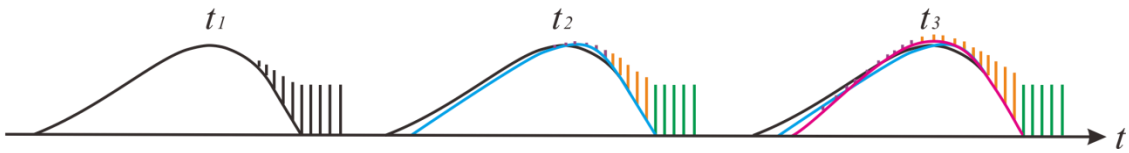

Figure 9-66. The interrelationship between dune profile and vegetation growth when sand is insufficient to eliminate surviving vegetation on the lee slope. Green bars are vegetation at the maximum growth and do not change between two successive times; orange bars are vegetation that continues to grow between two successive times; and magenta bars are newly-grown vegetation between two successive times.

An example of this process is shown in Figure 9-67. From 190 yr to 200 yr, the dune slice keeps migrating and the highest vertical position on the lee slope where vegetation can grow remains similar. Then after 210 yr, it stops migrating and sand starts to accumulate on the upper slope of the lee side, whilst vegetation encroaches further up even to the crest. Vegetation subsequently extends to the upper slope of the windward side at 220 yr and eventually stabilises the whole dune slice.

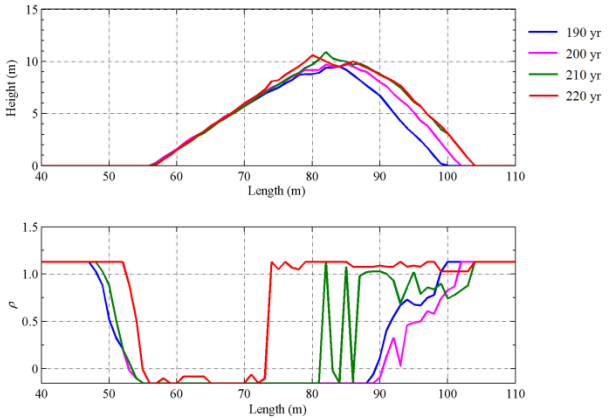

Figure 9-67. An example of a dune slice profile (upper panel) and vegetation change (lower panel) over time. H_0 = 5.2 m, D_0 = 0.6 m, $\tau_{E\_physioMax}$ = -2.0 m season^{-1}, and $\tau_{D\_physioMax}$ = 3.0 m season^{-1}. To facilitate comparison, dune profiles at different times all start from the same horizontal location.

9.8.3 Applications and Implications

Equation 9-3 can be used to estimate the time when an original barchan initiated the process of a barchan-to-parabolic dune transformation. Figure 9-68 shows the DEMs of two mobile parabolic dunes (D1 and D2) surveyed by a D-GPS in 2012. As discussed in Chapter 5, the broken relics of vegetated hummocks leaving behind the parabolic dunes are likely to indicate the location of the toe of the original barchans (back-ridges). The presence of a barchanoid field to the north of the surveyed dunes also suggests that there is a high possibility that this transformation scenario has happened for both dunes (Figure 4-2). Based on this assumption, the average width and the migration distance can be measured from their DEMs. The height of the original barchans is assumed to be the same as the height of the associated parabolic dunes measured. The sandy substratum thickness was estimated by digging in the deflation plain of a parabolic dune, which is approximately 0.6 m. The standard sand transport rate of 20 m^3 m^{-1} yr^{-1} is used. By substituting these values for their representative variables in Equation 9-1, the time when the original barchans started to transform into parabolic dunes D1 and D2 can be calculated - both of which are approximately 47 years (Table 9-3). Because of the absence of long-term historic remote sensing imagery, it is difficult to evaluate the accuracy of these hind-casts. Nonetheless, they represent a plausible time-scale. Further research is hence crucial on the comparison between long-term field measurements and modelling results.

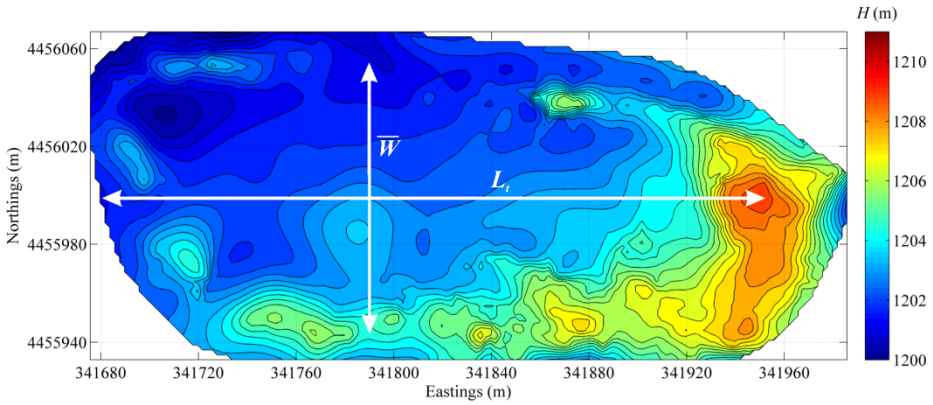

(a) D1

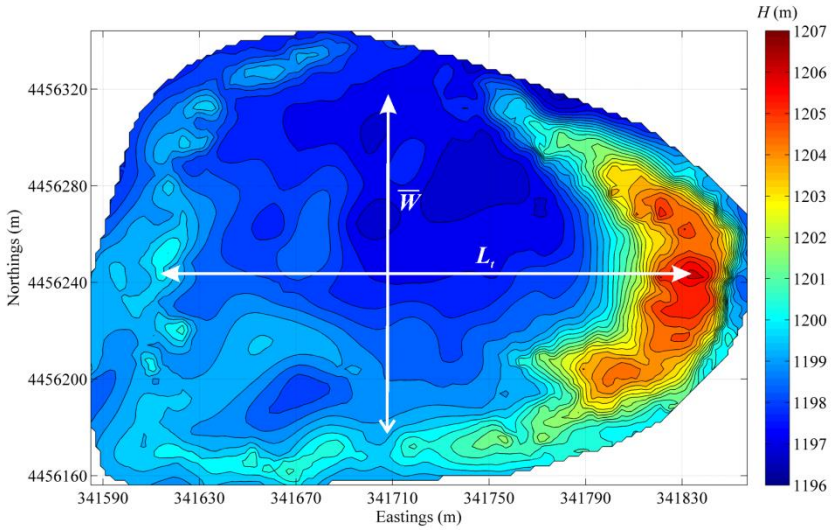

(b) D2

Figure 9-68. DEMs of measured parabolic dunes in 2012.

Table 9-3. Calculation of initiation times of barchan-to-parabolic dune transformations in the field.

Dune #	H_0 (m)	D_0 (m)	$\tau_{E\_physioMax}$ (m season^{-1})	$\tau_{D\_physioMax}$ (m season^{-1})	q (m^3 m^{-1} yr^{-1})	L_t (m)	$\overline{W}$ (m)	***t* (yr)**
D1	4	0.6	-2.0	3.0	20	270	110	**46.7**
D2	8	0.6	-2.0	3.0	20	220	140	**46.5**

If repeated topographic measurements are available, the derivation of Equation 9-3 provides a simpler approach to an estimation of *t* without resolving explicitly the environmental parameters of a dune system:

$$t = \Delta t \left[\left(\frac{\overline{W_1} L_{t2}}{L_{t1} \overline{W_2}} \right)^{1/0.64} - 1 \right]^{-1} + \Delta t \qquad (9\text{-}4)$$

where: Δt is the time interval between the two measurements, [yr]; L_{t1} and L_{t2} are migration distances from the original barchan at two investigated times respectively, [m]; and $\overline{W_1}$ and $\overline{W_2}$ are the average widths between arms or ridges at two investigated times respectively, [m]. This derived Equation 9-4 provides an easier approach to attain *t*, but it requires a relatively large temporal scale at a magnitude of decades and a relatively stable dune system.

9.9 Preliminary Explorations of Other Applications

9.9.1 Influence of Drought Events

Periodic drought events can influence the dune stabilisation and barchan-to-parabolic dune transformations significantly. Three key factors are explored here: drought duration, drought interval, and drought strength. The drought duration is the duration a drought event lasts. The drought interval is the period between two drought events when typical climate controls the region. The drought cycle consists of one drought duration and one drought interval. The drought strength is the magnitude of drought defined by a negative climatic impact. The simulation scenarios start from an initial 9.2 m high barchan over a sandy substratum of 0.6 m in depth. The maximum erosion and deposition tolerances are -2.5 and 3.0 m season^{-1} respectively. The standard potential transport rate of 20 m^3 m^{-1} yr^{-1} is used. The drought duration is explored in a range of [1, 5] yr with 1 year steps, and the drought interval is explored in a range of [10, 50] yr with 10 year steps. The drought strength or climatic impact varies in a range of [-1.2, -0.1] with 0.1 steps. This results in 300 simulation scenarios in total. All simulation scenarios start from a drought interval under typical climate regime, followed by a drought duration during which a climatic impact is imposed into the model. The cycle is repeated until the end of a simulation.

Figure 9-69 shows the relationship between the ratio of drought duration to drought cycle and the threshold of climatic impact. The threshold of climatic impact is the maximum climatic force or drought stress under which an initial barchan can still be transformed into a parabolic dune, while above which the initial barchan maintains its crescentic shape. The threshold of climatic impact can also be regarded as the maximum resistance of the system to climatic change when the catastrophic shift would happen. There is a strong logarithmic correlation between the threshold of climatic impact and the ratio of drought duration to drought cycle. As the drought duration to drought cycle ratio increases, the threshold

of climatic impact decreases at a lower rate. This indicates that a small increase in the relatively low drought duration to drought cycle ratio (which is commonly seen in a reality) can significantly reduce the capability of a dune system to be stabilised and to resist negative climatic forces.

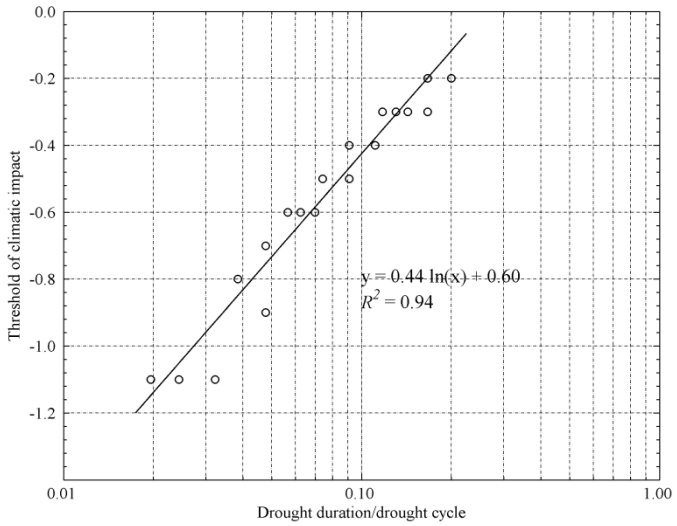

Figure 9-69. The relationship between the ratio of drought duration to drought cycle and the threshold of climatic impact.

9.9.2 Influence of Grazing Activity

The anthropogenic pressure, in particular, grazing activity, can retard the stabilisation of barchans and the barchan-to-parabolic dune transformations. The influence of grazing activity and the characteristics of vegetation on the transition time of a barchan into a parabolic dune are explored. All simulation scenarios start from an initial barchan at the height of 9.2 m on a sandy substratum of 0.6 m in depth. The standard potential sand transport rate of 20 m^3 m^{-1} yr^{-1} is used. The erosion tolerance is varied from -2.1, -2.3, to -2.5 m $season^{-1}$, at a constant deposition tolerance of 3.0 m $season^{-1}$, whilst the deposition tolerance is varied from 3.0, 3.1, to 3.2 m $season^{-1}$, at a constant erosion tolerance of -2.5 m $season^{-1}$. The forage demand is explored in a range of 1000 to 5000 yr^{-1} with 100 yr^{-1} steps. The domain size is 600 × 153 m^2, so the forage demand range is equivalent to a range of [0.011, 0.054] m^{-2} yr^{-1} with 0.001 m^{-2} yr^{-1} steps. This results in 205 simulation scenarios in total.

The relationships between the forage demand and the transition time of barchan-to-parabolic dune transformations under different deposition tolerances and different erosion tolerances are presented in Figure 9-70 and Figure 9-71 respectively. The last point in each line reflects the threshold of forage

demand above which an initial barchan cannot be stabilised and transformed into a parabolic dune within the simulation domain. A higher deposition tolerance significantly increases the threshold of forage demand, whereas the influence of the erosion tolerance seems insignificant. A small increase in the forage demand leads to more significant increase for a lower deposition tolerance, which means a dune system with a low deposition tolerance is more sensitive to grazing activity. However, there is no clear trend for the relationship between the forage demand and the transition time at different erosion tolerances, which suggests that the erosion tolerance is not crucial in controlling the transition time. It is likely that the stochastic nature of the simulations overwhelms the insignificant trend arising from different erosion tolerances.

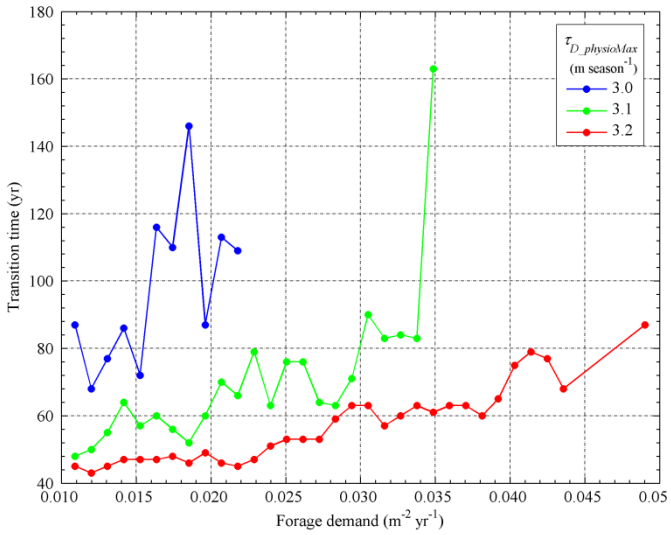

Figure 9-70. The relationship between the forage demand and the transition time under different deposition tolerances. H_0 = 9.2 m, D_0 = 0.6 m, q = 20 m^3 m^{-1} yr^{-1}, and $\tau_{E\_physioMax}$ = -2.5 m season^{-1}.

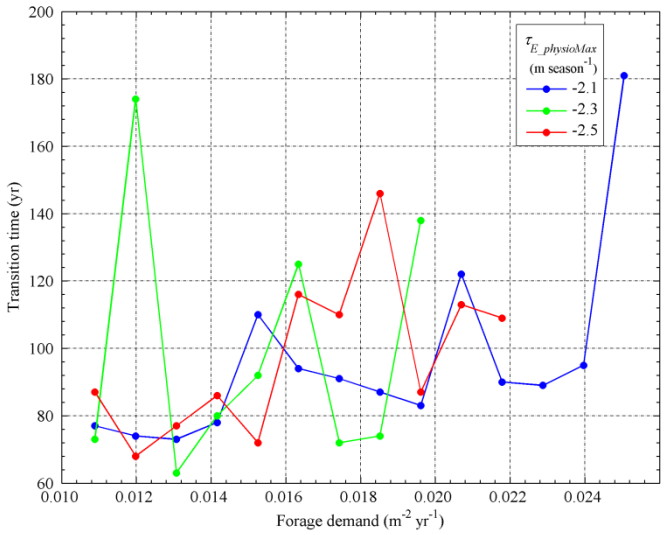

Figure 9-71. The relationship between the forage demand and the transition time under different erosion tolerances. H_0 = 9.2 m, D_0 = 0.6 m, q = 20 m^3 m^{-1} yr^{-1}, and $\tau_{D\_physioMax}$ = 3.0 m season^{-1}.

9.10 Discussion

The barchan-to-parabolic dune transformations have been successfully simulated on realistic temporal and spatial scales. This is partly due to the fact that the parameters used in the model have been customised to the local environmental conditions including the wind regime, sandy substratum thickness, and vegetation characteristics. In particular, the Extended-DECAL is intended to simulate perennial shrubs rather than grasses. Duran and Herrmann (2006) simulated the development of a parabolic dune from a barchan on a non-erodible surface under the influence of grasses. They proposed a dimensionless fixation index θ, determined by the initial barchan volume, wind strength, and vegetation growth rate (Equation 9-5), and suggested that a barchan can only be transformed into a parabolic dune when θ is smaller than 0.5, as was also reported by Reitz et al. (2010). The fixation index θ is defined as:

$$\theta = Q/(V^{\frac{1}{3}}V_v) \tag{9-5}$$

where: Q is the undisturbed saturated sand flux, [m^3 m^{-1} yr^{-1}], V is the initial barchan volume, [m^3], and V_v is the vegetation growth rate, [m yr^{-1}].

It is difficult to directly compare their θ with the modelling results presented in this chapter, because V_v is regarded as a vertical growth rate of plants in height, which is different from the vegetation effectiveness used in DECAL. Erosion and deposition in their model is, furthermore, treated as

undifferentiated absolute surface change impact on the vegetation growth, whereas vegetation in DECAL has different capabilities of withstanding erosion and sand burial. The growth forms of grasses and shrubs are also significantly different. In contrast to grasses, which grow rapidly and are usually short-lived, shrubs have a much more extended life cycle and can be influenced by changes of environmental and anthropogenic factors across different temporal scales. For example, the growth of a shrub is not only influenced by short-term sand transport events but also long-term seasonal and climatic changes.

The θ is, however, qualitatively comparable to the stabilising index (S_*) proposed in Section 9.8.1 in respect of how wind regime, sand availability, and vegetation characteristics influence the dune stabilisation and barchan-to-parabolic dune transformations. Given the same S_* (or the same normalised migration distance L_t', *cf.* Equation 9-3), a higher sand transport rate (q) or a lower sand availability (H_0D_0) needs a shorter time for an initial barchan to be transformed into a (barchanoid-) parabolic dune with the same L_t' - a system with a higher mobility. This is similar to a situation in which a larger Q or a smaller V results in a larger θ. The ratio of the erosion tolerance to the deposition tolerance ($\tau_{E\_physioMax} / \tau_{D\_physioMax}$) in S_* captures the impact of vegetation, whose increase (because of a decrease in the deposition tolerance, for example) requires less time for an initial barchan to reach the same L_t'. This is comparable with a situation in which a smaller V_v leads to a higher θ.

The Extended-DECAL incorporates the changes in vitality of plants at different seasons and at different ages, which can more realistically capture natural eco-geomorphic interactions across different temporal scales. This model can be easily adapted to different aeolian systems with different vegetation communities. It is possible, however, that grasses, shrubs, and trees coexist with one another, in which case a trade-off might be needed in order to determine an optimal modelling time scale. The Extended-DECAL can also be used as a tool to explore different aspects of external forces such as drought events and grazing activity, as briefly demonstrated in Section 9.9.

There are two potential mechanisms of the barchan-to-parabolic dune transformations that have been proposed by previous studies (*cf.* Section 2.3.2) – the 'horns-anchoring' mechanism and the 'nebkhas-initiation' mechanism. Here, the modelling results show that the 'horns-anchoring' mechanism is likely to control the barchan-to-parabolic dune transformation in the study region. Some of the processes involved in the transformation have been hypothesised by Barchyn and Hugenholtz (2012). They attribute the barchan-to-parabolic dune transformation to a smaller sand deposition on the slipface close to horns relative to the deposition tolerance of vegetation. Vegetation that survives sand burial on

the slipface near the horns anchors the dune surface therein, and causes a 'shear' that forces the slipface of the mobile barchanoid body in the middle to bend outwards. The resulting change in the planform brinkline angle decreases sand deposition on the slipface. Once the slipface deposition rate is below the deposition tolerance of vegetation, the portion of the dune can then be stabilised. As the dune is progressively stabilised inwards, it is eventually transformed into a parabolic shape. This hypothesis regards the batwing-shaped transforming dune as a clear-cut two parts - vegetated parabolic arms and bare crescentic body (Figure 9-72) – but this may be an oversimplification. The impact of different erosion tolerances pertaining to vegetation species has also been disregarded.

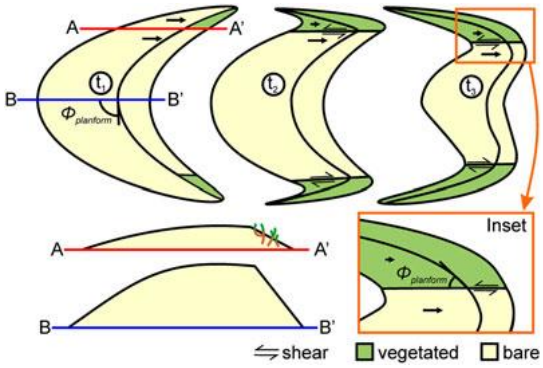

Figure 9-72. Hypothesis of the barchan-to-parabolic dune transformation proposed by Barchyn and Hugenholtz (2012). Timestep t_1: Cartoon profiles of barchan dunes illustrating how deposition rates on barchan horns (A–A') are less than those in the middle (B–B') due to lower planform brinkline angles ($\Phi_{planform}$). This can lead to preferential stabilisation of barchan horns and crest terminations, eventually leading to parabolic dune formation. Timestep t_2, t_3: Subsequent stabilisation of the crests causes differences in the velocity between the stabilised and active portions of the dune, causing shear to rotate the slipface to the outside of the dune and reduce the $\Phi_{planform}$ angles, prompting stabilisation due to lower deposition rates. The remainder of the dune subsequently stabilises inwards, a successive feedback. Arrows correspond to relative velocity.

The Extend-DECAL explores the impacts of both the erosion tolerance and the deposition tolerance of vegetation on the barchan-to-parabolic dune transformation. Modelling results show that there are much more complicated eco-geomorphic interactions and morpho-dynamics involved. Figure 9-73 and Figure 9-74 present an example that shows how vegetation interacts with the migrating dune and changes the dune morphology progressively. Four basic eco-geomorphic interaction zones can be identified, which bear different functionality in the barchan-to-parabolic dune transformation.

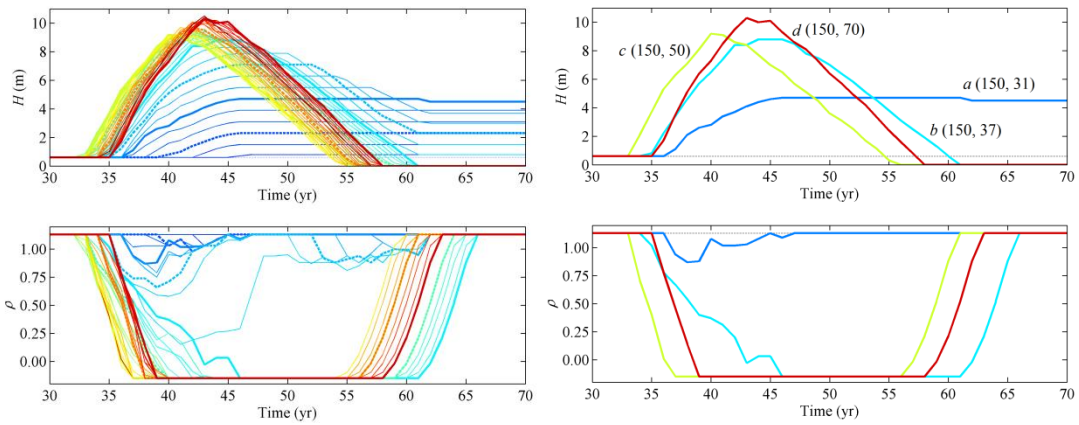

(a) (b)

Figure 9-73. The changes in height and vegetation effectiveness over time. q = 20 m^3 m^{-1} yr^{-1}, H_0 = 9.2 m, D_0 = 0.6 m, $\tau_{E\_physioMax}$ = -2.3 m season^{-1}, and $\tau_{D\_physioMax}$ = 3.0 m season^{-1}. (a) Each line/colour reflects a cell position along a transverse section from the horn tip (northings = 25 m) to the middle of the dune (northings = 70 m), also shown in a black line in Figure 9-74. (b) The *a*, *b*, *c*, and *d* reflect the boundaries between different eco-geomorphic interaction zones across the transverse section, also shown in snapshots in Figure 9-74.

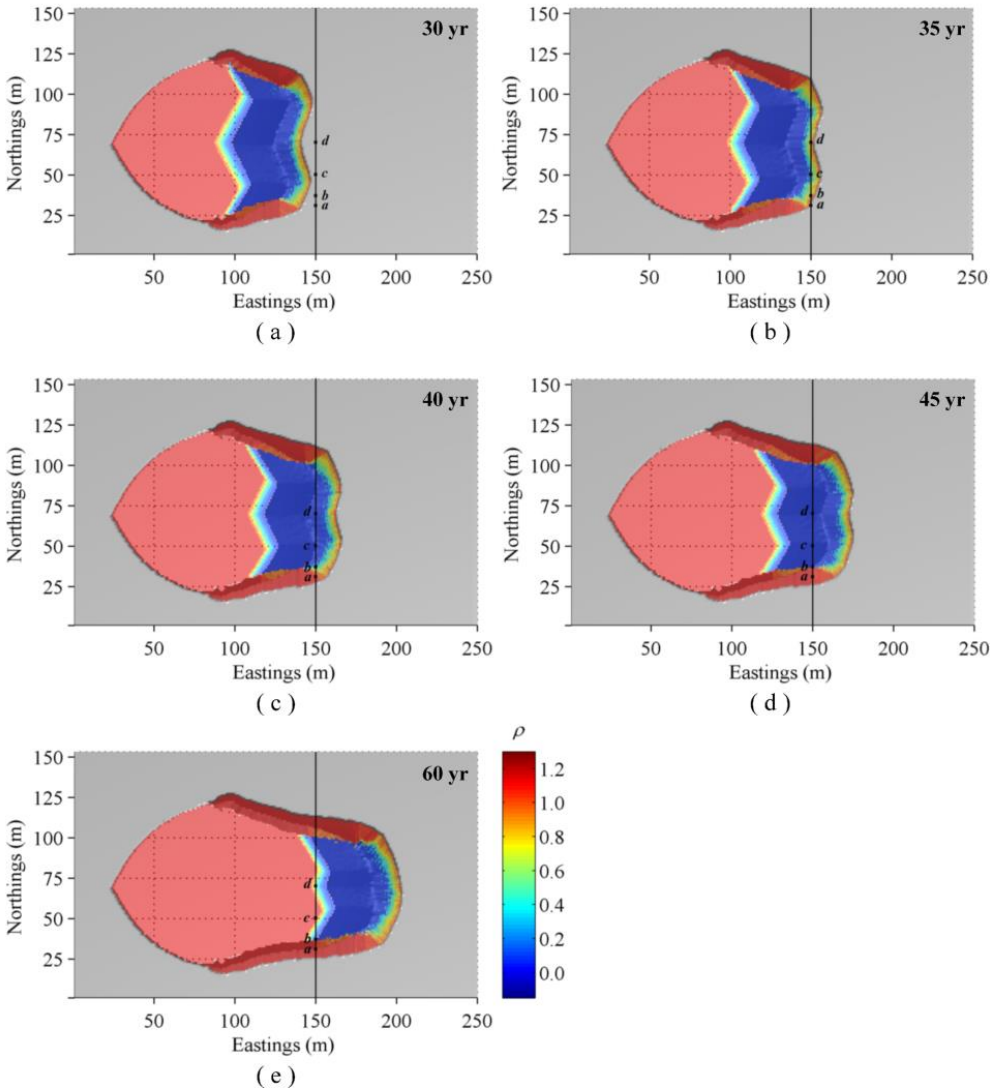

Figure 9-74. The eco-geomorphic interaction and the barchan-to-parabolic dune transformation. q = 20 m^3 m^{-1} yr^{-1}, H_0 = 9.2 m, D_0 = 0.6 m, $\tau_{E\_physioMax}$ = -2.3 m season^{-1}, and $\tau_{D\_physioMax}$ = 3.0 m season^{-1}. The *a*, *b*, *c*, and *d* reflect the boundaries between different eco-geomorphic interaction zones.

Four basic eco-geomorphic interaction zones may be identified going from the outer edge to the dune middle-line (examples shown as the black line in Figure 9-74):

Zone 1: from outer edge to point *a* (Figure 9-75a). Vegetation in this zone experiences minimal sand burial and declines slightly, because it is on the edge of the migrating lobe. But as the deposition rate decreases (see the slope of *H*), vegetation starts to recover and reaches its optimal state quickly while it continues to trap sand. Vegetation in the zone maintains a high vitality such that no erosion occurs. Going from the interacting edge towards *a*, sand availability increases slightly, and this zone eventually forms the outside slope of the parabolic arm, and point *a* increases the most in height forming the crest of this arm (Figure 9-74e).

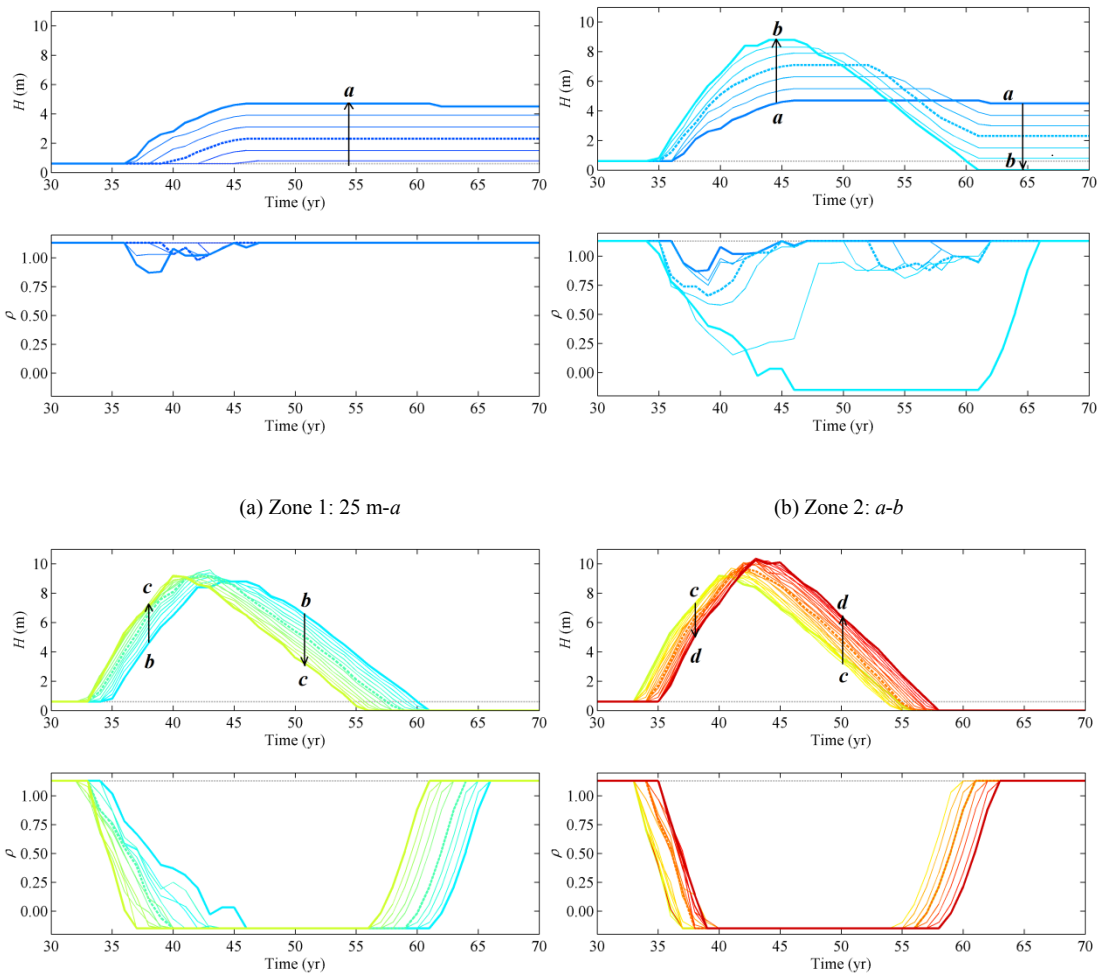

(a) Zone 1: 25 m-*a*

(b) Zone 2: *a*-*b*

(c) Zone 3: *b*-*c*

(d) Zone 4: *c*-*d*

Figure 9-75. Topography and vegetation change over time in different eco-geomorphic interaction zones. $q = 20$ m^3 m^{-1} yr^{-1}, $H_0 = 9.2$ m, $D_0 = 0.6$ m, $\tau_{E\_physioMax} = -2.3$ m season^{-1}, and $\tau_{D\_physioMax} = 3.0$ m season^{-1}. The *a*, *b*, *c*, and *d* are the boundaries of different eco-geomorphic interaction zones across the transverse section at 150 m of eastings shown in snapshots in Figure 9-74. Each line/colour represents a 1 × 1 m^2 cell along the transverse section. The arrow shows the location of cells from south to north.

Zone 2: from *a* to *b* (Figure 9-75b). As sand availability continues to increase, vegetation in this zone undergoes more severe sand burial and declines more significantly. Similar to Zone 1, vegetation recovers as the deposition rate decreases. However, because of more significant decline arising from more severe sand burial, vegetation also experiences slight erosion when no more sand is available for further trapping. Although the remobilisation of trapped sand decreases the local height, the recovery of vegetation in these cells is still quick enough to preserve partial sand. This zone then develops toward the inner slope of the transverse section of the arm. Going from *a* to *b*, increased sand availability leads to higher temporal maximum topography, but also results in more severe subsequent erosion. Point *b*

eventually becomes the inner boundary of the parabolic arm or the edge of the deflation plain (Figure 9-74e). Zone 1 and Zone 2 together comprise the transverse section of the arm.

Zone 3: from *b* to *c* (Figure 9-75c). As shown in Figure 9-74c, point *c* is the boundary between the crescentic-shaped body in the middle and the parabolic-shaped wing. The topography change over time in this zone is generally similar. Vegetation change, however, exhibits a gradient as sand burial increases. From *b* towards *c*, as sand deposition increases, the maximum height of the slip face where vegetation can survive decreases. Vegetation in this zone, nevertheless, is eliminated by sand burial eventually. Vegetation starts to revitalise only when these cells have been on the deflation plain where sedimentation balance is neutral (Figure 9-74e).

Zone 4: from *c* to *d* (Figure 9-75d). This zone comprises the transverse section of the crescentic-shaped body in the middle of the dune (Figure 9-74b & Figure 9-74c). The changes in both topography and vegetation display similar profiles. In contrast to Zone 3, vegetation in this zone survives only up to a limited and constant height on the slip-face.

In sum, the deposition tolerance of vegetation influences the eco-geomorphic interactions of all four zones, and it hence plays a significant role in controlling the barchan-to-parabolic dune transformation. The erosion tolerance only influences the formation and boundary of trailing arms in Zone 2, and is less significant as compared with the deposition tolerance. The increase in the maximum height that vegetation can reach from *c* to *b* in Zone 3 decelerates the migration rate of the parabolic-shaped wing progressively, which eventually slows down the crescentic body in the middle and leads to the transformation of the dune into the parabolic shape (*cf.* Section 9.8.2.2).

The key system parameters explored in this chapter can influence the relative proportions and locations of the four eco-geomorphic interaction zones and the associated morphologies of resulting parabolic dunes. A higher erosion tolerance of vegetation increases the portion of Zone 1, which then leads to the development of a larger arms-developing angle (*cf.* Section 9.8.2.3). A lower erosion tolerance of vegetation, however, results in a more significant sand loss by erosion in Zone 2, which results in thinner trailing arms or even no arms. An increase in the initial dune height or the substratum thickness decelerates the dune migration rate, which enables vegetation to survive sand burial better in Zone 2-3 and encourages a quicker barchan-to-parabolic dune transformation. A higher sand transport rate expands Zone 4 and narrows Zone 2, leading to a longer transition time.

The four eco-geomorphic interaction zones show much more complicated dynamics involved in the barchan-to-parabolic dune transformation, as compared with the hypothesis by Barchyn and Hugenholtz (2012). The erosion tolerance of vegetation cannot be omitted because it plays a crucial in forming trailing arms of resulting parabolic dunes, although it is overall less essential than the deposition tolerance in controlling the transformation.

The non-dimensional 'dune stabilising index' proposed in this chapter has been demonstrated to be able to capture the combined influence of the system controls on the barchan-to-parabolic dune transformation. The power-law relationship between the dune stabilising index and the normalised migration distance is likely to be a promising approach for extrapolating the historical trajectories of transforming dunes in the field. The accuracy, applicability, and limitations, however, need to be further examined by comparing the simulation results against real-world data.

The chapter explores the barchan-to-parabolic dune transformation from one single initial barchan in a whole domain. The interactions between neighbouring dunes, therefore, are disregarded. The spacing and arrangement of dunes, however, can be of particular importance in the evolution of a whole dunefield on a large spatial scale. The modelling results, for example, show that a negative arms-developing angle can occur when an initial barchan is migrating at a relatively high rate. These barchan-to-parabolic dune transformations require long transition duration, and the transition usually happens shortly before the dunes are completely stabilised. Therefore, if the barchans are closely-spaced laterally, they may have connected with their neighbouring dunes developing into transverse ridges before being able to transform into parabolic dunes. This might be the reason why a parabolic dune with a negative arms-developing angle is not commonly found in the field. The influence of dune spacing and arrangement on the barchan-to-parabolic dune transformation hence requires further research.

References

Baas, A.C.W., 2002. Chaos, fractals and self-organization in coastal geomorphology: simulating dune landscapes in vegetated environments. Geomorphology, 48(1-3), 309-328.

Bak, P., Tang, C., 1989. Earthquakes as a self-organized critical phenomenon. Journal of Geophysical Research: Solid Earth, 94(B11), 15635-15637.

Barchyn, T.E., Hugenholtz, C.H., 2012. A process-based hypothesis for the barchan-parabolic transformation and implications for dune activity modelling. Earth Surface Processes and Landforms, 37(13), 1456-1462.

Bouchaud, J.P., 2001. Power laws in economics and finance: some ideas from physics. Quantitative Finance, 1(1), 105-112.

Duran, O., Herrmann, H.J., 2006. Vegetation against dune mobility. Physical Review Letters, 97(18), 188001/188001-188004.

Mandelbrot, B., 1960. The Pareto-Lévy Law and the Distribution of Income. International Economic Review, 1(2), 79-106.

Pye, K., 1982. Morphological development of coastal dunes in a humid tropical environment, Cape Bedford and Cape Flattery, North Queensland. Geografiska Annaler Series a-Physical Geography, 64(3-4), 213-227.

Reitz, M.D., Jerolmack, D.J., Ewing, R.C., Martin, R.L., 2010. Barchan-parabolic dune pattern transition from vegetation stability threshold. Geophysical Research Letters, 37.

Chapter 10

Dune Reactivation and Parabolic-to-barchan Dune Transformations

---

This chapter:

- Presents dune reactivation and parabolic-to-barchan dune transformations under climatic changes and anthropogenic pressure;
- Explores how the characteristics of vegetation and the dune surface erodibility of an initial parabolic dune influence the dune reactivation and parabolic-to-barchan dune transformations under climatic changes arising from increased drought stress and wind strength;
- Examines the influence of grazing activity on the parabolic-to-barchan dune transformations, and how the characteristics of vegetation affect the reactivation threshold of a parabolic-to-barchan dune transformation.

10.1 Exploring Framework

10.1.1 Influence of Climatic Change on the Reactivation of Parabolic Dunes

The influence of climatic change on dune reactivation is explored from five initial parabolic dunes with different dune surface erodibility (*DSE*, *cf.* Section 8.3.2.1). As shown in Figure 10-1a, the five parabolic dunes are selected during a barchan-to-parabolic dune transformation from an initial barchan at the height 9.2 m on a sandy substratum of 0.6 m thick under the influence of vegetation with the maximum erosion tolerance ($\tau_{E\_physioMax}$) of -2.3 m season^{-1} and the maximum deposition tolerance ($\tau_{D\_physioMax}$) of 3.0 m season^{-1}. The selected parabolic dunes are dunes at 80, 90, 100, 110, and 120 yr (t_0) of the simulation respectively, and the dunes are then used as initial dunes to expose to different climatic impacts. The change in the dune surface erodibility from an initial barchan to a stabilised parabolic dune is present in Figure 10-1b, in which pink asterisks denote the five selected parabolic dunes. Figure 10-1c also shows

the associated dune surface erodibility of the five parabolic dunes. For the exploration of reactivation scenarios, the maximum erosion tolerance is varied in a range of -2.5 to -2.0 m season^{-1} (the negative sign denotes erosion), whilst the maximum deposition tolerance is selected in a range of 2.9 to 3.2 m season^{-1}. Both ranges are explored with a resolution of 0.1 m season^{-1} steps. The sand transport rate of 20 m^3 m^{-1} yr^{-1} is kept constant. The climatic impact (*CI*) is varied in a range of -0.10 to -0.46 with a resolution of 0.02. Multiple simulations are explored at the threshold of climatic impact when a parabolic dune can be reactivated into a barchan. More than 2000 simulations in total are hence analysed.

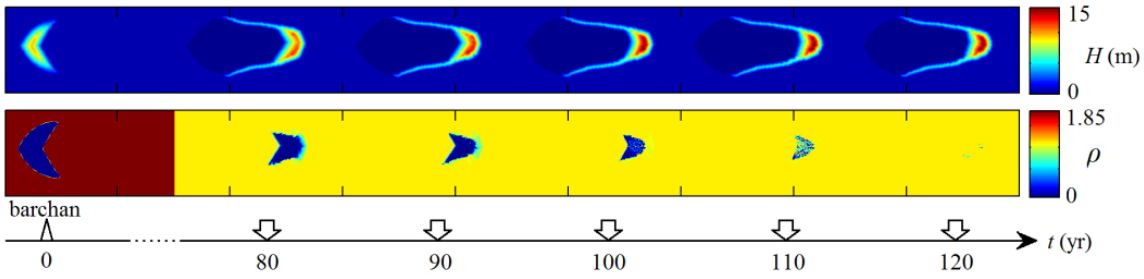

(a)

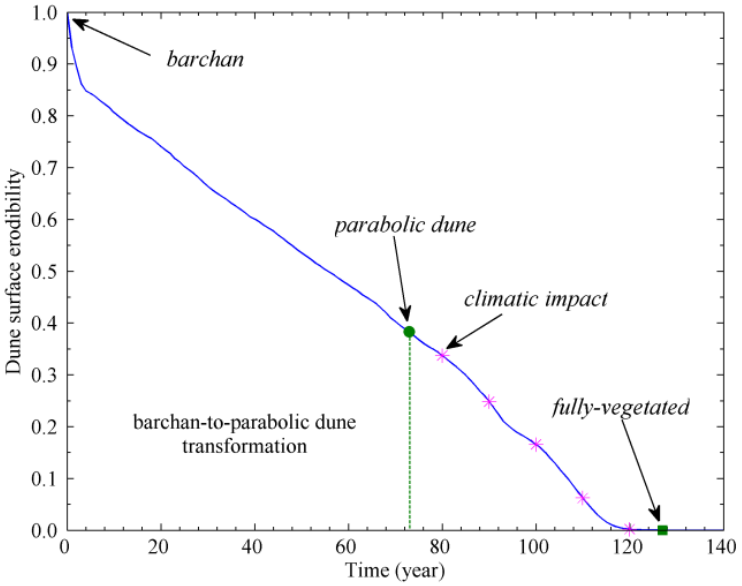

(b)

t_0	*DSE*
80	0.3370
90	0.2480
100	0.1654
110	0.0620
120	0.0018

(c)

Figure 10-1. The five stages of a parabolic dune for initiating a reactivation under climatic changes. The upper and lower panels in (a) denote the DEM and the vegetation effectiveness respectively. Pink asterisks in (b) denote parabolic dunes in (a), and the green dot denotes the time when the initial barchan is transformed into a typical parabolic dune.

10.1.2 Influence of Wind Strength on the Reactivation of Parabolic Dunes

The influence of an increase in wind strength on the reactivation of parabolic dunes is only limited to situations in which vegetation is insufficient to cease any sand transport. A fully-vegetated surface cannot only be reactivated by an increase in wind strength. To examine the influence of increased wind strength on the reactivation of parabolic dunes, the initial dune is selected at 80, 85, and 90 yr of the simulation in Figure 10-1 when parabolic dunes have relatively high mobility. The maximum erosion and deposition tolerances are varied in a range of -2.5 to -2.0 m season^{-1} and 2.9 to 3.2 m season^{-1} respectively with a resolution of 0.1 m season^{-1} steps. The sand transport rate is explored from 110 % to 250 % of the standard sand transport rate of 20 m^3 m^{-1} yr^{-1} with a step resolution of 10 % (i.e., 2 m^3 m^{-1} yr^{-1}). This results in 3240 simulation scenarios in total.

10.1.3 Influence of Grazing Stress on the Reactivation of Parabolic Dunes

Severe anthropogenic activity such as overgrazing can reactivate stabilising parabolic dunes and even transform them into highly mobile barchan dunes. All simulation scenarios start from an initial parabolic dune at 80 yr of the simulation in Figure 10-1 with a substratum thickness of 0.6 m. The deposition tolerance of vegetation is explored in a range of [2.9, 3.2] m season^{-1}, at a constant erosion tolerance of -2.5 m season^{-1}. On the other hand, to explore the impact of the erosion tolerance on the transformation, the erosion tolerance is then varied in a range of [-2.5, -2.0] m season^{-1}, at a constant deposition tolerance of 3.0 m season^{-1}. The forage demand is varied from 4000 to 6000 yr^{-1} with 100 yr^{-1} steps. The domain size of 400 × 153 m^2 is used, so the forage demand is then in a range of [0.065, 0.098] m^{-2} yr^{-1} with 0.002 m^{-2} yr^{-1} steps. This results in 189 simulation scenarios in total.

10.2 Climatic Change: an Increase in Drought Severity

This section first shows the resulting dune morphologies under drought from an initial parabolic dune, followed by detailed analysis of parameter controls on the parabolic-to-barchan dune transformations. Physical processes and mechanisms involved in the transformations are then explored.

10.2.1 Morphologies of Resulting Barchans under Climatic Change

As shown in Figure 10-2, the resulting dune morphologies from a relatively mobile parabolic dune (t_0 = 80 yr and 90 yr) under unfavourable changes of system controls, in particular, the changes in water availability, can be classified into four morphological categories. Under minor stress, a parabolic dune continues to be stabilised by vegetation and develops into a more elongated form. As stress increases, the less-vegetated lobe of a parabolic dune is reactivated significantly, moves forward quickly to separate from the more stabilised trailing arms, and transforms into a single barchan (in some scenarios accompanied by smaller barchans and parabolic dunes). Severe stress can not only reactivate the lobe of a parabolic dune but also the trailing arms and interdune areas to form a barchanoid and/or transverse dunefield.

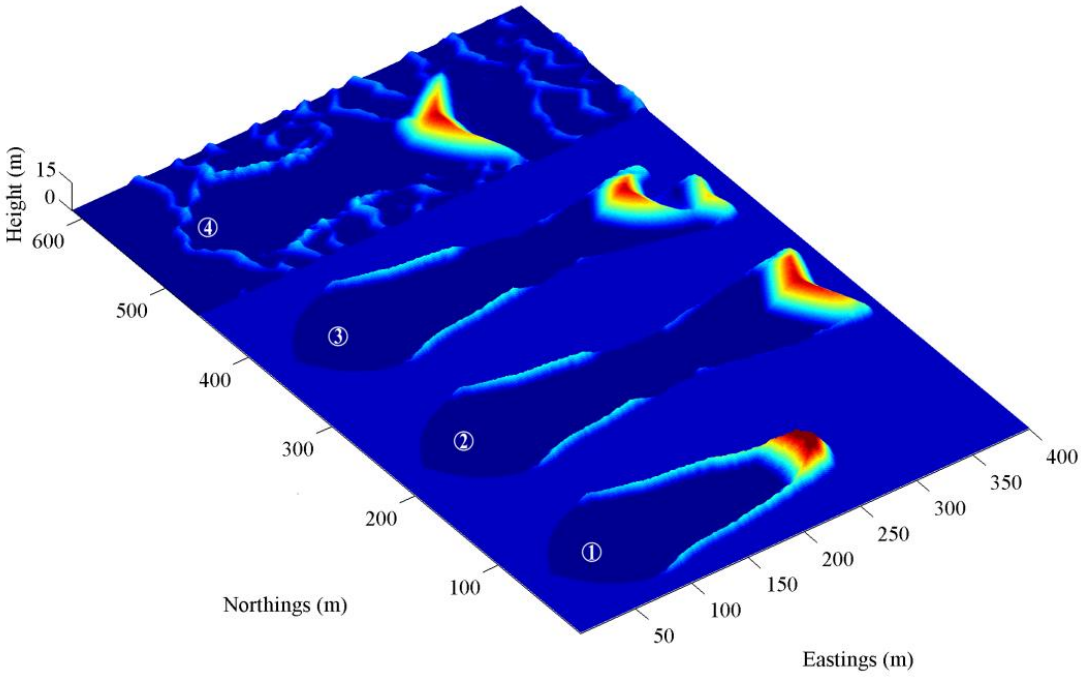

Figure 10-2. Resulting dune types at t_{stab} from an initial parabolic dune under climatic impacts. t_0 = 90 yr, $\tau_{E\_physioMax}$ = -2.0 m season^{-1}, and $\tau_{D\_physioMax}$ = 2.9 m season^{-1}. The climatic impact increases from -0.22, -0.28, -0.32, to -0.46 in sequence. (1) The parabolic dune continues to be stabilised and its lobe hardly changes in shape. (2) The lobe of parabolic dune is reactivated and separated from trailing arms to develop into a single barchan, whilst the trailing arms of parabolic dune remain intact. (3) The lobe of the parabolic dune is reactivated and separated from trailing arms to develop into multiple barchans, whilst the trailing arms of parabolic dune remain intact. (4) The whole dunefield is reactivated, and the trailing arms of the parabolic dune are destroyed.

Simulation scenarios that start with the initial parabolic dune at 80 yr can only be reactivated and transformed into a single barchan, occasionally accompanied with much smaller parabolic dunes in the downwind direction. An increase in the climatic impact can eventually lead to the destruction of the original arms of a parabolic dune and the activation of the entire domain, but never yields the development of multiple barchans (type 3 in Figure 10-2).

Simulation scenarios from the initial parabolic dunes at 90 yr show more variable morphological evolution. Examples in Figure 10-3 and Figure 10-4 show the evolution of dune morphology over time. As the climatic impact increases from -0.26 (Figure 10-3) to -0.40 (Figure 10-4), the initial parabolic dune transforms into multiple barchans (one large barchan following two smaller barchans) as compared with one single barchan in Figure 10-3. However, given enough time, the large barchan in the middle can catch up with smaller barchans in the front and merge into an even larger barchan. A larger climatic impact results in a quicker reactivation of the bare lobe leaving behind shorter arms. As a result, a larger reactive angle develops.

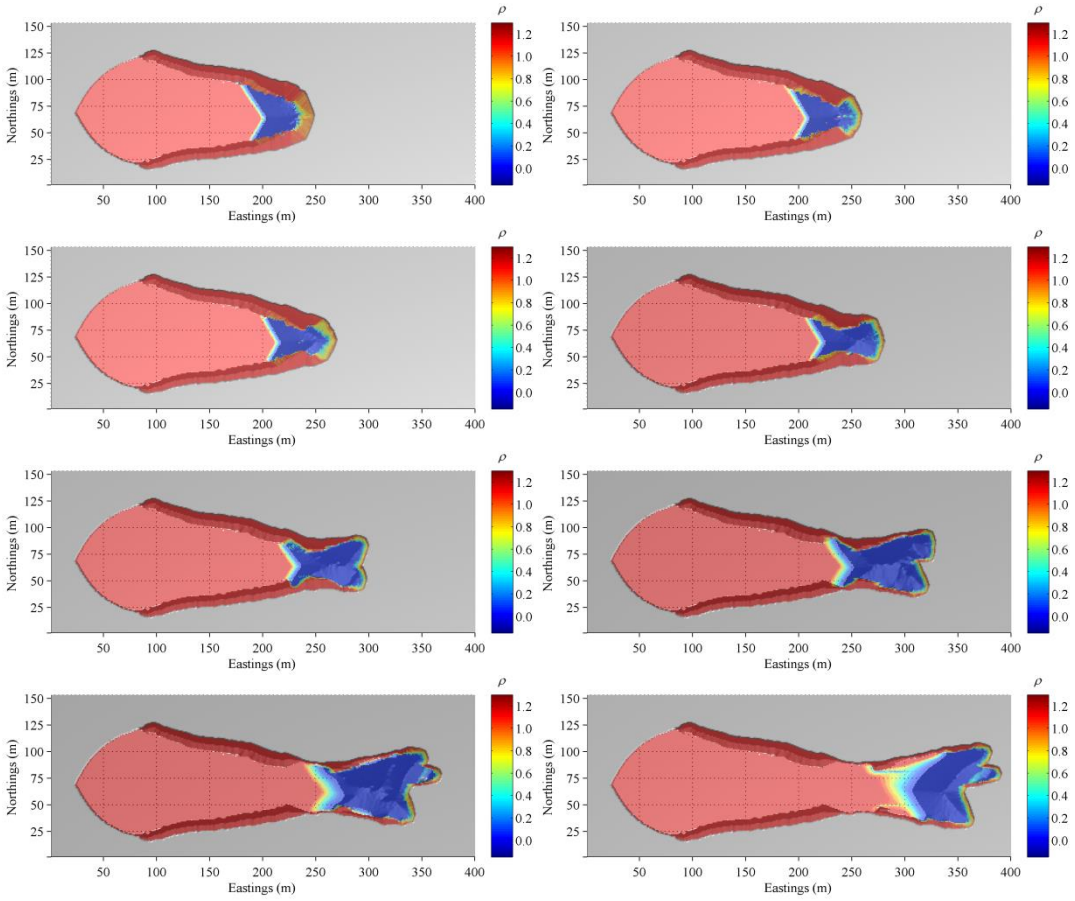

Figure 10-3. An example of a parabolic dune reactivation developing into a single barchan with 10 year steps. t_0 = 90 yr, q = 20 m^3 m^{-1} yr^{-1}, D_0 = 0.6 m, $\tau_{E\_physioMax}$ = -2.1 m season^{-1}, $\tau_{D\_physioMax}$ = 2.9 m season^{-1}, and CI = -0.26.

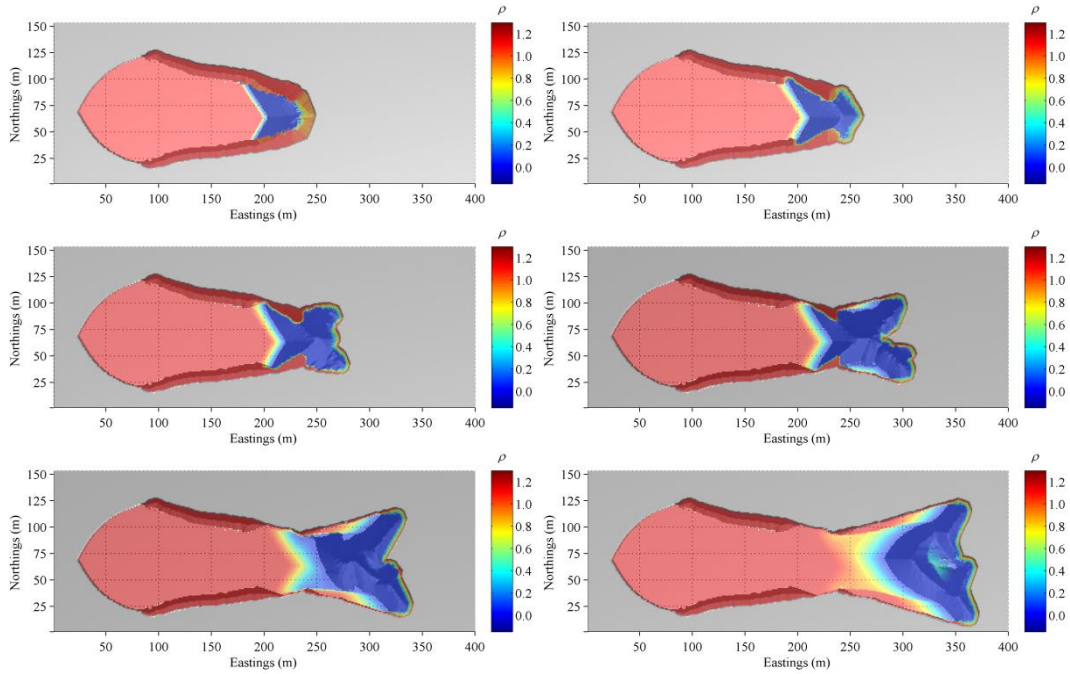

Figure 10-4. An example of a parabolic dune reactivation developing into multiple barchans with 10 year steps. t_0 = 90 yr, q = 20 m^3 m^{-1} yr^{-1}, D_0 = 0.6 m, $\tau_{E\_physioMax}$ = -2.1 m season^{-1}, $\tau_{D\_physioMax}$ = 2.9 m season^{-1}, and CI = -0.40.

Simulation scenarios from the initial parabolic dunes at 100 yr and 110 yr need a much stronger climatic impact in order to transform into barchans. The initial parabolic dune can only be transformed into a barchan with well-preserved original arms at a climatic impact of -0.44. A small further increase of the climatic impact to -0.46 reactivates the entire domain into a dune field with no remnant arms left behind. Simulations from the initial parabolic dune at 120 yr can only be either stabilised or fully-reactivated (no arms). In these situations, the erosion and deposition tolerances of vegetation are irrelevant to determining the threshold of climatic impact to reactive an initial parabolic dune.

10.2.2 Morphologies of Resulting Parabolic Dunes under Climatic Change

Although only very strong climatic impacts can reactivate and transform the initial parabolic dunes at 100 yr and 110 yr into barchans with preserved original arms, a large range of weaker climatic impacts encourages the simple parabolic dunes to evolve into more complicated dune morphologies. Figure 10-5 shows an example of morphological change from initial parabolic dunes at 100 yr under varying climatic impacts. As the climatic impact increases, parabolic dunes are partially reactivated and develop into more complicated imbricate forms, which are usually accompanied by the formation of nebkhas or nebkha ridges between trailing arms.

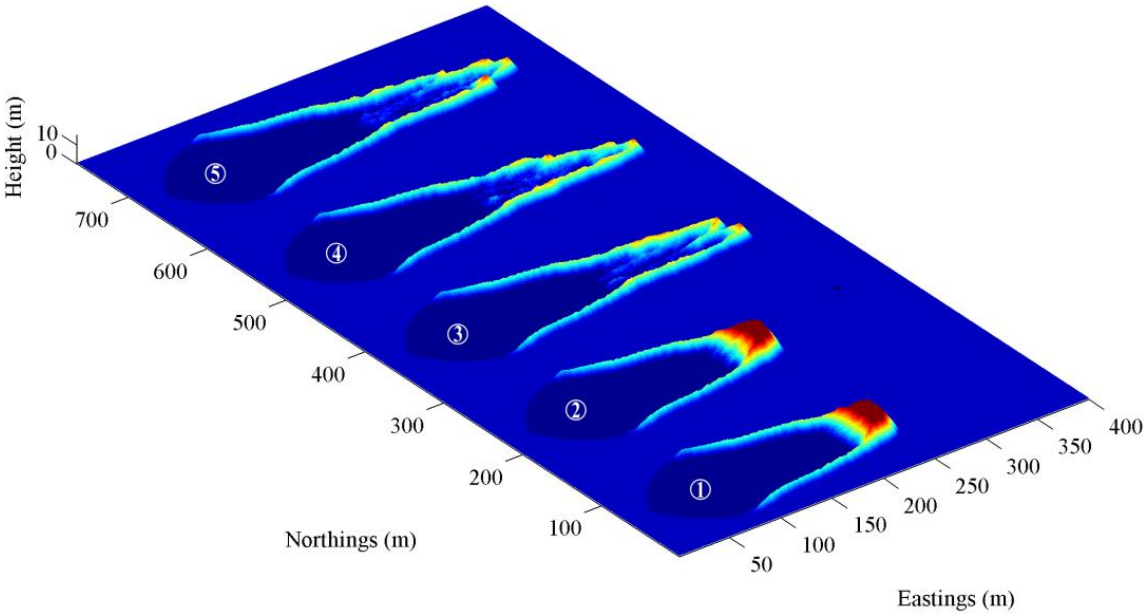

Figure 10-5. Fully-stabilised parabolic dunes under $\tau_{E\_physioMax}$ of -2.3 m season^{-1} and $\tau_{D\_physioMax}$ of 2.9 m season^{-1}. t_0 is 100 yr, and the climatic impact increases from -0.34 to -0.42 with a gradient of -0.02 from (1) to (5).

Examples of the morphologies of stabilised parabolic dunes under a different erosion tolerance and a different deposition tolerance are shown in Figure 10-6 and Figure 10-7 respectively. Given the same climatic impact and other parameters, an increase in the erosion tolerance or the deposition tolerance leads to quicker stabilisation of parabolic dunes and more lunate- or v- shaped morphology in comparison to their counterparts in Figure 10-5. Digitate parabolic dunes can also develop from blowout activity on lobes of existing parabolic dunes, such as the ones shown in Figure 10-7(1) and Figure 10-7(2).

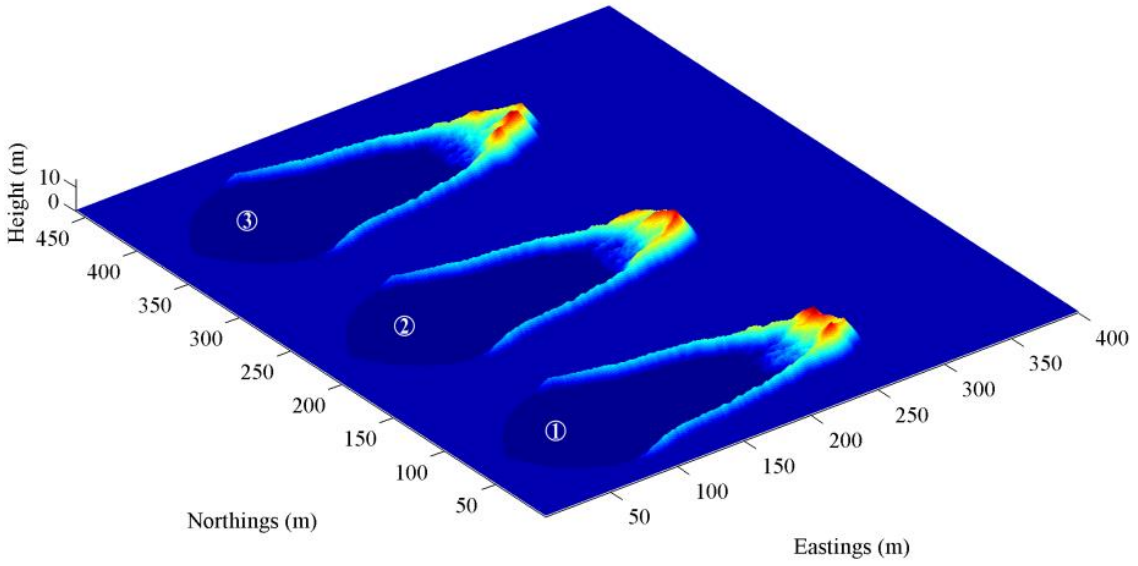

Figure 10-6. Fully-stabilised parabolic dunes under $\tau_{E\_physioMax}$ of -2.5 m season^{-1} and $\tau_{D\_physioMax}$ of 2.9 m season^{-1}. t_0 is 100 yr, and the climatic impact increases from -0.38 to -0.42 with a gradient of -0.02 from (1) to (3).

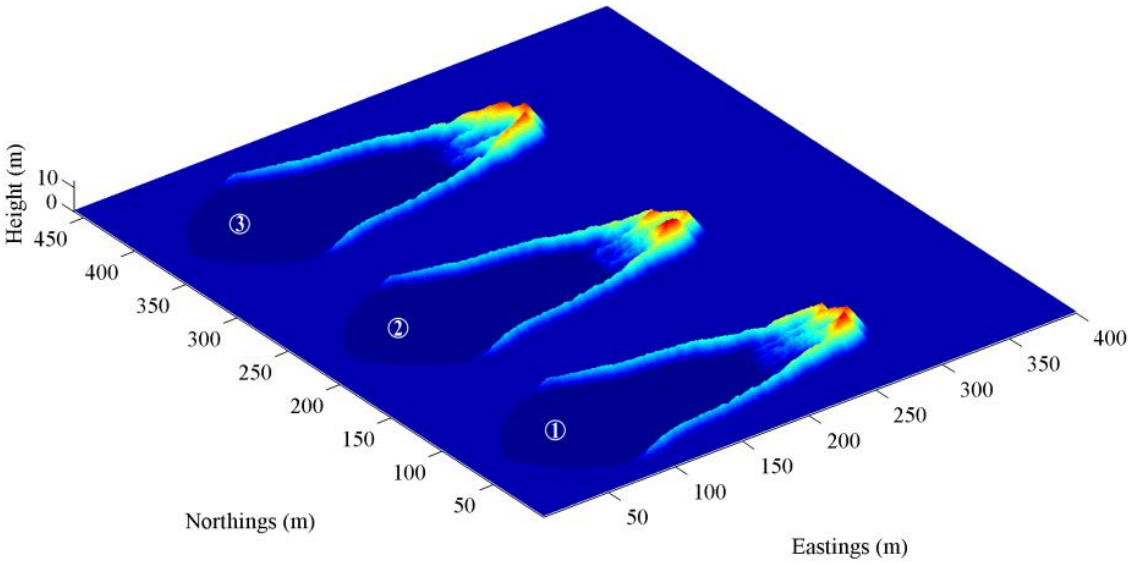

Figure 10-7. Fully-stabilised parabolic dunes under $\tau_{E\_physioMax}$ of -2.3 m season^{-1} and $\tau_{D\_physioMax}$ of 3.2 m season^{-1}. t_0 is 100 yr, and the climatic impact increases from -0.38 to -0.42 with a gradient of -0.02 from (1) to (3).

The stability of initial parabolic dunes also significantly contributes to the resulting dune morphologies (Figure 10-8). Given the same climatic impact, a less stabilised parabolic dune develops into a more elongated shape which usually has multiple lobes exhibiting complicated morphology. As the stability of the initial parabolic dune increases, lobes can only be partially reactivated. The development of blowouts on the lobe then leads to more digitate-shaped lobe morphology. An almost fully-stabilised parabolic dune is difficult to be reactivated without extreme stresses, and maintains a lunate-shaped lobe.

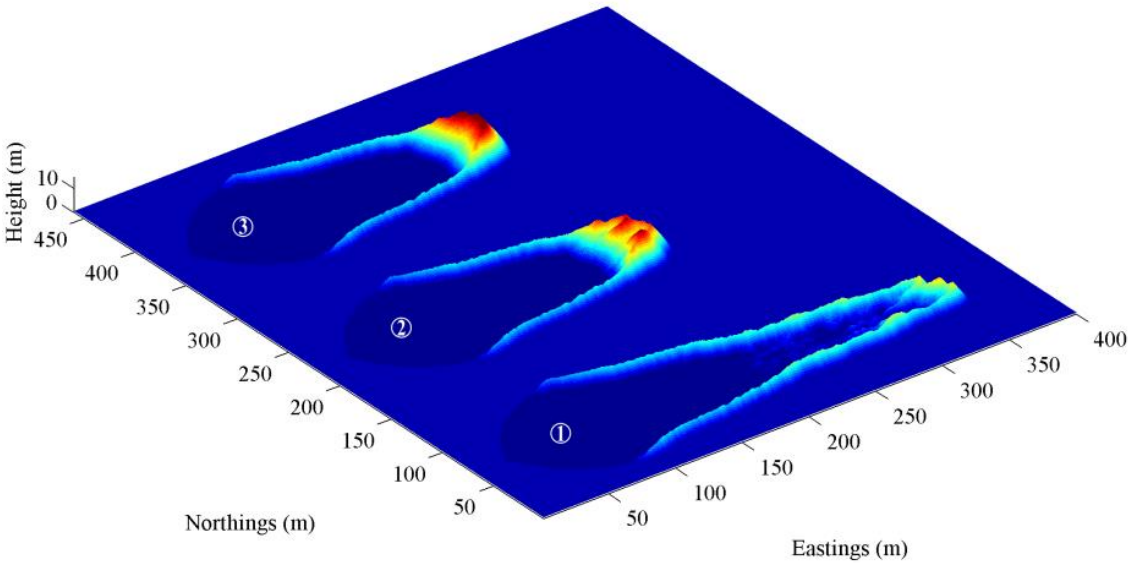

Figure 10-8. Fully-stabilised parabolic dunes from different initial parabolic dunes with different degrees of stability. From (1) to (3), the initial parabolic dune is at 100, 110, and 120 yr in sequence. $\tau_{E\_physioMax}$ and $\tau_{D\_physioMax}$ are -2.2 and 3.1 m season^{-1} respectively, and the climatic impact is -0.4.

10.2.3 Reactivation Threshold of Climatic Impact

The detailed analysis of the climatic impact on the parabolic-to-barchan dune transformations in the following sections is focused on initial parabolic dunes at 80 yr and 90 yr, because any more highly-vegetated parabolic dunes require a very strong climatic impact in order to be reactivated which is not common in reality. The reactivation threshold of climatic impact, the maximum tolerance to a climatic impact for a parabolic dune to maintain its shape, relates closely to the stability of a vegetated parabolic dunefield. Provided that all other system parameters are the same, a certain threshold of the climatic impact can sometimes result in the development of either barchans or stabilised parabolic dunes, because the threshold is the turning point between stabilisation and reactivation and hence the initial parabolic dune may evolve towards either direction under the intrinsic sensitivity of the stochastic CA model. Examples are shown in Table 10-1 and Figure 10-9. Because the climatic impact range has a resolution of 0.02, sometimes the turning point may be located in between two consecutive parameter values, with the lower value always resulting in stabilisation, and the higher value always yielding barchans.

Table 10-1. Examples of the reactivation threshold leading to the development of either barchans or stabilised parabolic dunes from the initial parabolic dune at 80 yr.

$\tau_{E\_physioMa}$	$\tau_{D\_physioMax}$	CI
-2.2	2.9	-0.12
-2.5	2.9	-0.12
-2.1	3	-0.14
-2.4	3	-0.14
-2.5	3	-0.14
-2.2	3.1	-0.16

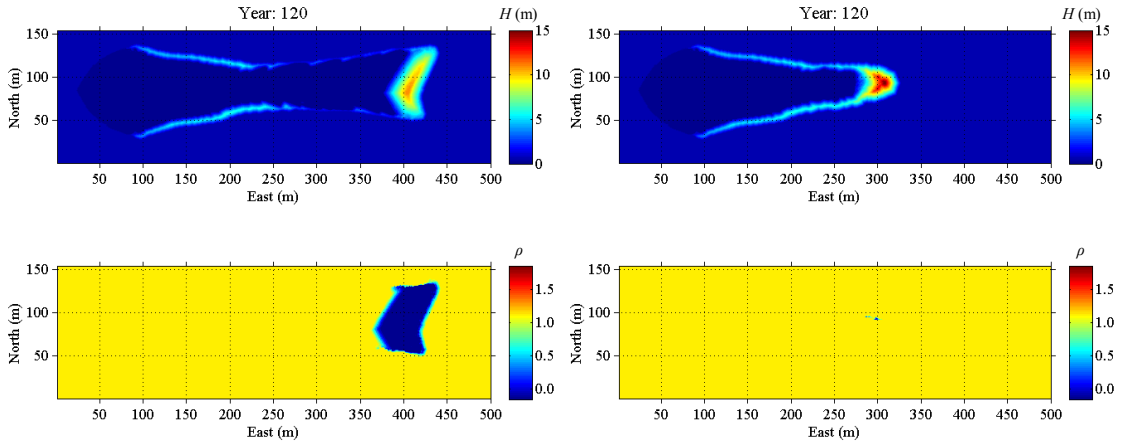

Figure 10-9. Two identical scenario simulations resulting in either a barchan (a) or a stabilised parabolic dune (b) under the same climatic impact of -0.12 and the same system parameters. t_0 = 80 yr, $\tau_{E\_physioMax}$ = -2.2 m season^{-1}, and $\tau_{D\_physioMax}$ = 2.9 m season^{-1}. The upper and lower panels denote the DEM and the vegetation effectiveness respectively.

As shown in Figure 10-10, the dune surface erodibility of the initial parabolic dune strongly controls the reactivation threshold of climatic impact. As the initial *DSE* decreases from 0.34 (t_0 = 80 yr) to 0.25 (t_0 = 90 yr), the reactivation threshold of climatic impact increases significantly. More stabilised parabolic dunes require more severe climatic impact to be reactivated and transformed into barchans. A high deposition tolerance of vegetation, meanwhile, facilitates dune stabilisation and requires a relatively great reactivation threshold, while the erosion tolerance of vegetation seems to play a minimal role in determining a dune reactivation threshold.

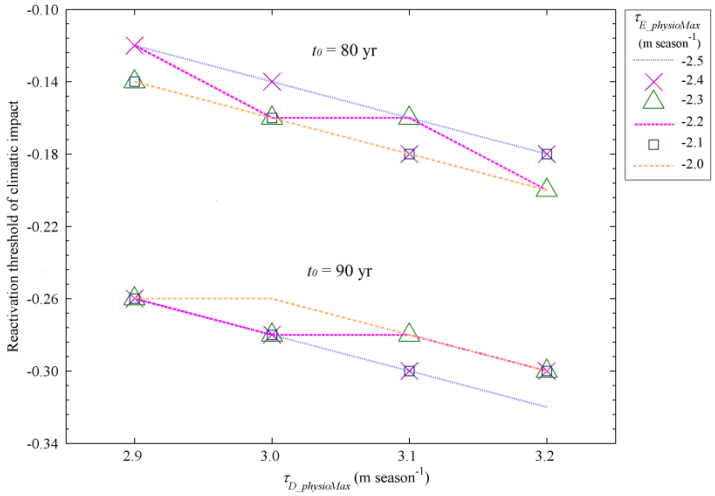

Figure 10-10. Influence of vegetation characteristics on the reactivation threshold of climatic impact.

As the stability of initial parabolic dunes increases further (*DSE* = 0.1654 when t_0 = 100 yr), there is no significant difference in the reactivation threshold of climatic impact under changes in the erosion and deposition tolerances of vegetation. Parabolic dunes cannot be reactivated and transformed into barchans unless the climatic impact is -0.44 or greater, regardless of the vegetation characteristics. When the climatic impact then increases to -0.46, the whole domain is activated into a dunefield and the trailing arms of the initial parabolic dune are destroyed. If the initial parabolic dune is almost fully-stabilised by vegetation (*DSE* = 0.0018 when t_0 = 120 yr), an extreme situation occurs in which the dune will either be stabilised completely or be reactivated into a barchan dunefield (without trailing arms left behind). Analysis of the influence of vegetation characterises (erosion and deposition tolerances) on the reactivation of parabolic dunes, therefore, is focussed on simulations starting from relatively mobile parabolic dunes at 80 yr and 90 yr.

10.2.4 Reactivation Angles

Figure 10-11 shows the influence of climatic impact on the reactivation angle of resulting barchans. As the climatic impact decreases, the reactivation angle becomes smaller. This means that a greater climatic impact results in a more severe lateral expansion and an associated larger size of dunes. A high vegetation erosion tolerance seems reduce the reactivation angle slightly when the climatic impact is relatively strong specifically greater than -0.25 in Figure 10-12a, and -0.30 in Figure 10-12c. The vegetation deposition tolerance, however, only influences the reactivation angle when a climatic impact is small and close to the reactivation threshold as shown in Figure 10-12b and Figure 10-12d. Nevertheless, the influence of vegetation erosion and deposition tolerances on the reactivation angle is generally minimal. Figure 10-13 shows the relationship between the climatic impact and the reactivation angle starting from parabolic dunes at 80 yr and 90 yr. There is a good linear correlation for both sets of data. Interestingly, the slopes of regression lines are similar, although the larger reactivation threshold of climatic impact for parabolic dunes at 90 yr limits the data set into a smaller range. Therefore, this correlation between the climatic impact and the reactivation angle seems independent of the stability of the initial parabolic dunes, and may be potentially used to estimate the severity of a climatic impact based on field measurements of reactivation angles. A large reactivation angle also means that the dune is more easily merged with any neighbouring dunes, which may result in the development of transverse dunes.

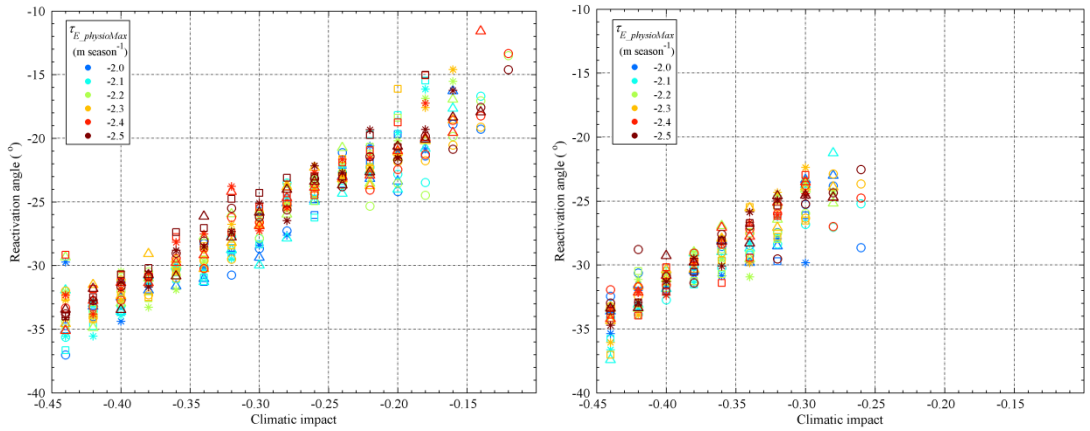

(a) t_0 = 80 yr (b) t_0 = 90 yr

Figure 10-11. Influence of the climatic impact on the reactivation angle. Marks of circles, triangles, asterisks, and squares denote $\tau_{D\_physioMax}$ of 2.9, 3.0, 3.1, and 3.2 m season^{-1} respectively.

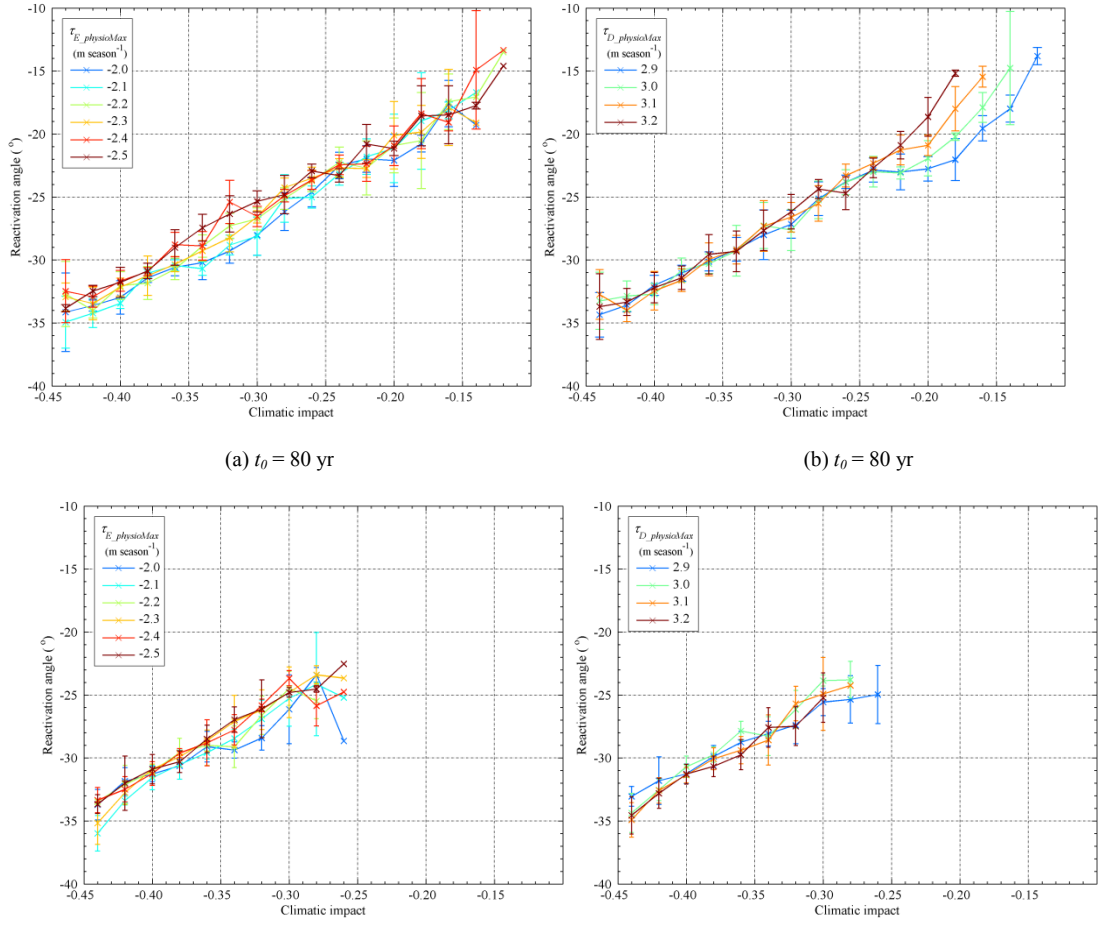

(a) t_0 = 80 yr (b) t_0 = 80 yr

(c) t_0 = 90 yr (d) t_0 = 90 yr

Figure 10-12. Influence of the climatic impact and the characteristics of vegetation on the reactivation angle. Colours labelled in the legend denote the erosion or deposition tolerance while crosses and whiskers denote means and standard deviations of the range of the deposition or erosion tolerance.

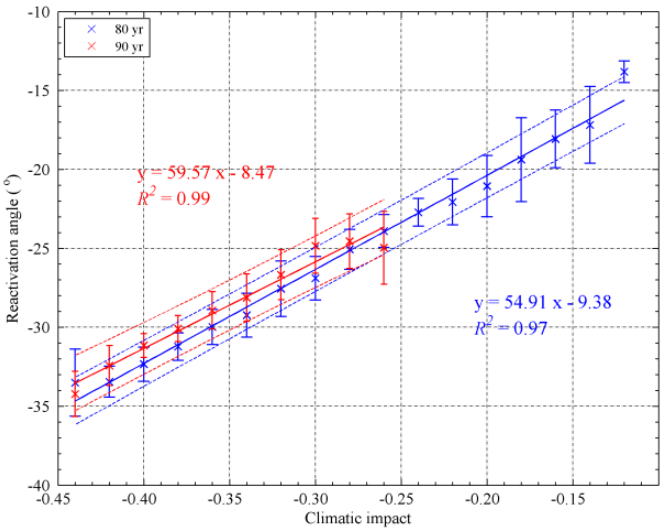

Figure 10-13. Influence of the climatic impact on the reactivation angle. Crosses denote means of simulations with different $\tau_{E\_physioMax}$ and $\tau_{D\_physioMax}$, and whiskers denote standard deviations. Lines show linear regressions with dashed lines denoting 95 % prediction intervals.

10.2.5 Transition Time

As the climatic impact increases, the transition time of parabolic dunes into barchans drops quickly first, then levels off and does not show significant decrease up to a certain climatic impact, which is approximately -0.26 for an initial parabolic dune at 80 yr, and -0.34 for an initial parabolic dune at 90 yr (Figure 10-14). More stabilised initial parabolic dunes require a longer time to be reactivated into barchans, and the transition time increases more significantly for a relatively small climatic impact. An increase in the deposition tolerance of vegetation discourages the reactivation of parabolic dunes and hence leads to longer transition duration. This impact becomes stronger as the climatic impact decreases. The erosion tolerance of vegetation, however, does not show an outstanding impact on a transition time.

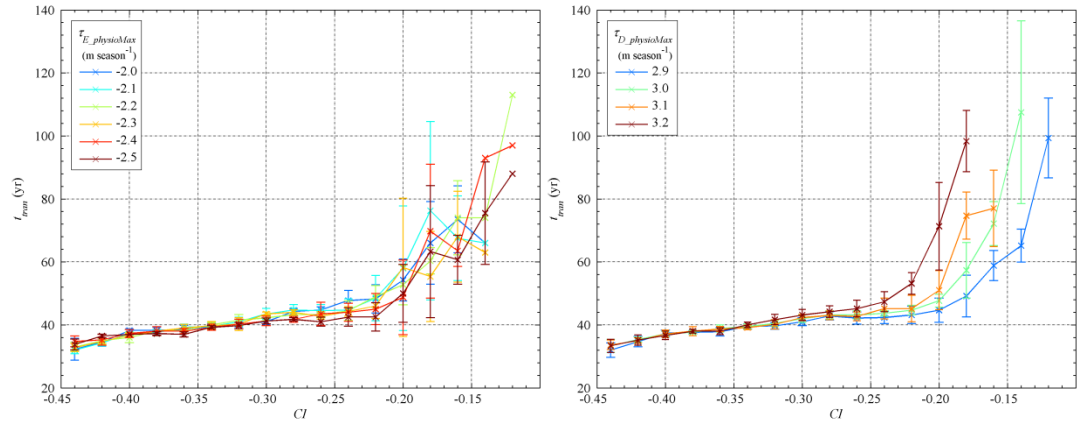

(a) t_0 = 80 yr

(b) t_0 = 80 yr

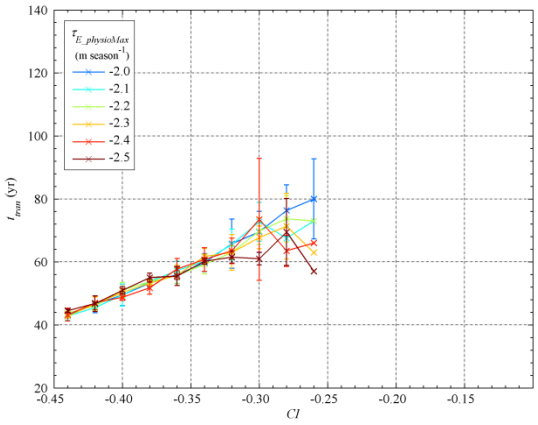

(c) t_0 = 90 yr

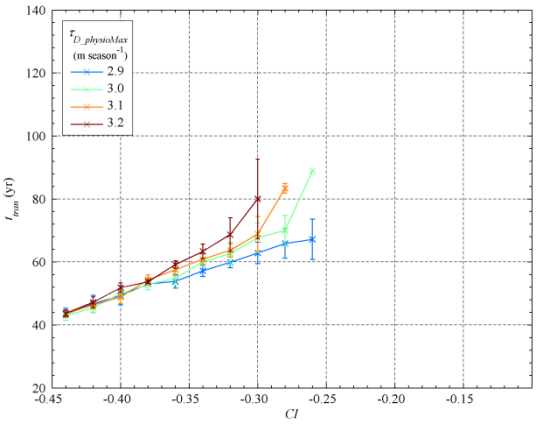

(d) t_0 = 90 yr

Figure 10-14. Influence of the climatic impact and the characteristics of vegetation on the dune transition time. Colours labelled in the legend denote the erosion or deposition tolerance, while crosses and whiskers denote means and standard deviations of the range of the deposition or erosion tolerance.

The relationship between the reactivation angle and the transition time is shown in Figure 10-15. As the stability of initial parabolic dunes increase, the minimal reactivation angle increases from approximately -10˚ for an initial parabolic dune at 80 yr to -20˚ for an initial parabolic dune at 90 yr. An increase in the reactivation angle significantly shortens the transition time until -22˚ for an initial parabolic dune at 80 yr and -34˚ for an initial parabolic dune at 90 yr respectively. Beyond this tipping angle, the transition time is very short and a further increase in reactivation angle does not reduce the transition time significantly any more. This tipping angle may, therefore, represent a boundary beyond which a catastrophic system shift occurs.

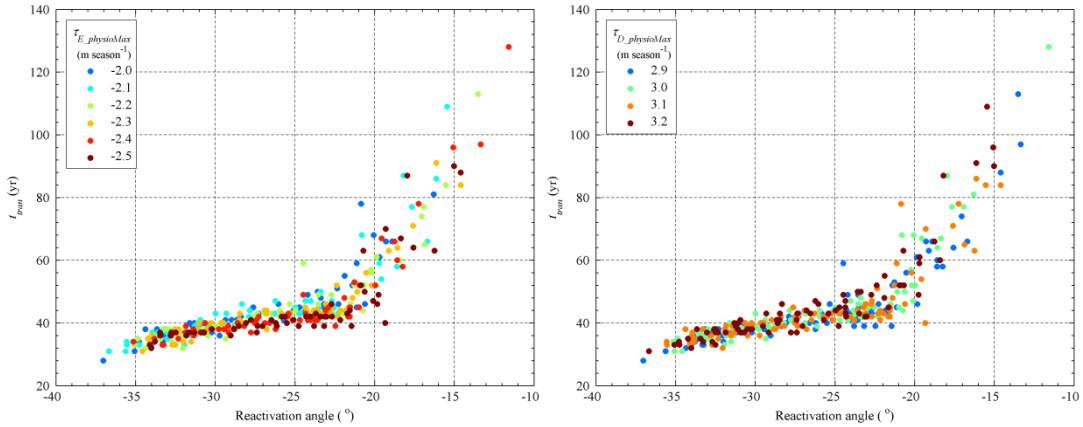

(a) t_0 = 80 yr

(b) t_0 = 80 yr

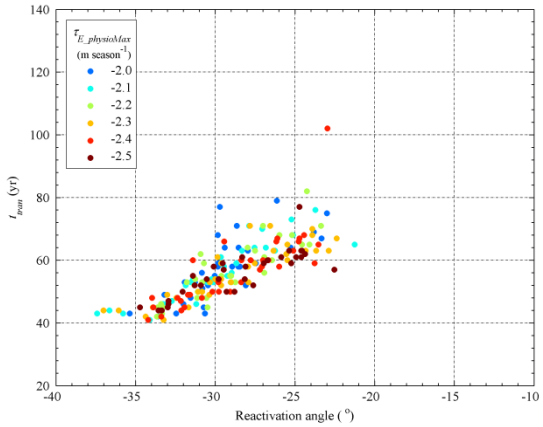

(c) t_0 = 90 yr

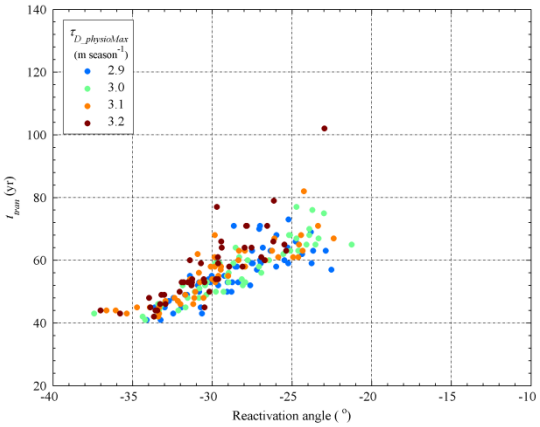

(d) t_0 = 90 yr

Figure 10-15. The relationship between the reactivation angle and the dune transformation time.

10.2.6 Dune Surface Erodibility

An increase in the climatic impact causes parabolic dunes to be transformed into barchans with a higher dune surface erodibility, as shown in Figure 10-16. As either the erosion tolerance or the deposition tolerance of vegetation increases, the dune surface erodibility at the transition time decreases. The changes in the erosion and deposition tolerances, however, result in a higher uncertainty for an initial parabolic dune at 90 yr in comparison with an initial parabolic dune at 80 yr. The erosion and deposition tolerances, meanwhile, are likely to play a more significant role in the dune reactivation from an initial parabolic dune with a greater vegetation cover (t_0 = 90 yr).

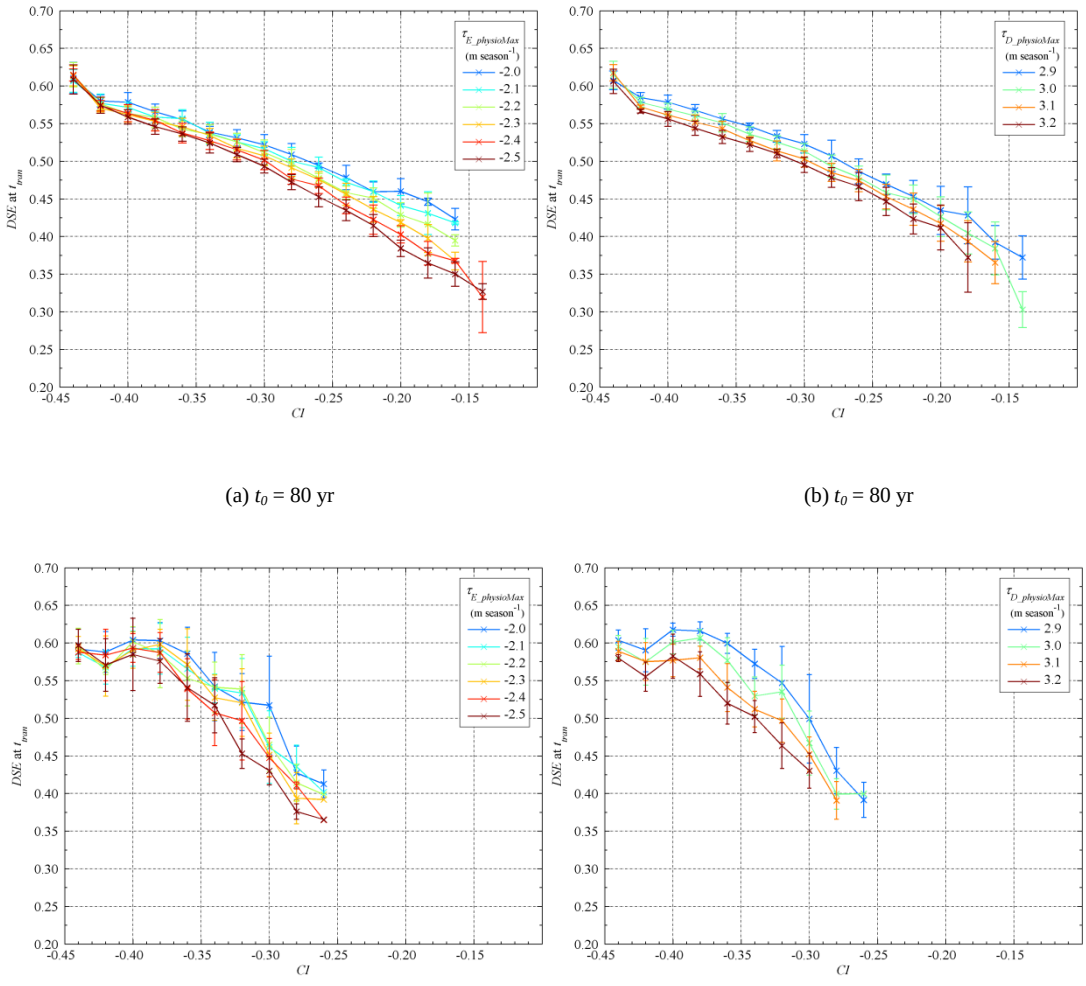

(a) t_0 = 80 yr

(b) t_0 = 80 yr

(c) t_0 = 90 yr

(d) t_0 = 90 yr

Figure 10-16. Influence of the climatic impact on the dune surface erodibility at the transformation time of parabolic dunes into barchans. Colours labelled in the legend denote the erosion or deposition tolerance, while crosses and whiskers denote means and standard deviations of the range of the deposition or erosion tolerance.

Figure 10-17 shows the relationship between the reactivation angle and the dune surface erodibility at the transition time. A larger reactivation angle is generally associated with a higher dune surface erodibility at the transition time. The influence of the erosion and the deposition tolerances does not show a clear trend. There is a more significant correlation between the reactivation angle and the dune surface erodibility at the transition time for an initial parabolic dune at 80 yr as compared with an initial parabolic dune at 90 yr. Nonetheless, the slopes of both regression lines are similar. Figure 10-18 presents the regression line acquired by fitting all the data of both sets, suggesting that the correlation may be independent of the degree of stability of an initial parabolic dune, although a more stabilised initial parabolic dune results in a wider distribution and a higher randomness.

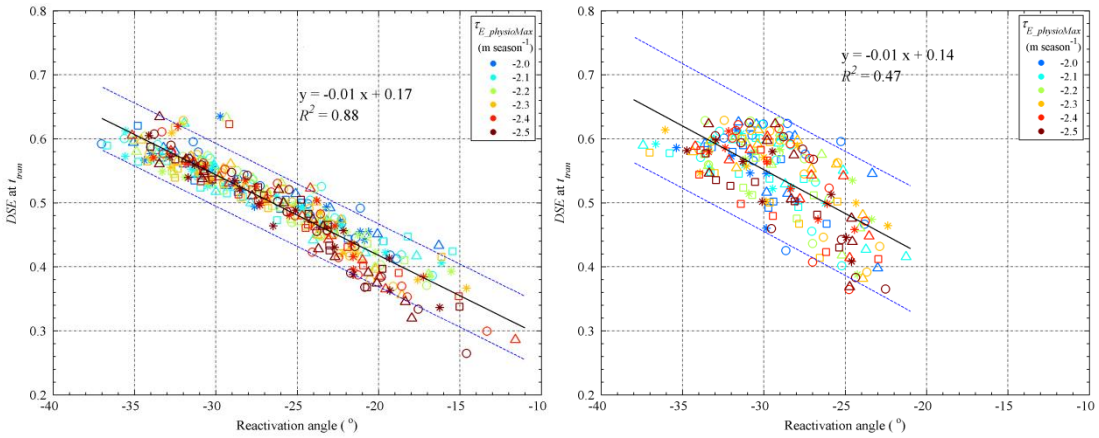

(a) t_0 = 80 yr (b) t_0 = 90 yr

Figure 10-17. The relationship between the reactivation angle and the dune surface erodibility at the transition time. Marks of circles, triangles, asterisks, and squares denote $\tau_{D\_physioMax}$ of 2.9, 3.0, 3.1, and 3.2 m season^{-1} respectively. The black line denotes the best-fit linear regression line, and the blue dotted lines denote 95 % prediction intervals.

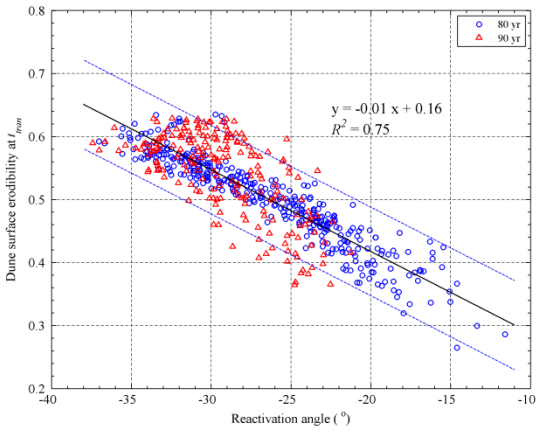

Figure 10-18. The relationship between the reactivation angle and the dune surface erodibility at the transition time. Blue circles and red triangles denote simulations from initial parabolic dunes at 80 yr and 90 yr respectively. The black line denotes the best-fit linear regression line, and the blue dotted lines denote 95 % prediction intervals.

10.3 Climatic Change: an Increase in Sand Transport Potential

10.3.1 Reactivation Threshold

The vegetation cover and the associated stability of an initial parabolic dune strongly control the reactivation threshold of sand transport rate (Figure 10-19). Here the model simulates a situation in which strong winds can only influence vegetation growth by changing the erosion and deposition balance, and thus excludes the situation in which vegetation is removed by high energy storms. Once a parabolic dune

has been fully-stabilised by vegetation, a sole increase in the potential sand transport rate of winds cannot remobilise the dune and initiate a parabolic-to-barchan dune transformation any more. A higher deposition tolerance of vegetation, meanwhile, increases the reaction threshold of sand transport rate slightly, although the influence of the erosion tolerance of vegetation seems minimal.

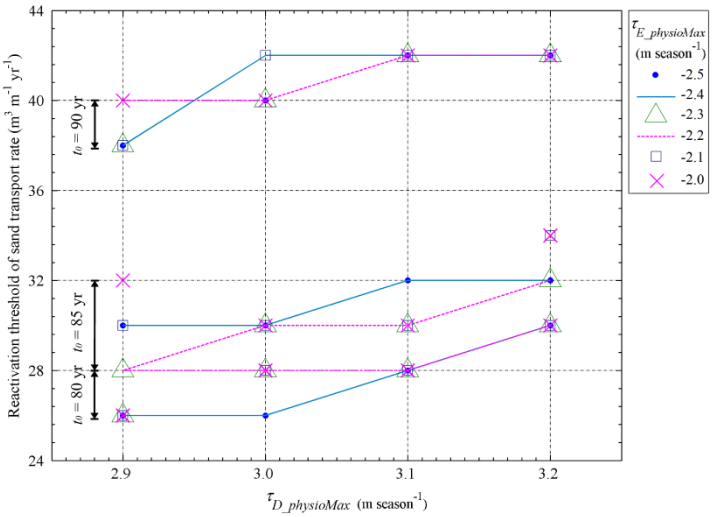

Figure 10-19. Influence of the vegetation characteristics on the reactivation threshold of climatic impact.

10.3.2 Reactivation Angles

The reactivation angle generally increases with the sand transport rate, but there is no outstanding trend with respect to the erosion and the deposition tolerances of vegetation (Figure 10-20). Although the reactivation threshold of sand transport rate varies for different initial parabolic dunes, the average reactivation angles under the same sand transport rate are similar and seem independent of the stability of the initial parabolic dunes (Figure 10-21). The slopes of regression lines derived from different initial parabolic dunes vary within a magnitude of 0.1. As a consequence, by comparing the reactivation angle of different mobile dunes, it is potentially possible to deduce the associated sand transport regime (Figure 10-22). For example, larger reactivation angles imply wind regime with higher sand transport rates.

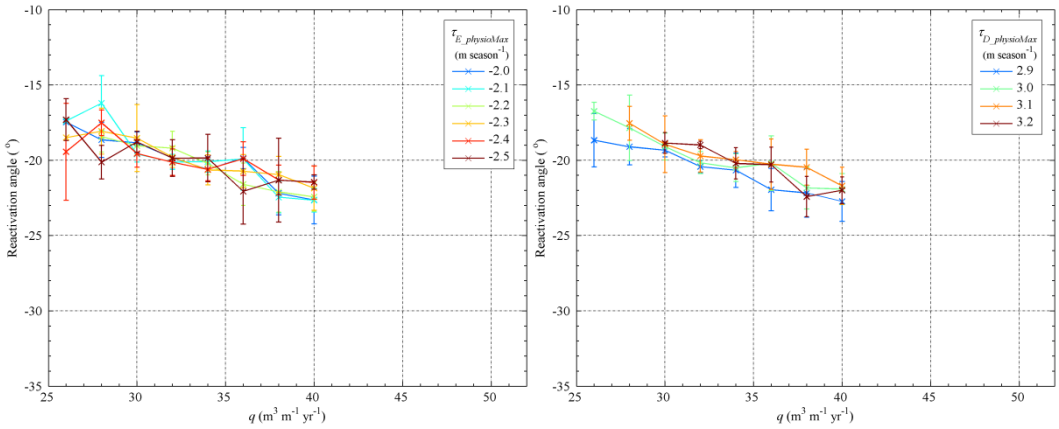

(a) t_0 = 80 yr (b) t_0 = 80 yr

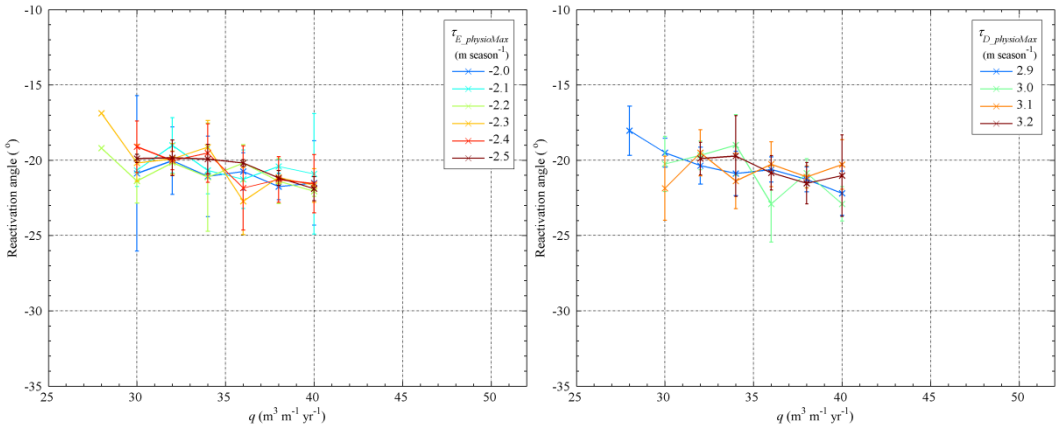

(c) t_0 = 85 yr (d) t_0 = 85 yr

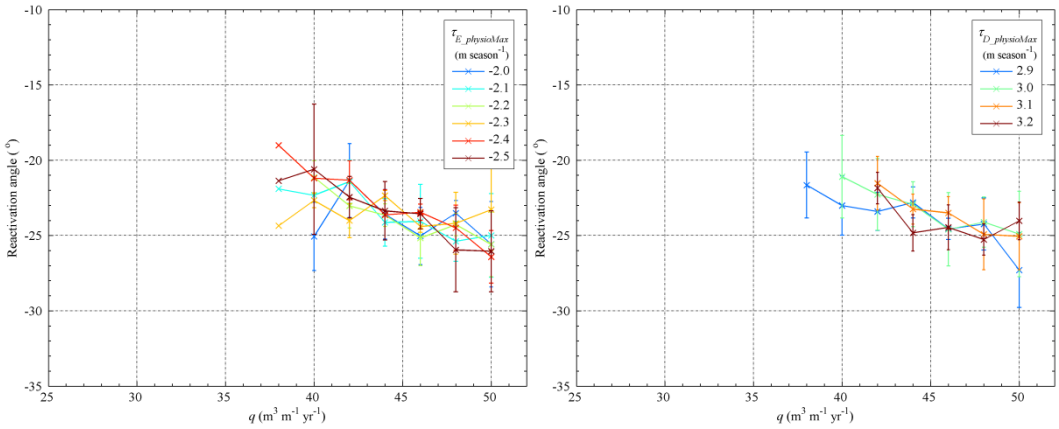

(e) t_0 = 90 yr (f) t_0 = 90 yr

Figure 10-20. The relationship between the sand transport rate and the reactivation angle under influence of different erosion and deposition tolerances. Colours labelled in the legend denote the erosion or deposition tolerance, while crosses and whiskers denote means and standard deviations of the range of the deposition or erosion tolerance.

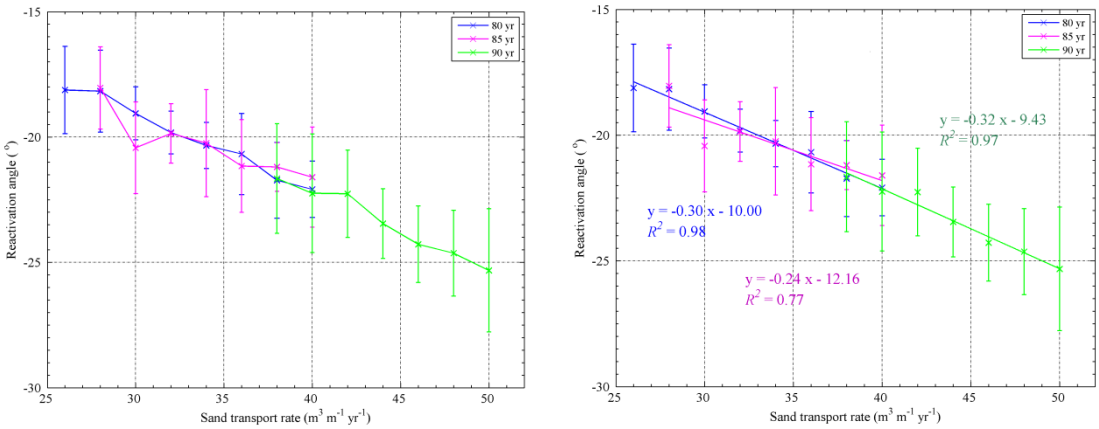

(a) (b)

Figure 10-21. The relationship between the sand transport rate and the reactivation angle under influence of different initial parabolic dunes with varying stability. Colours labelled in the legend denote initial parabolic dunes with different stability, and crosses and whiskers denote means and standard deviations respectively. Best-fit linear regression lines are shown in (b) with different colours denoting different initial parabolic dunes.

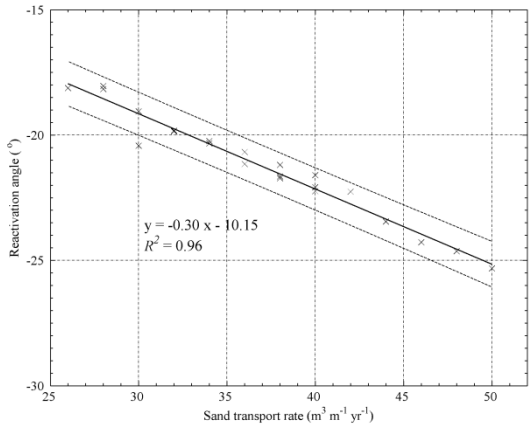

Figure 10-22. The relationship between the sand transport rate and the reactivation angle. Crosses denote means, and the black and blue dotted lines denote the best-fit linear regression line and 95 % prediction intervals respectively.

10.3.3 Transition Time

As the sand transport rate increases, the transition time of parabolic dunes into barchans decreases, as shown in Figure 10-23. The degree to which an increase in the sand transport rate shortens the transition time, however, dwindles rapidly. A parabolic-to-barchan dune transformation is hence sensitive to a change in the sand transport rate that is close to the reactivation threshold. A further increase in the sand transport rate would not significantly contribute to a quicker reactivation of parabolic dunes. Given the same sand transport rate, a more stabilised parabolic dune requires a longer transition time. The erosion

and the deposition tolerances only exert limited impacts on the transition time when the sand transport rate is relatively small, just above the reactivation threshold. A higher erosion tolerance of vegetation encourages a quicker barchan-to-parabolic dune transformation, whereas a higher deposition tolerance of vegetation prolongs the transition duration.

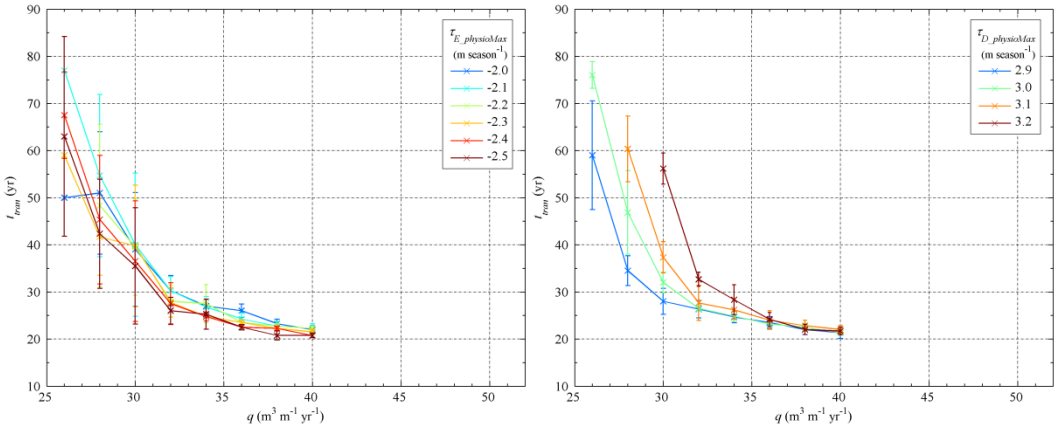

(a) t_0 = 80 yr

(b) t_0 = 80 yr

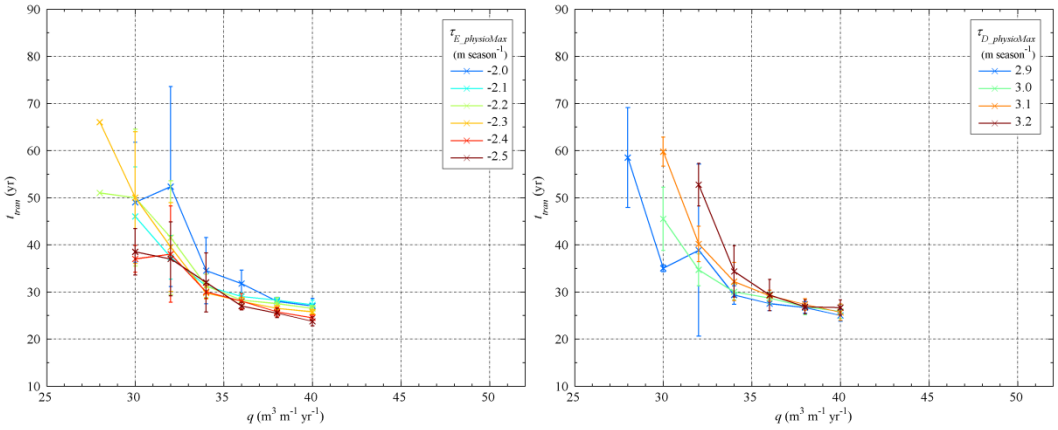

(c) t_0 = 85 yr

(d) t_0 = 85 yr

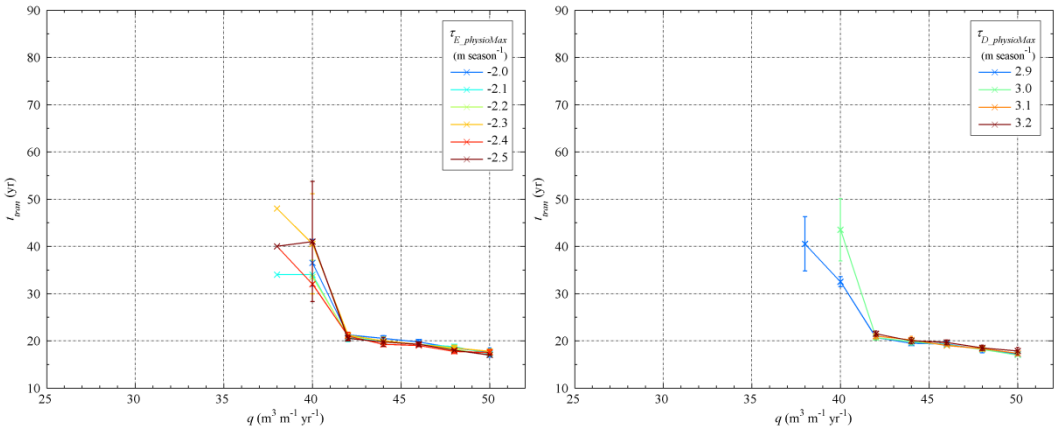

(e) t_0 = 90 yr

(f) t_0 = 90 yr

Figure 10-23. The relationship between the sand transport rate and the transformation time under influence of different erosion and deposition tolerances. Colours labelled in the legend denote the erosion or deposition tolerance, while crosses and whiskers denote means and standard deviations of the range of the deposition or erosion tolerance.

10.3.4 Dune Surface Erodibility

A higher sand transport rate transforms a parabolic dune into a barchan with greater dune surface erodibility at the transition time (Figure 10-24). A more stabilised parabolic dune is generally transformed into an incipient barchan, including arm remnants, with lower dune surface erodibility. Given the same sand transport rate, a higher erosion or deposition tolerance encourages the resulting barchans to have lower dune surface erodibility. Meanwhile, there is no significant correlation between the reactivation angle and the dune surface erodibility at the transition time, but high dune surface erodibility is associated with a large reactivation angle formed from a relatively stabilised initial parabolic dune (Figure 10-25).

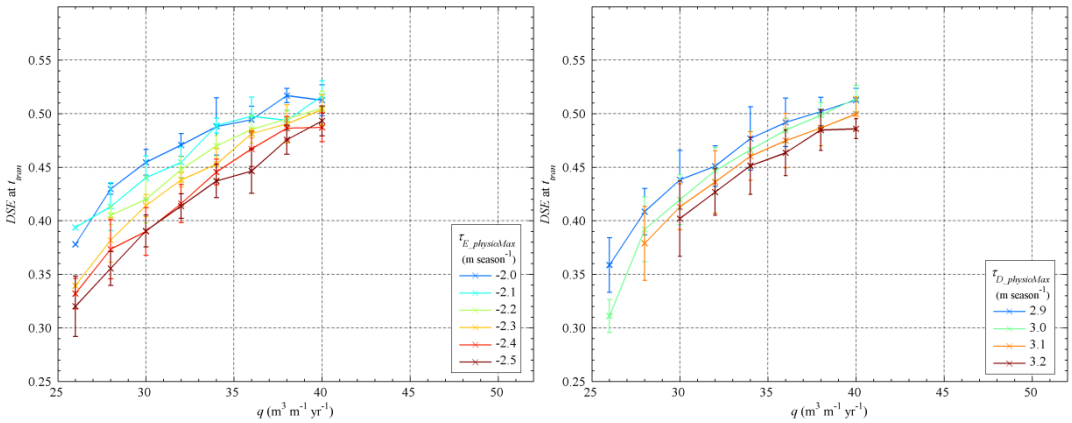

(a) t_0 = 80 yr (b) t_0 = 80 yr

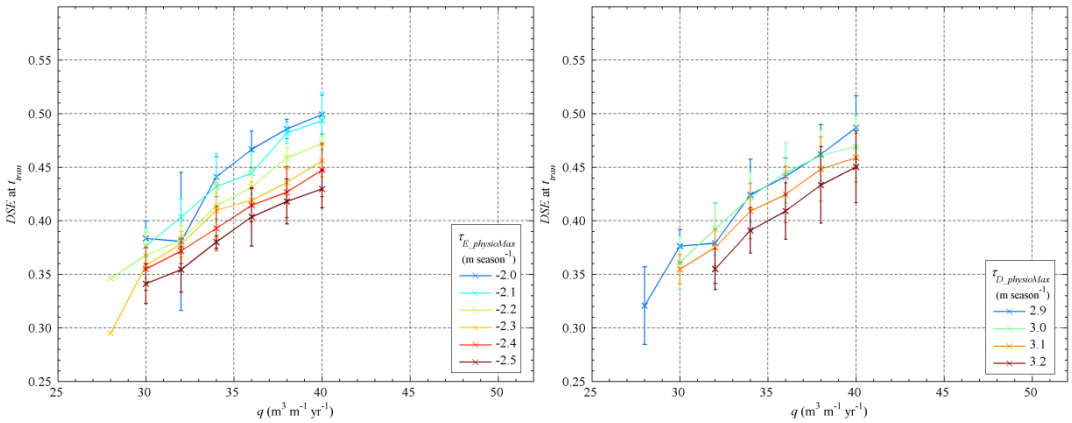

(c) t_0 = 85 yr (d) t_0 = 85 yr

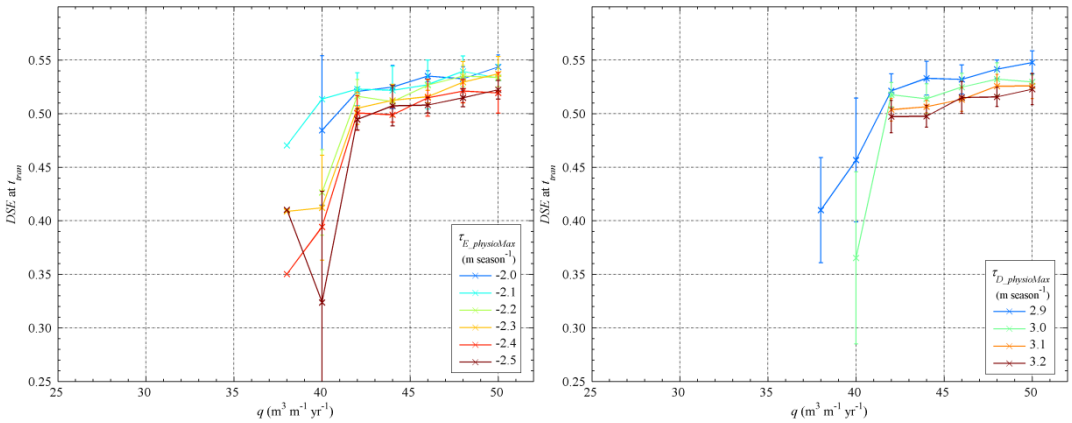

(e) t_0 = 90 yr (f) t_0 = 90 yr

Figure 10-24. The relationship between the sand transport rate and the dune surface erodibility under influence of different erosion and deposition tolerances. Colours labelled in the legend denote the erosion or deposition tolerance, while crosses and whiskers denote means and standard deviations of the range of the deposition or erosion tolerance.

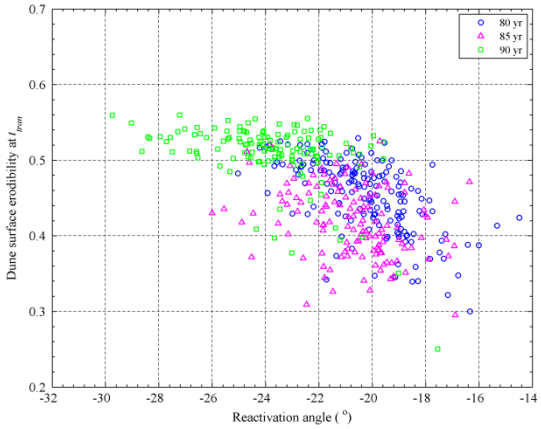

Figure 10-25. The relationship between the reactivation angle and the dune surface erodibility under influence of different initial parabolic dunes. The legend denotes different initial parabolic dunes.

10.4 Summary of Modelling Outcomes

Before moving forward to analyse the physical processes and mechanisms that control the parabolic-to-barchan dune transformations, the main outcomes of modelling simulations are summarised in Table 10-2. The table summarises how a change in surface erodibility of an initial parabolic dune, the erosion tolerance, and the deposition tolerance of vegetation can influence the key modelling measurements of a parabolic-to-barchan dune transformation.

Table 10-2. Summary of modelling outcomes.

Section 10.2: Drought			
Modelling Measurements	**Dune Surface Erodibility of an Initial Parabolic Dune**	$\tau_{E\_physioMax}$	$\tau_{D\_physioMax}$
Reactivation Threshold	positive	not significant	positive
Reactivation Angle	not significant	negative	negative close to threshold
Transition Time	positive	not significant	positive close to threshold
Dune Surface Erodibility at t_{tran}	not significant	negative	negative

Section 10.3: Sand Transport Potential			
Modelling Measurements	**Dune Surface Erodibility of an Initial Parabolic Dune**	$\tau_{D\_physioMax*}$	$\tau_{D\_physioMax*}$
Reactivation Threshold	positive	not significant	positive
Reactivation Angle	not significant	not significant	not significant
Transition Time	positive	negative close to threshold	positive close to threshold
Dune Surface Erodibility at t_{tran}	negative	negative	negative

Note: The 'positive' denotes that the modelling measurement (in row) increases as the parameter (in column) increases, whilst the 'negative' denotes an opposite trend. The 'not significant' means there is no pronounced trend between the parameter and the modelling measurement.

10.5 Processes and Mechanisms of the Parabolic-to-barchan Dune Transformation under Climatic Change

A barchan-to-parabolic dune transformation under climatic change can be conceptualised into stages illustrated by snapshots in Figure 10-26:

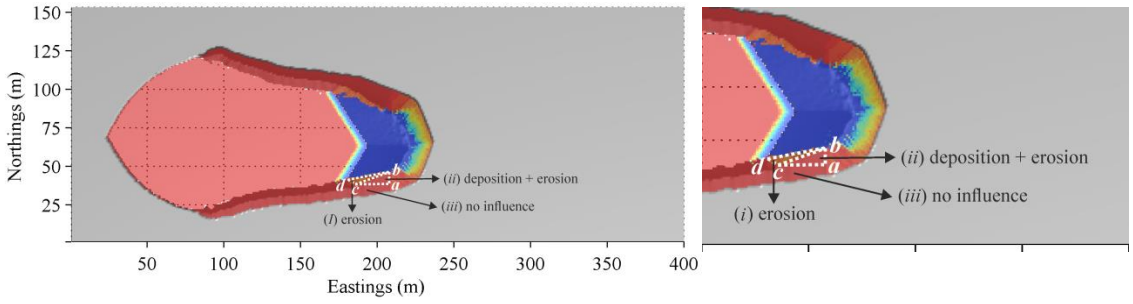

(a) t_0

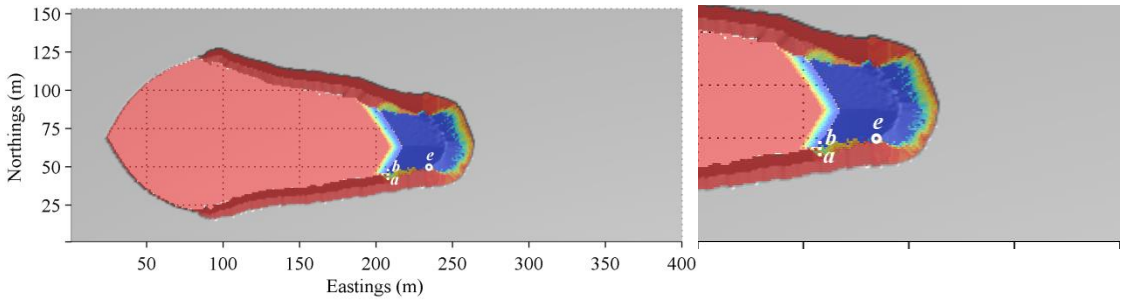

(b) 21 yr

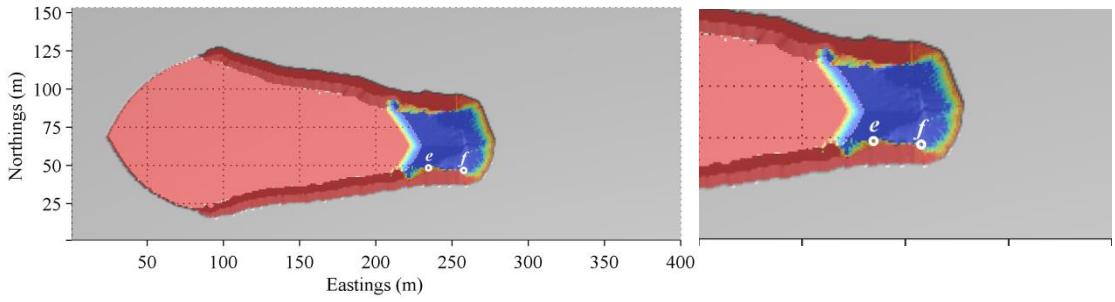

(c) 30 yr

Figure 10-26. (*To be continued*) Snapshots showing stages of the parabolic-to- barchan dune transformation. t_0 = 80 yr, q = 20 m^3 m^{-1} yr^{-1}, $\tau_{E\_physioMax}$ = -2.1 m $season^{-1}$, $\tau_{D\_physioMax}$ = 2.9 m $season^{-1}$, and CI = -0.14.

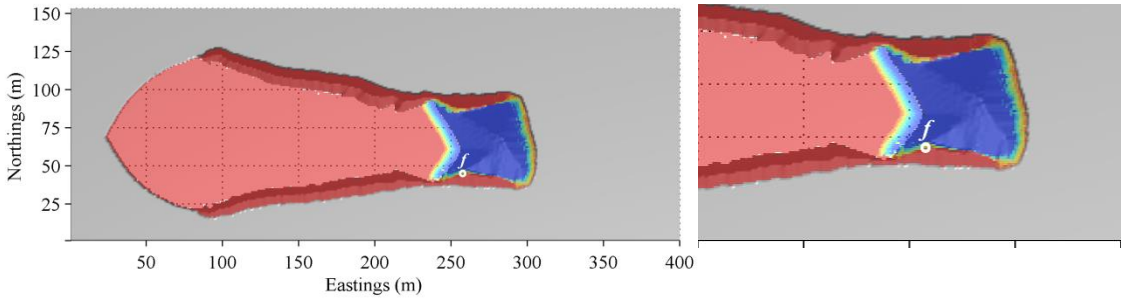

(d) 47 yr

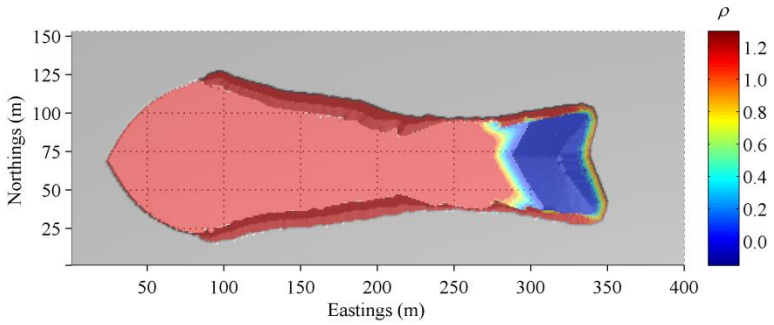

(e) 67 yr

Figure 10-26. (*Continued*) Snapshots showing stages of the parabolic-to- barchan dune transformation. t_0 = 80 yr, q = 20 m^3 m^{-1} yr^{-1}, $\tau_{E\_physioMax}$ = -2.1 m season^{-1}, $\tau_{D\_physioMax}$ = 2.9 m season^{-1}, and CI = -0.14.

The negative climatic impact reduces the capability of vegetation to withstand erosion and sand burial. More severe erosion causes vegetation on the inner slope of the arms close to the edges of the lobe to decline (*Zone i* outlined by Δ*bcd* in Figure 10-26a). The decline of vegetation in *Zone i* enables sand there to be transported and deposited onto *Zone ii* outlined by Δ*abc*. As the lobe migrates forward, the *Zone ii* ends up on the windward slope and undergoes erosion (*Line a-b* in Figure 10-26b). Beyond *Line a-c* in *Zone iii*, vegetation is able to withstand the climatic impact and neither erosion nor deposition occurs. The *Zone iii*, therefore, develops to be part of the arm.

The erosion of the arms provides more sand to be transported and deposited on the lee slope, thereby exerting a more severe negative impact on the vegetation there. More severe decline of vegetation on the edges of the lobe, meanwhile, further accelerates migration thereof as compared with the lobe in the middle. This is due to the fact that: (1) the vegetated area on the lower slope can maintain a steeper gradient than the bare surface on the upper slope, and the more severe decline of vegetation close to the lobe edges yields more abundant sand for advancing downwind (Figure 10-27); (2) a lower height on the lobe edges can lead to a faster migration rate (provided that the potential sand transport rate is the same),

which encourages the formation of a more rounded frontal edge of the dune lobe. However, the dune migration and the eco-geomorphic interaction in this stage are still controlled by the four eco-geomorphic interaction zones discussed in Figure 9-74.

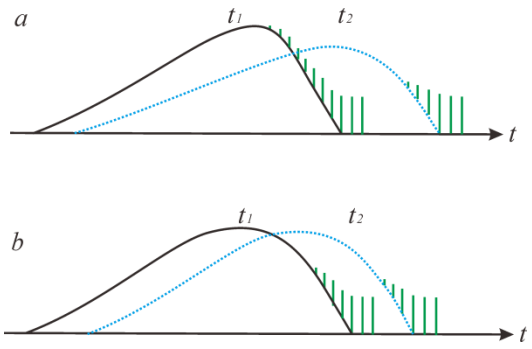

Figure 10-27. Different migration rates arising from the different maximum height where vegetation exists on the lee slope. Vegetation colonises a higher vertical position on the lee slope in the profile (a) than the profile (b). When vegetation declines to a similar position in height, the avalanching of sand on the upper slope in the profile (a) is more severe than that of the profile (b), because the vegetated area can maintain a steeper slope than the bare surface. This then results in a further and faster migration of the profile (a) as compared with the profile (b).

As *Line a-b* (Figure 10-26a) experiences stronger deposition, more severe erosion occurs when *Line a-b* is located on the windward slope as the lobe migrates forward. This is when a catastrophic shift begins. From that time onwards, severe erosion takes place on the vegetated edges of the lobe and the lobe is gradually separating from the trailing arms. The severe erosion provides more and more abundant sediment supply for sand transport from vegetated lobe edges along with incorporating sand from the sandy substratum underneath. This reinforces the vegetation decline on the lee slope and a faster migration rate on the lobe edges (because of a lower height). As a result, the maximum height that vegetation can reach on the lee slope decreases (see *Point e* and *Point f* in Figure 10-26c).

On the one hand, a faster migration of the lobe edges and lateral avalanching expand the frontal area, and vegetated edges of the lobe decrease in height because of vegetation decline arising from climatic impact; on the other hand, the vegetated edges that have already survived sand burial can only be eliminated by erosion because no sand supply is available upwind (since the reactivation angle is negative). As a result, an incipient crescentic ridge forms due to a faster migration rate on the edges as compared with the main body in the middle. At the same time, the middle of the parabolic ridge is

maintained because of a higher vertical location where vegetation has survived sand burial before the catastrophic shift occurred (see the *Point e* in Figure 10-26b&c). Continued erosion of vegetated edges lowers the height of the parabolic ridge due to the decrease in the maximum height vegetation can survive on the lee slope (see *Point f* in Figure 10-26c&d). The parabolic ridge eventually disappears when the vegetated lobe edges are no longer higher than the newly-created low ridge of the resulting barchan with a typical slip face (Figure 10-26d).

The initial parabolic dune transforms into a single barchan when the migration rate of the lobe edges is similar to the erosion rate of previously better-vegetated edges (or the parabolic ridge), as in the example described above. However, if the migration rate of the lobe edges is much faster than the erosion rate of the parabolic ridge, multiple barchans can develop (Figure 10-28). The lower erosion rate of the parabolic ridge slows down the migration rate of the main body in the middle, whereas the faster migration rate of lobe edges results in the escaping of sand from the main body and the formation of smaller sand piles downwind (because of severely deteriorated vegetation in the interdune areas incapable of deterring their fast migration). Continuous escaping of sand from the main body and the accumulation of sand on these piles can further lead to the development of barchans. The main body eventually transforms into a larger barchan as soon as the parabolic ridge has been completely eroded.

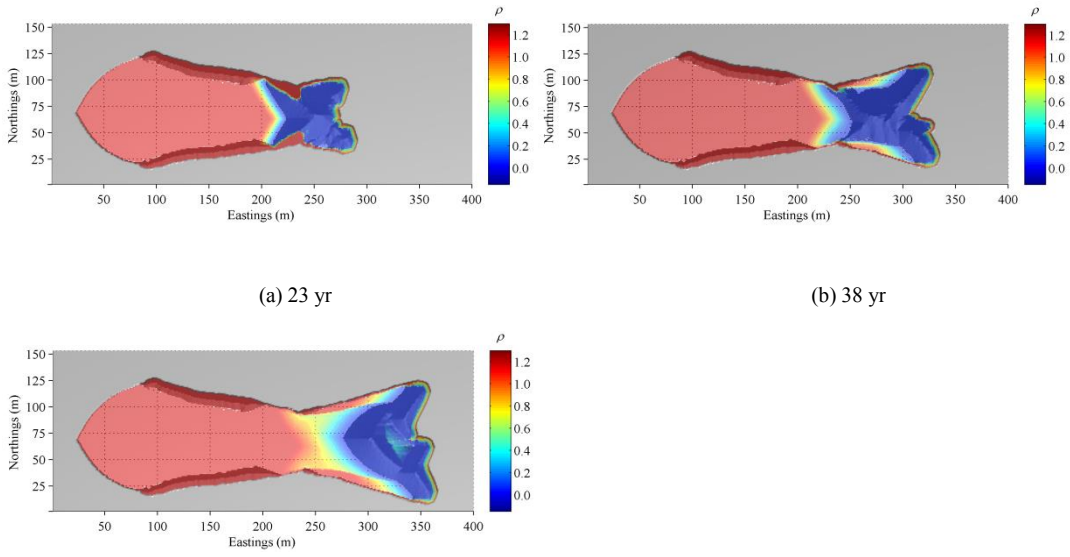

(a) 23 yr

(b) 38 yr

(a) 48 yr

Figure 10-28. Snapshots showing development of multiple barchans due to a faster migration rate of the lobe edges relative to the erosion rate of vegetated edges. t_0 = 90 yr, q = 20 m^3 m^{-1} yr^{-1}, $\tau_{E\_physioMax}$ = -2.1 m season^{-1}, $\tau_{D\_physioMax}$ = 2.9 m season^{-1}, and CI = -0.40.

A severe climatic change arising from the increase in either drought or wind energy can lead to the development of a larger reactivation angle, because 1) more severe vegetation decline on the lobe edges leads to a more severe lateral avalanching and a faster expansion of the frontal areas (the lee slope), and because 2) the *Point e* is at a lower height and the catastrophic shift happens more quickly, which also leads to shorter arms of the parabolic dune that is preserved. The reactivation angle seems independent of the stability of the initial parabolic dunes, indicating that although the different stability of an initial parabolic dune leads to different thresholds of climatic change, the degree to which climatic change can reactivate an initial parabolic dune is stronger than the influence arising from the different stability of an initial parabolic dune once the dune reactivation processes have been initiated.

A higher deposition tolerance reduces the difference in the migration rate on the lobe edges in comparison with the main body in the middle, thereby prolonging the transition duration of the parabolic-to-barchan dune transformation. The erosion tolerance of vegetation does not seem to impact the transformation significantly, but it is likely to influence the patterns of resulting barchans (a single barchan vs. multiple barchans) because of the effect on the erosion rate of the parabolic ridge. The characteristics of vegetation only play a significant role at a smaller climatic change. This suggests that the influence of severe climatic change on the dune transformation is independent from the flora in different regions.

10.6 Anthropogenic Pressure: Overgrazing

Grazing activity has been one of the major threats to a partially-vegetated dunefield, as the Ordos Plateau, due to its great vulnerability to environmental changes. The influence of grazing activity on the reactivation of parabolic dunes is explored in this section. Figure 10-29 exemplifies how grazing activity can lead to an initial parabolic dune being transformed into a highly mobile barchan. The general processes involved are in similar to that of the parabolic-to-barchan dune transformations arising from an increase in drought severity or wind energy. The greater impact of the vegetation on the lobe edges, as compared with the main body in the middle, results in a faster migration there, because of a gentler slope that bare surfaces can maintain (Figure 10-27) as well as a lower crest of the longitudinal profile. As sand is continuously incorporated into the migrating lobe from the sandy substratum and the eroded arms, the mobile lobe grows in size and expands laterally, transforming into a barchan eventually. In contrast to the

natural environmental changes which may only affect relatively weak and young plants, anthropogenic forces including grazing activity can exert a broader impact on any plant regardless of its size. As a result, well-vegetated interdune areas have also been reactivated slightly, leading to the development of low relief.

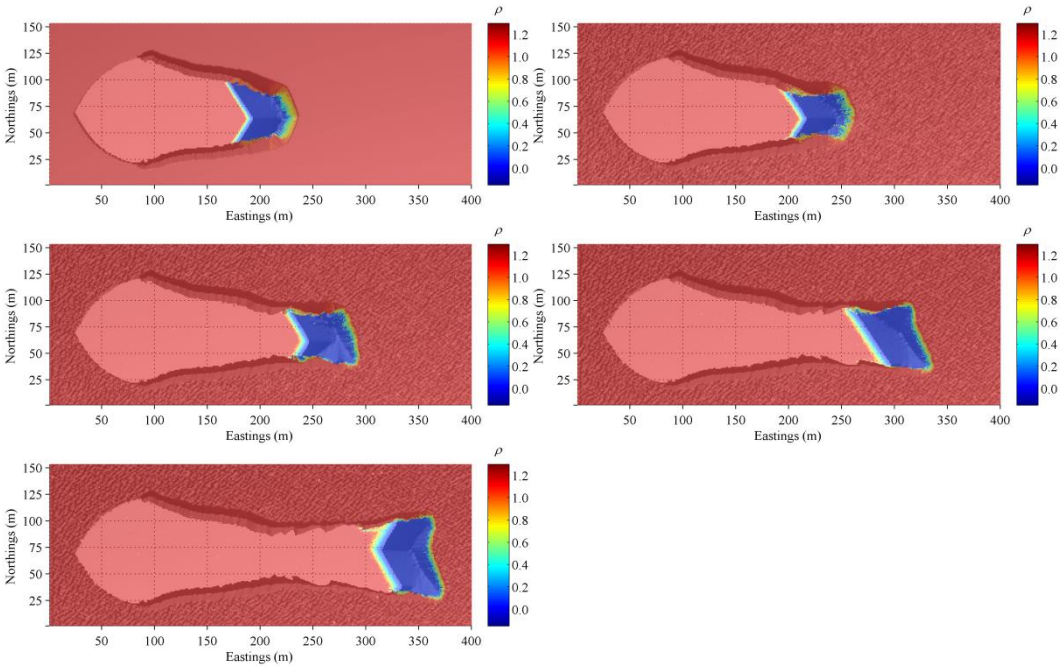

Figure 10-29. An example of the parabolic-to-barchan dune transformation arising from grazing activity. t_0 = 80 yr, q = 20 m^3 m^{-1} yr^{-1}, $\tau_{E\_physioMax}$ = -2.5 m $season^{-1}$, and $\tau_{D\_physioMax}$ = 3.0 m $season^{-1}$. The forage demand is 0.080 m^{-2} yr^{-1}. The interval between two snapshots is 20 yr.

As the forage demand increases, the transition time of the parabolic-to-barchan dune transformation decreases at a lower rate (Figure 10-30). This indicates a small increase in the forage demand just above the reactivation threshold can significantly shorten the transition time.

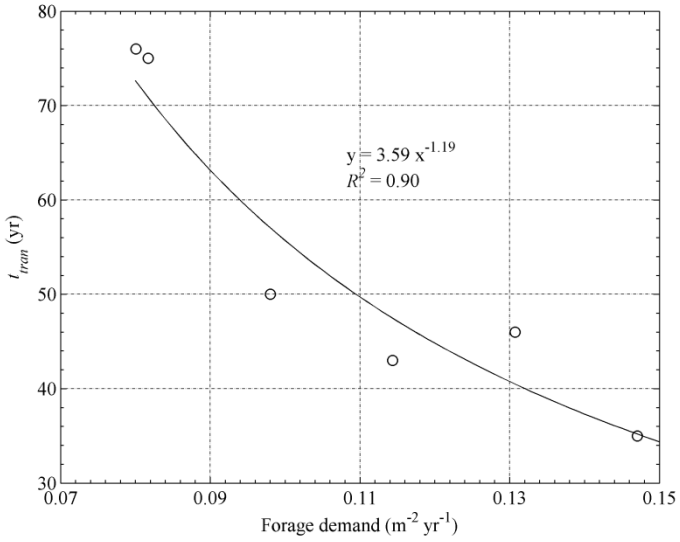

Figure 10-30. The relationship between the forage demand and the t_{tran} of the parabolic-to-barchan dune transformation. t_0 = 80 yr, q = 20 m^3 m^{-1} yr^{-1}, $\tau_{E\_physioMax}$ = -2.5 m $season^{-1}$, and $\tau_{D\_physioMax}$ = 3.0 m $season^{-1}$.

Figure 10-31 and Figure 10-32 show respectively the influence of the deposition tolerance and the erosion tolerance of vegetation on the forage demand threshold - the minimum forage demand that leads to the parabolic-to-barchan dune transformation. A higher deposition tolerance enables a dune system to withstand a larger forage demand before the dune stabilising processes are reversed, whereas the erosion tolerance seems to play a minimal role in determining the threshold of the parabolic-to-barchan dune transformation.

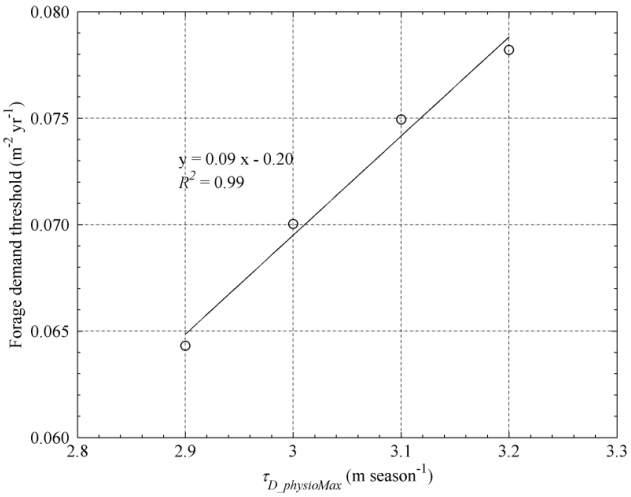

Figure 10-31. The relationship between the deposition tolerance of vegetation and the forage demand threshold for the parabolic-to-barchan dune transformation under $\tau_{E\_physioMax}$ of -2.5 m $season^{-1}$.

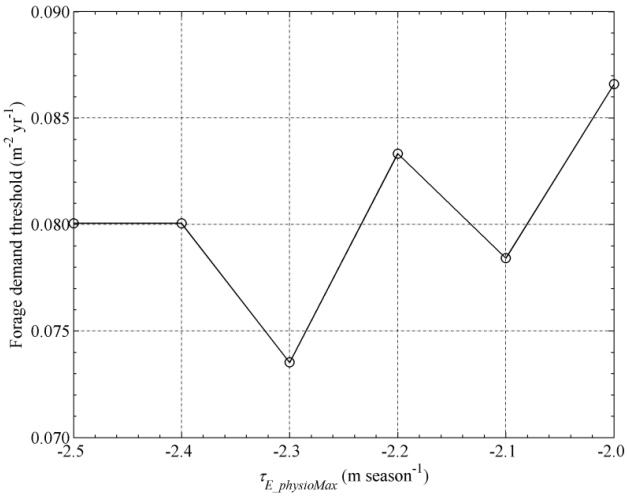

Figure 10-32. The relationship between the erosion tolerance of vegetation and the forage demand threshold for the parabolic-to-barchan dune transformation under $\tau_{D\_physioMax}$ of 3.0 m season^{-1}.

10.7 Discussion

Although some studies have reported that parabolic dunes can be reactivated and transformed into barchan and transverse dunes (*cf.* Section 2.3.4), few detailed research has been published so far (Nield and Baas, 2008). This chapter explores the possible scenarios in which an initial parabolic dune can be reactivated under climatic change arising from the increase in either drought or wind energy, or under grazing pressure. The modelling results show that the simulation scenarios are comparable to real-world situations regarding the realistic dune morphologies and the reasonable spatio-temporal scale. The processes and mechanisms of parabolic-to-barchan dune transformations have also been uncovered (*cf.* Section 10.4), which provides new insights into the change in eco-geomorphic interactions involved and into the possible linkage between field observations and dune transformation predictions.

The reactivation of an initial parabolic dune can lead to the development of more complicated imbricate dune morphology if the lobe of an initial parabolic dune is highly vegetated. This is because highly mobile initial parabolic dunes can be more easily reactivated and transformed into barchans, and can only continue to be stabilised under minor climatic impact. As a consequence, a highly mobile initial parabolic dune will either be reactivated into a barchan, or be stabilised as a lunate form. This suggests that the imbricate or digitate parabolic dunes can be developed in unidirectional wind regime, and multidirectional wind regime is hence not necessary (Pye and Tsoar, 1990).

The characteristics of eco-geomorphic interaction zones that control the parabolic-to-barchan dune transformation are different from the ones leading to the barchan-to-parabolic dune transformation. Following below, two transverse sections representing eco-geomorphic interaction zones of different stages involved in a parabolic-to-barchan dune transformation are discussed. The first transverse section, at 250 m eastings, represents a typical example showing how eco-geomorphic interaction zones respond to climatic change in an initial stage of the parabolic-to-barchan dune transformation when the transforming dune still maintains a parabolic shape. The second transverse section, at 325 m eastings, demonstrates typical eco-geomorphic interaction zones when the initial parabolic dune has transformed into a typical barchan dune with a slip face.

Figure 10-33 and Figure 10-34 show, as an example, how vegetation interacts with a migrating parabolic dune under climatic impact during the initial stage. Although the dune still maintains the parabolic shape, four basic eco-geomorphic interaction zones on a transverse line (the black line in Figure 10-34) exhibit different characteristics as the counterparts of the barchan-to-parabolic dune transformation shown in Figure 9-76. Figure 10-35 presents the temporal changes in height and vegetation effectiveness in the four zones, going from the outer edge to the dune middle-line. It can be seen that Zone 1, which develops into the outside slope of the arms, is almost eliminated (Figure 10-34). The Zone 2, which develops into the inner slope of the arms, is much thinner than the Zone 2 of the barchan-to-parabolic dune transformation due to much more severe impact of erosion (Figure 10-35b). As a result, trailing arms are no longer left behind. In contrast to the Zone 3 of the barchan-to-parabolic dune transformation, where vegetation dies solely because of sand burial (Figure 9-76c), vegetation in the Zone 3 of the parabolic-to-barchan dune transformation shown here declines slightly first due to sand burial, and then is eliminated by more severe erosion. The Zone 4 of the parabolic-to-barchan dune transformation in Figure 10-35d is similar to the counterpart of the barchan-to-parabolic dune transformation in which the maximum height where vegetation can survive is constant. In comparison to the barchan-to-parabolic dune transformation, the Zone 1 and Zone 2 of the initial parabolic dune - the only areas where vegetation is able to trap sand and stabilise the dune - are squeezed significantly under climatic impact. Consequently, the lobe expands in size due to the continuous incorporation of sand from its substratum underneath, and with only minimal loss to trailing arms.

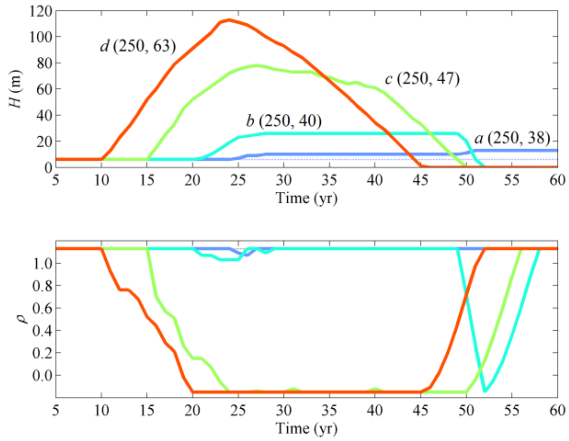

Figure 10-33. The changes in the height and the vegetation effectiveness over time under climatic impact. t_0 = 80 yr, q = 20 m^3 m^{-1} yr^{-1}, $\tau_{E\_physioMax}$ = -2.1 m season^{-1}, $\tau_{D\_physioMax}$ = 2.9 m season^{-1}, and CI = -0.14. The a, b, c, and d reflect the boundaries between different eco-geomorphic interaction zones across the transverse section at 250 m of eastings shown in snapshots in Figure 10-34.

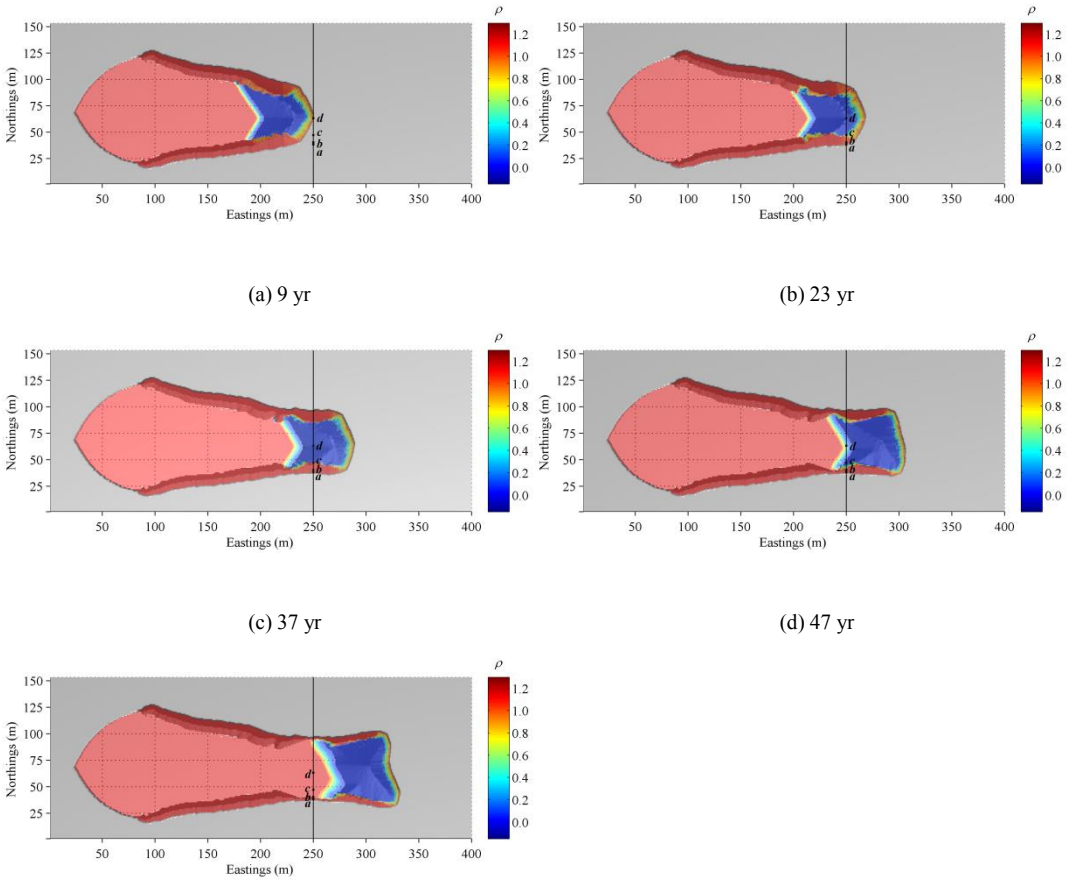

(a) 9 yr

(b) 23 yr

(c) 37 yr

(d) 47 yr

(c) 58 yr

Figure 10-34. The change in eco-geomorphic interaction under climatic impact. t_0 = 80 yr, q = 20 m^3 m^{-1} yr^{-1}, $\tau_{E\_physioMax}$ = -2.1 m season^{-1}, $\tau_{D\_physioMax}$ = 2.9 m season^{-1}, and CI = -0.14. The a, b, c, and d reflect boundaries between different eco-geomorphic interaction zones.

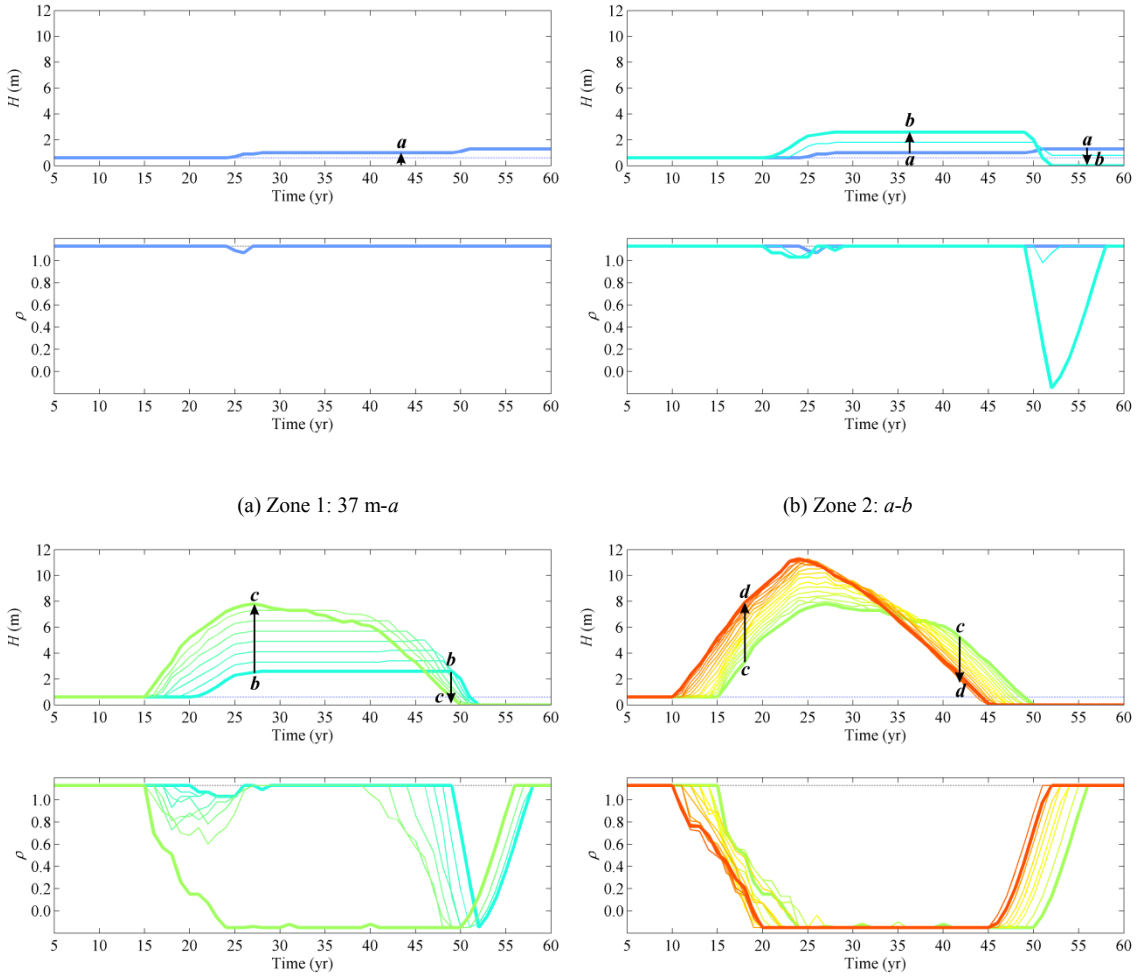

(a) Zone 1: 37 m-*a*

(b) Zone 2: *a*-*b*

(c) Zone 3: *b*-*c*

(d) Zone 4: *c*-*d*

Figure 10-35. Topography and vegetation change over time in different eco-geomorphic interaction zones under climatic impact. The *a*, *b*, *c*, and *d* are boundaries of different eco-geomorphic interaction zones across the transverse section at 250 m of eastings shown in snapshots in Figure 10-34. Each line/colour represents a 1 × 1 m^2 cell along the transverse section. The arrow shows the location of cells from south to north.

After the initial stage above, eco-geomorphic interaction zones when the parabolic dune has completed the transformation into a barchan are presented in Figure 10-36, Figure 10-37, and Figure 10-38. The characteristics of Zone 1 and Zone 2 are similar to their counterparts in the initial stage of the parabolic-to-barchan dune transformation under climatic impact in Figure 10-35. No outstanding arm is developed and the ridge is only 2 m in height (Figure 10-38a & b). Vegetation in Zone 2 declines slightly first because of sand burial and dies eventually because of erosion. The characteristics of Zone 3 are different from the counterparts of both the barchan-to-parabolic dune transformation (Figure 9-76c) and the initial stage of the parabolic-to-barchan dune transformation (Figure 10-35c). Vegetation in the Zone 3 can survive similar sand deposition and dies of further sand burial (Figure 10-38c). The *Point c* is the

tip of the barchan horn when it first encounters the migrating dune (Figure 10-37a), but it is the last to be eroded out of the deflation plain (Figure 10-37d). This indicates that the barchan dune is interacting with vegetation and expanding laterally. The Zone 4 shows similar characteristics of the counterpart of the barchan-to-parabolic dune transformation (Figure 10-38d & Figure 9-76d).

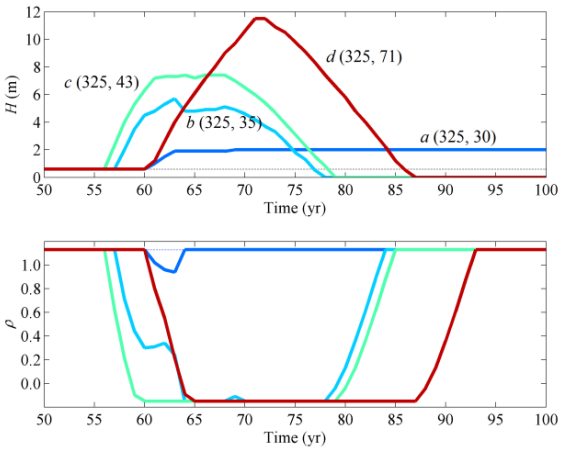

Figure 10-36. The changes in the height and the vegetation effectiveness over time under climatic impact. t_0 = 80 yr, q = 20 m^3 m^{-1} yr^{-1}, $\tau_{E\_physioMax}$ = -2.1 m season^{-1}, $\tau_{D\_physioMax}$ = 2.9 m season^{-1}, and CI = -0.14. The a, b, c, and d reflect the boundaries between different eco-geomorphic interaction zones across the transverse section at 325 m of eastings shown in snapshots in Figure 10-37.

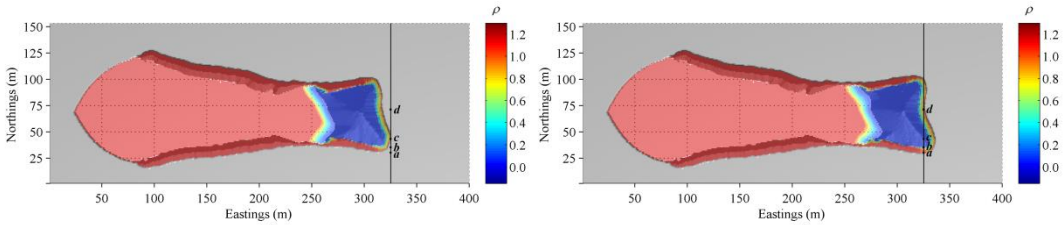

(a) 55 yr

(b) 60 yr

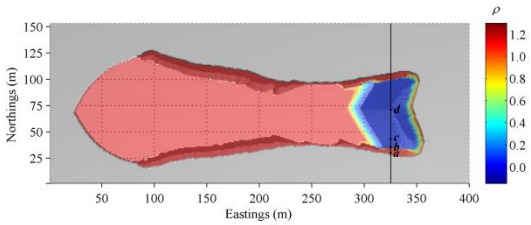

(c) 71 yr

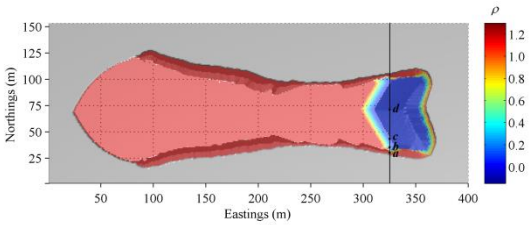

(d) 78 yr

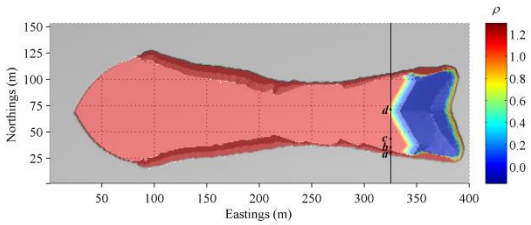

(c) 90 yr

Figure 10-37. The change in eco-geomorphic interaction under climatic impact. t_0 = 80 yr, q = 20 m^3 m^{-1} yr^{-1}, $\tau_{E\_physioMax}$ = -2.1 m season^{-1}, $\tau_{D\_physioMax}$ = 2.9 m season^{-1}, and CI = -0.14. The a, b, c, and d reflect boundaries between different eco-geomorphic interaction zones.

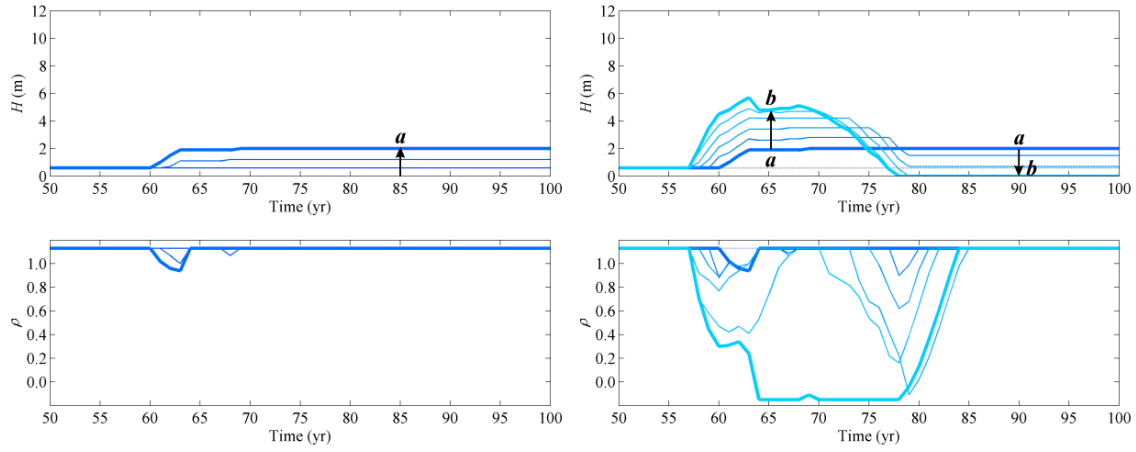

(a) Zone 1: 28 m-*a*

(b) Zone 2: *a*-*b*

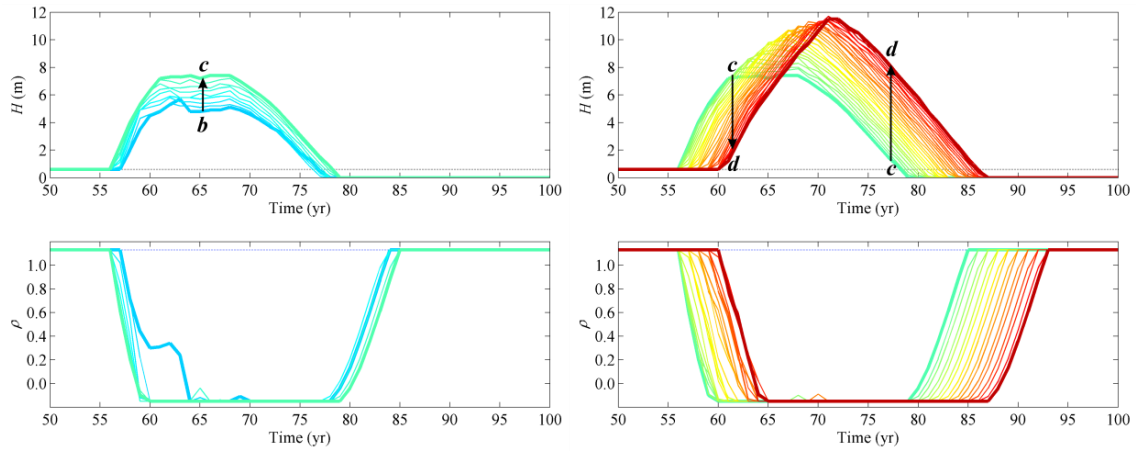

(c) Zone 3: *b*-*c*

(d) Zone 4: *c*-*d*

Figure 10-38. Topography and vegetation change over time in different eco-geomorphic interaction zones under climatic impact. The *a*, *b*, *c*, and *d* are boundaries of different eco-geomorphic interaction zones across the transverse section at 325 m of eastings shown in snapshots in Figure 10-37. Each line/colour represents a 1 × 1 m^2 cell along the transverse section. The arrow shows the location of cells from south to north.

As discussed above for both stages, the characteristics of four eco-geomorphic interaction zones closely relate to the processes of dune transformations, and may be potentially used to predict dune stability under climatic change in a real dunefield. Comparing modelling results herein against real-world data, however, requires further research. This chapter explores the parabolic-to-barchan dune transformation from an initial parabolic dune with similar shape but different levels of surface erodibility. A different shape of the initial parabolic dune may also influence the dune reactivation and transformation processes. The modelling results show that there is a reactivation lag of approximately 5 years between the start of climatic change and the dune morphological response, which may vary depending on the elongation ratio of an initial parabolic dune and the substratum thickness underneath. This lag is

equivalent to the reaction time in the conceptual dune remobilisation model of Hugenholtz and Wolfe (2005). Furthermore, the spacing and arrangement of initial parabolic dunes is likely to affect the processes of the reactivation and the parabolic-to-barchan dune transformation significantly due to interactions and collisions between migrating dunes, and hence requires further exploration.

References

Hugenholtz, C.H., Wolfe, S.A., 2005. Biogeomorphic model of dunefield activation and stabilization on the northern Great Plains. Geomorphology, 70(1-2), 53-70.

Nield, J.M., Baas, A.C.W., 2008. The influence of different environmental and climatic conditions on vegetated aeolian dune landscape development and response. Global and Planetary Change, 64(1–2), 76-92.

Pye, K., Tsoar, H., 1990. Aeolian sand and sand dunes. Unwin Hyman Ltd, London.

Chapter 11

General Discussion and Conclusions

Moving beyond the individual discussions in the previous chapters, this last chapter provides a general discussion regarding the methodology, strategies, contributions, limitations, and potential future research of this study as a whole, which is then followed by final conclusions to recap the main findings.

11.1 General Discussion

This thesis explores mechanisms and eco-geomorphic interactions of the barchan to parabolic dune transformations and the parabolic to barchan dune transformations. Dune transformations are a series of gradual processes over a relatively long period of time, at least in a magnitude of decades (Hugenholtz and Wolfe, 2005a; Tsoar and Blumberg, 2002). The absence of long-term field monitoring and remote sensing records regarding climatological, morphological, and ecological variables makes detailed empirical study on dune transformations difficult. To date, the fundamental mechanisms and eco-geomorphic interactions controlling both dune transformations remains poorly understood, although attempts have been made in various studies (Baas and Nield, 2007; Barchyn and Hugenholtz, 2012b; Duran and Herrmann, 2006; Livingstone and Warren, 1996; Muckersie and Shepherd, 1995; Robertson-Rintoul, 1990; Stetler and Gaylord, 1996; Tsoar and Blumberg, 2002; Wolfe and Hugenholtz, 2009). On the other hand, vegetated dunefields are quite often closely interacting with socio-economic activity, as on the Ordos Plateau, and there are growing public concerns about potential influence arising from environmental changes and urgent needs for planning judicious land-management practices responding to such changes. To bridge the gap between complex processes involved in dune transformations on a relatively long temporal scale and real-world monitoring records on a very limited temporal scale, this research has extended the DECAL model to incorporate key eco-geomorphic interactions informed by field measurements and remote sensing analysis to explore boundary conditions, parameter controls, and external forces on both dune transformations, and has improved greatly our understanding of the physical processes and mechanisms involved.

11.1.1 Applicability of the Extended-DECAL

This research has demonstrated how the Extended-DECAL can be adapted to a specific environment and can be customised and parameterised with real-world data to simulate possible scenarios under changes in a variety of natural and anthropogenic controls. The dynamic growth function introduced in the Extended-DECAL reflects the different capability of perennial shrubs to grow at different stages in their life cycles, and seems to capture the eco-geomorphic interactions of dune transformations at a reasonable temporal scale.

A considerable improvement has been made in the Extended-DECAL regarding incorporating natural growth curve of perennial vegetation species that is based on real-world field measurements in addition to the feedback between vegetation growth and sand transport (Baas and Nield, 2007; Duran et al., 2008; Nield and Baas, 2008b). Due to a lack of data and previous studies, an approach was used to regard the vegetation dimension as the proxy of vegetation age. More accurate results can, therefore, be achieved if the exact relationships between vegetation age, vegetation morphology, and the influence on sand transport are acquired. Despite these limitations, the natural growth curve of the dominant species Ordos Sagebrush is consistent with other studies suggesting that vegetation grows progressively, although is slightly different from sigmoid or exponential curves some studies have applied (Hugenholtz and Wolfe, 2005a; Hugenholtz and Wolfe, 2005b; Kutiel et al., 2004; Levin and Ben-Dor, 2004; Tsoar and Blumberg, 2002). The difference may be partly because the vegetation effectiveness used in the growth curve represents the impact of vegetation on sand transport rather than vegetation biomass, and the vegetation effectiveness can be influenced by a variety of factors including the vegetation structure and growth form, and partly because the vegetation growth used in these models is a change in overall canopy coverage in a certain area rather than the canopy change of a single plant. The growth form of the Ordos Sagebrush also resembles many shrubs and clumps of perennial grasses that dominate parabolic dune fields, such as marram grass (*Ammophila arenaria* and *Ammophila breviligulata*) which can be widely found across the Europe, and in some areas of South Africa, New Zealand, and Canada, and *Spinifex* species which colonies active parabolic dunes in Queensland of Australia (*cf.* Section 4.4).

The spatial resolution in a different dune system may be varied depending on the characteristics of the dominant vegetation species, which often involves a trade-off between different vegetation groups, especially when multiple vegetation species dominate a study region. Individual species may also adapt to climatic shifts in various behaviours. The erosion in the model influences vegetation growth through removing sediment and changing sedimentation balance. The erosion, however, can also remove nutrients

and create an inhospitable environment where little vegetation can survive (Mangan et al., 2004). The changes in chemical components of soil may also result in the changes in vegetation communities. The change of nutrients on vegetation growth and dune transformations is disregarded in the model and beyond the scope of this study, but it will be an important topic for further research.

A realistic vegetation seasonality differentiating the growing seasons from the non-growing seasons has also been incorporated into the model which has been disregarded by previous studies (Baas and Nield, 2007; Duran et al., 2008). In fact, seasonality is of particular importance in areas where dunes migrate periodically controlled by varying wind regime, temperature and precipitation, such as parabolic dunefields on Ceará and Sãn Franciso River Strand Plain in Brazil (Barbosa and Dominguez, 2004; Duran et al., 2008), on northern Great Plains in Canada (Hugenholtz et al., 2010; Wolfe and Hugenholtz, 2009), at Queensland coasts in Australia (Pye, 1983a; Pye, 1984), along Lake Michigan (Hansen et al., 2006), and at White Sands in New Mexico and eastern Colorado of the United States (Madole, 1995; McKee, 1966; Reitz et al., 2010). Because the study region represents a typical climate whereof windy seasons are associated with dry and cold, vegetation non-growing seasons, the modelling results may not be directly applicable to situations in which windy seasons coincide with vegetation growing seasons. The model, however, can be easily adapted to these environments to explore potential dune transformations. Nevertheless, it is very unlikely that active dune activity occurs in these areas since a greater vegetation cover can effectively inhibit the capability of strong winds to transport sand (Hesse and Simpson, 2006; Lancaster and Baas, 1998).

Simulated dune transformations herein are in a closed inland environment without external sediment supply. As such, the processes of dune transformations on the coast, in particular, behind high energy dispersive beaches, are likely to be significantly influenced by additional factors such as wave power, blowout activity, and coastline geometry (Duran and Moore, 2013; Eastwood et al., 2011). The modelling outcome may not be applicable to the third type of parabolic dunes (e.g., D5) in the study region where external sediment supply is available from the nearby seasonal river. The sand transport potential in the study region (q = 20 m^3 m^{-1} yr^{-1}), however, is comparable to many other parabolic dunefields such as Santa Catarina Island in Brazil (Bigarella et al., 2005), Anglesey of Wales in the United Kingdom (Ranwell, 1958), and Bigstick Sand Hills and Great Sand Hills of Saskatchewan in Canada (Hugenholtz et al., 2008; Wolfe and Lemmen, 1999).

11.1.2 System Controls on Barchan-to-parabolic Dune Transformations

The influence of primary controls on the barchan-to-parabolic dune transformation has been extensively explored, including the characteristics of vegetation (e.g., the capabilities of withstanding erosion and sand burial), the height of the initial barchan, the potential sand transport rate, and the substratum thickness. The results show that these parameters interact with each other, determining the processes of the dune transformation and the morphology of the resulting parabolic dunes in a complex manner.

Modelling results show that generally there are four types of parabolic dunes that are formed under various combinations of system parameters including chevron, lunate, typical, and elongated parabolic dunes, all of which, except chevron parabolic dunes, are end-members of dune stabilisation. Both the chevron and lunate parabolic dunes do not have evident trailing arms, but the chevron parabolic dunes are in the intermediate stage and largely bare, and thus have much higher mobility. The chevron parabolic dunes eventually develop into lunate or typical parabolic dunes. The outstanding difference between the chevron parabolic dunes and the lunate parabolic dunes is the migration form of their dune lobe. The chevron parabolic dunes migrate forward like an entity and their lobes do not change in shape over a long distance. Examples might be found in the parabolic dunefields along the Jafurah Desert in Saudi Arabia (Anton and Vincent, 1986) and in the Navajo County of Arizona (Stetler and Gaylord, 1996). In contrast, the lobes of the lunate parabolic dunes change in shape quickly. In effect, most lunate parabolic dunes start to develop only after their arms appear in the first place, like some parabolic dunes on the Canadian Prairies (Wolfe and Hugenholtz, 2009), at White Sands of New Mexico (McKee, 1966), and in the Horqin Desert of China (Yan, 2010). Elongated parabolic dunes in the model show a typical hairpin shape resembling those of the east coasts of Australia (Levin, 2011; Pye, 1983a; Pye, 1983b; Pye, 1984).

The capability of vegetation to withstand sand burial is a key factor governing a barchan-to-parabolic dune transformation, which has been observed by a few field studies (Hack, 1941; Hansen et al., 2006; McKee, 1966; Tsoar and Blumberg, 2002) and modelling explorations (Barchyn and Hugenholtz, 2012a; Barchyn and Hugenholtz, 2012b; Duran and Herrmann, 2006; Duran et al., 2008). This study also confirms that a slight increase in the deposition tolerance can significantly accelerate dune stabilisation and a barchan-to-parabolic dune transformation and lead to the development of less elongated dune morphology. The results, meanwhile, suggest that the erosion tolerance of vegetation also plays an important role, which has been disregarded by previous studies, although the transformation is less sensitive to a change in erosion tolerance in comparison to the deposition tolerance. For example, a

change of 0.1 m season^{-1} in the deposition tolerance leads to a deflection of a dune migrate rate from about 10 years, whilst the same change in the erosion tolerance only starts to alter the dune migration rate after more than 50 year. The influence of erosion tolerance is more pronounced when the deposition tolerance is relatively low, because the influence of erosion tolerance needs more time to manifest. Nevertheless, the erosion tolerance is crucial to develop long-walled trailing arms. This also explains why arms-developing angles are correlated well with the deposition tolerance, but they seem not to be influenced by the erosion tolerance.

Sand availability is another important control on the barchan-to-parabolic dune transformations (Arens et al., 2004; Livingstone and Warren, 1996). In a closed environment, sand supply is solely from the sandy substratum underneath the dunes besides sand stored in the dune bodies themselves, as is the case with the first and second types of parabolic dunes in the study region (*cf.* Section 5.4). A higher initial barchan dune or a thicker sandy substratum thickness encourages the stabilisation of barchan dunes into parabolic dunes. This is due to the fact that more sand available for sand transport slows down the dune migration rate, and enables vegetation to colonise the dune more easily. The research by Wiggs et al. (1995) has also found partially vegetated dunes of the Kalahari exhibit morphological changes in a similar degree as those much larger bare dunes in the Namib Desert, and reinforces that sand movement is a function of the dune size (Bagnold, 1941). Barchyn and Hugenholtz (2013) have shown that depth-limited blowouts migrate and elongate at a high rate and it is more difficult for plants to take root and stabilise their mobile lobes. The modelling simulations indicate similar results and found that small initial barchan dunes change in height more significantly before being stabilised as parabolic dunes. The substratum thickness seems play a more important role for relatively small dunes. There are several physical processes restraining one another. A smaller dune migrates at a higher rate, which inhibits the stabilisation by vegetation. A higher migration rate, however, also means that it can expose and incorporate more sand from the substratum on its way, which, on the other hand, can decelerate the migrating dune and encourage the stabilisation process. The sand from the dune, meanwhile, can be lost by forming trailing arms, and this sand loss from the dune lobe may accelerate dune migration substantially. These processes are significantly influenced by the characteristics of vegetation. A higher deposition tolerance of vegetation impedes the dune migration. Therefore, as the deposition tolerance of vegetation decreases, the importance of initial dune size becomes progressively overtaken by the sandy substratum thickness, and the erosion tolerance of vegetation plays an increasingly significant role. From

another point of view, as the height of the initial barchan increases, the characteristics of vegetation become less important.

The wind serves as the driving force in an aeolian system, and sand transport potential determines the potential capability of winds to transport sand (Nield and Baas, 2008b). It mobilises dunes by exerting two types of negative impacts on vegetation: burial and erosion (Lee and Ignaciuk, 1985; Maun, 1998). The simulation results show that as the sand transport potential increases, the transformations from barchan dunes to parabolic dunes generally have a greater sensitivity to all other system parameters, in particular, the erosion tolerance of vegetation and sandy substratum thickness, both of which play a more important role in a transformation when a system is more active and a dune maintains its mobility for a longer time. This is likely to indicate that dune mobility has a great spatial heterogeneity in a vegetated area under a relatively high energy wind regime. It also indicates that a stabilising dune in such an environment may be more easily activated by environmental stresses or human disturbances.

The proposed non-dimensional 'dune stabilising index (S_*)' captures the relationships between key parameters, and can assist in understanding a transforming dune system as a whole. It illustrates how the change in one parameter can be compromised by the change in another for a barchan-to-parabolic dune transformation. This extends significantly our understanding of the barchan-to-parabolic dune transformation to a more integrated level, as compared with focusing on limited parameter controls in previous studies (Barchyn and Hugenholtz, 2012b; Duran and Herrmann, 2006). The power-law relationship between the dune stabilising index and normalised migration distance provides a plausible approach for aiding paleoenvironmental reconstruction and predicting dune activity, as the example in Section 9.7.3 shows. This approach can be potentially used in areas where long-term remote sensing records are available, such as Whites Sand in New Mexico and dunefields in the Canadian prairies (Hugenholtz et al., 2010; Reitz et al., 2010). It also provides an indirect technique for monitoring climatic impacts on a dune system by detecting the degree of deviation from the known power-law relationship. For example, a higher L' or S_* may indicate that the stabilisation process is decelerated or accelerated by environmental changes. Although the exact relationship between the stabilising index and the normalised migration distance may vary to some degree in dune systems with different patterns of seasonality or vegetation communities, the role of each parameter in the barchan-to-parabolic dune transformation is likely to be the same. A verification of the approach using long term field data, however, is necessary before applying it to direct land-management practices.

The modelling results show that vegetation on the trailing arms is of particular importance in maintaining the parabolic-shaped dune morphology, akin to field observations by various studies (Livingstone and Warren, 1996; Muckersie and Shepherd, 1995; Robertson-Rintoul, 1990; Wolfe and Hugenholtz, 2009). Wide and high arms are associated with a faster transformation from an initial barchan to a parabolic dune. The vegetation zonation upwind of the stoss slope on the deflation plain (*cf.* Section 5.4) has also been replicated by the model. It is likely that the 'arms-anchoring' mechanism (*cf.* Section 2.3.2) controls the barchan-to-parabolic dune transformations in the study region, as discussed in Section 9.9 regarding the four eco-geomorphic zones identified. To what extent the formation of nebkhas can influence the barchan-to-parabolic dune transformation has not yet been explored, but the impact of small nebkhas below the spatial resolution (1 by 1 m^2) may be assumed to have been automatically incorporated into the modelling processes via the interaction between the vegetation growth and the sedimentation balance. The impact of large nebkhas has not been specifically simulated, but their influence on sand transport may be comparable with the combined effect of multiple neighbouring plants. The model, nevertheless, represents already the characteristics of more than 70 % of the overall plant population (*cf.* Section 5.3.3). The simulation results show that vegetation can temporally occupy the crest of the bare lobe of a highly mobile dune, in agreement with the findings by Tsoar and Blumberg (2002), but the vegetation can only thrive until the mobility of a dune decreases significantly (Wiggs et al., 1995).

The impacts of different parameter settings as well as the arrangement of dunes on the spatial heterogeneity of a dunefield are beyond the scope of this study, but are an important topic for future research. It may provide more effective strategies for vegetation restoration. For example, the modelling results indicate that separating individual barchan dunes from their neighbouring dunes may encourage the dune stabilisation and the transformation into parabolic dunes on a relatively large temporal scale.

The model has also been used to preliminarily explore the impacts of drought events and grazing activity on the barchan-to-parabolic dune transformation. It shows interestingly that there is a strong logarithmic relationship between the threshold of climatic impact and the ratio of the drought duration to the drought cycle. As the ratio increases, the threshold of climatic impact increases to a smaller degree. A stabilising dune system is more sensitive to the change in a relatively low ratio of the drought duration to the drought cycle. This agrees with findings by Hugenholtz and Wolfe (2005b) that small perturbations may extend the dune stabilisation time significantly on the southern Canadian prairies. Some dunes may even require centuries to completely stabilise (David et al., 1999; Olson, 1958; Wolfe, 1997). In

comparison to drought impact, grazing activity seems to exert a more severe impact and a relatively light forage demand can quickly reverse the processes of the dune stabilisation and the barchan-to-parabolic dune transformation. This suggests that controlling grazing activity is essential to restoring vegetation. The simulation results also show that a higher deposition tolerance can increase the resilience of a system to grazing activity and increase the threshold above which an initial barchan can no longer be stabilised into a parabolic dune. A system with a lower deposition tolerance of vegetation is more sensitive to a change in grazing activity.

11.1.3 System Controls on Parabolic-to-barchan Dune Transformations

Projections of more frequent drought in various regions may indicate more severe and prolonged droughts in the future (IPCC, 2013). This raises a great public concern on the activation of hitherto stabilised dunes, which has been observed at the Great Sand Dunes in Colorado (Marín et al., 2005). In this study, the parabolic-to-barchan dune reactivation and transformation have been explored from an initial parabolic dune with varying dune surface erodibility under changes in the drought severity and sand transport potential. The modelling results highlight that the relationship between erodibility and erosivity is susceptible to climatic changes (Thomas et al., 2005). Although for different reasons, the processes involved in the parabolic-to-barchan dune transformations are much alike. The modelling results shed important light on the eco-geomorphic interactions governing the parabolic-to-barchan dune transformations.

The modelling results suggest that the mobility of an initial parabolic dune at the outset of perturbations determines to a large extent the capacity of a system to absorb the environmental change and the propensity for reactivation and dune transformation. A slight increase in vegetation cover of an initial parabolic dune can increase the reactivation threshold of climatic impact (both drought stress and wind strength) significantly, consistent with findings suggested by Nield and Baas (2008a) that dune systems may exhibit a strong threshold response. Wiggs et al. (1995) have also found that an increase in water stress or wind strength can impair vegetation cover and a sparse vegetation cover raises the potential for surface mobility. A model proposed by Yizhaq et al. (2007) also indicates a similar behaviour that sufficiently high wind power can cause the decay of vegetation and activate stabilised dunes, and that changes in windiness and vegetation cover may shift the dune into a new state (Yizhaq et al., 2009). The modelling results suggest that there is positive feedback between the decline of vegetation

and the increase of sand availability (Brunsden and Thornes, 1979). A higher vegetation cover of initial parabolic dunes can dampen out small perturbations and enables the system to maintain the existing state (Hugenholtz and Wolfe, 2005a).

The modelling results show that the characteristics of vegetation play a less important role in the dune reactivation and parabolic-to-barchan dune transformations, as compared with the dune stabilisation and barchan-to-parabolic dune transformations. A higher deposition tolerance can increase the reactivation threshold of both climatic impact and sand transport rate slightly, but the influence of vegetation characteristics becomes negligible when the mobility of an initial parabolic dune is very low. As an extreme example, simulations from the initial parabolic dune at 120 yr can only be *either* stabilised *or* fully-reactivated by climatic impact, resembling observations by Nield and Baas (2008a). A highly vegetated parabolic dune cannot easily be reactivated and transformed into a barchan dune; instead, it results in more diverse dune morphologies and develops into a more complicated imbricated or nested parabolic dune. This seems to suggest that there is correlation between the complexity of dune morphology and the stability of the initial parabolic dunes. A long-term drought can, however, deplete vegetation and can reactive a dune significantly (Mangan et al., 2004). In contrast, stabilised parabolic dunes cannot be reactivated by increasing sand transport rate without catastrophic events such as fires or storms, because no sand is available for mobilisation. This indicates that under limited sand supply drought severity exerts more severe impacts on dune reactivation than windiness.

Beyond the threshold of a parabolic-to-barchan dune transformation, a small increase in either climatic impact or sand transport rate can accelerate the dune reactivation and transformation significantly, but a further increase would have a progressively decreased effect. A low erosion or deposition tolerance leads to the development of resulting barchan dunes with a higher dune surface erodibility. The influence of vegetation characteristics is more outstanding for an initial parabolic dune with higher stability. The different sensitivity caused by varying initial dune stability become less significant as the climatic impact increases, but does not show apparent change as the sand transport potential increases. This may be due to the fact that there is no significant difference in terms of sand availability even though vegetation cover is slightly different. As a result, vegetation characteristics play a less important role because of the limitation by sand availability even though sand transport potential increases substantially. In general, it seems that the transformation from more stabilised parabolic dunes to barchan dunes is more sensitive to changes in vegetation characteristics.

The modelling results also show that the characteristics of eco-geomorphic interaction zones involved in the dune reactivation are significantly different from that of dune stabilisation. Therefore, the change in the characteristics of eco-geomorphic interaction zones may indirectly reflect and predict the direction of an ongoing transformation. The reactivation angle is another interesting feature. There is a strong linear correlation between the climatic impact or the sand transport rate and the reactivation angle, independent of the stability of the initial parabolic dune and the reactivation threshold. The reactivation angle, therefore, may be potentially measured in the field and used as a proxy of environmental stresses. A large reactivation angle also means that the dune is more easily merged with any neighbouring dunes, which may result in the emergence of transverse dunes.

The response of dune morphology to environmental changes often involves time-lags. The modelling results suggest a reaction time of approximately 5 years before a dune starts to change its morphology in response to climatic change. Vegetation acts as a buffer between environmental changes and morphological responses, a prevalent phenomenon that has been observed in many studies. Lancaster and Helm (2000) have found that a lag between changes in precipitation and vegetation makes the dune mobility index incompetent to predict a short-term change in sand transport. Mangan et al. (2004) have contributed dunes at the High Plains remaining stable during the 1930s drought to the presence of plant rooting systems that can bind soil for a period of time even though the plants have died of drought. Hesse and Simpson (2006) found perennial plant cover predominantly controls the mobility of dunes in Australian. They also observed that the perennials have a response time longer than the inter-annual variations of precipitation, and seem to respond to cyclical droughts on a temporal scale of years to decades before impacting sand transport patterns over dunes. Compared with the response of dune morphology to environmental changes, vegetation is more sensitive and can thus be potentially used as an indicator for predicting the activation of vegetated parabolic dunes. In particular, the decline of vegetation on the lee slope and the windward slope close to the dune lobe is likely to be the first sign of dune reactivation and the subsequent parabolic-to-barchan dune transformation.

Under the same climatic environment, the transition time of the barchan-to-parabolic dune transformation depends on the size of the initial barchan. If environmental change occurs, some large barchans may have been transformed into the fully-vegetated parabolic dunes, whereas some smaller ones may still have a high mobility with relatively bare lobes. As a consequence, dunes respond to environmental change in different manners. Parabolic dunes with a high dune surface erodibility may be reactivated and transformed into barchans, whereas parabolic dunes with a relatively low dune surface

erodibility develop from simple forms into more complicated forms. The spatial arrangements and the history of dunes, therefore, play an important role in shaping the spatial heterogeneity of a dunefield. This may be an important reason why highly mobile barchans have been found to coexist with well-vegetated parabolic dunes in the field, such as dunefields in north-eastern Brazil (Yizhaq et al., 2007). Yizhaq et al. (2009) also suggest that the dune reactivation process is almost irreversible. Once reactivation of dunes occurs, it requires environmental stresses decreasing far below the levels of initial state to restore the stability of the system, the so-called hysteresis behaviour (Tsoar, 2005). The modelling results illustrate a similar behaviour that it is almost impossible for highly vegetated parabolic dunes to restore to the original state after they have been activated into barchans.

11.2 Conclusions

The outcome of each objective proposed in this study is summarised in Table 11-1. It illustrates how each objective has been achieved throughout this thesis. The Extended-DECAL introduces the 'dynamic' growth function and incorporates a range of functionalities to simulate eco-geomorphic interactions between perennial shrubs and dune morphology, including seasonality, climatic impact, and grazing pressure. Both the barchan-to-parabolic and the parabolic-to-barchan dune transformations have been replicated on realistic temporal and spatial scales. The fundamental mechanisms controlling both dune transformations have also been explored in detail.

Table 11-1. Thesis objectives and outcomes.

Objective	Outcome
(1) Explore how a CA model can be used to simulate interactions between different vegetation species and environmental conditions, in particular perennial grasses/shrubs that have relatively long life spans and strong seasonal growth patterns.	Various algorithms have been incorporated into the DECAL model to simulate the eco-geomorphic interactions between the growth of shrubs and sand transport, in particular the dynamic growth functions and the differentiation of shrub growth between growing and non-growing seasons (*cf.* Chapter 7).
(2) Explore how to utilise field investigations and remote sensing technique to help parameterise the model and predict potential dunefield evolutions under climatic changes.	The vegetation growth function and sand transport potential in the model have been successfully parameterised by field measurements (vegetation and DEMs, *cf.* Chapter 5) and remote sensing imagery interpretations (*cf.* Chapter 6).
(3) Investigate sensitivity of a barchan-to-parabolic dune transformation to changes in the sand availability (sandy substratum thickness and the size of barchan dunes), the wind regime, and the characteristics of vegetation species (the capability of withstanding wind erosion and sand burial).	The impacts of five key system parameters on a barchan-to-parabolic dune transformation have been fully explored. The modelling outcomes have been summarised in Table 9-1.
(4) Understand the fundamental eco-geomorphic processes during a barchan-to-parabolic dune transformation.	The physical processes that control a barchan-to-parabolic dune transformation have been investigated and clarified (*cf.* Section 9.8.2). The four eco-geomorphic interacting zones have been identified, which bear different functionality in the dune stabilisation (*cf.* Section 9.10).
(5) Explore how environmental parameters in a dune system interact and compromise with each other and fundamentally determine the processes of a barchan-to-parabolic dune transformation.	Stabilising index has been proposed to link the different parameters and to compare transformations across different dune systems (*cf.* Section 9.8.1).
(6) Investigate the processes and possibilities of the parabolic-to-barchan dune transformations under potential increases in drought stress and wind strength.	The impacts of drought stress and windiness on dune reactivation and the parabolic-to-barchan dune transformations have been established. The modelling outcomes have been summarised in Table 10-2.
(7) Understand the eco-geomorphic interactions that fundamentally govern the dune reactivation and parabolic-to-barchan dune transformations.	The physical processes that control a parabolic-to-barchan dune transformation have been investigated and clarified (*cf.* Section 10.5). The four eco-geomorphic interacting zones have been identified, which bear different functionality in the dune reactivation (*cf.* 10.7).
(8) Primarily explore the influence of period drought events and grazing activities on both dune stabilisation and reactivation.	The impacts of cyclical drought events and grazing activities on both dune stabilisation and reactivation have been explored (*cf.* Section 9.9 & 10.6).
(9) Explore the applicability of the Extended-DECAL in different aeolian systems.	This study has demonstrated how to customise the model by using real-world data to explore potential dune transformations (*cf.* 7.4.6). and assist in judicious land-management practices.

The characteristics of vegetation species, in particular the capability to withstand wind erosion and sand burial, play a key role in determining the transformation type and rate. The deposition tolerance of vegetation significantly influences the transition time and the resulting dune morphology of both dune transformations. A higher deposition tolerance encourages the stabilisation of a barchan, and leads to a faster dune transformation into a parabolic dune with no or relatively short arms - less elongated and more lunate dune morphology. Meanwhile, a higher deposition tolerance enables vegetation downwind of a partially-vegetated parabolic dune to resist stronger climatic impact, and hence results in gentler reactivation and a longer transition time into a barchan. In comparison with the deposition tolerance, the erosion tolerance of vegetation plays a less significant role in controlling the general direction of dune transformations, but the erosion tolerance is essential to the development of trailing arms of parabolic

dunes from an initial barchan and it influences the lateral expansion of a reactivated dune lobe into a highly mobile barchan.

Sand availability in a closed environment is primarily controlled by the size of dunes and the thickness of sandy substratum underneath. A higher sand availability generally decelerates dune migration and hence encourages the dune stabilisation and the barchan-to-parabolic dune transformation. In contrast, a high sand availability arising from larger surface erodibility of an initial parabolic dune increases sand transport and requires a smaller climatic impact to be reactivated into a barchan, because sand availability, instead of wind energy, is the limiting factor for sand transport in such an environment that dunes are surrounded by a well-vegetated interdune plain. An increase in potential sand transport rate accelerates the dune migration, thereby prolonging the transition time of the barchan-to-parabolic dune transformation, but shortens the transition time of the parabolic-to-barchan dune transformation.

The non-dimensional 'dunes stabilising index (S_*)' captures the key controls and the interactions of parameters that affect the processes of the barchan-to-parabolic dune transformation, and can be potentially used to reconstruct the history of stabilising dunes, and to predict dune activity. The arms-developing angle and the reactivation angle are closely related with the rate of dune stabilisation and reactivation respectively. They may be potentially identified and measured in the field, providing a useful linkage between field measurements and modelling simulations. The characteristics of eco-geomorphic interaction zones are more sensitive to the changes in environmental forces as compared with dune morphology, and may also be used as a proxy to monitor the stability of a dune system.

The Extended-DECAL has been used to preliminarily explore the impacts of drought events and grazing activity. The results show that a small increase in the ratio of the drought duration to the drought cycle can significantly reduce the capability of a dune system to be stabilised and to resist climatic impact. The modelling results indicate that the grazing activity, in comparison with climatic impact, can more easily result in dune reactivation and the transformation from vegetated parabolic dunes into barchan dunes.

The model can be easily adapted to a different dune environment, and be used to explore various scenarios under changes in both natural and anthropogenic controls. A relatively low computational demand enables extensive explorations of phase space and phase diagrams, detailed investigations of complicated interactions between relatively large numbers of system parameters, which can then assist in understanding various eco-geomorphic processes of a dune system in a more integrated manner.

References

Anton, D., Vincent, P., 1986. Parabolic dunes of the Jafurah Desert, Eastern Province, Saudi Arabia. Journal of Arid Environments, 11(3), 187-198.

Arens, S.M., Slings, Q., de Vries, C.N., 2004. Mobility of a remobilised parabolic dune in Kennemerland, The Netherlands. Geomorphology, 59(1-4), 175-188.

Baas, A.C.W., Nield, J.M., 2007. Modelling vegetated dune landscapes. Geophysical Research Letters, 34(6).

Bagnold, R.A., 1941. The physics of blown sand and desert dunes. Methuen & Co. Ltd, London.

Barbosa, L.M., Dominguez, J.M.L., 2004. Coastal dune fields at the São Francisco River strandplain, northeastern Brazil: morphology and environmental controls. Earth Surface Processes and Landforms, 29(4), 443-456.

Barchyn, T.E., Hugenholtz, C.H., 2012a. Predicting vegetation-stabilized dune field morphology. Geophysical Research Letters, 39.

Barchyn, T.E., Hugenholtz, C.H., 2012b. A process-based hypothesis for the barchan-parabolic transformation and implications for dune activity modelling. Earth Surface Processes and Landforms, 37(13), 1456-1462.

Barchyn, T.E., Hugenholtz, C.H., 2013. Reactivation of supply-limited dune fields from blowouts: A conceptual framework for state characterization. Geomorphology, 201(0), 172-182.

Bigarella, J.J., Klein, A.H.D., Menezes, J.T., Vintem, G., 2005. Sub-tropical coastal dunes: Examples from southern Brazil. Journal of Coastal Research, 113-137.

Brunsden, D., Thornes, J.B., 1979. Landscape Sensitivity and Change. Transactions of the Institute of British Geographers, 4(4), 463-484.

David, P.P., Wolfe, S.A., Huntley, D.J., Lemmen, D.S., 1999. Activity cycle of parabolic dunes based on morphology and chronology from Seward sand hills, Saskatchewan, Holocene Climate and Environmental Change in the Palliser Triangle: a Geoscientific Context for Evaluating the Impacts of Climate Change on the Southern Canadian Prairies. Geological Survey of Canada Bulletin 534, pp. 223-238.

Duran, O., Herrmann, H.J., 2006. Vegetation against dune mobility. Physical Review Letters, 97(18), 188001/188001-188004.

Duran, O., Moore, L.J., 2013. Vegetation controls on the maximum size of coastal dunes. Proceedings of the National Academy of Sciences of the United States of America, 110(43), 17217-17222.

Duran, O., Silva, M.V.N., Bezerra, L.J.C., Herrmann, H.J., Maia, L.P., 2008. Measurements and numerical simulations of the degree of activity and vegetation cover on parabolic dunes in north-eastern Brazil. Geomorphology, 102(3-4), 460-471.

Eastwood, E., Nield, J., Baas, A., Kocurek, G., 2011. Modelling controls on aeolian dune-field pattern evolution. Sedimentology, 58(6), 1391-1406.

Hack, J.T., 1941. Dunes of the Western Navajo Country. Geogr. Rev., 31(2), 240-263.

Hansen, E.C., Arbogast, A.F., Dijk, D.v., Yurk, B., 2006. Growth and Migration of Parabolic Dunes Along the Southeastern Coast of Lake Michigan. Journal of Coastal Research, 209-214.

Hesse, P.P., Simpson, R.L., 2006. Variable vegetation cover and episodic sand movement on longitudinal desert sand dunes. Geomorphology, 81(3-4), 276-291.

Hugenholtz, C.H., Bender, D., Wolfe, S.A., 2010. Declining sand dune activity in the southern Canadian prairies: Historical context, controls and ecosystem implications. Aeolian Research, 2(2-3), 71-82.

Hugenholtz, C.H., Wolfe, S.A., 2005a. Biogeomorphic model of dunefield activation and stabilization on the northern Great Plains. Geomorphology, 70(1-2), 53-70.

Hugenholtz, C.H., Wolfe, S.A., 2005b. Recent stabilization of active sand dunes on the Canadian prairies and relation to recent climate variations. Geomorphology, 68(1–2), 131-147.

Hugenholtz, C.H., Wolfe, S.A., Moorman, B.J., 2008. Effects of sand supply on the morphodynamics and stratigraphy of active parabolic dunes, Bigstick Sand Hills, southwestern Saskatchewan. Can. J. Earth Sci., 45(3), 321-335.

IPCC, 2013. Climate change 2013: the physical science basis. Contribution of working group I to the fifth assessment report of the intergovernmental panel on climate change. Cambridge University Press, New York.

Kutiel, P., Cohen, O., Shoshany, M., Shub, M., 2004. Vegetation establishment on the southern Israeli coastal sand dunes between the years 1965 and 1999. Landscape and Urban Planning, 67(1–4), 141-156.

Lancaster, N., Baas, A.C.W., 1998. Influence of vegetation cover on sand transport by wind: Field studies at Owens Lake, California. Earth Surface Processes and Landforms, 23(1), 69-82.

Lancaster, N., Helm, P., 2000. A test of a climatic index of dune mobility using measurements from the southwestern United States. Earth Surface Processes and Landforms, 25(2), 197-207.

Lee, J.A., Ignaciuk, R., 1985. The physiological ecology of strandline plants. Plant Ecol., 62(1), 319-326.

Levin, N., 2011. Climate-driven changes in tropical cyclone intensity shape dune activity on Earth's largest sand island. Geomorphology, 125(1), 239-252.

Levin, N., Ben-Dor, E., 2004. Monitoring sand dune stabilization along the coastal dunes of Ashdod-Nizanim, Israel, 1945–1999. Journal of Arid Environments, 58(3), 335-355.

Livingstone, I., Warren, A., 1996. Aeolian Geomorphology: An Introduction. Longman, Harlow.

Madole, R.F., 1995. Spatial and temporal patterns of late quaternary eolian deposition, Eastern Colorado, U.S.A. Quaternary Science Reviews, 14(2), 155-177.

Mangan, J., Overpeck, J., Webb, R., Wessman, C., Goetz, A.H., 2004. Response of Nebraska Sand Hills Natural Vegetation to Drought, Fire, Grazing, and Plant Functional Type Shifts as Simulated by the Century Model. Climatic Change, 63(1-2), 49-90.

Marín, L., Forman, S.L., Valdez, A., Bunch, F., 2005. Twentieth century dune migration at the Great Sand Dunes National Park and Preserve, Colorado, relation to drought variability. Geomorphology, 70(1–2), 163-183.

Maun, M.A., 1998. Adaptations of plants to burial in coastal sand dunes. Can. J. Bot.-Rev. Can. Bot., 76(5), 713-738.

McKee, E.D., 1966. Structures of dunes at white sands national monument, New Mexico. Sedimentology, 7(1), 3-69.

Muckersie, C., Shepherd, M.J., 1995. Dune phases as time-transgressive phenomena, Manawatu, New Zealand. Quaternary International, 26, 61-67.

Nield, J.M., Baas, A.C.W., 2008a. The influence of different environmental and climatic conditions on vegetated aeolian dune landscape development and response. Global and Planetary Change, 64(1–2), 76-92.

Nield, J.M., Baas, A.C.W., 2008b. Investigating parabolic and nebkha dune formation using a cellular automaton modelling approach. Earth Surface Processes and Landforms, 33(5), 724-740.

Olson, J.S., 1958. Rates of Succession and Soil Changes on Southern Lake Michigan Sand Dunes. Botanical Gazette, 119(3), 125-170.

Pye, K., 1983a. The coastal dune formations of northern Cape York Peninsula, Queensland. Proceedings of the Royal Society of Queensland, 94, 33-39.

Pye, K., 1983b. Dune formation on the humid tropical sector of the North Queensland Coast, Australia. Earth Surface Processes and Landforms, 8(4), 371-381.

Pye, K., 1984. Models of transgressive coastal dune building episodes and their relationship to Quaternary sea level changes: a discussion with reference to evidence from eastern Australia. In: M.W. Clark (Ed.), Coastal Research: UK Perspectives. Geo Books, Norwich, pp. 81-104.
Ranwell, D., 1958. Movement of vegetated sand dunes at Newborough Warren, Anglesey. Journal of Ecology, 46(1), 83-100.
Reitz, M.D., Jerolmack, D.J., Ewing, R.C., Martin, R.L., 2010. Barchan-parabolic dune pattern transition from vegetation stability threshold. Geophysical Research Letters, 37.
Robertson-Rintoul, M.J., 1990. A quantitative analysis of the near-surface wind flow pattern over coastal parabolic dunes. In: K.F. Nordstrom, N.P. Psuty, R.W.G. Carter (Eds.), Coastal Dunes Form And Processes. John Wiley & Sons Ltd., Chichester, pp. 57-78.
Stetler, L.D., Gaylord, D.R., 1996. Evaluating eolian-climatic interactions using a regional climate model from Hanford, Washington (USA). Geomorphology, 17(1–3), 99-113.
Thomas, D.S.G., Knight, M., Wiggs, G.F.S., 2005. Remobilization of southern African desert dune systems by twenty-first century global warming. Nature, 435(7046), 1218-1221.
Tsoar, H., 2005. Sand dunes mobility and stability in relation to climate. Physica A, 357(1), 50-56.
Tsoar, H., Blumberg, D.G., 2002. Formation of parabolic dunes from barchan and transverse dunes along Israel's Mediterranean coast. Earth Surface Processes and Landforms, 27(11), 1147-1161.
Wiggs, G.F.S., Thomas, D.S.G., Bullard, J.E., Livingstone, I., 1995. Dune mobility and vegetation cover in the Southwest Kalahari desert. Earth Surface Processes and Landforms, 20(6), 515-529.
Wolfe, S.A., 1997. Impact of increased aridity on sand dune activity in the Canadian Prairies. Journal of Arid Environments, 36(3), 421-432.
Wolfe, S.A., Hugenholtz, C.H., 2009. Barchan dunes stabilized under recent climate warming on the northern Great Plains. Geology, 37(11), 1039-1042.
Wolfe, S.A., Lemmen, D.S., 1999. Monitoring of dune activity in the Great Sand Hills region, Saskatchewan. In: D.S. Lemmen, R.E. Vance (Eds.), Holocene Climate and Environmental Change in the Palliser Triangle: a Geoscientific Context for Evaluating the Impacts of Climate Change on the Southern Canadian Prairies. Geological Survey of Canada Bulletin 534, pp. 199-210.
Yan, N., 2010. Surface process and morphological evolution of parabolic dunes. Msc., Beijing Normal University, Beijing, 42 pp.
Yizhaq, H., Ashkenazy, Y., Tsoar, H., 2007. Why Do Active and Stabilized Dunes Coexist under the Same Climatic Conditions? Physical Review Letters, 98(18), 188001.
Yizhaq, H., Ashkenazy, Y., Tsoar, H., 2009. Sand dune dynamics and climate change: A modeling approach. Journal of Geophysical Research: Earth Surface, 114(F1), F01023.